Multifunctional Amphiphilic Polyethers:

From Polyether Lipids to Tapered Structures

Dissertation zur Erlangung des Grades

“Doktor der Naturwissenschaften”

im Promotionsfach Chemie

am Fachbereich Chemie, Pharmazie und Geowissenschaften

der Johannes Gutenberg-Universität Mainz

Ann-Kathrin Maria Danner

geboren in Tübingen

Mainz, Mai 2018

JOHANNES GUTENBERG UNIVERSITÄT MAINZ

MATERIALS IN MAINZ SCIENCE

Dekan:

1. Berichterstatter:

2. Berichterstatter:

Tag der mündlichen Prüfung: 05. Juli 2018

Die als Dissertation vorgelegte Arbeit wurde in der Zeit von Mai 2015 bis Mai 2018 am Institut für Organische Chemie der Johannes Gutenberg-Universität Mainz im Arbeitskreis von Herrn Univ.-Prof. Dr. Holger Frey angefertigt.

Hiermit versichere ich gemäß § 10 Abs. 3d der Promotionsordnung vom 24.07.2007

Ich habe die jetzt als Dissertation vorgelegte Arbeit selbst angefertigt und alle benutzten Hilfsmittel (Literatur, Apparaturen, Material) in der Arbeit angegeben.

Ich habe oder hatte die jetzt als Dissertation vorgelegte Arbeit nicht als Prüfungsarbeit für eine andere staatliche oder andere wissenschaftliche Prüfung eingereicht.

Ich hatte weder die jetzt als Dissertation vorgelegt Arbeit noch Teile davon bei einer anderen Fakultät bzw. einem anderen Fachbereich als Dissertation eingereicht.

_____

Ann-Kathrin Danner

Für meine Familie

Danksagung

Vielen Dank!

Table of Contents

Motivation and Objectives

Due to their unique properties, aliphatic polyethers are an important and highly established class of polymers that are used for an immense variety of applications both in industry and academia. Especially polyethylene glycol (PEG), which is the gold standard for biomedical applications, is of enormous interest. The characteristic properties of PEG are its flexible and highly hydrophilic backbone as well as its chemical inertness.[1] Furthermore, PEG exhibits very low immunogenicity as well as toxicity and is therefore applied, *e.g.* in skin care products, food additives, laxatives and tablet formulations.[2,3] Moreover, bioconjugation and covalent attachment of PEG to the surface of nanocarriers, known as PEGylation, is commonly performed and serves to increase the aqueous solubility. In addition, PEGylation leads to improved pharmacokinetic properties due to reduced uptake by cells of the immune system, prolonged blood circulation times and decreased side effects.[4] In particular, PEG-lipids applied in liposomal nanocarriers result in sterically stabilized liposomes, so-called "stealth" liposomes, and thus have attracted considerable attention in biomedicine and nanotechnology.[5–7]

However, PEG only possesses two hydroxyl groups that are available for functionalization. This limits its utility for certain applications. Especially PEG-lipids applied in nanocarriers demand for the attachment of functional groups for active targeting or to enable labeling *via e.g.* radioactive labels or fluorescent markers, serving for carrier tracking. The attachment of several functional groups increases the loading capacity and leads to tailored properties whereas the aqueous solubility can be maintained.

Furthermore, the non-degradability of PEG is a drawback for numerous applications, especially in biomedicine. In order to avoid accumulation in tissue and enable renal clearance, the applied PEG segments must be below the renal threshold (<30 kDa), leading to a restriction of the applicable molecular weight.[8,9] PEGylation leads to sterically stabilized nanocarriers but also reduces the cellular uptake of the carriers and impedes drug release. Hence, a pH-dependent cleavage mechanism to facilitate cellular uptake and the release of cargo molecules is a promising strategy. Changes in the pH value occur in tumor tissue[10,11] and cellular compartments (endosome/lysosome),[12,13] which exhibit lower pH and thus could induce a triggered degradation of pH-sensitive PEG.

Moreover, the applied sterically stabilized nanocarriers often possess low stabilities *in vivo*, leading to reduced blood circulation times and fast renal clearance.[14,15] In this context, the stability of the stealth layer and particularly the stability of lipid anchorage of the PEG-lipids in the liposomal membrane is crucial.

In order to address these drawbacks, this thesis deals with the preparation of multifunctional PEGs (*mf*-PEGs) (**Scheme 1**). In this context, one major objective of this thesis is the synthesis of amphiphilic PEG-based lipids with numerous pendant functional groups that offer further options for modification. Furthermore, the thesis addresses the lack of degradability by preparing PEG-lipids with multiple pH-sensitive moieties to enable fragmentation of PEG. In addition, the need for enhanced stabilities of the nanocarriers is tackled *via* the evaluation of different lipid membrane anchors for PEG-lipids and the development of a cross-linking strategy.

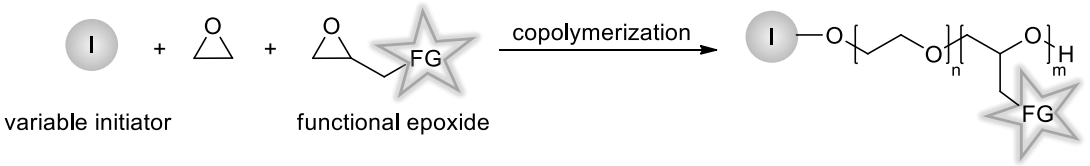

Scheme 1. Synthetic strategy to prepare multifunctional PEG (*mf*-PEG) *via* the copolymerization of ethylene oxide (EO) and an epoxide monomer, bearing a functional group (FG). Different initiators (I) can be used for the copolymerization, also influencing the characteristics of the copolymers.

In the following, the specific objectives of this thesis are summarized.

I) Polyether-lipids with variable hydrophobic initiators and different polymer architectures

Chapter 2.1 targets two major objectives: i) Synthesis of PEG-lipids that provide enhanced stabilities regarding lipid anchorage and ii) variation of polymer architecture to obtain multifunctional lipids. By applying initiators with different alkyl chain lengths for the polymerization, the stability of lipid anchorage in the lipid bilayer of liposomes can be evaluated. Moreover, the synthesis of hyperbranched polyglycerol (*hb*PG) *via* the slow monomer addition technique in a subsequent step to further extend the range of available structures that can be investigated, regarding their stability. This approach simultaneously introduces multiple functional groups. The investigations regarding stability of lipid

anchorage will be carried out in collaboration with Matthias Voigt of the Group of Prof. Dr. Mark Helm (Institute of Pharmacy and Biochemistry, Johannes Gutenberg-University Mainz).

II) pH-sensitive copolymers to obtain degradable PEG

The copolymerization of ethylene oxide (EO) and 3,4-epoxy-1-butene (EPB), presented in **chapter 2.2** leads to the introduction of pH-sensitive moieties to overcome the non-degradability of PEG. In order to obtain amphiphilic PEG-based structures, suitable for their incorporation in liposomes, a hydrophobic initiator is applied for the copolymerization, limiting the variety of solvents and counter ions that can be used for the anionic ring-opening polymerization (AROP). Both the conditions for the copolymerization as well as the pH-dependent hydrolysis of the copolymers and their incorporation into liposomes are explored.

III) PEG-lipids with multifunctional moieties for active targeting

Tailored epoxide monomers that are suitable for the anionic ring-opening polymerization (AROP) can be copolymerized with EO. A hydrophobic initiator is necessary to synthesize amphiphilic structures. In this context, the copolymerization of EO and mannose-carrying epoxides is investigated in **chapter 2.3** to introduce multiple target functions into the PEG-lipid. Mannose-moieties are known to target macrophages and dendritic cells (cells of the immune system) and should lead to PEG-lipids with the ability of active targeting.

IV) Multifunctional PEG-lipids enabling cross-linking

Post-polymerization modification is another strategy to prepare functional PEG-lipids. In **chapter 2.4** the copolymerization of EO and ethoxyethyl glycidyl ether (EEGE) is carried out. This leads to polymers with pendant hydroxyl groups that enable further functionalization. To this end, the attachment of multiple methacrylate moieties *via* enzyme catalyzed esterification and their suitability for cross-linking is studied. These multifunctional PEG-lipids should combine a tailored structure with adjustable functional moieties and the ability to prepare liposomes with enhanced stability.

V) Polyether-lipids for sterically stabilized nanoparticles

The suitability of polyglycerol as a multifunctional alternative for PEG-based lipids and the influence of pendant functional moieties on the stealth effect is explored in **chapter 3**.

For this purpose, EEGE is polymerized *via* the AROP, using cholesterol as hydrophobic initiator that leads to amphiphilic structures, enabling post-polymerization modification. The resulting polyglycerol-based lipids with pendant phosphonate groups serve as surfactants to stabilize polymer nanoparticles, prepared *via* the miniemulsion/solvent evaporation technique. The particles are prepared in a collaboration with the group of PD Dr. Frederik Wurm (Max Planck Institute for Polymer Research, Mainz). The protein corona and resulting stealth effect of the polyglycerol-decorated nanocarriers, as well as the influence of the attached functional groups on the stealth effect are investigated.

VI) Extending the scope of multifunctionality by applying the monomer-activated AROP

In **chapter 4**, the copolymerization of EO and epichlorohydrin (ECH) is performed using the monomer-activated AROP. This mild polymerization strategy has to be applied for epoxides like ECH that are prone to nucleophilic substitution and cannot be polymerized *via* the conventional AROP.[16] The copolymerization is studied using *in situ* ^{1}H NMR spectroscopy to determine the reactivity ratios of the comonomers and to gain detailed information about the polymer microstructure. Furthermore, the possibilities for post-polymerization modification of the pendant chlorine moieties is explored. These polymers should provide the possibility to attach different functional groups and hence they should represent a platform for various multifunctional PEGs.

References

(1) Herzberger, J.; Niederer, K.; Pohlit, H.; Seiwert, J.; Worm, M.; Wurm, F. R.; Frey, H. Polymerization of Ethylene Oxide, Propylene Oxide, and Other Alkylene Oxides: Synthesis, Novel Polymer Architectures, and Bioconjugation. *Chemical reviews* **2016**, *116*, 2170–2243.

(2) Hargreaves, A. E. *Chemical formulation: An overview of surfactant-based preparations used in everyday life*; RSC paperbacks; Royal Society of Chemistry: Cambridge, 2003.

(3) Dingels, C.; Schömer, M.; Frey, H. Die vielen Gesichter des Poly(ethylenglykol)s. *Chem. unserer Zeit* **2011**, *45*, 338–349.

(4) Pasut, G.; Veronese, F. M. State of the art in PEGylation: The great versatility achieved after forty years of research. *J. Control. Release* **2012**, *161*, 461–472.

(5) Pasut, G.; Paolino, D.; Celia, C.; Mero, A.; Joseph, A. S.; Wolfram, J.; Cosco, D.; Schiavon, O.; Shen, H.; Fresta, M. Polyethylene glycol (PEG)-dendron phospholipids

as innovative constructs for the preparation of super stealth liposomes for anticancer therapy. *J. Control. Release* **2015**, *199*, 106–113.

(6) Woodle, M. C. Surface-modified liposomes: Assessment and characterization for increased stability and prolonged blood circulation. *Chemistry and physics of lipids* **1993**, *64*, 249–262.

(7) Woodle, M. C.; Lasic, D. D. Sterically stabilized liposomes. *Biochim. Biophys. Acta, Rev. Biomembr.* **1992**, *1113*, 171–199.

(8) Knop, K.; Hoogenboom, R.; Fischer, D.; Schubert, U. S. Poly(ethylene glycol) in drug delivery: pros and cons as well as potential alternatives. *Angew. Chem. Int. Edit.* **2010**, *49*, 6288–6308.

(9) Harris, J. M.; Chess, R. B. Effect of pegylation on pharmaceuticals. *Nat. Rev. Drug. Discov.* **2003**, *2*, 214–221.

(10) Gerweck, L. E.; Vijayappa, S.; Kozin, S. Tumor pH controls the in vivo efficacy of weak acid and base chemotherapeutics. *Molecular cancer therapeutics* **2006**, *5*, 1275–1279.

(11) Patel, N. R.; Pattni, B. S.; Abouzeid, A. H.; Torchilin, V. P. Nanopreparations to overcome multidrug resistance in cancer. *Advanced drug delivery reviews* **2013**, *65*, 1748–1762.

(12) Sun, H.; Andresen, T. L.; Benjaminsen, R. V.; Almdal, K. Polymeric Nanosensors for Measuring the Full Dynamic pH Range of Endosomes and Lysosomes in Mammalian Cells. *j biomed nanotechnol* **2009**, *5*, 676–682.

(13) Benjaminsen, R. V.; Sun, H.; Henriksen, J. R.; Christensen, N. M.; Almdal, K.; Andresen, T. L. Evaluating nanoparticle sensor design for intracellular pH measurements. *ACS nano* **2011**, *5*, 5864–5873.

(14) Fritz, T.; Voigt, M.; Worm, M.; Negwer, I.; Müller, S. S.; Kettenbach, K.; Ross, T. L.; Roesch, F.; Koynov, K.; Frey, H. *et al.* Orthogonal Click Conjugation to the Liposomal Surface Reveals the Stability of the Lipid Anchorage as Crucial for Targeting. *Chemistry* **2016**, *22*, 11578–11582.

(15) Reibel, A. T.; Müller, S. S.; Pektor, S.; Bausbacher, N.; Miederer, M.; Frey, H.; Rösch, F. Fate of linear and branched polyether-lipids in vivo in comparison to their liposomal formulations by (18)f-radiolabeling and positron emission tomography. *Biomacromolecules* **2015**, *16*, 842–851.

(16) Carlotti, S.; Labbé, A.; Rejsek, V.; Doutaz, S.; Gervais, M.; Deffieux, A. Living/Controlled Anionic Polymerization and Copolymerization of Epichlorohydrin with Tetraoctylammonium Bromide−Triisobutylaluminum Initiating Systems. *Macromolecules* **2008**, *41*, 7058–7062.

Abstract

Polyethylene glycol (PEG) is the gold standard for biomedical applications and is applied for a wide range of products, ranging from cosmetics and food additives to highly sophisticated drug delivery systems.[1–3] In particular, the application of PEG in liposomes (PEGylation), leading to sterically stabilized nanocarriers that exhibit the "stealth effect", is a well-established strategy to improve the pharmacokinetic properties of these systems.[4–6] However, apart from its favorable properties for biomedicine and nanotechnology, PEG exhibits only two functional groups and possesses no degradability. Moreover, sterically stabilized liposomes often show low stability *in vivo*, leading to fast renal clearance. These drawbacks are addressed in this thesis, which aims at the synthesis of PEG and amphiphilic PEG-lipids with pendant functional groups, enabling, *e.g.*, active targeting. In addition, a synthetic strategy is provided to introduce multiple pH-sensitive moieties into PEG-lipids, resulting in pH-triggered fragmentation of PEG. To increase the stability of liposomes the hydrophobic membrane anchor is varied to influence the stability of lipid anchorage and the possibility for cross-linking of the stealth layer is evaluated.

Chapter 1 gives an overview of the characteristics and properties of polyethers and summarizes the synthetic concepts of the classic anionic ring-opening polymerization (AROP) and the monomer-activated AROP. Furthermore, synthetic options for the preparation of multifunctional PEGs (*mf*PEGs) are highlighted and various epoxide monomers for the copolymerization are introduced. Moreover, an introduction into liposomal research is given including preparation methods, differentiation of conventional and sterically stabilized liposomes as well as strategies to obtain stimuli-responsive behavior and active targeting of liposomes. In the final section, polymer nanoparticles and their synthesis are presented.

Chapter 2 deals with the synthesis of amphiphilic PEG-lipids, suitable for incorporation into liposomal nanocarriers. In **chapter 2.1** the synthesis of PEG-lipids and hyperbanched polyglycerol (*hb*PG) lipids with different hydrophobic initiators are presented. By varying the alkyl chain length of the initiator, different amphiphilic structures with tailored molecular weights and narrow size distributions are obtained. The properties of the different amphiphilic polyethers are studied and in a collaboration with Matthias Voigt (Group of Prof. Dr. Mark Helm, Institute of Pharmacy and Biochemistry, Johannes

Gutenberg-University Mainz) the stability of lipid anchorage is investigated to obtain liposomes with increased stability. **Chapter 2.2** addresses the non-degradability of PEG. In order to introduce degradation sites into PEG, copolymers of ethylene oxide (EO) and 3,4-epoxy-1-butene (EPB) are prepared *via* AROP to introduce multiple pH-sensitive moieties. An adaptation of the polymerization conditions (*i.e.* solvent, counter ion) enables the use of a hydrophobic initiator and leads to vinyl ether moieties directly after polymerization. The pH-dependent cleavage of the PEG-lipids is studied using ^{1}H NMR spectroscopy, showing full degradation between pH 3.5 and pH 4.5 in a time frame of 5 days to 32 days and the desired good stability at pH 7. In addition, the amphiphilic polyethers can be successfully incorporated into liposomal nanocarriers, leading to liposomes with sizes of 151 nm in diameter and narrow dispersity (0.216). Thus, the suitability of these structures for application in liposomal nanocarriers is established. In **Chapter 2.3** the copolymerization of EO and mannose-bearing epoxides is presented. Mannose-moieties are known to target macrophages and dendritic cells (cells of the immune system) and consequently are promising structures to obtain active targeting. The prepared amphiphilic polyether copolymers possess tailored molecular weights and an adjustable mannose content (0.6–5.4 mol%). Furthermore, the successful removal of the protecting groups is shown, rendering these structures advantageous for the preparation of liposomes which exhibit active targeting. In **Chapter 2.4** the synthesis of amphiphilic polyethers *via* the AROP of EO and ethoxyethyl glycidyl ether (EEGE) is presented. This strategy leads to numerous hydroxyl groups at the polymer backbone, which are available for functionalization. By performing an enzyme catalyzed esterification, the hydroxyl groups are converted into methacrylate groups, which allow for cross-linking after addition of a photoinitiator and irradiation with UV light. The functional polyether lipids are incorporated into liposomes, and first cross-linking experiments are performed.

Amphiphilic polyethers suitable for the stabilization of nanoparticles are introduced in **Chapter 3**. Cholesterol-based polyglycerols with pendant phosphonate groups are synthesized using the AROP strategy, followed by post-polymerization functionalization to attach an adjustable degree of functional moieties. These amphiphilic polyethers are used as surfactants for the preparation of polystyrene nanoparticles *via* the miniemulsion/solvent evaporation technique, performed in a collaboration of the Group of PD Dr. Frederik Wurm from the Max Planck Institute for Polymer Research, Mainz. The resulting nanocarriers are characterized using dynamic light scattering with respect to their size and isothermal

titration calorimetry to obtain information on the thermodynamic properties. Further investigations regarding the protein corona reveal a comparable stealth effect for the plain PGylated particles as well as PGylated particles carrying a low amount of phosphonate moieties (29 mol%) (in comparison to PEGylated nanocarriers). Furthermore, the results clearly show that the stealth effect decreases for higher amounts of attached phosphonate groups (43 mol%).

A different strategy to obtain *mf*PEGs is the copolymerization of EO and epichlorohydrin (ECH), presented in **Chapter 4**. Due to the reactive chloromethyl groups, the classical AROP is not applicable for the copolymerization of EO and ECH. Therefore, the monomer-activated polymerization method using aluminum-alkyl based activation is applied, leading to copolymers with moderate dispersities (1.27–1.44) and tailored comonomer content (6–33 mol% ECH). The reactivity ratios of ECH and EO are studied *via in situ* ^{1}H NMR kinetics study, revealing a strongly tapered, block-like structure of the copolymer. Furthermore, different functionalization reactions for the substitution of the chlorine moiety are carried out to investigate the possibility of attaching functional groups to these block-like tapered copolymers.

References

(1) Hargreaves, A. E. *Chemical formulation: An overview of surfactant-based preparations used in everyday life*; RSC paperbacks; Royal Society of Chemistry: Cambridge, 2003.

(2) Dingels, C.; Schömer, M.; Frey, H. Die vielen Gesichter des Poly(ethylenglykol)s. *Chem. unserer Zeit* **2011**, *45*, 338–349.

(3) Herzberger, J.; Niederer, K.; Pohlit, H.; Seiwert, J.; Worm, M.; Wurm, F. R.; Frey, H. Polymerization of Ethylene Oxide, Propylene Oxide, and Other Alkylene Oxides: Synthesis, Novel Polymer Architectures, and Bioconjugation. *Chemical reviews* **2016**, *116*, 2170–2243.

(4) Pasut, G.; Paolino, D.; Celia, C.; Mero, A.; Joseph, A. S.; Wolfram, J.; Cosco, D.; Schiavon, O.; Shen, H.; Fresta, M. Polyethylene glycol (PEG)-dendron phospholipids as innovative constructs for the preparation of super stealth liposomes for anticancer therapy. *J. Control. Release* **2015**, *199*, 106–113.

(5) Woodle, M. C.; Lasic, D. D. Sterically stabilized liposomes. *Biochim. Biophys. Acta, Rev. Biomembr.* **1992**, *1113*, 171–199.

(6) Woodle, M. C. Surface-modified liposomes: Assessment and characterization for increased stability and prolonged blood circulation. *Chemistry and physics of lipids* **1993**, *64*, 249–262.

Zusammenfassung

Polyethylenglykol (PEG) ist der Goldstandard für biomedizinische Anwendungen und wird für eine Vielzahl von Produkten verwendet, die von Kosmetik und Nahrungsmittelzusätzen bis hin zu hochentwickelten Wirkstofftransportsystemen reichen.[1–3] Besonders die Anwendung von PEG in Liposomen (PEGylierung), das zu sterisch stabilisierten Nanotransportern führt die den „stealth-Effekt“ (Tarnkappeneffekt) aufweisen, ist eine etablierte Strategie, um die pharmakokinetischen Eigenschaften dieser Systeme zu verbessen.[4–6] Allerdings besitzt PEG, trotz seiner herausragenden Eigenschaften für Biomedizin und Nanotechnologie nur zwei funktionelle Gruppen und zeigt keine Abbaubarkeit. Des Weiteren weisen sterisch stabilisierte Liposomen oft eine noch zu geringe *in vivo* Stabilität auf, die zu einer schnellen renalen Ausscheidung führt. Diese Nachteile werden in dieser Arbeit adressiert, in der die Synthese von PEG und amphiphilen PEG-Lipiden mit angefügten funktionellen Gruppen, die z.B. den aktiven Transport an einen Zielort ermöglichen, angestrebt wird. Darüber hinaus wird eine Synthesestrategie vorgestellt um zahlreiche pH-sensitive Gruppen in PEG-Lipide einzuführen, sodass diese zu einer pH-abhängigen Fragmentierung von PEG führen. Um die Stabilität der Liposomen zu erhöhen, wird der hydrophobe Membrananker, der die Stabilität der Lipidverankerung beeinflusst, variiert und die Möglichkeit einer Vernetzung der Tarnkappenhülle wird untersucht.

Kapitel 1 gibt einen Überblick über die Charakteristika und Eigenschaften von Polyethern und fasst die synthetischen Konzepte der klassischen anionischen Ringöffnungspolymerisation (AROP) und der monomer-aktivierten AROP zusammen. Darüber hinaus werden die synthetischen Möglichkeiten der Herstellung von multifunktionellen PEGs dargestellt und zahlreiche Epoxidmonomere für die Copolymerisation vorgestellt. Außerdem wird eine Einführung in die liposomale Forschung gegeben. Diese umfasst Herstellungsmethoden, die Unterscheidung von konventionellen und sterisch stabilisierten Liposomen und auch Strategien, um externes, Stimuli bedingtes Verhalten und aktiven Transport zum Zielkompartiment von Liposomen zu erhalten. Im letzten Abschnitt werden Polymernanopartikel und deren Synthese vorgestellt.

Kapitel 2 befasst sich mit der Synthese von amphiphilen PEG-Lipiden, welche für den Einbau in liposomale Nanotransporter geeignet sind. In **Abschnitt 2.1** wird die Synthese von PEG-Lipiden und hyperverzweigtem Polyglycerin (*hb*PG) mit verschiedenen hydrophoben Initiatoren vorgestellt. Indem die Alkylkettenlänge des Initiators variiert wurde, konnten verschiedene amphiphile Strukturen mit maßgeschneiderten Molekulargewichten und engen Größenverteilungen erhalten werden. Die Eigenschaften der unterschiedlichen, amphiphilen Polyether wurden näher charakterisiert und in einer Kooperation mit Matthias Voigt (Arbeitsgruppe von Prof. Dr. Mark Helm, Institut für Pharmazie und Biochemie, Johannes Gutenberg-Universität Mainz) wird die Stabilität der Lipidverankerung untersucht, um Liposomen mit erhöhter Stabilität zu erhalten. In **Unterkapitel 2.2** wird die Nichtabbaubarkeit von PEG adressiert. Hierfür wurden Copolymere aus Ethylenoxid (EO) und 3,4-Epoxy-1-Buten (EPB) mittels AROP hergestellt, um zahlreiche pH-sensitive Gruppen einzuführen. Die Anpassung der Polymerisations-bedingungen (d.h. Lösungsmittel, Gegenion) ermöglichte den Einsatz eines hydrophoben Initiators und führte dazu, dass nach der Polymerisation direkt die spaltbaren Vinylethergruppen erhalten wurden. Die pH-abhängige Spaltung der PEG-Lipide wurde mit Hilfe von ^{1}H NMR Spektroskopie untersucht und zeigte einen vollständigen Abbau bei pH 3,5 bis pH 4,5 in einem Zeitraum von 5 Tagen bis 32 Tagen und die erwünschte, gute Stabilität bei pH 7. Des Weiteren konnten die amphiphilen Polyether erfolgreich in liposomale Nanotransporter eingebaut werden, die zu Liposomen mit Durchmessern von 151 nm und engen Dispersitäten (0.216) führten. Somit konnte die Eignung dieser Strukturen für deren Einsatz in liposomale Nanotransporter aufgezeigt werden. In **Abschnitt 2.3** wird die Copolymerisation von EO und mannosehaltigen Epoxiden präsentiert. Mannosegruppen sind bekannt dafür, dass sie Makrophagen und Dendritische Zellen (Zellen des Immunsystems) ansteuern und sind deshalb vielversprechende Strukturen, um aktiven Transport zum Zielkompartiment zu vermitteln. Die hergestellten amphiphilen Polyether wiesen maßgeschneiderte Molekulargewichte und einen einstellbaren Mannosegehalt (0,6–5,4 mol%) auf. Darüber hinaus wurde die erfolgreiche Entfernung der Schutzgruppen nachgewiesen, sodass diese Strukturen vielversprechend für die Herstellung von Liposomen sind, die aktiven Transport zum Zielkompartiment aufweisen. In **Unterkapitel 2.4** wird die Synthese amphiphiler Polyether mittels AROP von EO und Ethoxyethylglycidylether (EEGE) vorgestellt. Diese Strategie führte zu zahlreichen Hydroxylgruppen entlang des Polymerrückgrats, die für Funktionalisierungen nutzbar sind. Mit Hilfe einer enzymkatalysierten Veresterung wurden

die Hydroxylgruppen in Methacrylatgruppen überführt, die eine Vernetzung nach der Zugabe eines Fotoinitiators und Bestrahlung mit UV-Licht ermöglichen. Die funktionellen Polyetherlipide wurden in Liposomen eingebaut und erste Vernetzungsversuche wurden durchgeführt.

In **Kapitel 3** werden amphiphile Polyether, die für die Stabilisierung von Nanopartikeln nutzbar sind, vorgestellt. Cholesterinbasiertes Polyglycerin mit angefügten Phosphonatgruppen wurde mit Hilfe der AROP Strategie synthetisiert, gefolgt von einer nach der Polymerisation folgenden Funktionalisierung, sodass einen einstellbarer Grad an funktionellen Gruppen angebracht werden konnte. Diese amphiphilen Polyether wurden als Tenside für die Herstellung von Polystyrolnanopartikeln mittels Miniemulsion/Lösungsmittelverdampfungstechnik verwendet. Diese wurden in einer Kooperation mit der Gruppe von PD Dr. Frederik Wurm des Max Planck Instituts für Polymerforschung in Mainz durchgeführt. Die resultierenden Nanotransporter wurden mit Hilfe von Lichtstreuung auf ihre Größe hin untersucht und mittels isothermer Titrationskalorimetrie wurden Informationen im Bezug auf deren thermischen Eigenschaften erhalten. Weitere Untersuchungen bezüglich der Proteinhülle zeigten vergleichbare Tarnkappeneffekte für PGylierte Partikel ohne als auch PGylierte Partikel mit niedrigen Gehalt von Phosphonatgruppen (29 mol%) (im Vergleich zu PEGylierten Nanotransportern). Darüber hinaus zeigen die Ergebnisse deutlich, dass der Tarnkappeneffekt für einen höheren Gehalt der angebrachten Phosphonatgruppen (43 mol%) verringert wurde.

Eine andere Strategie um multifunktionelle PEGs zu erhalten ist die Copolymerisation von EO und Epichlorhydrin (ECH), die in **Kapitel 4** vorgestellt wird. Aufgrund der reaktiven Chlormethylgruppen ist die klassische AROP für die Copolymerisation von EO und ECH nicht durchführbar. Aufgrund dessen wurde die monomeraktivierte Polymerisationsmethode angewendet. Diese führte zu Copolymeren mit moderaten Verteilungen (1,27–1,44) und maßgeschneidertem Comonomergehalt (6–33 mol% ECH). Das Reaktionsverhalten von ECH und EO wurde mittels *in situ* ^{1}H NMR Kinetikstudien untersucht. Diese zeigten, dass stark konisch zulaufende, blockartige Copolymerstrukturen erhalten wurden. Darüber hinaus wurden verschiedene Funktionalisierungsreaktionen zur Substitution der Chloridgruppen durchgeführt, um die Adressierbarkeit dieser funcktionallen Gruppen zu untersuchen.

Literaturverzeichnis

(1) Hargreaves, A. E. *Chemical formulation: An overview of surfactant-based preparations used in everyday life*; RSC paperbacks; Royal Society of Chemistry: Cambridge, 2003.

(2) Dingels, C.; Schömer, M.; Frey, H. Die vielen Gesichter des Poly(ethylenglykol)s. *Chem. unserer Zeit* **2011**, *45*, 338–349.

(3) Herzberger, J.; Niederer, K.; Pohlit, H.; Seiwert, J.; Worm, M.; Wurm, F. R.; Frey, H. Polymerization of Ethylene Oxide, Propylene Oxide, and Other Alkylene Oxides: Synthesis, Novel Polymer Architectures, and Bioconjugation. *Chemical reviews* **2016**, *116*, 2170–2243.

(4) Pasut, G.; Paolino, D.; Celia, C.; Mero, A.; Joseph, A. S.; Wolfram, J.; Cosco, D.; Schiavon, O.; Shen, H.; Fresta, M. Polyethylene glycol (PEG)-dendron phospholipids as innovative constructs for the preparation of super stealth liposomes for anticancer therapy. *J. Control. Release* **2015**, *199*, 106–113.

(5) Woodle, M. C.; Lasic, D. D. Sterically stabilized liposomes. *Biochim. Biophys. Acta, Rev. Biomembr.* **1992**, *1113*, 171–199.

(6) Woodle, M. C. Surface-modified liposomes: Assessment and characterization for increased stability and prolonged blood circulation. *Chemistry and physics of lipids* **1993**, *64*, 249–262.

Graphical Abstract

Chapter 2. Functional Polyether-based Lipids for Drug Delivery Systems

Chapter 2.1. Synthesis of Amphiphilic Polyethers Using Hydrophobic Initiators with Variable Alkyl Chain Length to Improve the Stability of Sterically Stabilized Liposomes

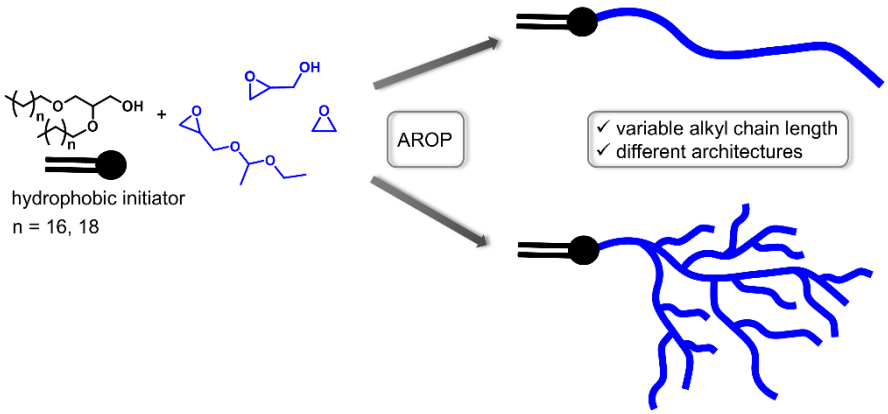

Chapter 2.2. Amphiphilic PEG with pH-sensitive Units Introduced *via* Anionic Ring-opening Copolymerization of EO and EPB Using a Hydrophobic Initiator

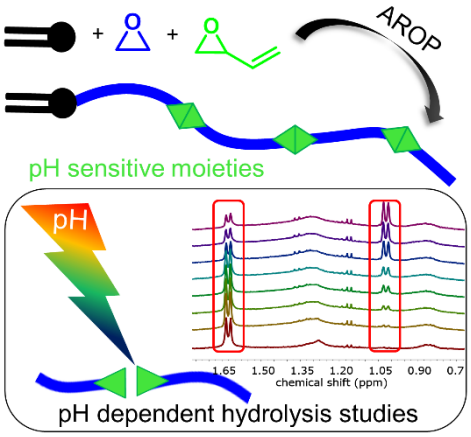

Chapter 2.3. Synthesis of Mannose-carrying Lipids *via* Anionic Copolymerization of Ethylene Oxide and Mannose-bearing Glycidyl Ethers

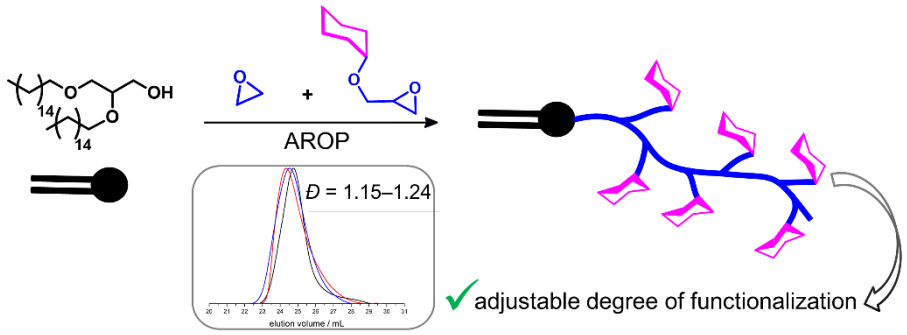

Chapter 2.4. Synthesis of Amphiphilic PEG Copolymers with Pendant Methacrylate Moieties to Enable Cross-linking of Liposomes

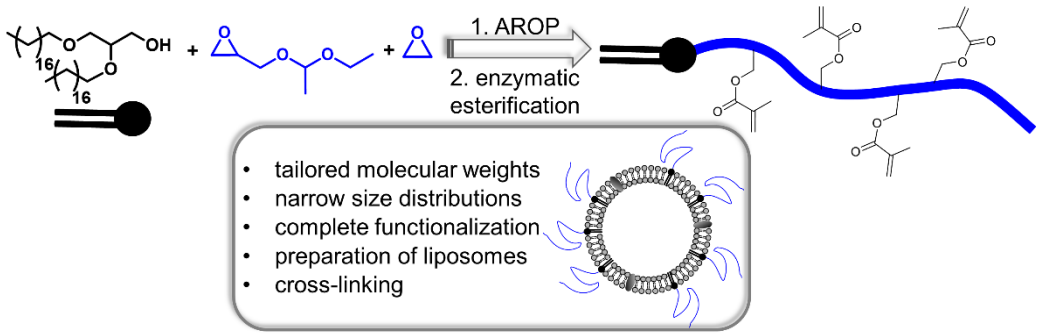

Chapter 3. Functional Polyether-based Surfactants

Chapter 3.1. Stealth Properties? How Adhesive Phosphonate Groups Control the Protein Corona of Polyglycerol-stabilized Nanocarriers

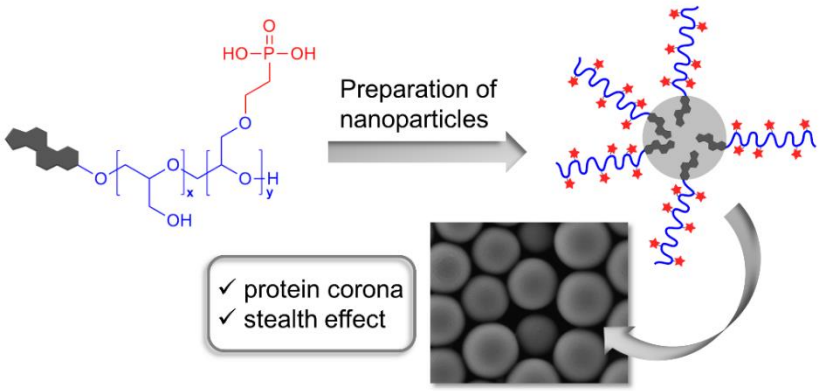

Chapter 4. Chloride-functional Poly(ethylene glycol) Copolymers

Chapter 4.1. Monomer-activated Copolymerization of Ethylene Oxide and Epichlorohydrin: *In Situ* Kinetics Evidences Tapered Block Copolymer Formation

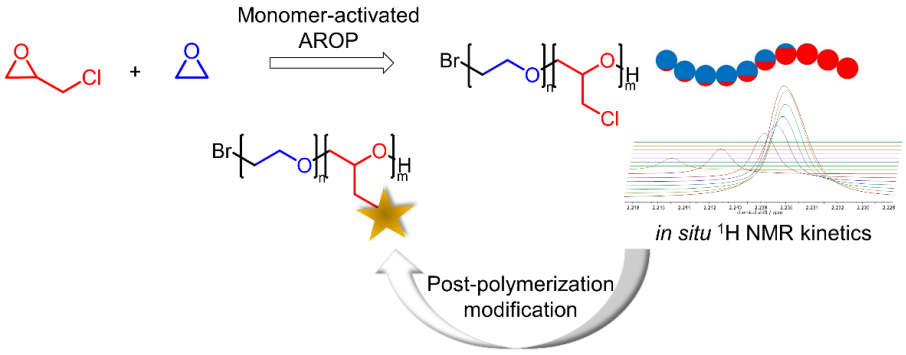

1. Introduction

This chapter gives an introduction into polyether chemistry including synthetic strategies and possible applications. Furthermore, characteristics and recent developments of liposomes and polymer nanoparticles applied as drug delivery systems are presented.

1.1 Aliphatic Polyethers

Aliphatic polyethers are an important class of polymers with unique properties that are exploited commercially for numerous applications. Polyethers possess a peculiar backbone that is water soluble due to the hydrophilicity of the C-O-C bond. Furthermore, the backbone is highly flexible, translating to low glass transition temperatures below –60 °C.[1] These properties distinguish polyethers from olefin- and vinyl-based polymers.[2]

In order to synthesize polyethers, a ring-opening polymerization (ROP) of three- to five-membered cyclic ethers can be performed in which epoxide (or oxirane respectively) monomers are most often used due to their convenient availability and high ring strain whereas oxetanes (four-membered ring) and oxolanes (five-membered ring) can only be polymerized *via* cationic polymerization methods.[3] Both ethylene oxide (EO) and propylene oxide (PO) are available in large quantities, since they are accessible by catalytic oxidation of the respective alkenes.[4–6] The ROP is driven by the ring strain of the epoxides, thus a polymerization *via* base- or acid-initiation as well as *via* a coordination mechanism is possible.[7]

EO is the simplest epoxide monomer. It possesses a low boiling point of 10.5 °C and its worldwide production capacity exceeds twenty-five million tons per year. It is synthesized *via* oxidation of ethylene with oxygen using a silver catalyst.[8,9] The first polymerization of EO was carried out by Charles Adolphe Wurtz in 1863 by applying alkali metal hydroxide or zinc chloride.[10] Consecutively, Staudinger and Schweitzer worked on EO-based polymers in the 1920s and already in the 1930s commercialization of these polymers emerged.[11] Depending on the targeted application, EO-based polymers are designated by different names. Polyethylene oxide (PEO) or polyoxy ethylene (POE) is used for polymers with high molecular weights > 30 000 g mol^{-1}, whereas polyethylene glycol (PEG) is utilized for lower molecular weights, especially for polymers applied in the biomedical and pharmaceutical sector. Furthermore, PEG is soluble in both organic solvents and water,

which renders it special compared to other aliphatic polyethers, *e.g.* polyoxymethylene (POM).[12] It is a semi-crystalline polymer that possesses a glass transition temperature (T_g) between −50 °C to −60 °C and a melting temperature (T_m) of up to 66 °C for higher molecular weights around 10 000 g mol^{-1}.[13] Due to its low immunogenicity and toxicity and thus good biocompatibility, PEG is used for a vast range of applications ranging from skin care products and food additives to tablet formulations, laxatives and further medical and pharmaceutical purposes.[14,15]

1.2. Polymerization Techniques

1.2.1 Anionic ring-opening polymerization (AROP)

As mentioned above, the oxyanionic ring-opening polymerization of EO was first reported by Wurtz[10] and studied in detail by Staudinger and Schweitzer.[11] In 1940, Flory investigated the size distribution of base-initiated PEG, demonstrating the high extent of control over molecular weights,[16] and in 1956 Szwarc was the first who described the living character of the anionic polymerization.[17] In general, the AROP is the "classical" method to polymerize EO. To this end, a nucleophilic initiator is applied for the ring-opening *via* S_N2 mechanism in which the high ring strain serves as driving force. The detailed mechanism is shown in **Scheme 1**.

In order to obtain narrow molecular weight distributions and the targeted molecular weight, electrophiles, *e.g.* water or oxidizing agents, *e.g.* O_2 have to be avoided. Hence, the polymerization should be carried out in vacuum or under inert atmosphere. As an initiator alkali metal alkoxides of sodium, potassium or cesium are applied. The bulky and "soft" alkali metals (like potassium or cesium) have a low tendency to aggregate and are therefore suitable counterions. In contrast, the "hard" lithium ion is unsuitable, because it forms strong aggregates with the "hard" oxygen of the alkoxide initiator and thus prevents polymerization. Partial deprotonation of the initiator is sufficient due to rapid proton exchange that occurs faster than initiation and propagation. Other possible initiators are hydrides, alkyls, aryls, hydroxides and amides.[18,19]

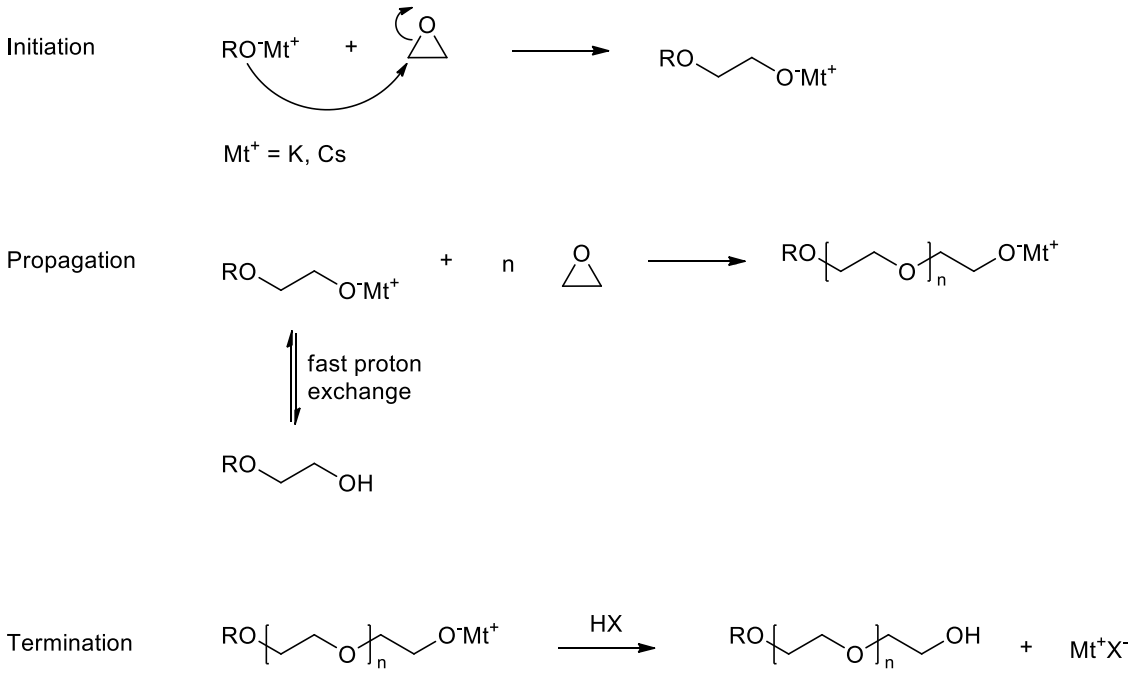

Scheme 1. Mechanism of the anionic ring-opening polymerization (AROP) of ethylene oxide (EO) with initiation, propagation and termination.

The polymerization can be carried out solvent free in bulk or in polar aprotic solvents like tetrahydrofuran (THF), dimethyl sulfoxide (DMSO) or 1,4-dioxane. Use of these solvents leads to free ions of the alkoxide and counterion (dissociated ion pair, **Scheme 2**) and thus high reactivity for polymerization, whereas solvents with low polarity lead to a very low rate of propagation due to an aggregation of the alkali metal alkoxide.[20–22] To suppress aggregation, cryptands (crown ethers) can be applied to increase the reactivity of the alkoxide *via* complexation of the alkali metal counterion.[23]

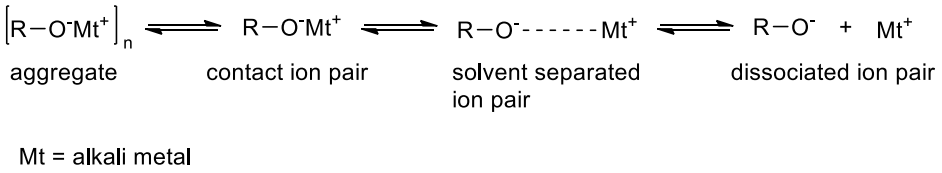

Scheme 2. Equilibrium of metal alkoxides in solution.

Using a functional initiator, various end groups can be introduced in the polymer. For example lipophilic alcohols like cholesterol or 1,2-dialkyl glycols applied as initiator result in amphiphilic polyethers. These structures possess particular advantages for surface modification of liposomes,[24,25] which will be highlighted in section 1.4.1. Further functional groups that can be introduced are, *e.g.* amines,[26,27] alkenes,[28,29] alkynes,[30] aldehydes,[31,32] hydroxyl groups[33] and catechols,[34,35] if suitable protecting groups are

applied in advance. In addition, the possibility to introduce an additional ω-functionalization relies on the use of an appropriate electrophile to terminate the polymerization resulting in α-ω-heterobifunctional PEGs.[36] A broad range of compounds for end-functionalization is available, *e.g.* mesylates,[37] methacrylates,[38,39] vinyl benzyl ethers[40] and propargyl ethers[33] can be attached.

In summary, the characteristics of the AROP are: strong bases are applied as initiator, polymers with Poisson-distributions of the molecular weight (and dispersities $Đ \leq 1.1$)[16] are obtained due to the living character of the polymerization and mono- or heterobifunctional structures can be prepared, depending on the initiator and terminating agent.

1.2.2 Monomer-activated method

The monomer-activated method for the polymerization of epoxides was developed by Carlotti and Deffieux and continues to be a major success for numerous functional or sensitive epoxides.[4,41] The polymerization of propylene oxide (PO) *via* the monomer-activated method was introduced in 2004 and enabled for the first time the synthesis of polypropylene oxide (PPO) with high molecular weights up to 170 000 g mol^{-1}.[41] As already reported by Inoue and co-workers[42–46] and Braune and Okuda,[47] the monomer activation occurs due to an interaction of the Lewis acid with the epoxide ring (**Figure 1**). Therefore, the electron density in the epoxide ring is decreased and a ring-opening is facilitated.

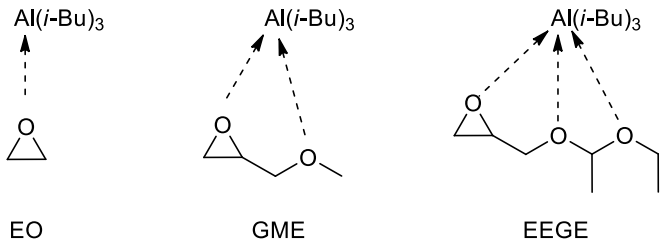

Figure 1. Complexation of triisobutylaluminum (TIBAL) by different epoxide monomers. Interaction of TIBAL with ethylene oxide (EO, left), glycidyl methyl ether (GME, middle) and ethoxyethyl glycidyl ether (EEGE, right).

During initiation, a so-called "ate complex" is formed by the Lewis acid (catalyst) and the weak nucleophile (initiator) as displayed in **Scheme 3**.[48] The ratio of catalyst and initiator must be > 1 to enable the formation of an "ate complex" and simultaneously allow for

activation of the epoxide ring. The amount of applied catalyst has to be increased with increasing coordination capability of the monomer. Nevertheless, low ratios are favored to obtain narrow molecular weight distributions.[41] As first initiating systems alkali metal alkoxides with trialkyl-aluminum species were used.[41] Improved initiator systems consist of organic salts, *i.e.* tetraalkyl ammonium halides or phosphonium salts as initiator and triisobutylaluminum as the catalyst.[48–52] By applying these initiator/catalyst systems transfer reactions are suppressed completely. In contrast, initiation *via* a hydride or *iso*-butyl group is observed. Hence, ill-defined chain ends or lower molecular weights can occur as a consequence.[53]

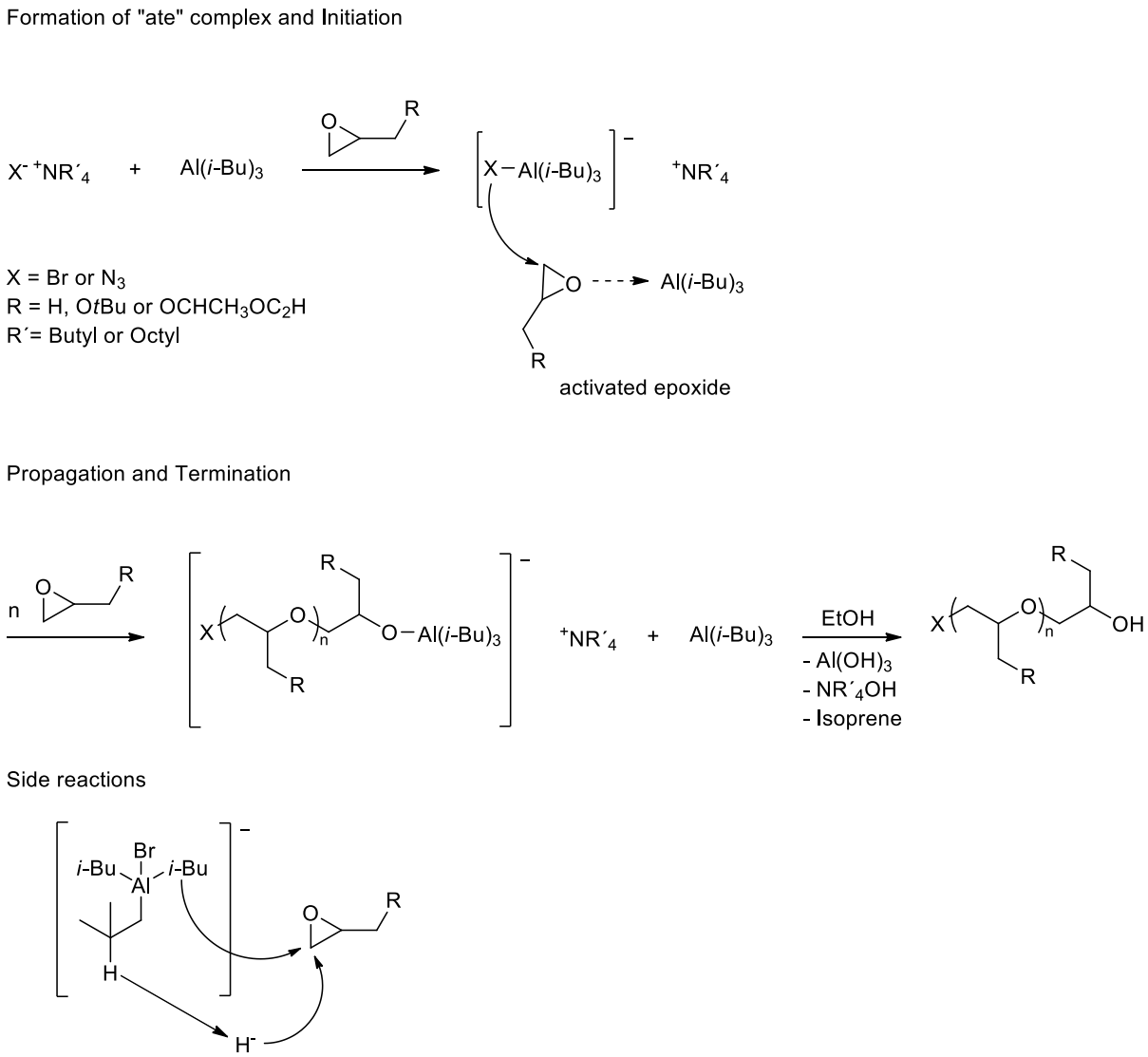

Scheme 3. Mechanism of the monomer-activated polymerization method including formation of “ate” complex, initiation, propagation and termination as well as side reactions.

Adequate solvents for the monomer-activation technique are aprotic and should possess no oxygen atoms due to their complexing properties that would lead to a complexation of the catalyst (aluminum compound), thereby blocking the activation of the epoxide. Consequently, cyclohexane, toluene, dichloromethane, chlorobenzene or fluorinated benzene are appropriate solvents.[41,48,52–55] In addition, the use of 2-methyltetrahydrofuran (MeTHF) was reported in literature.[56] Due to the strong activation of the epoxide ring, mild reaction conditions are applicable for the polymerization, *i.e.* low temperatures ranging from −30 °C to room temperature are sufficient. As mentioned above, the weak nucleophilicity of the "ate" complex that serves both as an initiator and propagating species suppresses transfer to monomer, resulting in high molecular weight polyethers, *e.g.* PPO (170 000 g mol^{-1}, $Đ$ = 1.34),[41] polyethoxyethyl glycidyl ether (PEEGE, 85 000 g mol^{-1}, $Đ$ = 1.27)[55] or PEG (up to 36 000 g mol^{-1}, $Đ \leq 1.41$).[54] Simultaneously, the size distribution remains fairly narrow. In addition, a higher polymerization rate for the monomer-activated technique compared to the AROP and a high tolerance of functional groups attached to the epoxide are observed.[41,54,57] Therefore, epichlorohydrin (ECH) can be polymerized without interaction of the active species with the chloromethyl group. Thus, polyepichlorohydrin (PECH) homopolymers with high molar masses (83 000 g mol^{-1}, $Đ \leq 1.25$) and copolymers with PO were prepared.[58] The reactive chloromethyl group of PECH offers a broad range of post-polymerization modifications. For example, Lynd and coworkers copolymerized EO and ECH, resulting in hydrolytically degradable methylene ethylene oxide (MEO) units after elimination of the chloride moieties.[59] Further modifications include azides and amines,[60] as well as hydroxyurethanes[61] and 1-butylimidazol leading to polyionic liquids.[62] Recent results on this topic are presented in chapter 4 of this thesis. Moreoever, glycidyl methacrylate,[63] allyl glycidyl ether (AGE),[64] epicyanohydrin[65] and fluorinated epoxides[52,53] were polymerized using the monomer-activated method. Also less reactive or sterically hindered epoxides like glycidyl methyl ether (GME)[63,66,67] and epoxides with hydrophobic alkyl chains[68,69] can be polymerized. In addition, phosphazene alkoxides can be applied as an initiator for the polymerization of PO with molecular weights up to 80 000 g mol^{-1}. In that case, a Lewis acid still serves as an activator.[57] Another approach uses Grignard reagents as deprotonating agent for 1-butanol. In this context, PO was polymerized in the presence of triisobutylaluminum as an activator and molecular weights between 2 500 and 10 000 g mol^{-1} were obtained.[56]

Recently, the influence of different polymerization techniques, *i.e.* conventional AROP vs. monomer-activated ROP, on the monomer distribution within the polymer backbone was investigated. Herzberger *et al.* found a strongly tapered structure for the statistical copolymerization of EO and EEGE *via* the monomer-activated method whereas the conventional AROP leads to random distributions of both monomers in the chain.[70] Furthermore, the reactivity ratios for different copolymerizations *via* the monomer-activated method are reported in literature, revealing random incorporation if two glycidyl ether monomers, *e.g.* glycidyl methyl ether (GME) and ethyl glycidyl ether (EGE) (r_{GME} = 0.98 and r_{EGE} = 0.95) are combined. A gradient structure is observed for the combination of EO and PO (r_{EO} = 2.05 and r_{PO} = 0.013) or PO and ECH (r_{PO} = 1.21 and r_{ECH} = 0.16).[54,58,71] **Figure 2** illustrates the monomer distribution for a random, gradient and block copolymer.

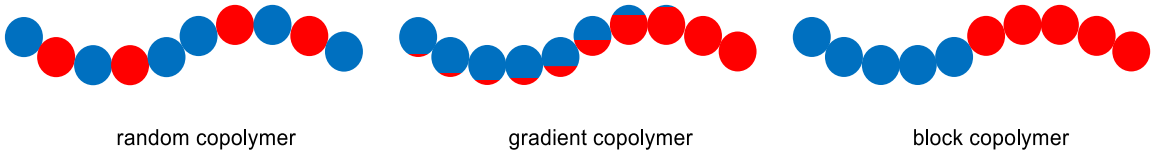

Figure 2. Illustration of the monomer distribution in a random copolymer (left), a gradient copolymer (middle) and a block copolymer (right).

However, the monomer-activated technique also leads to difficulties. Removal of residual initiator counterions (tetraalkyl ammonium salts) is challenging and time-consuming because precipitation often results in disappointing results. Further purification methods are long-term dialysis or column chromatography, but considerable product losses have to be taken into account. To obtain narrow molecular weight distributions the ratio of catalyst to initiator must be kept as low as possible and has to be adjusted for each monomer.[1,66] In addition, the direct determination of the molecular weight *via* ^{1}H NMR spectroscopy is not possible due to the initiators employed (bromide, chloride or azide), which do not enable a comparison of signal intensities. Therefore, the molecular weights are measured by size exclusion chromatography (SEC) or to obtain absolute values, end group functionalization or absolute methods (*e.g.* static light scattering) have to be conducted.[48,52]

In summary, the key-features of the monomer-activated method are the possibility to obtain polyethers from mono-substituted epoxides with higher molecular weights compared to the conventional AROP and the polymerization of unreactive or sensitive epoxides.

1.3. Multifunctional PEG (*mf*-PEG)

α-ω-bifunctional PEGs can be synthesized *via* the AROP of EO, using a functional initiator and terminating agent. Unfortunately, no further reactive groups are available for functionalization. In order to overcome this drawback, the copolymerization of EO and functional epoxide monomers is possible, leading to multifunctional PEG (*mf*-PEG) (**Scheme 4**).[72,73]

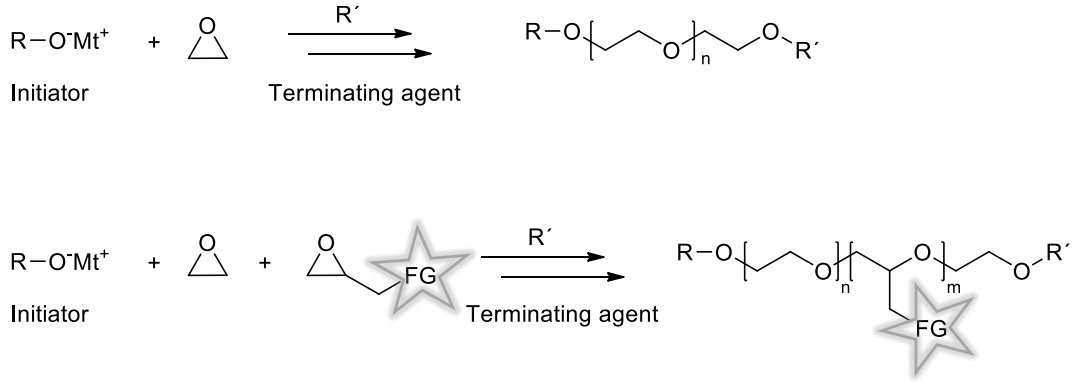

Scheme 4. Polymerization of ethylene oxide (EO) using a functional initiator (R-O$^-$) and terminating agent (R´) leading to α-ω-bifunctional PEG (top). Copolymerization of EO and an epoxide monomer, bearing a functional group (FG), leading to multifunctional PEG (*mf*-PEG).

Furthermore, the properties of PEG can be specifically tailored *via* the copolymerization of EO with substituted epoxides. For example, copolymerizing EO and PO offers the possibility to adjust or completely suppress the crystallinity of PEG and to tailor the solubility in aqueous solution.[74–76] In addition, good control of the monomer distribution can be obtained by either adding the monomers sequentially, leading to block copolymers or by adding the monomers simultaneously to afford random or gradient-like copolymers. The formation of gradient or block-like structures depends on the reactivity of the monomers and is different for each pair of monomers.[77–79]

The AROP of epoxides with substituents in α- and β-position or sterically hindered groups is not possible, whereas epoxides with alkyl chains can be polymerized but show a decrease of reactivity with increasing chain length.[80] In addition, nucleophilic ring-opening can occur at both methylene groups of the oxirane ring resulting in different polymeric structures (head-to-head, tail-to-tail, head-to-tail). Mostly regioregular head-to-tail connections are obtained due to steric reasons.[81] In case of substituted epoxides side

reactions can occur as shown in **Scheme 5**. A proton abstraction by the initiator or growing chain end resulting in a transfer of the negative charge to the monomer and thus formation of a double bond can occur which creates a new initiating species. This results in a complete loss of end-group functionalization and a decrease of the molecular weight.[18,82,83] The undesired transfer reactions can be minimized by applying lower polymerization temperatures or other polymerization techniques like the monomer-activated method (see previous section).[19,84] Due to the transfer reaction the maximum molecular weight, *e.g.* for PPO *via* AROP is limited to ~ 15 000 g mol^{-1} and for PEEGE to ~ 30 000 g mol^{-1}.[82,85]

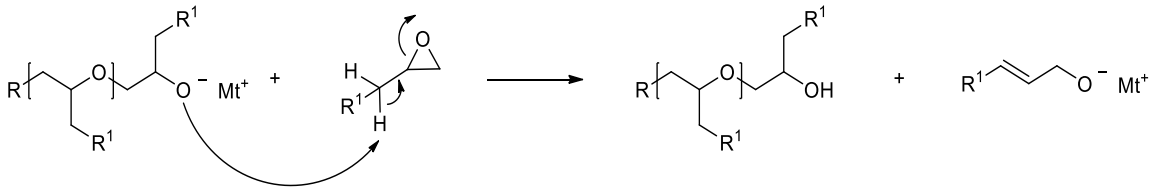

Scheme 5. Transfer reaction of the negative charge to the monomer leading to double bond formation and generation of a new initiating species.

The synthesis of functional epoxides is based on the oxidation of allylic structures or on the reaction of epichlorohydrin with alcohols to generate the desired glycidyl ethers. Furthermore, the functional groups often have to be protected to prevent an interaction with the polymerizing species.[1] EEGE is prepared using glycidol and ethyl vinyl ether in a published procedure.[86]

The monomer distribution of the AROP of EO and a monosubstituted epoxide monomer differs depending on the chosen monomer due to different steric and electronic properties. To gain a detailed understanding of the properties of the copolymers, it is necessary to know the monomer distribution in *mf*-PEGs. The comonomer distribution can be obtained *via* different methods. Especially *in-situ* monitoring of the copolymerization has gained increasing importance in recent years.[1,87] For this purpose, IR,[88–91] Raman,[92,93] UV[94,95] and ^{1}H and ^{13}C NMR spectroscopy[96–98] can be applied to determine the reactivity ratios of the comonomers in one single experiment. The preferential occurrence of a homopolymerization or rather a cross over reaction of the last monomer at the polymer chain end is described by the reactivity ratios r_1 and r_2. Hence, the reactivity ratios describe the copolymerization behavior of the chain ends M^{-} and are defined as: $r_1 = \frac{k_{11}}{k_{12}}$ and $r_2 = \frac{k_{22}}{k_{21}}$ in which k_{11} and k_{22} describe the rate constants for the homopolymerization of monomer

M_1 and monomer M_2 respectively and k_{12} and k_{21} stand for the cross-over reaction. Assuming, the number of active chain ends is constant during ionic copolymerizations, the copolymer composition equation (1) can be obtained and the copolymerization behavior for different reactivity ratios can be summarized as displayed in **Table 1**.[21,87,99]

$$\frac{d[M_1]}{d[M_2]} = \frac{[M_1]\cdot(r_1[M_1]+[M_2])}{[M_2]\cdot([M_1]+r_2[M_2])} \quad (1)$$

Table 1. Overview of the copolymerization behavior for different reactivity ratios.

$r_1 = 0$	No homopolymerization of M_1, only cross-over reactions
$r_1 < 1$	Cross-over reaction preferred
$r_1 = 1$	Equal chance of M_1 and M_1 to react with M_1^-
$r_1 > 1$	Homopolymerization preferred

In the copolymerization of EO and alkylene oxides the latter show a lower reactivity due to the steric hindrance resulting from the alkyl chains.[100] Furthermore, by increasing the alkyl chain length, the reactivity further decreases.[80] For example for the copolymerization of EO and PO the reactivity ratios are $r_{EO} = 2.8$ and $r_{PO} = 0.25$,[100] whereas the copolymerization of EO and butylene oxide (BO) leads to reactivity ratios of $r_{EO} = 6.46$ and $r_{BO} = 0.15$.[98] In contrast, the copolymerization of EO and glycidyl ethers leads to a fairly similar reactivity, *i.e.* reactivity ratios close to $r = 1$ and consequently a random monomer distribution.[79,101–104] This can be attributed to the additional oxygen atom in glycidyl ethers leading to an increased interaction with the counterion and an increased Lewis basicity, which lowers the transition state energy of the ring-opening.[78] In case of the copolymerization of EO and glycidyl amines, EO possesses a higher reactivity, resulting in the formation of a gradient structure. The alkyl chains attached to the nitrogen appear to shield the polar nitrogen atom effectively and consequently an activating interaction with the counterion is not possible.[97,105,106] The general structure of alkylene oxides, glycidyl ethers and glycidyl amines is given in **Figure 3**.

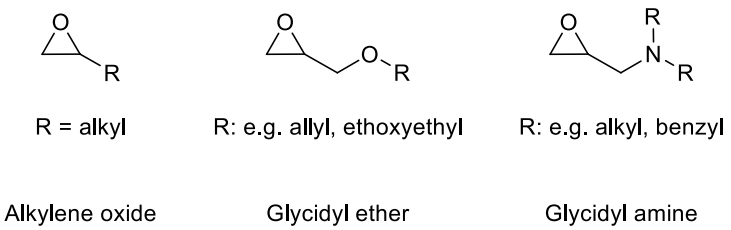

Figure 3. General structure of alkylene oxides (left), glycidyl ethers (middle) and glycidyl amines (right).

Currently, pH-, redox- and thermo-responsiveness of *mf*-PEGs are studied intensely. A selection of functional epoxides used for this purpose are shown in **Figure 4**. pH-responsive moieties are acetals and ketals, leading to free hydroxyl groups after acidic hydrolysis, as well as vinyl groups and *N*-alkyl amines.[27,107,108] For *N*-alkyl amines, a solubility switch from hydrophobic to hydrophilic *via* protonation at lower pH values is obtain.[105,106,109] *N*-allyl and *N*-benzyl protected epoxides serve for the introduction of primary amines into PEG, which subsequently offer the possibility for conjugation of substrates *via* amine chemistry.[97,105] Redox-responsive PEG is obtained by incorporating ferrocene as functional groups.[96,110] Another possibility are methyl thioethers that result in water-soluble sulfoxides or sulfones after oxidation.[77] This is an interesting strategy for redox-triggered drug delivery because oxidation occurs in oxidative inflammatory tissue.[111] Besides, thiol-ene click chemistry as post-polymerization modification of olefinic double bonds is usable for bioconjugation.[102,112–115] Thermo-responsive PEGs exhibit a LCST (lower critical solution temperature) behavior. The LCST behavior describes the loss of water solubility at elevated temperatures (cloud point $T_c \leq 100$ °C) due to dehydration and cleavage of hydrogen bonds. An introduction of functional groups allows for the adjustment of the cloud point. Regarding drug release strategies, *mf*-PEGs showing a LCST behavior at body temperature can be promising candidates for temperature-controlled drug release.[109,116] Moreover, hydroxyl-functional PEG can be obtained using EEGE as comonomer followed by acidic removal of the acetal protecting groups after polymerization. Thus, the hydrophilicity is increased and numerous hydroxyl groups at the backbone are available, *e.g.* for further functionalization.[117–119] Other possible comonomers are allyl glycidyl ether (AGE) and *tert*-butyl glycidyl ether. The deprotection is carried out with a palladium catalyst or trifluoracetic acid.[120] In addition, vicinal hydroxyl groups can be introduced by polymerizing 1,2-isopropylidene glyceryl glycidyl ether (IGG) followed by acidic hydrolysis of the protecting groups.[103]

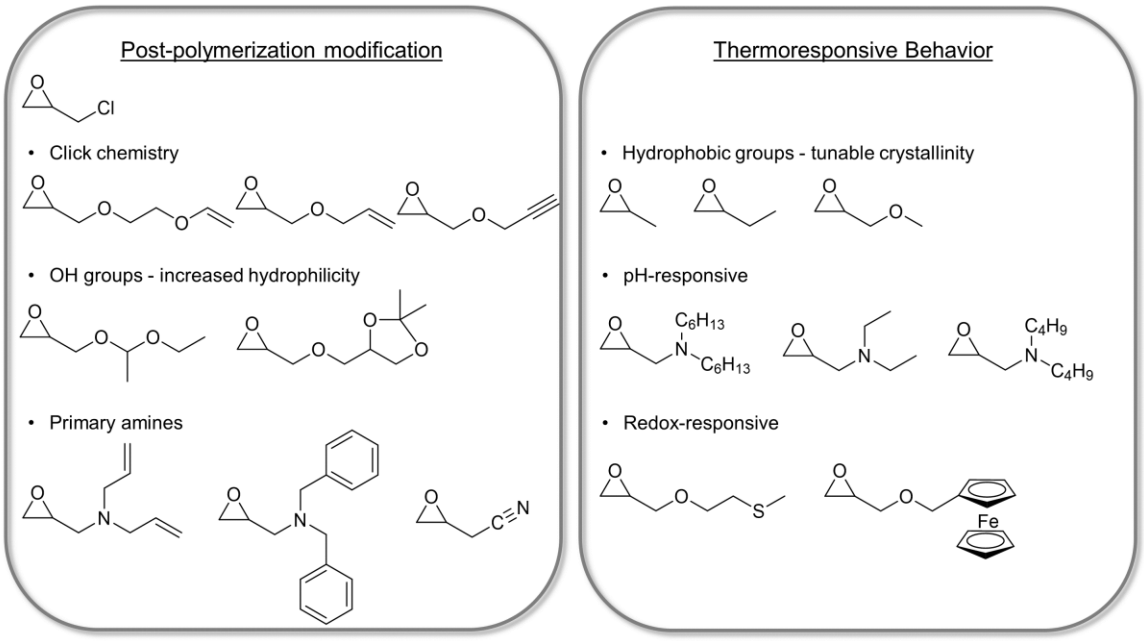

Figure 4. Overview of a selection of functional epoxides that can be copolymerized with ethylene oxide to obtain multifunctional PEGs. Depending on the functional groups of the epoxide, different properties can be installed, retaining typical PEG characteristics.

As mentioned earlier, PEG is suitable for biomedical applications due to its biocompatibility, low immunogenicity and high water-solubility.[121–123] Therefore, the attachment of PEG to bioactive molecules is highly interesting. This functionalization is a so-called "PEGylation". Due to the PEGylation antigenic activity can be reduced and blood circulation times are increased. In addition, enzymatic degradation and phagocytosis can be suppressed.[124–128] The described shielding effect of PEG also referred to as "stealth effect", may be due to the dense hydrate shell of PEG which forms a steric barrier and hence prevents unspecific protein adsorption.[129] Other recent observations suggest that a different composition of adsorbed proteins, especially a high amount of opsonins are found, which are supposed to lead to the stealth effect.[130]

1.4. Nanoparticles in Biomedicine

1.4.1 Liposomes

In 1965 Bangham *et al.* discovered that the formation of liposomes in water occurs spontaneously.[131] Since then these systems gained more and more importance especially in biomedicine.[132] Liposomes are nanocarriers consisting of natural phospholipids assembled in spherical structures with a size of 0.05-5.0 µm. They possess an aqueous core and a lipophilic bilayer membrane.[133,134] Liposomes are biocompatible and enable the encapsulation of hydrophobic and hydrophilic molecules due to their amphiphilic core-shell structure. Liposomes are interesting carrier systems in cosmetics,[135,136] food technology[137,138] and biomedical applications.[132,139] Until now, several liposome formulations are already approved as drug delivery systems for different diseases, *e.g.* hepatitis A,[140] fungal infections,[141] influenza[142] and various cancer types.[143–145] In addition, further potential systems are currently being tested in clinical trials.[139]

In general, different types of liposomes can be distinguished: multilamellar vesicles (MLVs), small unilamellar vesicles (SUVs), large unilamellar vesicles (LUVs) and giant unilamellar vesicles (GUVs, **Figure 5**).[134]

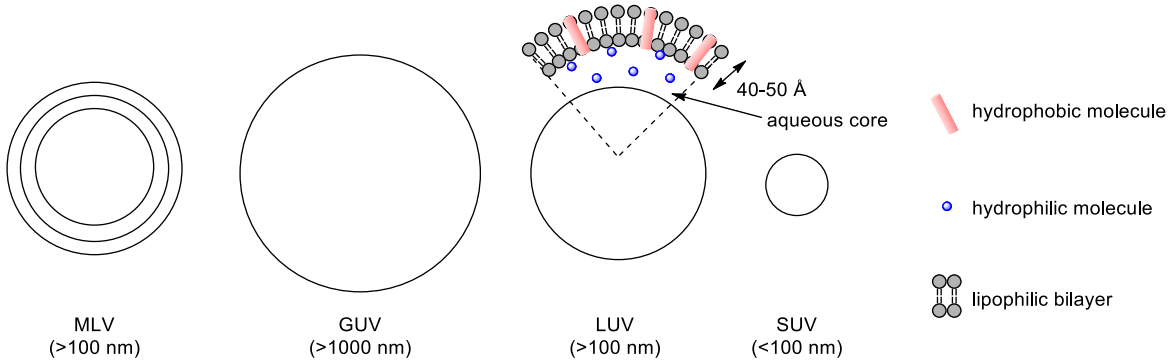

Figure 5. Overview of the different types of liposomes. From left to right: multilamellar vesicle (MLV), giant unilamellar vesicle (GUV), large unilamellar vesicle (LUV) and small unilamellar vesicle (SUV).

The size of a liposome plays an important role regarding its fate *in vivo*. Larger liposomes (> 100 nm) are taken up more rapidly by the reticulo-endothelial system (RES), also called mononuclear phagocytic system (MPS).[146] Furthermore, for multilamellar vesicles the drug entrapment and drug release as well as cell uptake differs, compared to unilamellar

vesicles.[147] Besides the lamellarity and size, the properties of a liposome are also influenced by the composition of lipids. The stability is decisively influenced by the phase transition temperature T_M of the phospholipid. Below T_M the phospholipid exists in the gel state which increases the stability of the liposome. If $T > T_M$ a transition to the fluid phase occurs. The fluid phase is less stable and shows an increase in water permeability of the liposome leading to a leakiness, which results in facile drug escape.[134] In general, phospholipids with unsaturated alkyl chains (*e.g.* 1,2-dioleoyl-*sn*-glycero-3-phosphocholine, DOPC) possess low T_M, whereas saturated lipids (*e.g.* 1,2-distearoyl-*sn*-glycero-3-phosphoethanolamine, DSPE) generally exhibit higher T_M. By adding cholesterol the stability of the bilayer can be further increased due to a reduced permeability for water soluble molecules.[148] In contrast, electrostatic repulsion between anionic and cationic head groups decreases the stability, resulting in an aggregation of liposomes. Nevertheless, cationic lipids are often used to encapsulate DNA or RNA for gene therapy. In addition, cationic lipids are also capable of influencing cell internalization based on an interaction between the negatively charged cell membranes and the positively charged liposomes.[149]

In order to prepare liposomes, different methods can be applied. Thin film hydration,[150] membrane extrusion,[151,152] reverse phase evaporation[153] and other novel methods like supercritical reverse phase evaporation,[154] micro hydrodynamic focusing,[155] and dual centrifugation[156,157] are the most commonly used methods. The size, lamellarity, polydispersity and encapsulation efficiency (EE) varies in dependency of the applied preparation method. Especially the novel methods enable scale-up and a good control over the properties, whereas the conventional techniques often miss narrow size distributions, a control of the EE and the possibility for scale-up.[139,155]

Conventional liposomes interact with plasma proteins upon application *in vivo*. This leads to an uptake by cells of the immune system, especially by macrophages of the MPS. The uptake occurs especially in liver (Kupffer cells) and spleen, resulting in reduced blood circulation times.[158] If cells of the MPS are the target of the liposomes, this passive targeting can be useful. However, to target different cells or tissues a rapid uptake has to be eliminated.[134,159,160] Consequently, the surface of the liposome has to be modified. For this purpose polyethylene glycol (PEG) is often used. PEGylated lipids are incorporated into the lipid bilayer to form so-called stealth liposomes or sterically stabilized liposomes (SSLs) respectively (**Figure 6**).

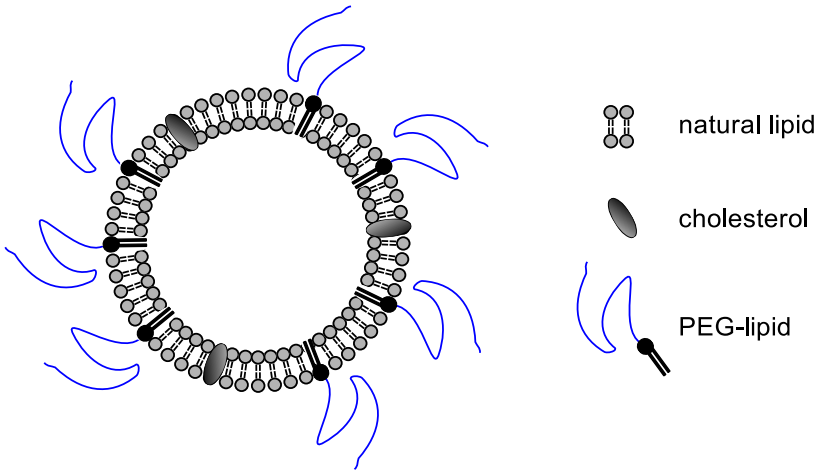

Figure 6. Schematic representation of a sterically stabilized liposome (SSL).

Stealth liposomes exhibit prolonged blood circulation times and improved safety profiles.[161,162] Besides, higher molecular weight PEGs or an increased molar content of PEG-lipids in the lipid bilayer lead to a better stealth effect. In the latter the PEG chains undergo a change from a "mushroom" to a "brush" confirmation, which shows a high impact on the protein binding at the liposomal surface.[163]

Also sterically stabilized liposomes passively accumulate. In contrast to the passive targeting of conventional liposomes to cells of the MPS, stealth liposomes accumulate in tumor tissue. This effect is described as enhanced permeability and retention (EPR) effect and was first reported by Maeda *et al.*.[164] The EPR effect describes characteristic pathophysiological transformations that are observed in tumor tissue, *i.e.* hypervascularization, enhanced permeability of blood vessels and enlarged gaps between endothelial cells.[165,166] These pathophysiological transformations enable a passive accumulation of long-circulating liposomes at the tumor site. In addition, lymphatic drainage is reduced, leading to a retention of the nanoparticles.[167,168] The state of the tumor and the specific cell line has a crucial impact on the sensitivity and passive targeting.[169] In addition, the size of the liposome also influences passive targeting, *i.e.* a diameter around 100 nm is assumed to represent an optimum.[170] With increasing complexity of the tumor tissue the distribution of nanoparticles throughout the tumor becomes more inhomogeneous, leading to an insufficient drug application and a possible multidrug resistance of the tumor.[171,172] Moreover, liposomes carrying a PEG stealth layer show retarded drug release at the tumor site.[173] These are challenges that still need to be overcome.

Introducing stimuli-responsive behavior to liposomes is a promising strategy to circumvent the encumbering effect of a stealth layer. Due to the stimuli-responsiveness a removal of the PEG chains, leading to a support of cell internalization and drug release can be obtained. In several tumor tissues the pH value is clearly lowered (pH ≤ 6.0) compared to healthy tissue, thus pH-sensitive liposomes (PSLs) subject to PEG shedding in tumor tissue and stable at physiological pH, are interesting. pH-sensitive moieties which have already been integrated in PEG-lipids are for example acetals,[174] orthoetsters,[175–177] hydrazone linkages[178–180] and vinyl ethers.[181,182] Recently, Worm *et al.* developed a synthetic strategy to integrate multiple vinyl ether moieties into PEG directly upon copolymerization of EO and 3,4-epoxy-1-butene (EPB).[183] In chapter 2.2 a polymerization strategy based on this method will be presented, targeting PEG-lipids with numerous pH-sensitive moieties. Besides, by employing PSLs accelerated blood clearance (ABC) can be overcome.[178,184] ABC describes an increased uptake of PEGylated nanocarriers by the liver due to an iterated administration of a drug delivery system.[184–186] Another possibility to obtain pH-sensitive drug delivery systems is the incorporation of so-called fusogenic lipids or peptides into nanocarriers. These lipids undergo a conformational change at lower pH facilitating an insertion into membranes and a fusion of the liposome with cell membranes.[187,188] For example fusogenic lipids can be applied to induce drug release from the endosomal cellular compartment into the cytoplasm.[189]

Furthermore, external stimuli can be utilized as triggers for drug release from liposomes *e.g.* thermosensitive liposomes release drugs upon locally applied mild hypothermia.[190] Another strategy are ecogenic liposomes, in which a stimulation *via* ultrasound leads to the release of encapsulated air and thus a disruption of the membrane.[191] In addition, the incorporation of magnetic nanoparticles resulting in magnetically sensitive liposomes is possible. Hence, an external magnetic field leads to drug release.[192]

Active targeting is a key strategy to further improve drug carrier systems. Therefore, targeting ligands with specific binding affinities towards receptors on cell surfaces can be applied. Ideally the receptors are exclusively expressed on the targeted cells which, eliminates undesired toxic effects or non-specific binding.[139] In addition, for PEGylated nanocarriers the target moiety is ideally attached at the end of the PEG chain to achieve better interaction with the desired receptor.[193] Targeting moieties that have been successfully attached and showed improved efficiency are *e.g.* antibodies,[194–197] folates,[198,199] aptamers[200] and mannose-moieties.[201] Cell internalization and cargo release

is also possible *via* cell penetrating peptides (CPPs) on the surface of a nanocarrier, although they do not have the already mentioned selectivity.[202,203] **Figure 7** shows a selection of targeting functions and stimuli-responsive moieties attached to a liposome.

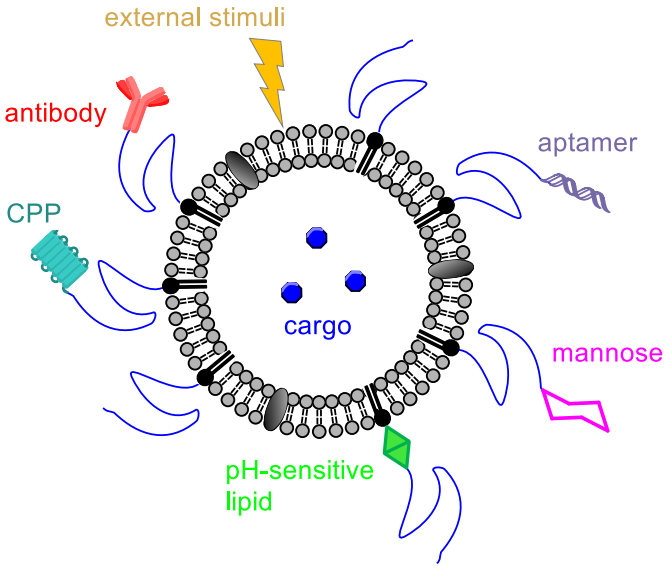

Figure 7. Schematic representation of stimuli-responsive moieties and different target functions attached to a stealth liposome.

Unfortunately, PEG-lipids only possess one functional hydroxyl group that is available for the attachment of functional groups like targeting moieties, fluorescent dyes or radioactive tracers. Thus, chemical modifications are limited and an introduction of numerous promising functional groups is not possible. Therefore, hyperbranched structures based on glycerol are promising candidates to attach numerous functional moieties. Recently, hyperbranched polyglycerol (*hb*PG) lipids have been synthesized and successfully functionalized with fluorescent labels as well as radioactive nuclides in order to investigate the fate of the liposomes *in vitro* and *in vivo*.[24,204,205] Schmidt and coworkers applied dynamic light scattering (DLS) to examine the behavior of liposomes modified with PEG-lipids and *hb*PG-lipids, respectively in human blood serum. The results showed no aggregation for liposomes modified with *hb*PG-lipids, whereas the PEG containing liposomes led to the formation of aggregates.[206] Nevertheless, first studies of liposomes with *hb*PG-lipids *via* positron emission tomography (PET) regarding their biodistribution showed low liposome stability *in vivo* and a rapid renal excretion of the lipids.[205] In contrast, recent results revealed a higher stability of liposomes modified with *hb*PG-lipids compared to PEG-lipids by changing the lipid anchorage of the polyether-based lipids from cholesterol to bis(alkyl)glycerol.[207] Another possibility to introduce multiple functional

groups is the copolymerization of EO and functional epoxide monomers leading to *mf*PEGs as described in the previous section.

Apte *et al.* combined a few of the already mentioned concepts and thereby achieved significant reduction of the tumor size of ovarian cancer in mouse models. For this purpose, they used non-cleavable PEG-lipids bearing CPPs and hydrazone-linked PEG-lipids carrying monoclonal antibodies at the polymer chain end. The pH-sensitive PEG-lipid was applied to prevent an uptake by the MPS during circulation and simultaneously obtain the detachment of PEG at the tumor site. Beyond, the attached antibody served as an active targeting moiety and the CPPs are exposed as recently as the PEG chains are cleaved and subsequently promote cell uptake.[208]

Nevertheless, the stability of liposomes during circulation has to be improved and more strategies to attach functional groups, leading to a selective targeting have to be developed. Moreover, studies to reach an uptake by specific cells and to promote drug release at the site of action have to be carried out.

1.4.2 Polymer nanoparticles

Nanoparticles are solid, colloidal particles with a diameter of 10 to 1 000 nm and the term is primarily used for nanospheres and nanocapsules. Nanospheres are solid particles, whereas nanocapsules are vesicular systems exhibiting a liquid core as shown in **Figure 8**.[209] The structure of the nanoparticle (nanocapsules or nanospheres) is determined *via* the preparation method and purification after nanoparticle preparation is important to ensure their suitability for medical applications.[210]

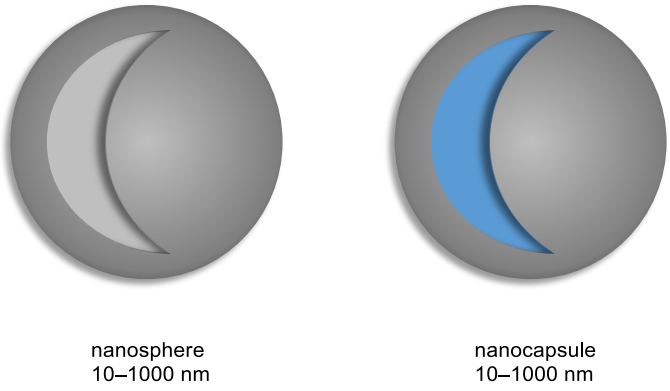

Figure 8. Schematic representation of a nanosphere exhibiting a solid mass (left) and a nanocapsule possessing a liquid core (right).

Within the last decades polymeric nanoparticles have gained increasing interest for biomedical applications. Nanoparticles are useful for the incorporation and conjugation of drugs and prodrugs, as stimuli-responsive drug delivery systems, imaging agents and for a combination of therapy and imaging (theranostics). In addition, they are applied for the treatment of cancer, neurodegenerative disorders and cardiovascular diseases.[211] The cell uptake of nanoparticles depends on the size and surface characteristics, which can be adjusted by the preparation method. Furthermore, non-specific cell uptake is influenced by the adsorption of proteins on the surface of the nanoparticles.[130]

For the preparation of nanoparticles two different methods can be distinguished, *i.e.* those methods, in which monomers are polymerized and those using preformed polymers.[212] A further classification into two different categories is possible: two-step strategies (preparation of an emulsification system and nanoparticle formation in the second step) and one-step strategies (preparation of nanoparticles without emulsification).[210] By polymerizing monomers to form the nanoparticles some challenges occur, *e.g.* formed byproducts can be toxic or monomer or unreacted initiator requires extensive purification.[213] Systems with preformed polymers avoid these drawbacks. Preformed polymers are used in solvent evaporation, nanoprecipitation, salting-out, dialysis and super-critical fluid technology. Methods in which monomers are polymerized are emulsion, mini- or microemulsion, interfacial or controlled/living radical polymerization.[211] A detailed description of all these different strategies is given elsewhere and will not be discussed in this thesis.[209,210] In the following, only the combined miniemulsion/solvent evaporation will be briefly presented. In the miniemulsion two (partially) immiscible liquids are mixed with the aid of amphiphilic surface-active molecules.[210] Thus, the miniemulsion consists of droplets in a continuous phase. The droplets are obtained by high shear forces *via* ultrasonication or high-pressure homogenizers. In order to obtain a high stability of the droplets a surfactant and co-stabilizer is necessary. The co-stabilizer is soluble in the droplet phase, but less soluble in the continuous phase compared to the rest of the droplet phase. This leads to osmotic pressure in the droplet in which the reactions take place, resulting in the formation of nanoparticles. When preformed polymers are used, a combination of the emulsion/solvent evaporation and miniemulsion technique can be performed.[214] In the first work of Gurny *et al.* nanoparticles of biocompatible polymers as drug carriers were prepared.[215] In the miniemulsion/solvent evaporation, the polymer is dissolved in a volatile solvent like dichloromethane or chloroform or ethyl acetate as less

toxic one. The organic solution is emulsified in the aqueous phase which normally contains a surfactant (as shown in **Figure 9**). The type of surfactant plays an important role regarding droplets/particle size and size distribution.[216] To obtain a dispersion of the nanodroplets *e.g.* ultrasonication can be applied.[217] Afterwards, the organic solvent is evaporated to obtain a polymer dispersion in water.

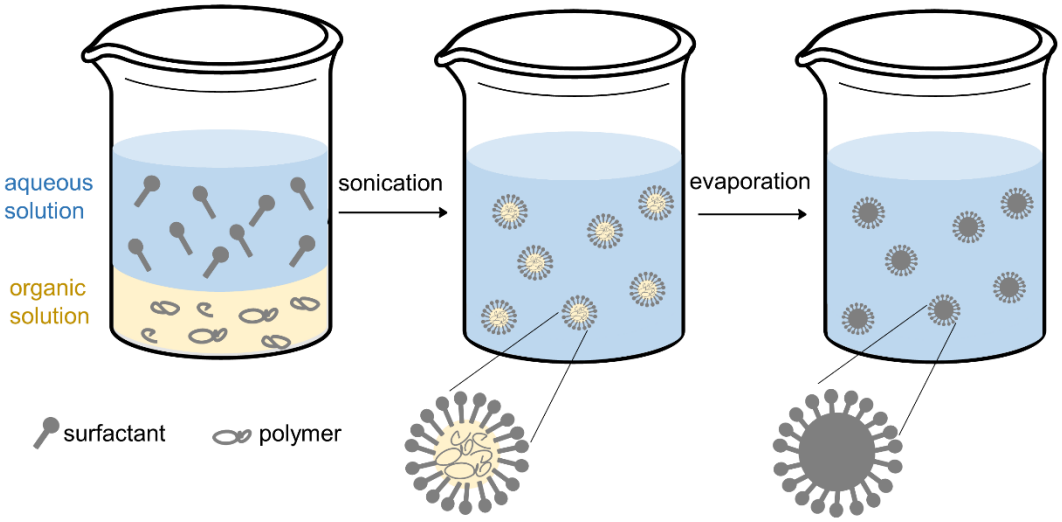

Figure 9. Schematic representation of the combined emulsion/solvent evaporation and miniemulsion technique.

With this technique nanoparticles of semiconducting polymers[218] and of biodegradable polymers like poly(lactide)s and poly(e-caprolactone)s[216] were prepared. Besides, the encapsulation of dye in methacrylate nanoparticles to obtain composite colorants[219] and polyphosphate nanoparticles loaded with paclitaxel which are promising for bone-cancer treatment[220] were obtained. Especially for biomedical applications, the surfactant has to be chosen carefully because its removal is challenging and normally it remains at the surface of the particle. Hence, surfactants which exhibit cell toxicity have to be avoided.[223,224]

Detailed characterization of nanoparticles is relevant for all subsequent pharmaceutical and biomedical applications. Size distribution, morphology, surface properties, stability and drug-polymer interactions are commonly investigated. Microscopic measurements can be carried out to investigate size, size distribution, shape and aggregation of the particles. To obtain information about structure and composition, infrared (IR) spectroscopy, mass (MS) spectrometry and nuclear magnetic resonance (NMR) spectroscopy can be performed. In addition, the hydrodynamic size distribution is determined *via* dynamic light scattering (DLS) and the surface charge is specified *via* zeta potential measurements.[210,221] In order

to investigate the binding affinities of proteins or protein mixtures on nanoparticles, isothermal titration calorimetry can be applied.[222] Subsequently, the formed protein corona of the nanoparticles can be examined *via* mass spectrometric analysis.[130] By analyzing the interaction of nanoparticles with plasma proteins, it is possible to gain a detailed understanding of the reciprocal interaction of nanocarriers and proteins as well as the correlation of the protein pattern and the stealth effect.[225] Schoettler *et al.* revealed that distinct proteins on the nanoparticle´s surface are necessary to avoid a non-specific cell uptake.[130] In chapter 3, these techniques are applied to investigate polystyrene nanoparticles prepared *via* the combined miniemulsion/solvent evaporation using an amphiphilic, linear polyglycerol with pendant phosphonate groups as surfactant.

1.5. References

(1) Herzberger, J.; Niederer, K.; Pohlit, H.; Seiwert, J.; Worm, M.; Wurm, F. R.; Frey, H. Polymerization of Ethylene Oxide, Propylene Oxide, and Other Alkylene Oxides: Synthesis, Novel Polymer Architectures, and Bioconjugation. *Chemical reviews* **2016**, *116*, 2170–2243.

(2) Jayakannan, M.; Ramakrishnan, S. Recent Developments in Polyether Synthesis. *Macromol. Rapid Commun.* **2001**, *22*, 1463.

(3) Penczek, S.; Kubisa, P.; Matyjaszewski, K. *Cationic ring-opening polymerization*; Advances in Polymer Science 68/69; Springer: Berlin, 1985.

(4) *Polymer science: A comprehensive reference;* Matyjaszewski, K.; Möller, M., Eds.; Elseiver: Amsterdam, 2012.

(5) Hadjichristidis, N.; Hirao, A. *Anionic Polymerization: Principles, Practice, Strength, Consequences and Applications*; Springer Japan, 2015.

(6) Fingerhut, A.; Serdyuk, O. V.; Tsogoeva, S. B. Non-heme iron catalysts for epoxidation and aziridination reactions of challenging terminal alkenes: Towards sustainability. *Green Chem.* **2015**, *17*, 2042–2058.

(7) Dudev, T.; Lim, C. Ring Strain Energies from ab Initio Calculations. *J. Am. Chem. Soc.* **1998**, *120*, 4450–4458.

(8) Dever, J. P.; George, K. F.; Hoffman, W. C.; Soo, H. Ethylene Oxide. In *Encyclopedia of chemical technology*; Kirk, R. E., Othmer, D. F., Eds.; Wiley: New York, NY, 2003.

(9) Ribeiro, L. G.; Taqueda, M. E. S. Stability Study on Ethylene Oxide Industrial Reaction from the Management of Critical Process Variables. *Chem. Eng. Technol.* **2015**, *38*, 2235–2242.

(10) Wurtz, C. A. Mémoire Sur L´oxyde D´éthylène Et Les Alcools Polyéthyléniques. *Ann. Chim. Phys.* **1863**, 317–354.

(11) Staudinger, H.; Schweitzer, O. Über Hochpolymere Verbindungen, 20. Mitteil.: Über Die Poly-Äthylenoxyde. *Ber. Dtsch. Chem. Ges. B* **1929**, 2395–2405.

(12) Israelachvili, J. The different faces of poly(ethylene glycol). *Proceedings of the National Academy of Sciences of the United States of America* **1997**, *94*, 8378–8379.

(13) Mandelkern, L.; Quinn, F. A.; Flory, P. J. Crystallization Kinetics in High Polymers. I. Bulk Polymers. *Journal of Applied Physics* **1954**, *25*, 830–839.

(14) Hargreaves, A. E. *Chemical formulation: An overview of surfactant-based preparations used in everyday life*; RSC paperbacks; Royal Society of Chemistry: Cambridge, 2003.

(15) Dingels, C.; Schömer, M.; Frey, H. Die vielen Gesichter des Poly(ethylenglykol)s. *Chem. unserer Zeit* **2011**, *45*, 338–349.

(16) Flory, P. J. Molecular Size Distribution in Ethylene Oxide Polymers. *J. Am. Chem. Soc.* **1940**, *62*, 1561–1565.

(17) Szwarc, M.; Levy, M.; Milkovich, R. Polymerization initiated by electron transfer to monomer. A new method of formation of block polymers 1. *J. Am. Chem. Soc.* **1956**, *78*, 2656–2657.

(18) Penczek, S.; Cypryk, M.; Duda, A.; Kubisa, P.; Slomkowksi, S. Living ring-opening polymerizations of heterocyclic monomers. *Prog. Polym. Sci.* **2007**, *32*, 247–282.

(19) Brocas, A.-L.; Mantzaridis, C.; Tunc, D.; Carlotti, S. Polyether synthesis: From activated or metal-free anionic ring-opening polymerization of epoxides to functionalization. *Prog. Polym. Sci.* **2013**, *38*, 845–873.

(20) Tieke, B. *Makromolekulare Chemie: Eine Einführung*, 2. ed; John Wiley & Sons: Hoboken, 2012.

(21) Odian, G. G. *Principles of polymerization*, 4. ed; Wiley-Interscience: Hoboken, NJ, NJ : WileyInterscience, 2004.

(22) Deffieux, A.; Boileau, S. Anionic polymerization of ethylene oxide with cryptates as counterions: 1. *Polymer* **1977**, *18*, 1047–1050.

(23) Stolarzewicz, A.; Neugebauer, D.; Grobelny, J. Potassium hydride — the new initiator for anionic polymerization of oxiranes. *Macromol. Rapid Commun.* **1996**, *17*, 787–793.

(24) Hofmann, A. M.; Wurm, F.; Hühn, E.; Nawroth, T.; Langguth, P.; Frey, H. Hyperbranched polyglycerol-based lipids via oxyanionic polymerization: toward multifunctional stealth liposomes. *Biomacromolecules* **2010**, *11*, 568–574.

(25) Hofmann, A. M.; Wurm, F.; Frey, H. Rapid Access to Polyfunctional Lipids with Complex Architecture via Oxyanionic Ring-Opening Polymerization. *Macromolecules* **2011**, *44*, 4648–4657.

(26) Wurm, F.; Klos, J.; Räder, H. J.; Frey, H. Synthesis and noncovalent protein conjugation of linear-hyperbranched PEG-poly(glycerol) alpha,omega(n)-telechelics. *J. Am. Chem. Soc.* **2009**, *131*, 7954–7955.

(27) Mangold, C.; Wurm, F.; Obermeier, B.; Frey, H. Hetero-Multifunctional Poly(ethylene glycol) Copolymers with Multiple Hydroxyl Groups and a Single Terminal Functionality. *Macromol. Rapid Comm.* **2010**, *31*, 258–264.

(28) Cammas, S.; Nagasaki, Y.; Kataoka, K. Heterobifunctional Poly(ethylene oxide): Synthesis of .alpha.-Methoxy-.omega.-amino and .alpha.-Hydroxy-.omega.-amino PEOs with the Same Molecular Weights. *Bioconjugate Chem.* **2002**, *6*, 226–230.

(29) Yue, J.; Li, X.; Mo, G.; Wang, R.; Huang, Y.; Jing, X. Modular Functionalization of Amphiphilic Block Copolymers via Radical-Mediated Thiol−Ene Reaction. *Macromolecules* **2010**, *43*, 9645–9654.

(30) Xie, Y.; Duan, S.; Forrest, M. L. Alkyne- and 1,6-elimination- succinimidyl carbonate - terminated heterobifunctional poly(ethylene glycol) for reversible "Click" PEGylation. *Drug discoveries & therapeutics* **2010**, *4*, 240–245.

(31) Studer, P.; Limal, D.; Breton, P.; Riess, G. Synthesis and characterization of poly(ethylene oxide)-block-poly(methylidene malonate 2.1.2) block copolymers bearing a mannose group at the PEO chain end. *Bioconjug. Chem.* **2005**, *16*, 223–229.

(32) Otsuka, H.; Nagasaki, Y.; Kataoka, K. Characterization of aldehyde-PEG tethered surfaces: Influence of PEG chain length on the specific biorecognition. *Langmuir* **2004**, *20*, 11285–11287.

(33) Hiki, S.; Kataoka, K. Versatile and selective synthesis of "click chemistry" compatible heterobifunctional poly(ethylene glycol)s possessing azide and alkyne functionalities. *Bioconjug. Chem.* **2010**, *21*, 248–254.

(34) Wilms, V. S.; Bauer, H.; Tonhauser, C.; Schilmann, A.-M.; Müller, M.-C.; Tremel, W.; Frey, H. Catechol-initiated polyethers: multifunctional hydrophilic ligands for PEGylation and functionalization of metal oxide nanoparticles. *Biomacromolecules* **2013**, *14*, 193–199.

(35) Thomas, A.; Bauer, H.; Schilmann, A.-M.; Fischer, K.; Tremel, W.; Frey, H. The "Needle in the Haystack" Makes the Difference: Linear and Hyperbranched Polyglycerols with a Single Catechol Moiety for Metal Oxide Nanoparticle Coating. *Macromolecules* **2014**, *47*, 4557–4566.

(36) Thompson, M. S.; Vadala, T. P.; Vadala, M. L.; Lin, Y.; Riffle, J. S. Synthesis and applications of heterobifunctional poly(ethylene oxide) oligomers. *Polymer* **2008**, *49*, 345–373.

(37) Akiyama, Y.; Otsuka, H.; Nagasaki, Y.; Kato, M.; Kataoka, K. Selective synthesis of heterobifunctional poly(ethylene glycol) derivatives containing both mercapto and acetal terminals. *Bioconjug. Chem.* **2000**, *11*, 947–950.

(38) Ishizu, K.; Furukawa, T. Synthesis of functionalized poly(ethylene oxide) macromonomers. *Polymer* **2001**, *42*, 7233–7236.

(39) Yagci, Y.; Ito, K. Macromolecular Architecture Based on Anionically Prepared Poly(ethylene oxide) Macromonomers. *Macromol. Symp.* **2005**, *226*, 87–96.

(40) Hayashi, H.; Iijima, M.; Kataoka, K.; Nagasaki, Y. pH-Sensitive Nanogel Possessing Reactive PEG Tethered Chains on the Surface. *Macromolecules* **2004**, *37*, 5389–5396.

(41) Billouard, C.; Carlotti, S.; Desbois, P.; Deffieux, A. "Controlled" High-Speed Anionic Polymerization of Propylene Oxide Initiated by Alkali Metal Alkoxide/Trialkylaluminum Systems. *Macromolecules* **2004**, *37*, 4038–4043.

(42) Aida, T.; Mizuta, R.; Yoshida, Y.; Inoue, S. Polymerization of epoxides catalysed by metalloporphine. *Makromol. Chem.* **1981**, *182*, 1073–1079.

(43) Aida, T.; Inoue, S. Metalloporphyrins as Initiators for Living and Immortal Polymerizations. *Acc. Chem. Res.* **1996**, *29*, 39–48.

(44) Aida, T.; Inoue, S. Living polymerization of epoxides with metalloporphyrin and synthesis of block copolymers with controlled chain lengths. *Macromolecules* **1981**, *14*, 1162–1166.

(45) Akatsuka, M.; Aida, T.; Inoue, S. High-Speed "Immortal" Polymerization of Epoxides Initiated with Aluminum Porphyrin. Acceleration of Propagation and Chain-Transfer Reactions by a Lewis Acid. *Macromolecules* **1994**, *27*, 2820–2825.

(46) Sugimoto, H.; Kawamura, C.; Kuroki, M.; Aida, T.; Inoue, S. Lewis Acid-Assisted Anionic Ring-Opening Polymerization of Epoxide by the Aluminum Complexes of Porphyrin, Phthalocyanine, Tetraazaannulene, and Schiff Base as Initiators. *Macromolecules* **1994**, *27*, 2013–2018.

(47) Braune, W.; Okuda, J. An Efficient Method for Controlled Propylene Oxide Polymerization: The Significance of Bimetallic Activation in Aluminum Lewis Acids. *Angew. Chem. Int. Ed.* **2003**, *42*, 64–68.

(48) Labbé, A.; Carlotti, S.; Billouard, C.; Desbois, P.; Deffieux, A. Controlled High-Speed Anionic Polymerization of Propylene Oxide Initiated by Onium Salts in the Presence of Triisobutylaluminum. *Macromolecules* **2007**, *40*, 7842–7847.

(49) Gervais, M.; Labbé, A.; Carlotti, S.; Deffieux, A. Direct Synthesis of α-Azido,ω-hydroxypolyethers by Monomer-Activated Anionic Polymerization. *Macromolecules* **2009**, *42*, 2395–2400.

(50) Deffieux, A.; Carlotti, S.; Desbois, P. New Perspectives in Living/Controlled Anionic Polymerization. *Macromol. Symp.* **2005**, *229*, 24–31.

(51) Carlotti, S.; Desbois, P.; Billouard, C.; Deffieux, A. Reactivity control in anionic polymerization of ethylenic and heterocyclic monomers through formation of 'ate' complexes. *Polym. Int.* **2006**, *55*, 1126–1131.

(52) Sakakibara, K.; Nakano, K.; Nozaki, K. Regio-controlled ring-opening polymerization of perfluoroalkyl-substituted epoxides. *Chem. Commun.* **2006**, 3334–3336.

(53) Sakakibara, K.; Nakano, K.; Nozaki, K. Regioregular Polymerization of Fluorine-Containing Epoxides. *Macromolecules* **2007**, *40*, 6136–6142.

(54) Rejsek, V.; Sauvanier, D.; Billouard, C.; Desbois, P.; Deffieux, A.; Carlotti, S. Controlled Anionic Homo- and Copolymerization of Ethylene Oxide and Propylene Oxide by Monomer Activation. *Macromolecules* **2007**, *40*, 6510–6514.

(55) Gervais, M.; Brocas, A.-L.; Cendejas, G.; Deffieux, A.; Carlotti, S. Synthesis of Linear High Molar Mass Glycidol-Based Polymers by Monomer-Activated Anionic Polymerization. *Macromolecules* **2010**, *43*, 1778–1784.

(56) Roos, K.; Carlotti, S. Grignard-based anionic ring-opening polymerization of propylene oxide activated by triisobutylaluminum. *European Polymer Journal* **2015**, *70*, 240–246.

(57) Brocas, A.-L.; Deffieux, A.; Le Malicot, N.; Carlotti, S. Combination of phosphazene base and triisobutylaluminum for the rapid synthesis of polyhydroxy telechelic poly(propylene oxide). *Polym. Chem.* **2012**, *3*, 1189.

(58) Carlotti, S.; Labbé, A.; Rejsek, V.; Doutaz, S.; Gervais, M.; Deffieux, A. Living/Controlled Anionic Polymerization and Copolymerization of Epichlorohydrin with Tetraoctylammonium Bromide−Triisobutylaluminum Initiating Systems. *Macromolecules* **2008**, *41*, 7058–7062.

(59) Lundberg, P.; Lee, B. F.; van den Berg, S. A.; Pressly, E. D.; Lee, A.; Hawker, C. J.; Lynd, N. A. Poly(ethylene oxide)-co-(methylene ethylene oxide): A hydrolytically-degradable poly(ethylene oxide) platform. *ACS Macro Lett.* **2012**, *1*, 1240–1243.

(60) Meyer, J.; Keul, H.; Möller, M. Poly(glycidyl amine) and Copolymers with Glycidol and Glycidyl Amine Repeating Units: Synthesis and Characterization. *Macromolecules* **2011**, *44*, 4082–4091.

(61) Brocas, A.-L.; Cendejas, G.; Caillol, S.; Deffieux, A.; Carlotti, S. Controlled synthesis of polyepichlorohydrin with pendant cyclic carbonate functions for isocyanate-free polyurethane networks. *J. Polym. Sci. A Polym. Chem.* **2011**, *49*, 2677–2684.

(62) Hu, H.; Yuan, W.; Lu, L.; Zhao, H.; Jia, Z.; Baker, G. L. Low glass transition temperature polymer electrolyte prepared from ionic liquid grafted polyethylene oxide. *J. Polym. Sci. A Polym. Chem.* **2014**, *52*, 2104–2110.

(63) Labbé, A.; Brocas, A.-L.; Ibarboure, E.; Ishizone, T.; Hirao, A.; Deffieux, A.; Carlotti, S. Selective Ring-Opening Polymerization of Glycidyl Methacrylate: Toward the Synthesis of Cross-Linked (Co)polyethers with Thermoresponsive Properties. *Macromolecules* **2011**, *44*, 6356–6364.

(64) Rodriguez, C. G.; Ferrier, R. C.; Helenic, A.; Lynd, N. A. Ring-Opening Polymerization of Epoxides: Facile Pathway to Functional Polyethers via a Versatile Organoaluminum Initiator. *Macromolecules* **2017**, *50*, 3121–3130.

(65) Herzberger, J.; Frey, H. Epicyanohydrin: Polymerization by Monomer Activation Gives Access to Nitrile-, Amino-, and Carboxyl-Functional Poly(ethylene glycol). *Macromolecules* **2015**, *48*, 8144–8153.

(66) Müller, S. S.; Moers, C.; Frey, H. A Challenging Comonomer Pair: Copolymerization of Ethylene Oxide and Glycidyl Methyl Ether to Thermoresponsive Polyethers. *Macromolecules* **2014**, *47*, 5492–5500.

(67) Labbé, A.; Carlotti, S.; Deffieux, A.; Hirao, A. Controlled Polymerization of Glycidyl Methyl Ether Initiated by Onium Salt/Triisobutylaluminum and Investigation of the Polymer LCST. *Macromol. Symp.* **2007**, *249-250*, 392–397.

(68) Brocas, A.-L.; Gervais, M.; Carlotti, S.; Pispas, S. Amphiphilic diblock copolymers based on ethylene oxide and epoxides bearing aliphatic side chains. *Polym. Chem.* **2012**, *3*, 2148.

(69) Gervais, M.; Brocas, A.-L.; Deffieux, A.; Ibarboure, E.; Carlotti, S. Rapid and controlled synthesis of hydrophobic polyethers by monomer activation. *Pure and Applied Chemistry* **2012**, *84*, 2610.

(70) Herzberger, J.; Leibig, D.; Liermann, J. C.; Frey, H. Conventional Oxyanionic versus Monomer-Activated Anionic Copolymerization of Ethylene Oxide with Glycidyl Ethers: Striking Differences in Reactivity Ratios. *ACS Macro Lett.* **2016**, *5*, 1206–1211.

(71) Heinen, S.; Rackow, S.; Schäfer, A.; Weinhart, M. A Perfect Match: Fast and Truly Random Copolymerization of Glycidyl Ether Monomers to Thermoresponsive Copolymers. *Macromolecules* **2017**, *50*, 44–53.

(72) Obermeier, B.; Wurm, F.; Mangold, C.; Frey, H. Multifunctional Poly(ethylene glycol)s. *Angew. Chem. Int. Edit.* **2011**, *50*, 7988–7997.

(73) Mangold, C.; Wurm, F.; Frey, H. Functional PEG-based polymers with reactive groups via anionic ROP of tailor-made epoxides. *Polym. Chem.* **2012**, *3*, 1714.

(74) Bailey, F. E.; Callard, R. W. Some properties of poly(ethylene oxide)1 in aqueous solution. *J. Appl. Polym. Sci.* **1959**, *1*, 56–62.

(75) Hamaide, T.; Goux, A.; Llauro, M.-F.; Spitz, R.; Guyot, A. Stat-poly(Ethylene oxide-co-propylene oxide). Synthesis, NMR characterization and crystallinity studies. Correlation with monte carlo simulation. *Angew. Makromol. Chemie* **1996**, *237*, 55–77.

(76) Louai, A.; Sarazin, D.; Pollet, G.; François, J.; Moreaux, F. Properties of ethylene oxide-propylene oxide statistical copolymers in aqueous solution. *Polymer* **1991**, *32*, 703–712.

(77) Herzberger, J.; Fischer, K.; Leibig, D.; Bros, M.; Thiermann, R.; Frey, H. Oxidation-Responsive and "Clickable" Poly(ethylene glycol) via Copolymerization of 2-(Methylthio)ethyl Glycidyl Ether. *J. Am. Chem. Soc.* **2016**, *138*, 9212–9223.

(78) Lee, B. F.; Wolffs, M.; Delaney, K. T.; Sprafke, J. K.; Leibfarth, F. A.; Hawker, C. J.; Lynd, N. A. Reactivity ratios, and mechanistic insight for anionic ring-opening copolymerization of epoxides. *Macromolecules* **2012**, *45*, 3722–3731.

(79) Niederer, K.; Schüll, C.; Leibig, D.; Johann, T.; Frey, H. Catechol Acetonide Glycidyl Ether (CAGE): A Functional Epoxide Monomer for Linear and Hyperbranched Multi-Catechol Functional Polyether Architectures. *Macromolecules* **2016**, *49*, 1655–1665.

(80) Stolarzewicz, A.; Neugebauer, D. Influence of substituent on the polymerization of oxiranes by potassium hydride. *Macromol. Chem. Phys.* **1999**, *200*, 2467–2470.

(81) Chisholm, M. H.; Navarro-Llobet, D. NMR Assignments of Regioregular Poly(propylene oxide) at the Triad and Tetrad Level. *Macromolecules* **2002**, *35*, 2389–2392.

(82) Price, C. C.; Carmelite, D. D. Reactions of Epoxides in Dimethyl Sulfoxide Catalyzed by Potassium t-Butoxide. *J. Am. Chem. Soc.* **1966**, *88*, 4039–4044.

(83) Price, C. C. Polyethers. *Acc. Chem. Res.* **1974**, *7*, 294–301.

(84) Allgaier, J.; Willbold, S.; Chang, T. Synthesis of Hydrophobic Poly(alkylene oxide)s and Amphiphilic Poly(alkylene oxide) Block Copolymers. *Macromolecules* **2007**, *40*, 518–525.

(85) Hans, M.; Keul, H.; Moeller, M. Chain transfer reactions limit the molecular weight of polyglycidol prepared via alkali metal based initiating systems. *Polymer* **2009**, *50*, 1103–1108.

(86) Fitton, A. O.; Hill, J.; Jane, D. E.; Millar, R. Synthesis of Simple Oxetanes Carrying Reactive 2-Substituents. *Synthesis* **1987**, 1140–1142.

(87) Mayo, F. R.; Lewis, F. M. Copolymerization. I. A Basis for Comparing the Behavior of Monomers in Copolymerization; The Copolymerization of Styrene and Methyl Methacrylate. *J. Am. Chem. Soc.* **1944**, *66*, 1594–1601.

(88) Shaikh, S.; Puskas, J. E.; Kaszas, G. A new high-throughput approach to measure copolymerization reactivity ratios using real-time FTIR monitoring. *J. Polym. Sci. A Polym. Chem.* **2004**, *42*, 4084–4100.

(89) Pasquale, A. J.; Long, T. E. Real-Time Monitoring of the Stable Free Radical Polymerization of Styrene via in-Situ Mid-Infrared Spectroscopy. *Macromolecules* **1999**, *32*, 7954–7957.

(90) Long, T. E.; Liu, H. Y.; Schell, B. A.; Teegarden, D. M.; Uerz, D. S. Determination of solution polymerization kinetics by near-infrared spectroscopy. 1. Living anionic polymerization processes. *Macromolecules* **1993**, *26*, 6237–6242.

(91) Fontoura, J. M. R.; Santos, A. F.; Silva, F. M.; Lenzi, M. K.; Lima, E. L.; Pinto, J. C. Monitoring and control of styrene solution polymerization using NIR spectroscopy. *J. Appl. Polym. Sci.* **2003**, *90*, 1273–1289.

(92) van den Brink, M.; Pepers, M.; van Herk, A. M.; German, A. L. On-line Monitoring and Composition Control of the Emulsion Copolymerization of VeoVA 9 and Butyl Acrylate by Raman Spectroscopy. *Polymer Reaction Engineering* **2001**, *9*, 101–133.

(93) Wang, C.; Vickers, T. J.; Schlenoff, J. B.; Mann, C. K. In situ Monitoring of Emulsion Polymerization using Fiber-Optic Raman Spectroscopy. *Appl Spectrosc* **2016**, *46*, 1729–1731.

(94) Quinebèche, S.; Navarro, C.; Gnanou, Y.; Fontanille, M. In situ mid-IR and UV–visible spectroscopies applied to the determination of kinetic parameters in the anionic copolymerization of styrene and isoprene. *Polymer* **2009**, *50*, 1351–1357.

(95) Alb, A. M.; Enohnyaket, P.; Drenski, M. F.; Head, A.; Reed, A. W.; Reed, W. F. Online Monitoring of Copolymerization Involving Comonomers of Similar Spectral Characteristics. *Macromolecules* **2006**, *39*, 5705–5713.

(96) Alkan, A.; Natalello, A.; Wagner, M.; Frey, H.; Wurm, F. R. Ferrocene-Containing Multifunctional Polyethers: Monomer Sequence Monitoring via Quantitative 13 C NMR Spectroscopy in Bulk. *Macromolecules* **2014**, *47*, 2242–2249.

(97) Obermeier, B.; Wurm, F.; Frey, H. Amino Functional Poly(ethylene glycol) Copolymers via Protected Amino Glycidol. *Macromolecules* **2010**, *43*, 2244–2251.

(98) Zhang, W.; Allgaier, J.; Zorn, R.; Willbold, S. Determination of the Compositional Profile for Tapered Copolymers of Ethylene Oxide and 1,2-Butylene Oxide by In-situ-NMR. *Macromolecules* **2013**, *46*, 3931–3938.

(99) Mayo, F. R.; Walling, C. Copolymerization. *Chem. Rev.* **1950**, *46*, 191–287.

(100) Heatley, F.; Yu, G.-e.; Booth, C.; Blease, T. G. Determination of reactivity ratios for the anionic copolymerization of ethylene oxide and propylene oxide in bulk. *European Polymer Journal* **1991**, *27*, 573–579.

(101) Lee, A.; Lundberg, P.; Klinger, D.; Lee, B. F.; Hawker, C. J.; Lynd, N. A. Physiologically relevant, pH-responsive PEG-based block and statistical copolymers withN,N-diisopropylamine units. *Polym. Chem.* **2013**, *4*, 5735–5742.

(102) Obermeier, B.; Frey, H. Poly(ethylene glycol-co-allyl glycidyl ether)s: A PEG-based modular synthetic platform for multiple bioconjugation. *Bioconjug. Chem.* **2011**, *22*, 436–444.

(103) Mangold, C.; Wurm, F.; Obermeier, B.; Frey, H. "Functional Poly(ethylene glycol)": PEG-Based Random Copolymers with 1,2-Diol Side Chains and Terminal Amino Functionality. *Macromolecules* **2010**, *43*, 8511–8518.

(104) Pang, X.; Jing, R.; Huang, J. Synthesis of amphiphilic macrocyclic graft copolymer consisting of a poly(ethylene oxide) ring and multi-poly(ε-caprolactone) lateral chains. *Polymer* **2008**, *49*, 893–900.

(105) Reuss, V. S.; Obermeier, B.; Dingels, C.; Frey, H. N,N -Diallylglycidylamine: A Key Monomer for Amino-Functional Poly(ethylene glycol) Architectures. *Macromolecules* **2012**, *45*, 4581–4589.

(106) Reuss, V. S.; Werre, M.; Frey, H. Thermoresponsive copolymers of ethylene oxide and N,N-diethyl glycidyl amine: Polyether polyelectrolytes and PEGylated gold nanoparticle formation. *Macromolecular rapid communications* **2012**, *33*, 1556–1561.

(107) Thomas, A.; Niederer, K.; Wurm, F.; Frey, H. Combining oxyanionic polymerization and click-chemistry: a general strategy for the synthesis of polyether polyol macromonomers. *Polym. Chem.* **2013**, *5*, 899.

(108) Southan, A.; Hoch, E.; Schönhaar, V.; Borchers, K.; Schuh, C.; Müller, M.; Bach, M.; Tovar, G. E. M. Side chain thiol-functionalized poly(ethylene glycol) by post-polymerization modification of hydroxyl groups: Synthesis, crosslinking and inkjet printing. *Polym. Chem.* **2014**, *5*, 5350–5359.

(109) Herzberger, J.; Kurzbach, D.; Werre, M.; Fischer, K.; Hinderberger, D.; Frey, H. Stimuli-Responsive Tertiary Amine Functional PEGs Based on N , N -Dialkylglycidylamines. *Macromolecules* **2014**, *47*, 7679–7690.

(110) Tonhauser, C.; Alkan, A.; Schömer, M.; Dingels, C.; Ritz, S.; Mailänder, V.; Frey, H.; Wurm, F. R. Ferrocenyl Glycidyl Ether: A Versatile Ferrocene Monomer for Copolymerization with Ethylene Oxide to Water-Soluble, Thermoresponsive Copolymers. *Macromolecules* **2013**, *46*, 647–655.

(111) Napoli, A.; Valentini, M.; Tirelli, N.; Müller, M.; Hubbell, J. A. Oxidation-responsive polymeric vesicles. *Nature materials* **2004**, *3*, 183–189.

(112) Lee, B. F.; Kade, M. J.; Chute, J. A.; Gupta, N.; Campos, L. M.; Fredrickson, G. H.; Kramer, E. J.; Lynd, N. A.; Hawker, C. J. Poly(allyl glycidyl ether)-A versatile and functional polyether platform. *Journal of polymer science. Part A, Polymer chemistry* **2011**, *49*, 4498–4504.

(113) Sokolovskaya, E.; Yoon, J.; Misra, A. C.; Bräse, S.; Lahann, J. Controlled microstructuring of janus particles based on a multifunctional poly(ethylene glycol). *Macromol. Rapid Comm.* **2013**, *34*, 1554–1559.

(114) Koyama, Y.; Umehara, M.; Mizuno, A.; Itaba, M.; Yasukouchi, T.; Natsume, K.; Suginaka, A. Synthesis of novel poly(ethylene glycol) derivatives having pendant amino groups and aggregating behavior of its mixture with fatty acid in water. *Bioconjug. Chem.* **1996**, *7*, 298–301.

(115) Mangold, C.; Dingels, C.; Obermeier, B.; Frey, H.; Wurm, F. PEG-based Multifunctional Polyethers with Highly Reactive Vinyl-Ether Side Chains for Click-Type Functionalization. *Macromolecules* **2011**, *44*, 6326–6334.

(116) Mangold, C.; Obermeier, B.; Wurm, F.; Frey, H. From an epoxide monomer toolkit to functional PEG copolymers with adjustable LCST behavior. *Macromol. Rapid Comm.* **2011**, *32*, 1930–1934.

(117) Thomas, A.; Müller, S. S.; Frey, H. Beyond poly(ethylene glycol): linear polyglycerol as a multifunctional polyether for biomedical and pharmaceutical applications. *Biomacromolecules* **2014**, *15*, 1935–1954.

(118) Taton, D.; Le Borgne, A.; Sepulchre, M.; Spassky, N. Synthesis of chiral and racemic functional polymers from glycidol and thioglycidol. *Macromol. Chem. Phys.* **1994**, *195*, 139–148.

(119) Li, Z.; Chau, Y. Synthesis of linear polyether polyol derivatives as new materials for bioconjugation. *Bioconjug. Chem.* **2009**, *20*, 780–789.

(120) Erberich, M.; Keul, H.; Möller, M. Polyglycidols with Two Orthogonal Protective Groups: Preparation, Selective Deprotection, and Functionalization. *Macromolecules* **2007**, *40*, 3070–3079.

(121) Abuchowski, A.; McCoy, J. R.; Palczuk, N. C.; van Es, T.; Davis, F. F. Effect of covalent attachment of polyethylene glycol on immunogenicity and circulating life of bovine liver catalase. *The Journal of biological chemistry* **1977**, *252*, 3582–3586.

(122) Abuchowski, A.; van Es, T.; Palczuk, N. C.; Davis, F. F. Alteration of immunological properties of bovine serum albumin by covalent attachment of polyethylene glycol. *The Journal of biological chemistry* **1977**, *252*, 3578–3581.

(123) Fruijtier-Pölloth, C. Safety assessment on polyethylene glycols (PEGs) and their derivatives as used in cosmetic products. *Toxicology* **2005**, *214*, 1–38.

(124) Harris, J. M.; Chess, R. B. Effect of pegylation on pharmaceuticals. *Nat. Rev. Drug. Discov.* **2003**, *2*, 214–221.

(125) Khandare, J.; Minko, T. Polymer–drug conjugates: Progress in polymeric prodrugs. *Prog. Polym. Sci.* **2006**, *31*, 359–397.

(126) Caliceti, P.; Veronese, F. M. Pharmacokinetic and biodistribution properties of poly(ethylene glycol)-protein conjugates. *Advanced drug delivery reviews* **2003**, *55*, 1261–1277.

(127) Roberts, M. J.; Bentley, M. D.; Harris, J. M. Chemistry for peptide and protein PEGylation. *Advanced drug delivery reviews* **2002**, *54*, 459–476.

(128) Ryan, S. M.; Mantovani, G.; Wang, X.; Haddleton, D. M.; Brayden, D. J. Advances in PEGylation of important biotech molecules: Delivery aspects. *Expert opinion on drug delivery* **2008**, *5*, 371–383.

(129) Pasut, G.; Veronese, F. M. State of the art in PEGylation: The great versatility achieved after forty years of research. *J. Control. Release* **2012**, *161*, 461–472.

(130) Schottler, S.; Becker, G.; Morsbach, S.; Steinbach, T.; Mohr, K.; Landfester, K.; Mailander, V.; Wurm, F. R. Protein adsorption is required for stealth effect of poly(ethylene glycol)- and poly(phosphoester)-coated nanocarriers. *Nature nanotechnology* **2016**, *11*, 372–377.

(131) Bangham, A. D.; Standish, M. M.; Watkins, J. C. Diffusion of univalent ions across the lamellae of swollen phospholipids. *Journal of Molecular Biology* **1965**, *13*, 238-IN27.

(132) Torchilin, V. P. Recent advances with liposomes as pharmaceutical carriers. *Nat. Rev. Drug. Discov.* **2005**, *4*, 145–160.

(133) Ferlay, J.; Shin, H.-R.; Bray, F.; Forman, D.; Mathers, C.; Parkin, D. M. Estimates of worldwide burden of cancer in 2008: GLOBOCAN 2008. *Int. J. Cancer* **2010**, *127*, 2893–2917.

(134) Sharma, A. Liposomes in drug delivery: Progress and limitations. *Int. J. Pharm.* **1997**, *154*, 123–140.

(135) Mu, L.; Sprando, R. L. Application of nanotechnology in cosmetics. *Pharmaceutical research* **2010**, *27*, 1746–1749.

(136) Betz, G.; Aeppli, A.; Menshutina, N.; Leuenberger, H. In vivo comparison of various liposome formulations for cosmetic application. *International journal of pharmaceutics* **2005**, *296*, 44–54.

(137) Mozafari, M. R.; Johnson, C.; Hatziantoniou, S.; Demetzos, C. Nanoliposomes and their applications in food nanotechnology. *Journal of liposome research* **2008**, *18*, 309–327.

(138) Taylor, T. M.; Davidson, P. M.; Bruce, B. D.; Weiss, J. Liposomal nanocapsules in food science and agriculture. *Critical reviews in food science and nutrition* **2005**, *45*, 587–605.

(139) Pattni, B. S.; Chupin, V. V.; Torchilin, V. P. New Developments in Liposomal Drug Delivery. *Chemical reviews* **2015**, *115*, 10938–10966.

(140) Usonis, V.; Bakasénas, V.; Valentelis, R.; Katiliene, G.; Vidzeniene, D.; Herzog, C. Antibody titres after primary and booster vaccination of infants and young children with a virosomal hepatitis A vaccine (Epaxal®). *Vaccine* **2003**, *21*, 4588–4592.

(141) Meunier, F.; Prentice, H. G.; Ringdén, O. Liposomal amphotericin B (AmBisome): Safety data from a phase II/III clinical trial. *The Journal of antimicrobial chemotherapy* **1991**, *28 Suppl B*, 83–91.

(142) Mischler, R.; Metcalfe, I. C. Inflexal V a trivalent virosome subunit influenza vaccine: Production. *Vaccine* **2002**, *20 Suppl 5*, B17-23.

(143) Park, J. W. Liposome-based drug delivery in breast cancer treatment. *Breast cancer research : BCR* **2002**, *4*, 95–99.

(144) Fassas, A.; Anagnostopoulos, A. The use of liposomal daunorubicin (DaunoXome) in acute myeloid leukemia. *Leukemia & lymphoma* **2005**, *46*, 795–802.

(145) Andreopoulou, E.; Gaiotti, D.; Kim, E.; Downey, A.; Mirchandani, D.; Hamilton, A.; Jacobs, A.; Curtin, J.; Muggia, F. Pegylated liposomal doxorubicin HCL (PLD; Caelyx/Doxil): Experience with long-term maintenance in responding patients with recurrent epithelial ovarian cancer. *Annals of oncology : official journal of the European Society for Medical Oncology* **2007**, *18*, 716–721.

(146) Allen, T. M.; Everest, J. M. Effect of liposome size and drug release properties on pharmacokinetics of encapsulated drug in rats. *The Journal of pharmacology and experimental therapeutics* **1983**, *226*, 539–544.

(147) Fröhlich, M.; Brecht, V.; Peschka-Süss, R. Parameters influencing the determination of liposome lamellarity by 31P-NMR. *Chemistry and physics of lipids* **2001**, *109*, 103–112.

(148) Vemuri, S.; Rhodes, C. T. Preparation and characterization of liposomes as therapeutic delivery systems: A review. *Pharmaceutica acta Helvetiae* **1995**, *70*, 95–111.

(149) Miller, C. R.; Bondurant, B.; McLean, S. D.; McGovern, K. A.; O'Brien, D. F. Liposome-cell interactions in vitro: Effect of liposome surface charge on the binding and endocytosis of conventional and sterically stabilized liposomes. *Biochemistry* **1998**, *37*, 12875–12883.

(150) Reeves, J. P.; Dowben, R. M. Formation and properties of thin-walled phospholipid vesicles. *Journal of cellular physiology* **1969**, *73*, 49–60.

(151) Frisken, B. J.; Asman, C.; Patty, P. J. Studies of Vesicle Extrusion. *Langmuir : the ACS journal of surfaces and colloids* **2000**, *16*, 928–933.

(152) Popa, R.; Vrânceanu, M.; Nikolaus, S.; Nirschl, H.; Leneweit, G. Entrance effects at nanopores of nanocapsules functionalized with poly(ethylene glycol) and their flow through nanochannels. *Langmuir* **2008**, *24*, 13030–13036.

(153) Szoka, F.; Papahadjopoulos, D. Procedure for preparation of liposomes with large internal aqueous space and high capture by reverse-phase evaporation. *Proceedings of the National Academy of Sciences of the United States of America* **1978**, *75*, 4194–4198.

(154) Otake, K.; Imura, T.; Sakai, H.; Abe, M. Development of a New Preparation Method of Liposomes Using Supercritical Carbon Dioxide. *Langmuir : the ACS journal of surfaces and colloids* **2001**, *17*, 3898–3901.

(155) Jahn, A.; Vreeland, W. N.; Gaitan, M.; Locascio, L. E. Controlled vesicle self-assembly in microfluidic channels with hydrodynamic focusing. *J. Am. Chem. Soc.* **2004**, *126*, 2674–2675.

(156) Massing, U.; Cicko, S.; Ziroli, V. Dual asymmetric centrifugation (DAC)--a new technique for liposome preparation. *J. Control. Release* **2008**, *125*, 16–24.

(157) Meier, S.; Pütz, G.; Massing, U.; Hagemeyer, C. E.; Elverfeldt, D. von; Meissner, M.; Ardipradja, K.; Barnert, S.; Peter, K.; Bode, C. *et al.* Immuno-magnetoliposomes targeting activated platelets as a potentially human-compatible MRI contrast agent for targeting atherothrombosis. *Biomaterials* **2015**, *53*, 137–148.

(158) Awasthi, V. D.; Garcia, D.; Goins, B. A.; Phillips, W. T. Circulation and biodistribution profiles of long-circulating PEG-liposomes of various sizes in rabbits. *Int. J. Pharm.* **2003**, *253*, 121–132.

(159) Woodle, M. C.; Lasic, D. D. Sterically stabilized liposomes. *Biochim. Biophys. Acta, Rev. Biomembr.* **1992**, *1113*, 171–199.

(160) Barenholz, Y. Liposome application: problems and prospects. *Curr. Opin. Colloid. In.* **2001**, *6*, 66–77.

(161) Pasut, G.; Paolino, D.; Celia, C.; Mero, A.; Joseph, A. S.; Wolfram, J.; Cosco, D.; Schiavon, O.; Shen, H.; Fresta, M. Polyethylene glycol (PEG)-dendron phospholipids as innovative constructs for the preparation of super stealth liposomes for anticancer therapy. *J. Control. Release* **2015**, *199*, 106–113.

(162) Woodle, M. C. Surface-modified liposomes: Assessment and characterization for increased stability and prolonged blood circulation. *Chemistry and physics of lipids* **1993**, *64*, 249–262.

(163) Lee, H.; Larson, R. G. Adsorption of Plasma Proteins onto PEGylated Lipid Bilayers: The Effect of PEG Size and Grafting Density. *Biomacromolecules* **2016**, *17*, 1757–1765.

(164) Maeda, H.; Wu, J.; Sawa, T.; Matsumura, Y.; Hori, K. Tumor vascular permeability and the EPR effect in macromolecular therapeutics: a review. *J. Control. Release* **2000**, *65*, 271–284.

(165) Knop, K.; Hoogenboom, R.; Fischer, D.; Schubert, U. S. Poly(ethylene glycol) in drug delivery: pros and cons as well as potential alternatives. *Angew. Chem. Int. Edit.* **2010**, *49*, 6288–6308.

(166) Maeda, H.; Bharate, G. Y.; Daruwalla, J. Polymeric drugs for efficient tumor-targeted drug delivery based on EPR-effect. *Eur. J. Pharm. Biopharm.* **2009**, *71*, 409–419.

(167) Matsumura, Y.; Maeda, H. A new concept for macromolecular therapeutics in cancer chemotherapy: mechanism of tumoritropic accumulation of proteins and the antitumor agent smancs. *Cancer Res.* **1986**, *46*, 6387–6392.

(168) Fang, J.; Nakamura, H.; Maeda, H. The EPR effect: Unique features of tumor blood vessels for drug delivery, factors involved, and limitations and augmentation of the effect. *Advanced drug delivery reviews* **2011**, *63*, 136–151.

(169) Yuan, F.; Dellian, M.; Fukumura, D.; Leunig, M.; Berk, D. A.; Torchilin, V. P.; Jain, R. K. Vascular permeability in a human tumor xenograft: Molecular size dependence and cutoff size. *Cancer Res.* **1995**, *55*, 3752–3756.

(170) Nagayasu; Uchiyama; Kiwada. The size of liposomes: A factor which affects their targeting efficiency to tumors and therapeutic activity of liposomal antitumor drugs. *Advanced drug delivery reviews* **1999**, *40*, 75–87.

(171) Patel, N. R.; Pattni, B. S.; Abouzeid, A. H.; Torchilin, V. P. Nanopreparations to overcome multidrug resistance in cancer. *Advanced drug delivery reviews* **2013**, *65*, 1748–1762.

(172) Bae, Y. H. Drug targeting and tumor heterogeneity. *J. Control. Release* **2009**, *133*, 2–3.

(173) Hong, R. L.; Huang, C. J.; Tseng, Y. L.; Pang, V. F.; Chen, S. T.; Liu, J. J.; Chang, F. H. Direct comparison of liposomal doxorubicin with or without polyethylene glycol coating in C-26 tumor-bearing mice: Is surface coating with polyethylene glycol beneficial? *Clinical cancer research : an official journal of the American Association for Cancer Research* **1999**, *5*, 3645–3652.

(174) Wong, J. B.; Grosse, S.; Tabor, A. B.; Hart, S. L.; Hailes, H. C. Acid cleavable PEG-lipids for applications in a ternary gene delivery vector. *Molecular bioSystems* **2008**, *4*, 532–541.

(175) Masson, C.; Garinot, M.; Mignet, N.; Wetzer, B.; Mailhe, P.; Scherman, D.; Bessodes, M. pH-sensitive PEG lipids containing orthoester linkers: New potential tools for nonviral gene delivery. *J. Control. Release* **2004**, *99*, 423–434.

(176) Li, W.; Huang, Z.; MacKay, J. A.; Grube, S.; Szoka, F. C. Low-pH-sensitive poly(ethylene glycol) (PEG)-stabilized plasmid nanolipoparticles: Effects of PEG chain length, lipid composition and assembly conditions on gene delivery. *The journal of gene medicine* **2005**, *7*, 67–79.

(177) Guo, X.; Szoka, F. C. Steric stabilization of fusogenic liposomes by a low-pH sensitive PEG--diortho ester--lipid conjugate. *Bioconjug. Chem.* **2001**, *12*, 291–300.

(178) Chen, D.; Liu, W.; Shen, Y.; Mu, H.; Zhang, Y.; Liang, R.; Wang, A.; Sun, K.; Fu, F. Effects of a novel pH-sensitive liposome with cleavable esterase-catalyzed and pH-responsive double smart mPEG lipid derivative on ABC phenomenon. *Int. J. Nanomed.* **2011**, *6*, 2053–2061.

(179) Chen, D.; Jiang, X.; Huang, Y.; Zhang, C.; Ping, Q. pH-Sensitive mPEG-Hz-Cholesterol Conjugates as a Liposome Delivery System. *Journal of Bioactive and Compatible Polymers* **2010**, *25*, 527–542.

(180) Zhang, L.; Wang, Y.; Yang, Y.; Liu, Y.; Ruan, S.; Zhang, Q.; Tai, X.; Chen, J.; Xia, T.; Qiu, Y. *et al.* High Tumor Penetration of Paclitaxel Loaded pH Sensitive Cleavable Liposomes by Depletion of Tumor Collagen I in Breast Cancer. *ACS applied materials & interfaces* **2015**, *7*, 9691–9701.

(181) Shin, J. Acid-triggered release via dePEGylation of DOPE liposomes containing acid-labile vinyl ether PEG–lipids. *J. Control. Release* **2003**, *91*, 187–200.

(182) Shin, J.; Shum, P.; Grey, J.; Fujiwara, S.-i.; Malhotra, G. S.; González-Bonet, A.; Hyun, S.-H.; Moase, E.; Allen, T. M.; Thompson, D. H. Acid-labile mPEG-vinyl ether-1,2-dioleylglycerol lipids with tunable pH sensitivity: Synthesis and structural effects on hydrolysis rates, DOPE liposome release performance, and pharmacokinetics. *Mol. Pharm.* **2012**, *9*, 3266–3276.

(183) Worm, M.; Leibig, D.; Dingels, C.; Frey, H. Cleavable Polyethylene Glycol: 3,4-Epoxy-1-butene as a Comonomer to Establish Degradability at Physiologically Relevant pH. *ACS Macro Lett.* **2016**, *5*, 1357–1363.

(184) Abu Lila, A. S.; Kiwada, H.; Ishida, T. The accelerated blood clearance (ABC) phenomenon: Clinical challenge and approaches to manage. *J. Control. Release* **2013**, *172*, 38–47.

(185) Dams, E. T.; Laverman, P.; Oyen, W. J.; Storm, G.; Scherphof, G. L.; van der Meer, J. W.; Corstens, F. H.; Boerman, O. C. Accelerated blood clearance and altered biodistribution of repeated injections of sterically stabilized liposomes. *The Journal of pharmacology and experimental therapeutics* **2000**, *292*, 1071–1079.

(186) Laverman, P.; Carstens, M. G.; Boerman, O. C.; Dams, E. T.; Oyen, W. J.; van Rooijen, N.; Corstens, F. H.; Storm, G. Factors affecting the accelerated blood clearance of polyethylene glycol-liposomes upon repeated injection. *The Journal of pharmacology and experimental therapeutics* **2001**, *298*, 607–612.

(187) Deshpande, P. P.; Biswas, S.; Torchilin, V. P. Current trends in the use of liposomes for tumor targeting. *Nanomedicine (London, England)* **2013**, *8*, 1509–1528.

(188) Andreev, O. A.; Engelman, D. M.; Reshetnyak, Y. K. Targeting diseased tissues by pHLIP insertion at low cell surface pH. *Frontiers in physiology* **2014**, *5*, 97.

(189) Farhood, H.; Serbina, N.; Huang, L. The role of dioleoyl phosphatidylethanolamine in cationic liposome mediated gene transfer. *BBA-Biomembranes* **1995**, *1235*, 289–295.

(190) Landon, C. D.; Park, J.-Y.; Needham, D.; Dewhirst, M. W. Nanoscale Drug Delivery and Hyperthermia: The Materials Design and Preclinical and Clinical Testing of Low Temperature-Sensitive Liposomes Used in Combination with Mild Hyperthermia in the Treatment of Local Cancer. *The open nanomedicine journal* **2011**, *3*, 38–64.

(191) Paul, S.; Nahire, R.; Mallik, S.; Sarkar, K. Encapsulated microbubbles and echogenic liposomes for contrast ultrasound imaging and targeted drug delivery. *Computational mechanics* **2014**, *53*, 413–435.

(192) Reimhult, E. Nanoparticle-triggered release from lipid membrane vesicles. *New biotechnology* **2015**, *32*, 665–672.

(193) Kirpotin, D.; Park, J. W.; Hong, K.; Zalipsky, S.; Li, W. L.; Carter, P.; Benz, C. C.; Papahadjopoulos, D. Sterically stabilized anti-HER2 immunoliposomes: Design and targeting to human breast cancer cells in vitro. *Biochemistry* **1997**, *36*, 66–75.

(194) Sofou, S.; Sgouros, G. Antibody-targeted liposomes in cancer therapy and imaging. *Expert opinion on drug delivery* **2008**, *5*, 189–204.

(195) Sapra, P.; Allen, T. M. Ligand-targeted liposomal anticancer drugs. *Progress in lipid research* **2003**, *42*, 439–462.

(196) Lopes de Menezes, D. E.; Kirchmeier, M. J.; Gagne, J.-F.; Pilarski, L. M.; Allen, T. M. Cellular Trafficking and Cytotoxicity of Anti-Cd19-Targeted Liposomal Doxorubicin in B Lymphoma Cells. *Journal of liposome research* **1999**, *9*, 199–228.

(197) Blume, G.; Cevc, G.; Crommelin, M.D.J.A.; Bakker-Woudenberg, I.A.J.M.; Kluft, C.; Storm, G. Specific targeting with poly(ethylene glycol)-modified liposomes: Coupling of homing devices to the ends of the polymeric chains combines effective target binding with long circulation times. *BBA-Biomembranes* **1993**, *1149*, 180–184.

(198) Gabizon, A.; Tzemach, D.; Gorin, J.; Mak, L.; Amitay, Y.; Shmeeda, H.; Zalipsky, S. Improved therapeutic activity of folate-targeted liposomal doxorubicin in folate

receptor-expressing tumor models. *Cancer chemotherapy and pharmacology* **2010**, *66*, 43–52.

(199) Yamada, A.; Taniguchi, Y.; Kawano, K.; Honda, T.; Hattori, Y.; Maitani, Y. Design of folate-linked liposomal doxorubicin to its antitumor effect in mice. *Clinical cancer research : an official journal of the American Association for Cancer Research* **2008**, *14*, 8161–8168.

(200) Baek, S. E.; Lee, K. H.; Park, Y. S.; Oh, D.-K.; Oh, S.; Kim, K.-S.; Kim, D.-E. RNA aptamer-conjugated liposome as an efficient anticancer drug delivery vehicle targeting cancer cells in vivo. *J. Control. Release* **2014**, *196*, 234–242.

(201) Shao, J.; Ma, J. K. H. Characterization of a mannosylphospholipid liposome system for drug targeting to alveolar macrophages. *Drug delivery* **1997**, *4*, 43–48.

(202) Gupta, B.; Levchenko, T. S.; Torchilin, V. P. TAT Peptide-Modified Liposomes Provide Enhanced Gene Delivery to Intracranial Human Brain Tumor Xenografts in Nude Mice. *oncol res* **2006**, *16*, 351–359.

(203) Pappalardo, J. S.; Quattrocchi, V.; Langellotti, C.; Di Giacomo, S.; Gnazzo, V.; Olivera, V.; Calamante, G.; Zamorano, P. I.; Levchenko, T. S.; Torchilin, V. P. Improved transfection of spleen-derived antigen-presenting cells in culture using TATp-liposomes. *J. Control. Release* **2009**, *134*, 41–46.

(204) Fritz, T.; Hirsch, M.; Richter, F. C.; Müller, S. S.; Hofmann, A. M.; Rusitzka, Kristiane A K; Markl, J.; Massing, U.; Frey, H.; Helm, M. Click modification of multifunctional liposomes bearing hyperbranched polyether chains. *Biomacromolecules* **2014**, *15*, 2440–2448.

(205) Reibel, A. T.; Müller, S. S.; Pektor, S.; Bausbacher, N.; Miederer, M.; Frey, H.; Rösch, F. Fate of linear and branched polyether-lipids in vivo in comparison to their liposomal formulations by (18)f-radiolabeling and positron emission tomography. *Biomacromolecules* **2015**, *16*, 842–851.

(206) Mohr, K.; Müller, S. S.; Müller, L. K.; Rusitzka, K.; Gietzen, S.; Frey, H.; Schmidt, M. Evaluation of multifunctional liposomes in human blood serum by light scattering. *Langmuir* **2014**, *30*, 14954–14962.

(207) Wagener, K.; Worm, M.; Pektor, S.; Schinnerer, M.; Thiermann, R.; Miederer, M.; Frey, H.; Rösch, F. Comparison of Linear and Hyperbranched Polyether Lipids for Liposome Shielding by 18F-Radiolabeling and Positron Emission Tomography. *Biomacromolecules* **2018,** DOI: 10.1021/acs.biomac.8b00115.

(208) Apte, A.; Koren, E.; Koshkaryev, A.; Torchilin, V. P. Doxorubicin in TAT peptide-modified multifunctional immunoliposomes demonstrates increased activity against both drug-sensitive and drug-resistant ovarian cancer models. *Cancer biology & therapy* **2014**, *15*, 69–80.

(209) Rao, J. P.; Geckeler, K. E. Polymer nanoparticles: Preparation techniques and size-control parameters. *Prog. Polym. Sci.* **2011**, *36*, 887–913.

(210) Crucho, C. I. C.; Barros, M. T. Polymeric nanoparticles: A study on the preparation variables and characterization methods. *Materials science & engineering. C, Materials for biological applications* **2017**, *80*, 771–784.

(211) Banik, B. L.; Fattahi, P.; Brown, J. L. Polymeric nanoparticles: The future of nanomedicine. *Wiley interdisciplinary reviews. Nanomedicine and nanobiotechnology* **2016**, *8*, 271–299.

(212) Brayner, R. *Nanomaterials: A danger or a promise? ; a chemical and biological perspective*; Springer: London, 2013.

(213) Lockman, P. R.; Mumper, R. J.; Khan, M. A.; Allen, D. D. Nanoparticle technology for drug delivery across the blood-brain barrier. *Drug development and industrial pharmacy* **2002**, *28*, 1–13.

(214) Landfester, K. Miniemulsion polymerization and the structure of polymer and hybrid nanoparticles. *Angew. Chem. Int. Edit.* **2009**, *48*, 4488–4507.

(215) Gurny, R.; Peppas, N. A.; Harrington, D. D.; Banker, G. S. Development of Biodegradable and Injectable Latices for Controlled Release of Potent Drugs. *Drug development and industrial pharmacy* **1981**, *7*, 1–25.

(216) Musyanovych, A.; Schmitz-Wienke, J.; Mailänder, V.; Walther, P.; Landfester, K. Preparation of biodegradable polymer nanoparticles by miniemulsion technique and their cell interactions. *Macromol. Biosci.* **2008**, *8*, 127–139.

(217) Vauthier, C.; Bouchemal, K. Methods for the preparation and manufacture of polymeric nanoparticles. *Pharmaceutical research* **2009**, *26*, 1025–1058.

(218) Landfester, K.; Montenegro, R.; Scherf, U.; Güntner, R.; Asawapirom, U.; Patil, S.; Neher, D.; Kietzke, T. Semiconducting Polymer Nanospheres in Aqueous Dispersion Prepared by a Miniemulsion Process. *Adv. Mater.* **2002**, *14*, 651–655.

(219) Zhao, X.; Meng, Q.; Liu, J.; Li, Q. Hydrophobic dye/polymer composite colorants synthesized by miniemulsion solvent evaporation technique. *Dyes and Pigments* **2014**, *100*, 41–49.

(220) Alexandrino, E. M.; Ritz, S.; Marsico, F.; Baier, G.; Mailänder, V.; Landfester, K.; Wurm, F. R. Paclitaxel-loaded polyphosphate nanoparticles: a potential strategy for bone cancer treatment. *J. Mater. Chem. B* **2014**, *2*, 1298.

(221) Lin, P.-C.; Lin, S.; Wang, P. C.; Sridhar, R. Techniques for physicochemical characterization of nanomaterials. *Biotechnology advances* **2014**, *32*, 711–726.

(222) Muller, J.; Bauer, K. N.; Prozeller, D.; Simon, J.; Mailander, V.; Wurm, F. R.; Morsbach, S.; Landfester, K. Coating nanoparticles with tunable surfactants facilitates control over the protein corona. *Biomaterials* **2017**, *115*, 1–8.

(223) Carrio, A.; Schwach, G.; Coudane, J.; Vert, M. Preparation and degradation of surfactant-free PLAGA microspheres. *J. Control. Release* **1995**, *37*, 113–121.

(224) Yang, C. Y.; Tsay, S. Y.; Tsiang, R. C. Encapsulating aspirin into a surfactant-free ethyl cellulose microsphere using non-toxic solvents by emulsion solvent-evaporation technique. *Journal of microencapsulation* **2001**, *18*, 223–236.

(225) Schottler, S.; Landfester, K.; Mailander, V. Controlling the Stealth Effect of Nanocarriers through Understanding the Protein Corona. *Angewandte Chemie (International ed. in English)* **2016**, *55*, 8806–8815.

2. Functional Polyether-based Lipids for Drug Delivery Systems

2.1 Synthesis of Amphiphilic Polyethers Using Hydrophobic Initiators with Variable Alkyl Chain Length to Improve the Stability of Sterically Stabilized Liposomes

Ann-Kathrin Danner,[a,b] Ulrike Kemmer-Jonas [a] and Holger Frey [a,*]

[a]Institute of Organic Chemistry, Johannes Gutenberg-University Mainz, Duesbergweg 10-14, 55128 Mainz, Germany.

[b]Graduate School Materials Science in Mainz, Staudinger Weg 9, 55128 Mainz, Germany.

E-Mail: hfrey@uni-mainz.de

Unpublished results.

Abstract

The stability of sterically stabilized liposomes is crucial for their successful application as drug delivery system. In this work amphiphilic polyethers with different architectures which are suitable for liposomal incorporation are synthesized. Therefore, dialkyl-based glycerol with varied alkyl chain lengths serves as hydrophobic membrane anchor and is applied as initiator for the anionic ring-opening polymerization (AROP) of ethylene oxide (EO) and ethoxyethyl glycidyl ether (EEGE) respectively. The AROP leads to copolymers with defined molecular weights (1160–6200 g mol^{-1}) and narrow size distributions (1.05–1.30). Linear polyglycerol (*lin*PG) is obtained from PEEGE *via* acidic treatment and used as macroinitiator for hypergrafting of glycidol leading to hyperbranched polyglycerol (*hb*PG). The synthesized linear and hyperbranched polyether lipids are characterized using NMR spectroscopy, matrix-assisted laser desorption/ionization time-of-flight mass spectrometry (MALDI-ToF MS) as well as size exclusion chromatography (SEC) and differential scanning calorimetry (DSC). Furthermore, the polyether-lipids are functionalized by attaching alkyne moieties to enable click-chemistry *via* azide-alkyne cycloaddition. Due to the long alkyl chains of the initiator these amphiphilic polyethers are promising candidates for liposomes with increased stability.

Table of Contents Graphics

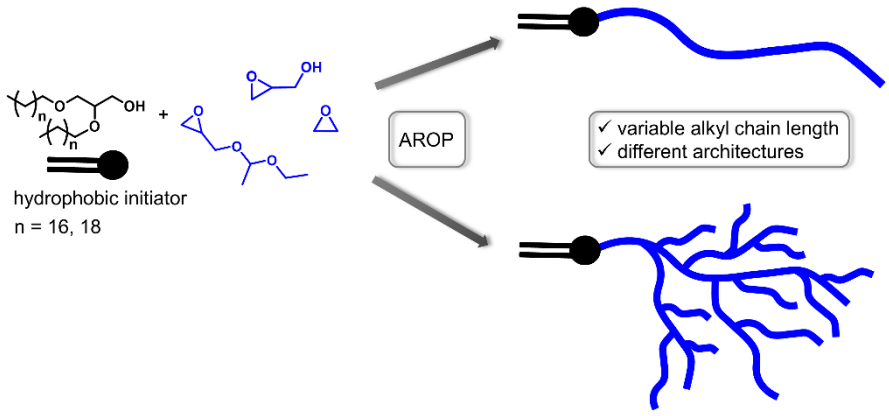

Introduction

In the last decades liposomes received high attention due to their great potential as pharmaceutical carriers.[1] Liposomes consist of phospholipids arranged in a spherical bilayer structure exhibiting an aqueous core. Due to their structure, hydrophilic as well as hydrophobic molecules can be incorporated, rendering them suitable for versatile applications.[2] Conventional liposomes interact with plasma proteins upon administration, leading to a fast elimination from the blood stream and thus a short half-life.[3] In order to improve their pharmacokinetic properties surface modification is a common strategy to avoid a rapid clearance. Therefore, polyethylene glycol (PEG) is often attached to the liposomal surface, also known as PEGylation to obtain long-circulating liposomes or rather so-called stealth liposomes. Such surface modifications lead to an improved circulation time and safety profile.[4,5] In addition, these carriers passively accumulate in tumor tissue due to pathophysiological transformations of the tissue. This phenomena is known as enhanced permeability and retention (EPR) effect.[6,7] Nowadays, numerous PEGylated liposomes are FDA-approved and play an important role in biomedical applications.[8] The attachment of functional moieties leading to active targeting, *i.e.* directed drug delivery can further improve the efficacy of liposomes.[9] Numerous target functions have already been successfully attached, *e.g.* aptamers,[10] antibodies[11,12] and folates.[13,14] Unfortunately, PEG possesses only two terminal hydroxyl groups which are available for functionalization, limiting the attachment of multiple functional moieties.[15] Hence, hyperbranched polyglycerol (*hb*PG) is a promising alternative due to the multitude of hydroxyl groups available for post-polymerization modifications. Furthermore, *hb*PG is highly water-soluble and exhibits good biocompatibility.[16] Recently, Hofmann *et al.* prepared amphiphilic *hb*PGs with molecular weights of 3000–5000 g mol^{-1} using different hydrophobic initiators (cholesterol, 1,2-bis-*n*-tetradecyl glyceryl ether (BisTD), 1,2-bis-*n*-hexadecyl glyceryl ether (BisHD) and 1,2-bis-*n*-octadecyl glyceryl ether (BisOD)). Hypergrafting of glycidol was carried out by applying isopropylidene glyceryl glycidyl ether (IGG) as macroinitiator.[17] These different structures were investigated regarding their effect on liposomal properties, *e.g.* aggregation behavior in blood serum[18] or surface modification after liposome formation.[19] In addition, Fritz *et al.* investigated the stability of lipid anchorage of different hyperbranched polyether-based lipids. A comparison of cholesterol and BisHD as hydrophobic membrane anchor for these lipids was carried out.

The results showed that the anchorage in the lipid bilayer is less stable for cholesterol-based amphiphiles compared to dialkyl-based amphiphiles.[20] These findings were also confirmed *via* non-invasive small animal positron emission tomography (PET) imaging carried out for ^{18}F-radiolabeled polyether-lipids to study the biodistribution *in vivo*. The investigations revealed a higher steric stabilization of liposomes carrying BisHD-*hb*PG[21] compared to liposomes with cholesterol-based *hb*PG.[22] Thus, a prolonged blood circulation time for BisHD-*hb*PG is obtained. In general, the stability of lipid anchorage is important to guarantee a good stability of the liposome and an effective active targeting. Therefore, investigating the influence of different alkyl chain lengths of the hydrophobic dialkyl-based anchor on the stability of lipid anchorage is of great interest. For this purpose, PEG and *hb*PG-lipids with 1,2-bis-*n*-octadecyl glyceryl ether (BisOD) and 1,2-bis-*n*-icosanyl glyceryl ether (BisID) respectively as hydrophobic membrane anchor are synthesized (**Scheme 1**) and the molecular weights are varied in the same range as previous studies to enable a valuable comparison.

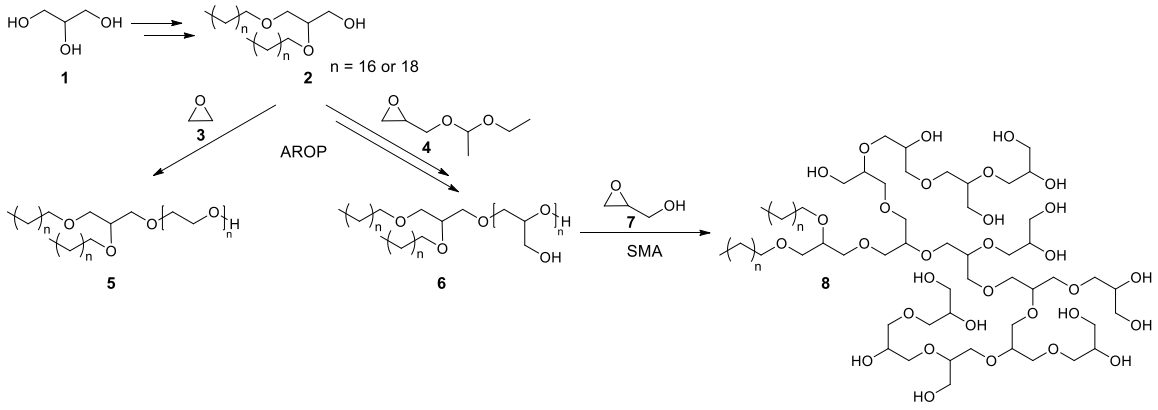

Scheme 1. Synthetic strategy to synthesize amphiphilic polyethylene glycol (PEG) (**5**) and amphiphilic hyperbranched polyglycerol (*hb*PG) (**8**). Dialkyl-based glyceryl ether with different alkyl chain lengths (octadecane or rather icosane) (**2**) is applied as initiator for the anionic ring-opening polymerization (AROP) of ethylene oxide (EO) (left, **3**), leading to amphiphilic PEG (**5**) and ethoxyethyl glycidyl ether (EEGE) (right, **4**), leading to amphiphilic linear polyglycerol (*lin*PG) (**6**). *Lin*PG (**6**) is used as macroinitiator for hypergrafting of glycidol (**7**) *via* the slow monomer addition (SMA) technique to obtain hyperbranched polyglycerol (*hb*PG) (**8**).

Results and Discussion

The anionic ring-opening polymerization (AROP) was applied to synthesize well-defined polymers of ethylene oxide (EO) or ethoxyethyl glycidyl ether (EEGE) with tailored molecular weights. 1,2-bis-*n*-octadecyl glyceryl ether (BisOD) and 1,2-bis-*n*-icosanyl glyceryl ether (BisID) were used as initiator for the polymerization to obtain amphiphilic polyether-based lipids (**Scheme 1**). The initiators were prepared in a straight forward two-step procedure based on the work of Stauch e*t al.*[23] performing a Williamson etherification using 1-*O*-benzyl glycerol and octadecyl bromide or rather iscosane bromide followed by hydrogenation to remove the benzyl protecting group (**Scheme S1**). The combination of a hydrophobic initiator and a hydrophilic polyether results in polymers with amphiphilic behavior, which are suitable for the integration into liposomes to obtain sterically stabilized nanocarriers. The polymerization of EEGE leads to linear structures (PEEGE) with acetal-protected hydroxyl groups, which can be released upon acidic treatment. The resulting linear polyglycerol (*lin*PG) exhibits numerous hydroxyl groups and can be used as macroinitiator to prepare hyperbranched polyglycerol (*hb*PG). Hofmann *et al*. prepared block copolymers of PEG and *hb*PG in which polyisopropylidene glyceryl glycidyl ether (PIGG) was applied as macroinitiator to synthesize *hb*PG.[17] Herein, we use *lin*PG as an alternative macroinitiator resulting likewise in *hb*PG. The *hb*PG-lipids as well as the PEG-based lipids can be further functionalized with alkyne-moieties enabling the attachment of functional moieties, *e.g.* a dye, *via* azide-alkyne cycloaddition.

A. Synthesis of amphiphilic polyethers

For the polymerization of EO, the AROP was carried out in dry tetrahydrofuran (THF) and potassium naphthalenide was used as base to deprotonate the initiator. The deprotonation process was followed by color change of the initiator solution. The polymerization was carried out at 60 °C for 24 h to obtain full conversion. Tailored molecular weights between 3000 and 7000 g mol^{-1} were envisaged *via* the amount of employed initiator. The specified molecular weight range was targeted to enable a comparison of the resulting polyether lipids with the results from previous studies.[20–22] To polymerize EEGE the AROP was performed solvent-free in bulk under slightly reduced pressure and at elevated temperatures (100 °C) for 7 days. High temperatures were necessary to enable a polymerization clearly above the melting point of the initiator and to increase the overall reactivity. In addition,

cesium hydroxide was used as base for deprotonation to ensure a good reactivity for the polymerization due to the formation of a dissociated ion pair.[24,25] Acidic treatment with diluted HCl (1.0 mol L^{-1}) led to the removal of the acetal-protecting groups. The free hydroxyl groups were deprotonated using cesium hydroxide and glycidol was added *via* the slow monomer addition (SMA) approach over a time period of 16 h to obtain well-defined hyperbranched polyglycerol (*hb*PG). SMA was carried out in *N*-methyl-2-pyrrolidone (NMP) to guarantee a good solubility of the macroinitiator and the resulting *hb*PG.

The successful polymerization of all polymers was confirmed using ^{1}H NMR spectroscopy. The spectra display the typical resonances for the polyether backbone as well as the signals for the incorporated hydrophobic initiator. In addition, the removal of the acetal protecting groups of PEEGE was verified *via* the disappearance of the characteristic acetal signal. Furthermore, ^{1}H NMR spectroscopy was applied to determine the average molecular weights of the synthesized polyether-based lipids *via* end group analysis (see **Table 1**). The polymers exhibit molecular weights in a range of 3190–6200 g mol^{-1} (1660–2890 g mol^{-1} for BisOD-*lin*PG macroinitiator). In case of the prepared BisOD-PEGs and BisOD-*lin*PGs, the molecular weights were in close proximity to the aspired values. Due to difficulties regarding the solubility and steric hindrance of BisID during the polymerization and therefore less reactivity of the active chain end, the resulting molecular weights were lower compared to the targeted molecular weights. Furthermore, due to not well-resolved signals in the NMR spectrum of BisID-*lin*PG the formation of aggregates is assumed. Hence, a determination of the molecular weight *via* ^{1}H NMR spectroscopy was not possible for BisID-*lin*PG.

In addition, matrix-assisted laser desorption/ionization time-of-flight mass spectrometry (MALDI-ToF MS) verified the successful polymerization using the hydrophobic initiators BisOD and BisID (**Figure S12**, **Figure S19**, **Figure S32** and **Figure S39**). Mass discrimination effects are observable especially for the synthesized *lin*PGs because the molecular weights are underestimated compared to the calculated molecular weights *via* ^{1}H NMR spectroscopy.

Table 1. Properties of the synthesized BisOD-PEG, BisOD-*lin*PG, BisOD-*hb*PG, BisID-PEG and BisID-*lin*PG.

#	**Composition**[a]	M_n^{th}	M_n^{NMR}	$M_w/M_n^{SEC,\ b}$	T_g^c	T_m^c
		g mol^{-1}	g mol^{-1}		°C	°C
1	BisOD-PEG$_{63}$	3500	3400	1.07	-	52
2	BisOD-PEG$_{81}$	5180	4180	1.10	-	54
3	BisOD-PEG$_{88}$	5000	4450	1.07	-	55
4	BisOD-PEG$_{127}$	7030	6200	1.07	-	58
5	BisOD-*lin*PG$_{14}$	2080	1660	1.30	–21	57
6	BisOD-*lin*PG$_{19}$	2070	1970	1.26	–21	56
7	BisOD-*lin*PG$_{31}$	2220	2890	1.30	–23	59
8	BisOD-*hb*PG$_{35}$[d]	8500	3190	1.29	n.d.	n.d.
9	BisOD-*hb*PG$_{47}$[e]	5000	4070	1.37	–20	56
10	BisOD-*hb*PG$_{68}$[d]	7500	5640	1.56	n.d.	n.d.
11	BisOD-*hb*PG$_{78}$[e]	7500	6370	1.46	–20	39
12	BisOD-*hb*PG$_{81}$[e]	7500	6590	1.24	–20	42
13	BisID-PEG$_{62}$	3520	3380	1.17	-	51
14	BisID-PEG$_{72}$	7040	3820	1.15	-	55
15	BisID-PEG$_{84}$	5060	4350	1.17	-	55
16	BisID-PEG$_{120}$	7040	5930	1.20	-	56
17	BisID-*lin*PG$_6$	2500	1130[f]	1.22	–42[g]	66
18	BisID-*lin*PG$_{11}$	2500	1500[f]	1.05	–21	71

[a]determined using ^{1}H NMR spectroscopy.
[b]obtained from SEC measurements in DMF using PEG standards.
[c]determined using DSC measurements.
[d]BisOD-*lin*PG$_{19}$ applied as macroinitiator.
[e]BisOD-*lin*PG$_{31}$ applied as macroinitiator.
[f]value obtained from SEC measurements. Determination *via* ^{1}H NMR measurement was not possible due to the formation of aggregates/micelles.
[g]solvents could not be removed completely. Additional minor ascending slopes (T_g at 1 °C and 17 °C) were detected. Remeasuring was not possible due to a lack of sample.
n.d. Thermal properties were not determined for #8 and #10. The entire samples were used for liposome preparation.

The amphiphilic polyethers were further characterized using size exclusion chromatography (SEC) indicating monomodal and narrow size distributions in a range of 1.07–1.20 for BisOD-PEG and BisID-PEG, 1.22–1.30 for *lin*PGs and moderate size distributions of 1.24–1.56 for *hb*PGs. SEC measurements were performed in DMF using PEG standards. Moreover, the SEC elugrams reveal shifts to lower elution volume for higher molecular weights as displayed in **Figure 1**, **Figure S40** and **Figure S42**. The determined molecular weights for BisOD-PEGs and BisOD-*lin*PGs are in good agreement with the molecular weight calculated *via* ^{1}H NMR spectroscopy. The molecular weights obtained *via* SEC for the synthesized *hb*PGs differ from the ones calculated by ^{1}H NMR spectroscopy due to the globular structure of *hb*PG and thus differences in the hydrodynamic volume of the prepared *hb*PG and the PEG standards used for calibration. Furthermore, some of the different *hb*PGs exhibit a similar elution volume because the hydrodynamic volume increases only marginal with higher molecular weights. In addition, for BisID-PEGs the SEC measurements reveal lower molecular weights as calculated *via* ^{1}H NMR spectroscopy due to an increased amphiphilic character of the polymer (compared to BisOD-PEG), which also influences the hydrodynamic volume and leads to an underestimation of the molecular weight.

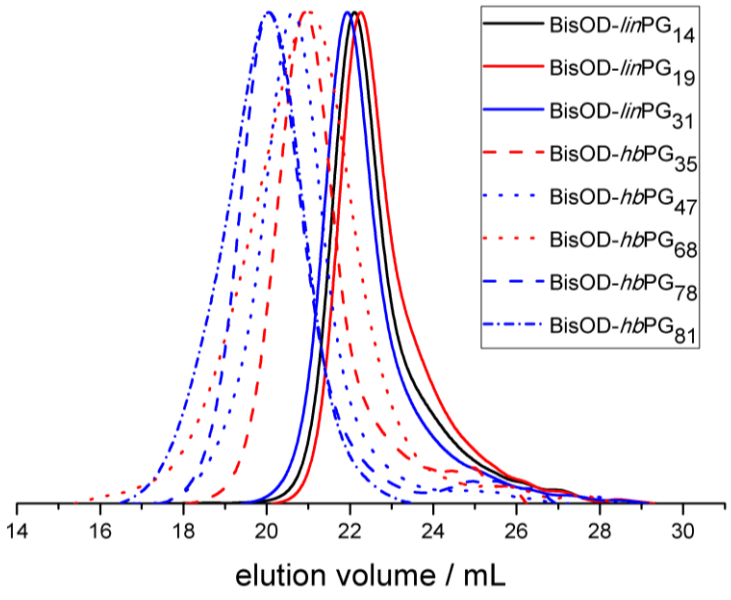

Figure 1. SEC traces (DMF, PEG standard, RI signal) of the synthesized BisOD-*lin*PGs and BisOD-*hb*PGs. The colors indicate the respective macroinitiator applied for the synthesis of BisOD-*hb*PG.

By applying differential scanning calorimetry (DSC) the thermal properties of the amphiphilic polyethers were investigated. BisOD-PEGs and BisID-PEGs exhibit no glass transition temperature T_g but possess a melting temperature T_m in the range of 51–58 °C (**Table 1**). In general, the T_m of PEG differs depending on the molecular weight.[26] The commercially available PEG-4400 exhibited a T_g of –57 °C and a T_m of 59 °C.[27] Consequently, the determined T_ms are in close proximity to the value of PEG-4400. A T_g was not detectable due to the predominant melting endotherm. BisOD-*lin*PG possesses a T_g in the range of –23 °C to –21 °C and a T_m between 56 °C and 59 °C. The measured value for the T_g is close to the value reported in literature (T_g of –27 °C for *lin*PG_{53}).[28] As expected, the T_g is increased in comparison to the T_g of PEG due to the formation of numerous hydrogen bonds. Surprisingly, a T_m is detected although *lin*PG is highly amorphous and already a copolymer of P($EG_{0.77}$-*co*-$G_{0.23}$) leads to an amorphous material where no T_m is observed (T_g –53 °C, no T_m).[29] However, the measured T_m is in close proximity to the melting point (mp) of the applied initiator BisOD (mp: 65.6–66.6 °C). Therefore, the T_m can be attributed to the initiator assuming a clustering of the initiator segments due to the differences in hydrophilicity and thus segregation of the initiator and polyether segments. A similar result is obtained for BisID-*lin*PGs, possessing a T_g between –42 °C and –21 °C and a melting endotherm in the range of 66–71 °C. The measured T_m can be attributed to the initiator BisID which exhibits a melting point of 70.3–71.6 °C. The synthesized BisOD-*hb*PGs exhibit a T_g of –20 °C and a T_m between 39 °C and 56 °C. As expected, the value of the T_g is in the same range as the T_g of the amphiphilic *lin*PGs. In contrast, the T_m decreases with increasing molecular weight of BisOD-*hb*PG. With higher molecular weights the amorphous *hb*PG structure becomes more dominant, leading to decreased T_ms.

B. Functionalization with propargyl bromide

The polyether-based lipids were functionalized with propargyl bromide to attach alkyne-moieties. An alkyne-group enables a copper(I)-catalyzed azide alkyne cycloaddition (CuAAC) with functional groups, *e.g.* dyes or other azide-bearing molecules. This reaction is known from literature and was adapted for the synthesized amphiphilic polyethers.[22] Therefore, the terminal hydroxyl group of PEG or hydroxyl groups of *hb*PG were deprotonated using sodium hydride (NaH). In case of the functionalization of *hb*PG, the degree of functionalization was controlled *via* the amount of applied propragyl bromide.

The successful functionalization was proven *via* ^{1}H NMR spectroscopy due to the appearance of the characteristic resonances for the propargyl group (methylene protons at 3.95 ppm and alkyne proton at 2.13 ppm) as shown in **Figure 2**. Comparing the signal intensity of the initiator (0.94–0.90 ppm) and the alkyne proton (2.13 ppm), complete functionalization (in case of PEG-lipids) or rather the degree of functionalization (in case of *hb*PG-lipids) was calculated. End group analysis was also applied to calculate the molecular weight of the functionalized polymers. Due to the amphiphilic character of the polymers, the determined molecular weight *via* ^{1}H NMR spectroscopy differs from the theoretical values.

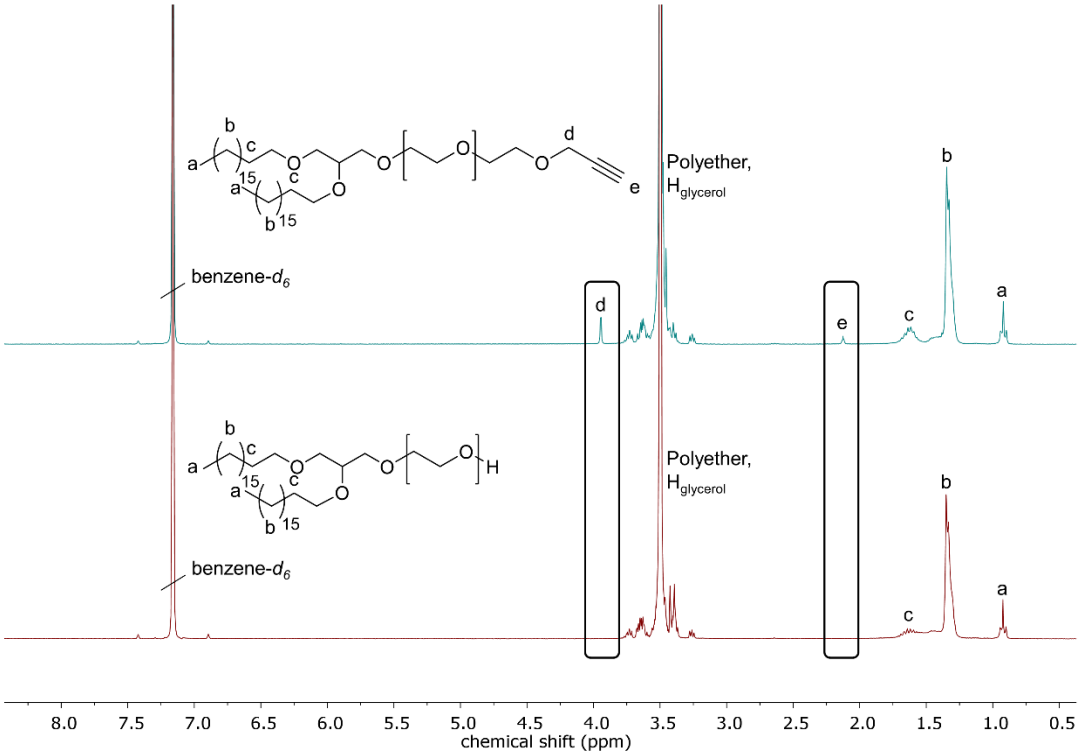

Figure 2. ^{1}H NMR spectra (benzene-d_6, 300 MHz) of BisOD-PEG$_{81}$ (bottom, red) and BisOD-PEG$_{81}$-alkyne (top, green). The appearing signals for the propargyl group (signal d and signal e) are emphasized in black boxes.

In **Table 2** the characteristics of the functionalized BisOD-PEG-alkyne, BisOD-*hb*PG-alkyne and BisID-PEG-alkyne are summarized and an overview of the amount of attached alkyne moieties is given.

SEC measurements reveal monomodal and narrow (PEG-alkyne) or rather moderate (*hb*PG-alkyne) size distributions for all functionalized polymers as displayed in **Figure 3** as well as **Figure S41** and **Figure S43**. Moreover, the successful attachment of alkyne-

moieties to BisOD-*hb*PG is proven due to the shift of the SEC traces to lower elution volume translating to higher molecular weights (**Figure 3**).

Table 2. Summary of the functionalized BisOD-PEG-alkyne, BisOD-*hb*PG-alkyne and BisID-PEG-alkyne.

#	Composition	M_n^{th} g mol^{-1}	M_n^{NMR} g mol^{-1}	$M_w/M_n^{SEC, a}$	alkyne moieties^{NMR} %[b]
1	BisOD-PEG$_{63}$-alkyne	3440	3680	1.14	100
2	BisOD-PEG$_{81}$-alkyne	4220	4650	1.10	100
3	BisOD-PEG$_{88}$-alkyne	4490	4420	1.09	100
4	BisOD-PEG$_{127}$-alkyne	6240	5910	1.08	100
8	BisOD-*hb*PG$_{35}$-alkyne	3230	2850	1.34	3
9	BisOD-*hb*PG$_{68}$-alkyne	5680	6900	1.33	4
10	BisID-PEG$_{62}$-alkyne	3420	3340	1.36	100
11	BisID-PEG$_{72}$-alkyne	3860	5450	1.13	100
12	BisID-PEG$_{84}$-alkyne	4390	4230	1.16	100
13	BisID-PEG$_{120}$-alkyne	5970	4480	1.20	100

[a]obtained from SEC measurement in DMF using PEG standards.
[b]related to the total amount of free hydroxyl groups.

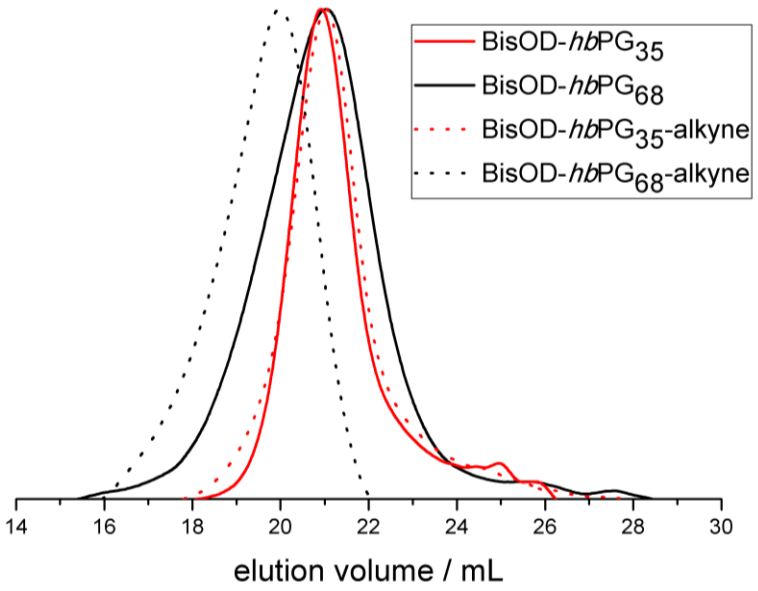

Figure 3. SEC traces (DMF, PEG standard, RI signal) of the synthesized BisOD-*hb*PGs (solid traces) and the functionalized BisOD-*hb*PGs-alkyne (dotted traces).

As mentioned above, these amphiphilic polyethers are suitable for the integration into liposomal nanocarriers to obtain stealth liposomes. The liposomes will be prepared *via* dual centrifugation (DC).[30] Afterwards, the attached alkyne-moieties enable a copper-catalyzed cycloaddition to attach *e.g.* dyes which facilitates further investigations regarding the stability of lipid anchorage especially in *in vitro* and *in vivo* experiments. These investigations are currently on-going and are carried out in cooperation with Matthias Voigt (Group of Prof. Dr. Mark Helm) from the Institute of Pharmacy and Biochemistry.

Conclusion

In this work, the AROP of EO and EEGE respectively by applying hydrophobic initiators with variable alkyl chain lengths to obtain amphiphilic PEG and PEEGE was presented. PEEGE led to *lin*PG after acidic treatment. The obtained *lin*PG served as macroinitiator to synthesize *hb*PG by adding glycidol using the slow monomer addition technique. The prepared polymers exhibit monomodal and narrow size distributions. The successful polymerization was further confirmed by ^{1}H NMR spectroscopy and MADLI-ToF MS. DSC measurements revealed a high crystallinity for both, BisHD-PEG and BisID-PEG and an amorphous structure for *lin*PG and *hb*PG. Alkyne-moieties were introduced *via* post-polymerization modification, enabling further attachment of functional groups, which possess an azide-moiety and undergo a cycloaddition (click chemistry). These amphiphilic structures are tailored for the integration into liposomal structures. Further investigations are conducted to study the stability of lipid anchorage and hence find the optimal polyether-based lipid to prepare stealth liposomes with increased stability profiles.

Acknowledgments

A. Danner is a recipient of a DFG-funded position through the Excellence Initiative by the Graduate School Materials Science in Mainz (GSC 266). The authors thank Maria Müller for DSC, Monika Schmelzer for SEC measurements and Dr. Elena Berger-Nicoletti for

MALDI-ToF MS. In addition, Maria Golowin and Yannick Wohlleben are acknowledged for technical assistance.

References

(1) Torchilin, V. P. Recent advances with liposomes as pharmaceutical carriers. *Nat. Rev. Drug. Discov.* **2005**, *4*, 145–160.

(2) Pattni, B. S.; Chupin, V. V.; Torchilin, V. P. New Developments in Liposomal Drug Delivery. *Chem. Rev.* **2015**, *115*, 10938–10966.

(3) Awasthi, V. D.; Garcia, D.; Goins, B. A.; Phillips, W. T. Circulation and biodistribution profiles of long-circulating PEG-liposomes of various sizes in rabbits. *Int. J. Pharm.* **2003**, *253*, 121–132.

(4) Pasut, G.; Paolino, D.; Celia, C.; Mero, A.; Joseph, A. S.; Wolfram, J.; Cosco, D.; Schiavon, O.; Shen, H.; Fresta, M. Polyethylene glycol (PEG)-dendron phospholipids as innovative constructs for the preparation of super stealth liposomes for anticancer therapy. *J. Control. Release* **2015**, *199*, 106–113.

(5) Woodle, M. C. Surface-modified liposomes: Assessment and characterization for increased stability and prolonged blood circulation. *Chemistry and physics of lipids* **1993**, *64*, 249–262.

(6) Maeda, H.; Bharate, G. Y.; Daruwalla, J. Polymeric drugs for efficient tumor-targeted drug delivery based on EPR-effect. *Eur. J. Pharm. Biopharm.* **2009**, *71*, 409–419.

(7) Maeda, H.; Wu, J.; Sawa, T.; Matsumura, Y.; Hori, K. Tumor vascular permeability and the EPR effect in macromolecular therapeutics: a review. *J. Control. Release* **2000**, *65*, 271–284.

(8) Milla, P.; Dosio, F.; Cattel, L. PEGylation of Proteins and Liposomes: A Powerful and Flexible Strategy to Improve the Drug Delivery. *CDM* **2012**, *13*, 105–119.

(9) Torchilin, V. P. Liposomes as targetable drug carriers. *Critical reviews in therapeutic drug carrier systems* **1985**, *2*, 65–115.

(10) Baek, S. E.; Lee, K. H.; Park, Y. S.; Oh, D.-K.; Oh, S.; Kim, K.-S.; Kim, D.-E. RNA aptamer-conjugated liposome as an efficient anticancer drug delivery vehicle targeting cancer cells in vivo. *J. Control. Release* **2014**, *196*, 234–242.

(11) Sapra, P.; Allen, T. M. Ligand-targeted liposomal anticancer drugs. *Progress in lipid research* **2003**, *42*, 439–462.

(12) Sofou, S.; Sgouros, G. Antibody-targeted liposomes in cancer therapy and imaging. *Expert opinion on drug delivery* **2008**, *5*, 189–204.

(13) Yamada, A.; Taniguchi, Y.; Kawano, K.; Honda, T.; Hattori, Y.; Maitani, Y. Design of folate-linked liposomal doxorubicin to its antitumor effect in mice. *Clinical cancer research : an official journal of the American Association for Cancer Research* **2008**, *14*, 8161–8168.

(14) Gabizon, A.; Tzemach, D.; Gorin, J.; Mak, L.; Amitay, Y.; Shmeeda, H.; Zalipsky, S. Improved therapeutic activity of folate-targeted liposomal doxorubicin in folate receptor-expressing tumor models. *Cancer chemotherapy and pharmacology* **2010**, *66*, 43–52.

(15) Sawant, R. R.; Torchilin, V. P. Challenges in development of targeted liposomal therapeutics. *The AAPS journal* **2012**, *14*, 303–315.

(16) Kainthan, R. K.; Janzen, J.; Levin, E.; Devine, D. V.; Brooks, D. E. Biocompatibility testing of branched and linear polyglycidol. *Biomacromolecules* **2006**, *7*, 703–709.

(17) Hofmann, A. M.; Wurm, F.; Hühn, E.; Nawroth, T.; Langguth, P.; Frey, H. Hyperbranched polyglycerol-based lipids via oxyanionic polymerization: toward multifunctional stealth liposomes. *Biomacromolecules* **2010**, *11*, 568–574.

(18) Mohr, K.; Müller, S. S.; Müller, L. K.; Rusitzka, K.; Gietzen, S.; Frey, H.; Schmidt, M. Evaluation of multifunctional liposomes in human blood serum by light scattering. *Langmuir* **2014**, *30*, 14954–14962.

(19) Fritz, T.; Hirsch, M.; Richter, F. C.; Müller, S. S.; Hofmann, A. M.; Rusitzka, Kristiane A K; Markl, J.; Massing, U.; Frey, H.; Helm, M. Click modification of multifunctional liposomes bearing hyperbranched polyether chains. *Biomacromolecules* **2014**, *15*, 2440–2448.

(20) Fritz, T.; Voigt, M.; Worm, M.; Negwer, I.; Müller, S. S.; Kettenbach, K.; Ross, T. L.; Roesch, F.; Koynov, K.; Frey, H. *et al.* Orthogonal Click Conjugation to the Liposomal Surface Reveals the Stability of the Lipid Anchorage as Crucial for Targeting. *Chem. Eur. J.* **2016**, *22*, 11578–11582.

(21) Wagener, K.; Worm, M.; Pektor, S.; Schinnerer, M.; Thiermann, R.; Miederer, M.; Frey, H.; Rösch, F. Comparison of Linear and Hyperbranched Polyether Lipids for Liposome Shielding by 18F-Radiolabeling and Positron Emission Tomography. *Biomacromolecules* **2018,** DOI: 10.1021/acs.biomac.8b00115.

(22) Reibel, A. T.; Müller, S. S.; Pektor, S.; Bausbacher, N.; Miederer, M.; Frey, H.; Rösch, F. Fate of linear and branched polyether-lipids in vivo in comparison to their liposomal formulations by (18)f-radiolabeling and positron emission tomography. *Biomacromolecules* **2015**, *16*, 842–851.

(23) Stauch, O.; Uhlmann, T.; Fröhlich, M.; Thomann, R.; El-Badry, M.; Kim, Y.-K.; Schubert, R. Mimicking a Cytoskeleton by Coupling Poly(N -isopropylacrylamide) to the Inner Leaflet of Liposomal Membranes: Effects of Photopolymerization on Vesicle Shape and Polymer Architecture. *Biomacromolecules* **2002**, *3*, 324–332.

(24) Brocas, A.-L.; Mantzaridis, C.; Tunc, D.; Carlotti, S. Polyether synthesis: From activated or metal-free anionic ring-opening polymerization of epoxides to functionalization. *Prog. Polym. Sci.* **2013**, *38*, 845–873.

(25) Penczek, S.; Cypryk, M.; Duda, A.; Kubisa, P.; Slomkowski, S. Living ring-opening polymerizations of heterocyclic monomers. *Prog. Polym. Sci.* **2007**, *32*, 247–282.

(26) Mandelkern, L. The Crystallization Of Flexible Polymer Molecules. *Chem. Rev.* **1956**, *56*, 903–958.

(27) Müller, S. S.; Moers, C.; Frey, H. A Challenging Comonomer Pair: Copolymerization of Ethylene Oxide and Glycidyl Methyl Ether to Thermoresponsive Polyethers. *Macromolecules* **2014**, *47*, 5492–5500.

(28) Schömer, M.; Frey, H. Water-Soluble "Poly(propylene oxide)" by Random Copolymerization of Propylene Oxide with a Protected Glycidol Monomer. *Macromolecules* **2012**, *45*, 3039–3046.

(29) Mangold, C.; Wurm, F.; Obermeier, B.; Frey, H. Hetero-Multifunctional Poly(ethylene glycol) Copolymers with Multiple Hydroxyl Groups and a Single Terminal Functionality. *Macromol. Rapid Comm.* **2010**, *31*, 258–264.

(30) Massing, U.; Cicko, S.; Ziroli, V. Dual asymmetric centrifugation (DAC)--a new technique for liposome preparation. *J. Control. Release* **2008**, *125*, 16–24.

Supporting Information

Synthesis of Amphiphilic Polyethers Using Hydrophobic Initiators with Variable Alkyl Chain Length to Improve the Stability of Sterically Stabilized Liposomes

Ann-Kathrin Danner,[a,b] Ulrike Kemmer-Jonas [a] and Holger Frey [a,*]

[a]Institute of Organic Chemistry, Johannes Gutenberg-University Mainz, Duesbergweg 10-14, 55128 Mainz, Germany.

[b]Graduate School Materials Science in Mainz, Staudinger Weg 9, 55128 Mainz, Germany.

E-Mail: hfrey@uni-mainz.de

1. Materials and Methods

1.1 Reagents

Unless mentioned otherwise, all chemicals were obtained from *Sigma Aldrich*, *Acros Organics*, *Fisher Scientific* or *TCI Europe*. Deuterated solvents (pyridine-d_5, benzene-d_6 or chloroform-*d*) were purchased from *Deutero GmbH*. Ethylene oxide (EO) was received from *Sigma Aldrich* and must be handled with high precaution. Ethoxyethyl glycidyl ether (EEGE) was synthesized according to literature[1] and was dried over CaH_2 for at least 30 min and freshly cryo-transferred prior to use. For the anionic ring-opening polymerization (AROP) dry THF was stored over benzophenone/sodium.

1.2 Instrumentation

^{1}H, ^{13}C NMR and 2D spectra were measured on a Bruker Avance III HD 300 (300 MHz, 5 mm, BBFO probe, and B-ACS 60 auto sampler) or rather a Bruker Avance II spectrometer operated at 400 MHz (5 mm BBFO smart probe and SampleXPress 60 auto sampler) at 296 K. Pyridine-d_5, benzene-d_6 or chloroform-*d* was used as solvent. The NMR spectra were referenced internally to the respective signals of the deuterated solvent. Analysis of all spectra was carried out using the software MestReNova version 9.0. SEC measurements were performed in dimethylformamide (DMF) with 0.25 g L^{-1} lithium bromide on an Agilent 1100 Series equipped with PSS HEMA 300/100/40 column, RI and UV detector (275 nm). Monodisperse linear PEG standards from *Polymer Standard Service GmbH* (PSS) were applied for calibration. For all SEC traces the RI signal is displayed. Analysis was performed by applying the software PSS WinGPC Unity. DSC measurements were performed on a Perkin Elmer 8200 differential scanning calorimeter. Calibration was carried out using the melting points of indium (T_m = 156.6 °C) and Milli-Q water (T_m = 0 °C). 4 to 8 mg of each sample were measured in a temperature range of –95 to 100 °C (first cycle, heating rate 20 °C min^{-1}) or rather –90 to 80 °C (second cycle, heating rate 10 °C min^{-1}) for all PEG samples. All *lin*PGs were measured in a temperature range of -90 to 90 °C with a heating rate of 10 °C min^{-1} (first cycle) or rather 20 °C min^{-1} (second cycle). The values for the second cycle were used to determine glass transition temperature T_g and melting temperature T_m. Matrix-assisted laser desorption/ionization time-of-flight mass spectrometry (MALDI-ToF MS) measurements were carried out on a Shimadzu

Axima CFR MALDI-ToF mass spectrometer which is equipped with a nitrogen laser (3 ns laser pulses at 337 nm). For the measurements dithranol was used as matrix.

1.3 Handling of Ethylene Oxide (EO)

The gaseous, flammable and highly toxic ethylene oxide (EO) must be handled carefully and has to be stored in pressure-proof gas bottles. It has to be used only in an adequate fume hood under appropriate safety precautions. Polymerizations in which EO is involved are performed in flame-dried glassware to enable the conversion of EO inside the sealed and evacuated glass apparatus and to guarantee secure handling via cryo-transfer techniques. To avoid abrupt detachment of the septum and hence release of EO the maximum batch-sizes of 8 g EO in a 500 mL flask must not be exceeded.

2. Synthesis

2.1 Synthesis of ethoxyethyl glycidyl ether (EEGE)

EEGE was synthesized as described in literature.[1]

^{1}H NMR, COSY (300 MHz, chloroform-*d*, δ): 4.75–4.68 (qd, *J* = 5.3 Hz; 3.4 Hz, 1H, acetal H), 3.86–3.29 (m, 4H, -CHC*H*$_2$OCOCH$_2$-, -CHCH$_2$OCOC*H*$_2$-) 3.13–3.07 (m, 1H, CH$_2$OC*H*CH$_2$-), 2.77–2.74 (ddd, *J* = 5.1 Hz; 4.1 Hz; 1.0 Hz, 1H, C*H*$_2$OCHCH$_2$-), 2.61–2.55 (ddd, *J* = 10.7 Hz; 5.1 Hz; 2.7 Hz, 1H, C*H*$_2$OCHCH$_2$-), 1.29–1.26 (dd, *J* = 5.4 Hz; 4.7 Hz, 3H, -OCHC*H*$_3$), 1.18–1.13 (td, *J* = 7.1 Hz; 0.9 Hz, 3H, -OCH$_2$C*H*$_3$).

2.2 Synthesis of 1,2-bis-*n*-octadecyl glyceryl ether (BisOD)

The synthesis was carried out according to literature.[2]

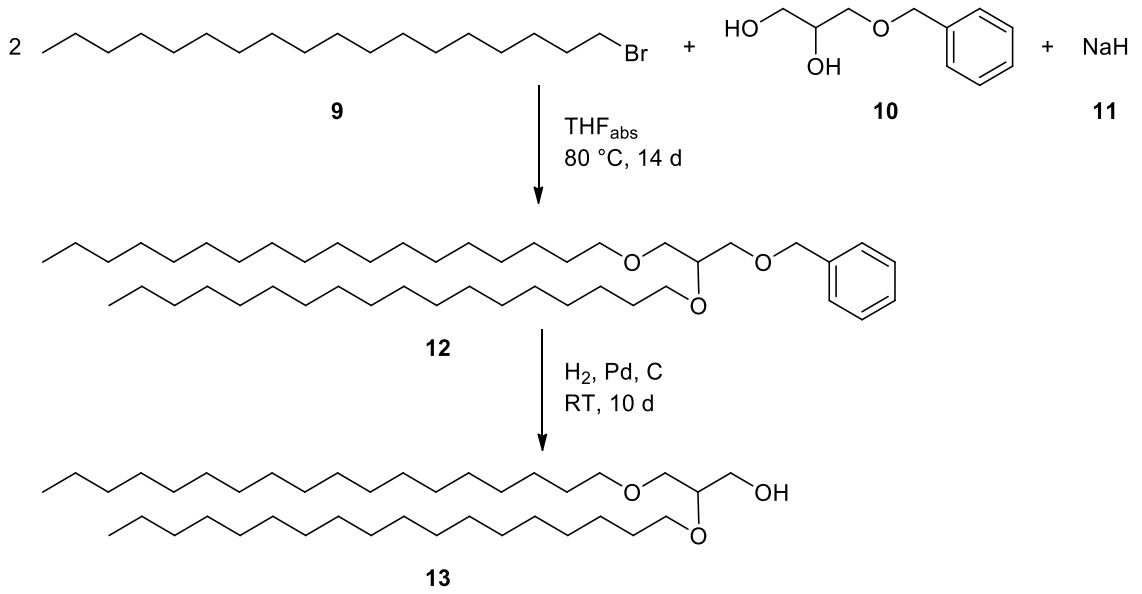

Scheme S1. Synthesis of 1,2-bis-n-octadecyl glyceryl ether (BisOD) (**13**).

mp: 65.6–66.6 °C.

^{1}H NMR, COSY (400 MHz, chloroform-*d*, δ): 3.74–3.41 (m, 9H, glycerol H), 1.59–1.53 (m, 4H, -OCH$_2$C*H$_2$*-), 1.31–1.25 (m, 60H, -OCH$_2$CH$_2$(C*H$_2$*)$_{15}$CH$_3$), 0.88 (t, *J* = 13.1 Hz; 7.2 Hz, 6H; -O(CH$_2$)$_{17}$C*H$_3$*).

^{13}C NMR, HSQC, HMBC (101 MHz, chloroform-*d*, δ): 78.4 (glycerol C), 72.0 (-O*C*H$_2$CH$_2$-), 71.1 (glycerol C), 70.6 (-O*C*H$_2$CH$_2$-), 63.3 (glycerol C), 32.1 (-OCH$_2$CH$_2$(*C*H$_2$)$_{17}$CH$_3$), 30.3 (-OCH$_2$*C*H$_2$-), 29.9-29.5 (-OCH$_2$CH$_2$(*C*H$_2$)$_{17}$CH$_3$), 26.3 (-OCH$_2$CH$_2$(*C*H$_2$)$_{17}$CH$_3$), 22.9 (-OCH$_2$CH$_2$(*C*H$_2$)$_{17}$CH$_3$), 14.3 (-O(CH$_2$)$_{19}$*C*H$_3$).

2.3 Polymer synthesis of BisOD-PEG

The synthesis is described for BisOD-PEG$_{81}$ as a representative example.

1,2-Bis-*n*-octadecyl glyceryl ether (BisOD) (0.2 g, 0.36 mmol, 1 eq.) was placed in a dry Schlenk flask and dissolved in benzene (10 mL). The solution was stirred at 60 °C for 30 min and dried in vacuo for 16 h to remove moisture. Dry tetrahydrofuran (approx. 10 mL) was cryo-transferred to the Schlenk flask to dissolve the initiator. Afterwards, the initiator was deprotonated with a 0.5 M solution of potassium naphthalenide in THF (0.36 mL, 0.18 mmol, 0.5 eq.) while stirring. The solution was cooled down to –80 °C and ethylene oxide (EO) (1.70 mL, 37.57 mmol, 105 eq.) was cryo-transferred using a graduated ampule. The polymerization was carried out at 60 °C for 24 h. In order to quench the polymerization, an excess of ethanol was added. The solvent was removed under

reduced pressure, the crude product was dissolved in methanol and precipitated twice in cold diethyl ether to obtain the pure product. Yield: 99%.

^{1}H NMR, COSY (400 MHz, benzene-d_6, δ): 3.67–3.30 (m, 359H, polyether backbone and glycerol H), 1.66–1.56 (m, 4H, -OCH_2CH_2-), 1.44–1.28 (m, 58H, -$OCH_2CH_2(CH_2)_{15}CH_3$), 0.92–0.89 (m, 6H, -$O(CH_2)_{17}CH_3$).

^{13}C NMR, HSQC, HMBC (101 MHz, benzene-d_6, δ): 79.0 (glycerol C), 73.4 (polyether backbone and glycerol C), 72.4-70.9 (polyether backbone and glycerol C), 62.2 (polyether backbone and glycerol C), 32.6 (-$OCH_2CH_2(CH_2)_{14}CH_2CH_3$), 31.1–30.1 (-$OCH_2CH_2$- and -$OCH_2CH_2(CH_2)_{14}CH_2CH_3$), 27.0 (-$OCH_2CH_2(CH_2)_{14}CH_2CH_3$), 23.4 (-$OCH_2CH_2(CH_2)_{14}CH_2CH_3$), 14.64 (-$O(CH_2)_{17}CH_3$).

2.4 Functionalization of BisOD-PEG with propargyl bromide

The functionalization is described for BisOD-PEG_{81}-alkyne as a representative example.

BisOD-PEG_{81} (0.3 g, 0.074 mmol, 1 eq.) was placed in a dry Schlenk flask and dissolved in dry THF. The solution was cooled to 0 °C and sodium hydride (0.005 g, 0.223 mmol, 3 eq.) was added while stirring. Subsequently, propargyl bromide (0.020 mL, 0.223 mmol, 3 eq.) was added and the solution was stirred for 24 h at room temperature. The reaction mixture was filtered and the solvent was slightly reduced under reduced pressure. The remaining solution was precipitated twice in cold diethyl ether and the pure product was dried in vacuo. Yield: 66%.

^{1}H NMR, COSY (300 MHz, benzene-d_6, δ): 3.95–3.94 (d, J = 2.4 Hz, 2H, -OCH_2CCH), 3.77–3.24 (m, 374H, polyether backbone and glycerol H), 2.13–2.12 (t, J = 2.4 Hz, 1H, -OCH_2CCH), 1.69–1.57 (m, 12H, -OCH_2CH_2-), 1.47–1.30 (m, 60H, -$OCH_2CH_2(CH_2)_{15}CH_3$), 0.94–0.90 (m, 6H, -$O(CH_2)_{17}CH_3$).

2.5 Polymer synthesis of BisOD-*lin*PG

The polymerization is described for BisOD-*lin*PG_{19} as representative example.

1,2-Bis-*n*-octadecyl glyceryl ether (BisOD) (0.25 g, 0.42 mmol, 1 eq.) and cesium hydroxide (0.06 g, 0.38 mmol, 0.9 eq.) were placed in a dry Schlenk flask and dissolved in benzene (10 mL). The solution was stirred at 60 °C for 30 min to enable the formation of the alkoxide and dried for 16 h under vacuum. The alkoxide was heated to 100 °C in vacuo to liquefy the initiator. Subsequently, EEGE (1.28 mL, 8.39 mmol, 20 eq.) was added via syringe and the polymerization was carried out under reduced pressure for 7 days. Methanol (5 mL) was added to quench the polymerization and to dissolve the crude product. Afterwards, 1N HCl (3 mL) was added to remove the acetal protecting groups. The solution was stirred at 40 °C for 10 days and subsequently precipitated in cold diethyl ether to obtain the pure product. Yield: 97%.

^{1}H NMR, COSY (400 MHz, pyridine-d_5, δ): 4.41–3.83 (m, polyether backbone and glycerol H), 1.67–1.62 (m, 4H, -OCH_2CH_2-), 1.44–1.27 (m, 62H, -$OCH_2CH_2(CH_2)_{15}CH_3$), 0.90–0.87 (m, 6H, -$O(CH_2)_{17}CH_3$).

^{13}C NMR, HSQC, HMBC (101 MHz, pyridine-d_5, δ): 81.9–81.7 (polyether backbone and glycerol C), 73.4 (polyether backbone and glycerol C), 72.7–72.4 (polyether backbone and glycerol C), 65.0 (polyether backbone and glycerol C), 62.8–62.7 (polyether backbone and glycerol C), 30.5 (-$OCH_2CH_2(CH_2)_{15}CH_3$).

2.6 Synthesis of BisOD-*hb*PG

Hypergrafting of glycidol is described for the macroinitiator BisOD-*lin*PG_{19} as representative example.

The macroinitiator BisOD-*lin*PG_{19} (0.15 g, 0.076 mmol, 1 eq.) was placed in a Schlenk flask, dissolved in benzene (2 mL) and dried for 16 h in vacuo. Afterwards, BisOD-*lin*PG_{19} was again dissolved in benzene (2 mL) and cesium hydroxide (0.022 g, 0.13 mmol, 1.7 eq. (equates to a degree of deprotonation of 10% of hydroxyl groups)) was added. The solution was stirred at 80 °C for 2 h to allow the formation of the alkoxide. Afterwards, the alkoxide was dried for 16 h under reduced pressure. The macroinitiator was dissolved in *N*-methyl-2-pyrrolidone (NMP) (1 mL) and a solution of glycidol (0.37 mL, 5.7 mmol, 75 eq.) (15%) in NMP was added to the initiator solution over a time period of 16 h (0.1 ml per h) at 100 °C. The solution was stirred for additional 2 h to ensure complete conversion of

glycidol. Subsequently, the solvent was removed under reduced pressure and the crude product was dialyzed for 16 h against methanol (500 MWCO). The solvent was removed under reduced pressure and the product was dried in vacuo. Yield: 47%.

^{1}H NMR, COSY (400 MHz, pyridine-d_5, δ): 6.39–6.22 (m, 64H, hydroxyl groups of *hb*PG), 4.36–3.53 (m, 340H, polyether backbone, glycidol H) 1.69–1.61 (m, 4H, -OCH$_2$C*H$_2$*-(BisOD)), 1.45–1.26 (m, 58H, -OCH$_2$CH$_2$(C*H$_2$*)$_{15}$CH$_3$(BisOD)), 0.90–0.87 (m, 6H, -O(CH$_2$)$_{17}$C*H$_3$*(BisOD)).

2.7 Functionalization of BisOD-*hb*PG with propargyl bromide

The functionalization is described for BisOD-*hb*PG$_{68}$ as representative example.

BisOD-*hb*PG$_{68}$ (0.18 g, 0.032 mmol, 1 eq.) was placed in a Schlenk flask and dissolved in dimethylformamide (DMF) (5 mL). The solution was cooled to 0 °C and sodium hydride (0.005 g, 0.22 mmol, 7 eq.) was added. The solution was stirred for 1 h at 0 °C to ensure complete deprotonation. Subsequently, propargyl bromide (0.064 mL, 0.064 mmol, 2 eq.) and the mixture was allowed to slowly reach room temperature. The solution was stirred at room temperature for 3 days. Afterwards, water (0.5 mL) was added and the solvent was removed under reduced pressure. The crude product was dialyzed against methanol (500 MWCO) for 3 h. The solvent was removed under reduced pressure and the product was dried in vacuo for 2 h. Yield: 83%.

^{1}H NMR, COSY (400 MHz, pyridine-d_5, δ): 6.17–5.16 (m, 134 H, hydroxyl groups of *hb*PG), 4.61 (s, 8H, -OC*H$_2$*CCH) 4.38–3.45 (m, 500H, polyether backbone, glycidol H), 2.70 (s, 0.2H, -OCH$_2$CC*H*), 1.73–1.63 (m, 4H, -OCH$_2$C*H$_2$*- (BisOD)), 1.45–1.26 (m, 88H, -OCH$_2$CH$_2$(C*H$_2$*)$_{15}$CH$_3$ (BisOD)), 0.90–0.87 (m, 6H, -O(CH$_2$)$_{17}$C*H$_3$* (BisOD)).

2.8 Synthesis of 1,2-bis-*n*-icosanyl glyceryl ether (BisID)

The synthesis was carried out as displayed in **Scheme S1**.

Dry tetrahydrofuran (THF) was placed in three-necked round bottom flask equipped with Dimroth condenser and sealed precision glass (KPG) stirrer. Under argon atmosphere and stirring 3-benzyloxy-1,2-propanediol (2.7 mL, 0.017 mol, 1 eq.), sodium hydride (1.62 g, 0.068 mol, 4 eq.) and 1-bromoicosane (24.42 g, 0.068 mol, 4 eq.) was added. The reaction mixture was stirred at 80 °C for 9 days. Additional NaH was added (1.00 g, 0.042 mol, 2.5 eq) and the solution was stirred for another 23 days. The solvent was removed under

reduced pressure to obtain a total volume of 250 mL. Water (250 mL) and diethyl ether (250 mL) was added and the mixture was stirred overnight at room temperature. To neutralize the reaction mixture, sulfuric acid (1 mol·L^{-1}, 15 mL, 0.015 mol) was added and again stirred overnight. The organic phase was extracted three times with diethyl ether (150 mL each) and dried over sodium sulfate. The solvent was removed under reduced pressure and the crude product was purified using flash column chromatography (petroleum ether/diethyl ether 40:1). The intermediate 1,2-bis-*n*-icosanyl-3-benzyl glyceryl ether (4.97 g, 0.007 mol) was obtained as colorless solid. Yield: 41%.

1,2-Bis-*n*-icosanyl-3-benzyl glyceryl ether (4.97 g, 0.007 mol, 1 eq.) was dissolved in dichloromethane. Palladium on activated charcoal was added (5 weight percent). Hydrogen was introduced and the mixture was stirred at room temperature for 20 days. The catalyst was removed via filtration over celite®. Afterwards the solvent was removed under reduced pressure to obtain 1,2-bis-*n*-icosanyl glyceryl ether (1.84 g, 0.003 mol) as colorless solid. Yield: 42%.

mp: 70.3–71.6 °C.

^{1}H NMR, COSY (400 MHz, chloroform-*d*, δ): 3.74–3.41 (m, 9H, glycerol H), 1.60–1.52 (m, 4H, -$OCH_2C\mathit{H_2}$-), 1.34–1.21 (m, 68H, -$OCH_2CH_2(C\mathit{H_2})_{17}CH_3$), 0.89–0.86 (m, 6H, -$O(CH_2)_{19}C\mathit{H_3}$).

^{13}C NMR, HSQC, HMBC (101 MHz, chloroform-*d*, δ): 78.4 (glycerol C), 72.0 (-OCH_2CH_2-), 71.1 (glycerol C), 70.6 (-OCH_2CH_2-), 63.25 (glycerol C), 32.1 (-$OCH_2CH_2(CH_2)_{17}CH_3$), 30.2 (-OCH_2CH_2-), 29.9–29.5 (-$OCH_2CH_2(CH_2)_{17}CH_3$), 26.3 (-$OCH_2CH_2(CH_2)_{17}CH_3$), 22.9 (-$OCH_2CH_2(CH_2)_{17}CH_3$), 14.3 (-$O(CH_2)_{19}CH_3$).

2.9 Polymer synthesis of BisID-PEG

The synthesis is described for BisID-PEG_{62} as a representative example.

1,2-Bis-*n*-icosanyl glyceryl ether (BisID) (0.2 g, 0.307 mmol, 1 eq.) was placed in a dry Schlenk flask and dissolved in benzene (10 mL). The solution was stirred at 60 °C for at least 30 min and dried in vacuo for 16 h to remove moisture. Dry tetrahydrofuran (approx. 10 mL) was cryo-transferred to the Schlenk flask to dissolve the initiator. Afterwards, the solution was stirred and the initiator was deprotonated with a 0.5 M solution of potassium naphthalenide in THF (0.31 mL, 0.153 mmol, 0.5 eq.). The solution was cooled down to –90 °C and ethylene oxide (EO) (0.95 mL, 20.919 mmol, 68 eq.) was cryo-transferred

using a graduated ampule. The polymerization was carried out at 60 °C for 24 h. Subsequently, the reaction mixture was heated to 80 °C for 16 h. To quench the polymerization, an excess of ethanol was added and the solvent was removed under reduced pressure. The crude product was dissolved in methanol and precipitated three times in cold diethyl ether to obtain the pure product. Yield: 95%.

^{1}H NMR, COSY (400 MHz, benzene-d_6, δ): 3.73–3.31 (m, 256H, polyether backbone and glycerol H), 1.67–1.58 (m, 4H, -OCH_2CH_2-), 1.45–1.27 (m, 70H, -$OCH_2CH_2(CH_2)_{15}CH_3$), 0.93–0.89 (m, 6H, -$O(CH_2)_{19}CH_3$).

^{13}C NMR, HSQC, HMBC (101 MHz, benzene-d_6, δ): 79.0 (glycerol C), 73.4 (polyether backbone and glycerol C), 72.4–70.8 (polyether backbone and glycerol C), 62.1 (polyether backbone and glycerol C), 32.6 (-$OCH_2CH_2(CH_2)_{16}CH_2CH_3$), 31.1–30.1 (-$OCH_2CH_2$- and -$OCH_2CH_2(CH_2)_{16}CH_2CH_3$ (BisID)), 27.0 (-$OCH_2CH_2(CH_2)_{16}CH_2CH_3$ (BisID)), 23.4 (-$OCH_2CH_2(CH_2)_{16}CH_2CH_3$ (BisID)), 14.6 (-$O(CH_2)_{19}CH_3$ (BisID)).

2.10 Functionalization of BisID-PEG with propargyl bromide

The functionalization is described for BisID-PEG_{62}-alkyne as a representative example.

BisID-PEG_{62} (0.2 g, 0.059 mmol, 1 eq.) was placed in a Schlenk flask and dissolved in dry THF (10 mL). The solution was cooled to 0 °C and sodium hydride (0.004 g, 0.178 mmol, 3 eq.) was added. Afterwards, propargyl bromide (0.016 mL, 0.178 mmol, 3 eq.) was added and the solution was stirred for 24 h at room temperature. The reaction mixture was filtered and the solvent was reduced under reduced pressure. The remaining solution was precipitated twice in cold diethyl ether and the pure product was dried in vacuo. Yield: 61%.

^{1}H NMR, COSY (300 MHz, benzene-d_6, δ): 3.95–3.94 (d, J = 2.4 Hz, 2H, -OCH_2CCH), 3.77–3.24 (m, 245H, polyether backbone and glycerol H), 2.12–2.11 (t, J = 2.4 Hz, 1H, -OCH_2CCH), 1.69–1.57 (m, 4H, -OCH_2CH_2-), 1.49–1.28 (m, 67H, -$OCH_2CH_2(CH_2)_{15}CH_3$), 0.94–0.90 (m, 6H, -$O(CH_2)_{17}CH_3$).

2.11 Polymer synthesis of BisID-*lin*PG

The synthesis is described for BisID-*lin*PG_6 as a representative example.

1,2-Bis-*n*-icosanyl glyceryl ether (BisID) (0.15 g, 0.23 mmol, 1 eq.) and cesium hydroxide (0.03 g, 0.21 mmol, 0.9 eq.) were placed in a dry Schlenk flask and dissolved in benzene (10 mL). The solution was stirred at 60 °C for 30 min to enable the formation of the alkoxide and dried for 16 h under vacuum. The initiator was heated to 100 °C under reduced pressure to liquefy the initiator. Subsequently, EEGE (0.88 mL, 5.75 mmol, 25 eq.) was added and the polymerization was carried out in vacuo for 7 days. Methanol (3 mL) was added to quench the polymerization and to dissolve the crude product. Afterwards, 1N HCl (3 mL) was added to remove the acetal protecting groups. The solution was stirred at 40 °C for 7 days and subsequently precipitated in cold diethyl ether to obtain the pure product. Yield: 18%.

^{1}H NMR, COSY (400 MHz, pyridine-d_5, δ): 4.40–3.45-3.30 (m, 165H, polyether backbone and glycerol H), 1.73–1.63 (m, 4H, -OCH_2CH_2-), 1.45–1.26 (m, 66H, -$OCH_2CH_2(CH_2)_{17}CH_3$), 0.91–0.88 (m, 6H, -$O(CH_2)_{19}CH_3$).

^{13}C NMR, HMBC, HSQC (101 MHz, benzene-d_6, δ): 82.0–81.8, (polyether backbone and glycerol C), 79.1 (polyether backbone and glycerol C), 73.6–73.5 (polyether backbone and glycerol C), 72.8–72.2 (polyether backbone and glycerol C), 71.2–70 8 (polyether backbone and glycerol C), 65.1 (polyether backbone and glycerol C), 62.8 (polyether backbone and glycerol C), 32.7 (-$OCH_2CH_2(CH_2)_{16}CH_2CH_3$ (BisID)), 31.3-30.2 (-OCH_2CH_2- and -$OCH_2CH_2(CH_2)_{16}CH_2CH_3$ (BisID)), 27.2 (-$OCH_2CH_2(CH_2)_{16}CH_2CH_3$ (BisID)), 23.5 (-$OCH_2CH_2(CH_2)_{16}CH_2CH_3$ (BisID)), 14.9 (-$O(CH_2)_{19}CH_3$ (BisID)).

3. Characterization Data

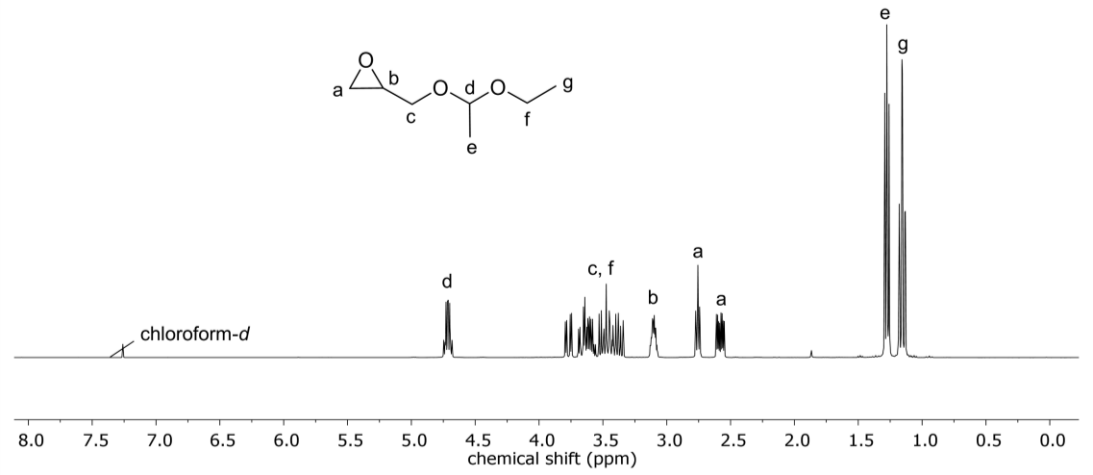

Figure S1. [1]H NMR (chloroform-*d*, 300 MHz) of ethoxyethyl glycidyl ether (EEGE).

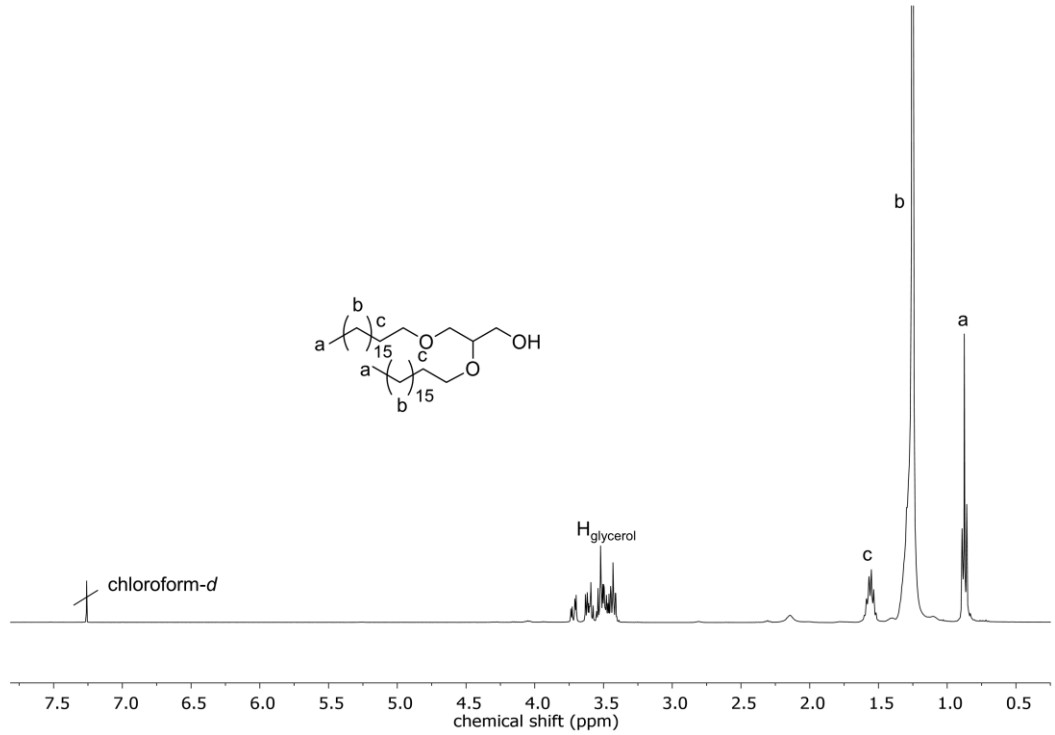

Figure S2. [1]H NMR (chloroform-*d*, 400 MHz) of 1,2-bis-*n*-octadecyl glyceryl ether (BisOD).

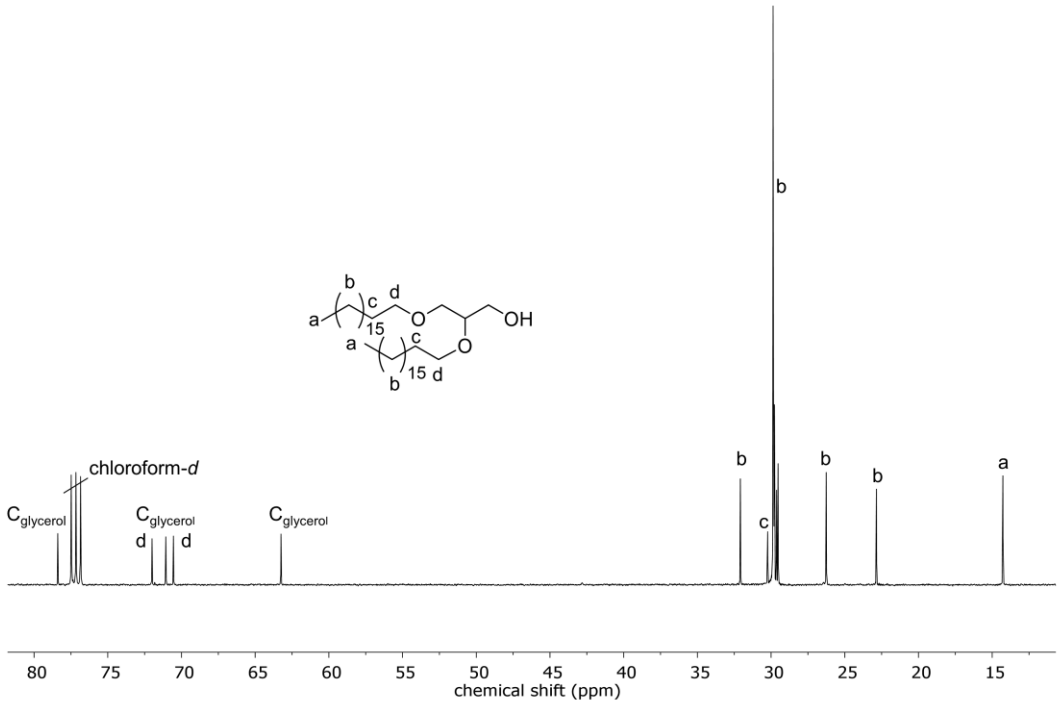

Figure S3. ^{13}C NMR (chloroform-*d*, 101 MHz) of 1,2-bis-*n*-octadecyl glyceryl ether (BisOD).

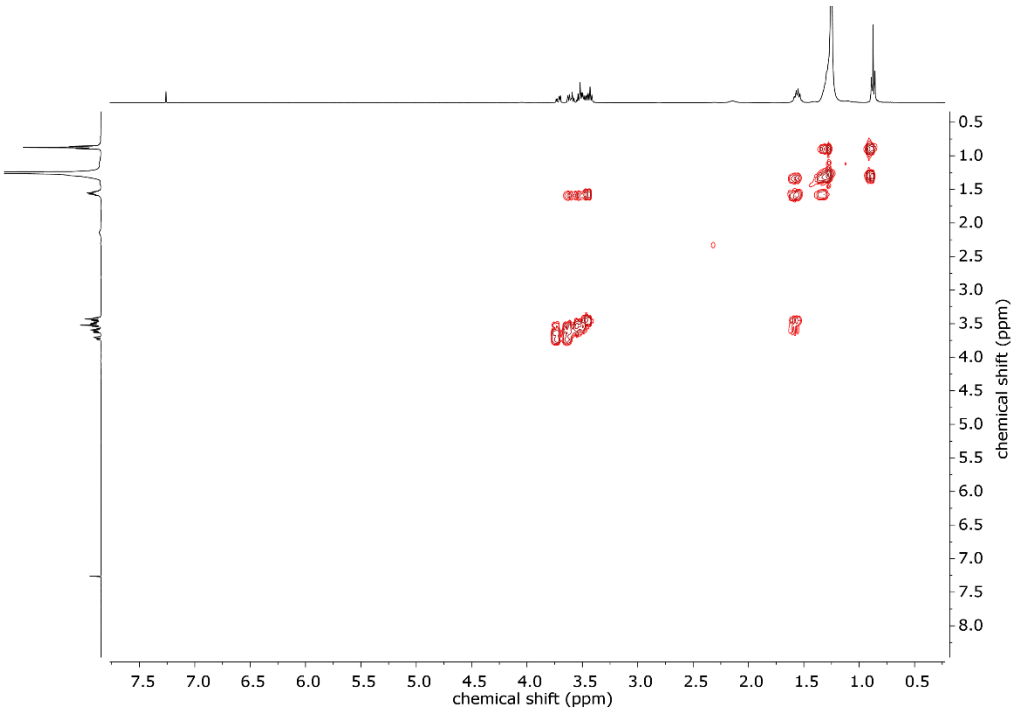

Figure S4. COSY NMR (chloroform-*d*, 400 MHz) of 1,2-bis-*n*-octadecyl glyceryl ether (BisOD).

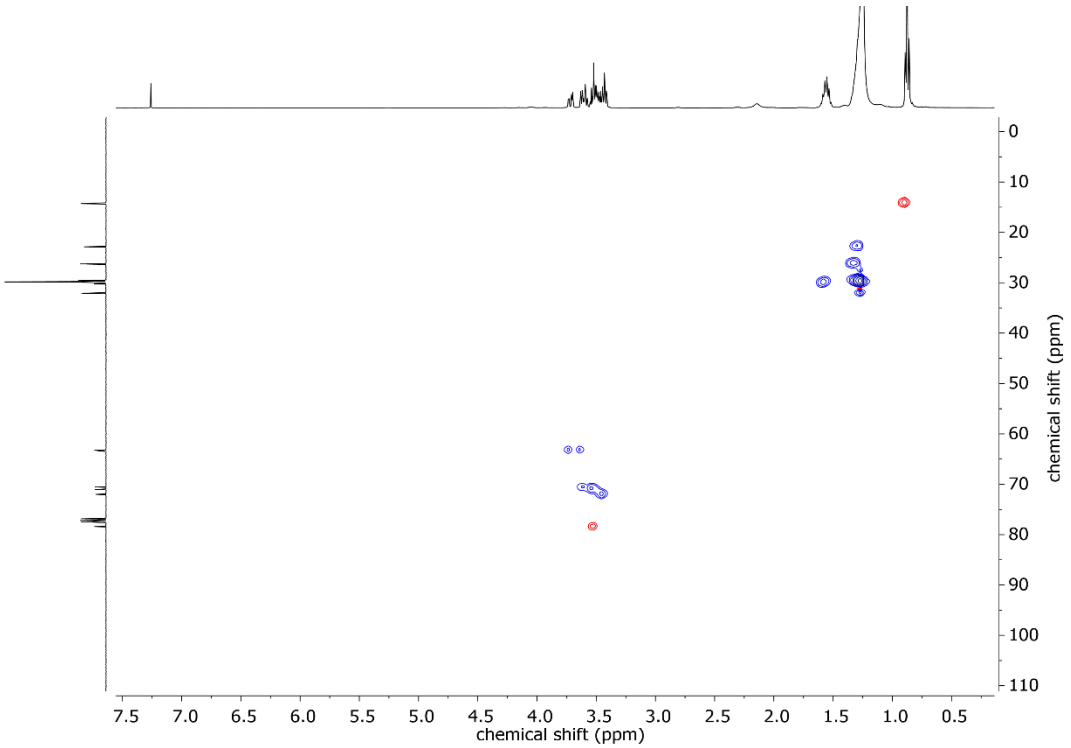

Figure S5. HSQC NMR (chloroform-*d*) of 1,2-bis-*n*-octadecyl glyceryl ether (BisOD).

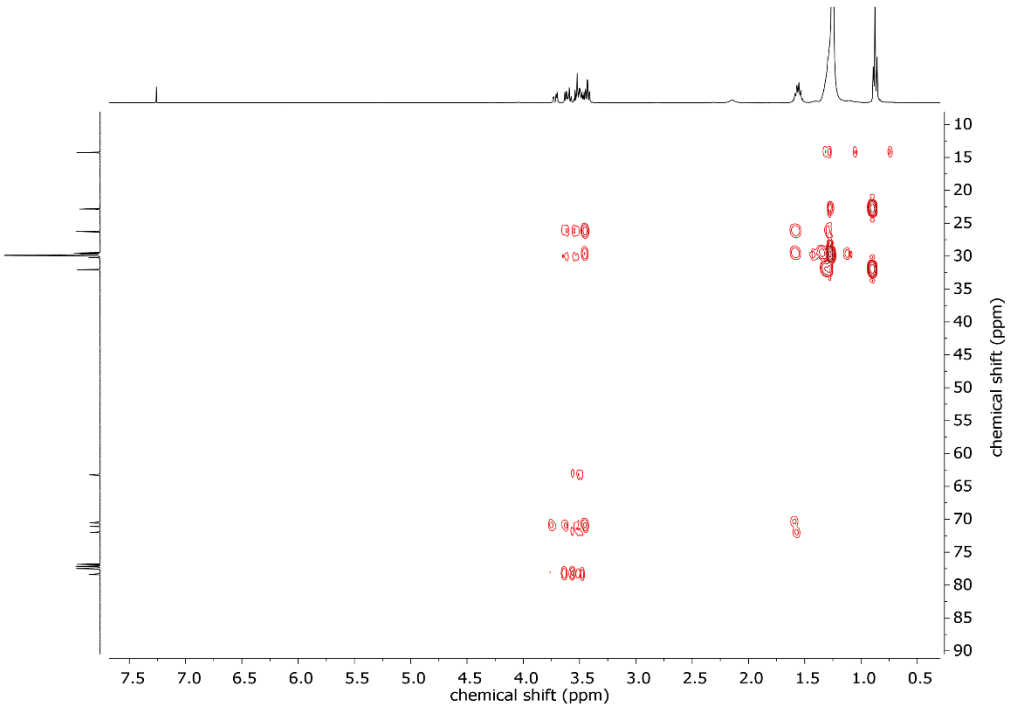

Figure S6. HMBC NMR (chloroform-*d*) of 1,2-bis-*n*-octadecyl glyceryl ether (BisOD).

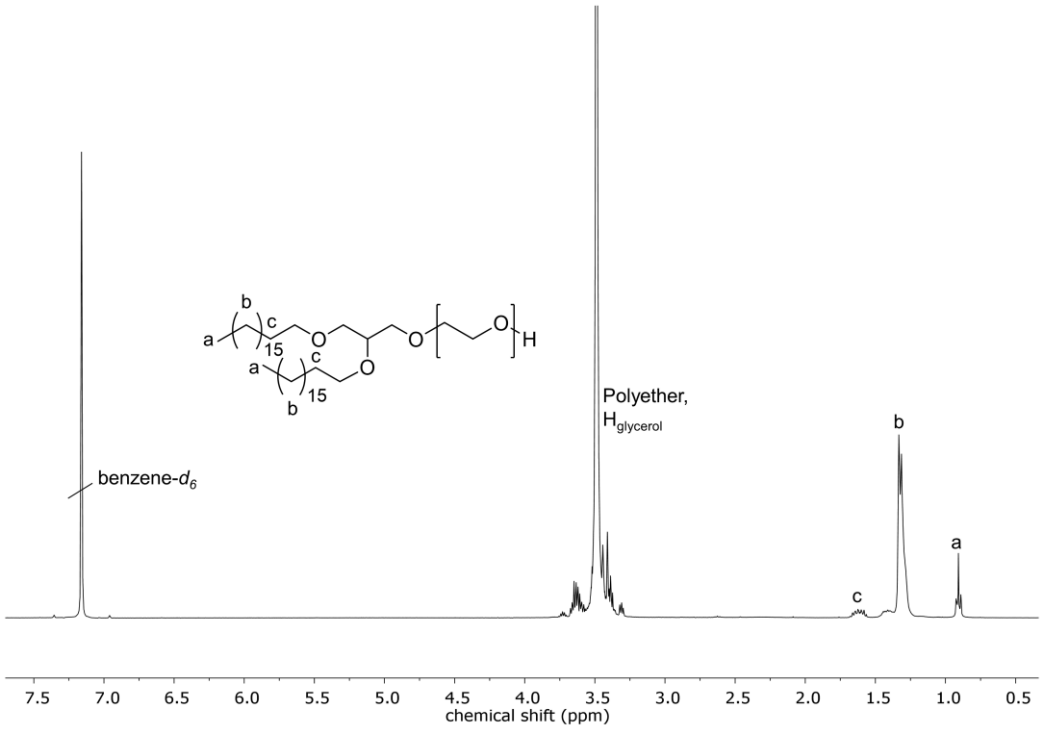

Figure S7. ^{1}H NMR (benzene-d_6, 400 MHz) of BisOD-PEG$_{81}$.

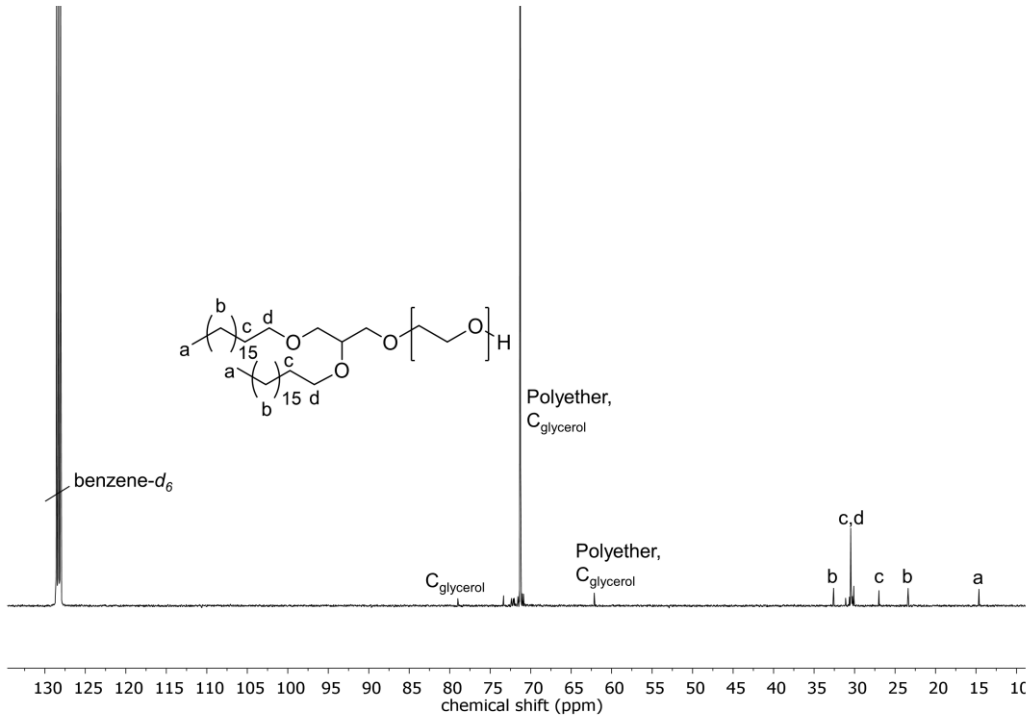

Figure S8. ^{13}C NMR (benzene-d_6, 101 MHz) of BisOD-PEG$_{81}$.

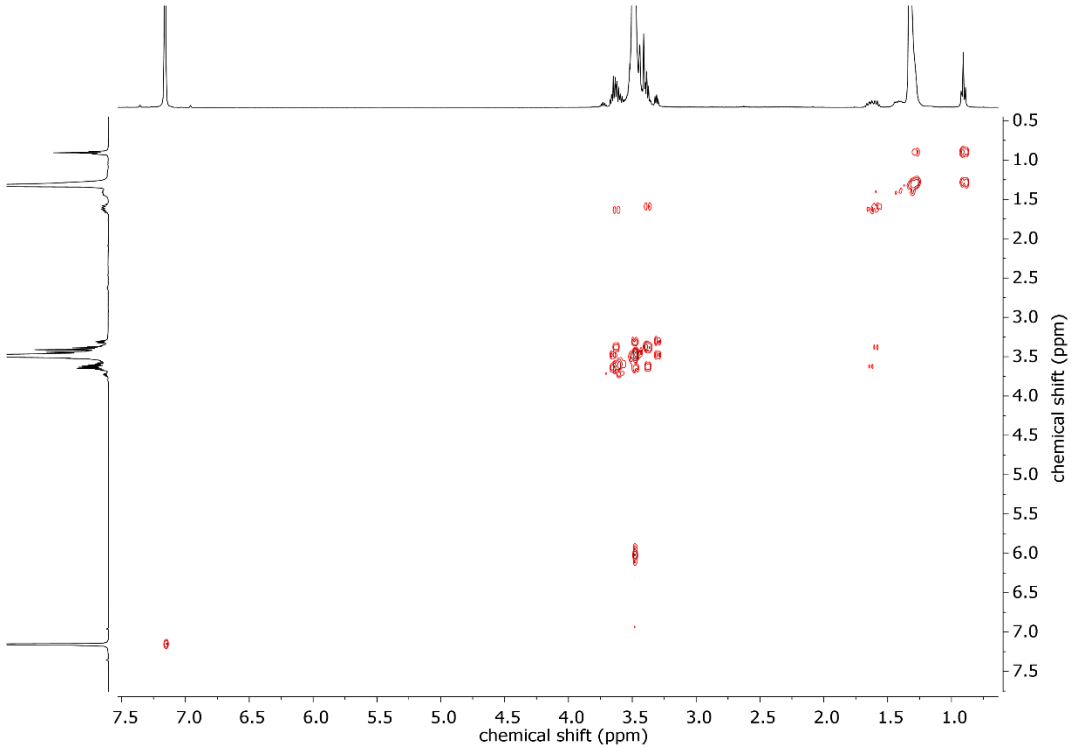

Figure S9. COSY NMR (benzene-d_6, 400 MHz) of BisOD-PEG$_{81}$.

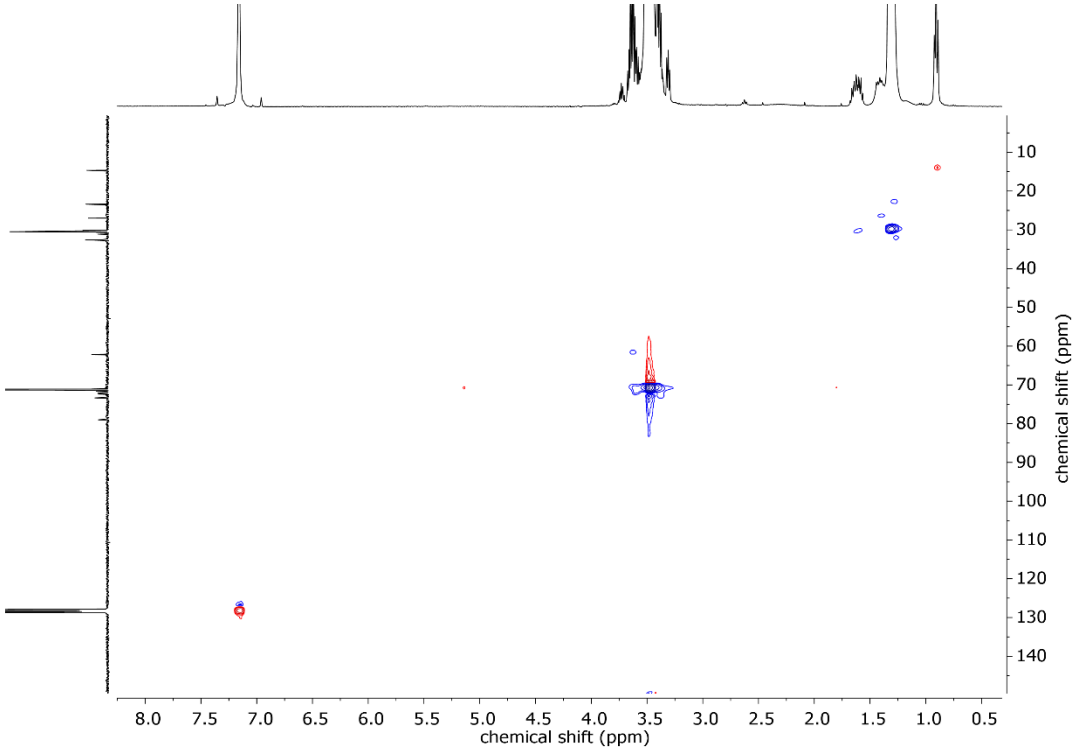

Figure S10. HSQC NMR (benzene-d_6) of BisOD-PEG$_{81}$.

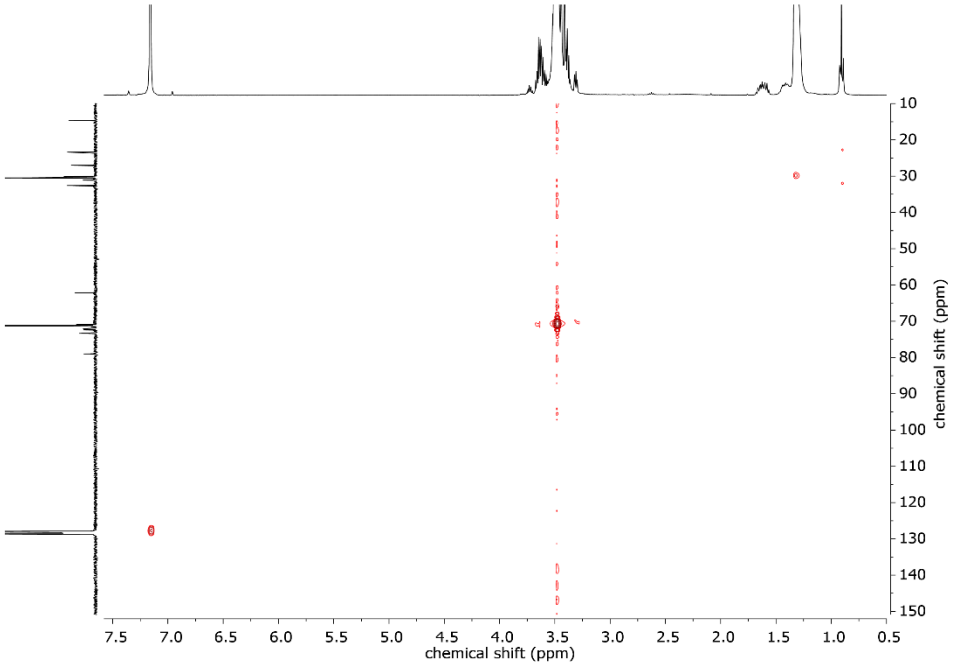

Figure S11. HMBC NMR (benzene-d_6) of BisOD-PEG$_{81}$.

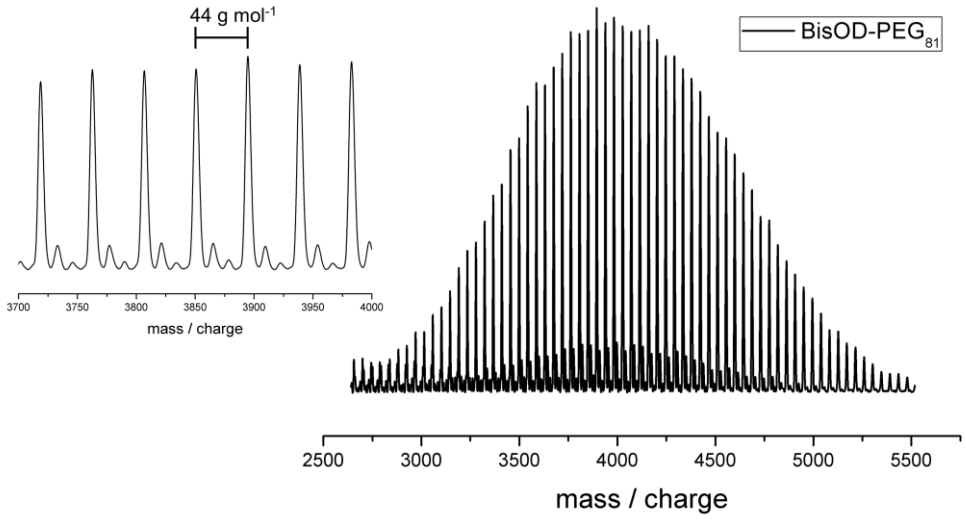

Figure S12. MALDI-ToF MS of BisOD-PEG$_{81}$ with K^+ as counter ion and dithranol as matrix.

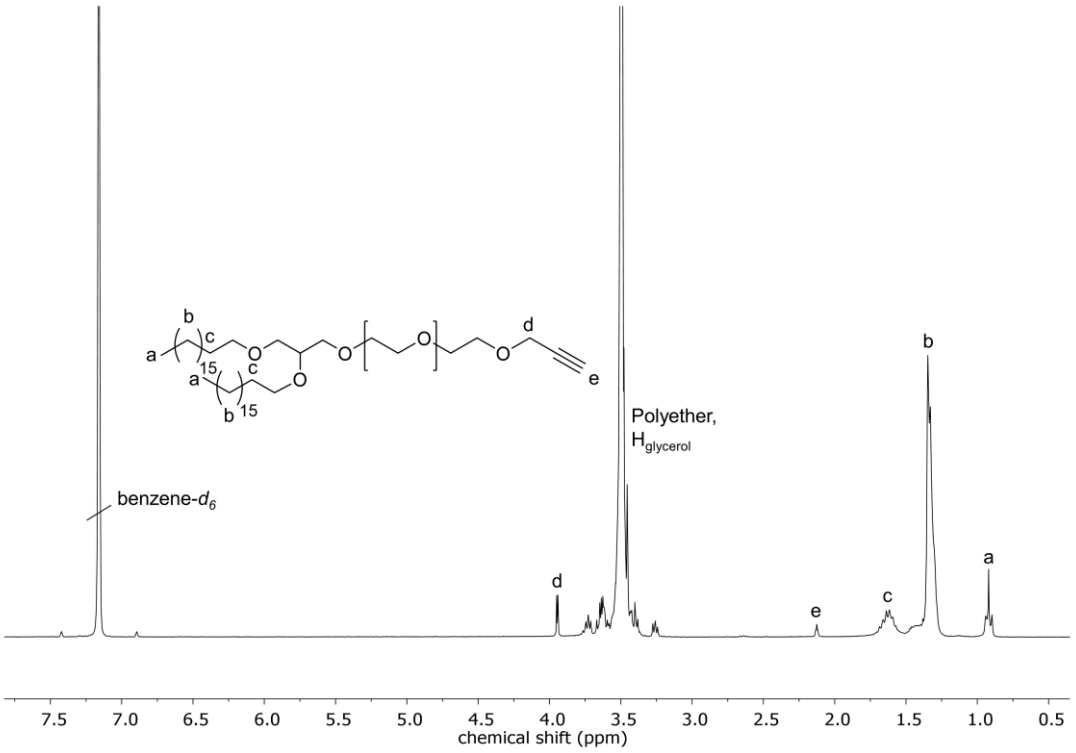

Figure S13. ^{1}H NMR (benzene-d_6, 300 MHz) of BisOD-PEG$_{81}$-alkyne.

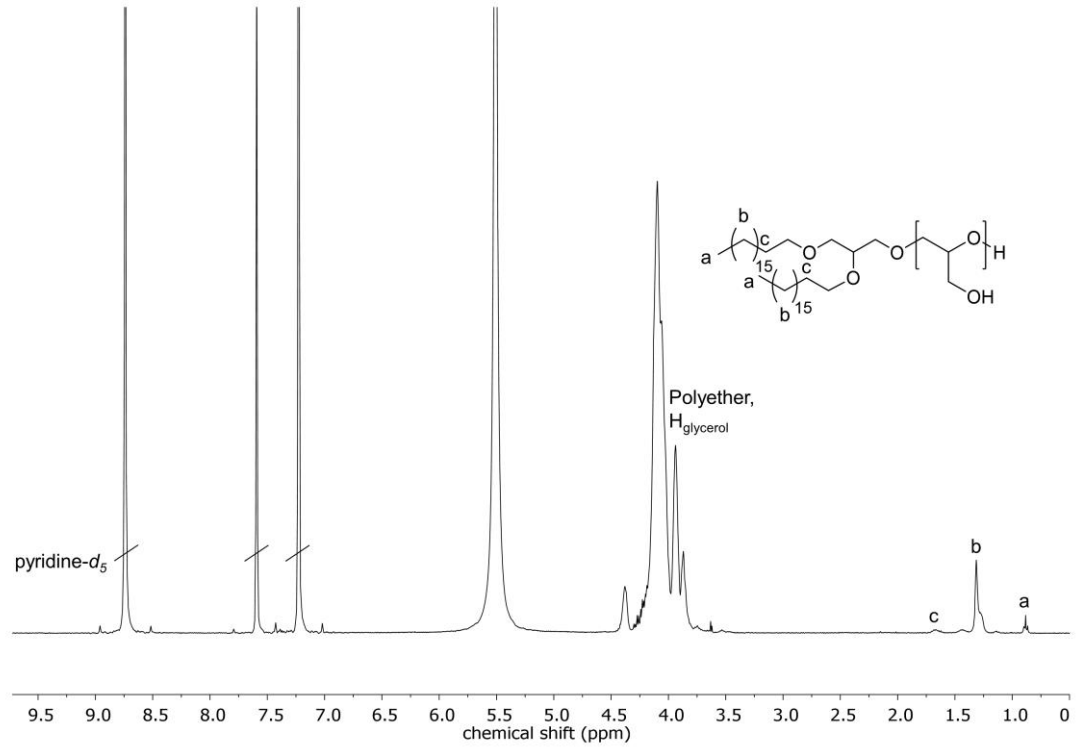

Figure S14. ^{1}H NMR (pyridine-d_5, 400 MHz) of BisOD-*lin*PG$_{19}$.

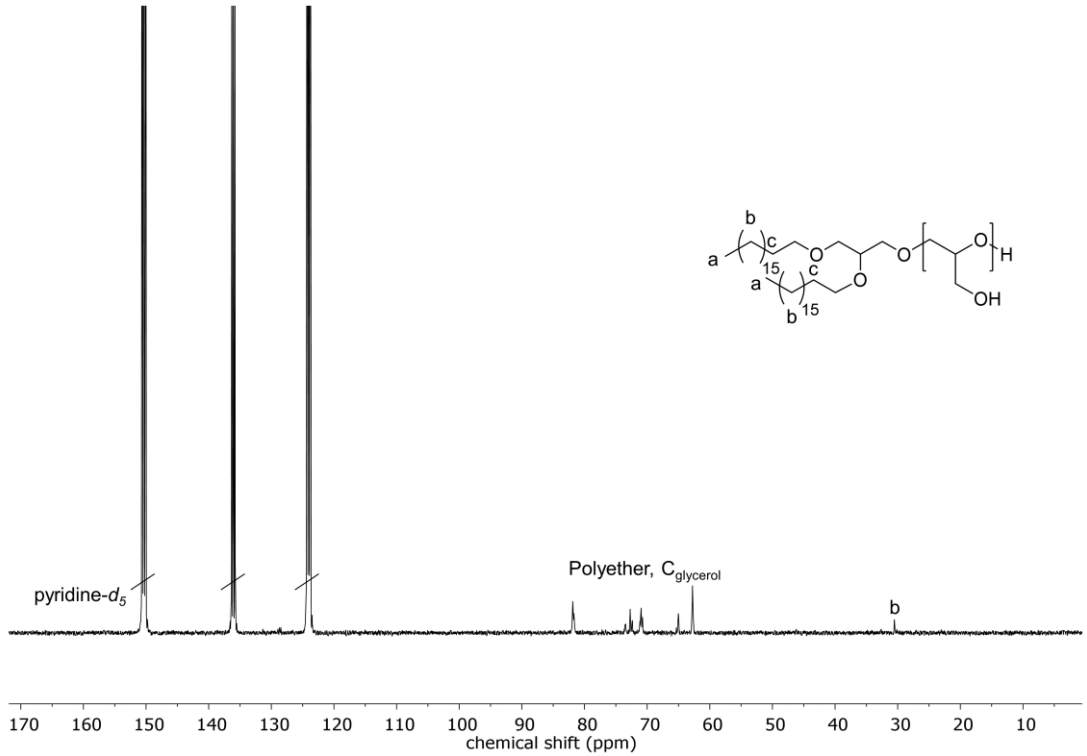

Figure S15. ^{13}C NMR (pyridine-d_5, 101 MHz) of BisOD-*lin*PG$_{19}$.

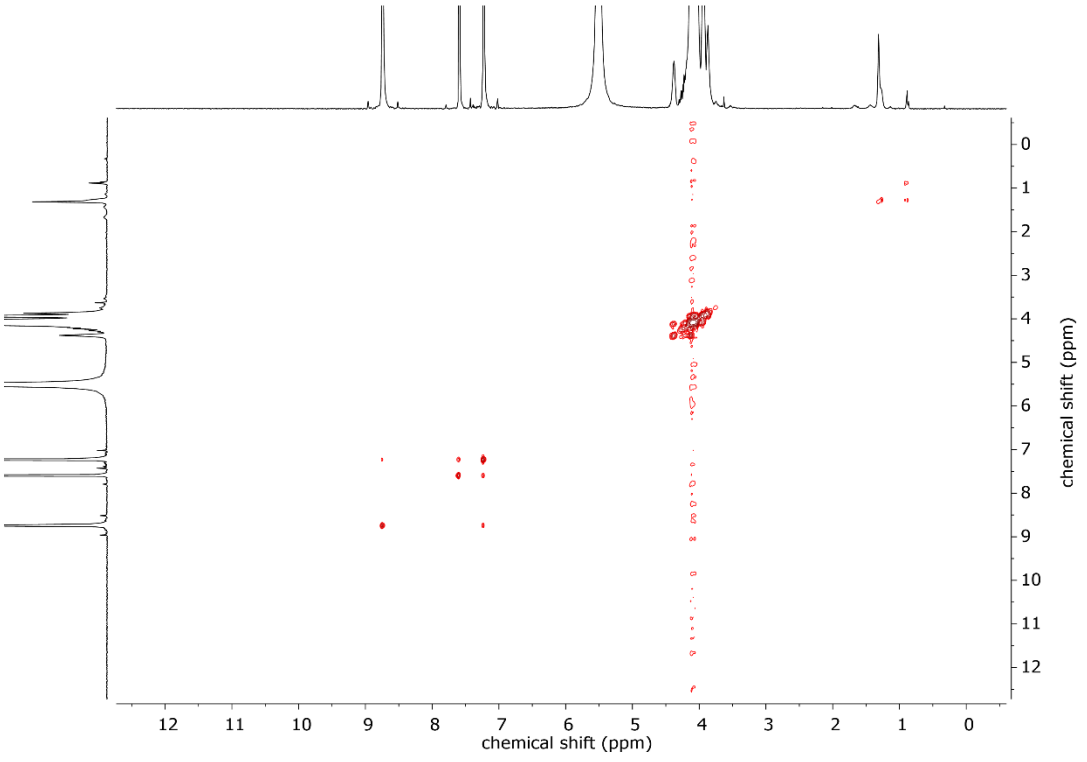

Figure S16. COSY NMR (pyridine-d_5, 400 MHz) of BisOD-*lin*PG$_{19}$.

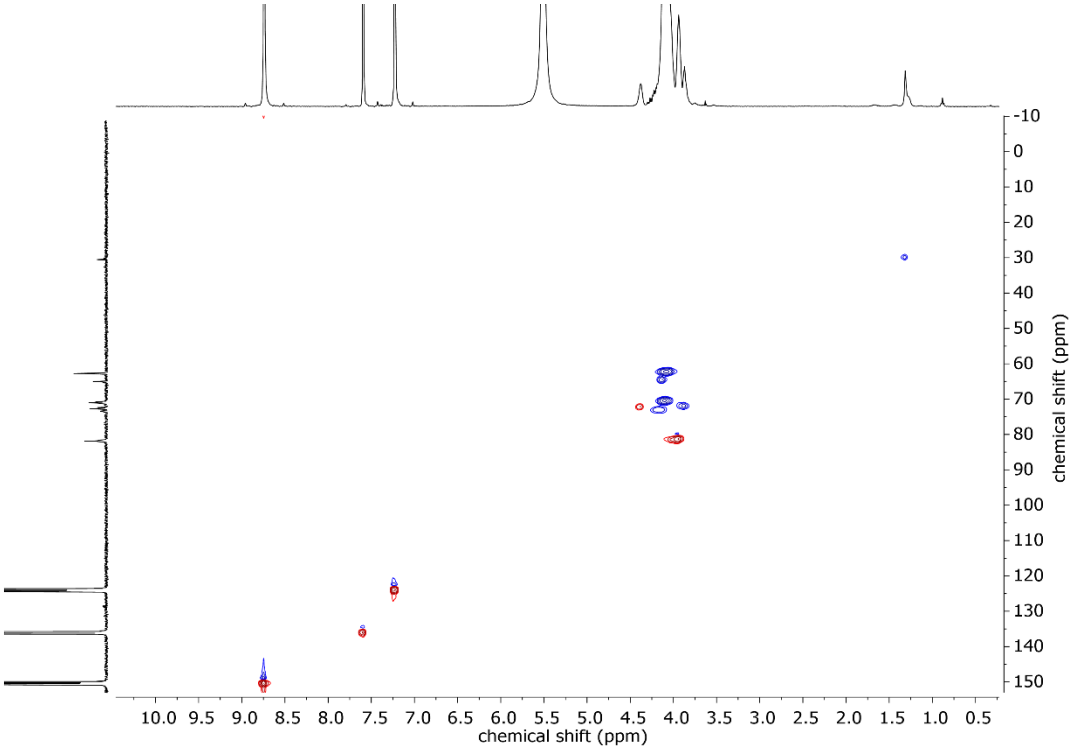

Figure S17. HSQC NMR (pyridine-d_5) of BisOD-*lin*PG$_{19}$.

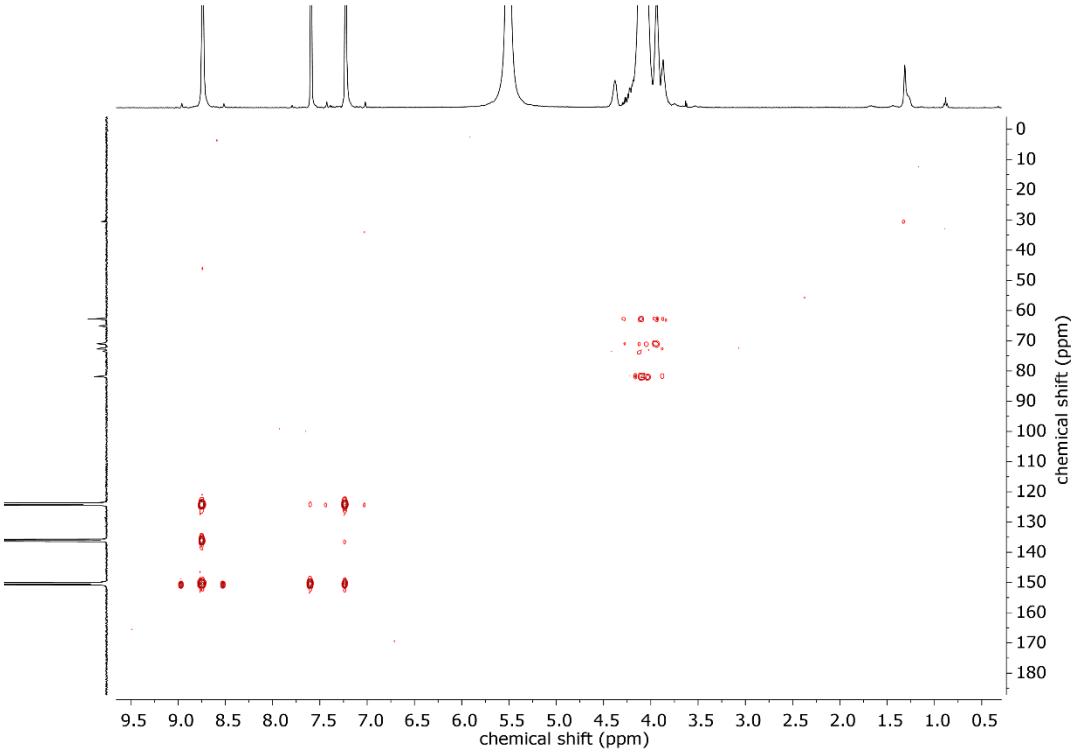

Figure S18. HMBC NMR (pyridine-d_5) of BisOD-*lin*PG$_{19}$.

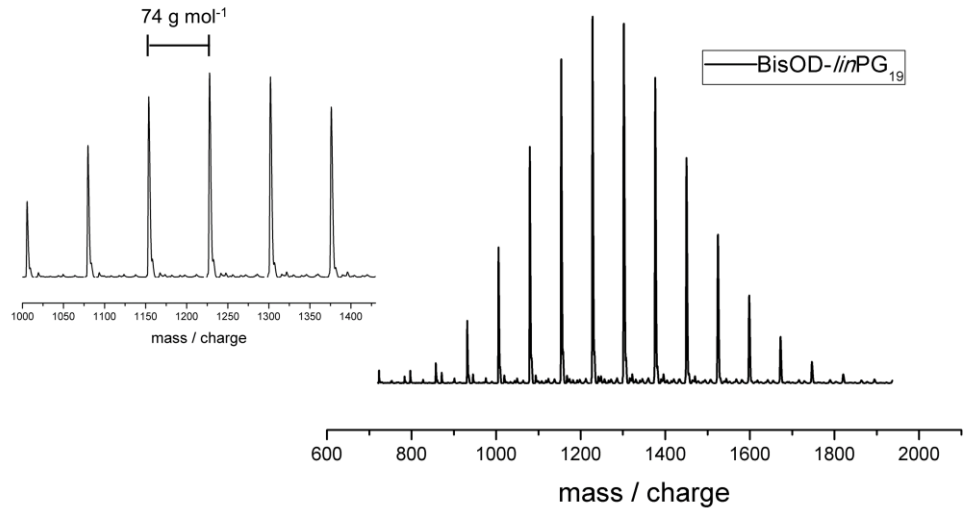

Figure S19. MALDI-ToF MS of BisOD-*lin*PG_{19} with K^+ as counter ion and dithranol as matrix.

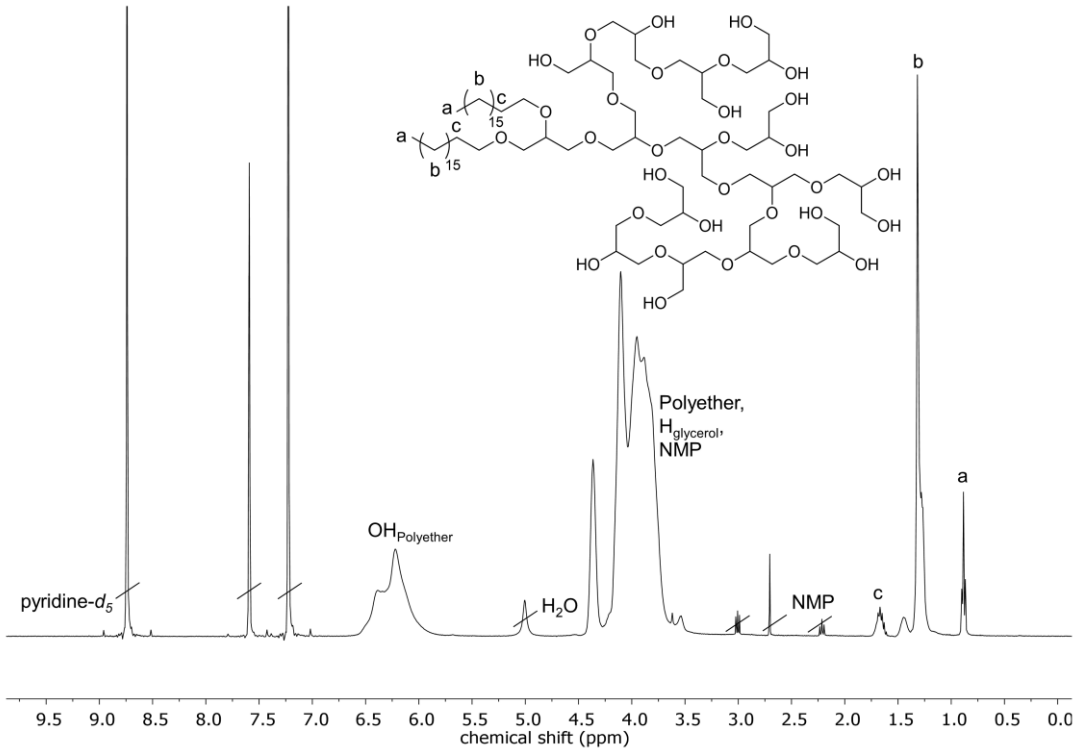

Figure S20. ^{1}H NMR (pyridine-d_5, 400 MHz) of BisOD-*hb*PG_{68}.

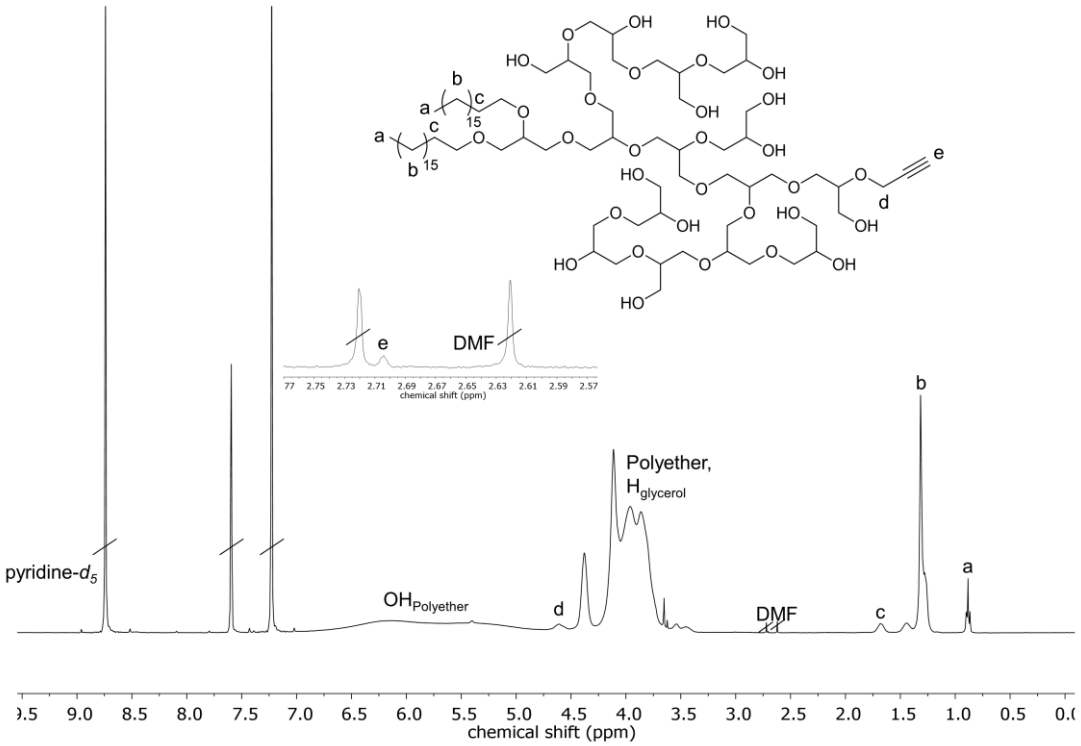

Figure S21. ^{1}H NMR (pyridine-d_5, 400 MHz) of BisOD-*hb*PG_{68}-alkyne.

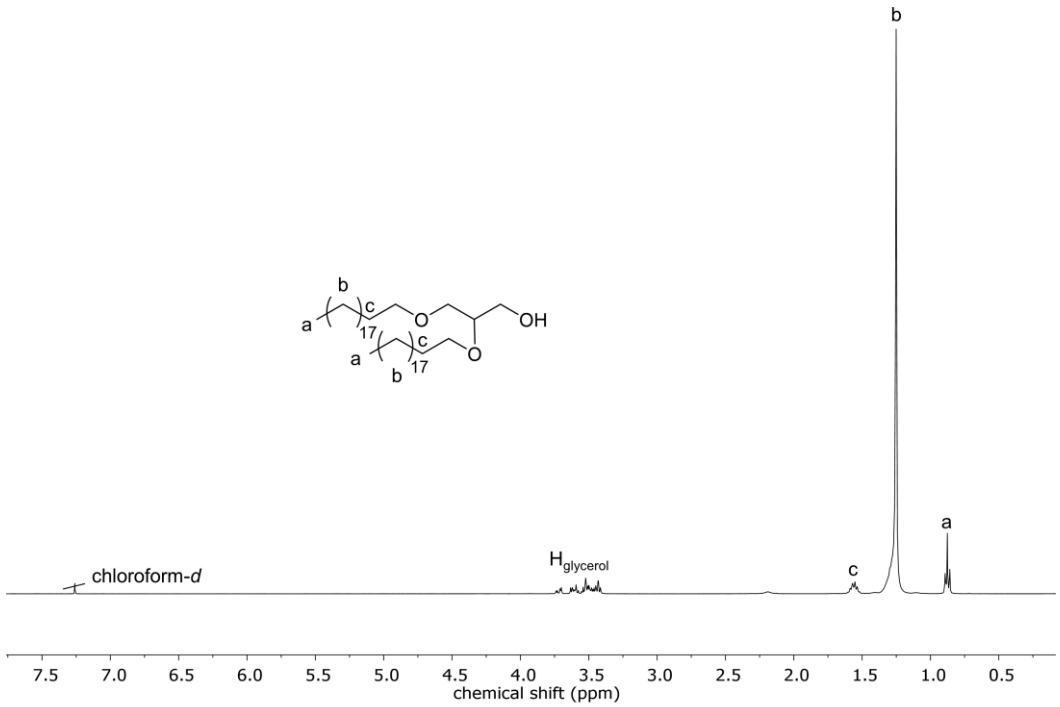

Figure S22. ^{1}H NMR (chloroform-*d*, 400 MHz) of 1,2-bis-*n*-icosanyl glyceryl ether (BisID).

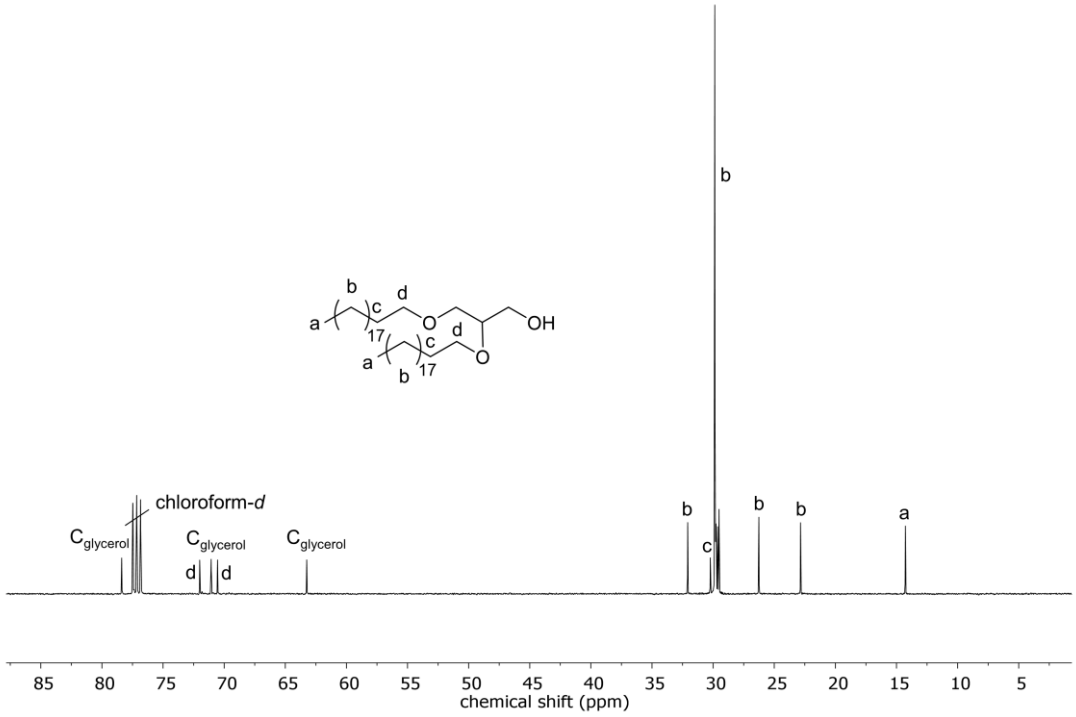

Figure S23. ^{13}C NMR (chloroform-*d*, 101 MHz) of 1,2-bis-*n*-icosanyl glyceryl ether (BisID).

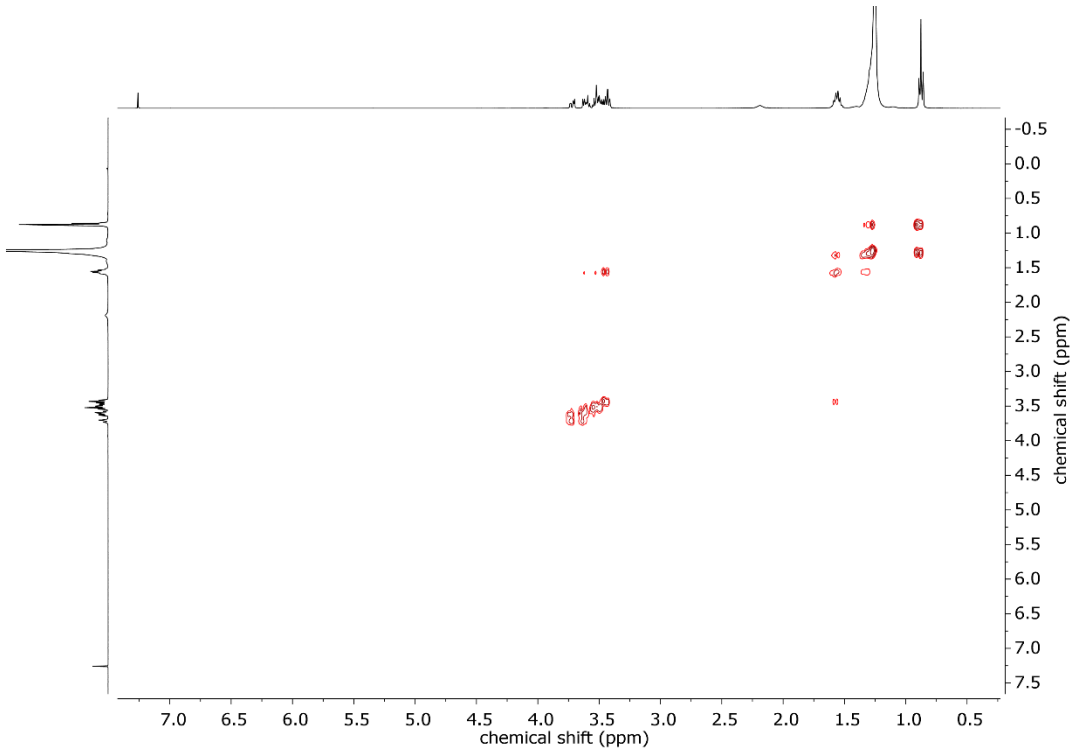

Figure S24. COSY NMR (chloroform-*d*, 400 MHz) of 1,2-bis-*n*-icosanyl glyceryl ether (BisID).

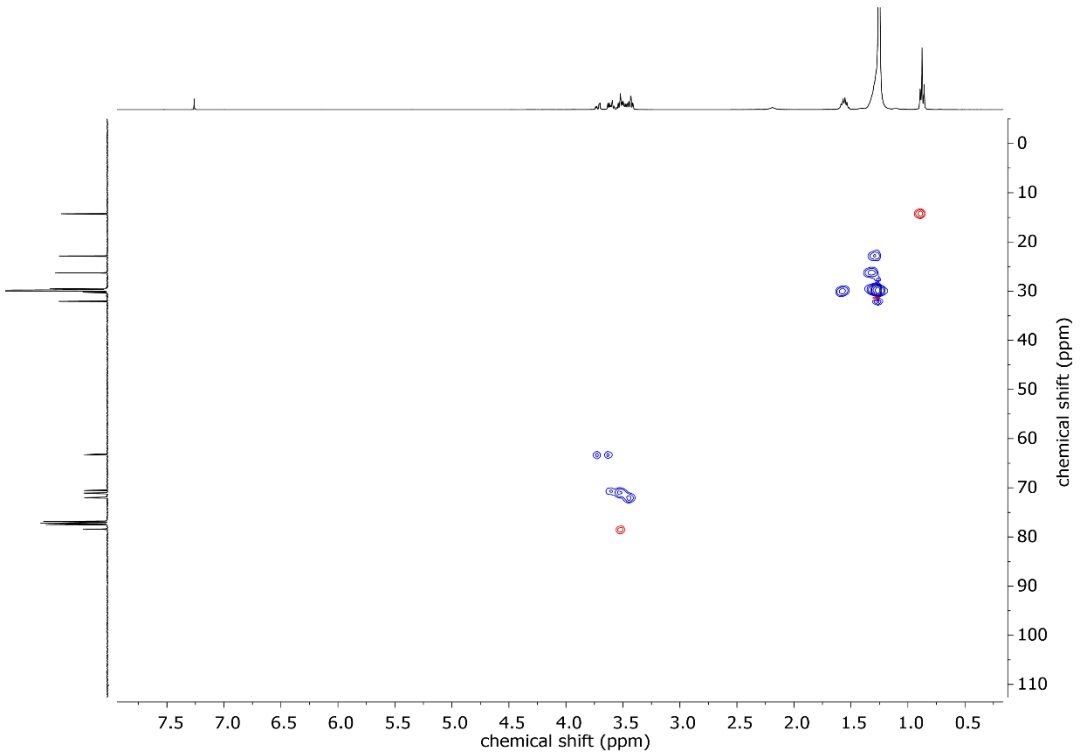

Figure S25. HSQC (chloroform-*d*) of 1,2-bis-*n*-icosanyl glyceryl ether (BisID).

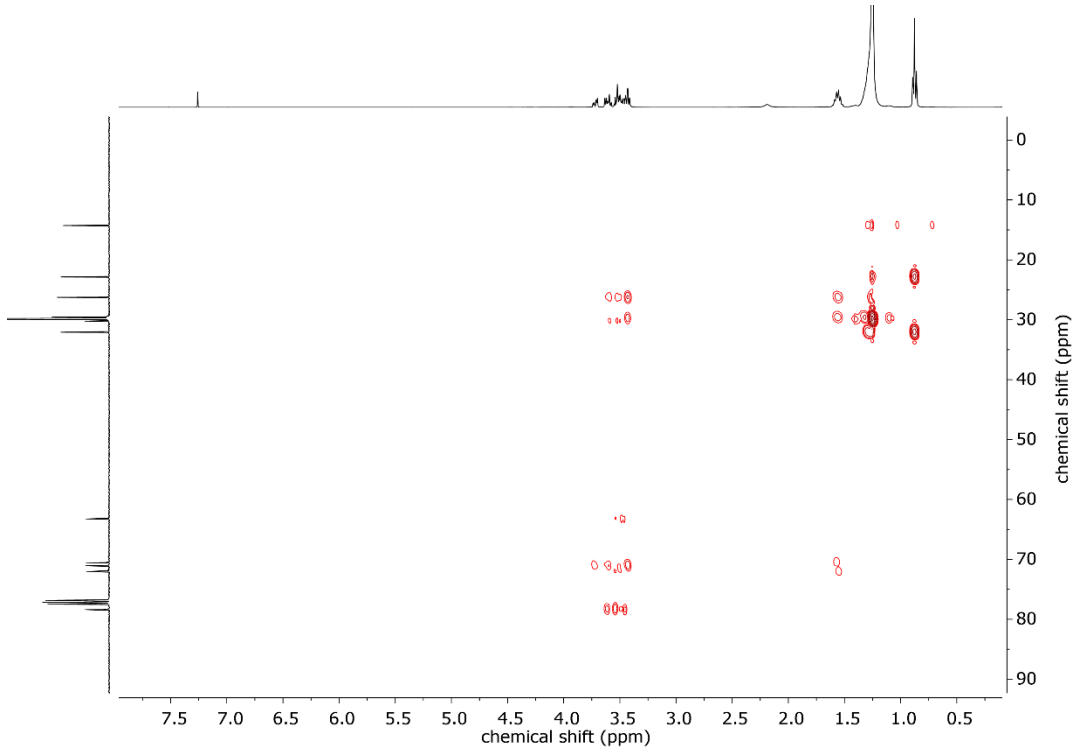

Figure S26. HMBC (chloroform-*d*) of 1,2-bis-*n*-icosanyl glyceryl ether (BisID).

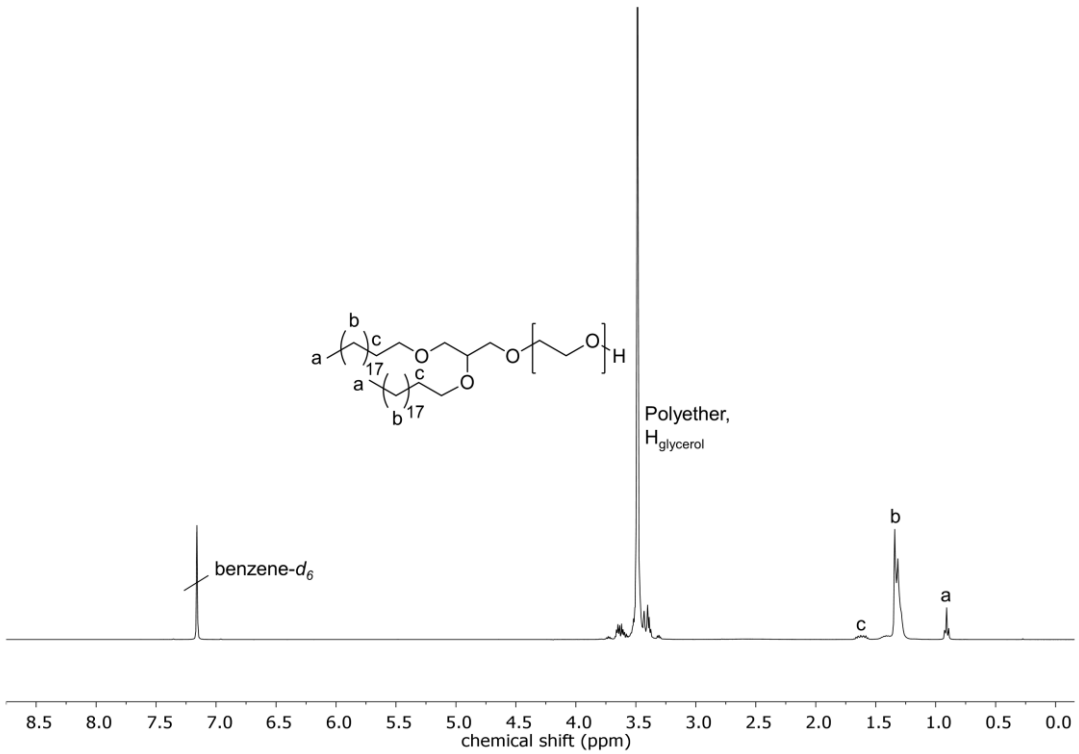

Figure S27. ^{1}H NMR (benzene-d_6, 400 MHz) of BisID-PEG$_{62}$.

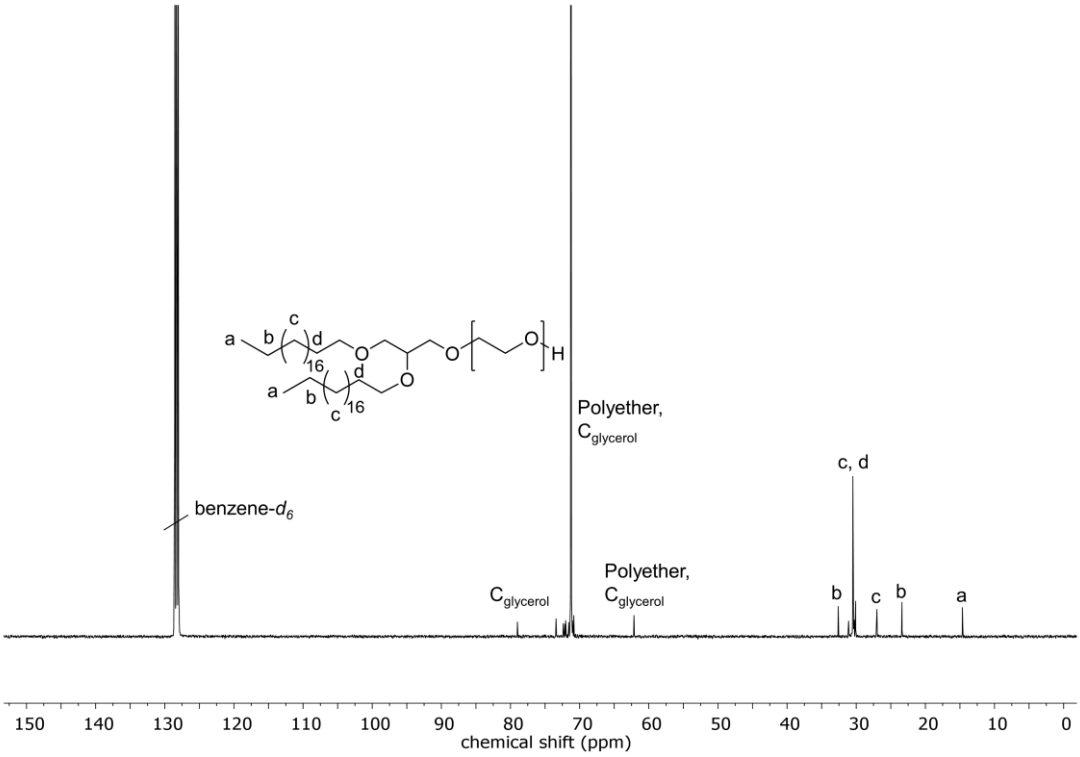

Figure S28. ^{13}C NMR (benzene-d_6, 101 MHz) of BisID-PEG$_{62}$.

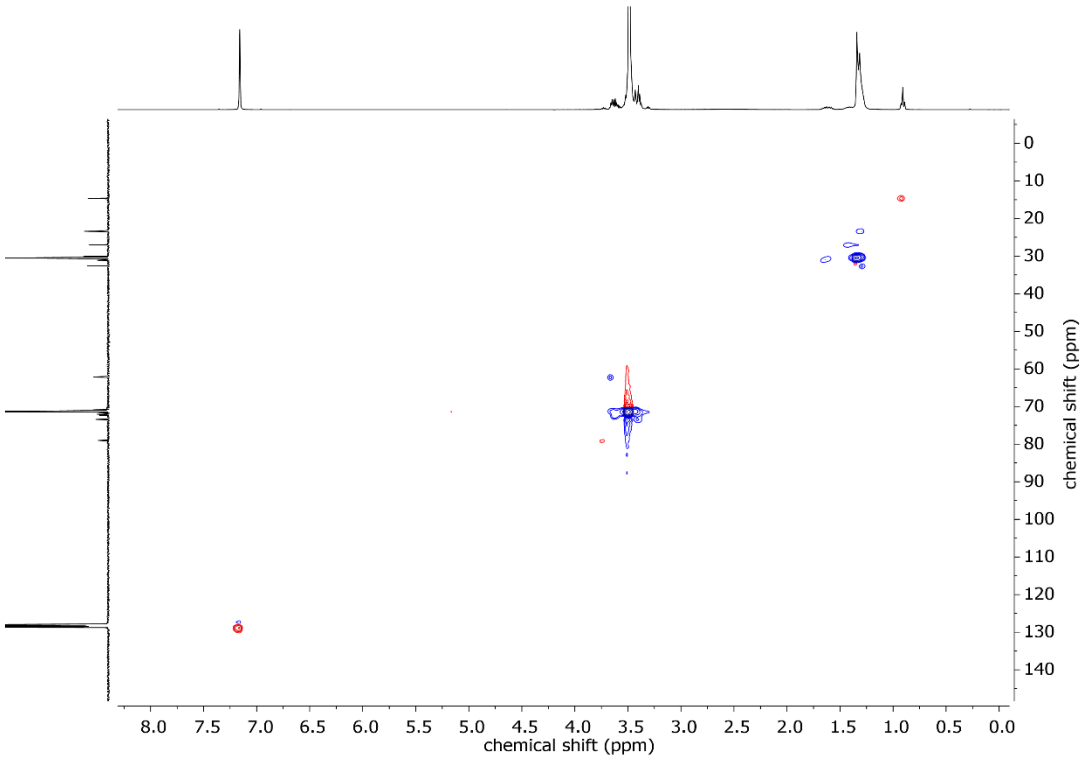

Figure S29. COSY NMR (benzene-d_6, 400 MHz) of BisID-PEG$_{62}$.

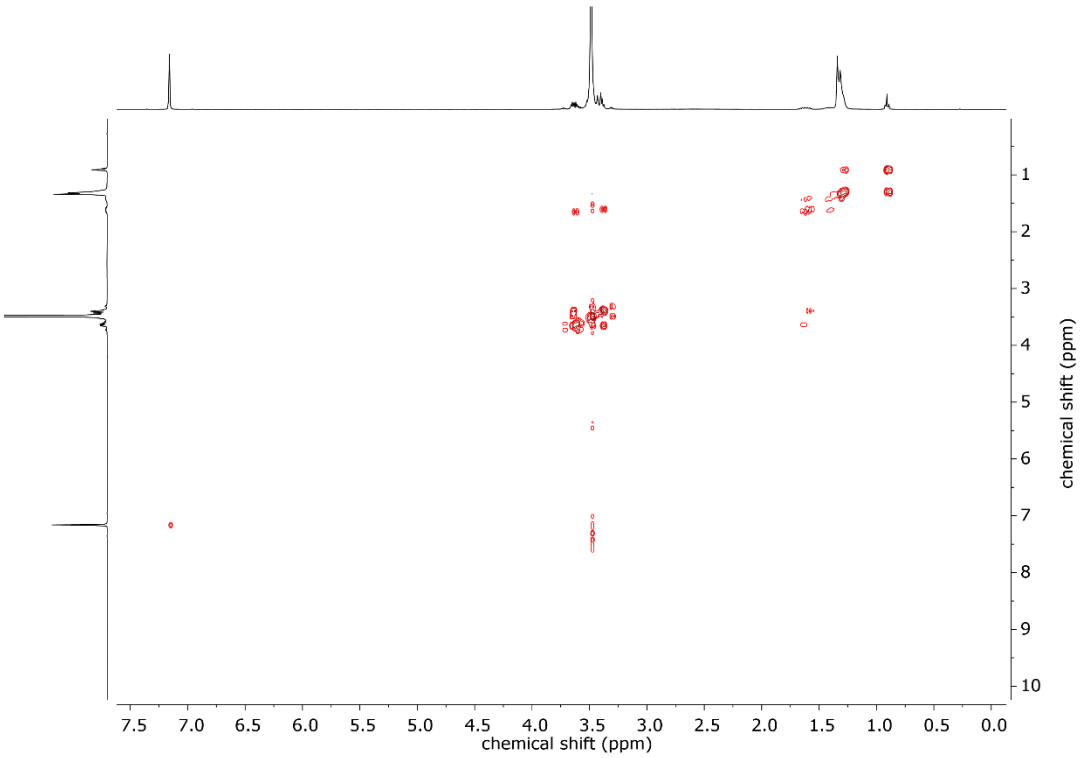

Figure S30. HSQC NMR (benzene-d_6) of BisID-PEG$_{62}$.

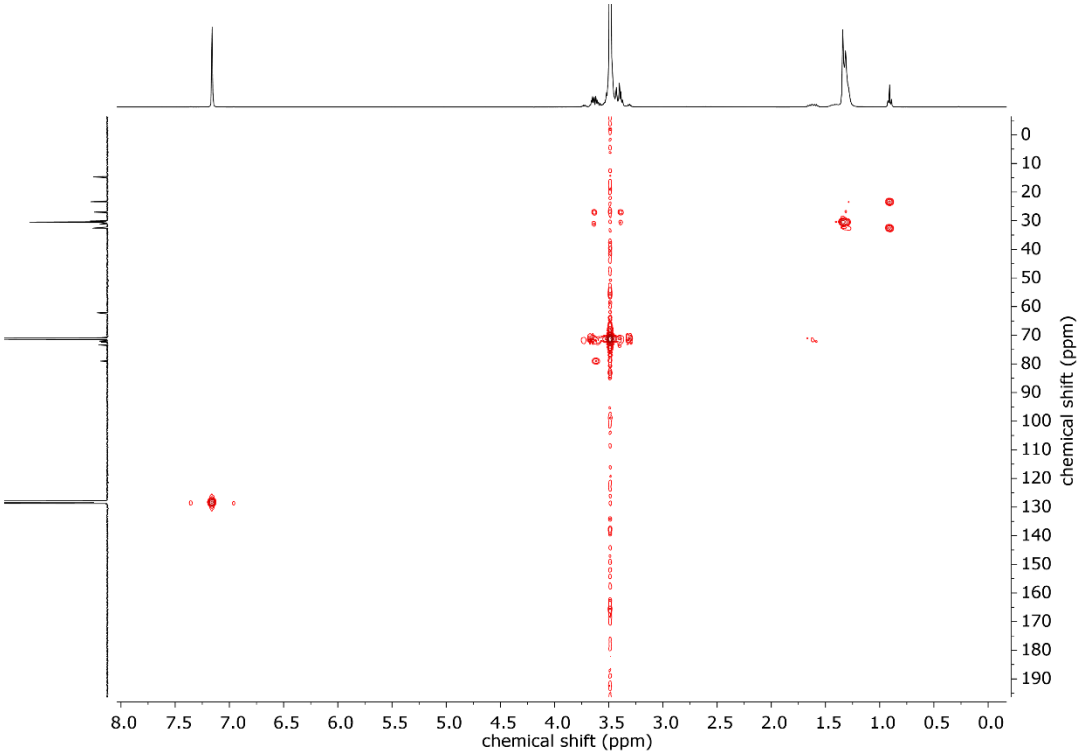

Figure S31. HMBC (benzene-d_6) of BisID-PEG$_{62}$.

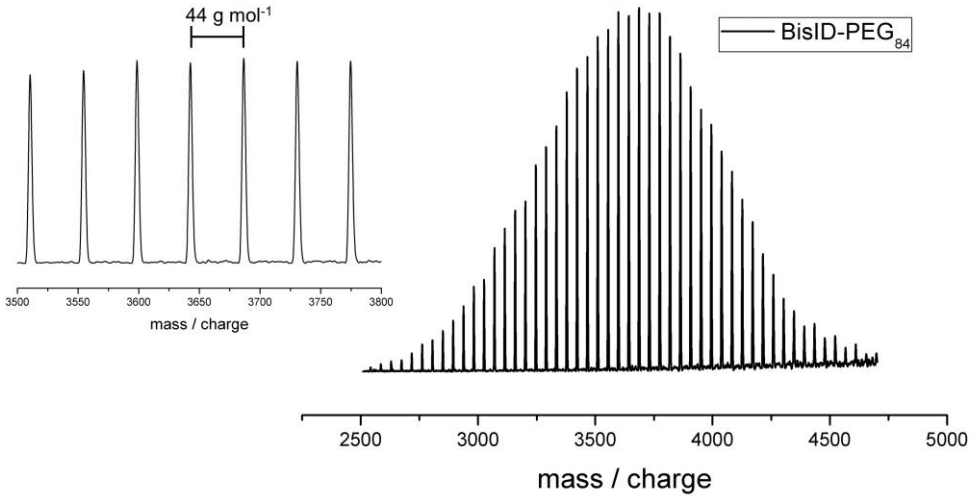

Figure S32. MALDI-ToF MS of BisID-PEG$_{84}$ with K^+ as counter ion and dithranol as matrix.

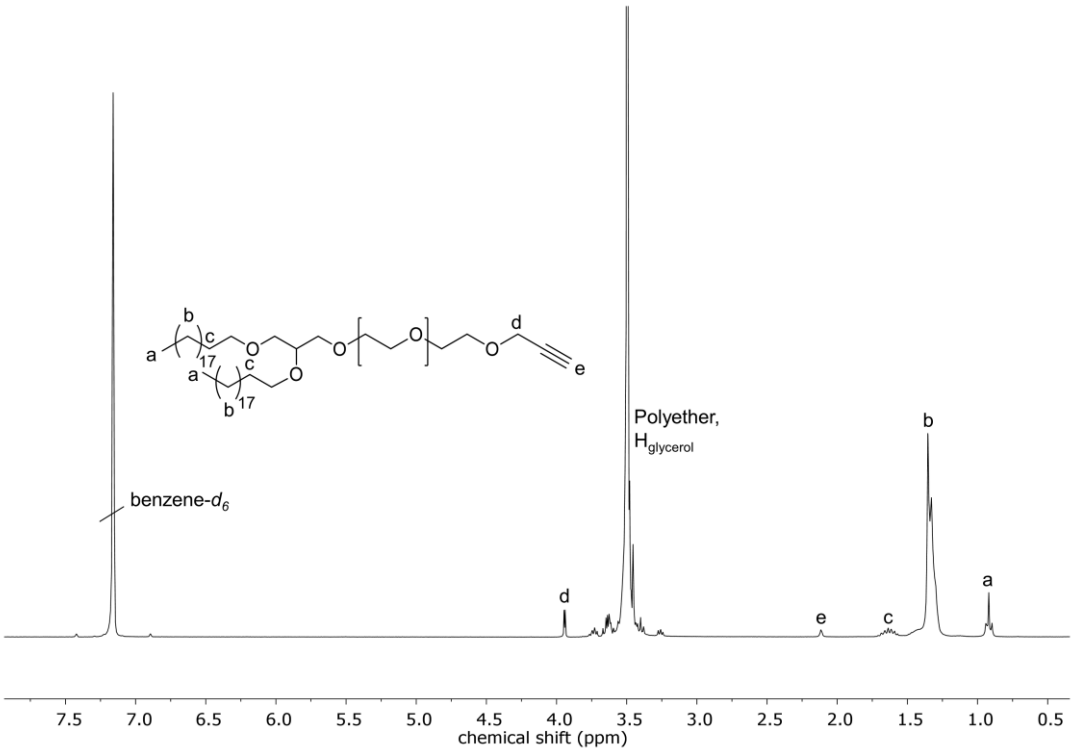

Figure S33. ^{1}H NMR (benzene-d_6, 300 MHz) of BisID-PEG$_{62}$-alkyne.

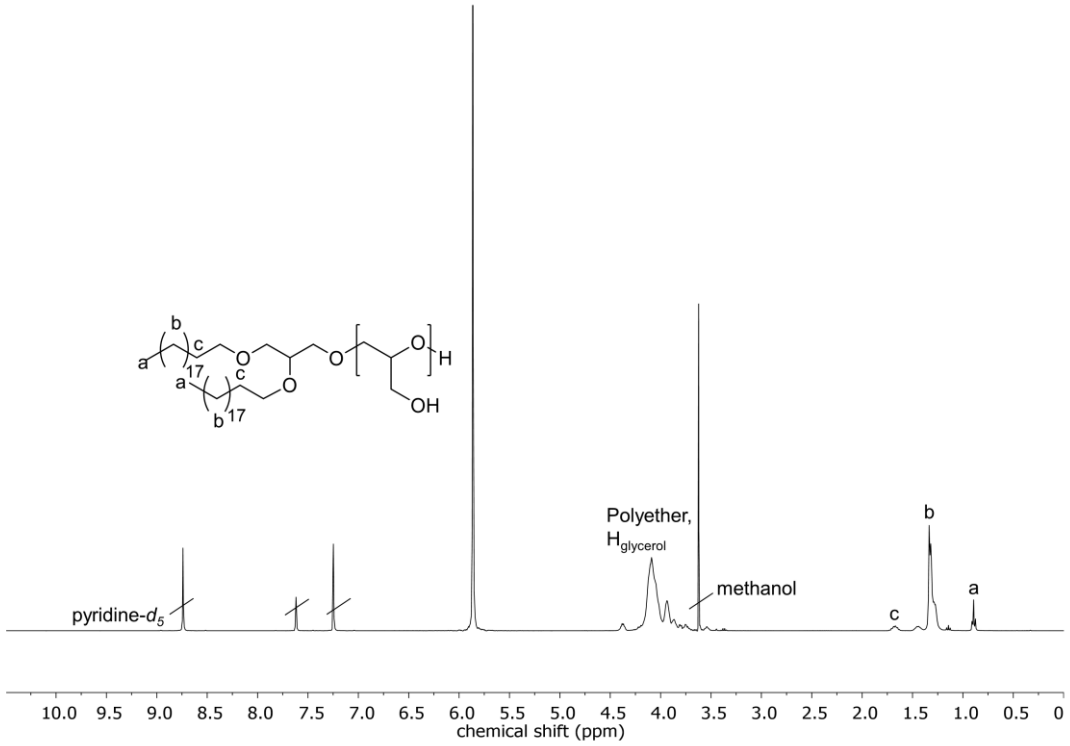

Figure S34. ^{1}H NMR (pyridine-d_5, 400 MHz) of BisID-*lin*PG$_6$.

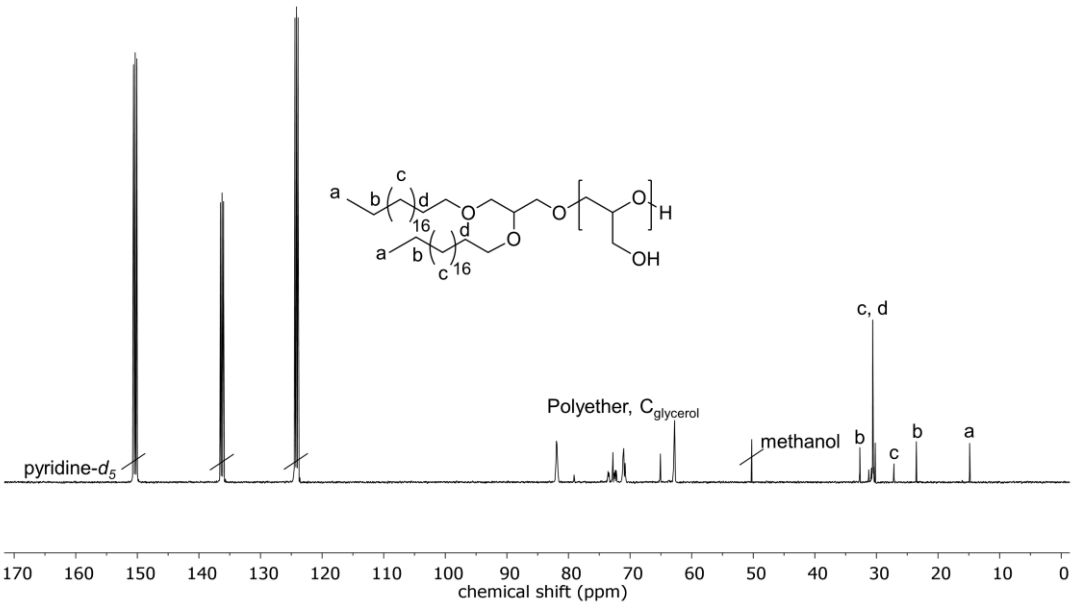

Figure S35. ^{13}C NMR (pyridine-d_5, 101 MHz) of BisID-*lin*PG$_6$.

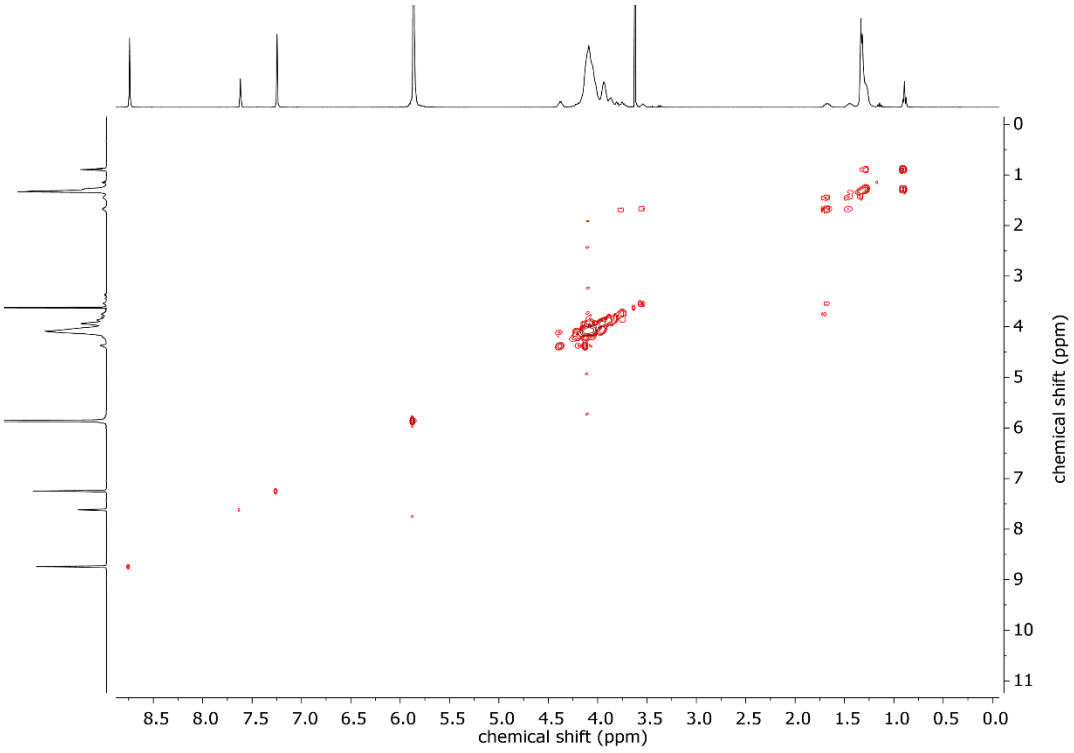

Figure S36. COSY NMR (pyridine-d_5, 400 MHz) of BisID-*lin*PG$_6$.

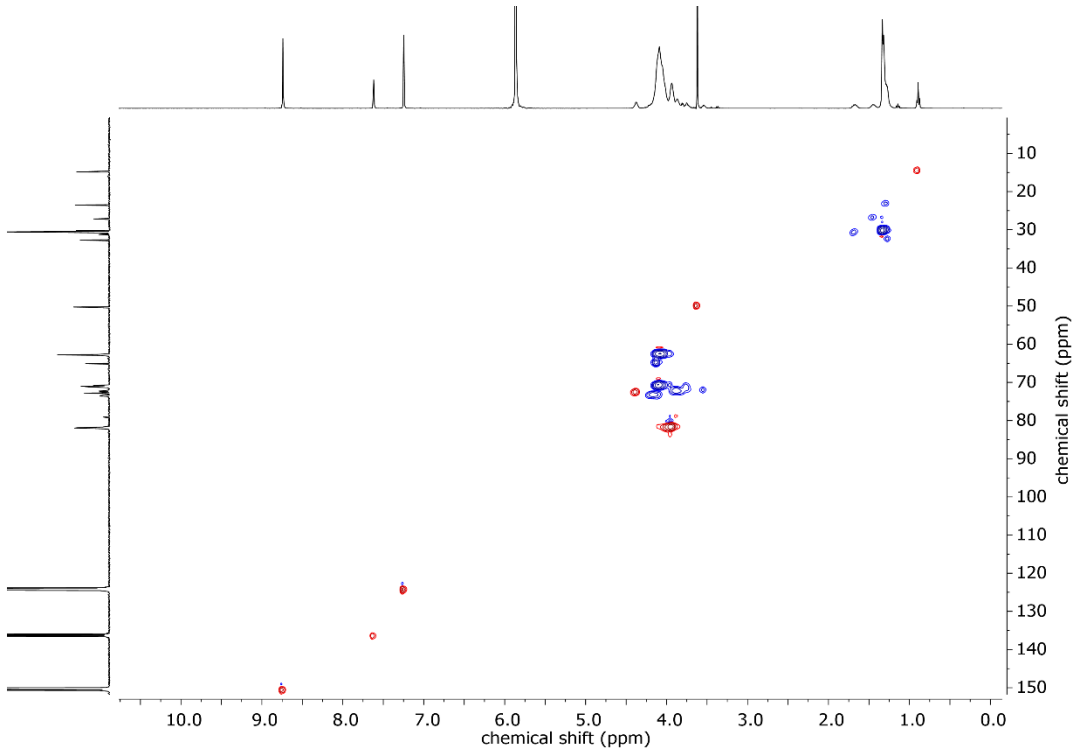

Figure S37. HSQC NMR (pyridine-d_5) of BisID-*lin*PG$_6$.

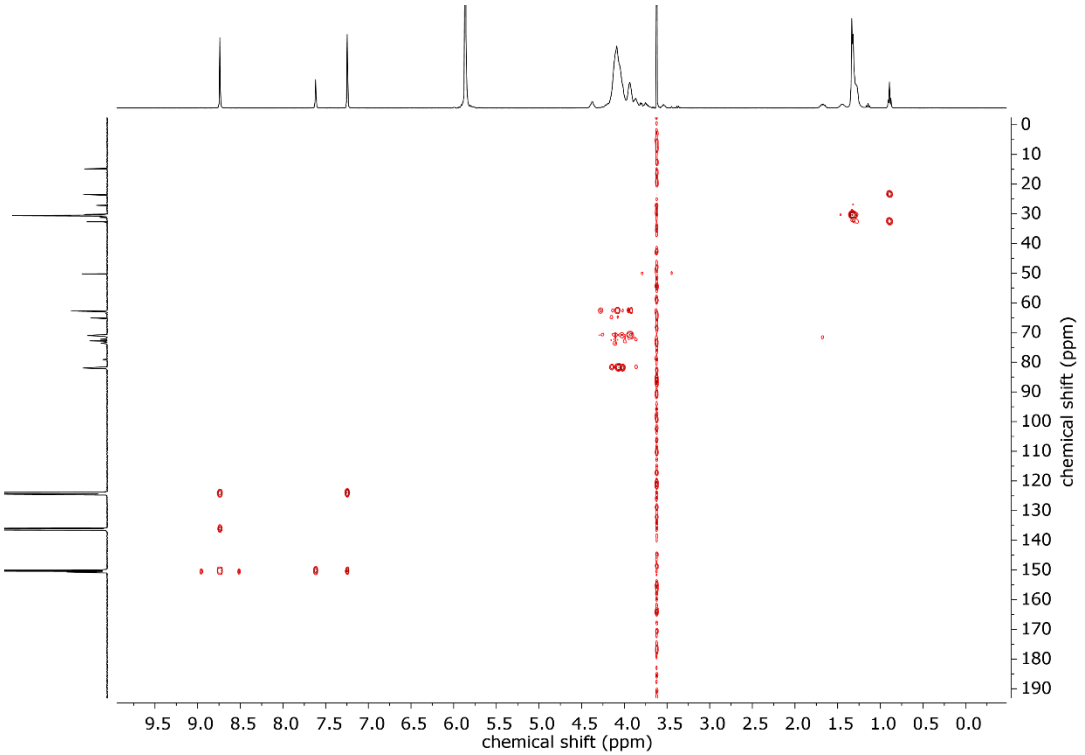

Figure S38. HMBC NMR (pyridine-d_5) of BisID-*lin*PG$_6$.

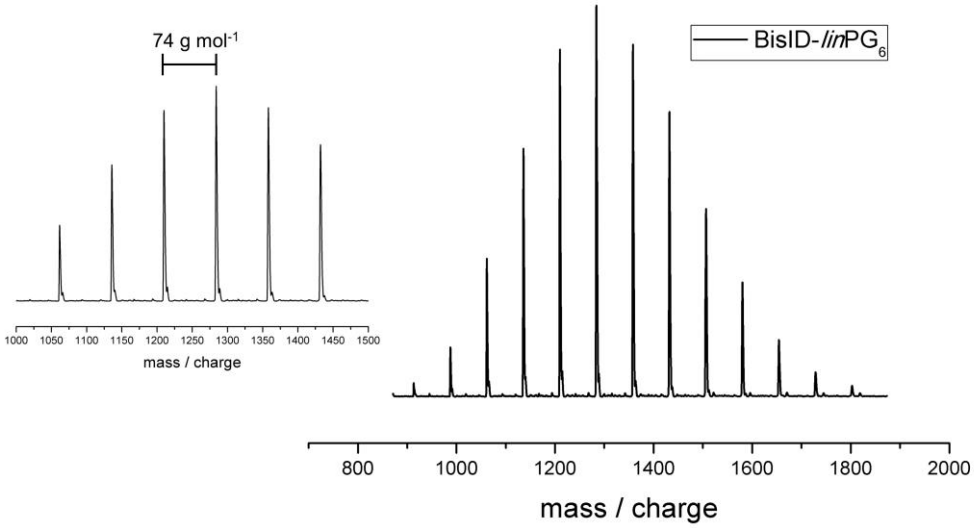

Figure S39. MALDI-ToF MS of BisID-*lin*PG_6 with K^+ as counter ion and dithranol as matrix.

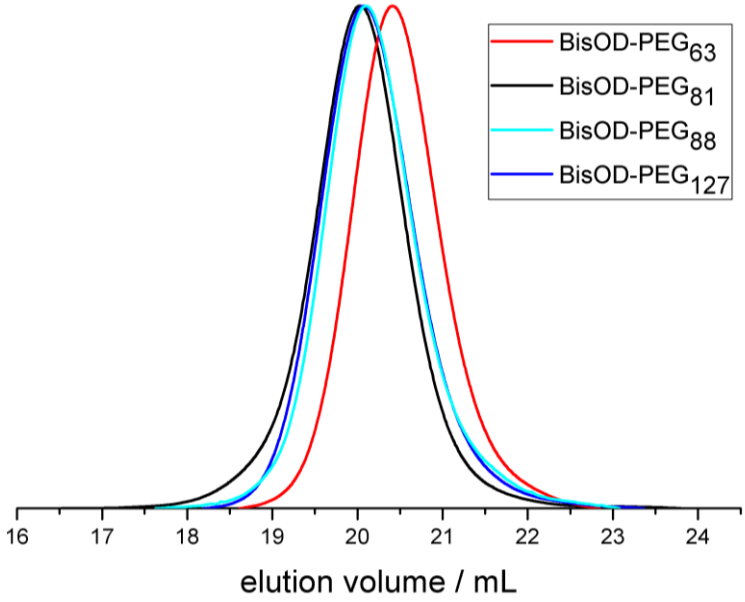

Figure S40. SEC traces (DMF, PEG standard, RI signal) of the synthesized BisOD-PEGs.

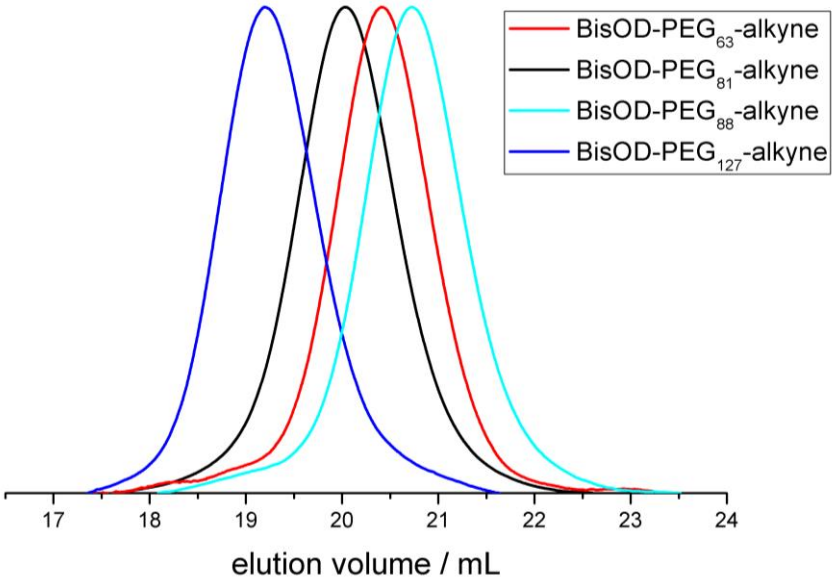

Figure S41. SEC traces (DMF, PEG standard, RI signal) of the synthesized BisOD-PEG-alkyne.

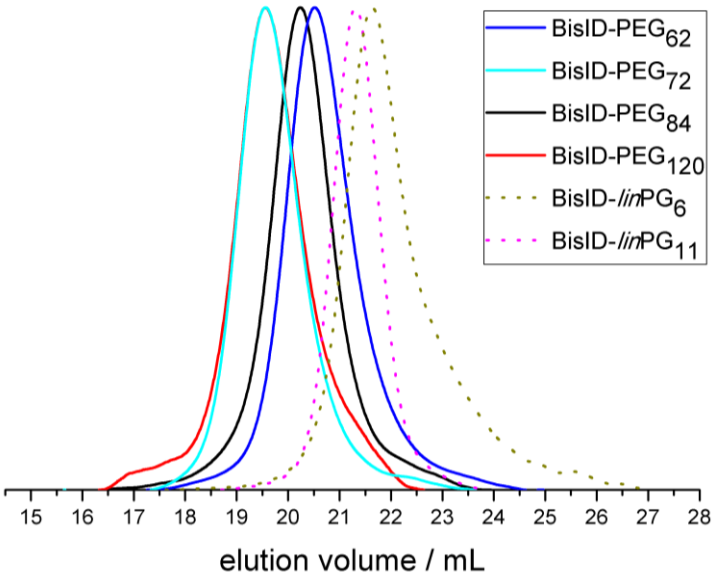

Figure S42. SEC traces (DMF, PEG standard, RI signal) of the synthesized BisID-PEGs and BisID-*lin*PGs.

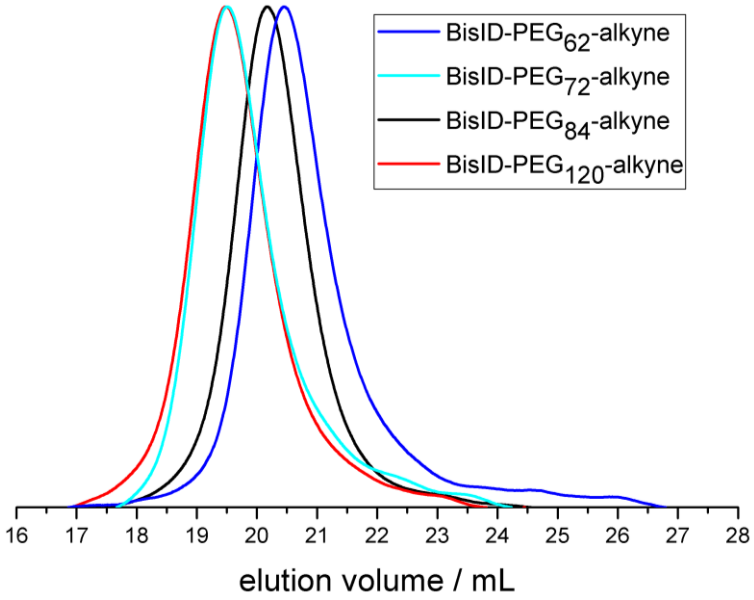

Figure S43. SEC traces (DMF, PEG standard, RI signal) of the functionalized BisID-PEG-alkyne**.**

4. References

(1) Fitton, A. O.; Hill, J.; Jane, D. E.; Millar, R. Synthesis of Simple Oxetanes Carrying Reactive 2-Substituents. *Synthesis* **1987**, 1140–1142.

(2) Stauch, O.; Uhlmann, T.; Fröhlich, M.; Thomann, R.; El-Badry, M.; Kim, Y.-K.; Schubert, R. Mimicking a Cytoskeleton by Coupling Poly(N -isopropylacrylamide) to the Inner Leaflet of Liposomal Membranes: Effects of Photopolymerization on Vesicle Shape and Polymer Architecture. *Biomacromolecules* **2002**, *3*, 324–332.

2.2 Amphiphilic PEG with pH-sensitive Units Introduced *via* Anionic Ring-opening Copolymerization of EO and EPB Using a Hydrophobic Initiator

Ann-Kathrin Danner,[a,b] Larissa Bessler[a] and Holger Frey[a, *]

[a]Institute of Organic Chemistry, Johannes Gutenberg-University Mainz, Duesbergweg 10-14, 55128 Mainz, Germany.

[b]Graduate School Materials Science in Mainz, Staudinger Weg 9, 55128 Mainz, Germany.

E-Mail: hfrey@uni-mainz.de

To be submitted to *Macromolecular Rapid Communications*.

Abstract

The synthesis of amphiphilic and pH-sensitive polyethylene glycol (PEG) copolymers, using a hydrophobic initiator and incorporating vinyl ether moieties into the backbone is presented. Crown ether assisted anionic ring-opening polymerization (AROP) of ethylene oxide and 3,4-epoxy-1-butene (EPB) with potassium as a counterion enabled the use of 1,2-bis-*n*-octadecyl glyceryl ether (BisOD) as an initiator, which can be inserted in lipid membranes. The AROP leads to copolymers with defined molecular weights (2540–4470 g mol^{-1}) and narrow molecular weight distributions (1.09–1.26). Furthermore, the reaction conditions directly resulted in the primary formation of vinyl moieties instead of allyl groups. Hence, post-polymerization isomerization is not required. In order to investigate the pH sensitivity and cleavage of the copolymers ^{1}H NMR kinetic studies were performed and the degradation products are analyzed using size exclusion chromatography (SEC). Due to the hydrophobic anchor structure, the copolymers can be integrated into liposomes, which renders them promising candidates for drug delivery systems.

Table of Contents Graphics

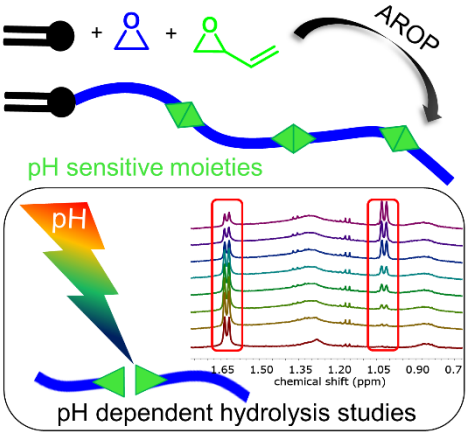

Introduction

Numerous PEGylated liposomes are FDA-approved and therefore play an important role in medical applications.[1] Polyethylene glycol (PEG), which is used for PEGylation possesses several advantageous characteristics, such as excellent biocompatibility and prolonged blood circulation times. Nevertheless, the introduction of cleavable moieties enabling biodegradability of PEG maybe beneficial to further tune pharmacokinetics of PEGylated lipids or drugs and aid to overcome the molecular weight threshold of 30 kDa for application of PEG in the body. The cleavage of sensitive units may take place either in reductive intracellular compartments of the cell with the aid of redox-responsive groups,[2] in tumor tissue[3,4] or in the endosomal/lysosomal compartment *via* acid-cleavable moieties.[5,6] Examples for degradable units are *e.g.* ortho esters,[7–9] *cis*-aconitic acids,[10] hydrazones[11,12] or silyl ethers[13]. In order to generate an oxidation-responsive polyether, the copolymerization of EO and 2-(methylthio)ethyl glycidyl ether can be applied.[14] Furthermore, cleavable acetal moieties can be introduced into the PEG chain, but unfortunately only one or two degradable moieties can be integrated and acetals show cleavage at rather low pH values of 4 or below.[15] To obtain multiple acetal groups as cleavage sites, the synthesis of hyperbranched polyether-lipids is an option.[16] By introducing one single pH-sensitive vinyl ether group in PEG-lipids[17–21] the hydrolysis rate of vinyl ethers can be adjusted *via* the substitution pattern, and vinyl ethers are therefore highly promising as pH-sensitive units.[22–24] In this context, Lynd and coworkers copolymerized ethylene oxide (EO) and epichlorohydrin (ECH), followed by an elimination of the methyl chloride moiety, leading to the formation of methylene ethylene oxide (MEO) units and thus cleavable PEG.[25] Unfortunately, due to the disparate reactivities of EO and ECH, the monomer-activated polymerization of EO and ECH leads to the formation of tapered block-copolymers.[26] Therefore, polymer cleavage leads to long PEG segments that are still present after degradation. Consequently, a rather random distribution of the comonomer along the PEG chain is necessary.

Recently, Worm *et al.* introduced the anionic ring-opening copolymerization of 3,4-epoxy-1-butene (EPB) and EO leading to well-defined structures with pH-cleavable vinyl groups. The copolymers exhibited narrow molecular weight distributions, a defined end group for bioconjugation and the possibility to adjust the amount of incorporated cleavable units. In

addition, the polymers showed excellent storage stability, despite their cleavage at physiological pH of around 5 in buffer solution.[27]

The use of crown ethers for oxyanionic polymerization has been studied in various works, especially for the AROP of propylene oxide (PO)[28–31] and recently for the copolymerization of PO and *N*,*N*-diethyl glycidyl amine (DEGA). Addition of a crown ether leads to a separation of the counter ion from the chain end and thus higher reactivity of the propagating species. By applying this strategy high molecular weights PPO were obtained and copolymers of PO and DEGA as well as PDEGA homopolymers were prepared.[32]

Transferring the synthetic approach from Worm *et al.*[27] to amphiphilic structures, which enable the preparation of PEGylated "stealth" liposomes[33,34] with defined pH-dependent cleavage sites is promising to obtain drug delivery systems with triggered release. However, the copolymerization is restricted to initiators that are soluble in DMSO, and thus the range of applications is limited. Hence, the strategy of Worm *et al.*[27] has to be modified to enable the synthesis of amphiphilic copolymers, using a hydrophobic initiator. By changing the solvent, the counter ion has to be adapted as well, which requires further adjustments to avoid the occurrence of β-elimination.[27] In this context, crown ethers can be applied to complex the counter ion and suppress interaction with the growing chain end. **Scheme 1** shows the synthetic approach developed in this work for the copolymerization of ethylene oxide (EO) and 3,4-epoxy-1-butene (EPB) in the presence of a highly nonpolar initiator.

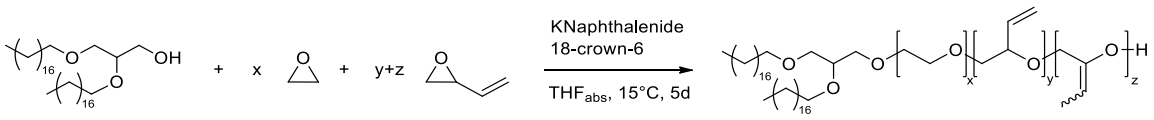

Scheme 1. Copolymerization of ethylene oxide (EO) and 3,4-epoxy-1-butene (EPB) with 1,2-bis-*n*-octadecyl glyceryl ether (BisOD) as initiator.

Results and Discussion

The anionic ring-opening polymerization (AROP) was applied to synthesized well-defined copolymers of ethylene oxide (EO) and 3,4-epoxy-1-butene (EPB) resulting in P(EPB-*co*-EG). The AROP strategy enables the synthesis of copolymers with tailored molecular weights and adjustable EPB content. 1,2-Bis-*n*-octadecyl glyceryl ether (BisOD) was used as an initiator for the statistical copolymerization to obtain amphiphilic polyether-based lipids BisOD-p(EPB-*co*-EG) (**Scheme 1**). The initiator was synthesized in a straight forward two-step procedure based on the work of Stauch e*t al*.

The AROP was carried out in dry tetrahydrofuran (THF) instead of DMSO due to the insolubility of the hydrophobic initiator BisOD in polar solvents. Potassium naphthalenide was used for deprotonation of the initiator. This process was followed by a color change of the initiator solution. In addition, 18-crown-6 was added to complex the potassium cation to suppress β-elimination, which was reported to be a problematic side reaction by Worm *et al*.[27] The amount of employed crown ether was 1.75 eq. or 2.25 eq. with respect to the amount of applied potassium to ensure full complexation of the cation. The ratio for complexation was chosen according to values given in literature (ratio 28-crown-6 to $K^+ \geq 1.5$).[31] The reaction was carried out at different temperatures, *i.e.* at 5, 10, 15 and 20 °C. All polymerizations led to a higher ratio of vinyl groups instead of allyl groups and still high conversion with only marginal β-elimination (≤ 12 mol%). Therefore, the polymerization was also generally permitted to run for 5 days. Subsequently, for the removal of 18-crown-6, liquid-liquid extraction was applied using dichloromethane and saturated sodium bicarbonate solution.

Successful copolymerization was confirmed by ^{1}H NMR spectroscopy. In this context, the characteristic olefinic NMR signals for allyl and vinyl groups as well as the broad polyether backbone signal and the initiator signals were observed. Due to different signals for the vinyl and allyl groups in the ^{1}H NMR spectrum, the degree of isomerization was determined, revealing a vinyl content between 60 and 80% after the polymerization as shown in **Table 1**. However, (*E*)- and (*Z*)-isomers of the vinyl groups are indistinguishable due to overlap of these signals with the initiator signal. Furthermore, ^{1}H NMR spectroscopy was applied to determine the molecular weights of the synthesized polyether-based lipids. The copolymers exhibit molecular weights in a range of 2540–4470 g mol^{-1} and were

slightly lower than expected from the monomer/initiator ratio, which is due to the occurring β-elimination (see **Table 1**). In addition, the EPB content incorporated in the copolymers was also calculated using ^{1}H NMR spectroscopy by comparison of the signal intensity of the initiator both with the polyether backbone and the olefinic proton signals of EPB. The amount of EPB was varied between 2.3 and 5.9 mol% to obtain a sufficient concentration of cleavage sites, albeit minimizing the amount of small PEG segments after cleavage, since oligomers of PEG (oligo(ethylene glycol) ≤ 400 g mol^{-1}) are toxic in biomedical applications due to enzyme catalyzed oxidation processes.[35,36]

Table 1. Properties of the synthesized BisOD-PEG and copolymers BisOD-p(EPB-*co*-EG).

#	Composition[a]	EPB[th] mol%	M_n[th] g mol^{-1}	M_n[a] g mol^{-1}	M_w/M_n[b]	Vinyl/Allyl[a] %
1	BisOD-PEG	0	5180	4180	1.09	-
2	BisOD-p(EPB$_{0.023}$-*co*-EG$_{0.977}$)	6.7	7460	3790	1.11	59:41
3	BisOD-p(EPB$_{0.026}$-*co*-EG$_{0.974}$)	3.3	7330	3990	1.09	75:25
4	BisOD-p(EPB$_{0.030}$-*co*-EG$_{0.970}$)	10	7590	2540	1.13	77:23
5	BisOD-p(EPB$_{0.031}$-*co*-EG$_{0.969}$)	5.3	7410	5260	1.12	63:37
6	BisOD-p(EPB$_{0.034}$-*co*-EG$_{0.966}$)	6.7	7460	2680	1.09	63:37
7	BisOD-p(EPB$_{0.037}$-*co*-EG$_{0.963}$)	3.3	7330	3870	1.10	74:26
8	BisOD-p(EPB$_{0.040}$-*co*-EG$_{0.960}$)	5.3	7410	3080	1.14	77:23
9	BisOD-p(EPB$_{0.045}$-*co*-EG$_{0.955}$)	6.7	7460	3290	1.23	56:44
10	BisOD-p(EPB$_{0.059}$-*co*-EG$_{0.941}$)	10	7590	4470	1.26	60:40

[a]determined using ^{1}H NMR spectroscopy.
[b]obtained via SEC measurements.

The copolymers were further characterized using size exclusion chromatography (SEC) indicating monomodal and narrow molecular weight distributions with dispersity ranging

from 1.09 to 1.26 (calculated *via* SEC using PEG standard) for all copolymers. Furthermore, the SEC elugram reveals a shift to lower elution volume for higher molecular weights as shown in **Figure 1**. The molecular weight determined *via* size exclusion chromatography (SEC) differs from the value calculated from ^{1}H NMR spectroscopy (see **Table S1**). Molecular weights measured by SEC are underestimated due to differences of the hydrodynamic volume of the polymers and the PEG standard used for calibration. In addition, the amphiphilic character of the copolymers may also influence the hydrodynamic volume and lead to an underestimation of the molecular weight.

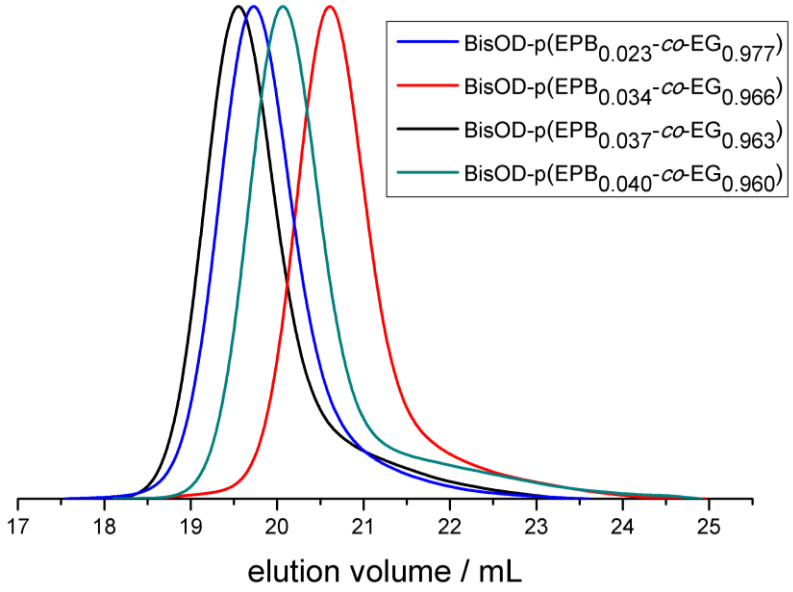

Figure 1. Selection of SEC traces (DMF, PEG standard, RI signal) of BisOD-p(EPB-*co*-EG).

Using differential scanning calorimetry (DSC), the thermal properties of all copolymers were investigated. All copolymers exhibit a glass transition temperature T_g and a melting temperature T_m, indicating crystalline materials, as expected, considering the small amount of comonomer incorporated. The T_g was generally between –70 and –56 °C, and the melting temperature T_m of the copolymers ranged from 30 to 42 °C (**Table S2** and **Figure S9**). The T_m decreases with increasing amount of EPB units incorporated in the copolymers due to frequent disruption of the PEG segments. In contrast, BisOD-PEG exhibits no T_g but possesses a T_m at 54 °C. The DSC measurements revealed only a marginal influence of the EPB content in the copolymers on the T_g.

Cleavage of the vinyl groups of the EPB monomer units was investigated at different pH values. For these studies, the amphiphilic copolymer was dissolved in D_2O at a defined pH

value and incubated at 37 °C. The kinetics of the hydrolysis was measured directly in the NMR tube. ^{1}H NMR spectra were recorded manually over a time period of 768 h to monitor the cleavage of the vinyl groups. Following this procedure, the stability of the copolymers was investigated at pH 3.5, which can be translated to pD 3.9, pH 4.0 or rather pD 4.9, pH 4.5, which equals pD 4.9 and pH 7.0 or rather pD 7.4. The hydrolysis was monitored *via* the decrease of the signal intensity of EPB units and in the same time increase of the signals of the ketone end groups (see **Figure 2**). As expected, the degradation was faster at lower pH and decreased with increasing pH value. At pH 3.5 the amphiphilic polyether was fully degraded after 5 days although a fraction of allyl groups was still present before hydrolysis. Hydrolysis at pH 4.0 was carried out for12 days to reach full degradation and at pH 4.5 complete fragmentation was obtained after 32 days. In comparison Worm *et al.* reported half-lives of 12 h (pD 4.4), 28 h (pD 4.9) and 112 h (pD 5.4) for fully isomerized copolymers.[27]

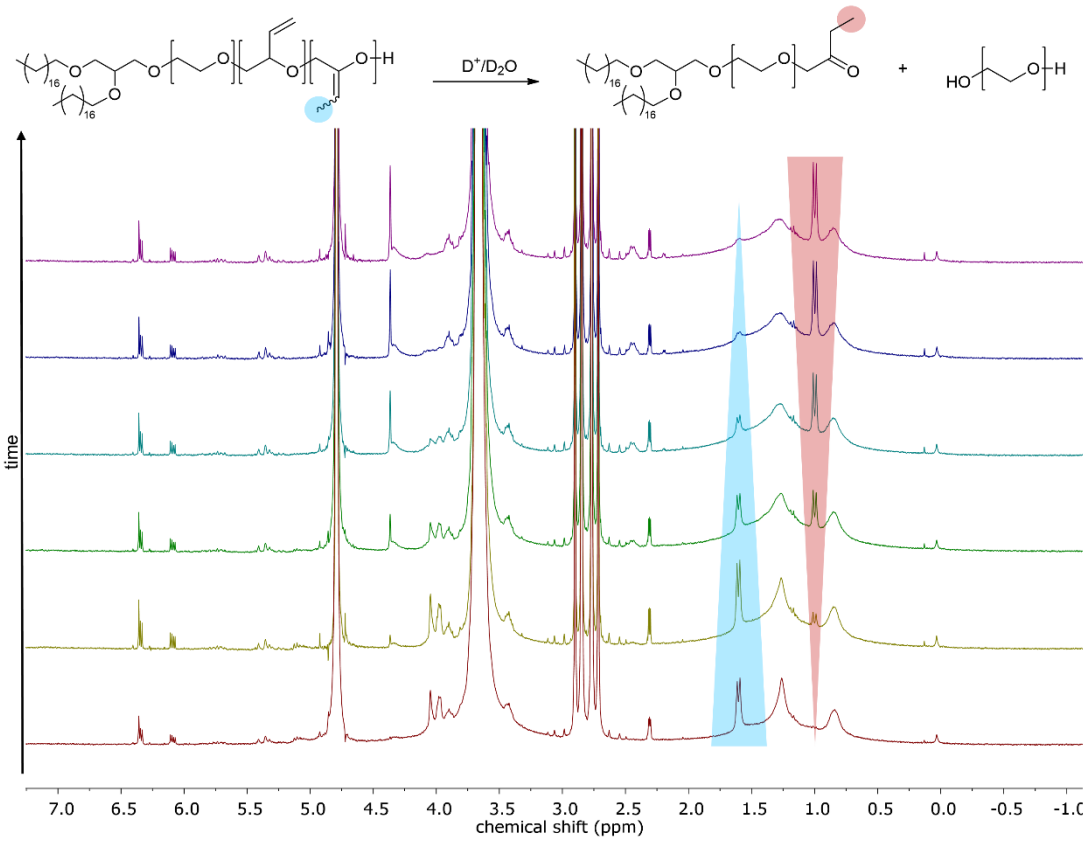

Figure 2. Reaction scheme for the hydrolysis of BisOD-p(EPB-*co*-EG) to ketone end groups and PEG fragments (top). Selection of ^{1}H NMR (D_2O, 300 MHz) spectra of the hydrolysis of BisOD-p($EPB_{0.032}$-*co*-$EG_{0.968}$) at pH 3.5 and incubation at 37 °C (bottom). The decrease of the signal intensity of the vinyl moieties and the increase of the signal intensity of the ketone end groups is highlighted by colored arrows.

At pH 7.0 the copolymer showed very good stability, and even after 768 h at 37 °C no degradation was observed in the ^{1}H NMR spectrum (**Figure S12**). This was also confirmed *via* SEC measurements, revealing a narrow and monomodal size distribution (**Figure S13**). Furthermore, the degradation products of all copolymers after full hydrolysis were studied. To this end, the amphiphilic polyethers were dissolved in diluted hydrochloric acid (c = 0.1 mol L^{-1}) and stirred for 24 h. After removal of the solvent the hydrolyzed copolymers were investigated *via* SEC. The measurement revealed degradation products around 1000 g mol^{-1} with moderate dispersities between 1.48 and 1.79 depending on the amount of incorporated EPB (see **Figure 3** and **Table S3**). As expected, the hydrolyzed copolymers exhibit lower molecular weights with higher EPB content and *vice versa*. Thus, the molecular weight of the hydrolysis fragments can be adjusted *via* the amount of incorporated EPB, which is relevant for biomedical applications, as described above. In addition, the amphiphilic copolymers exhibit excellent storage stability and were still stable after 5 months storage at 4 °C (**Figure S14**).

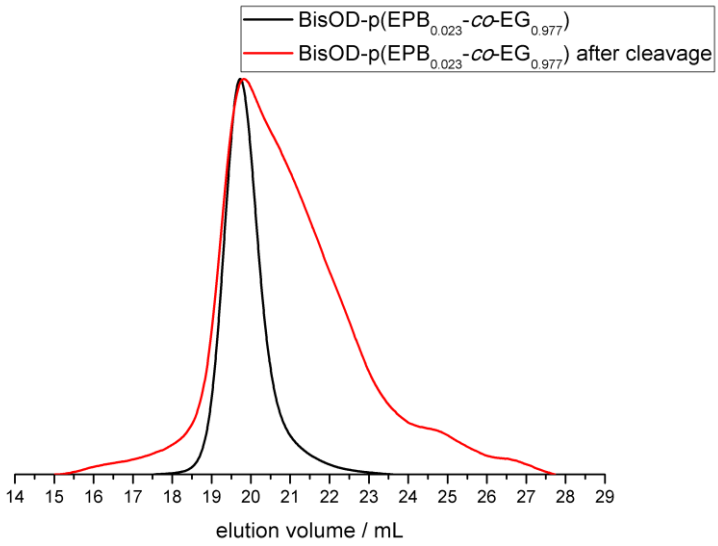

Figure 3. SEC elugram (DMF, PEG standard, RI signal) of BisOD-p(EPB$_{0.023}$-*co*-EG$_{0.977}$) after copolymerization (black) and after hydrolysis with diluted HCl (0.1 mol L^{-1}).

These amphiphilic polyethers can be applied in drug delivery systems, particularly in liposomes. As a proof of principle, liposomal nanocarriers were prepared in which the pH-sensitive polyether-based lipid BisOD-p(EPB$_{0.023}$-*co*-EG$_{0.977}$) was integrated. Liposome preparation was carried out in analogy to previous reported procedures[37] using a dual centrifuge (DC),[38] which enables the preparation of liposomes in small batch sizes.[39] For

that purpose, a lipid composition of 50 mol% egg-phosphatidylcholine (EPC), 45 mol% cholesterol and 5 mol% BisOD-p(EPB$_{0.023}$-*co*-EG$_{0.977}$) was applied to obtain pH-sensitive liposomes (L1). The formulated nanoparticular suspension was investigated *via* light scattering (DLS), using a zeta-sizer and revealing a size of 151.4 nm in diameter and narrow dispersity (PDI 0.216). The polydispersity index was obtained from cumulant analysis and is unrelated to the polydispersities obtained from SEC measurements (M_w/M_n). For comparison also liposomes without pH-sensitive polyether lipids were prepared (55 mol% EPC and 45 mol% cholesterol) (L2). As shown in **Figure 4**, the liposomal formulation without BisOD-p(EPB$_{0.023}$-*co*-EG$_{0.977}$) exhibits larger particles (190.0 nm) with a broader dispersity (0.292).

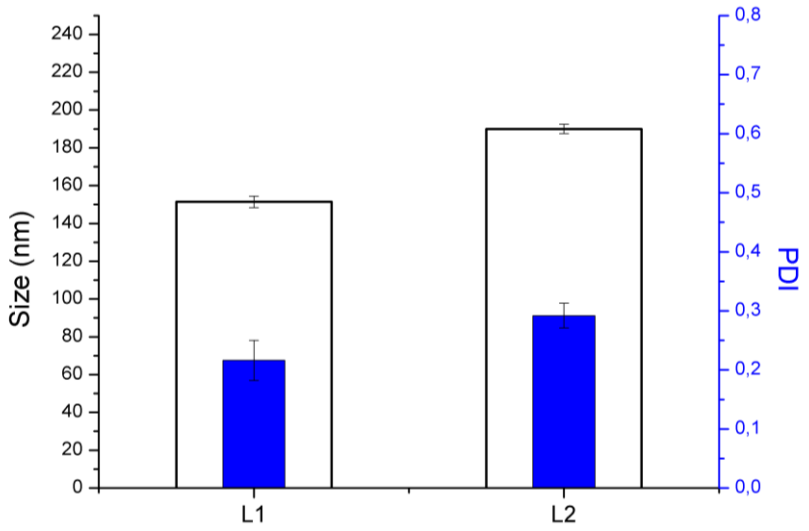

Figure 4. Diameters of liposomes (white bar, left axis) and PDI (blue bar, right axis) of liposomal formulation determined by dynamic light scattering (error bar show standard deviation (SD) from a technical triplicate). L1 represents the formulated nanoparticular suspension with integrated polyether lipid BisOD-p(EPB$_{0.023}$-*co*-EG$_{0.977}$). L2 represents a nanoparticular suspension consisting of EPC and cholesterol.

This first results demonstrate the suitability of the prepared pH-sensitive lipids for their incorporation into liposomes, rendering them promising candidates for drug delivery applications. Future work will aim at an investigation of the cleavage of the pH-sensitive moieties after liposomal formulation and their impact on pharmacokinetic properties.

Conclusion

The copolymerization of EO and EPB was reported by Worm *et al*.[27] In this work, we used a hydrophobic initiator, which can be incorporated into lipid membranes, for the copolymerization, leading to amphiphilic and pH-sensitive PEG. For this purpose, the reaction conditions had to be adjusted, *i.e.* the polymerization was carried out in tetrahydrofuran (THF) as a less polar solvent compared to dimethyl sulfoxide (DMSO), which required the use of potassium as a counter ion. To suppress the occurring β-elimination, crown ethers were necessary to complex the counter ion. These alterations of the polymerization conditions led to the primary formation of vinyl ethers (allyl groups still present in the copolymer were ≤44%), thus isomerization *via* Wilkinson´s catalyst was avoided. The β-elimination could not be suppressed completely, but could be limited to ≤12 mol%. Nevertheless, all polymers exhibit monomodal and narrow size distributions with dispersities between 1.09 and 1.26 and well-defined molecular weights of 2540–4470 $g \cdot mol^{-1}$. Despite the one-step procedure, omitting a second isomerization step, pH dependent hydrolysis resulted in full degradation at pH 3.5, pH 4.0 and pH 4.5 in a time frame of 5 to 32 days and excellent stability at pH 7.0. After 768 h at 37 °C the polyether lipids were still stable and no degradation was observed. Furthermore, as proof of principal the copolymer was integrated successfully into liposomal nanocarriers, leading to particles with diameters of 151.4 nm and narrow size distributions. Due to the good biocompatibility of PEG and the pH-sensitive moieties these polyether lipids are promising candidates for drug delivery systems that exhibit a triggered pH-dependent release.

Acknowledgments

A. Danner is a recipient of a DFG-funded position through the Excellence Initiative by the Graduate School Materials Science in Mainz (GSC 266). The authors thank Matthias Voigt for liposome preparation and characterization. Furthermore, the authors thank Maria Müller for DSC and Monika Schmelzer for SEC measurements.

References

(1) Milla, P.; Dosio, F.; Cattel, L. PEGylation of Proteins and Liposomes: A Powerful and Flexible Strategy to Improve the Drug Delivery. *CDM* **2012**, *13*, 105–119.

(2) Jones, D. P.; Carlson, J. L.; Mody, V. C.; Cai, J.; Lynn, M. J.; Sternberg, P. Redox state of glutathione in human plasma. *Free Radical Biology and Medicine* **2000**, *28*, 625–635.

(3) Gerweck, L. E.; Vijayappa, S.; Kozin, S. Tumor pH controls the in vivo efficacy of weak acid and base chemotherapeutics. *Molecular cancer therapeutics* **2006**, *5*, 1275–1279.

(4) Patel, N. R.; Pattni, B. S.; Abouzeid, A. H.; Torchilin, V. P. Nanopreparations to overcome multidrug resistance in cancer. *Advanced drug delivery reviews* **2013**, *65*, 1748–1762.

(5) Sun, H.; Andresen, T. L.; Benjaminsen, R. V.; Almdal, K. Polymeric Nanosensors for Measuring the Full Dynamic pH Range of Endosomes and Lysosomes in Mammalian Cells. *j biomed nanotechnol* **2009**, *5*, 676–682.

(6) Benjaminsen, R. V.; Sun, H.; Henriksen, J. R.; Christensen, N. M.; Almdal, K.; Andresen, T. L. Evaluating nanoparticle sensor design for intracellular pH measurements. *ACS nano* **2011**, *5*, 5864–5873.

(7) Chen, H.; Zhang, H.; McCallum, C. M.; Szoka, F. C.; Guo, X. Unsaturated cationic ortho esters for endosome permeation in gene delivery. *Journal of medicinal chemistry* **2007**, *50*, 4269–4278.

(8) Huang, Z.; Guo, X.; Li, W.; MacKay, J. A.; Szoka, F. C. Acid-triggered transformation of diortho ester phosphocholine liposome. *J. Am. Chem. Soc.* **2006**, *128*, 60–61.

(9) Masson, C.; Garinot, M.; Mignet, N.; Wetzer, B.; Mailhe, P.; Scherman, D.; Bessodes, M. pH-sensitive PEG lipids containing orthoester linkers: New potential tools for nonviral gene delivery. *J. Control. Release* **2004**, *99*, 423–434.

(10) DuBois Clochard, M.-C.; Rankin, S.; Brocchini, S. Synthesis of soluble polymers for medicine that degrade by intramolecular acid catalysis. *Macromol. Rapid Commun.* **2000**, *21*, 853–859.

(11) Kale, A. A.; Torchilin, V. P. Design, synthesis, and characterization of pH-sensitive PEG-PE conjugates for stimuli-sensitive pharmaceutical nanocarriers: The effect of substitutes at the hydrazone linkage on the ph stability of PEG-PE conjugates. *Bioconjug. Chem.* **2007**, *18*, 363–370.

(12) Sawant, R. M.; Hurley, J. P.; Salmaso, S.; Kale, A.; Tolcheva, E.; Levchenko, T. S.; Torchilin, V. P. "SMART" drug delivery systems: Double-targeted pH-responsive pharmaceutical nanocarriers. *Bioconjug. Chem.* **2006**, *17*, 943–949.

(13) Parrott, M. C.; Luft, J. C.; Byrne, J. D.; Fain, J. H.; Napier, M. E.; Desimone, J. M. Tunable bifunctional silyl ether cross-linkers for the design of acid-sensitive biomaterials. *J. Am. Chem. Soc.* **2010**, *132*, 17928–17932.

(14) Herzberger, J.; Fischer, K.; Leibig, D.; Bros, M.; Thiermann, R.; Frey, H. Oxidation-Responsive and "Clickable" Poly(ethylene glycol) via Copolymerization of 2-(Methylthio)ethyl Glycidyl Ether. *J. Am. Chem. Soc.* **2016**, *138*, 9212–9223.

(15) Dingels, C.; Müller, S. S.; Steinbach, T.; Tonhauser, C.; Frey, H. Universal concept for the implementation of a single cleavable unit at tunable position in functional poly(ethylene glycol)s. *Biomacromolecules* **2013**, *14*, 448–459.

(16) Müller, S. S.; Fritz, T.; Gimnich, M.; Worm, M.; Helm, M.; Frey, H. Biodegradable hyperbranched polyether-lipids with in-chain pH-sensitive linkages. *Polym. Chem.* **2016**, *7*, 6257–6268.

(17) Boomer, J. A.; Inerowicz, H. D.; Zhang, Z.-Y.; Bergstrand, N.; Edwards, K.; Kim, J.-M.; Thompson, D. H. Acid-Triggered Release from Sterically Stabilized Fusogenic Liposomes via a Hydrolytic DePEGylation Strategy †. *Langmuir : the ACS journal of surfaces and colloids* **2003**, *19*, 6408–6415.

(18) Boomer, J. A.; Qualls, M. M.; Inerowicz, H. D.; Haynes, R. H.; Patri, V. S.; Kim, J.-M.; Thompson, D. H. Cytoplasmic delivery of liposomal contents mediated by an acid-labile cholesterol-vinyl ether-PEG conjugate. *Bioconjug. Chem.* **2009**, *20*, 47–59.

(19) Kim, H.-K.; Thompson, D. H.; Jang, H. S.; Chung, Y. J.; van den Bossche, J. pH-responsive biodegradable assemblies containing tunable phenyl-substituted vinyl ethers for use as efficient gene delivery vehicles. *ACS applied materials & interfaces* **2013**, *5*, 5648–5658.

(20) Shin, J. Acid-triggered release via dePEGylation of DOPE liposomes containing acid-labile vinyl ether PEG–lipids. *J. Control. Release* **2003**, *91*, 187–200.

(21) Shin, J.; Shum, P.; Grey, J.; Fujiwara, S.-i.; Malhotra, G. S.; González-Bonet, A.; Hyun, S.-H.; Moase, E.; Allen, T. M.; Thompson, D. H. Acid-labile mPEG-vinyl ether-1,2-dioleylglycerol lipids with tunable pH sensitivity: Synthesis and structural effects on hydrolysis rates, DOPE liposome release performance, and pharmacokinetics. *Mol. Pharm.* **2012**, *9*, 3266–3276.

(22) Kresge, A. J.; Leibovitch, M. Kinetics and mechanism of the acid-catalyzed hydrolysis of 1,1-dimethoxyethene (ketene dimethyl acetal) and trimethoxyethene in aqueous solution. *J. Am. Chem. Soc.* **1992**, *114*, 3099–3102.

(23) Kresge, A. J.; Tobin, J. B. Vinyl ether hydrolysis. 25. Effect of ?: - and ?-trimethylsilyl substitution. *J. Phys. Org. Chem.* **1991**, *4*, 587–591.

(24) Leibovitch, M.; Kresge, A. J.; Peterson, M. R.; Csizmadia, I. G. Ab initio investigation of the structure and reactivity of vinyl ethers. *Journal of Molecular Structure: THEOCHEM* **1991**, *230*, 349–385.

(25) Lundberg, P.; Lee, B. F.; van den Berg, S. A.; Pressly, E. D.; Lee, A.; Hawker, C. J.; Lynd, N. A. Poly(ethylene oxide)-co-(methylene ethylene oxide): A hydrolytically-degradable poly(ethylene oxide) platform. *ACS Macro Lett.* **2012**, *1*, 1240–1243.

(26) Danner, A.-K.; Leibig, D.; Vogt, L.-M.; Frey, H. *Monomer-activated Copolymerization of Ethylene Oxide and Epichlorohydrin: In Situ Kinetics Evidences Tapered Block Copolymer Formation*; Mainz, 2018.

(27) Worm, M.; Leibig, D.; Dingels, C.; Frey, H. Cleavable Polyethylene Glycol: 3,4-Epoxy-1-butene as a Comonomer to Establish Degradability at Physiologically Relevant pH. *ACS Macro Lett.* **2016**, *5*, 1357–1363.

(28) Ding, J.; Heatley, F.; Price, C.; Booth, C. Use of crown ether in the anionic polymerization of propylene oxide—2. Molecular weight and molecular weight distribution. *European Polymer Journal* **1991**, *27*, 895–899.

(29) Sato, K.; Sukegawa, T.; Oyaizu, K.; Nishide, H. Synthesis of Poly(TEMPO-Substituted Glycidyl Ether) by Utilizing t -BuOK/18-Crown-6 for an Organic Cathode-Active Material. *Macromol. Symp.* **2015**, *351*, 90–96.

(30) Stolarzewicz, A.; Neugebauer, D.; Grobelny, Z. Influence of the kind of crown ether on the anionic polymerization of (phenoxymethyl)oxirane initiated by potassium tert-butoxide. *Macromol. Chem. Phys.* **1995**, *196*, 1301–1306.

(31) Ding, J.; Price, C.; Booth, C. Use of crown ether in the anionic polymerization of propylene oxide—1. Rate of polymerization. *European Polymer Journal* **1991**, *27*, 891–894.

(32) Blankenburg, J.; Wagner, M.; Frey, H. Well-Defined Multi-Amino-Functional and Stimuli-Responsive Poly(propylene oxide) by Crown Ether Assisted Anionic Ring-Opening Polymerization. *Macromolecules* **2017**, *50*, 8885–8893.

(33) Woodle, M. C.; Lasic, D. D. Sterically stabilized liposomes. *Biochim. Biophys. Acta, Rev. Biomembr.* **1992**, *1113*, 171–199.

(34) Papahadjopoulos, D.; Allen, T. M.; Gabizon, A.; Mayhew, E.; Matthay, K.; Huang, S. K.; Lee, K.-D.; Woodle, M. C.; Lasic, D. D.; Redemann, C. *et al.* Sterically stabilized liposomes: Improvements in pharmacokinetics and antitumor therapeutic efficacy. *Proc. Natl. Acad. Sci. U.S.A.* **1991**, *88*, 11460–11464.

(35) Knop, K.; Hoogenboom, R.; Fischer, D.; Schubert, U. S. Poly(ethylene glycol) in drug delivery: pros and cons as well as potential alternatives. *Angew. Chem. Int. Edit.* **2010**, *49*, 6288–6308.

(36) Harris, J. M.; Chess, R. B. Effect of pegylation on pharmaceuticals. *Nat. Rev. Drug. Discov.* **2003**, *2*, 214–221.

(37) Fritz, T.; Voigt, M.; Worm, M.; Negwer, I.; Müller, S. S.; Kettenbach, K.; Ross, T. L.; Roesch, F.; Koynov, K.; Frey, H. *et al.* Orthogonal Click Conjugation to the Liposomal Surface Reveals the Stability of the Lipid Anchorage as Crucial for Targeting. *Chemistry* **2016**, *22*, 11578–11582.

(38) Massing, U.; Cicko, S.; Ziroli, V. Dual asymmetric centrifugation (DAC)--a new technique for liposome preparation. *J. Control. Release* **2008**, *125*, 16–24.

(39) Fritz, T.; Hirsch, M.; Richter, F. C.; Müller, S. S.; Hofmann, A. M.; Rusitzka, Kristiane A K; Markl, J.; Massing, U.; Frey, H.; Helm, M. Click modification of multifunctional liposomes bearing hyperbranched polyether chains. *Biomacromolecules* **2014**, *15*, 2440–2448.

Supporting Information

Amphiphilic PEG with pH-sensitive Units Introduced *via* Anionic Ring-opening Copolymerization of EO and EPB Using a Hydrophobic Initiator

Ann-Kathrin Danner,[a,b] Larissa Bessler[a] and Holger Frey[a, *]

[a]Institute of Organic Chemistry, Johannes Gutenberg-University Mainz, Duesbergweg 10-14, 55128 Mainz, Germany.

[b]Graduate School Materials Science in Mainz, Staudinger Weg 9, 55128 Mainz, Germany.

E-Mail: hfrey@uni-mainz.de

1. Materials and Methods

1.1 Reagents

All chemicals were purchased from *Sigma Aldrich*, *Acros Organics*, *Fisher Scientific* or *TCI Europe* unless mentioned otherwise. Egg phosphatidylcholine (EPB) was kindly provided by *Lipoid GmbH*. Deuterated solvents (benzene-d_6, D_2O, chloroform-*d*) were obtained from *Deutero GmbH*. Ethylene oxide (EO) was obtained from *Sigma Aldrich* and must be carefully handled. 3,4-Epoxy-1-butene (EPB) was purchased from *abcr GmbH* and was dried over CaH_2 for at least 30 min and freshly distilled before usage. For the anionic ring-opening polymerization (AROP) THF was dried and stored over benzophenone/sodium.

1.2 Characterization

^1H and ^{13}C NMR spectra as well as 2D NMR spectra were recorded using a Bruker Avance III HD 300 (300 MHz, 5 mm, BBFO probe, and B-ACS 60 auto sampler) or a Bruker Avance II spectrometer operated at 400 MHz (5 mm BBFO smart probe and SampleXPress 60 auto sampler) at 296 K. Benzene-d_6, chloroform-*d* or D_2O was employed as solvent and the spectra were referenced internally to proton signals of the deuterated solvent. All spectra were analyzed using the software MestReNova version 9.0. SEC measurements were carried out in dimethylformamide with 0.25 g L^{-1} lithium bromide on an Agilent 1100 Series equipped with PSS HEMA 300/100/40 column, RI and UV detector (275 nm). Monodisperse linear PEG standards from *Polymer Standard Service GmbH* (PSS) were employed for calibration. RI signal is shown for all SEC traces, analysis was carried out using the software PSS WinGPC Unity. DSC measurements were performed on a Perkin Elmer 8200 differential scanning calorimeter and calibration was carried out using the melting points of indium (T_m = 156.6 °C) and Milli-Q water (T_m = 0 °C). 3 to 4 mg of each sample were measured in a temperature range of –95 to 100 °C (first cycle, heating rate 20 °C min^{-1}) or from –95 to 80 °C (second cycle, heating rate 10 °C min^{-1}) respectively. The values obtained from the second cycle were used to determine glass transition temperature T_g and melting temperature T_m. Liposomes were prepared using a Rotana 460 dual centrifugation (DC) from *Hettich*. Light scattering was performed on a Malvern Zetasizer Nano ZS using disposable polystyrene cuvettes. 10 µL of the purified liposome solution was diluted in 1 mL phosphate-buffered saline (PBS). After equilibration to 25 °C,

three measurements were carried out at a scattering angle of 173°. The software Zetasizer version 6.20 from *Malvern Instruments* was used for analysis.

1.3 Handling of Ethylene Oxide (EO)

The toxic, flammable and gaseous ethylene oxide (EO) must be handled with high precaution and has to be stored in pressure-proof gas bottles. It must be used only in an adequate fume hood under appropriate safety precautions. Reactions containing EO are carried out in flame-dried glassware to convert EO inside the sealed and evacuated glass apparatus and to guarantee secure handling *via* cryo-transfer techniques. Maximum batch-sizes of EO are 5 g in a 250 mL flask which must not be exceeded to avoid abrupt detachment of the septum and thus release of EO.

2. Synthesis

2.1 Synthesis of 1,2-bis-*n*-octadecyl glyceryl ether (BisOD)

The synthesis was carried out in orientation and with adaptation to literature.[1]

Dry tetrahydrofuran (THF) was placed in three-necked round bottom flask equipped with Dimroth condenser and sealed precision glass (KPG) stirrer. Under argon atmosphere and stirring 3-benzyloxy-1,2-propanediol (5.4 mL, 0.034 mol, 1 eq.), sodium hydride (3.24 g, 0.135 mol, 4 eq.) and 1-bromooctadecane (45.05 g,0.135 mol, 4 eq.) was added. The reaction mixture was stirred at 80 °C for 14 days. Solvent was removed under reduced pressure to obtain a total volume of 250 mL. Water (200 mL) and diethyl ether (200 mL) was added and the mixture was stirred overnight at room temperature. To neutralize the reaction mixture, sulfuric acid (1 mol·L^{-1}, 11 mL, 0,011 mol) was added and again stirred overnight. The organic phase was extracted three times with diethyl ether (150 mL each) and dried over sodium sulfate. The solvent was removed under reduced pressure and the crude product was purified using flash column chromatography (petroleum ether/diethyl ether 10:1). The intermediate 1,2-bis-*n*-octadecyl-3-benzyl glyceryl ether (7.26 g, 0.014 mol) was obtained as colorless solid. Yield: 41%.

1,2-Bis-*n*-octadecyl-3-benzyl glyceryl ether (7.26 g, 0.014 mol, 1 eq.) was dissolved in dichloromethane. Palladium on activated charcoal was added (5 weight percent). Hydrogen

was introduced and the mixture was stirred at room temperature for 10 days. The catalyst was removed *via* filtration over celite®. Afterwards the solvent was removed under reduced pressure to obtain 1,2-bis-*n*-octadecyl glyceryl ether (6.52 g, 0.012 mol) as colorless solid. Yield: 87%.

mp: 65.6–66.6 °C.

^{1}H NMR, COSY (400 MHz, chloroform-*d*, δ): 3.74–3.41 (m, 9H, glycerol H), 1.59–1.53 (m, 4H, -OCH_2CH_2-), 1.31–1.25 (m, 60H, -$OCH_2CH_2(CH_2)_{15}CH_3$), 0.88 (t, *J* = 13.1 Hz; 7.2 Hz, 6H; -$O(CH_2)_{17}CH_3$).

^{13}C NMR, HSQC, HMBC (101 MHz, chloroform-*d*, δ): 78.4 (glycerol C), 72.0 (-OCH_2CH_2-), 71.06 (glycerol C), 70.6 (-OCH_2CH_2-), 63.3 (glycerol C), 32.1 (-$OCH_2CH_2(CH_2)_{15}CH_3$), 30.2 (-OCH_2CH_2-), 29.7–29.5 (-$OCH_2CH_2(CH_2)_{15}CH_3$), 26.3 (-$OCH_2CH_2(CH_2)_{15}CH_3$), 22.9 (-$OCH_2CH_2(CH_2)_{15}CH_3$), 14.3 (-$O(CH_2)_{17}CH_3$).

2.2 Polymer synthesis of BisOD-PEG

1,2-Bis-*n*-octadecyl glyceryl ether (BisOD) (0.2 g, 0.36 mmol, 1 eq.) was placed in a dry Schlenk flask and dissolved in benzene (10 mL). The solution was stirred at 60 °C for 30 min and dried in vacuo for 16 h to remove moisture. Dry tetrahydrofuran (approx. 10 mL) was cryo-transferred to the Schlenk flask to dissolve the initiator. Afterwards, the initiator was deprotonated with a 0.5 M solution of potassium naphthalide in THF (0.36 mL, 0.18 mmol, 0.5 eq.) while stirring. The solution was cooled down to –80 °C and ethylene oxide (EO) (1.70 mL, 37.57 mmol, 105 eq.) was cryo-transferred using a graduated ampule. The polymerization was carried out at 60 °C for 24 h. To quench the polymerization, an excess of ethanol was added. The solvent was removed under reduced pressure, the crude product was dissolved in methanol and precipitated twice in cold diethyl ether to obtain the pure product. Yield: 99%.

^{1}H NMR, COSY (400 MHz, benzene-d_6, δ): 3.67–3.30 (m, 359H, polyether backbone and glycerol H), 1.66–1.56 (m, 4H, -OCH_2CH_2-), 1.44–1.28 (m, 58H, -$OCH_2CH_2(CH_2)_{15}CH_3$), 0.92–0.89 (m, 6H, -$O(CH_2)_{17}CH_3$).

^{13}C NMR, HSQC, HMBC (101 MHz, benzene-d_6, δ): 79.0 (glycerol C), 73.4 (polyether backbone and glycerol C), 72.4–70.9 (polyether backbone and glycerol C), 62.2 (polyether backbone and glycerol C), 32.6 (-$OCH_2CH_2(CH_2)_{14}CH_2CH_3$ (BisOD)), 31.1–301

(-OCH_2CH_2- and -$OCH_2CH_2(CH_2)_{14}CH_2CH_3$ (BisOD)), 27.0 (-$OCH_2CH_2(CH_2)_{14}CH_2CH_3$ (BisOD)), 23.4 (-$CH_2CH_2(CH_2)_{14}CH_2CH_3$ (BisOD)), 14.6 (-$O(CH_2)_{17}CH_3$ (BisOD)).

2.3 Copolymer synthesis of BisOD-p(EPB-*co*-EG)

1,2-Bis-*n*-octadecyl glyceryl ether (BisOD) (0.1 g, 0.17 mmol, 1 eq.) and 18-crown-6 (79.8 mg, 0.30 mmol, 1.8 eq.) was placed in a dry Schlenk flask and dissolved in benzene (10 mL). The solution was stirred at 60 °C for 30 min and dried in vacuo for 16 h to remove moisture. Tetrahydrofuran (approx. 10 mL) was cryo-transferred to the Schlenk flask to dissolve the initiator. Afterwards, the solution was stirred and the initiator was deprotonated with a 0.5 M solution of potassium naphthalide in THF (0.27 mL, 0.13 mmol, 0.8 eq.). 3,4-Epoxy-1-butene (EPB) (0.14 mL, 1.68 mmol, 10 eq.) was injected into the Schlenk flask with a syringe at –80 °C. Subsequently, EO (1.10 mL, 23.50 mmol, 140 eq.) was cryo-transferred using a graduated ampule. The polymerization was carried out at 15 °C for 5 days. To quench the polymerization, an excess of ethanol was added. The solvent was removed under reduced pressure and the crude product was dissolved in dichloromethane (250 mL) and extracted three times with saturated sodium bicarbonate solution (30 mL) to remove residual crown ether. The solution was dried over magnesium sulfate and the solvent was removed under reduced pressure to obtain the pure product. Yield: 97%.

^{1}H NMR, COSY (400 MHz, benzene-d_6, δ): 6.16–5.97 (m, CH_2=C*H*C- (β-elimination)), 5.86–5.72 (m, -CHC*H*=CH_2 (allyl)), 5.31–5.02 (m, -CHCH=CH_2 (allyl)), 4.78–4.73 (q, J = 6.7 Hz; -OC=C*H*CH_3 (vinyl)), 4.02–3.93 (m, -CH_2C*H*CH=CH_2, -CH_2C=CHCH_3 and CH_3CH=COC$H_2$$CH_2$-), 3.76–3.31 (m, polyether backbone), 1.74–1.72 (m, CH_3CH=CO- (vinyl)), 1.69–1-58 (m, -OCH_2CH_2- (BisOD)), 1.44–1.29 (m, -$OCH_2CH_2(CH_2)_{15}CH_3$ (BisOD)), 0.94–0.90 (m, 6H -$OCH_2CH_2(CH_2)_{15}CH_3$ (BisOD)).

^{13}C NMR, HSQC, HMBC (100.6 MHz, benzene-d_6, δ): 107.6 (-OC=*C*HCH_3 (vinyl)), 79.0 (-CH_2*C*HCH=CH_2), 73.4–68.7 (polyether backbone and glycerol C), 62.2 (polyether backbone and glycerol C), 32.6 (-$OCH_2CH_2(CH_2)_{14}CH_2CH_3$ (BisOD)), 31.1–30.1 (-OCH_2CH_2- and -$OCH_2CH_2(CH_2)_{14}CH_2CH_3$ (BisOD)), 27.0 (-$OCH_2CH_2(CH_2)_{14}CH_2CH_3$ (BisOD)), 23.4 (-$OCH_2CH_2(CH_2)_{14}CH_2CH_3$ (BisOD)), 14.7 (-$O(CH_2)_{17}CH_3$ (BisOD)), 10.72 (*C*H_3CH=CO- (vinyl)).

2.4 ^{1}H NMR Kinetics

Deuterated phosphate/citrate phosphate buffer solutions were prepared as reported earlier.[2] In order to obtain the respective pD value, the equation pD = pH + 0.4 was employed.[3] For ^{1}H NMR kinetic studies at pH 3.5 equates to pD 3.9, pH 4.0 or pD 4.4 respectively, pH 4.5 which can be translated to pD 4.9 and pH 7.0 which equals to pD 7.4, the copolymer (23.5 mg) was dissolved in 0.7 mL of deuterated buffer and transferred instantly to a NMR tube. ^{1}H NMR spectra were recorded manually at selected intervals and in between the NMR tube was placed in an oil bath at 37 °C.

2.5 SEC Hydrolysis Studies

The copolymer BisOD-p(EPB-*co*-EG) (5 mg) was dissolved in diluted hydrochloric acid (2.5 mL, c_{HCl} = 0.1 mol L^{-1}) and mixed for 24 h under exposure to air. In order to prepare the diluted hydrochloric acid, 0.01 mL $HCl_{conc.}$ was dissolved in H_2O (2.49 mL). Afterwards the solvent was removed by lyophilization and the cleaved copolymer was analyzed *via* size exclusion chromatography (SEC) measured in DMF.

2.6 Liposome preparation

Liposomes were prepared according to literature.[4] The prepared liposomal formulations had the following compositions: L1: 50 mol% egg-phosphatidylcholine (EPC), 45 mol% cholesterol and 5 mol% BisOD-p($EPB_{0.023}$-*co*-$EG_{0.977}$), L2: 55 mol% EPC and 45 mol% cholesterol. Dual centrifugation was carried out for 20 min followed by two additional centrifugation steps for 2 min each and in between the vial was turned inside the sample holder to yield uniform mixing.

3. Characterization Data

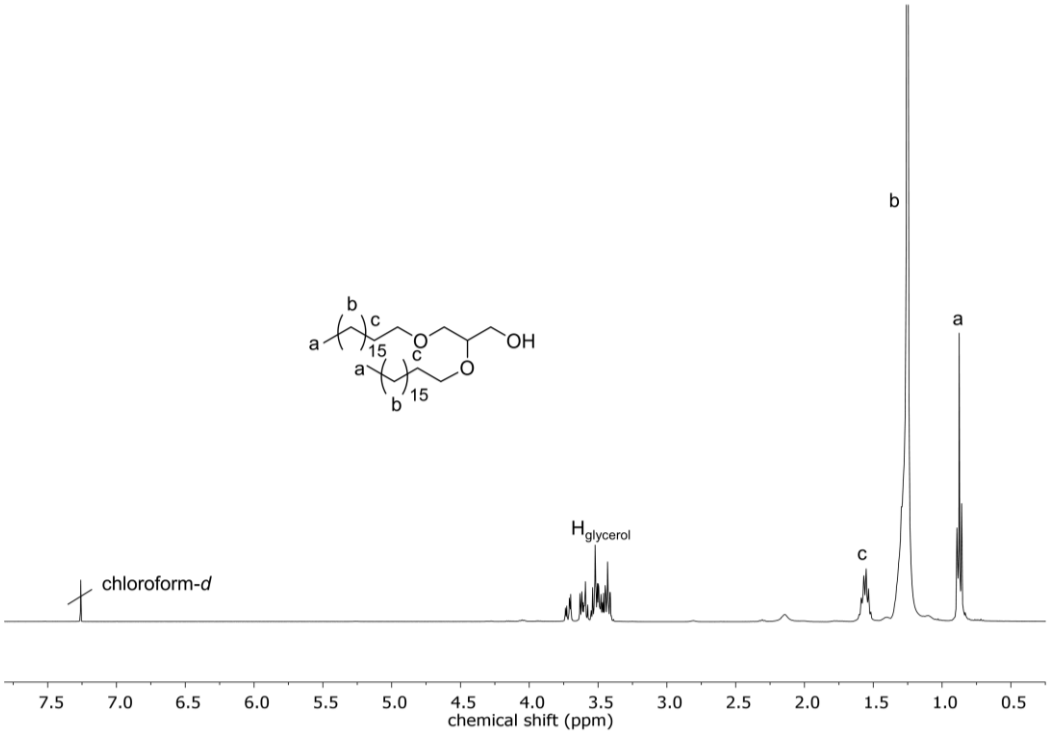

Figure S1. ^{1}H NMR (chloroform-*d*, 400 MHz) of 1,2-bis-*n*-octadecyl glyceryl ether (BisOD).

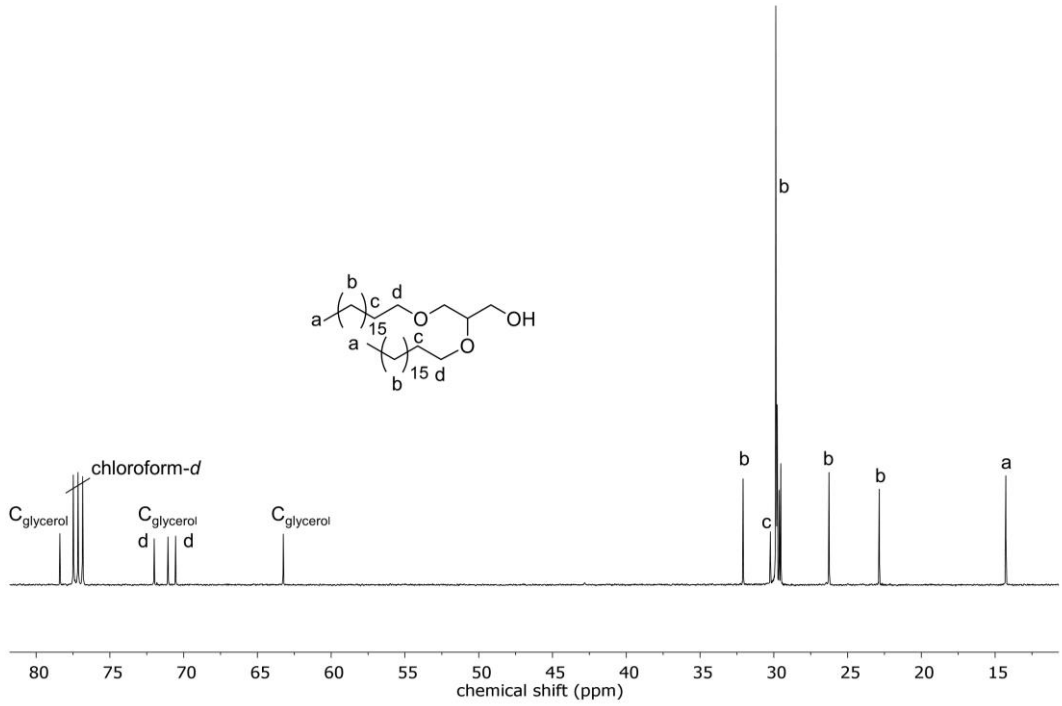

Figure S2. ^{13}C NMR (chloroform-*d*, 101 MHz) of 1,2-bis-*n*-octadecyl glyceryl ether (BisOD).

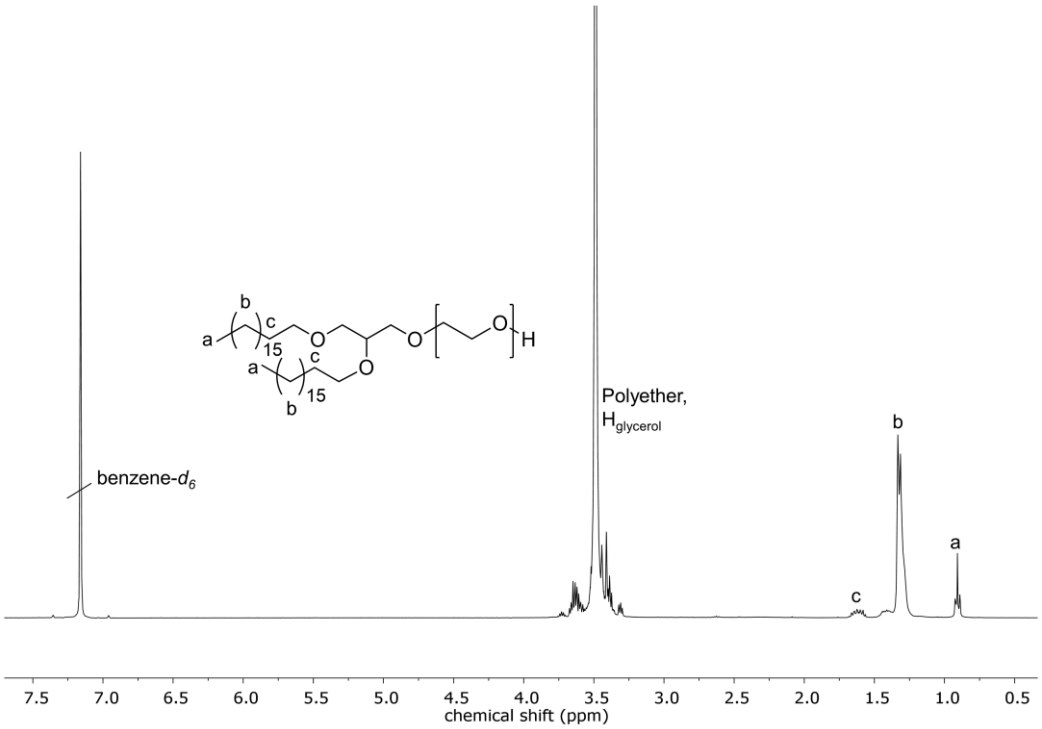

Figure S3. ^{1}H NMR (benzene-d_6, 400 MHz) of BisOD-PEG.

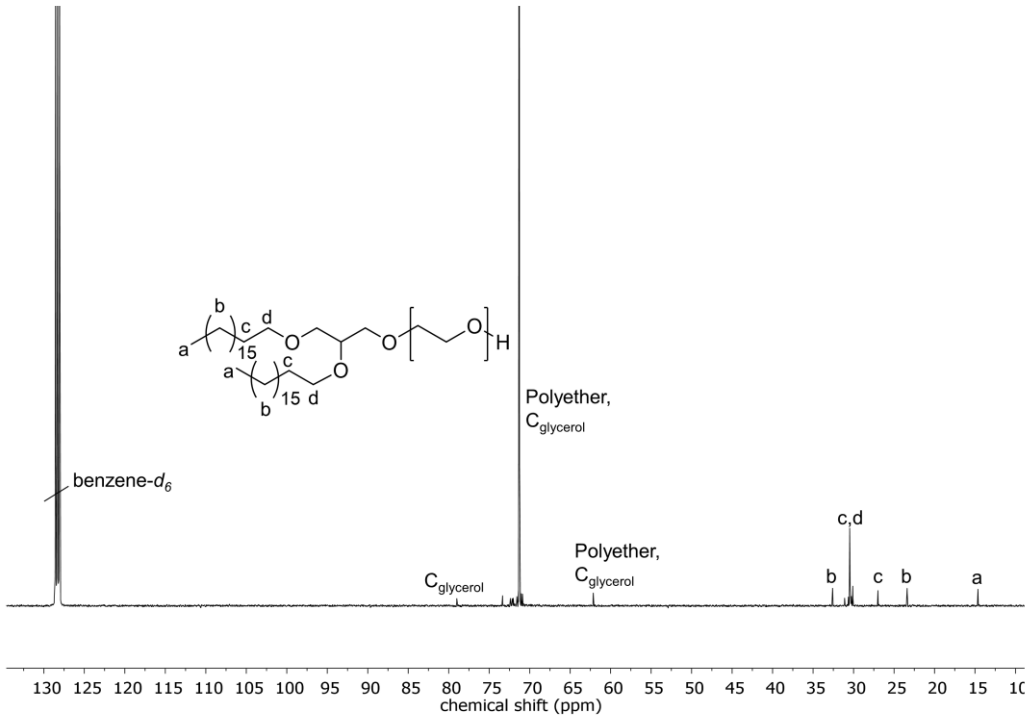

Figure S4. ^{13}C NMR (benzene-d_6, 101 MHz) of BisOD-PEG.

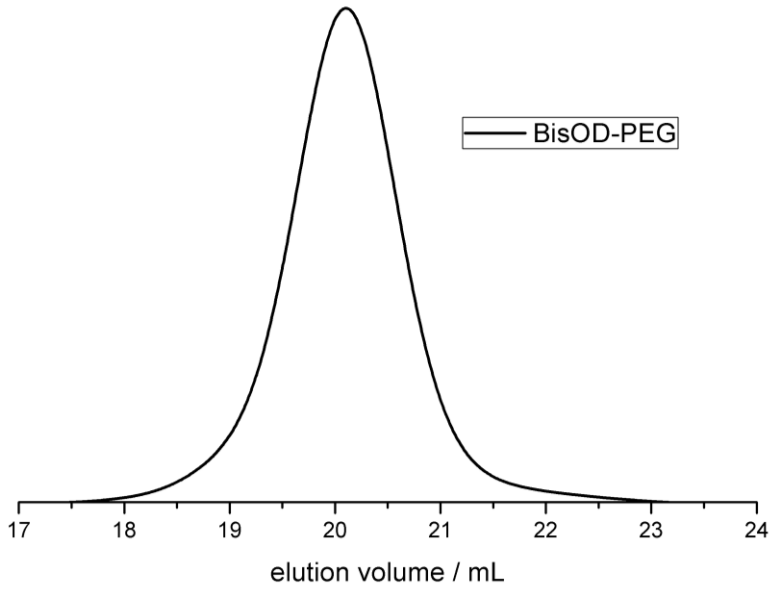

Figure S5. SEC elugram (DMF, PEG standard, RI signal) of BisOD-PEG.

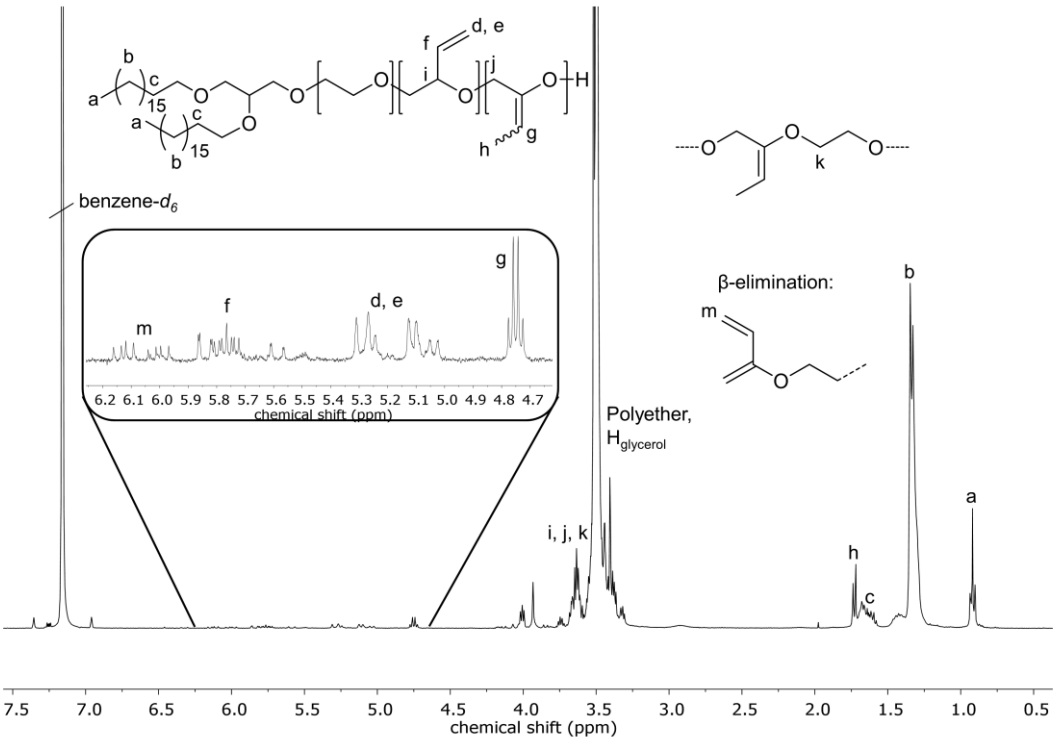

Figure S6. ^{1}H NMR (benzene-d_6, 400 MHz) of BisOD-p(EPB$_{0.023}$-*co*-EG$_{0.977}$).

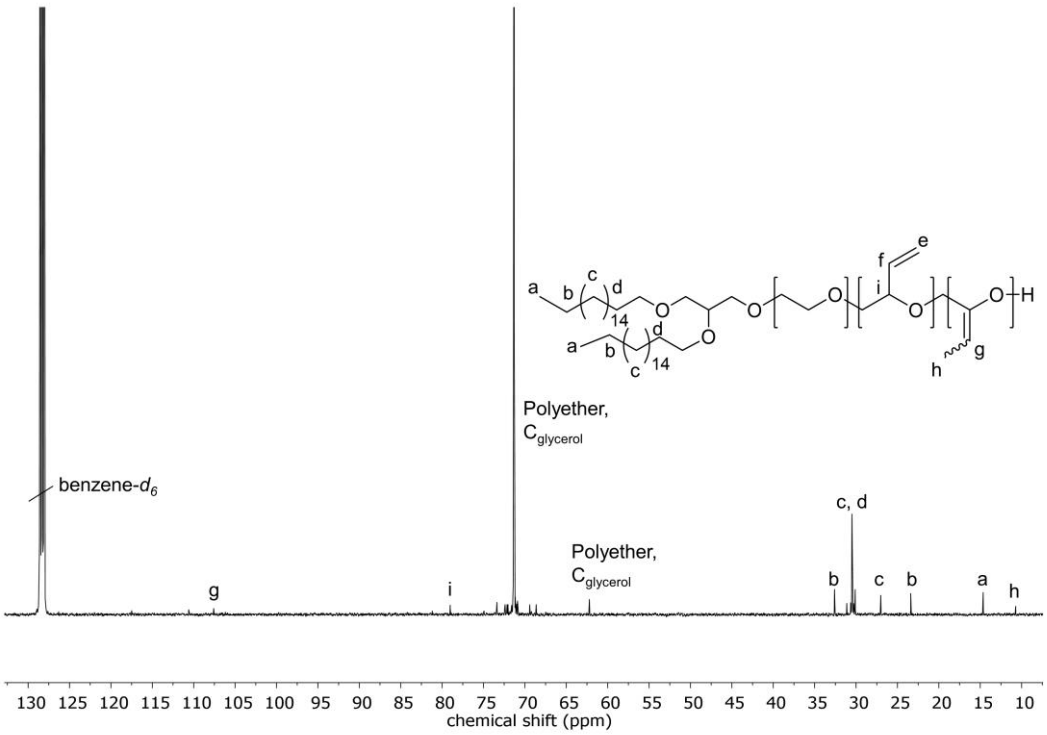

Figure S7. ^{13}C NMR (benzene-d_6, 101 MHz) of BisOD-p(EPB$_{0.023}$-*co*-EG$_{0.977}$).

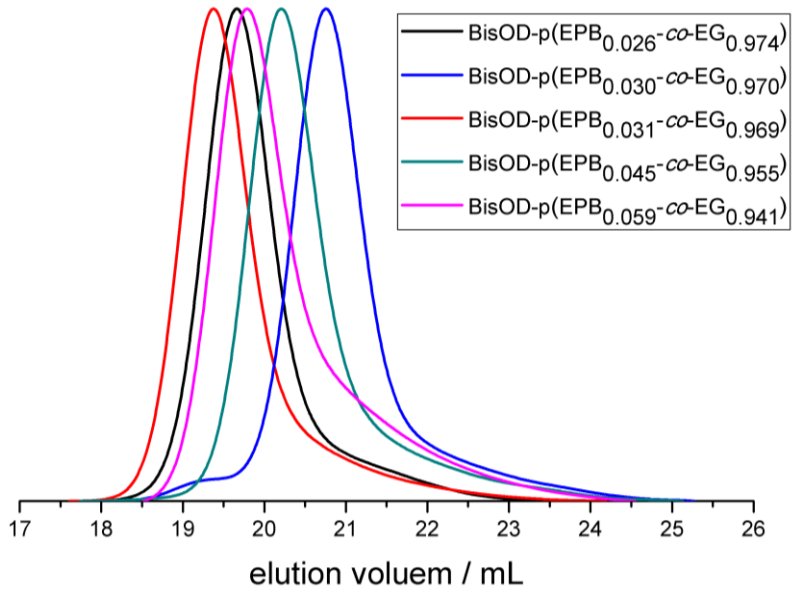

Figure S8. SEC elugram (DMF, PEG standard, RI signal) of BisOD-p(EPB-*co*-EG).

Table S1. Overview of the molecular weights calculated *via* ^{1}H NMR spectroscopy and SEC measurement as well as the amount of β-elimination determined by ^{1}H NMR spectroscopy.

#	**Composition**[a]	M_n^{NMR}	M_n^{SEC}	**β-elimination**^{NMR}
		g mol^{-1}	g mol^{-1}	mol%
1	BisOD-PEG	4180	3970	-
2	BisOD-p(EPB$_{0.023}$-*co*-EG$_{0.977}$)	3790	3030	8
3	BisOD-p(EPB$_{0.026}$-*co*-EG$_{0.974}$)	3990	2770	8
4	BisOD-p(EPB$_{0.030}$-*co*-EG$_{0.970}$)	2540	1880	10
5	BisOD-p(EPB$_{0.031}$-*co*-EG$_{0.969}$)	5260	3010	9
6	BisOD-p(EPB$_{0.034}$-*co*-EG$_{0.966}$)	2680	2030	5
7	BisOD-p(EPB$_{0.037}$-*co*-EG$_{0.963}$)	3870	2840	11
8	BisOD-p(EPB$_{0.040}$-*co*-EG$_{0.960}$)	3080	2160	12
9	BisOD-p(EPB$_{0.045}$-*co*-EG$_{0.955}$)	3290	2780	7
10	BisOD-p(EPB$_{0.059}$-*co*-EG$_{0.941}$)	4470	3110	11

[a]determined using ^{1}H NMR spectroscopy.

Table S2. Overview of the thermal properties of BisOD-PEG and BisOD-p(EPB-*co*-EG).

#	**Composition**[a]	M_n^{NMR}	T_g[b]	T_m[b]
		g mol^{-1}	°C	°C
1	BisOD-PEG	4180	-	54
2	BisOD-p(EPB$_{0.023}$-*co*-EG$_{0.977}$)	3790	–56	42
3	BisOD-p(EPB$_{0.026}$-*co*-EG$_{0.974}$)	3990	–58	38
4	BisOD-p(EPB$_{0.030}$-*co*-EG$_{0.970}$)	2540	–70	39
5	BisOD-p(EPB$_{0.031}$-*co*-EG$_{0.969}$)	5260	–61	36
6	BisOD-p(EPB$_{0.034}$-*co*-EG$_{0.966}$)	2030	–70	39
7	BisOD-p(EPB$_{0.037}$-*co*-EG$_{0.963}$)	2840	–57	37
8	BisOD-p(EPB$_{0.040}$-*co*-EG$_{0.960}$)	3080	–58	33
9	BisOD-p(EPB$_{0.045}$-*co*-EG$_{0.955}$)	3290	–59	30
10	BisOD-p(EPB$_{0.059}$-*co*-EG$_{0.941}$)	4470	–62	30

[a]determined using ^{1}H NMR spectroscopy.
[b]obtained *via* DSC measurements.

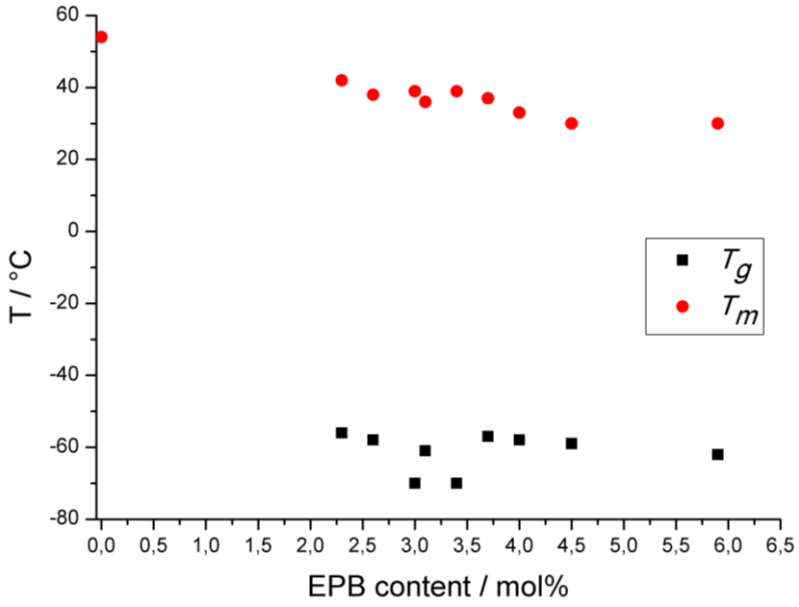

Figure S9. Thermal properties of the synthesized polymers. Glass transition temperatures T_g vs. EPB content (mol%) (▪) and melting temperatures T_m vs. EPB content (mol%) (●).

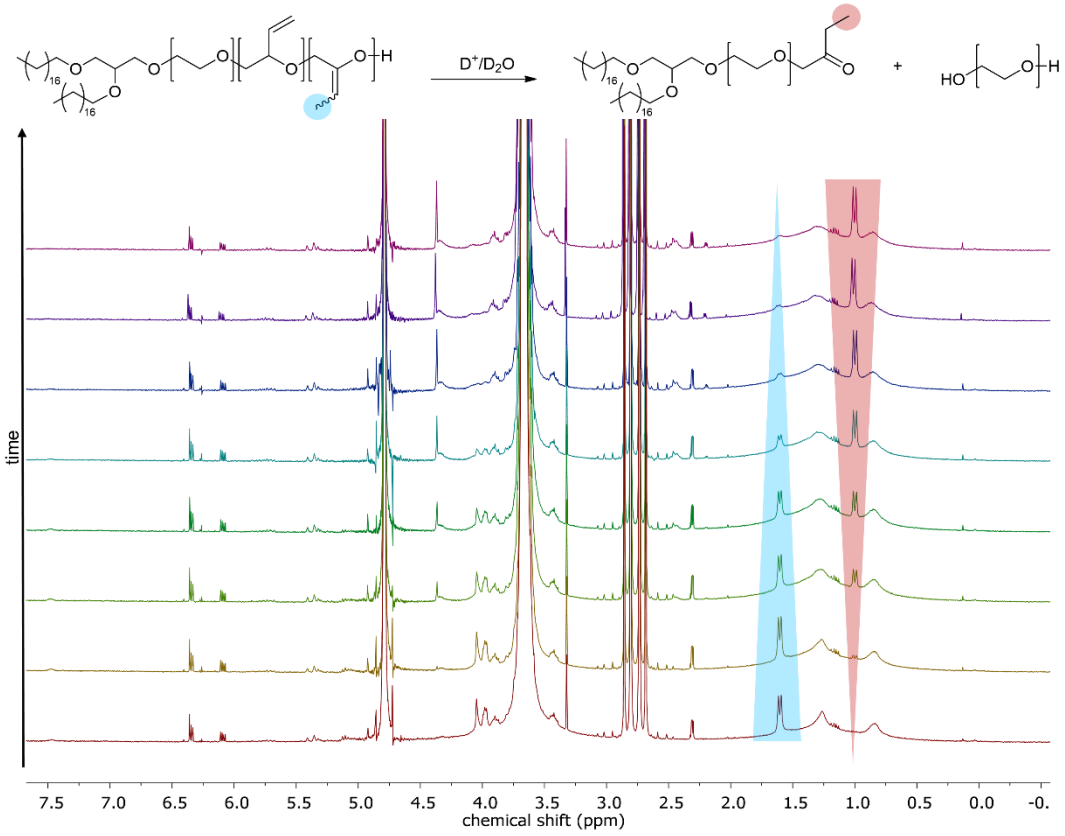

Figure S10. Reaction scheme for the hydrolysis of BisOD-p(EPB-*co*-EG) to ketone end groups and PEG fragments (top). Selection of ^{1}H NMR (D_2O, 300 MHz) spectra of the hydrolysis of BisOD-p($EPB_{0.030}$-*co*-$EG_{0.970}$) at pH 4.0 and incubation at 37 °C (bottom).

The decrease of the signal intensity of the vinyl moieties and the increase of the signal intensity of the ketone end groups is highlighted by colored arrows.

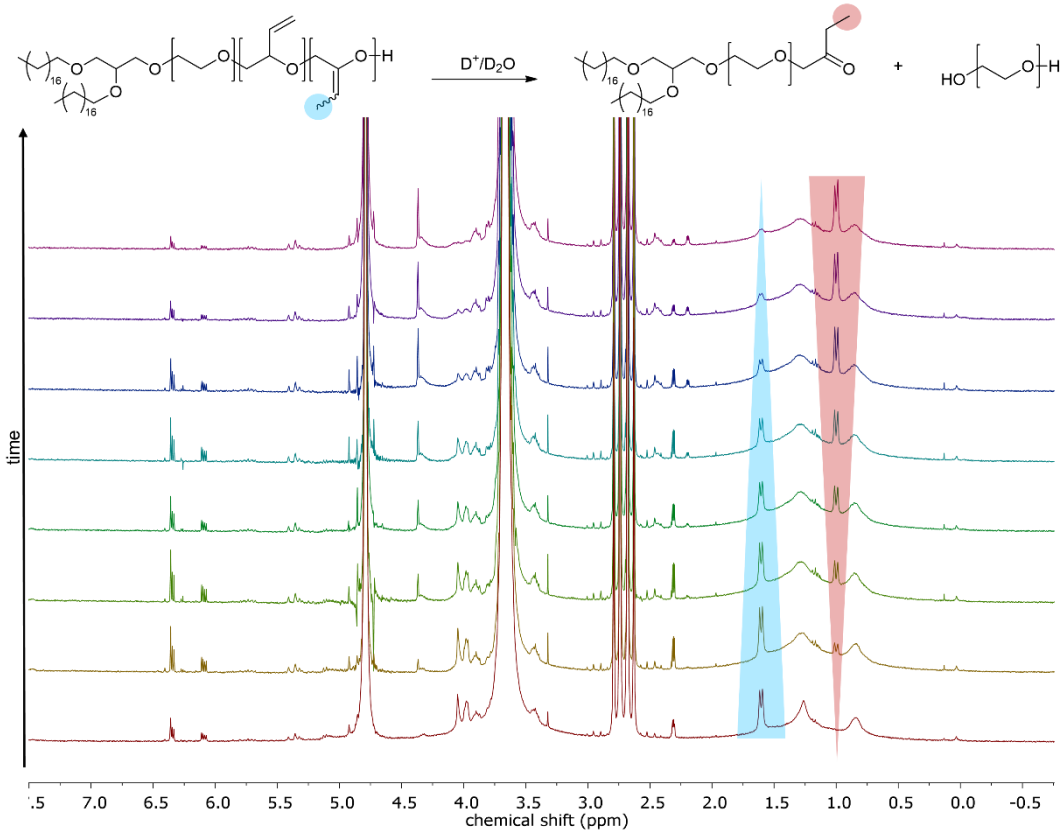

Figure S11. Reaction scheme for the hydrolysis of BisOD-p(EPB-*co*-EG) to ketone end groups and PEG fragments (top). Selection of ^{1}H NMR (D_2O, 300 MHz) spectra of the hydrolysis of BisOD-p($EPB_{0.030}$-*co*-$EG_{0.970}$) at pH 4.5 and incubation at 37 °C (bottom). The decrease of the signal intensity of the vinyl moieties and the increase of the signal intensity of the ketone end groups is highlighted by colored arrows.

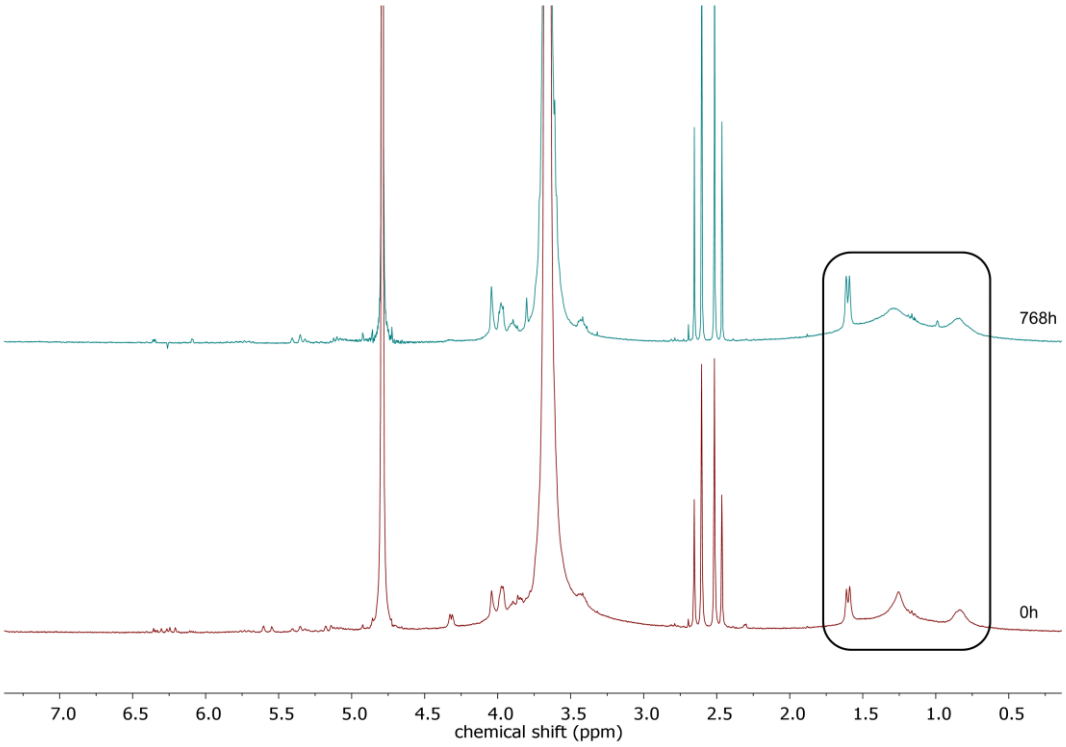

Figure S12. Selection of ^{1}H NMR (D_2O, 300 MHz) spectra of the hydrolysis of BisOD-p($EPB_{0.030}$-*co*-$EG_{0.970}$) at pH 7.0 and incubation at 37 °C, before hydrolysis (0 h) (red, bottom) and after 32 days (768 h) (green, top).

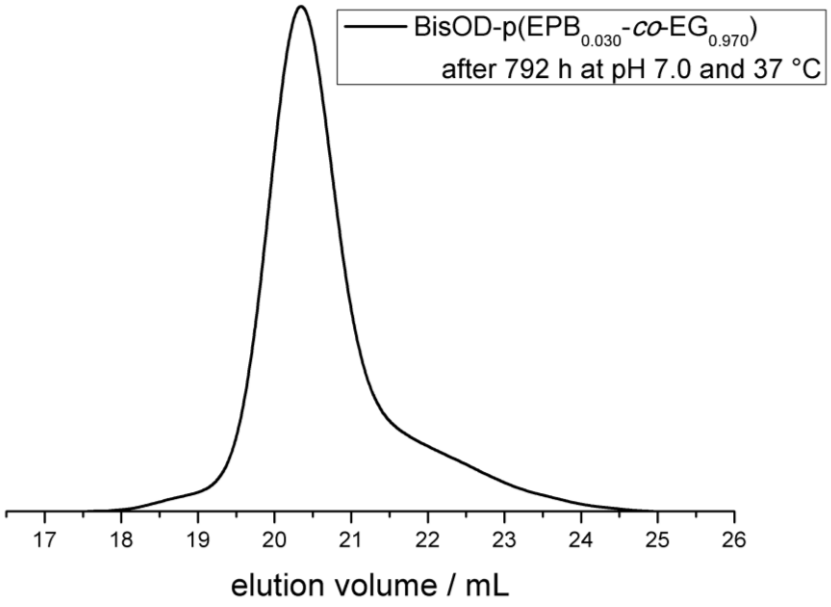

Figure S13. SEC elugram (DMF, PEG standard, RI signal) of BisOD-p($EPB_{0.030}$-*co*-$EG_{0.970}$) after incubation at pH 7 and 37 °C for 792 h.

Table S3. Overview of the properties of BisOD-p(EPB-*co*-EG) after hydrolysis with diluted HCl (0.1 mol L^{-1}).

#	Composition[a]	M_n[b] g mol^{-1}	M_n[c] g $mo\lambda^{-1}$	M_w/M_n[c]
2	BisOD-p($EPB_{0.023}$-*co*-$EG_{0.977}$)	3790	1430	1.79
3	BisOD-p($EPB_{0.026}$-*co*-$EG_{0.974}$)	3990	1100	1.57
4	BisOD-p($EPB_{0.030}$-*co*-$EG_{0.970}$)	2540	1030	1.67
5	BisOD-p($EPB_{0.031}$-*co*-$EG_{0.969}$)	5260	1120	1.68
6	BisOD-p($EPB_{0.034}$-*co*-$EG_{0.966}$)	2030	1100	1.50
7	BisOD-p($EPB_{0.037}$-*co*-$EG_{0.963}$)	2840	1130	1.63
8	BisOD-p($EPB_{0.040}$-*co*-$EG_{0.960}$)	3080	940	1.63
9	BisOD-p($EPB_{0.045}$-*co*-$EG_{0.955}$)	3290	990	1.48
10	BisOD-p($EPB_{0.059}$-*co*-$EG_{0.941}$)	4470	880	1.60
11	BisOD-p($EPB_{0.032}$-*co*-$EG_{0.968}$)	4850	1460	1.54

[a]determined using ^{1}H NMR spectroscopy.
[b]determined using ^{1}H NMR spectroscopy before hydrolysis.
[c]measured after hydrolysis using SEC (DMF, PEG standard, RI detector).

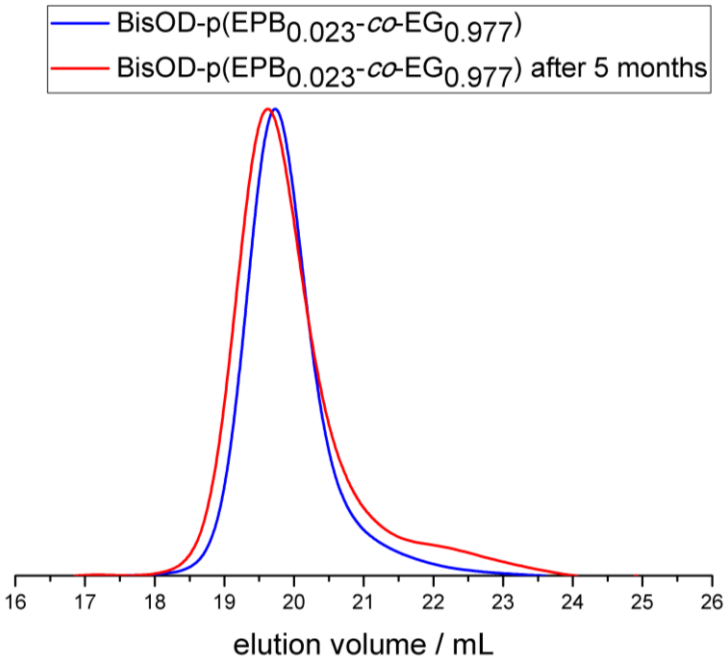

Figure S14. SEC elugram (DMF, PEG standard, RI signal) of BisOD-p($EPB_{0.023}$-*co*-$EG_{0.977}$) after copolymerization and of BisOD-p($EPB_{0.023}$-*co*-$EG_{0.977}$) after 5 months stored in a refrigerator at 4 °C.

4. References

(1) Hofmann, A. M.; Wurm, F.; Hühn, E.; Nawroth, T.; Langguth, P.; Frey, H. Hyperbranched polyglycerol-based lipids via oxyanionic polymerization: toward multifunctional stealth liposomes. *Biomacromolecules* **2010**, *11*, 568–574.

(2) Worm, M.; Leibig, D.; Dingels, C.; Frey, H. Cleavable Polyethylene Glycol: 3,4-Epoxy-1-butene as a Comonomer to Establish Degradability at Physiologically Relevant pH. *ACS Macro Lett.* **2016**, *5*, 1357–1363.

(3) Glasoe, P. K.; Long, F. A. Use of glass electrodes to measure acidities in deuterium oxide 1,2. *J. Phys. Chem.* **1960**, *64*, 188–190.

(4) Fritz, T.; Voigt, M.; Worm, M.; Negwer, I.; Müller, S. S.; Kettenbach, K.; Ross, T. L.; Roesch, F.; Koynov, K.; Frey, H. *et al.* Orthogonal Click Conjugation to the Liposomal Surface Reveals the Stability of the Lipid Anchorage as Crucial for Targeting. *Chem. Eur. J.* **2016**, *22*, 11578–11582.

2.3 Synthesis of Mannose-carrying Lipids *via* Anionic Copolymerization of Ethylene Oxide and Mannose-bearing Glycidyl Ethers

Ann-Kathrin Danner,[a,b] Jens Langhanki,[a] Till Opatz[a] and Holger Frey[a,*]

[a]Institute of Organic Chemistry, Johannes Gutenberg-University Mainz, Duesbergweg 10-14, 55128 Mainz, Germany.

[b]Graduate School Materials Science in Mainz, Staudinger Weg 9, 55128 Mainz, Germany.

E-Mail: hfrey@uni-mainz.de

To be submitted.

Abstract

Mannosylated nanocarriers are able to target cells of the immune system due to the high amount of mannose receptors that are expressed on these cells. Hence, integration of mannose-moieties in polyethylene glycol (PEG) offers a promising strategy for PEGylated liposomes with the ability to target specific cells. Herein, the anionic ring-opening copolymerization (AROP) of ethylene oxide (EO) and mannose-bearing glycidyl ethers, using 1,2-bis-*n*-hexadecyl glyceryl ether (BisHD) as initiator, is introduced to obtain multifunctional amphiphilic PEG. The synthesized copolymers exhibit molecular weights between 6330 and 8970 g mol^{-1} and narrow size distributions with polydispersities of 1.15–1.24. Furthermore, the amount of incorporated mannose-bearing glycidyl ether is systematically varied between 1 and 5 mol%. The properties of the copolymers are investigated *via* NMR spectroscopy and size exclusion chromatography (SEC). In addition, the thermal properties of the copolymers are studied, using differential scanning calorimetry (DSC) and revealing a melting temperature for all copolymers.

Table of Contents Graphics

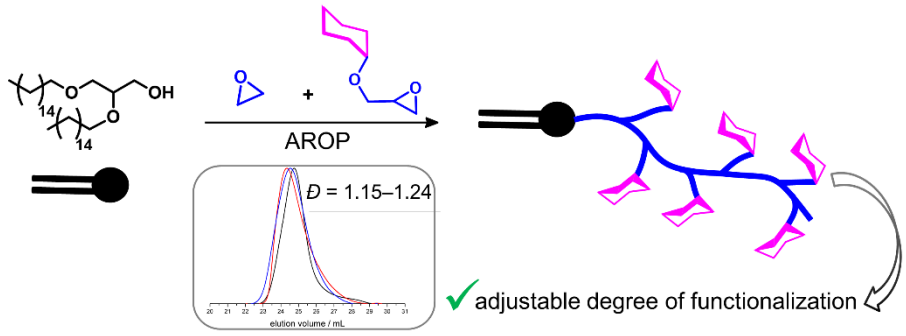

Introduction

Mannosylation of nanocarriers is gaining more and more significance in biomedical applications due to their ability to specifically target mannose receptors (lectins), which are greatly expressed on macrophages[1] and dendritic cells (DCs)[2–4] to wit cells of the immune system.[5] Hence, receptor-mediated drug targeting for selective drug delivery and improved pharmacokinetics are achieved.[6] Different carriers with mannose-moieties are already known in literature, *e.g.* polyester nanoparticles (NPs),[7–9] polyanhydride NPs,[10] pH-sensitive dextran NPs[11] and non-PEGylated liposomes.[6,12,13] Mannosylated liposomes show cell-specific targeting and higher uptake compared to non-mannosylated liposomes.[6,13] Furthermore, the so-called cluster glycoside effect plays an important role to obtain an effective uptake into cells. This effect describes the enhanced binding of multivalent glycoside ligands to cell receptors (lectins) compared to monovalent ligands.[14]

Polyethylene glycol (PEG) is highly water-soluble, non-toxic and biocompatible.[15] It is used for PEGylation of liposomes which leads to prolonged blood circulation times and reduced side effects of toxic drugs due to its "shielding" properties.[16,17] PEG offers the possibility for α- and ω-functionalization but unfortunately lacks further functionalities.[18] Therefore, the development of multifunctional PEG is highly promising, leading to an introduction of numerous functional groups, which can serve *e.g.* for active targeting of liposomes.[19,20] Multifunctional PEG is obtained *via* the copolymerization of ethylene oxide (EO) and epoxide monomers.[21] The copolymerization of EO and glycidyl propargyl ether (GPgE) led to multiple alkyne moieties in the polyether backbone, which provide the possibility to attach mannose-moieties to the PEG chain by performing a copper(I)-catalyzed azide-alkyne cycloaddition.[22] The copolymers were synthesized using the monomer-activated method which unfortunately leads to rather broad size distributions. Furthermore, the applied cycloaddition requires a toxic copper catalyst, which is a disadvantage for biomedical purposes. Besides, several groups already reported ω-functionalization of PEG with monomannose[23–25] and functional epoxides with galactopyranoside, glucofuranoside and glucopyranoside were applied for post-polymerization functionalization of polypeptides.[26]

In order to avoid post-polymerization and a toxic catalyst, it would be an appealing approach to develop a method to integrate multiple mannose-moieties directly during

polymerization. Consequently, target functions can be introduced into the polyether backbone very easily to obtain the already mentioned advantages of PEG and the ability of targeting cells of the immune system. By applying the anionic ring-opening polymerization (AROP) narrow size distributions can be reached. Hence, a mannose-bearing glycidyl ether with protected hydroxyl groups is necessary for the copolymerization with EO. To the best of our knowledge a direct copolymerization of EO and mannose-bearing epoxides is not known, yet. For this purpose, we synthesized two mannose-bearing glycidyl ethers with different protecting groups and investigated the copolymerization with EO, using a hydrophobic initiator, which enables their incorporation into liposomes due to the resulting amphiphilic structure.

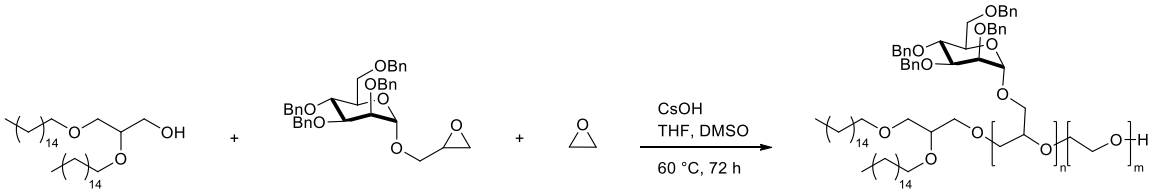

Scheme 1. Anionic ring-opening copolymerization of ethylene oxide (EO) and 1-(oxiran-2-ylmethyl)-2,3,4,6-tetra-*O*-benzyl-*α*-D-mannopyranose using 1,2-bis-*n*-hexadecyl glyceryl ether (BisHD) as initiator.

Results and Discussion

Two different mannose-bearing glycidyl ethers were synthesized by allylation of the hydroxyl group in position 1 followed by a prilezahev epoxidation with *meta*-chloroperoxybenzoic acid (mCPBA). In order to protect the free hydroxyl groups, benzyl and acetonide-protecting groups respectively were applied to obtain 1-(oxiran-2-ylmethyl)-2,3,4,6-tetra-*O*-benzyl-*α*-D-mannopyranose (**4**) and 1-(oxiran-2-ylmethyl)-2,3:4,6-di-*O*-isopropyliden-*α*-D-mannopyranose (**6**) (**Scheme S1**).

For the anionic ring-opening polymerization (AROP) of ethylene oxide (EO) and 1-(oxiran-2-ylmethyl)-2,3,4,6-tetra-*O*-benzyl-*α*-D-mannopyranose (2,3,4,6-tetra-*O*-benzyl-*α*-D-mannopyranose glycidyl ether, BMGE) 1,2-bis-*n*-hexadecyl glyceryl ether (BisHD) was used as initiator. By applying the AROP strategy, a good control of the molecular weight as well as content of incorporated comonomer BMGE is obtained. Due to the hydrophobic initiator,

the copolymerization leads to amphiphilic polyethers BisHD-p(BMGE-*co*-EG) that allow for the preparation of functional liposomes. In general, this copolymerization offers the possibility to introduce and adjust the degree of mannose-moieties to enable a selective binding to lectin receptors on the cell surface.[5,27,28] The copolymerization was carried out in a mixture of dry tetrahydrofuran (THF) and dimethyl sulfoxide (DMSO) (5:1) at 60 °C for 3 days to obtain full conversion. The addition of DMSO increased the solvation of the propagating chain end and thus led to a higher reactivity of the alkoxide. The BMGE ratio was set to 1, 2, 3 and 5 mol% respectively and molecular weights between 5500 and 7700 g mol^{-1} were envisaged for the copolymers. The obtained amphiphilic polyethers were characterized *via* ^{1}H NMR spectroscopy and size exclusion chromatography (SEC) and had molecular weights between 6330 and 8970 g mol^{-1} (calculated *via* ^{1}H NMR spectroscopy) and low polydispersities in a range of 1.15 to 1.24 (determined by SEC using PEG standards).

The ^{1}H NMR spectrum shows typical resonances for the polyether backbone and the initiator. Furthermore, the characteristic signals for BMGE are displayed confirming the successful copolymerization (**Figure S13**). The amount of functional moieties integrated in the polyether backbone was calculated by ^{1}H NMR and thus varied between 0.6 mol% and 5.4 mol%. The signal of the benzyl protecting groups was used to calculate the degree of incorporated BMGE by comparing the signal intensity of the methyl groups of the initiator at 0.94–0.91 ppm with the benzyl protecting groups at 7.44–7.22 ppm. In addition, the molecular weight of the copolymers was determined using ^{1}H NMR spectroscopy. To further prove the successful copolymerization, diffusion ordered spectroscopy (DOSY) was performed. DOSY is a powerful tool to characterize copolymers and especially to confirm the copolymer formation.[29,30] The DOSY NMR spectrum of the copolymer with the related ^{1}H spectrum projected on top is shown in **Figure S18**. As displayed, the ^{1}H NMR signals of PEG and PBMGE exhibit the same diffusion coefficient, translating to an effective copolymerization of both monomers.

Further characterization was carried out using SEC measurements. SEC was performed in THF using a PEG standard for calibration. Narrow and monomodal size distributions were obtained for all copolymers with polydispersities ≤ 1.24. The molecular weights determined *via* SEC were underestimated compared to the molecular weights calculated *via* ^{1}H NMR spectroscopy and the theoretical values. This is due to the differences in the hydrodynamic volume of the copolymers and the PEG standards, which were used for

calibration. The SEC measurements reveal a shift to lower elution volume for higher molecular weights as displayed in **Figure 1** and **Figure S27**. Comparing the RI and UV elugram of the copolymer, the SEC curve shows an overlap for both signals, indicating a successful copolymerization of the applied monomers (**Figure S19**). Characterization data like molecular weight, content of incorporated mannose-based glycidyl ethers, polydispersity and thermal properties of the synthesized copolymers are summarized in **Table 1.**

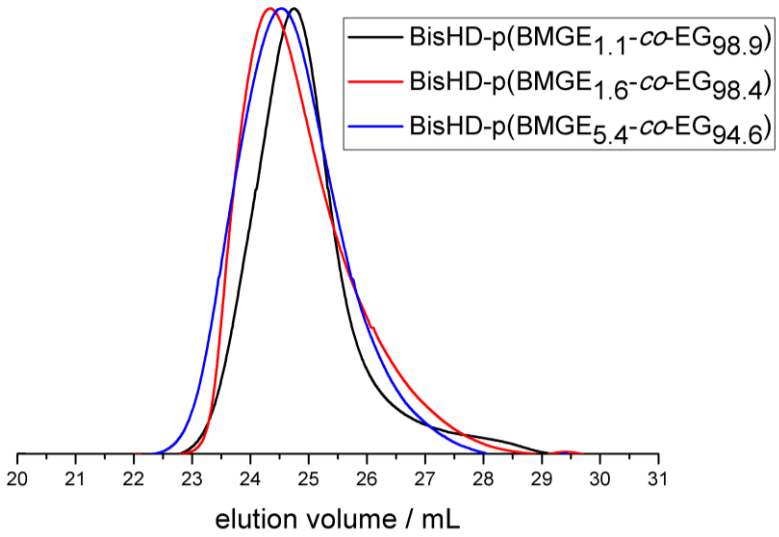

Figure 1. SEC traces (THF, PEG standard, RI signal) of the synthesized copolymers BisHD-p(BMGE-*co*-EG).

The thermal properties of the copolymers were analyzed using differential scanning calorimetry (DSC). All copolymers exhibited a melting temperature T_m in a range of 27 °C to 53 °C (see **Table 1**). Due to the predominant melting endotherm, a T_g was not detectable. The T_m decreases with increasing amount of introduced mannose-moieties. In comparison, PEG-4400 exhibits a T_g of –57 °C and a T_m of 59 °C.[31] Hence, the T_m of the copolymers is clearly decreased due to the interruption of PEG by BMGE and therefore a shortening of the formed PEG segments. Therefore, we assume a statistical distribution of the BMGE monomer along the backbone. This is in agreement with literature where the reactivity of EO and glycidyl ethers, *e.g.* ethoxyethyl glycidyl ether (EEGE), was compared, revealing a comparable reactivity in the AROP (reactivity ratios of r_{EO} = 1.05 and r_{EEGE} = 0.94) and hence a statistical monomer distribution.[32] A statistical monomer distribution along the

backbone should be also favorable regarding the steric hindrance of the space demanding protecting groups of the mannose-bearing glycidyl ether.

Table 1. Summary of the synthesized copolymers BisHD-p(BMGE-*co*-EG) and their properties.

Composition[a]	M_n^{th} g mol^{-1}	M_n^{NMR} g mol^{-1}	$M_w/M_n^{SEC,b}$	**mannose** mol% th / NMR	T_m °C
BisHD-p(BMGE$_{0.6}$-*co*-EG$_{99.4}$)	5500	6580	1.15	1/0.6	53
BisHD-p(BMGE$_{0.7}$-*co*-EG$_{99.3}$)	5500	7230	1.18	1/0.7	51
BisHD-p(BMGE$_{1.1}$-*co*-EG$_{98.9}$)	5500	8970	1.21	1/1.1	53
BisHD-p(BMGE$_{1.6}$-*co*-EG$_{98.4}$)	6050	8670	1.24	2/1.6	48
BisHD-p(BMGE$_{2.8}$-*co*-EG$_{97.2}$)	6600	7990	1.19	3/2.8	32
BisHD-p(BMGE$_{3.2}$-*co*-EG$_{96.8}$)	7700	6330	1.19	5/3.2	35
BisHD-p(BMGE$_{5.4}$-*co*-EG$_{94.6}$)	6600	7390	1.23	3/5.4	27

[a]determined using ^{1}H NMR spectroscopy.
[b]measured in THF using a PEG standard.

The benzyl protecting groups can be removed *via* hydrogenation after polymerization to obtain BisHD-p(MGE-*co*-EG). Therefore, the polymer was dissolved in methanol and hydrogenated for 6 days. By using palladium hydroxide on activated charcoal instead of palladium on activated charcoal, the effectiveness of the performed hydrogenation was improved and the reaction time was reduced from 10 to 6 days. The catalyst was removed *via* filtration, using celite®. Unfortunately, the resulting mannose-moieties showed a strong adhesion during filtration, leading to loss and a reduced yield (26%). The successful removal of the benzyl protecting groups was confirmed *via* ^{1}H NMR spectroscopy, showing the disappearance of the respective signals to wit the signals for the benzyl protecting groups including the signal of the adjacent methylene groups vanish (**Figure 2**). Due to the increased hydrophilicity of the resulting BisHD-p(MGE-*co*-EG) aggregated are formed in

deuterated methanol, leading to not well-resolved signals in the ^{1}H NMR spectrum. Nevertheless, the disappearance of the signals for the benzyl protecting groups can be confirmed. In general, the removal of the benzyl protecting groups was very time-consuming. Hence, we assume the formation of entanglements due to the flexible polyether backbone and thus steric hindrance during hydrogenation.

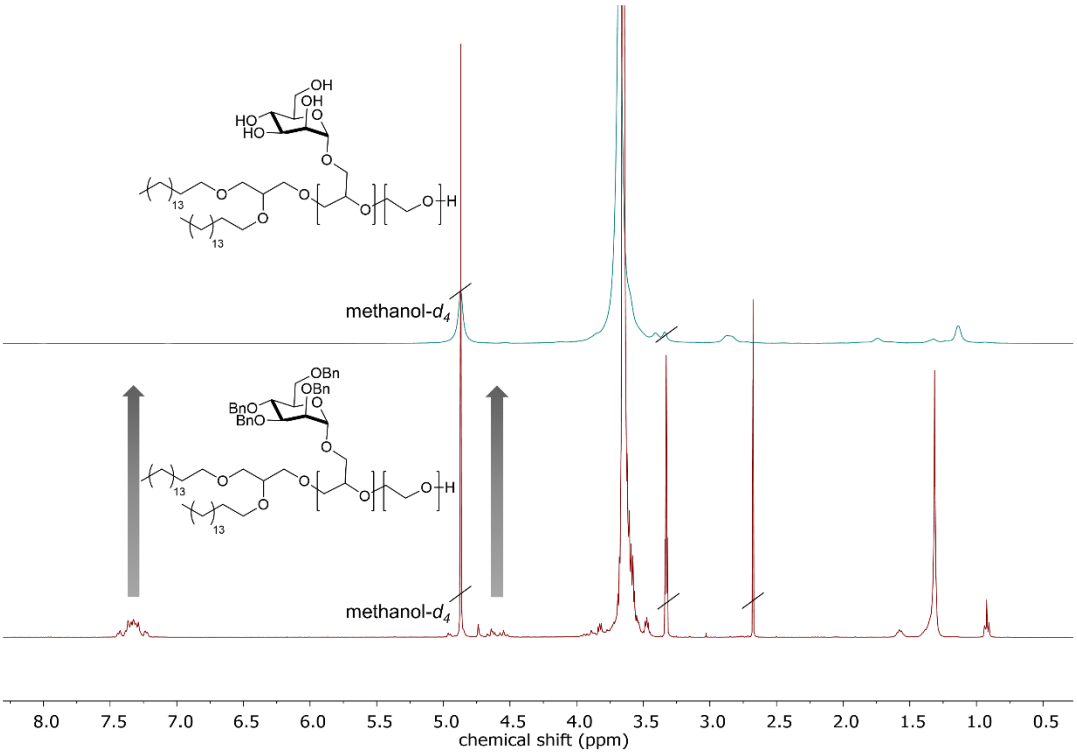

Figure 2. ^{1}H NMR spectra (methanol-d_4, 400 MHz) of BisHD-p(BMGE$_{1.1}$-*co*-EG$_{98.9}$) before hydrogenation and BisHD-p(MGE$_{1.1}$-*co*-EG$_{98.9}$) after hydrogenation.

Moreover, a copolymerization of EO and 1-(oxiran-2-ylmethyl)-2,3:4,6-di-*O*-isopropyliden-*α*-D-mannopyranose (2,3:4,6-di-*O*-isopropyliden-*α*-D-mannopyranose glycidyl ether, IMGE) was performed. Due to the nature of the protecting groups, we expected less steric hindrance during polymerization and therefore a faster copolymerization, an easier incorporation of a higher amount of the comonomer IMGE and facile deprotection. The successful copolymerization was confirmed using NMR spectroscopy (**Table S1**). Unfortunately, SEC measurements revealed a bimodal size distribution for all synthesized copolymers (**Figure S28**). Thus, undefined polymers which are not suitable for biomedical applications were obtained. This can be attributed to a cleavage of the labile ketal protecting groups during polymerization, leading to free hydroxyl groups. Consequently, a new initiator species is formed, which is available for polymerization. By reducing the reaction

time from 4 or 6 days respectively to 3 days the occurring side reaction did not occur and a copolymer BisHD-p(IMGE-*co*-EG) with a monomodal size distribution, exhibiting a low polydispersity (*Đ* = 1.19) was obtained.

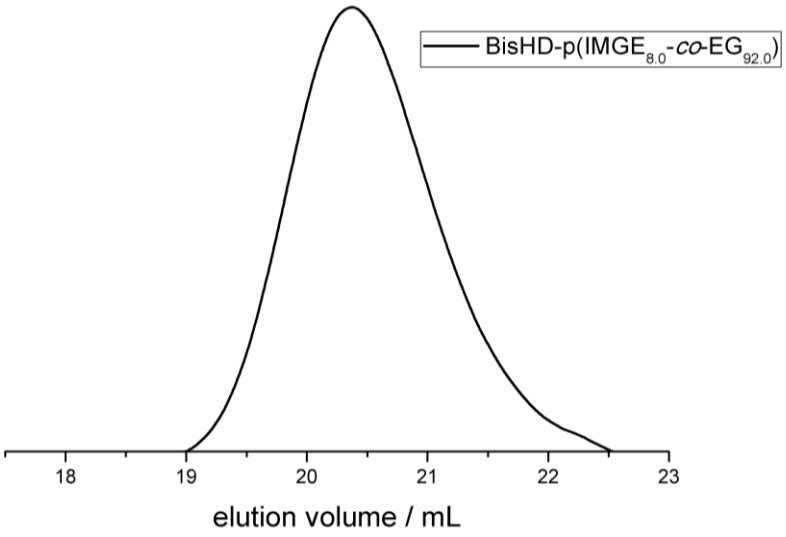

Figure 3. SEC traces (THF, PEG standard, RI signal) of the synthesized copolymer BisHD-p($IMGE_{8.0}$-*co*-$EG_{92.0}$).

The ^{1}H NMR spectrum displays the characteristic signals for IMGE as well as the resonances for the polyether backbone and the initiator (**Figure S21**). Furthermore, the amount of incorporated IMGE was calculated, using ^{1}H NMR spectroscopy, revealing an incorporation of 8 mol% IMGE. Thus, the amount of mannose-moieties introduced to the amphiphilic polyether is higher compared to the prepared copolymers, in which BMGE was applied as functional epoxide. Therefore, IMGE is especially promising as comonomer if a degree of functionalization > 6 mol% is targeted. In addition, DOSY NMR measurement confirmed the successful copolymerization of EO and IMGE, since the ^{1}H NMR signals of PEG and PIMGE exhibit the same diffusion coefficient (**Figure S26**). **Table 2** gives an overview of the obtained molecular weight, characteristics given by SEC and the amount of incorporated comonomer IMGE for the synthesized copolymer BisHD-p($IMGE_{8.0}$-*co*-$EG_{92.0}$).

Table 2. Summary of the synthesized copolymer BisHD-p(IMGE$_{8.0}$-co-EG$_{92.0}$).

Composition[a]	M_n^{th} g mol^{-1}	M_n^{NMR} g mol^{-1}	$M_w/M_n^{SEC,b}$	**mannose** mol% th / NMR[a]
BisHD-p(IMGE$_{8.0}$-*co*-EG$_{92.0}$)	5760	1250	1.19	3.0/8.0

[a]determined using ^{1}H NMR spectroscopy.
[b]measured in THF using a PEG standard.

As can be seen in **Table 2**, the obtained molecular weight (calculated *via* ^{1}H NMR spectroscopy) was much lower than the targeted molecular weight. Hence, full conversion was not reached after a reaction time of 3 days. Moreover, due to the incomplete conversion the amount of incorporated comonomer IMGE is higher than the theoretical value. Therefore, further investigations have to be carried out to optimize the reactions conditions.

Conclusion

In summary, the copolymerization of EO and BMGE *via* the AROP was investigated and aimed to introduce mannose-moieties directly during polymerization leading to multifunctional PEG. This strategy enables an incorporation of a variable amount of mannose-groups and combines the already mentioned advantages of PEG and the ability of targeting cells of the immune system. The degree of functionalization was varied between 0.6 mol% and 5.4 mol% and the copolymers had defined molecular weights (6330–8970 g mol^{-1}) and showed narrow size distributions (1.15–1.24). DOSY NMR measurements confirmed the successful copolymerization of both monomers. In addition, the copolymerization of EO and IMGE was possible. However, the reaction conditions for this copolymerization have to be further improved to obtain full conversion. In future work the effectiveness of targeting lectin receptors and internalization efficiencies in cells (*in vitro* studies) will be investigated.

Acknowledgments

A. Danner is a recipient of a DFG-funded position through the Excellence Initiative by the Graduate School Materials Science in Mainz (GSC 266). The authors thank Monika Schmelzer for SEC measurements, Ulrike Kemmer-Jonas for DSC measurements and Yannick Wohlleben for support in the laboratory.

References

(1) Chellat, F.; Merhi, Y.; Moreau, A.; Yahia, L.'H. Therapeutic potential of nanoparticulate systems for macrophage targeting. *Biomaterials* **2005**, *26*, 7260–7275.

(2) Guermonprez, P.; Valladeau, J.; Zitvogel, L.; Théry, C.; Amigorena, S. Antigen presentation and T cell stimulation by dendritic cells. *Annual review of immunology* **2002**, *20*, 621–667.

(3) McGreal, E. P.; Miller, J. L.; Gordon, S. Ligand recognition by antigen-presenting cell C-type lectin receptors. *Current opinion in immunology* **2005**, *17*, 18–24.

(4) van Vliet, S. J.; García-Vallejo, J. J.; van Kooyk, Y. Dendritic cells and C-type lectin receptors: Coupling innate to adaptive immune responses. *Immunology and cell biology* **2008**, *86*, 580–587.

(5) Irache, J. M.; Salman, H. H.; Gamazo, C.; Espuelas, S. Mannose-targeted systems for the delivery of therapeutics. *Expert opinion on drug delivery* **2008**, *5*, 703–724.

(6) Kawakami, S.; Wong, J.; Sato, A.; Hattori, Y.; Yamashita, F.; Hashida, M. Biodistribution characteristics of mannosylated, fucosylated, and galactosylated liposomes in mice. *Biochimica et Biophysica Acta (BBA) - General Subjects* **2000**, *1524*, 258–265.

(7) Ghotbi, Z.; Haddadi, A.; Hamdy, S.; Hung, R. W.; Samuel, J.; Lavasanifar, A. Active targeting of dendritic cells with mannan-decorated PLGA nanoparticles. *Journal of drug targeting* **2011**, *19*, 281–292.

(8) Fievez, V.; Plapied, L.; Des Rieux, A.; Pourcelle, V.; Freichels, H.; Wascotte, V.; Vanderhaeghen, M.-L.; Jerôme, C.; Vanderplasschen, A.; Marchand-Brynaert, J. *et al.* Targeting nanoparticles to M cells with non-peptidic ligands for oral vaccination. *European journal of pharmaceutics and biopharmaceutics : official journal of Arbeitsgemeinschaft für Pharmazeutische Verfahrenstechnik e.V* **2009**, *73*, 16–24.

(9) Nahar, M.; Jain, N. K. Preparation, characterization and evaluation of targeting potential of amphotericin B-loaded engineered PLGA nanoparticles. *Pharmaceutical research* **2009**, *26*, 2588–2598.

(10) Carrillo-Conde, B.; Song, E.-H.; Chavez-Santoscoy, A.; Phanse, Y.; Ramer-Tait, A. E.; Pohl, N. L. B.; Wannemuehler, M. J.; Bellaire, B. H.; Narasimhan, B. Mannose-

functionalized "pathogen-like" polyanhydride nanoparticles target C-type lectin receptors on dendritic cells. *Mol. Pharm.* **2011**, *8*, 1877–1886.

(11) Cui, L.; Cohen, J. A.; Broaders, K. E.; Beaudette, T. T.; Fréchet, J. M. J. Mannosylated dextran nanoparticles: A pH-sensitive system engineered for immunomodulation through mannose targeting. *Bioconjug. Chem.* **2011**, *22*, 949–957.

(12) Barratt, G.; Tenu, J.-P.; Yapo, A.; Petit, J.-F. Preparation and characterisation of liposomes containing mannosylated phospholipids capable of targetting drugs to macrophages. *BBA-Biomembranes* **1986**, *862*, 153–164.

(13) Shao, J.; Ma, J. K. H. Characterization of a mannosylphospholipid liposome system for drug targeting to alveolar macrophages. *Drug delivery* **1997**, *4*, 43–48.

(14) Lundquist, J. J.; Toone, E. J. The Cluster Glycoside Effect. *Chem. Rev.* **2002**, *102*, 555–578.

(15) Herzberger, J.; Niederer, K.; Pohlit, H.; Seiwert, J.; Worm, M.; Wurm, F. R.; Frey, H. Polymerization of Ethylene Oxide, Propylene Oxide, and Other Alkylene Oxides: Synthesis, Novel Polymer Architectures, and Bioconjugation. *Chemical reviews* **2016**, *116*, 2170–2243.

(16) Knop, K.; Hoogenboom, R.; Fischer, D.; Schubert, U. S. Poly(ethylene glycol) in drug delivery: pros and cons as well as potential alternatives. *Angew. Chem. Int. Edit.* **2010**, *49*, 6288–6308.

(17) Sharma, A. Liposomes in drug delivery: Progress and limitations. *Int. J. Pharm.* **1997**, *154*, 123–140.

(18) Thompson, M. S.; Vadala, T. P.; Vadala, M. L.; Lin, Y.; Riffle, J. S. Synthesis and applications of heterobifunctional poly(ethylene oxide) oligomers. *Polymer* **2008**, *49*, 345–373.

(19) Thomas, A.; Müller, S. S.; Frey, H. Beyond poly(ethylene glycol): linear polyglycerol as a multifunctional polyether for biomedical and pharmaceutical applications. *Biomacromolecules* **2014**, *15*, 1935–1954.

(20) Hofmann, A. M.; Wurm, F.; Hühn, E.; Nawroth, T.; Langguth, P.; Frey, H. Hyperbranched polyglycerol-based lipids via oxyanionic polymerization: toward multifunctional stealth liposomes. *Biomacromolecules* **2010**, *11*, 568–574.

(21) Obermeier, B.; Wurm, F.; Mangold, C.; Frey, H. Multifunctional Poly(ethylene glycol)s. *Angew. Chem. Int. Edit.* **2011**, *50*, 7988–7997.

(22) Herzberger, J.; Leibig, D.; Langhanki, J.; Moers, C.; Opatz, T.; Frey, H. "Clickable PEG" via anionic copolymerization of ethylene oxide and glycidyl propargyl ether. *Polym. Chem.* **2017**, *8*, 1882–1887.

(23) Studer, P.; Limal, D.; Breton, P.; Riess, G. Synthesis and characterization of poly(ethylene oxide)-block-poly(methylidene malonate 2.1.2) block copolymers bearing a mannose group at the PEO chain end. *Bioconjug. Chem.* **2005**, *16*, 223–229.

(24) Muthiah, M.; Vu-Quang, H.; Kim, Y.-K.; Rhee, J. H.; Kang, S. H.; Jun, S. Y.; Choi, Y.-J.; Jeong, Y. Y.; Cho, C.-S.; Park, I.-K. Mannose-poly(ethylene glycol)-linked SPION targeted to antigen presenting cells for magnetic resonance imaging on lymph node. *Carbohydrate polymers* **2013**, *92*, 1586–1595.

(25) Kim, N.; Jiang, D.; Jacobi, A. M.; Lennox, K. A.; Rose, S. D.; Behlke, M. A.; Salem, A. K. Synthesis and characterization of mannosylated pegylated polyethylenimine as a carrier for siRNA. *International journal of pharmaceutics* **2012**, *427*, 123–133.

(26) Gharakhanian, E. G.; Deming, T. J. Versatile Synthesis of Stable, Functional Polypeptides via Reaction with Epoxides. *Biomacromolecules* **2015**, *16*, 1802–1806.

(27) Freichels, H.; Wagner, M.; Okwieka, P.; Meyer, R. G.; Mailänder, V.; Landfester, K.; Musyanovych, A. (Oligo)mannose functionalized hydroxyethyl starch nanocapsules: En route to drug delivery systems with targeting properties. *J. Mater. Chem. B* **2013**, *1*, 4338.

(28) Kikkeri, R.; Lepenies, B.; Adibekian, A.; Laurino, P.; Seeberger, P. H. In vitro imaging and in vivo liver targeting with carbohydrate capped quantum dots. *J. Am. Chem. Soc.* **2009**, *131*, 2110–2112.

(29) Bakkour, Y.; Darcos, V.; Li, S.; Coudane, J. Diffusion ordered spectroscopy (DOSY) as a powerful tool for amphiphilic block copolymer characterization and for critical micelle concentration (CMC) determination. *Polym. Chem.* **2012**, *3*, 2006.

(30) Groves, P. Diffusion ordered spectroscopy (DOSY) as applied to polymers. *Polym. Chem.* **2017**, *8*, 6700–6708.

(31) Müller, S. S.; Moers, C.; Frey, H. A Challenging Comonomer Pair: Copolymerization of Ethylene Oxide and Glycidyl Methyl Ether to Thermoresponsive Polyethers. *Macromolecules* **2014**, *47*, 5492–5500.

(32) Herzberger, J.; Leibig, D.; Liermann, J. C.; Frey, H. Conventional Oxyanionic versus Monomer-Activated Anionic Copolymerization of Ethylene Oxide with Glycidyl Ethers: Striking Differences in Reactivity Ratios. *ACS Macro Lett.* **2016**, *5*, 1206–1211.

Supporting Information

Synthesis of Mannose-carrying Lipids *via* Anionic Copolymerization of Ethylene Oxide and Mannose-bearing Glycidyl Ethers

Ann-Kathrin Danner,[a,b] Jens Langhanki,[a] Till Opatz[a] and Holger Frey[a,*]

[a]Institute of Organic Chemistry, Johannes Gutenberg-University Mainz, Duesbergweg 10-14, 55128 Mainz, Germany.

[b]Graduate School Materials Science in Mainz, Staudinger Weg 9, 55128 Mainz, Germany.

E-Mail: hfrey@uni-mainz.de

1. Materials and Methods

1.1 Reagents

All chemicals were bought from *Sigma Aldrich*, *Acros Organics*, *Fisher Scientific* or *TCI Europe* unless mentioned otherwise. Deuterated solvents (methanol-d_4, benzene-d_6, chloroform-*d*) were purchased from *Deutero GmbH*. Dry DMSO over molecular sieve was obtained from *Acros Organics*. Ethylene oxide (EO) was obtained from *Sigma Aldrich* and must be handled with high precaution. 1-(oxiran-2-ylmethyl)-2,3,4,6-tetra-*O*-benzyl-α-D-mannopyranose and 1-(oxiran-2-ylmethyl)-2,3:4,6-di-*O*-isopropyliden-α-D-manno-pyranose were dissolve in benzene and dried in vacuo for 16 h prior to use. For the anionic ring-opening polymerization (AROP) tetrahydrofuran (THF) was dried and stored over benzophenone/sodium.

1.2 Instrumentation

^{1}H NMR, ^{13}C NMR and 2D NMR spectra were measured using a Bruker Avance III HD 300 spectrometer (300 MHz, 5 mm, BBFO probe, and B-ACS 60 auto sampler) or a Bruker Avance II 400 spectrometer operated at 400 MHz (5 mm BBFO smart probe and SampleXPress 60 auto sampler) or a Bruker Avance III 600 spectrometer (600 MHz, 5 mm TCl-CryoProbe with z-gradient and ATM and SampleXPRess Lite 16 auto sampler) at 296 K. Methanol-d_4, benzene-d_6 and chloroform-*d* were used as solvent and the spectra were referenced internally to proton signals of the deuterated solvent. All spectra were analyzed using the software MestReNova version 9.0. SEC measurements were carried out in tetrahydrofuran (THF) with 0.25 g L^{-1} lithium bromide on an Agilent 1100 Series equipped with PSS HEMA 300/100/40 column, RI and UV detector (275 nm). Monodisperse linear PEG standards from *Polymer Standard Service GmbH* (PSS) were used for calibration. RI signal is shown for all SEC traces unless otherwise mentioned and analysis was carried out using the software PSS WinGPC Unity. DSC measurements were performed on a Perkin Elmer 8200 differential scanning calorimeter and calibration was carried out using the melting points of indium (T_m = 156.6 °C) and Milli-Q water (T_m = 0 °C). 8 to 9 mg of each sample were measured in a temperature range of –90 to 100 °C with a heating rate of 20 °C min^{-1}. The values for the second cycle were used to determine the glass transition temperature T_g and melting temperature T_m.

1.3 Handling of Ethylene Oxide (EO)

The flammable, toxic and gaseous ethylene oxide (EO) must be handled carefully and has to be stored in pressure-proof gas bottles. It must be used in an adequate fume hood under appropriate safety precautions. Reactions containing EO are carried out in flame-dried glassware to convert EO inside the sealed and evacuated glass apparatus and to guarantee secure handling via cryo-transfer techniques. Maximum batch-sizes of EO are 5 g in a 250 mL flask which must not be exceeded to avoid abrupt detachment of the septum and thus release of EO.

2. Synthesis

2.1 Synthesis of 1,2-Bis-*n*-hexadecyl glyceryl ether (BisHD)

The synthesis was carried out according to literature.[1]

mp: 58.5–59.7 °C.

^{1}H NMR, COSY (400 MHz, chloroform-*d*, δ): 3.74–3.41 (m, 9H, glycerol H), 1.59–1.54 (m, 4H, -OCH$_2$C*H$_2$*-), 1.32–1.25 (m, 52H, -OCH$_2$CH$_2$(C*H$_2$*)$_{13}$CH$_3$), 0.87 (m, 6H, -O(CH$_2$)$_{15}$C*H$_3$*).

^{13}C NMR, HSQC, HMBC (100.6 MHz, chloroform-*d*, δ): 78.4 (glycerol C), 72.0 (-O*C*H$_2$CH$_2$-), 71.1 (glycerol C), 70.6 (-O*C*H$_2$CH$_2$-), 63.3 (glycerol C), 32.1 (-OCH$_2$CH$_2$(*C*H$_2$)$_{13}$CH$_3$), 30.2 (-OCH$_2$*C*H$_2$-), 29.9-29.5 (-OCH$_2$CH$_2$(*C*H$_2$)$_{13}$CH$_3$), 26.3 (-OCH$_2$CH$_2$(*C*H$_2$)$_{13}$CH$_3$), 22.9 (-OCH$_2$CH$_2$(*C*H$_2$)$_{13}$CH$_3$), 14.3 (-O(CH$_2$)$_{15}$*C*H$_3$).

2.2. Monomer synthesis

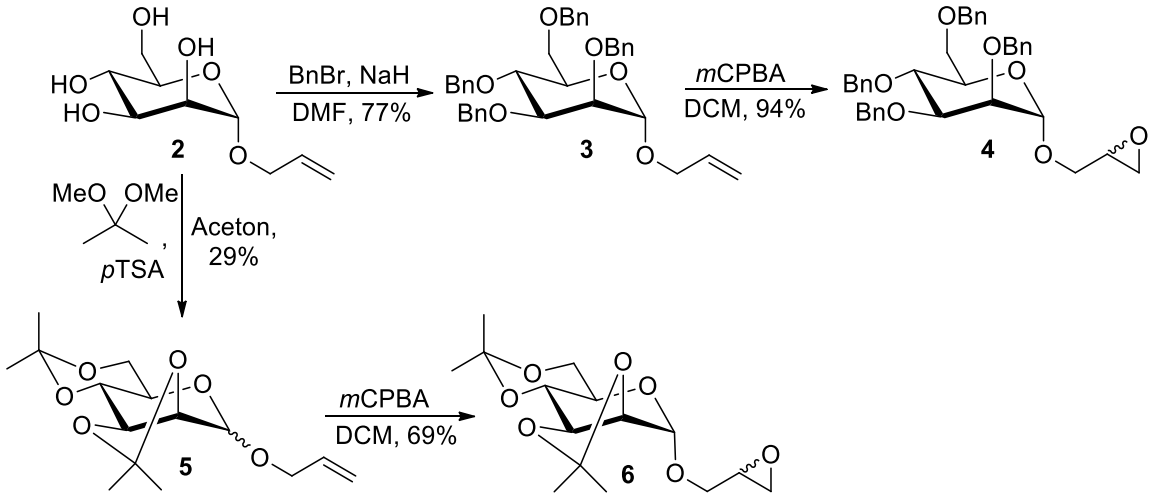

Scheme S1. Synthetic strategy to obtain 1-(oxiran-2-ylmethyl)-2,3,4,6-tetra-*O*-benzyl-*α*-D-mannopyranose (**4**) and 1-(oxiran-2-ylmethyl)-2,3:4,6-di-*O*-isopropyliden-*α*-D-mannopyranose (**6**).

2.2.1 Allyl-*α*-D-mannopyranose **2**

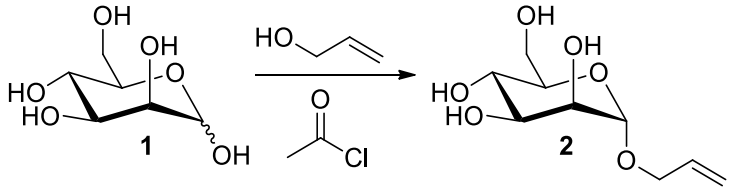

A solution of *α*-D-mannopyranose (**1**, 5.00 g, 27.8 mmol, 1 eq.) in allylalcohol (48.4 g, 56.9 mL, 833 mmol, 30 eq.) was treated with acetyl chloride (5.41 g, 4.92 mL, 69.4 mmol, 1.5 eq.) under stirring at room temperature. The reaction mixture was heated to 100 °C and stirred at that temperature for 16 hours. Subsequently the reaction mixture was cooled to room temperature and treated with solid $NaHCO_3$ until pH = 7. The mixture was filtered over a bed of Celite, which was washed thoroughly with toluene. The solvents were removed under reduced pressure and the residue was purified by flash column chromatography (ethyl acetate/ methanol, 10:1) to give the title compound (4.75 g, 21.6 mmol, 78%) as a colorless viscous oil.

R_f = 0.32 (silica gel, ethyl acetate/ methanol, 10:2).

^{1}H-NMR, COSY (400 MHz, CD_3OD) δ (ppm) = 5.94 (dddd, ^3J = 17.3 Hz, ^3J = 10.7 Hz, ^3J = 6.0 Hz, ^3J = 5.1 Hz, 1H, Man–O–CH_2–C*H*), 5.30 (*pseudo* dq, ^2J = 17.2 Hz, J = 1.7 Hz, 1H, O–CH_2–CH=C$H_{2,a}$), 5.17 (*pseudo* dq, ^2J = 10.4 Hz, J = 1.5 Hz, 1H, O–CH_2–

CH=C$H_{2,b}$), 4.97 (d, ^3J = 1.7 Hz, 1H, H-1), 4.22 (*pseudo* ddt, ^2J = 13.1 Hz, ^3J = 5.1 Hz, ^4J = 1.6 Hz, 1H, O–C$H_{2,a}$–CH=CH_2), 4.00 (*pseudo* ddt, ^2J = 13.1 Hz, ^3J = 5.9 Hz, ^4J = 1.4 Hz, 1H, O–C$H_{2,b}$–CH=CH_2), 3.86–3.78 (m, 2H, H-2, H-6$_a$), 3.72–3.67 (m, 2H, H-3, H-6$_b$), 3.61 (*pseudo* t, ^3J = 9.5 Hz, 1H, H-4), 3.53 (ddd, ^3J = 9.8 Hz, ^3J = 5.8 Hz, ^3J = 2.3 Hz, 1H, H-5).

^{13}C-NMR, HSQC, HMBC (100.6 MHz, CD_3OD) δ (ppm) = 135.5 (Man–O–CH_2–*C*H), 117.3 (O–CH_2–CH=*C*H_2), 100.7 (C-1), 74.7 (C-5), 72.6 (C-3), 72.2 (C-2), 68.8 (Man–O–*C*H_2–CH), 68.6 (C-4), 62.9 (C-6).

IR (ATR) $\tilde{\nu}$ (cm^{-1}) = 3344, 2923, 1453, 1422, 1412, 1261, 1129, 1096, 1053, 1024, 975, 925, 879, 810.

$[\boldsymbol{\alpha}]_{\boldsymbol{D}}^{\mathbf{24}}$ = +62.5° (c = 1.00, H_2O).

ESI-MS: *m/z* (%) = 243.1 (100) $[M + Na]^+$, 244.2 (11) $[M(^{13}C_1) + Na]^+$.

The spectral data are in accordance with literature.[2]

2.2.2 Allyl-2,3,4,6-tetra-*O*-benzyl-*α*-D-mannopyranose **3**

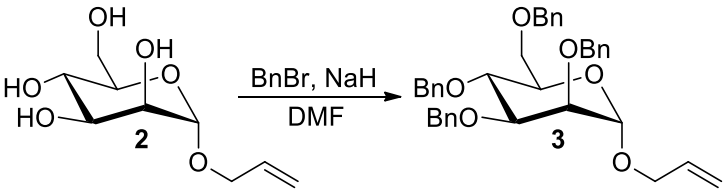

A suspension of NaH (3.18 g, 79.5 mmol, 7.0 eq., 60% in mineral oil) in dimethylformamide (32 mL) was treated with a solution of allyl-*α*-D-mannopyranose (**2**, 2.50 g, 11.3 mmol, 1.0 eq.) in dimethylformamide (32 mL) at 0 °C and was stirred at this temperature for 30 minutes. Subsequently benzylbromide (13.60 g, 9.45 mL, 79.5 mmol, 7.0 eq.) was added dropwise at 0 °C and the resulting mixture was stirred at room temperature for 16 hours. Afterwards the reaction mixture was cooled to 0 °C and water (50 mL) as well as diethylether (50 mL) was added slowly. The separated organic phase was washed with water (3 × 50 mL), brine (50 mL) and was dried over anhydrous Na_2SO_4. The solvent was removed *in vacuo* and the residue was purified by flash column chromatography (cyclohexane/ethyl acetate, gradient 0% to 15% ethyl acetate, Isolera

Flash Purification System) to afford the title compound (5.07 g, 8.73 mmol, 77%) as a colorless oil.

R_f = 0.46 (cyclohexane/ethyl acetate 4:1).

^{1}H-NMR, COSY (400 MHz, $CDCl_3$) δ (ppm) = 7.41–7.14 (m, 20H, H-Ar), 5.85 (dddd, ^3J = 16.8 Hz, ^3J = 10.7 Hz, ^3J = 6.1 Hz, ^3J = 5.0 Hz, 1H, Man–O–CH_2–C*H*), 5.22 (*pseudo* dq, ^2J = 17.2 Hz, ^4J = 1.7 Hz, 1H, O–CH_2–CH=C$H_{2,a}$), 5.15 (*pseudo* dq, ^2J = 10.4 Hz, ^4J = 1.5 Hz, 1H, O–CH_2–CH=C$H_{2,b}$), 4.93 (d, ^3J = 1.9 Hz, 1H, H-1), 4.89 (d, ^2J = 10.7 Hz, 1H, C-4–O–C$H_{2,a}$–Ph), 4.76 (d, ^2J = 12.5 Hz, 1H, C-2–O–C$H_{2,a}$–Ph), 4.72 (d, ^2J = 12.5 Hz, 1H, C-2–O–C$H_{2,b}$–Ph), 4.68 (d, ^2J = 12.1 Hz, 1H, C-6–O–C$H_{2,a}$–Ph), 4.63 (s, 2H, C-3–O–CH_2–Ph), 4.55 (d, ^2J = 12.1 Hz, 1H, C-6–O–C$H_{2,b}$–Ph), 4.51 (d, ^2J = 10.7 Hz, 1H, C-4–O–C$H_{2,b}$–Ph), 4.17 (*pseudo* ddt, ^2J = 13.0 Hz, ^3J = 5.0 Hz, ^4J = 1.6 Hz, 1H, O–C$H_{2,a}$–CH=CH_2), 4.04–3.91 (m, 3H, O–C$H_{2,b}$–CH=CH_2, H-3, H-5), 3.82 (dd, ^3J = 3.1 Hz, ^3J = 1.9 Hz, 2H, H-2), 3.81–3.71 (m, 3H, H-4, 2 × H-6).

^{13}C-NMR, HSQC, HMBC (100.6 MHz, $CDCl_3$) δ (ppm) = 138.8, 138.7, 138.7, 138.6 (4 × C_q), 134.1 (Man–O–CH_2–*C*H), 128.6, 128.6, 128.6, 128.6, 128.3, 128.1, 128.0, 127.9, 127.8, 127.7 (C-Ar), 117.5 (O–CH_2–CH=*C*H_2), 97.3 (C-1), 80.5 (C-5), 75.4 (C-4–O–*C*H_2–Ph), 75.2 (C-3), 74.9 (C-2), 73.6 (C-6–O–*C*H_2–Ph), 72.8 (C-2–O–*C*H_2–Ph), 72.4 (C-3–O–*C*H_2–Ph), 72.1 (C-4), 69.5 (C-6), 68.1 (Man–O–*C*H_2–CH).

IR (ATR) $\tilde{\nu}$ (cm^{-1}) = 3063, 3030, 2908, 2864, 1496, 1453, 1395, 1207, 1092, 1058, 1027, 914, 734, 696.

$[\boldsymbol{\alpha}]_{\boldsymbol{D}}^{\mathbf{24}}$ = +33.2° (c = 0.50, $CHCl_3$).

ESI-MS: *m/z* (%) = 598.4 (100) $[M + H]^+$, 599.2 (36) $[M(^{13}C_1) + H]^+$, 523.3 (4) [M – O–CH_2–CH=CH_2]$^+$, 431.3 (15) [M – O–CH_2–CH=CH_2 – Bn]$^+$.

The spectral data are in accordance with literature.[3]

2.2.3 1-(Oxiran-2-ylmethyl)-2,3,4,6-tetra-*O*-benzyl-*α*-D-mannopyranose **4**

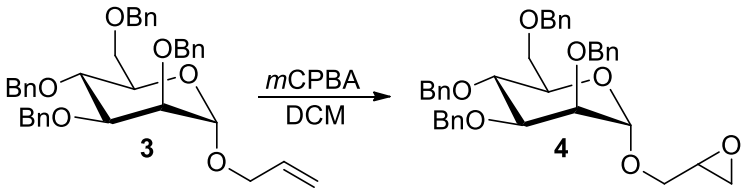

A solution of mannopyranose **3** (4.96 g, 8.55 mmol, 1.0 eq.) in dichloromethane (220 mL) was treated with *m*CPBA (2.21 g, 12.8 mmol, 1.5 eq.) at 0 °C under stirring. The reaction mixture was stirred for 18 hours at room temperature, but TLC (cyclohexane/ethyl acetate 4:1) still showed starting material. Again *m*CPBA (500 mg, 2.90 mmol, 0.3 eq.) was added and the reaction mixture was stirred for 24 hours at room temperature. Subsequently TLC showed complete conversion and the reaction mixture was diluted with ethyl acetate (200 mL) and transferred into a 2 L Erlenmeyer flask. Then saturated $Na_2S_2O_3$-solution (300 mL) was added and the mixture was vigorously stirred for 20 minutes. The separated organic layer was washed with saturated $NaHCO_3$-solution (150 mL) and dried over anhydrous Na_2SO_4. The solvent was removed *in vacuo* and the residue was filtrated over silica gel (cyclohexane/ethyl acetate 5:1, then 1:1) to afford the title compound (4.79 g, 8.03 mmol, 94%, mixture of both epimers (A,B) in ratio 1:0.6).

R_f = 0.27 (Cyclohexane/Ethylacetate 4:1).

NMR-signals that can be assigned to epimer A:

^{1}H-NMR, COSY (400 MHz, $CDCl_3$) δ (ppm) = 7.41–7.15 (m, 20H, H-Ar), 4.92 (d, ^3J = 1.9 Hz, 1H, H-1), 4.89 (d, ^2J = 10.8 Hz, 1H, C-4–O–C$H_{2,a}$–Ph), 4.79–4.70 (m, 2H, C-2–O–CH_2–Ph), 4.69–4.62 (m, 3H, C-6–O–C$H_{2,a}$–Ph, C-3–O–CH_2–Ph), 4.57–4.49 (m, 2H, C-6–O–C$H_{2,b}$–Ph, C-4–O–C$H_{2,b}$–Ph), 4.03–3.96 (m, 1H, H-4), 3.96–3.91 (m, 1H, H-5), 3.83 (dd, ^3J = 3.1 Hz, ^3J = 1.9 Hz, H-2), 3.81–3.71 (m, 3H, H-3, 2 × H-6), 3.67 (dd, ^2J = 4.1 Hz, ^3J = 2.6 Hz, 2H, Man–O–CH_2), 3.16–3.10 (m, 1H, Man–O–CH$_2$–C*H*), 2.79–2.74 (m, 1H, Man–O–CH$_2$–CH(O)C$H_{2,a}$), 2.59 (dd, ^2J = 5.1 Hz, ^3J = 2.7 Hz, 1H, Man–O–CH$_2$–CH(O)C$H_{2,b}$).

^{13}C-NMR, HSQC, HMBC (100.6 MHz, $CDCl_3$) δ (ppm) = 138.6, 138.5, 138.5, 138.4 (4 × C_q), 128.5, 128.5, 128.4, 128.1, 127.9, 127.9, 127.8, 127.7 (C-Ar), 98.2 (C-1), 80.2 (C-5), 75.3 (C-4–O–*C*H$_2$–Ph), 75.0 (C-4), 74.7 (C-2), 73.5 (C-6–O–*C*H$_2$–Ph), 72.8 (C-2–O–*C*H$_2$–Ph), 72.3 (C-3–O–*C*H$_2$–Ph), 72.1 (C-3), 69.3 (C-6), 67.2 (Man–O–*C*H$_2$), 50.2 (Man–O–CH$_2$–*C*H), 44.5 (Man–O–CH$_2$–CH(O)*C*H$_2$).

NMR-signals that can be assigned to epimer B:

^{1}H-NMR, COSY (400 MHz, $CDCl_3$) δ (ppm) = 7.41–7.15 (m, 20H, H-Ar), 4.94 (d, ^3J = 1.9 Hz, 1H, H-1), 4.90 (d, ^2J = 10.8 Hz, 1H, C-4–O–C$H_{2,a}$–Ph), 4.79–4.70 (m, 2H, C-2–O–CH_2–Ph), 4.69–4.62 (m, 3H, C-6–O–C$H_{2,a}$–Ph, C-3–O–CH_2–Ph), 4.57–4.49 (m, 2H, C-6–O–C$H_{2,b}$–Ph, C-4–O–C$H_{2,b}$–Ph), 4.03–3.96 (m, 1H, H-4), 3.96–3.91 (m, 1H, H-5), 3.90 (dd, ^2J = 3.0 Hz, ^3J = 2.0 Hz, 1H, Man–O–C$H_{2,a}$), 3.87 (dd, ^3J = 2.9 Hz, ^3J = 1.9 Hz, H-2), 3.81–3.71 (m, 3H, H-3, 2 × H-6), 3.33 (dd, ^2J = 11.6 Hz, ^3J = 6.7 Hz,1H, Man–O–C$H_{2,b}$), 3.16–3.10 (m, 1H, Man–O–CH_2–C*H*), 2.79–2.74 (m, 1H, Man–O–CH_2–CH(O)C$H_{2,a}$), 2.53 (dd, ^2J = 4.9 Hz, ^3J = 2.7 Hz, 1H, Man–O–CH_2–CH(O)C$H_{2,b}$).

^{13}C-NMR, HSQC, HMBC (100.6 MHz, $CDCl_3$) δ (ppm) = 138.6, 138.5, 138.5, 138.4 (4 × C_q), 128.5, 128.5, 128.4, 128.1, 127.9, 127.9, 127.8, 127.7 (C-Ar), 98.4 (C-1), 80.2 (C-5), 75.3 (C-4–O–*C*H_2–Ph), 75.0 (C-4), 74.6 (C-2), 73.5 (C-6–O–*C*H_2–Ph), 72.8 (C-2–O–*C*H_2–Ph), 72.3 (C-3–O–*C*H_2–Ph), 72.2 (C-3), 69.4 (C-6), 68.9 (Man–O–*C*H_2), 50.7 (Man–O–CH_2–*C*H), 44.7 (Man–O–CH_2–CH(O)*C*H_2).

IR (ATR) $\tilde{\nu}$ (cm^{-1}) = 3030, 2912, 2868, 1496, 1453, 1363, 1280, 1207, 1092, 1052, 1027, 909, 843, 735, 696.

$[\boldsymbol{\alpha}]_{\boldsymbol{D}}^{\mathbf{24}}$ = +29.6° (c = 1.00, $CHCl_3$).

ESI-MS: *m/z* (%) = 619.6 (100) $[M + Na]^+$, 620.3 (15) $[M(^{13}C_1) + Na]^+$, 615.3 (98) $[M + NH_4]^+$, 616.2 (15) $[M(^{13}C_1) + NH_4]^+$.

2.2.4 Allyl-2,3:4,6-di-*O*-isopropyliden-α,β-D-mannopyranose **5**

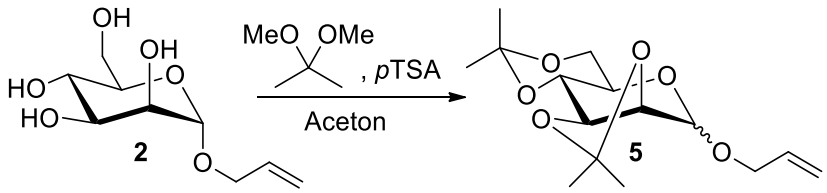

A suspension of allyl-α-D-mannopyranose (**2**, 5.68 g, 25.5 mmol, 1.0 eq.) in acetone (72 mL) was treated with *para*-toluenesulfonic acid (480 mg, 2.52 mmol, 0.1 eq.) and 2,2-dimethoxy propane (24.0 mmol, 196 mmol, 7.5 eq.) and stirred for 16 hours at room temperature. Subsequently triethylamine (1.5 mL) was added and the solvents were removed *in vacuo*. The residue was taken up in a mixture of diethylether (200 mL) and saturated $NaHCO_3$-solution (200 mL) and was extracted. The separated organic phase was

dried over anhydrous Na_2SO_4 and filtered. The solvent was removed in vacuo and the residue was purified by flash column chromatography (cyclohexane/ethyl acetate, gradient 0% to 20% ethyl acetate with an addition of 3% triethylamine, Isolera Flash Purification System) to afford the title compound (2.08 g, 6.93 mmol, 27%, pure α-anomer) as a colorless oil. Furthermore a mixture of both anomeres in α:β ratio 1:2.2 (154 mg, 2%) could be obtained.

R_f = 0.47 (cyclohexane/ethyl acetate 5:1), α-anomer.

R_f = 0.31 (cyclohexane/ethyl acetate 5:1), β-anomer.

NMR-signals that can be assigned to the α-anomer:

^{1}H-NMR, COSY 600 MHz, $CDCl_3$) δ (ppm) = 5.90 (dddd, ^3J = 16.9 Hz, ^3J = 10.4 Hz, ^3J = 6.3 Hz, ^3J = 5.3 Hz, 1H, Man–O–CH_2–C*H*), 5.30 (*pseudo* dq, ^2J = 17.2 Hz, J = 1.6 Hz, 1H, O–CH_2–CH=C$H_{2,a}$), 5.22 (*pseudo* dq, ^2J = 10.4 Hz, J = 1.4 Hz, 1H, O–CH_2–CH=C$H_{2,b}$), 5.07 (br s, 1H, H-1), 4.21–4.15 (m, 3H, H-2, H-3, Man–O–C$H_{2,a}$), 3.99 (ddt, ^2J = 12.7 Hz, ^3J = 6.3 Hz, ^4J = 1.3 Hz, 1H, Man–O–C$H_{2,b}$), 3.88 (dd, ^2J = 10.7 Hz, ^3J = 5.6 Hz, 1H, H-6_a), 3.79–3.72 (m, 2H, H-4, H-6_b), 3.61 (*pseudo* dt, ^3J = 10.3 Hz, ^3J = 5.6 Hz, 1H, H-5), 1.56 (s, 3H, C-2,C-3–C_q–CH_3), 1.52 (s, 3H, C-4,C-6–C_q–CH_3), 1.43 (s, 3H, C-4,C-6–C_q–CH_3), 1.38 (s, 3H, C-2,C-3–C_q–CH_3).

^{13}C-NMR, HSQC, HMBC (150.9 MHz, $CDCl_3$) δ (ppm) = 133.6 (Man–O–CH_2–*C*H), 118.2 (Man–O–CH_2–CH=*C*H_2), 109.6 (C-2,C-3–C_q), 99.8 (C-4,C-6–C_q), 97.1 (C-1), 76.2 (C-2), 75.0 (C-3), 72.9 (C-4), 68.3 (Man–O–*C*H_2), 62.2 (C-6), 61.5 (C-5), 29.2 (C-4,C-6–C_q–*C*H_3), 28.3 (C-2,C-3–C_q–*C*H_3), 26.3 (C-2,C-3–C_q–*C*H_3), 18.9 (C-4,C-6–C_q–*C*H_3).

NMR-signals that can be assigned to the β-anomer:

^{1}H-NMR, COSY 600 MHz, $CDCl_3$) δ (ppm) = 5.97–5.86 (m, 1H, Man–O–CH_2–C*H*), 5.34–5.30 (m, 1H, O–CH_2–CH=C$H_{2,a}$), 5.25–5.22 (*m*, 1H, O–CH_2–CH=C$H_{2,b}$), 4.84 (d, ^3J = 2.5 Hz 1H, H-1), 4.40 (*pseudo* ddt, ^2J = 13.1 Hz, ^3J = 4.9 Hz, ^4J = 1.5 Hz, 1H, Man–O–C$H_{2,a}$), 4.29 (dd, ^3J = 5.9 Hz, ^3J = 2.5 Hz, 1H, H-2), 4.18–4.13 (m, 2H, H-3, Man–O–C$H_{2,b}$), 4.02 (dd, ^3J = 10.3 Hz, ^3J = 7.6 Hz, 1H, H-4), 3.93 (dd, ^2J = 10.9 Hz, ^3J = 5.5 Hz, 1H, H-6_a), 3.81–3.75 (m, 1H, H-6_b), 3.23 (*pseudo* dt, ^3J = 10.3 Hz, ^3J = 5.5 Hz, 1H, H-5), 1.55 (s, 3H, C-2:C-3–C_q–CH_3), 1.52 (s, 3H, C-4:C-6–C_q–CH_3), 1.42 (s, 3H, C-4:C-6–C_q–CH_3), 1.35 (s, 3H, C-2:C-3–C_q–CH_3).

^{13}C-NMR, HSQC, HMBC (150.9 MHz, $CDCl_3$) δ (ppm) = 133.7 (Man–O–CH_2–*C*H), 118.4 (Man–O–CH_2–CH=*C*H_2), 111.2 (C-2:C-3–C_q), 99.8 (C-4:C-6–C_q), 97.4 (C-1), 76.6 (C-3), 74.7 (C-2), 72.3 (C-4), 70.2 (Man–O–*C*H_2), 66.0 (C-5), 62.6 (C-6), 29.1 (C-4:C-6–C_q–*C*H_3), 28.0 (C-2:C-3–C_q–*C*H_3), 26.3 (C-2:C-3–C_q–*C*H_3), 19.0 (C-4:C-6–C_q–*C*H_3).

IR (ATR) $\tilde{\nu}$ (cm^{-1}) = 2989, 2937, 2915, 2876, 1571, 1458, 1381, 1370, 1242, 1218, 1198, 1166, 1114, 1073, 1041, 923, 852, 809, 785.

$[\boldsymbol{\alpha}]_{\boldsymbol{D}}^{\mathbf{28}}$ = +12.5° (c = 1.00, $CHCl_3$).

ESI-MS: *m/z* (%) = measurement not possible (The substance decomposes due to the acidic conditions on the HPLC-column.)

HRMS (ESI): calculated for $[C_{15}H_{24}O_6 + Na]^+$: 323.1465 found: 323.1464.

The spectral data are in accordance with literature.[4]

2.2.5 1-(Oxiran-2-ylmethyl)-2,3:4,6-di-*O*-isopropyliden-α-D-mannopyranose **6**

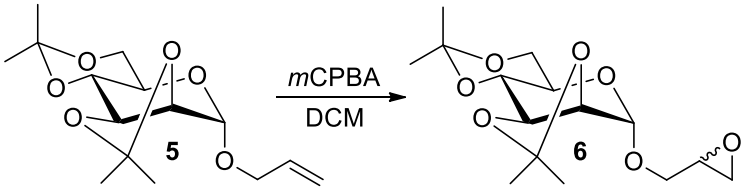

A solution of mannopyranose **5** (1.20 g, 4.00 mmol, 1.0 eq.) in dichloromethane (100 mL) was treated with *m*CPBA (1.04 g, 6.00 mmol, 1.5 eq.) at 0 °C under stirring. The reaction mixture was stirred for 18 hours at room temperature, but TLC (cyclohexane/ethyl acetate 5:1) still showed starting material. Again *m*CPBA (300 mg, 1.74 mmol, 0.4 eq.) was added and the reaction mixture was stirred for 18 hours at room temperature. Subsequently, TLC showed complete conversion and the reaction mixture was diluted with ethyl acetate (200 mL) and transferred into a 2 L Erlenmeyer flask. Then saturated $Na_2S_2O_3$-solution (300 mL) was added and the mixture was vigorously stirred for 20 minutes. The separated organic layer was washed with saturated $NaHCO_3$-solution (150 mL) and dried over anhydrous Na_2SO_4. The solvent was removed *in vacuo* and the residue was purified by flash column chromatography (cyclohexane/ethyl acetate, gradient 0% to 40% ethyl acetate with an addition of 2% triethylamine, Isolera Flash Purification System) to afford the title

compound (875 mg, 2.77 mmol, 69%, mixture of both epimers in ratio 1:0.9) as a colorless oil.

R_f = 0.24 (cyclohexane/ethyl acetate 5:1).

NMR-signals that can be assigned to the epimer A:

^{1}H-NMR, COSY (400 MHz, $CDCl_3$) δ (ppm) = 5.08 (br s, 1H, H-1), 4.24 (*pseudo* d, ^3J = 5.6 Hz, 1H, H-2), 4.18–4.13 (m, 1H, H-3), 3.92 (dd, ^2J = 11.6 Hz, ^3J = 3.0 Hz, 1H, Man–O–C$H_{2,a}$), 3.90–3.84 (m, 1H, H-6$_a$), 3.79–3.71 (m, 2H, H-4, H-6$_b$), 3.65–3.58 (m, 1H, H-5), 3.39 (dd, ^2J = 11.6 Hz, ^3J = 6.6 Hz, Man–O–C$H_{2,b}$), 3.19–3.14 (m, 1H, Man–O–CH_2–C*H*), 2.85–2.80 (m, 1H, Man–O–CH_2–CH(O)C$H_{2,a}$), 2.59 (dd, ^2J = 4.9 Hz, ^3J = 2.6 Hz, 1H, Man–O–CH_2–CH(O)C$H_{2,b}$).

^{13}C-NMR, HSQC, HMBC (100.6 MHz, $CDCl_3$) δ (ppm) = 109.5 (C-2:C-3–C_q), 99.7 (C-4:C-6–C_q), 98.1 (C-1), 75.9 (C-2), 74.8 (C-3), 72.6 (C-4), 68.8 (Man–O–CH_2), 62.0 (C-6), 61.5 (C-5), 50.5 (Man–O–CH_2–*C*H), 44.5 (Man–O–CH_2–CH(O)*C*H_2), 29.1 (C-4:C-6–C_q–*C*H_3), 28.2 (C-2:C-3–C_q–*C*H_3), 26.1 (C-2:C-3–C_q–*C*H_3), 18.8 (C-4:C-6–C_q–*C*H_3).

NMR-signals that can be assigned to the epimer B:

^{1}H-NMR, COSY (400 MHz, $CDCl_3$) δ (ppm) = 5.08 (br s, 1H, H-1), 4.21 (*pseudo* d, ^3J = 5.7 Hz, 1H, H-2), 4.18–4.13 (m, 1H, H-3), 3.90–3.84 (m, 1H, H-6$_a$),), 3.79–3.71 (m, 3H, H-4, H-6$_b$, Man-O–C$H_{2,a}$), 3.68–3.65 (m, 1H, Man–O–C$H_{2,b}$), 3.65–3.58 (m, 1H, H-5), 3.19–3.14 (m, 1H, Man–O–CH_2–C*H*), 2.85–2.80 (m, 1H, Man–O–CH_2–CH(O)C$H_{2,a}$), 2.66 (dd, ^2J = 5.0 Hz, ^3J = 2.6 Hz, 1H, Man–O–CH_2–CH(O)C$H_{2,b}$).

^{13}C-NMR, HSQC, HMBC (100.6 MHz, $CDCl_3$) δ (ppm) = 109.5 (C-2:C-3–C_q), 99.7 (C-4:C-6–C_q), 98.1 (C-1), 75.9 (C-2), 74.8 (C-3), 72.6 (C-4), 67.8 (Man–O–CH_2), 62.0 (C-6), 61.5 (C-5), 50.1 (Man–O–CH_2–*C*H), 29.1 (C-4:C-6–C_q–*C*H_3), 28.2 (C-2:C-3–C_q–*C*H_3), 26.1 (C-2:C-3–C_q–*C*H_3), 18.8 (C-4:C-6–C_q–*C*H_3).

IR (ATR) $\tilde{\nu}$ (cm^{-1}) = 2990, 2938, 2917, 1381, 1371, 1219, 1198, 1166, 1137, 1114, 1081, 1042, 1021, 906, 850, 809, 784, 758.

$[\boldsymbol{\alpha}]_{\boldsymbol{D}}^{\mathbf{28}}$ = +10.5° (c = 1.00, $CHCl_3$).

ESI-MS: *m/z* (%) = 339.1 (100) $[M + Na]^+$, 340.2 (8) $[M(^{13}C_1) + Na]^+$, 317.2 (6) $[M + H]^+$.

HRMS (ESI): calculated for $[C_{15}H_{24}O_7 + Na]^+$: 339.1414 found: 339.1414.

2.3 Copolymer synthesis of BisHD-p(BMGE-*co*-EG)

The synthetic procedure is described for BisHD-p($BMGE_{1.1}$-*co*-$EG_{98.9}$) as representative example.

1,2-Bis-*n*-hexadecyl glyceryl ether (BisHD) (0.15 g, 0.278 mmol, 1 eq.) and CsOH (0.038 g, 0.250 mmol, 0.9 eq.) was placed in a dry Schlenk flask and dissolved in benzene (10 mL). The solution was stirred at 60 °C for at least 30 min to from the alkoxide and dried under vaccum for 16 h to remove moisture. Tetrahydrofuran (approx. 15 mL) was cryo-transferred to the Schlenk flask to dissolve the initiator. 1-(Oxiran-2-ylmethyl)-2,3,4,6-tetra-*O*-benzyl-*α*-D-mannopyranose (0.166 g, 0.278 mmol, 1 eq.) was dissolved in benzene (3 mL) and dried in vacuo for 16 h. Subsequently, it was dissolved in dry DMSO (3 mL) and injected into the Schlenk flask with a syringe at –80 °C. EO (1.25 mL, 27.551 mmol, 99 eq.) was cryo-transferred using a graduated ampule. The polymerization was carried out at 60 °C for 3 days. To quench the polymerization, an excess of ethanol was added. The solvent was removed under reduced pressure, the crude product was dissolved in THF and precipitated in cold diethyl ether to obtain the pure product. Yield: 63%.

^{1}H NMR, COSY (400 MHz, methanol-d_4, δ): 7.44–7.22 (m, H_{benzyl}), 4.96–4.95 (m, -OC*H*O-), 4.74–4.52 (m, -CH_2Bn), 3.97–3.43 (m, polyether backbone), 1.58–1.56 (m, -OCH_2CH_2- (BisHD)), 1.42–1.26 (m, -$OCH_2CH_2(CH_2)_{13}CH_3$ (BisHD)), 0.94–0.91 (m, 6H -$OCH_2CH_2(CH_2)_{15}CH_3$ (BisHD))

^{13}C NMR, HSQC, HMBC (100.6 MHz, methanol-d_4, δ): 129.4–128.7 (C_{benzyl}), 79.3 ($C_{glycerol}$), 73.7 (-CH_2Bn), 71.9–71.4 (polyether backbone, $C_{mannose}$, $C_{glycerol}$), 62.2 ($C_{glycerol}$), 33.1 (-$OCH_2CH_2(CH_2)_{13}CH_3$), 31.1–30.5 (-$OCH_2CH_2(CH_2)_{13}CH_3$), 27.3–27 (-$OCH_2CH_2(CH_2)_{13}CH_3$), 23.8 (-$OCH_2CH_2(CH_2)_{13}CH_3$), 14.5 (-$O(CH_2)_{15}CH_3$).

2.4 Removal of benzyl protecting groups

The procedure is described for BisHD-p($BMGE_{1.1}$-*co*-$EG_{98.9}$) as an example.

BisHD-p($BMGE_{1.1}$-co-$EG_{98.9}$) (0.201 g, 0.0224 mmol, 1 eq.) was dissolved in methanol (10 mL) and palladium hydroxide on activated charcoal (5 weight percent) was added. Hydrogen was introduced (40-50 bar) and the mixture was stirred at room temperature for 6 d. Afterwards, the catalyst was removed via filtration over celite®. The solvent was removed under reduced pressure and the pure product was obtained. Yield: 26%.

^{1}H NMR, COSY (400 MHz, methanol-d_4, δ): 3.89–3.41 (m, polyether backbone), 1.92–1.63 (m, -OCH_2CH_2-CH_2- (BisHD)), 1.32–1.13 (m, -$OCH_2CH_2(CH_2)_{13}CH_3$ (BisHD)), 1.00–0.93 (m, 6H -$OCH_2CH_2(CH_2)_{15}CH_3$ (BisHD)).

2.5 Copolymer synthesis of BisHD-p(IMGE-*co*-EG)

The synthetic procedure is described for BisHD-p($IMGE_{8.0}$-*co*-$EG_{92.0}$).

1,2-Bis-*n*-hexadecyl glyceryl ether (BisHD) (0.05 g, 0.093 mmol, 1 eq.) and CsOH (0.013 g,0.083 mmol, 0.9 eq.) was placed in a dry Schlenk flask and dissolved in benzene (10 mL). The solution was stirred at 60 °C for at least 30 min to from the alkoxide and dried under vaccum for 16 h to remove moisture. Tetrahydrofuran (approx. 15 mL) was cryo-transferred to the Schlenk flask to dissolve the initiator. 1-(Oxiran-2-ylmethyl)-2,3:4,6-di-*O*-isopropyliden-*α*-D-mannopyranose (0.088 g, 0.278 mmol, 3 eq.) was dissolved in benzene (3 mL) and dried in vacuo for 16 h. Subsequently, it was dissolved in dry DMSO (2 mL) and injected into the Schlenk flask with a syringe at –80 °C. EO (0.40 mL, 8.998 mmol, 97 eq.) was cryo-transferred using a graduated ampule. The polymerization was carried out at 60 °C for 3 days. To quench the polymerization, an excess of ethanol was added. The solvent was removed under reduced pressure, the crude product was dissolved in THF and precipitated in cold diethyl ether to obtain the pure product. Yield: 42%.

^{1}H NMR, COSY (400 MHz, benzene-d_6, δ): 5.26–5.22 (m, -OC*H*O-), 4.37–3.81 (m, $H_{mannose}$), 3.75–3.39 (m, polyether backbone, $H_{glycerol}$, $H_{mannose}$), 1.55–1.54 (m, -OCH_2CH_2-(BisHD)), 1.48 (s, CH_3CO-), 1.34–1.25 (m, -$OCH_2CH_2(CH_2)_{13}CH_3$ (BisHD)), 0.94–0.91 (m, 6H, -$OCH_2CH_2(CH_2)_{13}CH_3$ (BisHD)).

^{13}C NMR, HSQC, HMBC (100.6 MHz, benzene-d_6, δ): 109.5 ($C_{mannose}$), 99.9 ($C_{mannose}$), 98.7 (-O*C*HO-), 79.0–78.7 ($C_{mannose}$, $C_{glycerol}$), 77.0 ($C_{mannose}$), 75.9 ($C_{mannose}$), 73.8–73.5 ($C_{mannose}$), 73.4–70.4 (polyether backbone, $C_{glycerol}$), 67.9–67.6 ($C_{mannose}$, $C_{glycerol}$), 62.8–62.1 ($C_{mannose}$, $C_{glycerol}$), 40.9 (-$OCH_2CH_2(CH_2)_{13}CH_3$ (BisHD)), 32.6 (-$OCH_2CH_2(CH_2)_{13}CH_3$ (BisHD)), 31.1-30.3 (-$OCH_2CH_2(CH_2)_{13}CH_3$ (BisHD)), 30.1 (-OCCH_3), 27.0-26.7 (-$OCH_2CH_2(CH_2)_{13}CH_3$ (BisHD)), 23.4 (-$OCH_2CH_2(CH_2)_{13}CH_3$ (BisHD)), 19.1 (-$OCH_2CH_2(CH_2)_{13}CH_3$ (BisHD)), 14.7 (-$O(CH_2)_{15}CH_3$ (BisHD)).

3. Characterization Data

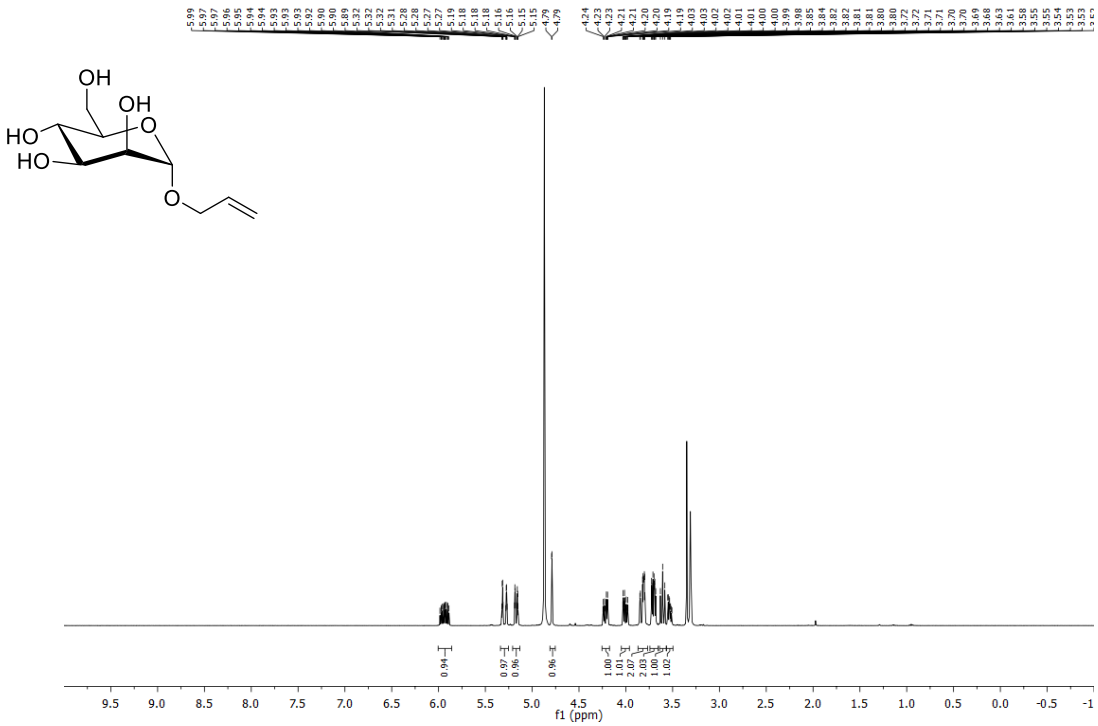

Figure S1. ^{1}H NMR spectrum (chloroform-*d*, 400 MHz) of allyl-*α*-D-mannopyranose (**2**).

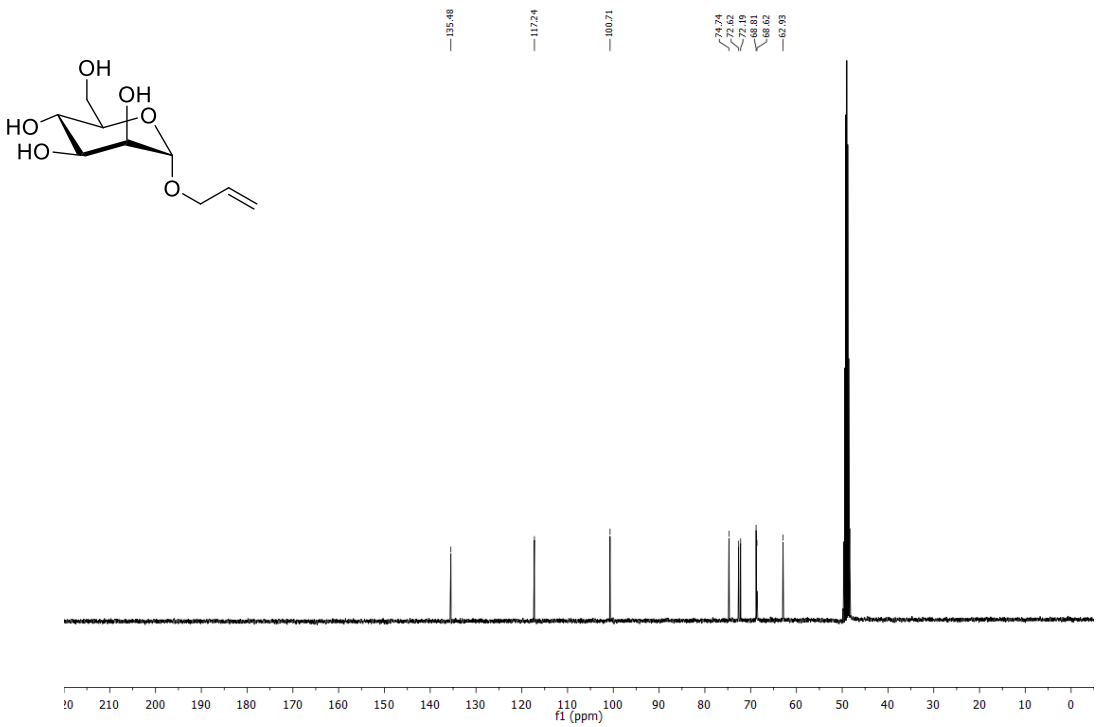

Figure S2. ^{13}C NMR spectrum (chloroform-*d*, 100.6 MHz) of allyl-*α*-D-mannopyranose (**2**).

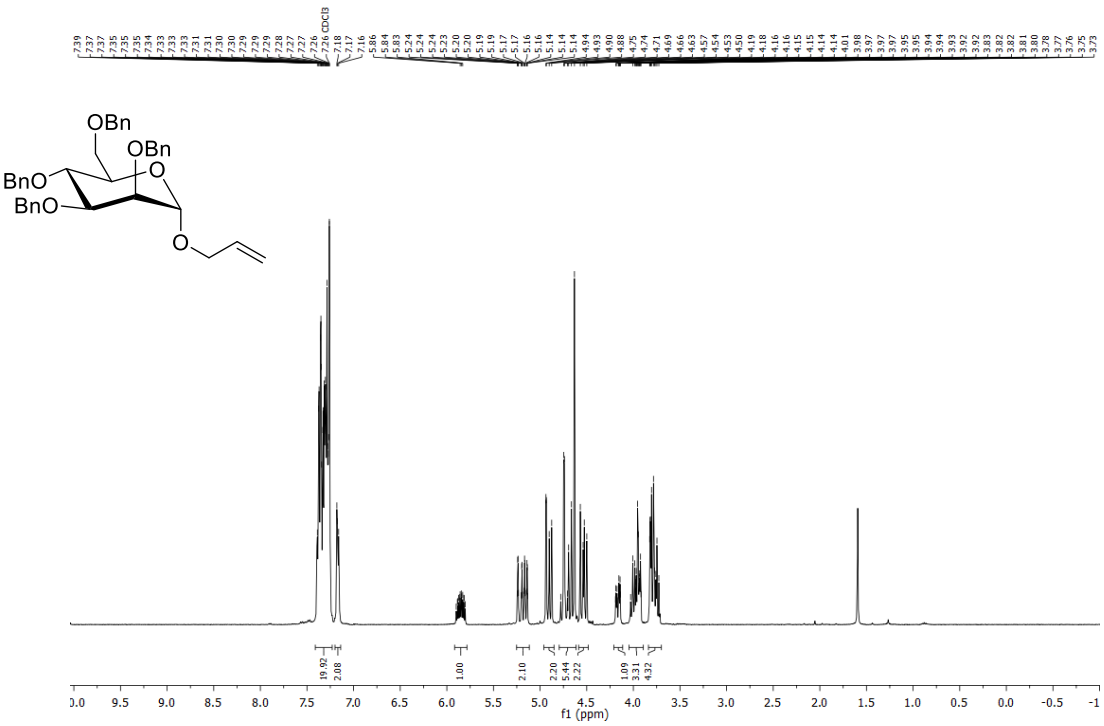

Figure S3. ^{1}H NMR spectrum (chloroform-*d*, 400 MHz) of allyl-2,3,4,6-tetra-*O*-benzyl-*α*-D-mannopyranose (**3**).

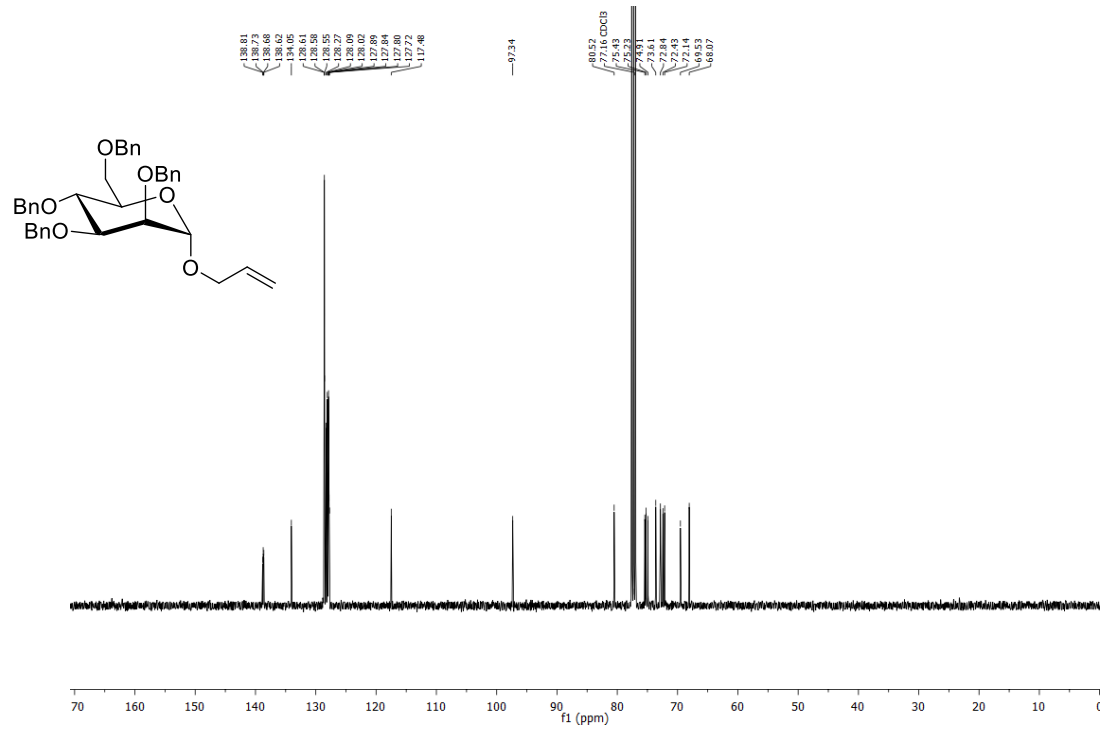

Figure S4. ^{13}C NMR spectrum (chloroform-*d*, 100.6 MHz) of allyl-2,3,4,6-tetra-*O*-benzyl-*α*-D-mannopyranose (**3**).

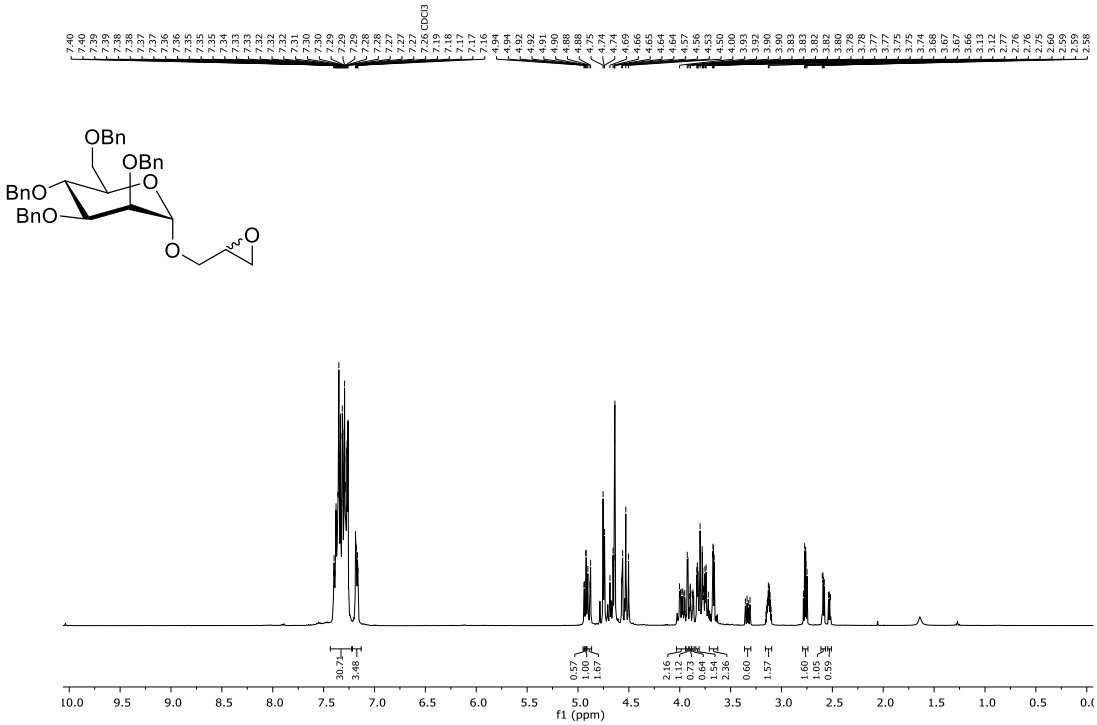

Figure S5. ^{1}H NMR spectrum (chloroform-*d*, 400 MHz) of 1-(oxiran-2-ylmethyl)-2,3,4,6-tetra-*O*-benzyl-*α*-D-mannopyranose (**4**).

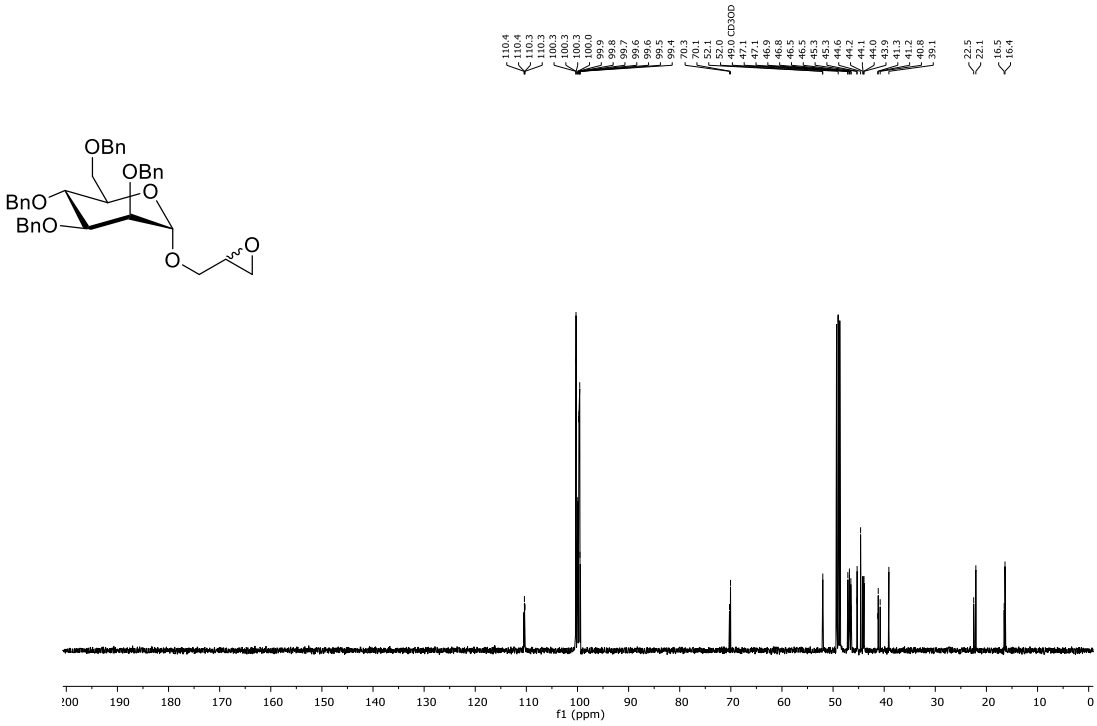

Figure S6. ^{13}C NMR spectrum (chloroform-*d*, 100.6 MHz) of 1-(oxiran-2-ylmethyl)-2,3,4,6-tetra-*O*-benzyl-*α*-D-mannopyranose (**4**).

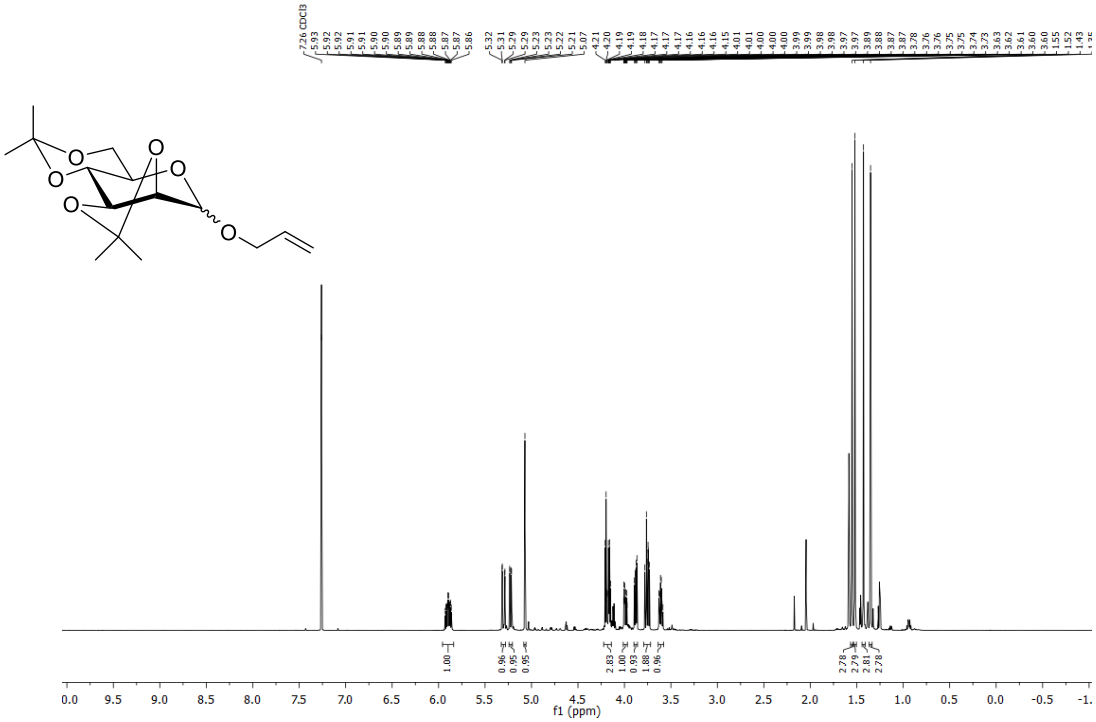

Figure S7. ^{1}H NMR spectrum (chloroform-*d*, 600 MHz) of allyl-2,3:4,6-di-*O*-isopropyliden-*α*,*β*-D-mannopyranose (**5**).

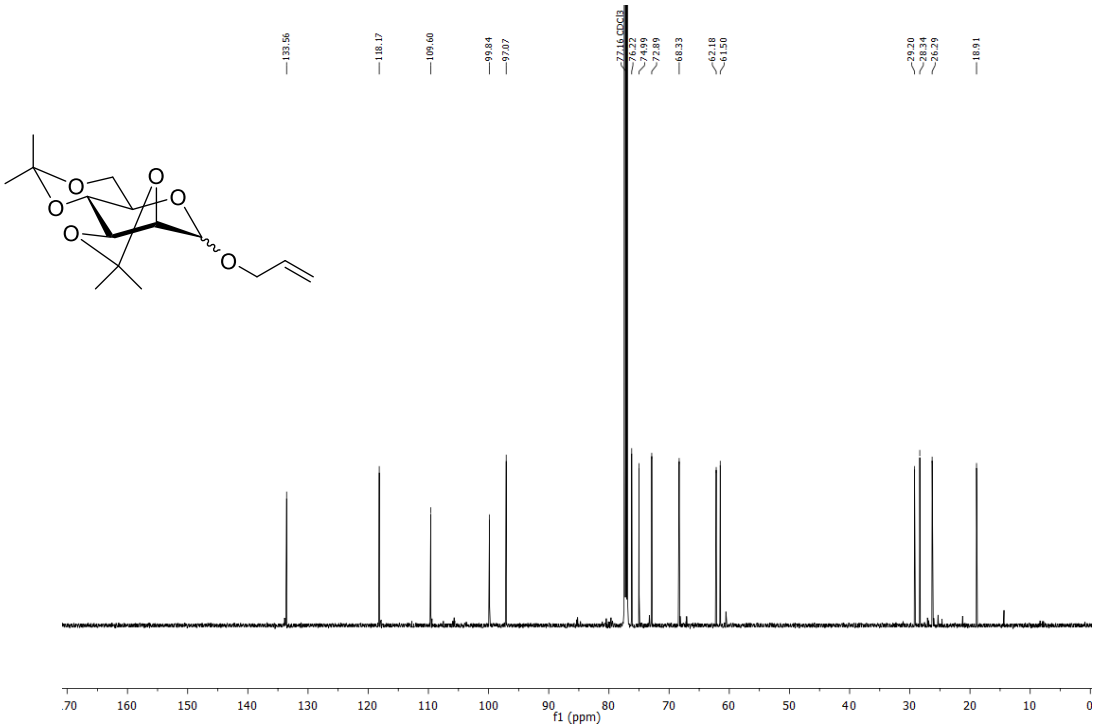

Figure S8. ^{13}C NMR spectrum (chloroform-*d*, 151 MHz) of allyl-2,3:4,6-di-*O*-isopropyliden-*α*,*β*-D-mannopyranose (**5**).

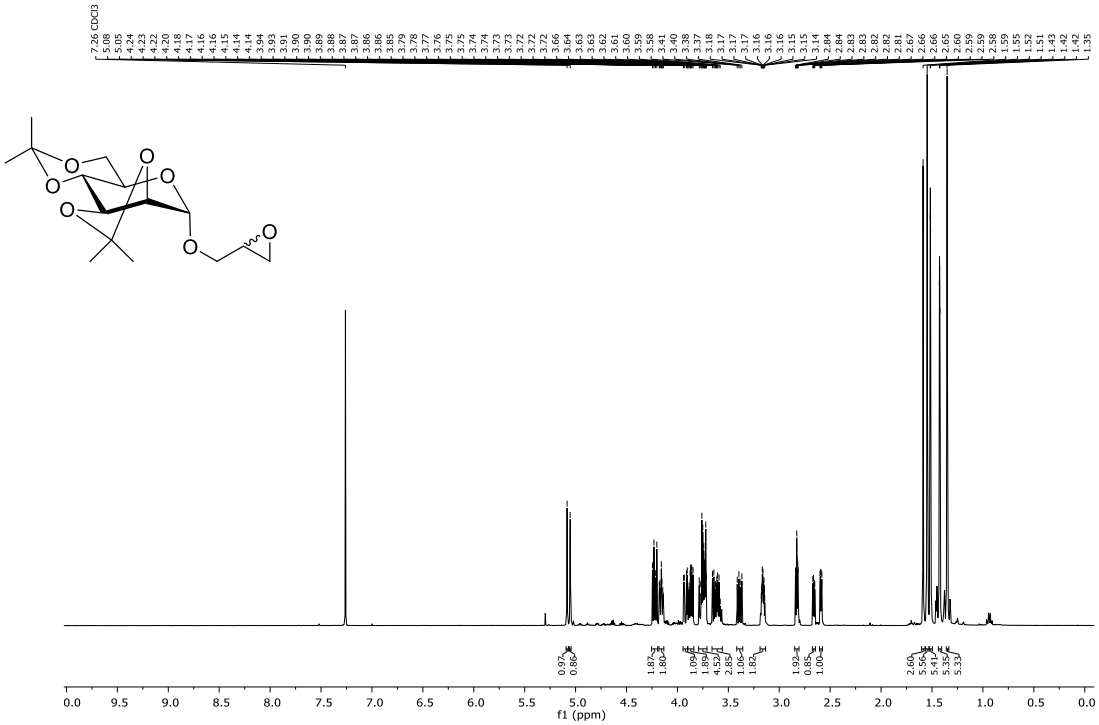

Figure S9. ^{1}H NMR spectrum (chloroform-*d*, 400 MHz) of 1-(oxiran-2-ylmethyl)-2,3:4,6-di-*O*-isopropyliden-*α*-D-mannopyranose (**6**).

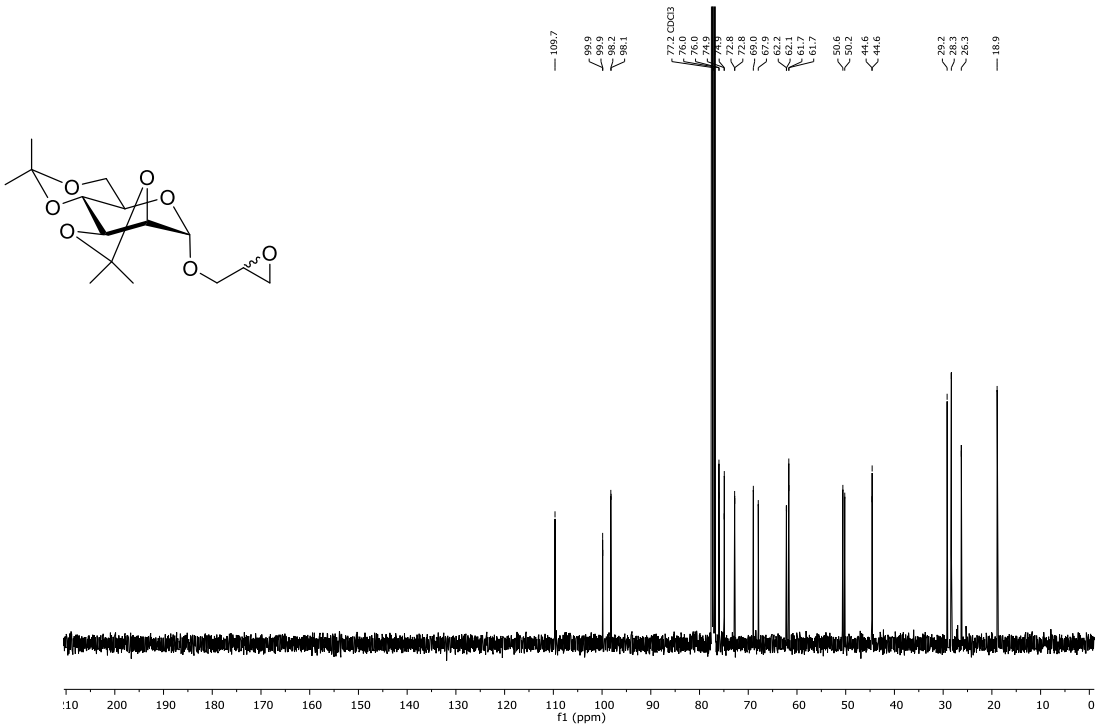

Figure S10. ^{13}C NMR spectrum (chloroform-*d*, 100.6 MHz) of 1-(oxiran-2-ylmethyl)-2,3:4,6-di-*O*-isopropyliden-*α*-D-mannopyranose (**6**).

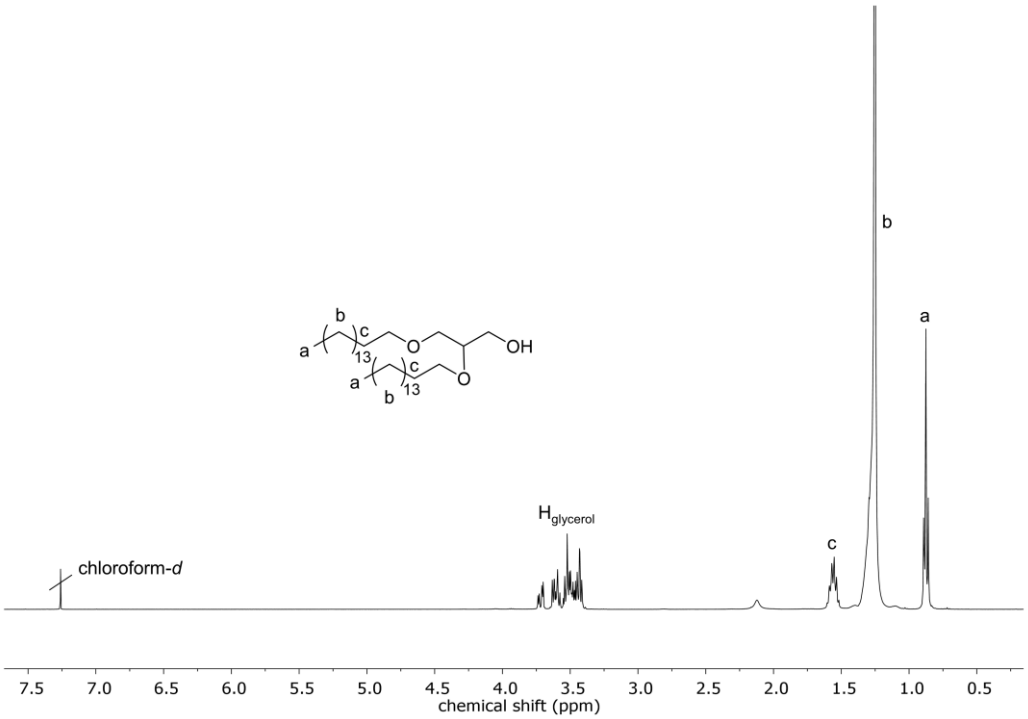

Figure S11. ^{1}H NMR (chloroform-*d*, 400 MHz) of 1,2-bis-*n*-hexadecyl glyceryl ether (BisHD).

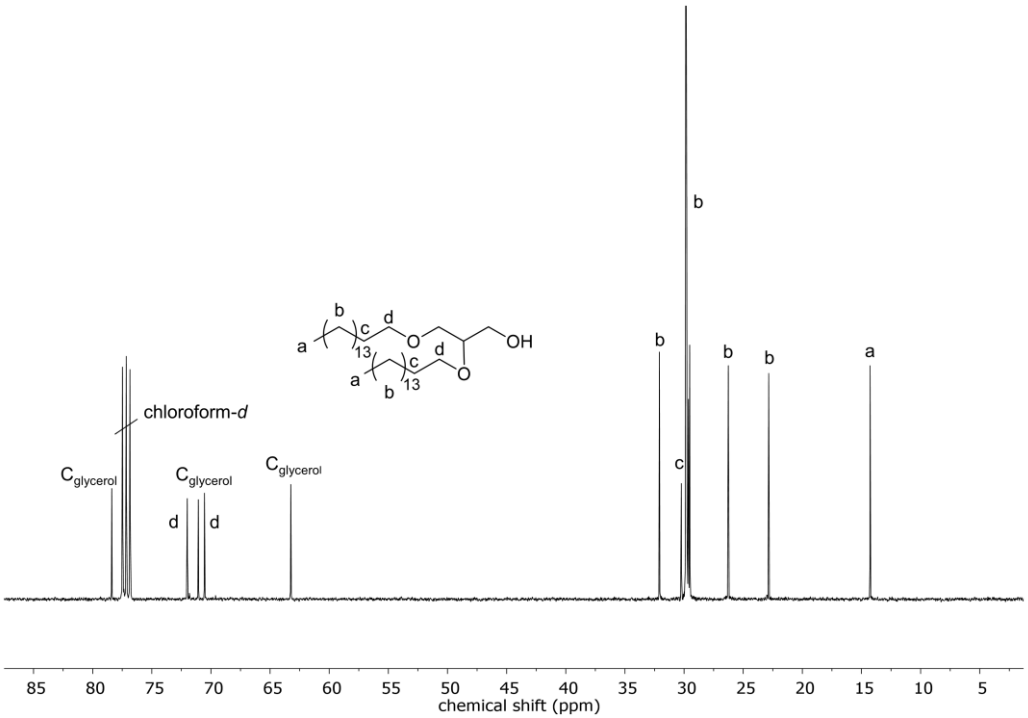

Figure S12. ^{13}C NMR (chloroform-*d*, 100.6 MHz) of 1,2-bis-*n*- hexadecyl glyceryl ether (BisHD).

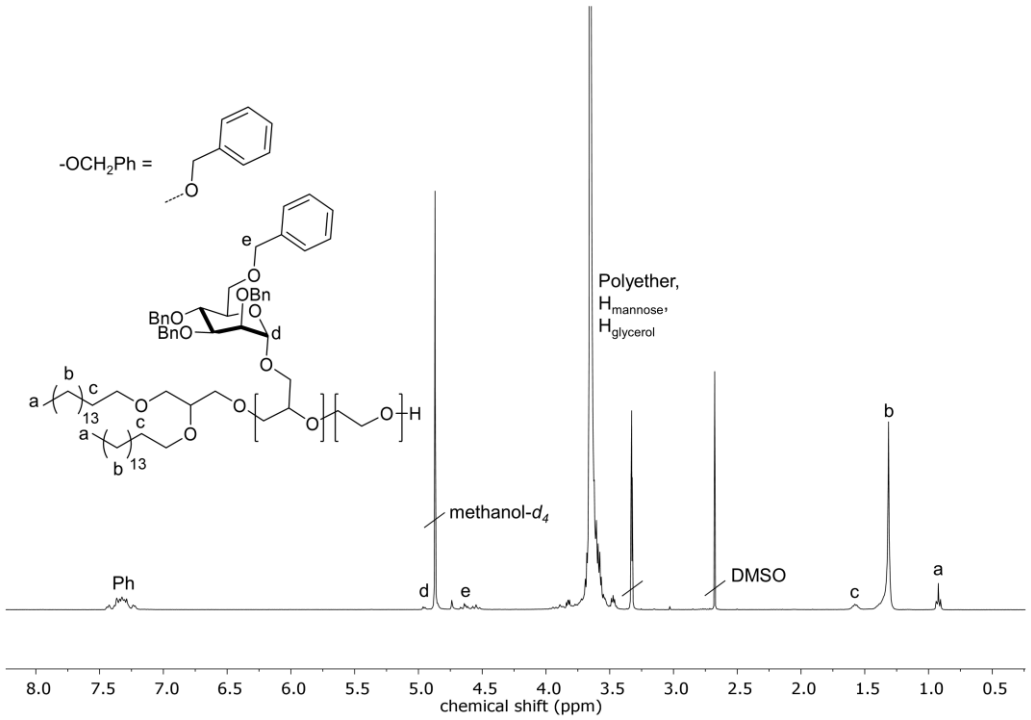

Figure S13. ^{1}H NMR (methanol-d_4, 400 MHz) of BisHD-p(BMGE$_{1.1}$-*co*-EG$_{98.9}$).

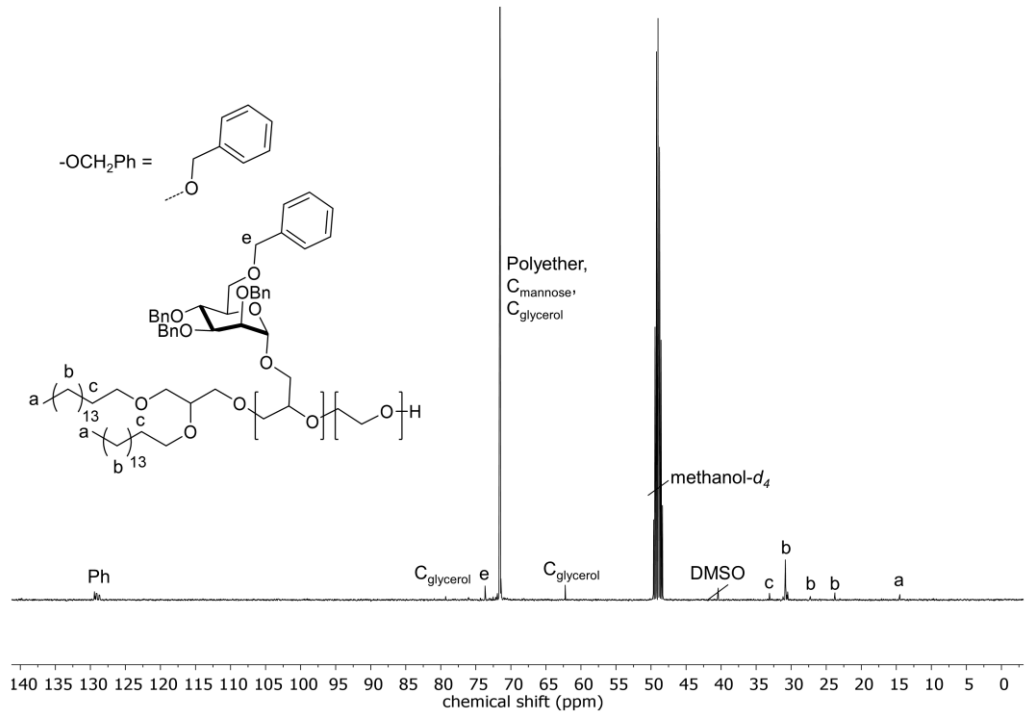

Figure S14. ^{13}C NMR (methanol-d_4, 100.6 MHz) of BisHD-p(BMGE$_{1.1}$-*co*-EG$_{98.9}$).

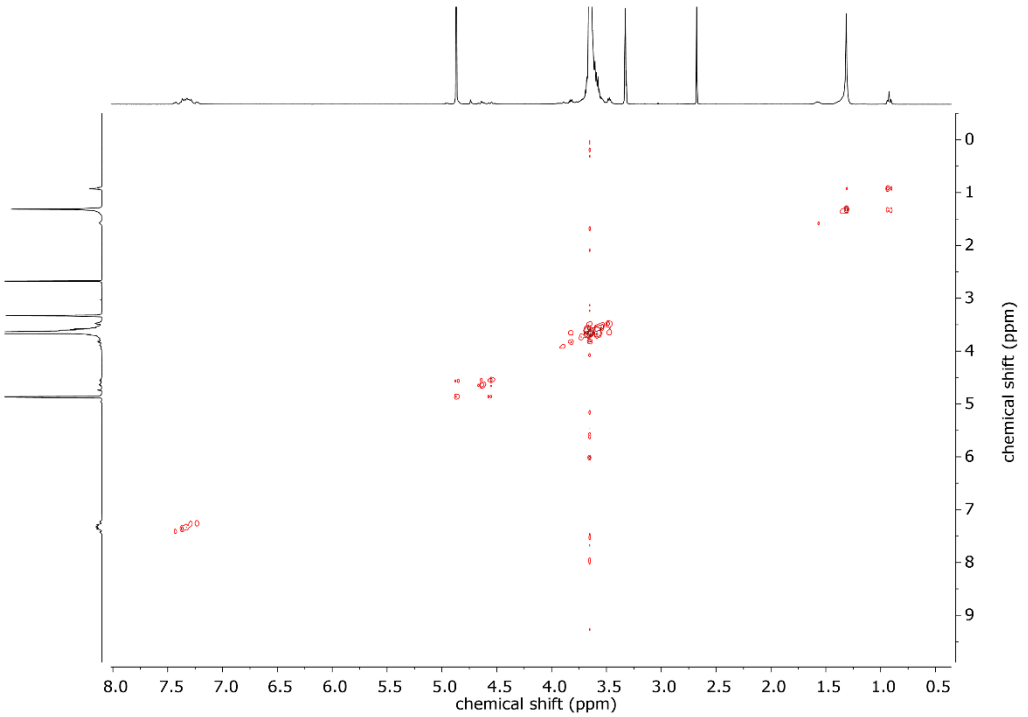

Figure S15. COSY NMR (methanol-d_4, 400 MHz) of BisHD-p(BMGE$_{1.1}$-*co*-EG$_{98.9}$).

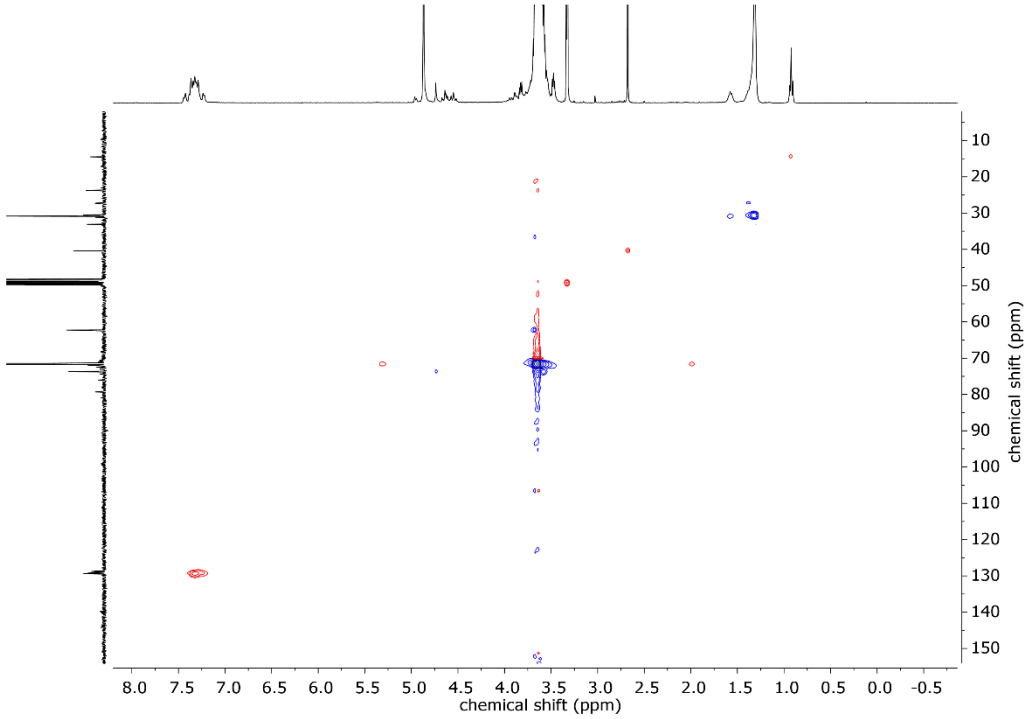

Figure S16. HSQC NMR (methanol-d_4) of BisHD-p(BMGE$_{1.1}$-*co*-EG$_{98.9}$).

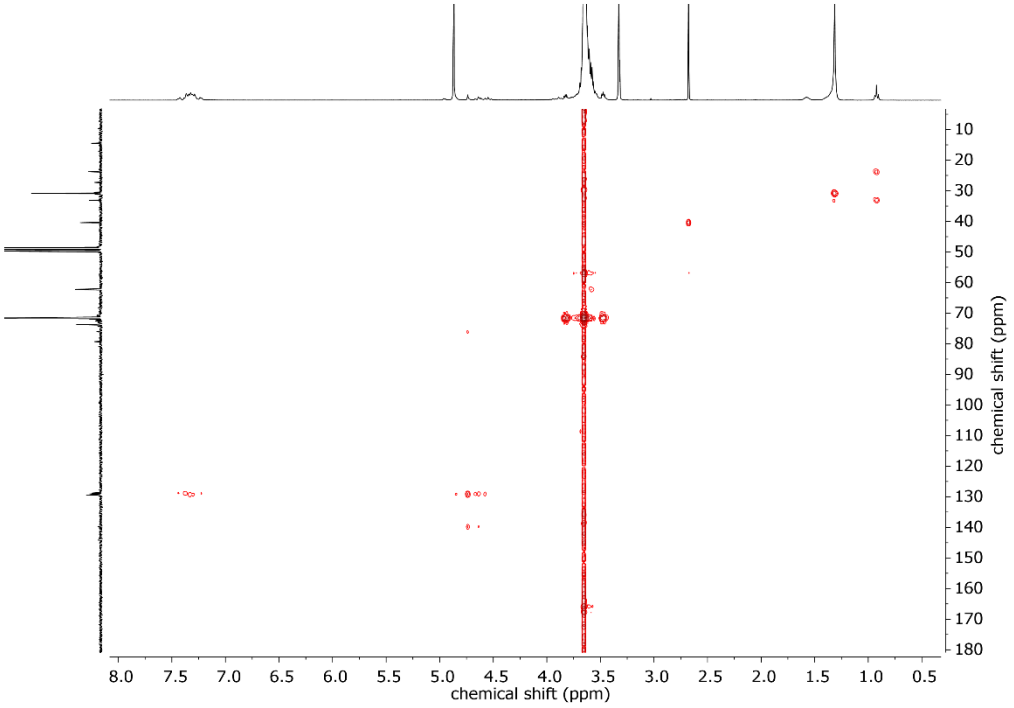

Figure S17. HMBC NMR (methanol-d_4) of BisHD-p(BMGE$_{1.1}$-*co*-EG$_{98.9}$).

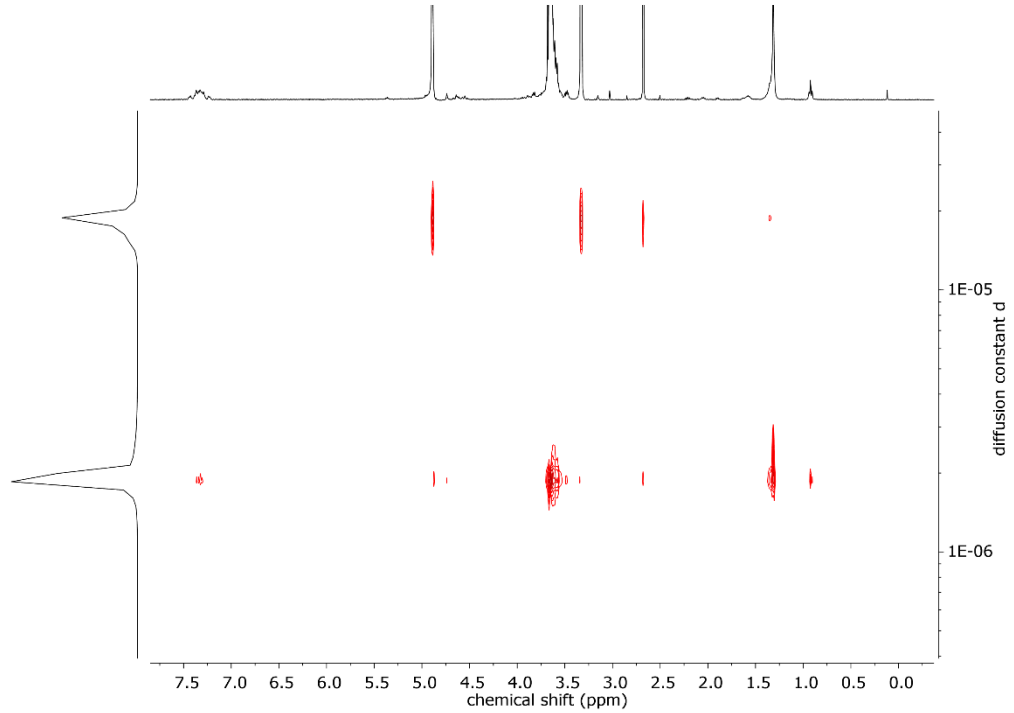

Figure S18. DOSY NMR (methanol-d_4, 400 MHz) of BisHD-p(BMGE$_{0.7}$-*co*-EG$_{99.3}$).

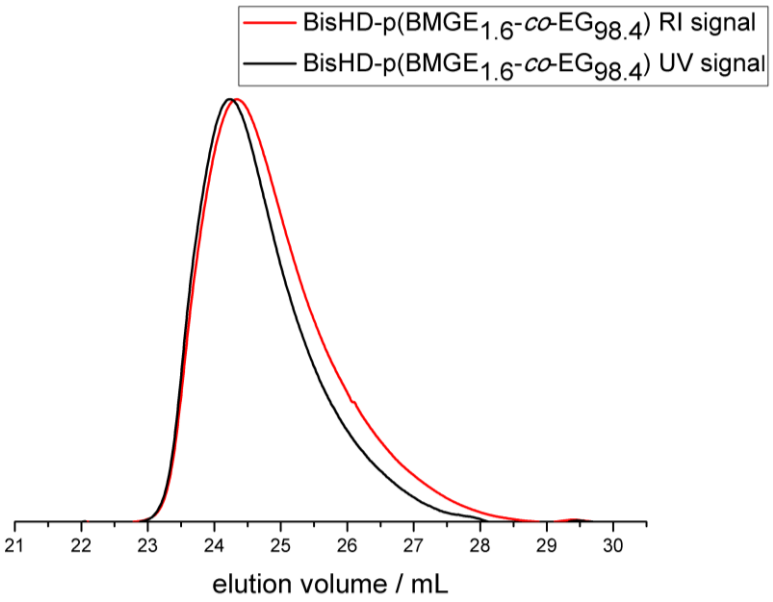

Figure S19. SEC elugram of BisHD-p(BMGE$_{1.6}$-co-EG$_{98.4}$) measured in THF using PEG standards. The RI signal is shown in red and the UV signal is represented by the black curve.

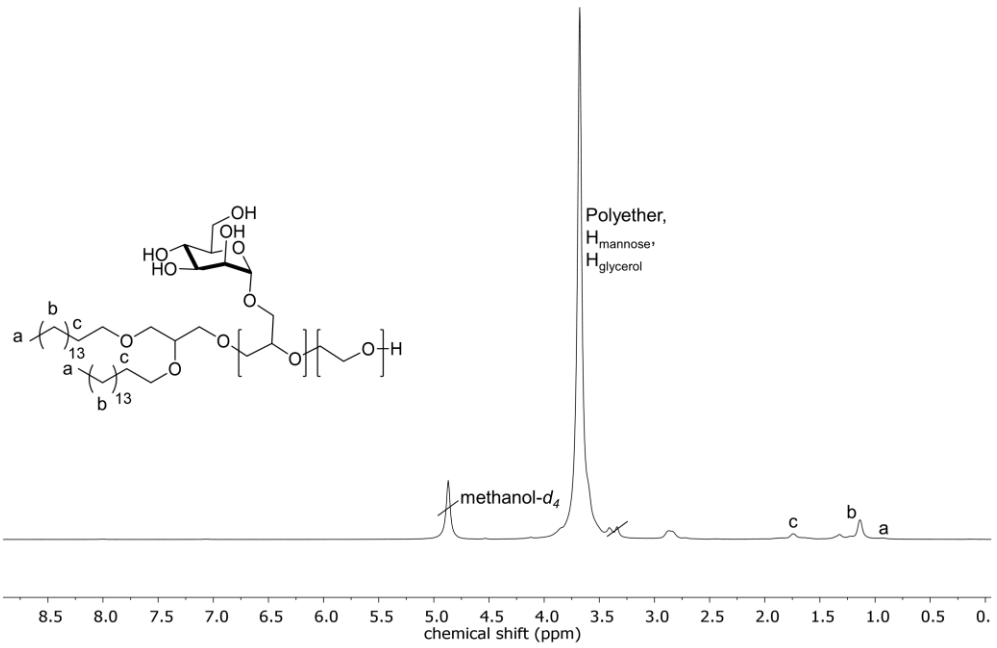

Figure S20. ^{1}H NMR (methanol-d_4, 400 MHz) of BisHD-p(MGE$_{1.1}$-*co*-EG$_{98.9}$).

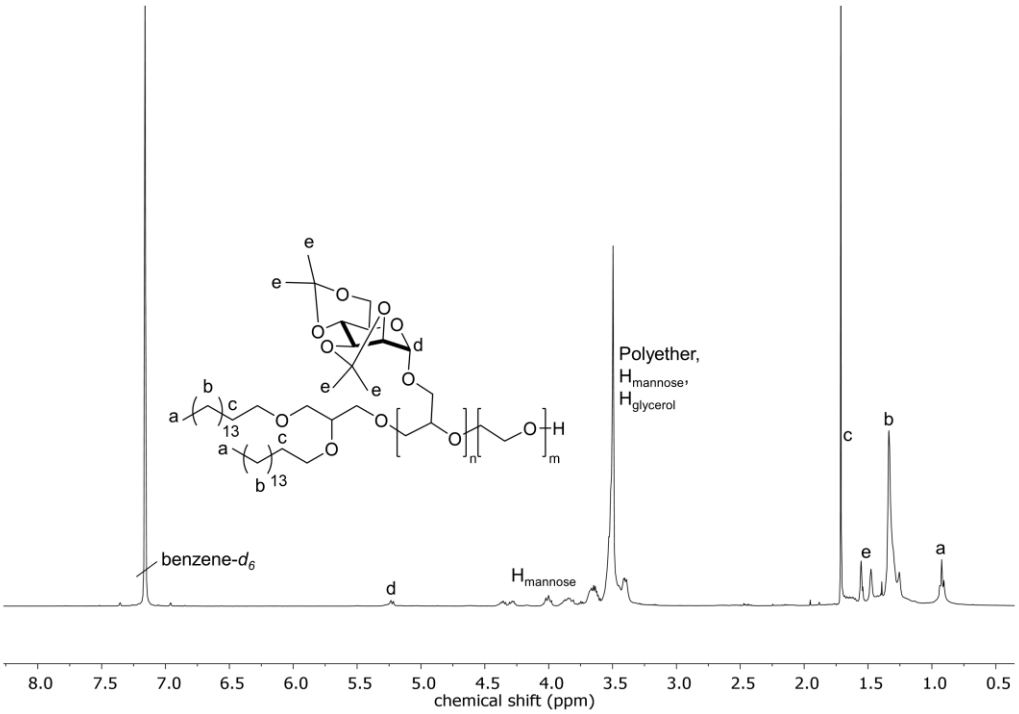

Figure S21. ^{1}H NMR (benzene-d_6, 400 MHz) of BisHD-p(IMGE$_{8.0}$-*co*-EG$_{92.0}$).

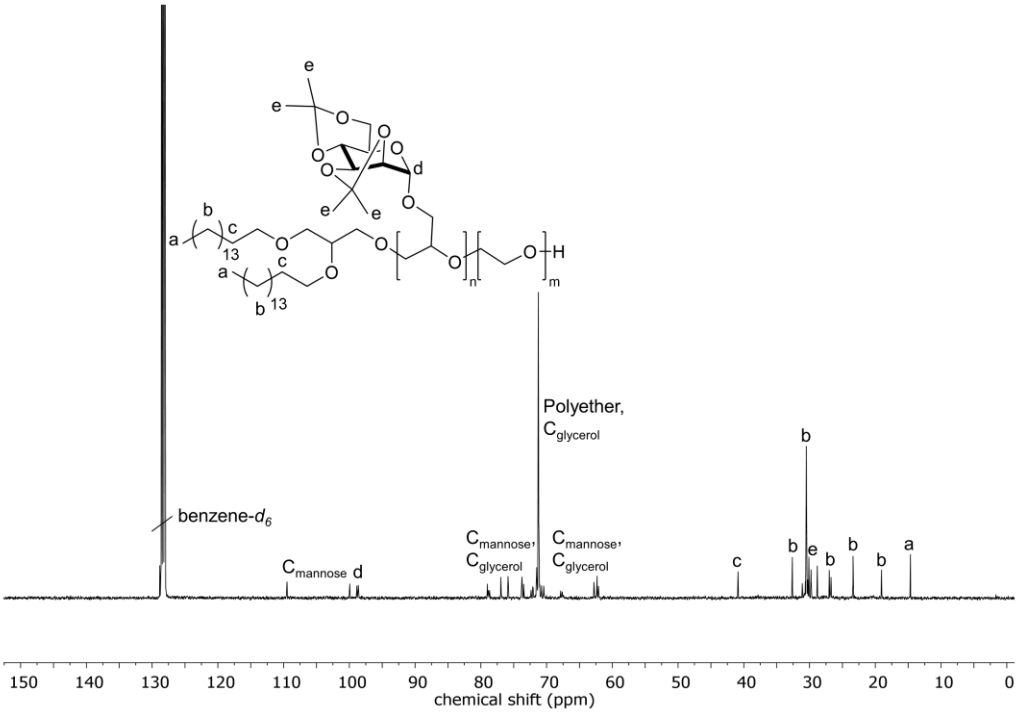

Figure S22. ^{13}C NMR (benzene-d_6, 100.6 MHz) BisHD-p(IMGE$_{8.0}$-*co*-EG$_{92.0}$).

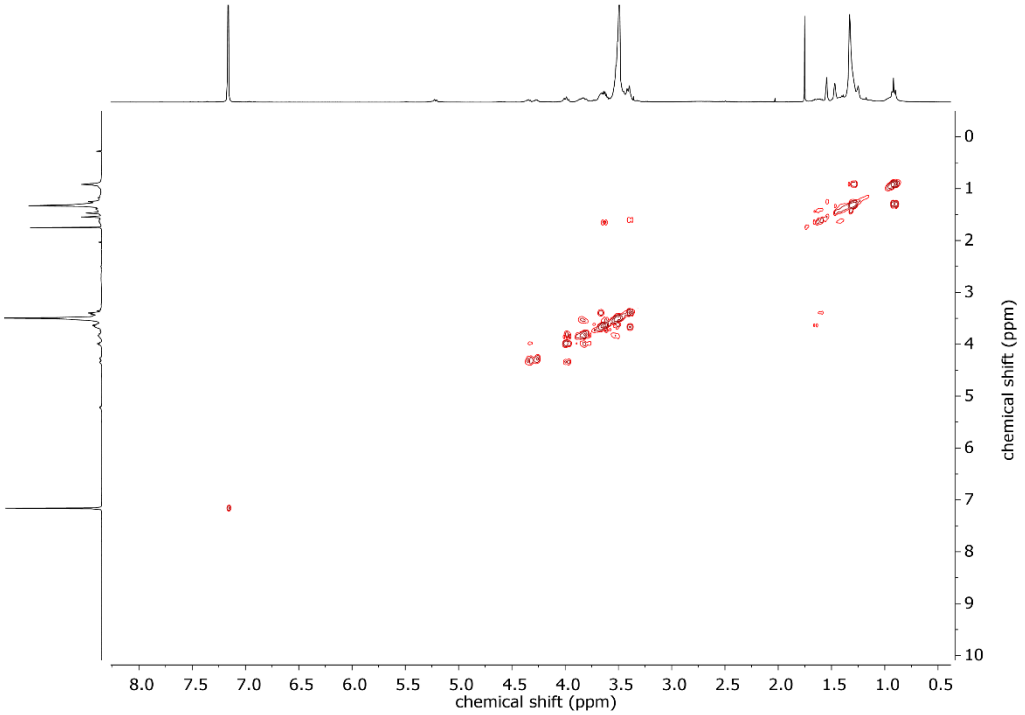

Figure S23. COSY NMR (benzene-d_6, 400 MHz) BisHD-p(IMGE$_{8.0}$-*co*-EG$_{92.0}$)

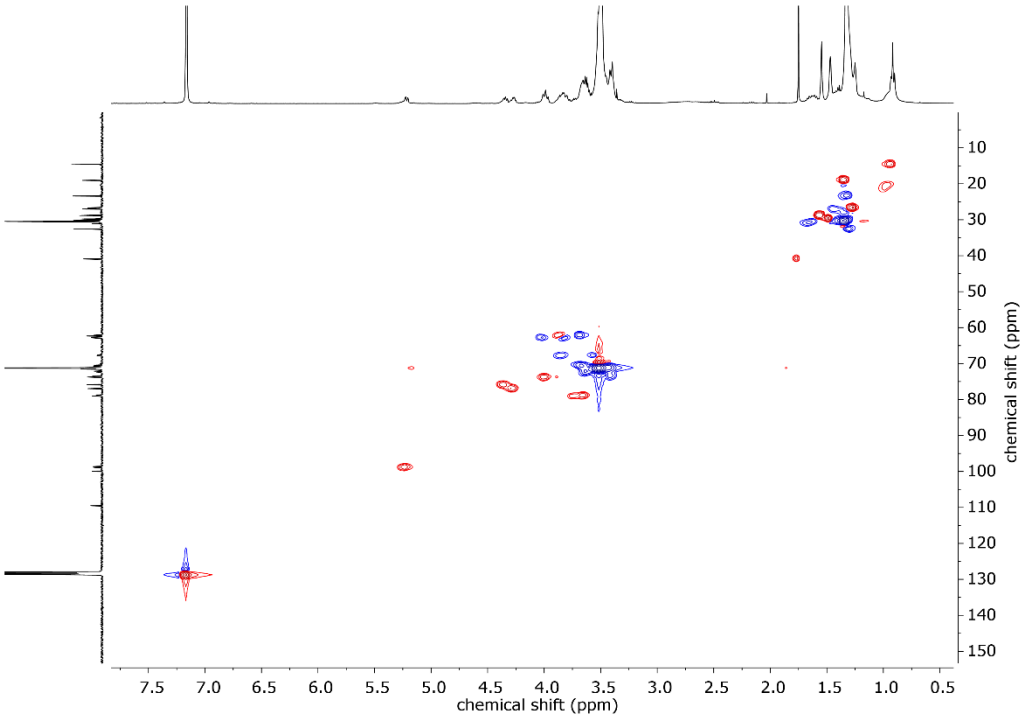

Figure S24. HSQC NMR (benzene-d_6) of BisHD-p(IMGE$_{8.0}$-*co*-EG$_{92.0}$).

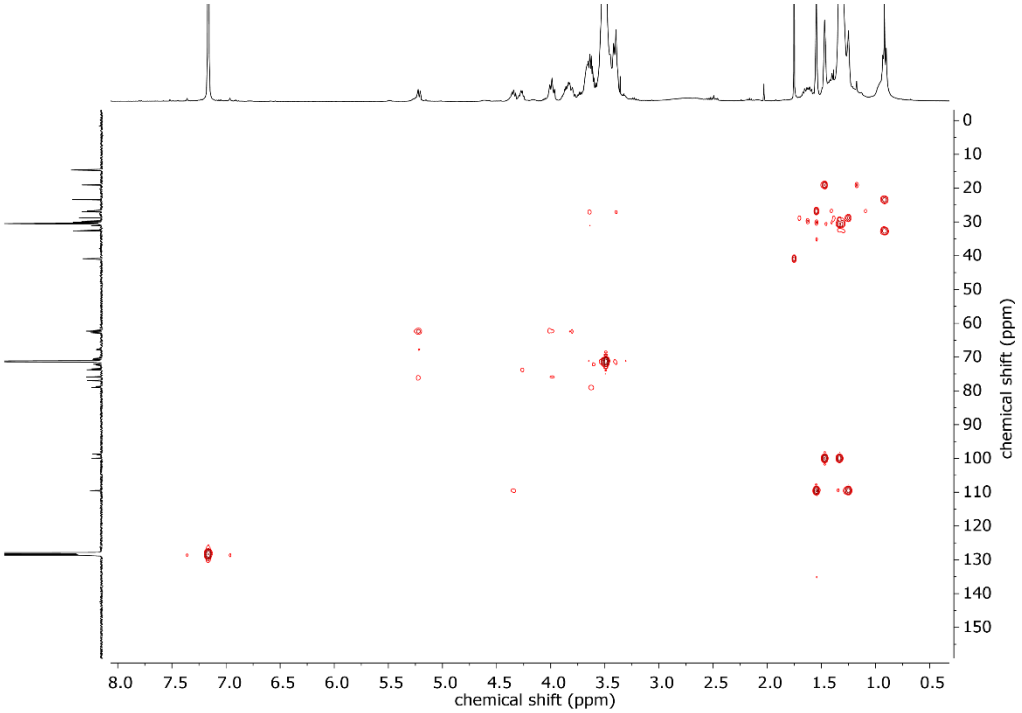

Figure S25. HMBC NMR (benzene-d_6) of BisHD-p(IMGE$_{8.0}$-*co*-EG$_{92.0}$).

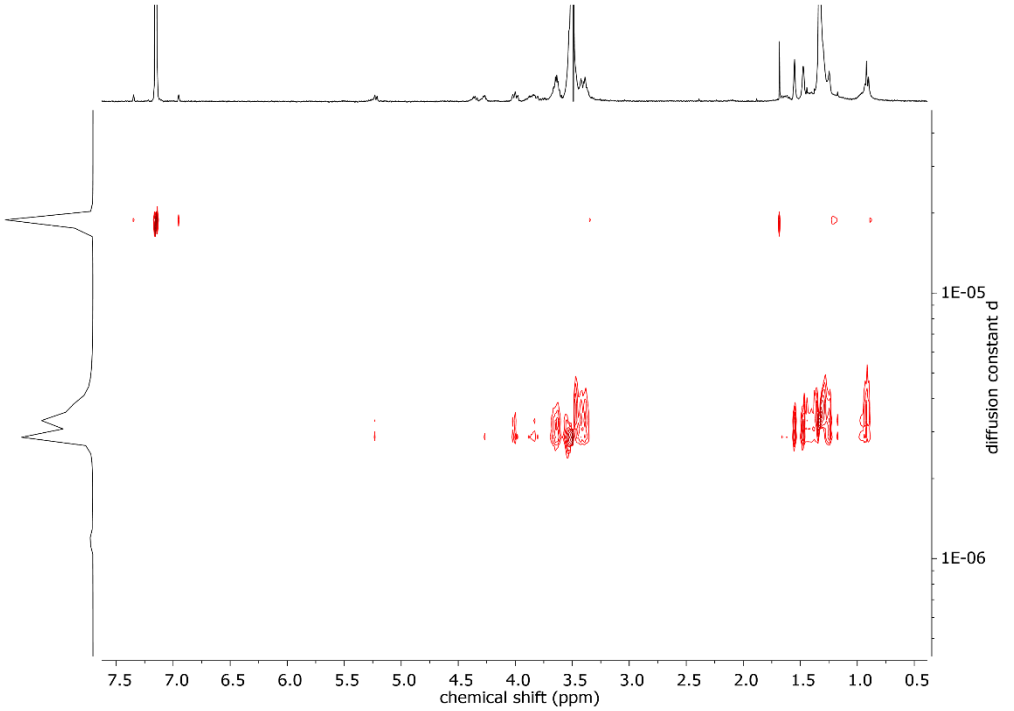

Figure S26. DOSY NMR (benzene-d_6, 400 MHz) of BisHD-p(IMGE$_{8.0}$-*co*-EG$_{92.0}$).

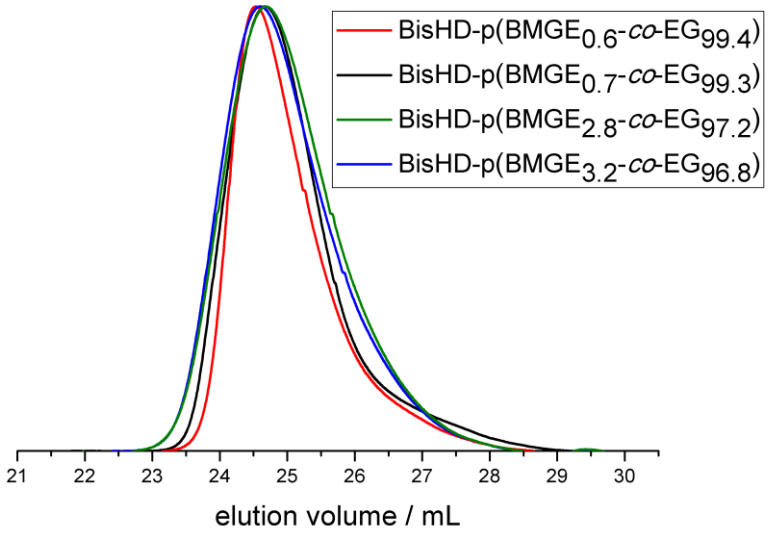

Figure S27. SEC traces (THF, PEG standard, RI signal) of the synthesized copolymers BisHD-p(BMGE-*co*-EG).

Table S1. Overview of the molecular weights calculated via ^{1}H NMR spectroscopy and SEC measurement for the copolymers BisHD-p(IMGE-*co*-EG) as well as the incorporated amount of mannose-moieties.

Composition[a]	M_n^{th} g mol^{-1}	M_n^{NMR} g mol^{-1}	$M_w/M_n^{SEC,b}$	**mannose** mol% th / NMR[a]
BisHD-p(IMGE$_{3.3}$-*co*-EG$_{96.7}$)	5760	8480	1.16	3.0/3.3
BisHD-p(IMGE$_{3.8}$-*co*-EG$_{96.2}$)	5760	4790	1.64	3.0/3.8
BisHD-p(IMGE$_{5.4}$-*co*-EG$_{94.6}$)	6310	5950	1.22	5.0/5.4
BisHD-p(IMGE$_{6.3}$-*co*-EG$_{93.7}$)	6310	5420	1.25	5.0/6.3

[a]determined using ^{1}H NMR spectroscopy.
[b]measured in THF using a PEG standard.

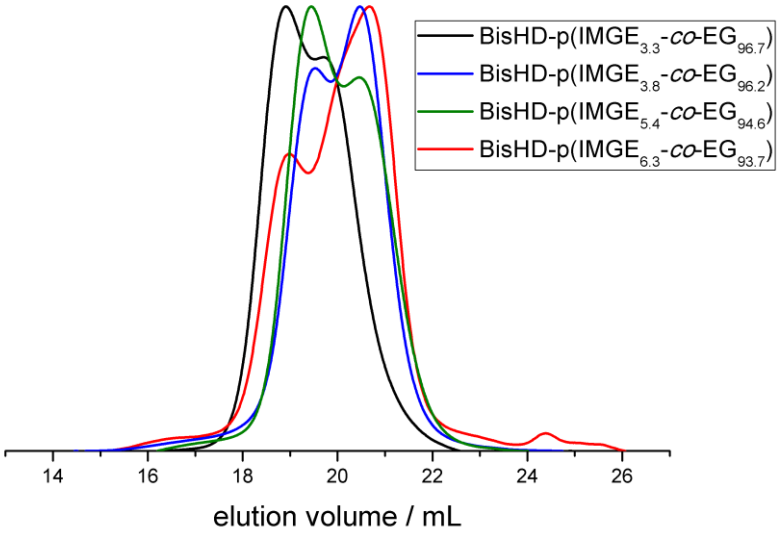

Figure S28. SEC traces (THF, PEG standard, RI signal) of the copolymers BisHD-p(IMGE-*co*-EG).

4. References

(1) Hofmann, A. M.; Wurm, F.; Hühn, E.; Nawroth, T.; Langguth, P.; Frey, H. Hyperbranched polyglycerol-based lipids via oxyanionic polymerization: toward multifunctional stealth liposomes. *Biomacromolecules* **2010**, *11*, 568–574.

(2) Hartmann, M.; Horst, A. K.; Klemm, P.; Lindhorst, T. K. A kit for the investigation of live Escherichia coli cell adhesion to glycosylated surfaces. *Chem. Commun.* **2010**, *46*, 330–332.

(3) Zeng, J.; Vedachalam, S.; Xiang, S.; Liu, X.-W. Direct C-glycosylation of organotrifluoroborates with glycosyl fluorides and its application to the total synthesis of (+)-varitriol. *Organic letters* **2011**, *13*, 42–45.

(4) Chernyak, A. Y.; Levinsky, A. B.; Dmitriev, B. A.; Kochetkov, N. K. A new type of carbohydrate-containing synthetic antigen: Synthesis of carbohydrate-containing polyacrylamide copolymers having the specificity of O:3 and O:4 factors of Salmonella. *Carbohydrate Research* **1984**, *128*, 269–282.

2.4 Synthesis of Amphiphilic PEG Copolymers with Pendant Methacrylate Moieties to Enable Cross-linking of Liposomes

Ann-Kathrin Danner,[a,b] Hannah Maus[a] and Holger Frey[a,*]

[a]Institute of Organic Chemistry, Johannes Gutenberg-University Mainz, Duesbergweg 10-14, 55128 Mainz, Germany.

[b]Graduate School Materials Science in Mainz, Staudinger Weg 9, 55128 Mainz, Germany.

E-Mail: hfrey@uni-mainz.de

Unpublished results.

Abstract

The anionic ring-opening copolymerization (AROP) of ethylene oxide (EO) and ethoxyethyl glycidyl ether (EEGE) was applied to synthesize amphiphilic polyethers, enabling post-polymerization modification of the pendant hydroxyl groups. The AROP and subsequent acidic treatment to remove the acetal protecting groups led to BisOD-p(G-*co*-EG) with defined molecular weights (2540–4470 g mol^{-1}) and narrow size distributions with polydispersities of 1.09 to 1.26. Furthermore, enzymatic esterification of the available hydroxyl groups resulted in an entire functionalization. Hence, methacrylate carrying polyether lipids were obtained, which were incorporated in liposomal nanocarriers. Light scattering revealed diameters of 173–229 nm and moderate polydispersities (0.17–0.45) for the liposome formulations. Addition of a photoinitiator allows for cross-linking *via* UV light of the pendant methacrylate groups. The demonstrated possibility for cross-linking renders these copolymers interesting for the preparation of stabilized drug delivery systems.

Table of Contents Graphics

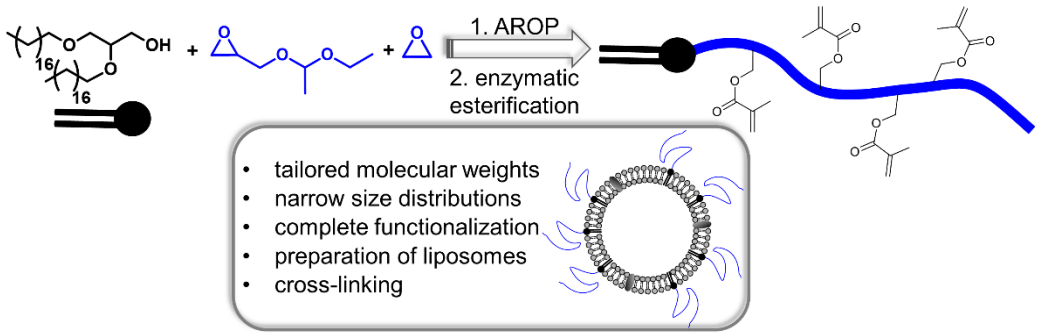

Introduction

Since the early 1970s liposomes have become the most common and well-investigated nanocarriers for biomedical applications.[1,2] Liposomes consist of phospholipids arranged in a bilayer structure, forming spherical vesicles and resembling biological membranes.[3] The first generation of liposomes or rather conventional liposomes undergo a rapid clearance from the blood stream after administration. To overcome this drawback surface modification, leading to a protective layer on the liposomal surface is a widespread strategy.[4] Therefore, polyethylene glycol (PEG) is applied due to its biocompatibility and the ability to increase the circulation time of the nanocarrier. The so-called PEGylation results in improved pharmacokinetic properties due to steric stabilization.[5,6] Furthermore, these "stealth" liposomes tend to accumulate in tumor tissue, which is known as enhanced permeability and retention (EPR) effect.[7,8] Based on these advantages multitudinous PEGylated liposomes are FDA-approved and thus are highly relevant nanocarriers in drug delivery.[9] However, under physiological conditions also stealth liposomes are prone to osmotic rupture, lipid hydrolysis, aggregation and fusion to reduce their curvature.[10–13] In addition, charged proteins are able to interrupt electrostatic interactions and degradative enzymes can digest lipids.[14] Therefore, the stability of liposomes still possesses potential for improvements. Recently, Helm and coworkers revealed the relevance of lipid anchorage as crucial to obtain a stable anchorage of PEG-based lipids in the liposomal membrane and hence successful steric stabilization.[15] Positron emission tomography (PET) imaging of ^{18}F-radiolabeled polyether-lipids confirmed these results, revealing a higher steric stabilization of liposomes, carrying dialkyl-based polyethers compared to liposomes with cholesterol-based polyethers.[16] A different approach to enhance the stability of liposomes is a cross-linking of components of the lipid bilayer. Besides increasing the stability, the leakage of entrapped molecules inside the liposome can be reduced, leading to better controllable drug carriers.[17,18] Therefore, Ringsdorf and coworkers used amphiphiles with diacetylene and butadiene moieties which undergo polymerization upon irradiation with UV light to prepare stabilized vesicles. The results showed increased stability against organic solvents and reduced leakage of encapsulated markers.[17] Several groups conducted similar experiments to prepare cross-linked liposomes and confirming the enhanced stability.[18,19] For example, Smith *et al.* cross-linked the lipid bilayer of a liposome *via* UV irradiation of diyne lipids.[18] Another possibility to stabilize liposomes is a cross-linking of

the polymer stealth layer incorporated into the liposome. Furthermore, facilitating a reversibility of cross-linking would be beneficial for drug release after administration. In this context, the attachment of cross-linkable units *via* esterification of polyether lipids is a promising strategy to prepare stabilized liposomes. In general, enzyme catalyzed reactions are of great interest due to the high reactivity as well as selectivity of enzymes.[20] *Candida antarctica lipase B* (CALB) catalyzes the hydrolysis of triglycerides *in vivo*. Nevertheless, methyl- and ethyl esters as well as acrylates and methacrylates are also suitable as substrates for CALB.[21–23]

Herein, we synthesize polyether-based lipids with pendant methacrylate groups. The amphiphilic polyethers are suitable for the incorporation into liposomes and enable cross-linking due to the attached double bonds, which should lead to stabilized nanocarriers.

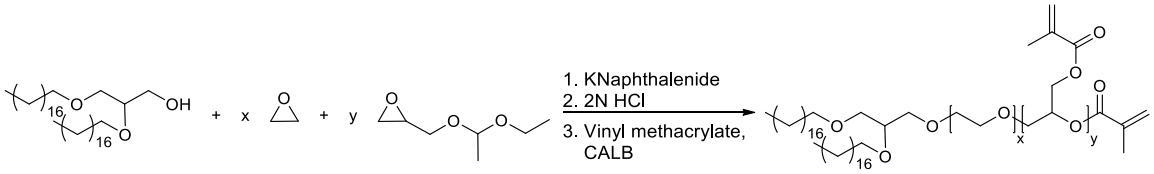

Scheme 1. Copolymerization of ethylene oxide (EO) and ethoxyethyl glycidyl ether (EEGE) with 1,2-bis-*n*-octadecyl glyceryl ether (BisOD) as initiator and subsequent enzyme catalyzed esterification with vinyl methacrylate to obtain BisOD-p(G^{MA}-*co*-EG).

Results and Discussion

In order to access dialkyl-based lipids the hydrophobic initiator 1,2-bis-*n*-octadecyl glyceryl ether (BisOD) was synthesized using a two-step protocol known from literature.[24] Subsequently, BisOD was applied for the anionic ring-opening polymerization (AROP) of ethylene oxide (EO) and ethoxyethyl glycidyl ether (EEGE) resulting in amphiphilic polyether-based lipids BisOD-p(EEGE-*co*-EG) and followed by removal of the protecting groups BisOD-p(G-*co*-EG) was obtained. Applying the AROP strategy, copolymers with adjustable molecular weights and tailored comonomer content can be synthesized (**Scheme 1**).

A. Synthesis and characterization of BisOD-p(G-*co*-EG)

The conditions for the AROP were adopted with little modifications from Mangold *et al*.[25] The polymerization was carried out in dry tetrahydrofuran (THF) to ensure a good solubility of the initiator and the formation of a dissociated ion pair to obtain a high reactivity for polymerization.[26,27] Potassium naphthalenide was used for deprotonation to generate the alkoxide. The reaction was performed at 80 °C for 3–5 days to achieve full conversion. In order to remove the acetal protecting groups, the polymer was treated with 2N HCl and stirred at 40 °C for 3 days. The successful removal of the protecting groups was confirmed *via* the disappearance of the respective signals d, e and f in the ^{1}H NMR spectrum as shown in **Figure 1** and the appearance of the characteristic bond stretching vibration of the free hydroxyl groups in the IR spectrum (**Figure S32**). Furthermore, NMR spectroscopy verified the effective copolymerization, *i.e.* the broad polyether backbone signal as well as EEGE and initiator signals could be assigned. The molecular weights of the obtained polyether lipids and the comonomer ratios were determined *via* end group analysis of the respective ^{1}H NMR spectrum of BisOD-p(EEGE-*co*-EG). The copolymers exhibit molecular weights in the range of 2130–4990 g mol^{-1} and were lower as the aspired value. In contrast, the ratio of incorporated comonomer EEGE varied between 12 and 26 mol% and therefore was higher as intended as can be seen in **Table 1**. This discrepancies may be due to occurring deviations in measuring the appropriate EO volume, resulting in different comonomer ratios upon polymerization.

Size exclusion chromatography (SEC) was performed to further characterize the synthesized polyethers. For all polyether lipids monomodal and narrow size distributions with molecular weight dispersities ranging from 1.09 to 1.26 (measured in DMF using PEG standards) were obtained. The molecular weights determined *via* SEC were overestimated compared to the values received *via* ^{1}H NMR spectroscopy due to differences in the hydrodynamic volume of the polyethers and the PEG standards applied for calibration. In addition, the elugram displays shifts of the SEC traces to higher elution volume for lower molecular weights, which additionally confirms the successful removal of the acetal protecting groups of BisOD-p(EEGE-*co*-EG), resulting in BisOD-p(G-*co*-EG) (**Figure 2**).

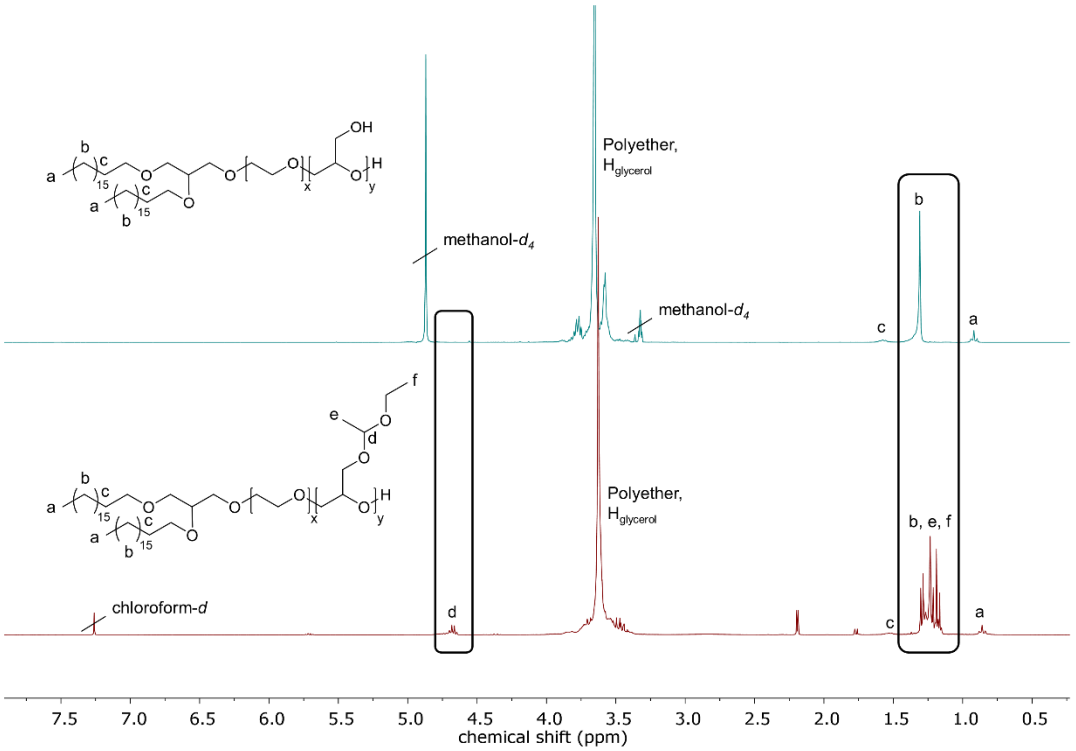

Figure 1. ^{1}H NMR spectra (300 MHz) of BisOD-p(EEGE$_{0.12}$-*co*-EG$_{0.88}$) (bottom, red) measured in chloroform-*d* and BisOD-p(G$_{0.12}$-*co*-EG$_{0.88}$) (top, green) measured in methanol-d_4. The disappearing signals of EEGE (bottom, signal d, e and f) are emphasized in black boxes.

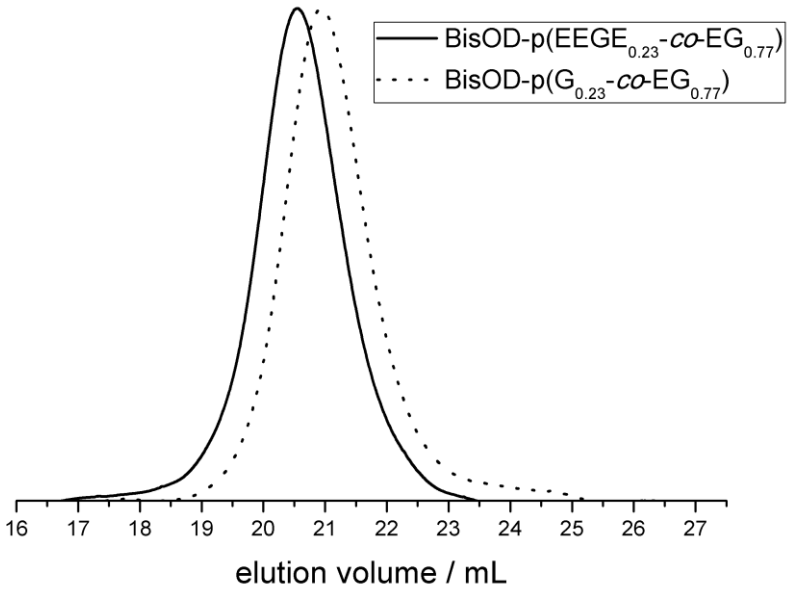

Figure 2. SEC traces (DMF, PEG standard, RI signal) of BisOD-p(EEGE$_{0.23}$-*co*-EG$_{0.77}$) (solid line) and BisOD-p(G$_{0.23}$-*co*-EG$_{0.77}$) (dotted line).

Differential scanning calorimetry (DSC) was applied to determine the thermal properties of the synthesized polyether lipids. For BisOD-PEG a melting temperature of 54 °C was determined whereas no glass transition temperature T_g was detected due to the predominant melting endotherm. BisOD-*lin*PG possesses a T_g of –21 °C and a T_m of 56 °C. As expected, the T_g is increased compared to the T_g of PEG based on the formation of hydrogen bonds. The measured T_m can be attributed to the melting point of the applied initiator BisOD of 65.6–66.6 °C. All copolymers exhibit a distinct T_g ranging from –53 to –45 °C due to the incorporation of the amorphous polyglycerol. As expected, the T_g increases with higher amount of polyglycerol in the copolymer. The free hydroxyl groups form hydrogen bonds, reducing the flexibility of the polyether chains and thus leading to an increase of the T_g. Surprisingly, the measured T_m of the copolymers (38–48 °C) increases with increasing amount of incorporated glycerol. In literature, the T_m decreases with increasing amount of polyglycerol and is absent for an incorporation of glycerol ≥ 23 mol%.[25] By incorporating polyglycerol a frequent disruption of the PEG segments is obtained which reduces the crystallinity.

Table 1. Properties of the synthesized BisOD-PEG, BisOD-*lin*PG and copolymers BisOD-p(G-*co*-EG).

#	**Composition**[a]	M_n^{th}	M_n^{NMR}	M_w/M_n[b]	G^{th}	T_g[c]	T_m[c]
		g mol^{-1}	g mol^{-1}		mol%	°C	°C
1	BisOD-PEG	5180	4180	1.09	0	-	54
2	BisOD-*lin*PG	2070	1970	1.26	100	–21	56
3	BisOD-p($G_{0.12}$-*co*-$EG_{0.88}$)	7510	4170	1.14	10	–53	39
4	BisOD-p($G_{0.13}$-*co*-$EG_{0.87}$)	7670	3610	1.12	16	–49	38
5	BisOD-p($G_{0.18}$-*co*-$EG_{0.82}$)	7670	4990	1.17	16	–49	40
6	BisOD-p($G_{0.23}$-*co*-$EG_{0.77}$)	5300	2130	1.18	10	–46	48
7	BisOD-p($G_{0.26}$-*co*-$EG_{0.74}$)	6020	2200	1.16	13	–45	47

[a]determined using ^{1}H NMR spectroscopy.
[b]obtained *via* SEC measurements in DMF using PEG standards.
[b]obtained *via* DSC measurements.

B. Enzymatic functionalization

An enzyme catalyzed reaction was carried out to functionalize the free hydroxyl groups of BisOD-p(G-*co*-EG). In order to introduce methacrylate groups *via* esterification of vinyl methacrylate, the enzyme *candida antarctica lipase B* (CALB) was used to catalyze the reaction, resulting in BisOD-p(G^{MA}-*co*-EG). The reaction was carried out at room temperature and butylated hydroxytoluene (BHT) was added to avoid cross-linking. Full conversion was reached in toluene after a reaction time of 7 days by using an excess of vinyl methacrylate. In general, a non-polar solvent is favorable to permit increased reactivity of the enzyme.[28] The formation of formaldehyde during functionalization results in an irreversible reaction and thus allows for a high yield of the functionalized polymers.

The successful functionalization was confirmed *via* NMR and IR spectroscopy. In the IR spectrum the bond stretching vibration of the free hydroxyl groups (3390 cm^{-1}) vanishes whereas the characteristic C=C (1639 cm^{-1}) and C=O (1718 cm^{-1}) stretching vibration appears (**Figure S33**). Furthermore, ^{1}H NMR spectroscopy reveals the occurrence of the vinyl signals for the vinyl group at 6.10 ppm and 5.56 ppm as well as the methyl group at 1.93 ppm adjacent to the vinyl function (**Figure 3**). In addition, a shift for the methylene group of the former polyglycerol to low field (4.36–4.10 ppm) is observed due to the attachment of the ester groups.

The degree of functionalization was determined *via* ^{1}H NMR spectroscopy, comparing the signal intensity of the vinyl groups of the attached methacrylate and the signal intensity of the methyl groups of the initiator at 0.87 ppm, revealing complete functionalization of the available hydroxyl groups. Due to inaccuracies occurring from ^{1}H NMR integration, the calculated degree of functionalization is higher than the theoretical value. Furthermore, monomodal and narrow dispersities (1.10–1.26) were verified *via* SEC measurements. A shift of the SEC traces to lower elution volume translating to higher molecular weights additionally confirmed the successful esterification in quantitative yields.

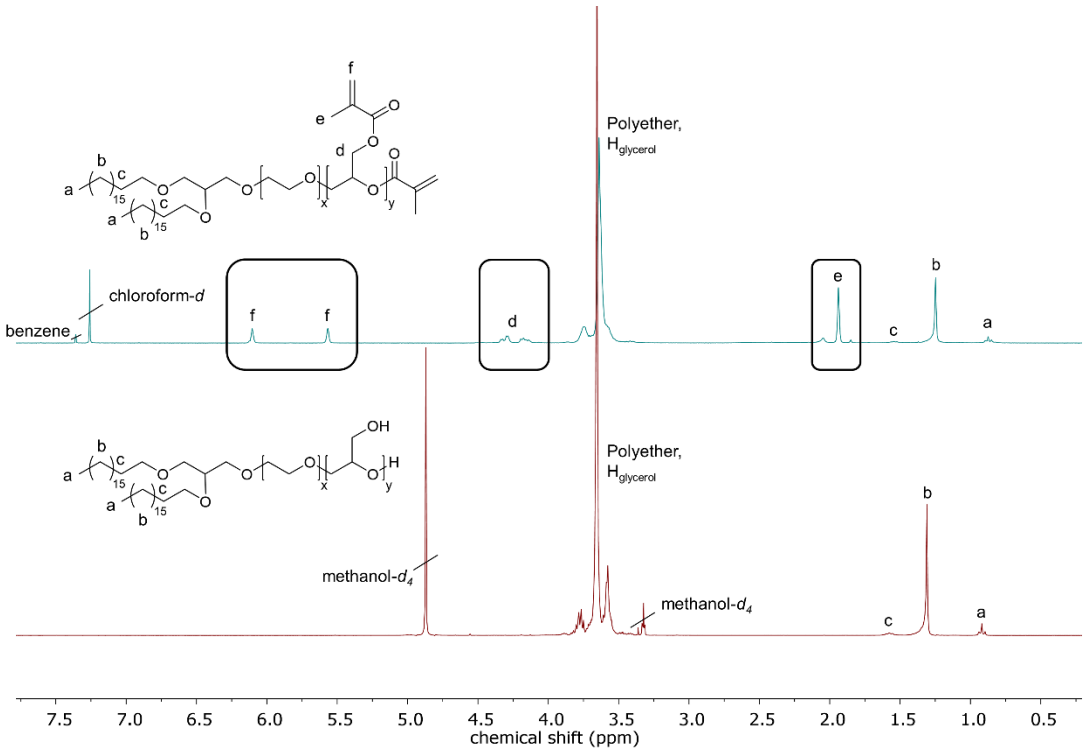

Figure 3. ^{1}H NMR spectra (300 MHz) of BisOD-p($G_{0.12}$-*co*-$EG_{0.88}$) (bottom, red) measured in methanol-d_4 and BisOD-p($G^{MA}_{0.12}$-*co*-$EG_{0.88}$) (top, green) measured in chloroform-*d*. The signals for the methacrylate groups (top, signal d, e and f) are highlighted with black boxes.

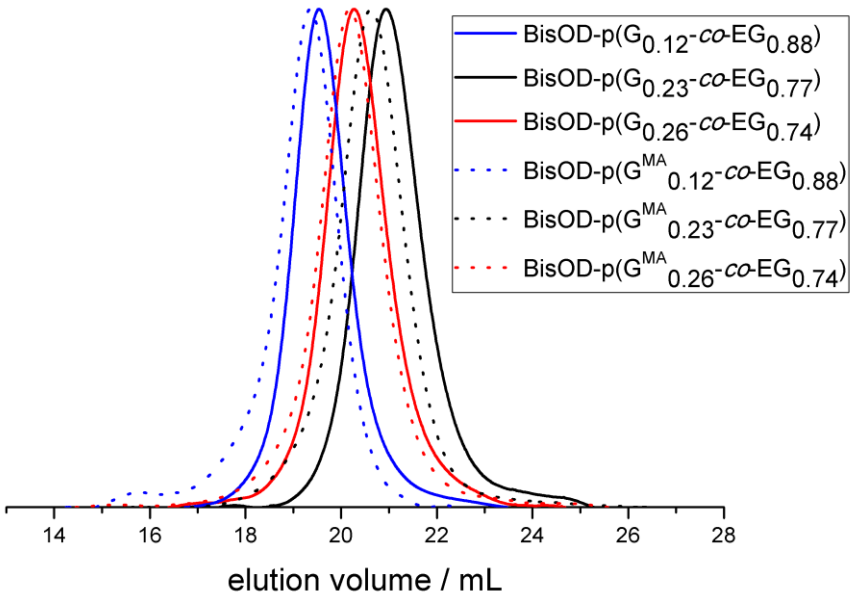

Figure 4. SEC traces (DMF, PEG standard, RI signal) of BisOD-p(G-*co*-EG) (solid lines) and BisOD-p(G^{MA}-*co*-EG) (dotted lines).

DSC measurements revealed a T_g of −59 and −58 °C for the functionalized polyether lipids BisOD-p(G^{MA}-*co*-EG). In comparison to BisOD-p(G-*co*-EG) the T_g is clearly decreased due to the disappearance of hydrogen bonds and hence an increased flexibility of the polyether chains. Furthermore, BisOD-p(G^{MA}-*co*-EG) exhibit a melting endotherm ranging from 22–28 °C which is diminished compared to the determined T_m of BisOD-p(G-*co*-EG) and can be attributed to the introduction of the methacrylate groups.

Table 2. Properties of the functionalized copolymers BisOD-p(G^{MA}-*co*-EG).

#	Composition[a]	M_n^{th}	M_n^{NMR}	M_w/M_n^{SEC}	MA^{NMR}	T_g[b]	T_m[b]
		g mol^{-1}	g mol^{-1}		mol%	°C	°C
8	BisOD-p(G$^{MA}_{0.12}$-*co*-EG$_{0.88}$)	4670	4780	1.24	12	–58	28
9	BisOD-p(G$^{MA}_{0.23}$-*co*-EG$_{0.77}$)	2520	2610	1.20	26	[c]	[c]
10	BisOD-p(G$^{MA}_{0.26}$-*co*-EG$_{0.74}$)	2650	2740	1.26	39	–59	22

[a]determined using ^{1}H NMR spectroscopy.
[b]obtained *via* DSC measurements.
[c]not determined.

C. Liposome preparation

The functionalized polyether lipids BisOD-p(G^{MA}-*co*-EG) are suitable for the incorporation into liposomes. Therefore, the dialkyl-based initiator BisOD serves as hydrophobic membrane anchor and the polyether chains lead to a steric stabilization of the liposome. dual centrifugation (DC) was applied to prepare the liposomes. Using DC the preparation of small liposomes (≤100 nm) with narrow size distributions is possible.[29] In order to prepare the liposomes a composition of 55 mol% egg-phosphatidylcholine-3 (EPC-3), 40 mol% cholesterol and 5 mol% BisOD-p(G$^{MA}_{0.12}$-*co*-EG$_{0.88}$) (#8), BisOD-p(G$^{MA}_{0.23}$-*co*-EG$_{0.77}$) (#9) and BisOD-p(G$^{MA}_{0.26}$-*co*-EG$_{0.74}$) (#10) respectively, was used. The obtained liposomal formulation after dual centrifugation was characterized *via* light scattering (using a zeta-sizer), revealing diameters between 173 nm and 229 nm and polydispersities (PDI) ranging from 0.17 to 0.45 (**Figure 5**). It is important to mention that the polydispersities obtained from SEC measurements (M_w/M_n) and the PDI obtained from light scattering are unrelated.

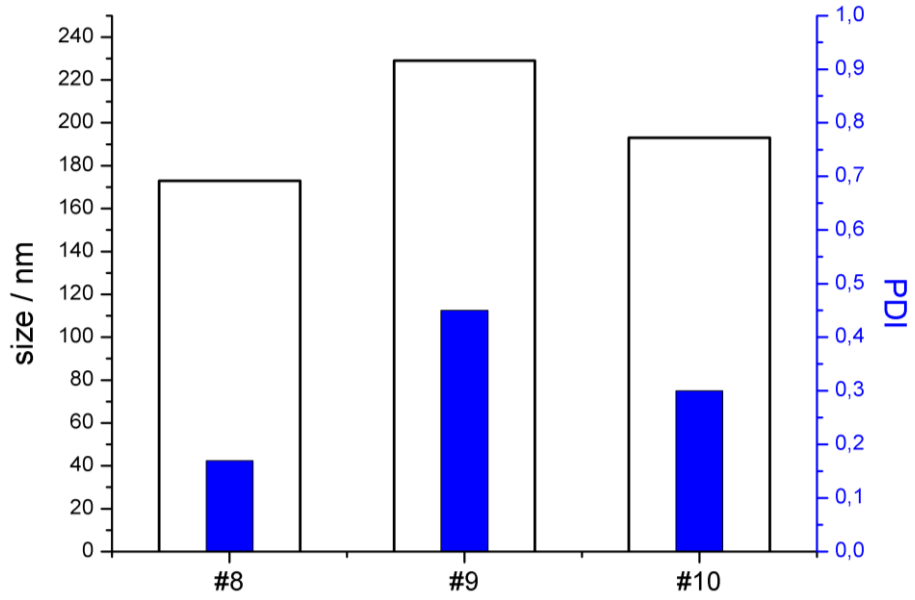

Figure 5. Properties of the prepared liposomal formulations using egg-phosphatidylcholine-3 (EPC-3), cholesterol and BisOD-p($G^{MA}_{0.12}$-*co*-$EG_{0.88}$) (#8), BisOD-p($G^{MA}_{0.23}$-*co*-$EG_{0.77}$) (#9) and BisOD-p($G^{MA}_{0.26}$-*co*-$EG_{0.74}$) (#10) respectively.

In order to investigate the possibility of cross-linking of the introduced methacrylate groups, 2-hydroxy-2-methylpropiophenone served as photo initiator and was added to liposomal solutions with different concentrations. The solutions were irradiated with UV light for 10 minutes and subsequently characterized *via* light scattering. As can be seen in **Figure S37** the measured size distribution for the liposome formulation of BisOD-p($G^{MA}_{0.12}$-*co*-$EG_{0.88}$) (#8) is almost identical for the sample before cross-linking (red curve) and after cross-linking in a diluted solution of 1:1000 with PBS buffer (green curve). In case of a dilution of 1:10, liposomes with larger sizes are observed (blue curve) which can be attributed to the formation of aggregates, *i.e.* cross-linking occurs among different individual liposomes.

Concerning these results we assume that cross-linking after incorporation of BisOD-p(G^{MA}-*co*-EG) into liposomes is feasible. Depending on the concentration of the liposome formulation, cross-linking occurs within a single or among different liposomes. Nevertheless, further studies regarding cross-linking and subsequent investigations, evaluating the stability of the liposomes *in vitro* and *in vivo* are necessary. In general, the stability should be enhanced after cross-linking but due to the ester groups a cleavage after administration should be possible by esterases, which will be necessary to obtain a release of the cargo.[30]

Conclusion

In this work, we presented the copolymerization of ethylene oxide (EO) and ethoxyethyl glycidyl ether (EEGE) by applying a hydrophobic dialkyl-based initiator to obtain amphiphilic polyethers. Polyether lipids with defined molecular weights of 2130–4990 g mol^{-1} and narrow size distributions were achieved. The amount of incorporated comonomer glycidol was calculated by end group analysis *via* ^{1}H NMR spectroscopy. The resulting BisOD-p(G-*co*-EG) was modified *via* CALB catalyzed esterification and quantitative yields of functionalized hydroxyl groups were obtained. Due to the amphiphilic character, the polyether lipids with pendant methacrylate groups could be integrated into liposomes. The liposome formulations were prepared *via* dual centrifugation and characterized *via* light scattering, using a zeta-sizer and revealing liposomal diameters ranging from 173 nm to 229 nm and moderate polydispersities (0.17–0.45). The vinyl moieties permit cross-linking after liposome preparation and irradiation with UV light. The excellent biocompatibility of PEG and its stealth effect as well as the possibility for cross-linking, render these polyether lipids promising candidates for drug delivery systems with enhanced stability.

Acknowledgments

A. Danner is a recipient of a DFG-funded position through the Excellence Initiative by the Graduate School Materials Science in Mainz (GSC 266). The authors thank Maria Müller for DSC and Monika Schmelzer for SEC measurements. Furthermore, the authors thank Prof. Dr. Mark Helm and Matthias Voigt for provision of the dual centrifuge for liposome preparation.

References

(1) Pattni, B. S.; Chupin, V. V.; Torchilin, V. P. New Developments in Liposomal Drug Delivery. *Chemical reviews* **2015**, *115*, 10938–10966.

(2) Sawant, R. R.; Torchilin, V. P. Challenges in development of targeted liposomal therapeutics. *The AAPS journal* **2012**, *14*, 303–315.

(3) Vemuri, S.; Rhodes, C. T. Preparation and characterization of liposomes as therapeutic delivery systems: A review. *Pharmaceutica acta Helvetiae* **1995**, *70*, 95–111.

(4) Torchilin, V. P. Recent advances with liposomes as pharmaceutical carriers. *Nat. Rev. Drug. Discov.* **2005**, *4*, 145–160.

(5) Woodle, M. C. Surface-modified liposomes: Assessment and characterization for increased stability and prolonged blood circulation. *Chemistry and physics of lipids* **1993**, *64*, 249–262.

(6) Pasut, G.; Paolino, D.; Celia, C.; Mero, A.; Joseph, A. S.; Wolfram, J.; Cosco, D.; Schiavon, O.; Shen, H.; Fresta, M. Polyethylene glycol (PEG)-dendron phospholipids as innovative constructs for the preparation of super stealth liposomes for anticancer therapy. *J. Control. Release* **2015**, *199*, 106–113.

(7) Maeda, H.; Bharate, G. Y.; Daruwalla, J. Polymeric drugs for efficient tumor-targeted drug delivery based on EPR-effect. *Eur. J. Pharm. Biopharm.* **2009**, *71*, 409–419.

(8) Maeda, H.; Wu, J.; Sawa, T.; Matsumura, Y.; Hori, K. Tumor vascular permeability and the EPR effect in macromolecular therapeutics: a review. *J. Control. Release* **2000**, *65*, 271–284.

(9) Milla, P.; Dosio, F.; Cattel, L. PEGylation of Proteins and Liposomes: A Powerful and Flexible Strategy to Improve the Drug Delivery. *CDM* **2012**, *13*, 105–119.

(10) Taira, M. C.; Chiaramoni, N. S.; Pecuch, K. M.; Alonso-Romanowski, S. Stability of liposomal formulations in physiological conditions for oral drug delivery. *Drug delivery* **2004**, *11*, 123–128.

(11) Moghimi, S. M.; Szebeni, J. Stealth liposomes and long circulating nanoparticles: Critical issues in pharmacokinetics, opsonization and protein-binding properties. *Progress in lipid research* **2003**, *42*, 463–478.

(12) Yuet, P. K.; Blankschtein, D. Effect of Surfactant Tail-Length Asymmetry on the Formation of Mixed Surfactant Vesicles. *Langmuir : the ACS journal of surfaces and colloids* **1996**, *12*, 3819–3827.

(13) Lin, C.-M.; Li, C.-S.; Sheng, Y.-J.; Wu, D. T.; Tsao, H.-K. Size-dependent properties of small unilamellar vesicles formed by model lipids. *Langmuir* **2012**, *28*, 689–700.

(14) Boyer, C.; Zasadzinski, J. A. Multiple lipid compartments slow vesicle contents release in lipases and serum. *ACS nano* **2007**, *1*, 176–182.

(15) Fritz, T.; Voigt, M.; Worm, M.; Negwer, I.; Müller, S. S.; Kettenbach, K.; Ross, T. L.; Roesch, F.; Koynov, K.; Frey, H. *et al.* Orthogonal Click Conjugation to the Liposomal Surface Reveals the Stability of the Lipid Anchorage as Crucial for Targeting. *Chemistry* **2016**, *22*, 11578–11582.

(16) Wagener, K.; Worm, M.; Pektor, S.; Schinnerer, M.; Thiermann, R.; Miederer, M.; Frey, H.; Rösch, F. Comparison of Linear and Hyperbranched Polyether Lipids for Liposome Shielding by 18F-Radiolabeling and Positron Emission Tomography. *Biomacromolecules* **2018,** DOI: 10.1021/acs.biomac.8b00115.

(17) Hupfer, B.; Ringsdorf, H.; Schupp, H. Liposomes from polymerizable phospholipids. *Chemistry and physics of lipids* **1983**, *33*, 355–374.

(18) Smith, C. E.; Kong, H. Cross-linkable liposomes stabilize a magnetic resonance contrast-enhancing polymeric fastener. *Langmuir* **2014**, *30*, 3697–3704.

(19) Liu, S.; O'Brien, D. F. Stable Polymeric Nanoballoons: Lyophilization and Rehydration of Cross-linked Liposomes. *J. Am. Chem. Soc.* **2002**, *124*, 6037–6042.

(20) Zaks, A.; Klibanov, A. M. Enzyme-catalyzed processes in organic solvents. *Proceedings of the National Academy of Sciences of the United States of America* **1985**, *82*, 3192–3196.

(21) Warwel, S.; Steinke, G.; Klaas, M. An efficient method for lipase-catalysed preparation of acrylic and methacrylic acid esters. *Biotechnol Tech* **1996**, *10*, DOI: 10.1007/BF00184030.

(22) Theil, F.; Bjrkling, F. Specificity of Candida antarctica lipase B (SP 435) in the presence of lipase A in a double enantioselective transesterification. *Biotechnol Lett* **1993**, *15*, 605–608.

(23) Anderson, E. M.; Larsson, K. M.; Kirk, O. One Biocatalyst–Many Applications: The Use of Candida Antarctica B-Lipase in Organic Synthesis. *Biocatalysis and Biotransformation* **1998**, *16*, 181–204.

(24) Stauch, O.; Uhlmann, T.; Fröhlich, M.; Thomann, R.; El-Badry, M.; Kim, Y.-K.; Schubert, R. Mimicking a Cytoskeleton by Coupling Poly(N -isopropylacrylamide) to the Inner Leaflet of Liposomal Membranes: Effects of Photopolymerization on Vesicle Shape and Polymer Architecture. *Biomacromolecules* **2002**, *3*, 324–332.

(25) Mangold, C.; Wurm, F.; Obermeier, B.; Frey, H. Hetero-Multifunctional Poly(ethylene glycol) Copolymers with Multiple Hydroxyl Groups and a Single Terminal Functionality. *Macromol. Rapid Comm.* **2010**, *31*, 258–264.

(26) Odian, G. G. *Principles of polymerization*, 4. ed; Wiley-Interscience: Hoboken, NJ, NJ : WileyInterscience, 2004.

(27) Penczek, S.; Cypryk, M.; Duda, A.; Kubisa, P.; Slomkowski, S. Living ring-opening polymerizations of heterocyclic monomers. *Prog. Polym. Sci.* **2007**, *32*, 247–282.

(28) Laane, C.; Boeren, S.; Vos, K.; Veeger, C. Rules for optimization of biocatalysis in organic solvents. *Biotechnology and bioengineering* **1987**, *30*, 81–87.

(29) Massing, U.; Cicko, S.; Ziroli, V. Dual asymmetric centrifugation (DAC)--a new technique for liposome preparation. *J. Control. Release* **2008**, *125*, 16–24.

(30) Williams, F. M. Clinical significance of esterases in man. *Clinical pharmacokinetics* **1985**, *10*, 392–403.

Supporting Information

Synthesis of Amphiphilic PEG Copolymers with Pendant Methacrylate Moieties to Enable Cross-linking of Liposomes

Ann-Kathrin Danner,[a,b] Hannah Maus[a] and Holger Frey[a,*]

[a]Institute of Organic Chemistry, Johannes Gutenberg-University Mainz, Duesbergweg 10-14, 55128 Mainz, Germany.

[b]Graduate School Materials Science in Mainz, Staudinger Weg 9, 55128 Mainz, Germany.

E-Mail: hfrey@uni-mainz.de

1. Materials and Methods

1.1 Reagents

All applied chemicals were purchased from *Sigma Aldrich*, *Acros Organics*, *Fisher Scientific* or *TCI Europe* unless otherwise noted. Deuterated solvents (benzene-d_6, methanol-d_4, pyridine-d_5, chloroform-*d*) were received from *Deutero GmbH*. Ethylene oxide (EO) was obtained from *Sigma Aldrich* and must be handled with care. Ethoxyethyl glycidyl ether (EEGE) was synthesized as reported in literature.[1] EEGE was dried over CaH_2 for 30 min and cryo-transferred prior to use. Anhydrous THF used for the anionic ring-opening polymerization (AROP) was previously dired over sodium.

1.2 Methods

NMR spectroscopy was carried out on a Bruker Avance III HD 300 (300 MHz, 5 mm, BBFO probe, and B-ACS 60 auto sampler) and a Bruker Avance II spectrometer operated at 400 MHz (5 mm BBFO smart probe and SampleXPress 60 auto sampler) at 296 K. Benzene-d_6, methanol-d_4, pyridine-d_5 or chloroform-*d* was applied as solvent and the NMR spectra were referenced internally to the respective signals of the deuterated solvent. The software MestReNova version 9.0 was used for the analysis of all spectra. SEC measurements were performed using dimethylformamide (DMF) with 0.25 g L^{-1} lithium bromide on an Agilent 1100 Series equipped with PSS HEMA 300/100/40 column, RI and UV detector (275 nm). Monodisperse linear PEG standards from *Polymer Standard Service GmbH* (PSS) were applied for calibration. The RI signal is displayed for all SEC traces and the software PSS WinGPC Unity was used for analysis. DSC measurements were carried out on a Perkin Elmer 8200 differential scanning calorimeter. Calibration was obtained using the melting points of indium (T_m = 156.6 °C) and MilliQ water (T_m = 0 °C). 4 to 6 mg of each polymer sample were measured in a temperature range of –95 to 100 °C (first cycle, heating rate 20 °C min^{-1}) and –95 to 70 °C (second cycle, heating rate 10 °C min^{-1}) respectively. The values obtained from the second cycle were used to determine the glass transition temperature T_g and the melting temperature T_m. Infrared spectroscopy was carried out on a Nicolet iS10 fourier transformation spectrometer obtained from *Thermo Scientific*. Liposomes were prepared using a Rotana 460 dual centrifugation (DC) from *Hettich*. Centrifugation was carried out for 20 min followed by additional two centrifugation steps for 2 min each. Light scattering was performed on a Malvern Zetasizer Nano ZS using

disposable polystyrene cuvettes. 1 µL of the liposome solution was diluted in 1 mL phosphate-buffered saline (PBS). After equilibration to 25 °C, the measurement was carried out at a scattering angle of 173°. The software Zetasizer version 6.20 from *Malvern Instruments* was used for analysis.

1.3 Handling of Ethylene Oxide (EO)

The toxic, gaseous and flammable ethylene oxide (EO) must be handled with high precaution and must be stored in pressure-proof gas bottles. EO must be only used in an appropriate fume hood and under adequate safety precautions. Polymerizations of EO are performed in flame-dried glassware to facilitate the conversion of EO inside the sealed and evacuated glass apparatus and to guarantee safe handling via cryo-transfer techniques. The maximum batch-size of 8 g EO in a 500 mL flask must not be exceeded to avoid abrupt detachment of the septum and release of EO.

2. Synthesis

2.1 Synthesis of ethoxyethyl glycidyl ether (EEGE)

EEGE was synthesized according to literature.[1]

^{1}H NMR, COSY (300 MHz, chloroform-*d*, δ): 4.75–4.68 (qd, *J* = 5.3 Hz; 3.4 Hz, 1H, acetal H), 3.86–3.29 (m, 4H, -CHC*H*$_2$OCOCH$_2$-, -CHCH$_2$OCOC*H*$_2$-) 3.13–3.07 (m, 1H, CH$_2$OC*H*CH$_2$-), 2.77–2.74 (ddd, *J* = 5.1 Hz; 4.1 Hz; 1.0 Hz, 1H, C*H*$_2$OCHCH$_2$-), 2.61–2.55 (ddd, *J* = 10.7 Hz; 5.1 Hz; 2.7 Hz, 1H, C*H*$_2$OCHCH$_2$-), 1.29–1.26 (dd, *J* = 5.4 Hz; 4.7 Hz, 3H, -OCHC*H*$_3$), 1.18–1.13 (td, *J* = 7.1 Hz; 0.9 Hz, 3H, -OCH$_2$C*H*$_3$).

2.2 Synthesis of 1,2-bis-*n*-octadecyl glyceryl ether (BisOD)

The synthesis of BisOD (**5**) was carried out as described in chapter 2.2 and in adaptation to literature.[2]

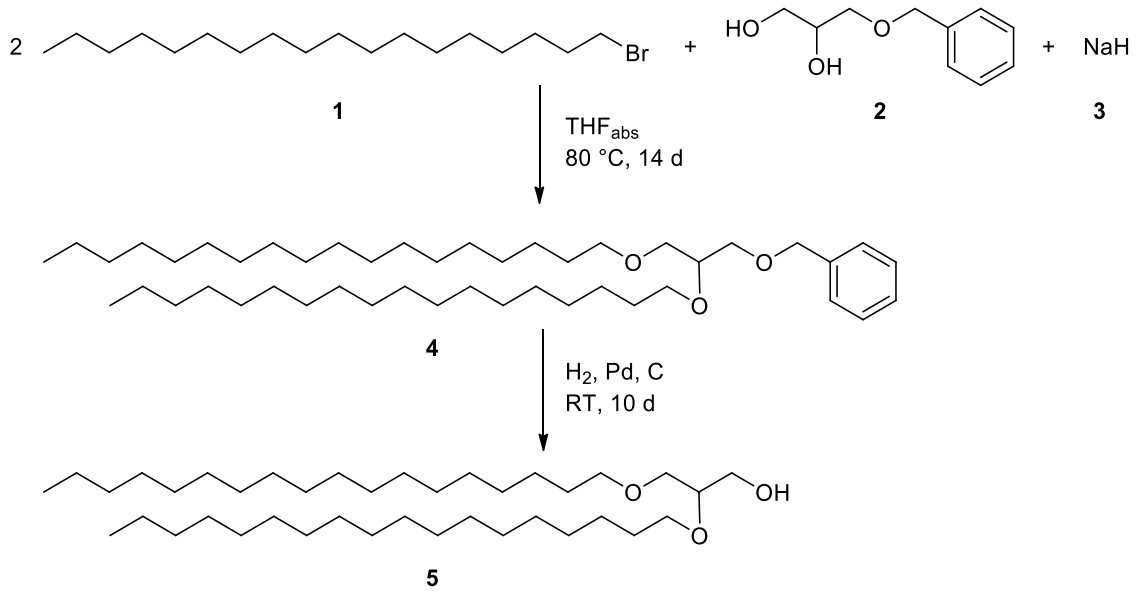

Scheme S1. Synthesis of 1,2-bis-*n*-octadecyl glyceryl ether (BisOD) (**5**).

mp: 65.6–66.6 °C.

^{1}H NMR, COSY (400 MHz, chloroform-*d*, δ): 3.74–3.41 (m, 9H, glycerol H), 1.59–1.53 (m, 4H, -OCH$_2$C*H$_2$*-), 1.31–1.25 (m, 60H, -OCH$_2$CH$_2$(C*H$_2$*)$_{15}$CH$_3$), 0.88 (t, *J* = 13.1 Hz; 7.2 Hz, 6H; -O(CH$_2$)$_{17}$C*H$_3$*).

^{13}C NMR, HSQC, HMBC (101 MHz, chloroform-*d*, δ): 78.4 (glycerol C), 72.0 (-O*C*H$_2$CH$_2$-), 71.1 (glycerol C), 70.6 (-O*C*H$_2$CH$_2$-), 63.3 (glycerol C), 32.1 (-OCH$_2$CH$_2$(*C*H$_2$)$_{17}$CH$_3$), 30.2 (-OCH$_2$*C*H$_2$-), 29.7–29.5 (-OCH$_2$CH$_2$(*C*H$_2$)$_{17}$CH$_3$), 26.3 (-OCH$_2$CH$_2$(*C*H$_2$)$_{17}$CH$_3$), 22.9 (-OCH$_2$CH$_2$(*C*H$_2$)$_{17}$CH$_3$), 14.3 (-O(CH$_2$)$_{19}$*C*H$_3$).

2.3 Polymer synthesis of BisOD-PEG

1,2-Bis-*n*-octadecyl glyceryl ether (BisOD) (0.2 g, 0.36 mmol, 1 eq.) was placed in a dry Schlenk flask and dissolved in benzene (10 mL). The solution was stirred at 60 °C for 30 min and dried under vacuum for 16 h to remove moisture. To dissolve the initiator dry tetrahydrofuran (THF) (approx. 10 mL) was cryo-transferred to the Schlenk flask. Subsequently, the initiator was deprotonated with a 0.5 M solution of potassium naphthalenide in THF (0.36 mL, 0.18 mmol, 0.5 eq.) while stirring. Subsequently, the solution was cooled to –80 °C and ethylene oxide (EO) (1.70 mL, 37.57 mmol, 105 eq.) was cryo-transferred using a graduated ampule. The polymerization was carried out at 60 °C for 24 h. An excess of ethanol was added to quench the polymerization and the

solvent was removed under reduced pressure. The crude product was dissolved in methanol and precipitated twice in cold diethyl ether to obtain the pure product. Yield: 99%.

^{1}H NMR, COSY (400 MHz, benzene-d_6, δ): 3.67–3.30 (m, 359H, polyether backbone and glycerol H), 1.66–1.56 (m, 4H, -OCH_2CH_2-), 1.44–1.28 (m, 58H, -$OCH_2CH_2(CH_2)_{15}CH_3$), 0.92–0.89 (m, 6H, -$O(CH_2)_{17}CH_3$).

^{13}C NMR, HSQC, HMBC (101 MHz, benzene-d_6, δ): 79.0 (glycerol C), 73.4 (polyether backbone and glycerol C), 72.4–70.9 (polyether backbone and glycerol C), 62.2 (polyether backbone and glycerol C), 32.6 (-$OCH_2CH_2(CH_2)_{14}CH_2CH_3$ (BisOD)), 31.1–30.1 (-OCH_2CH_2- and -$OCH_2CH_2(CH_2)_{14}CH_2CH_3$ (BisOD)), 27.0 (-$OCH_2CH_2(CH_2)_{14}CH_2CH_3$ (BisOD)), 23.4 (-$OCH_2CH_2(CH_2)_{14}CH_2CH_3$ (BisOD)), 14.6 (-$O(CH_2)_{17}CH_3$ (BisOD)).

2.4 Polymer synthesis of BisOD-*lin*PG

1,2-Bis-*n*-octadecyl glyceryl ether (BisOD) (0.25 g, 0.42 mmol, 1 eq.) and cesium hydroxide (0.06 g, 0.38 mmol, 0.9 eq.) were placed in a dry Schlenk flask and dissolved in benzene (10 mL). The solution was stirred at 60 °C for 30 min to enable the formation of the alkoxide and dried for 16 h under vacuum. The alkoxide was heated to 100 °C in vacuo to liquefy the initiator. Subsequently, EEGE (1.28 mL, 8.39 mmol, 20 eq.) was added via syringe and the polymerization was carried out *in vacuo* for 7 days. Methanol (5 mL) was added to quench the polymerization and to dissolve the crude product. Afterwards, 2N HCl (3 mL) was added to remove the acetal protecting groups. The solution was stirred at 40 °C for 10 days and subsequently precipitated in cold diethyl ether to obtain the pure product. Yield: 97%.

^{1}H NMR, COSY (400 MHz, pyridine-d_5, δ): 4.41–3.83 (m, polyether backbone and glycerol H), 1.67–1.62 (m, 4H, -OCH_2CH_2-), 1.44–1.27 (m, 62H, -$OCH_2CH_2(CH_2)_{15}CH_3$), 0.90–0.87 (m, 6H, -$O(CH_2)_{17}CH_3$).

^{13}C NMR, HSQC, HMBC (101 MHz, pyridine-d_5, δ): 81.9–81.7 (polyether backbone and glycerol C), 73.4 (polyether backbone and glycerol C), 72.7–72.4 (polyether backbone and glycerol C), 65.0 (polyether backbone and glycerol C), 62.8–62.7 (polyether backbone and glycerol C), 30.5 (-$OCH_2CH_2(CH_2)_{15}CH_3$).

2.5 Copolymer synthesis of BisOD-p(G-*co*-EG)

The polymerization is described for BisOD-p($G_{0.12}$-*co*-$EG_{0.88}$) as representative example.

1,2-Bis-*n*-octadecyl glyceryl ether (BisOD) (0.15 g, 0.25 mmol, 1 eq.) was placed in a dry Schlenk flask and dissolved in benzene (10 mL). The solution was dried under reduced pressure for 24 h to remove moisture. The initiator was dissolved in anhydrous tetrahydrofuran (THF) (15 mL) and subsequently deprotonated by adding a 0.5 M solution of potassium naphthalenide in THF (0.25 mL, 0.13 mmol, 0.5 eq.) while stirring. The initiator solution was cooled to −80 °C and ethylene oxide (EO) (1.50 mL, 33.03 mmol, 132 eq.) was cryo-transferred using a graduated ampule. Subsequently, ethoxyethyl glycidyl ether (EEGE) (0.020 mL, 0.223 mmol, 3 eq.) was added and the polymerization was carried out for 4 days at 80 °C. The polymerization was quenched by adding an excess of ethanol and the solvent was removed under reduced pressure. The crude polymer was dissolved in methanol (10 mL) and 2N HCl (6 mL) was added. The solution was stirred at 40 °C for 3 days. Afterwards, the solvent was removed under reduced pressure, the polymer was dissolved in methanol (2 mL) and precipitated in cold diethyl ether (45 mL) to obtain the pure product BisOD-p($G_{0.12}$-*co*-$EG_{0.88}$).

BisOD-p($EEGE_{0.12}$-*co*-$EG_{0.88}$)

^{1}H NMR, COSY (300 MHz, chloroform-*d*, δ): 4.72–4.65 (m, 8H, acetal H), 3.75–3.41 (m, 310H, polyether backbone, -CHC*H*$_2$OCOCH$_2$-, -CHCH$_2$OCOC*H*$_2$- and glycerol H), 1.55–1.49 (m, 3H, -OCH$_2$C*H*$_2$-), 1.37–1.15 (m, 99H, -OCH$_2$CH$_2$(C*H*$_2$)$_{15}$CH$_3$), -OCHC*H*$_3$, -OCH$_2$C*H*$_3$), 0.88–0.84 (m, 6H, -O(CH$_2$)$_{17}$C*H*$_3$).

^{13}C NMR, HSQC, HMBC (75 MHz, chloroform-*d*, δ): 99.7 (acetal C), 79.8 (glycerol C), 71.4–69.7 (polyether backbone and glycerol C), 62.7 (polyether backbone and glycerol C), 61.1 (polyether backbone and glycerol C), 60.7 (-CH*C*H$_2$OCOCH$_2$-, -CHCH$_2$OCO*C*H$_2$-), 58.5 (polyether backbone and glycerol C), 32.1 (-OCH$_2$CH$_2$(CH$_2$)$_{14}$*C*H$_2$CH$_3$), 29.8–29.5 (-OCH$_2$*C*H$_2$- and -OCH$_2$CH$_2$(*C*H$_2$)$_{14}$CH$_2$CH$_3$), 22.8 (-OCH$_2$CH$_2$(CH$_2$)$_{14}$*C*H$_2$CH$_3$), 20.1–19.9 (-OCH*C*H$_3$, -OCH$_2$*C*H$_3$), 18.5 (-OCH*C*H$_3$, -OCH$_2$*C*H$_3$), 15.4 (-OCH*C*H$_3$, -OCH$_2$*C*H$_3$), 14.2 (-O(CH$_2$)$_{17}$*C*H$_3$).

IR (ATR) $\tilde{\nu}$ (cm^{-1}) = 2865, 1457, 1379, 1348, 1298, 1249, 1097, 999, 948, 874.

BisOD-p($G_{0.12}$-*co*-$EG_{0.88}$)

^{1}H NMR, COSY (300 MHz, methanol-d_4, δ): 3.81–3.54 (m, 488H, polyether backbone and glycerol H), 1.60–1.55 (m, 5H, -OCH_2CH_2-), 1.35–1.31 (m, 63H, -$OCH_2CH_2(CH_2)_{15}CH_3$), 0.94–0.90 (m, 6H, -$O(CH_2)_{17}CH_3$).

^{13}C NMR, HSQC, HMBC (75 MHz methanol-d_4, δ): 81.1 (polyether backbone and glycerol C), 73.7 (polyether backbone and glycerol C), 72.2–71.5 (polyether backbone and glycerol C), 70.5 (polyether backbone and glycerol C), 62.8 (polyether backbone and glycerol C), 62.2 (polyether backbone and glycerol C), 33.1 (-$OCH_2CH_2(CH_2)_{14}CH_2CH_3$ (BisOD)), 31.2–30.5 (-OCH_2CH_2- and -$OCH_2CH_2(CH_2)_{14}CH_2CH_3$ (BisOD)), 27.3 (-$OCH_2CH_2(CH_2)_{14}CH_2CH_3$ (BisOD)), 23.8 (-$(CH_2)_{14}CH_2CH_3$ (BisOD)), 14.5 (-$O(CH_2)_{17}CH_3$ (BisOD)).

IR (ATR) $\tilde{\nu}$ (cm^{-1}) = 3450, 2916, 2866, 1464, 1350, 1296, 1249, 1090, 948, 845.

2.6 Enzymatic functionalization to obtain BisOD-p(G^{MA}-*co*-EG)

The reaction is described for BisOD-p($G^{MA}_{0.12}$-*co*-$EG_{0.88}$) as representative example.

BisOD-p($G_{0.12}$-*co*-$EG_{0.88}$) (0.20 g, 0.05 mmol, 1 eq.) was placed in a flask and dissolved in toluene (8 mL). Subsequently, a spatula tip of butylated hydroxytoluene (BHT), *candida antarctica lipase B* (CALB) (80 mg) and vinyl methacrylate (0.30 mL, 2.50 mmol, 50 eq.) was added. The solution was mixed on a shaking plate under exclusion of light for 7 days. The solution was filtered and the solvent was reduced under vacuum. The crude product was precipitated in cold diethyl ether to obtain the pure product BisOD-p($G^{MA}_{0.12}$-*co*-$EG_{0.88}$). Yield: 72%.

^{1}H NMR, COSY (300 MHz, chloroform-*d*, δ): 6.10 (s, 9H, CH_2CCOO-), 5.57 (d, *J* = 2.0 Hz, 9H, CH_2CCOO-), 4.34–4.07 (m, 20H, -$COOCH_2$CH-), 3.86–3.40 (m, 242H, polyether backbone and glycerol H), 1.94 (s, 27H, CH_3C-), 1.61–1.45 (m, 3H, -OCH_2CH_2-), 1.30–1.25 (m, 39H, -$OCH_2CH_2(CH_2)_{15}CH_3$), 0.89–0.85 (m, 6H, -$O(CH_2)_{17}CH_3$).

^{13}C NMR, HSQC, HMBC (75 MHz, chloroform-*d*, δ): 136.3 (CH_2CCOO-), 125.9 (CH_2CCOO-), 71.1–70.1 (polyether backbone and glycerol C), 64.4 (-$COOCH_2$CH-), 29.9 (-$OCH_2CH_2(CH_2)_{14}CH_2CH_3$), 18.5 ($CH_3$C-).

IR (ATR) $\tilde{\nu}$ (cm^{-1}) = 2865, 1718, 1639, 1453, 1350, 1320, 1297, 1251, 1099, 943, 856, 815.

2.7 Liposome preparation

BisOD-p($G_{0.12}$-*co*-$EG_{0.88}$) (112 µL, 40 mg mL^{-1}), egg-phosphatidylcholine-3 (EPC-3) (121 µL, 100 mg mL^{-1}) and cholesterol (350 µL, 12.5 mg mL^{-1}) was each dissolved in ethanol and mixed in a flask to obtain a solution of 55 mol% EPC-3, 40 mol% cholesterol and 5 mol% BisOD-p($G_{0.12}$-*co*-$EG_{0.88}$). The solvent was removed via lyophilisation, the dried lipids were dissolved in phosphate-buffered saline (PBS) (39 µL) and ceramic beads (300 mg) were added. The sample was centrifuged for 20 min at 2500 rpm. Subsequently, additional PBS (120 µL) was added to obtain a final lipid concentration of 132 mg mL^{-1}. The sample was centrifuged for additional 2 min at 2500 rpm. To obtain optimal homogenization of the sample, the vial was rotated by 180° and again centrifuged for 2 min at 2500 rpm to obtain the liposomes.

2.8 Cross-linking of liposomes

The liposomal formulations (1 µL) were diluted with phosphate-buffered saline (PBS) to obtain a lipid concentration of 13.2 mg mL^{-1} and 0.132 mg mL^{-1} respectively. 2-Hydroxy-2-methylpropiophenone in ethanol (1 wt%) was added as photoinitiator and the sample was irradiated with UV light for 10 min to achieve cross-linking of the methacrylate groups.

3. Characterization Data

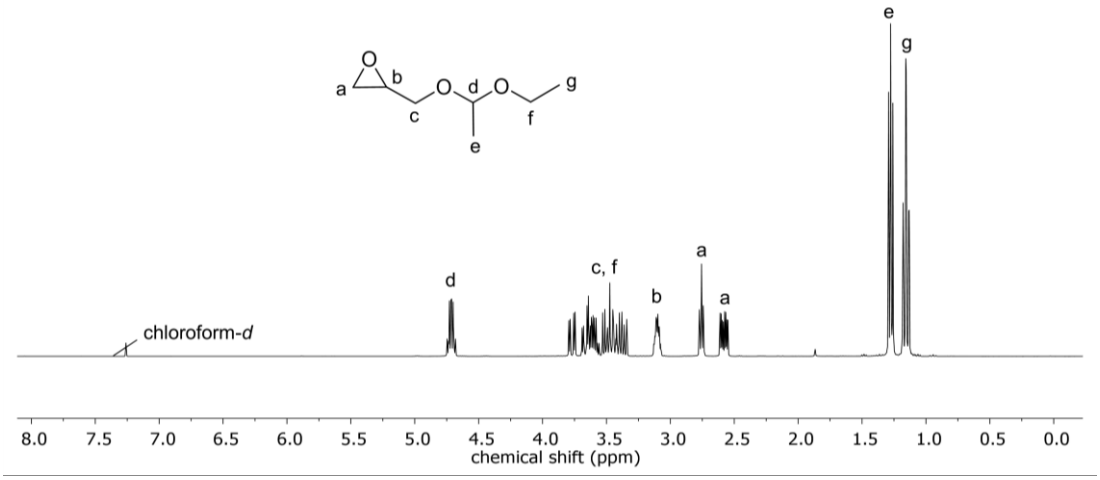

Figure S1. [1]H NMR (chloroform-*d*, 300 MHz) of ethoxyethyl glycidyl ether (EEGE).

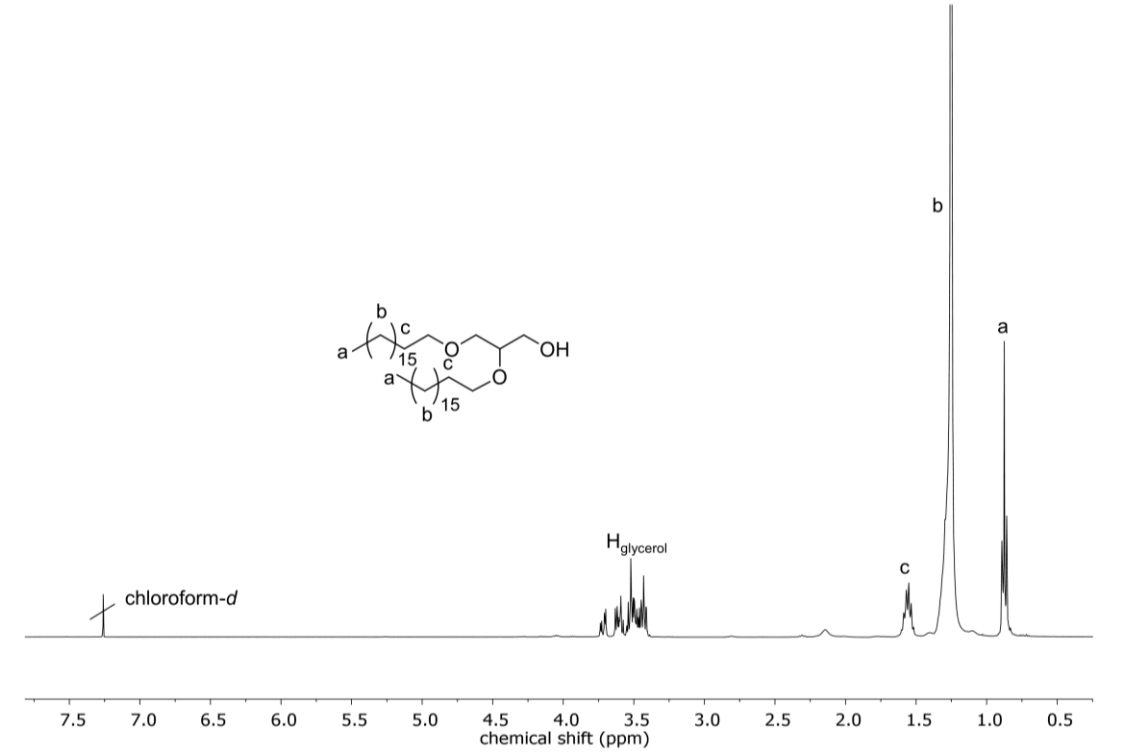

Figure S2. [1]H NMR (chloroform-*d*, 400 MHz) of 1,2-bis-*n*-octadecyl glyceryl ether (BisOD).

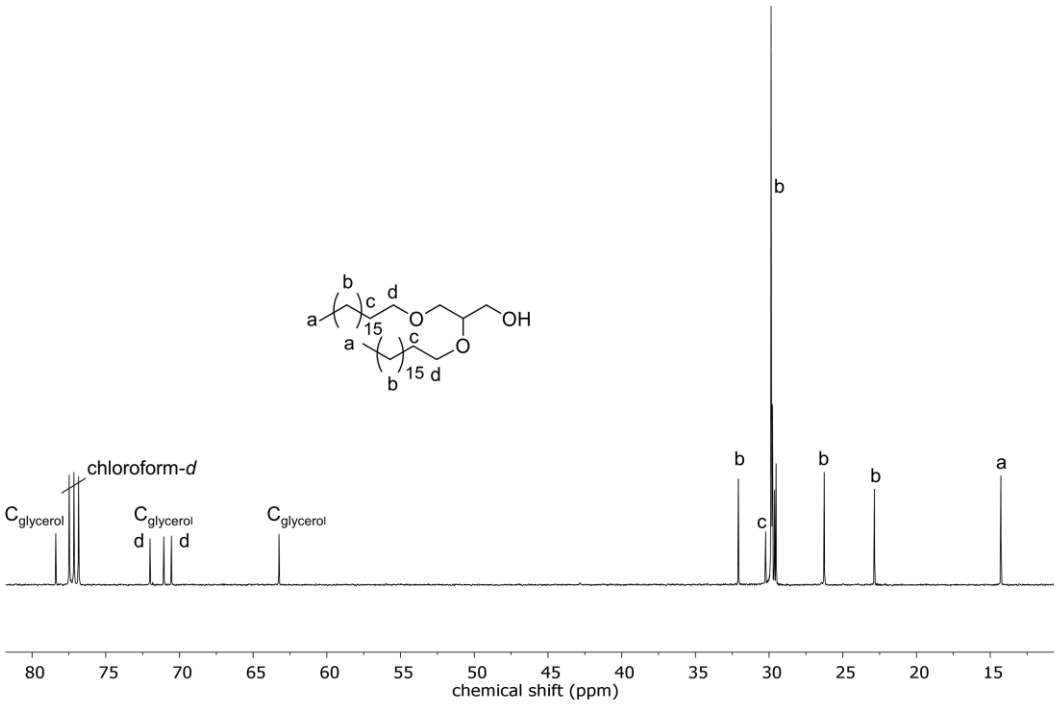

Figure S3. ^{13}C NMR (chloroform-*d*, 101 MHz) of 1,2-bis-*n*-octadecyl glyceryl ether (BisOD).

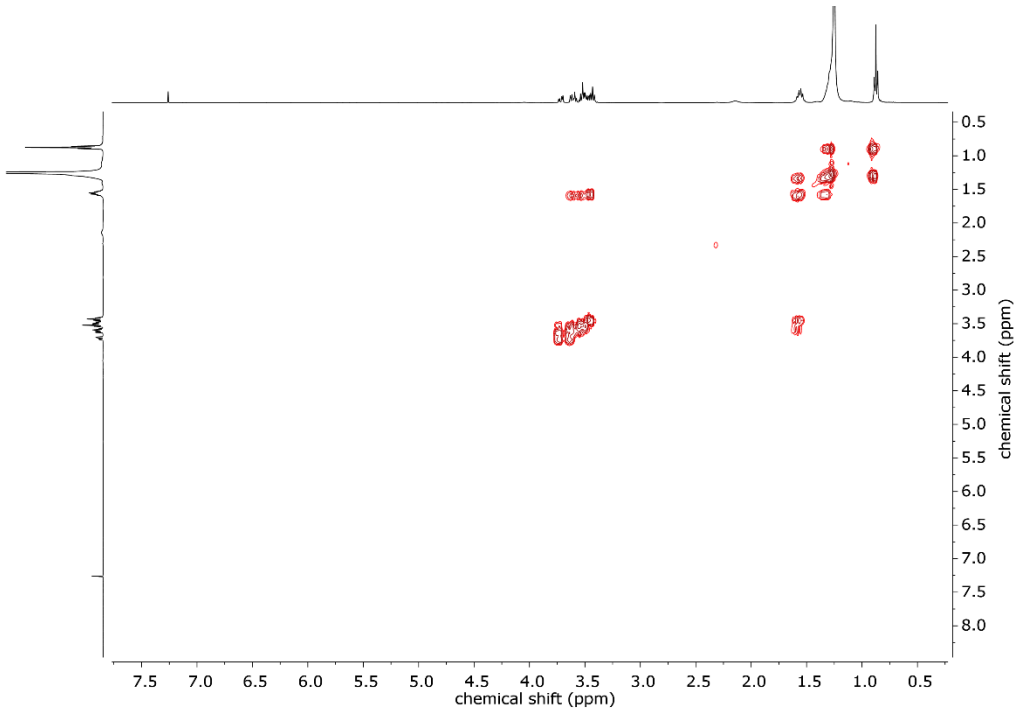

Figure S4. COSY NMR (chloroform-*d*, 400 MHz) of 1,2-bis-*n*-octadecyl glyceryl ether (BisOD).

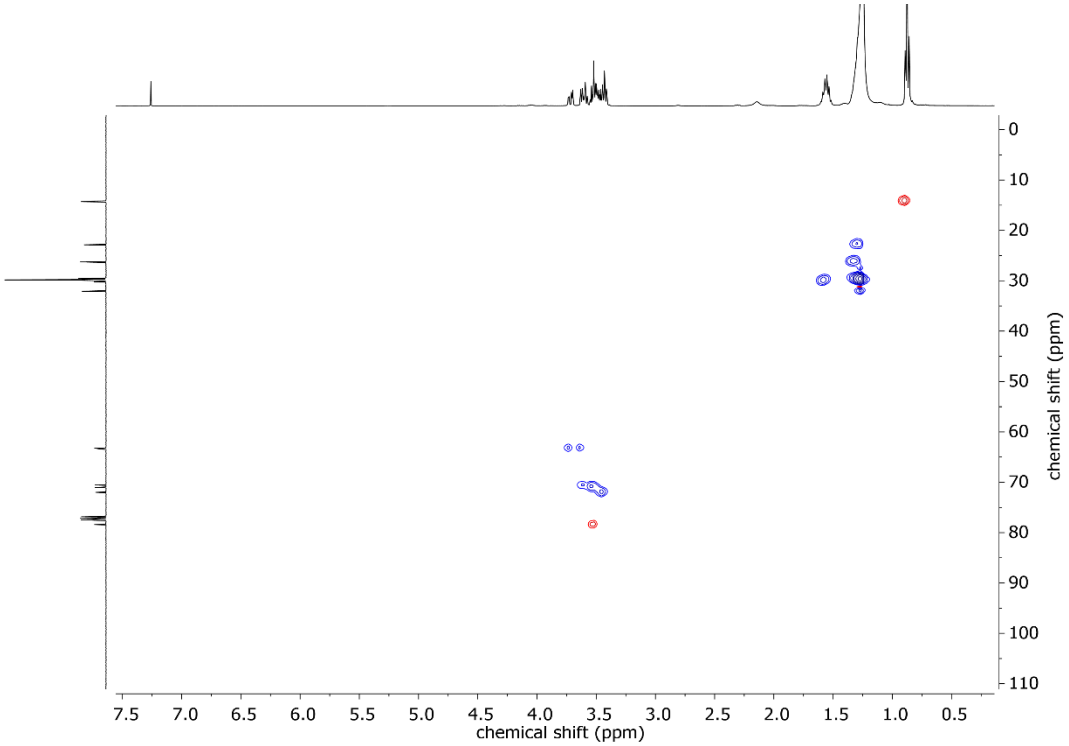

Figure S5. HSQC NMR (chloroform-*d*) of 1,2-bis-*n*-octadecyl glyceryl ether (BisOD).

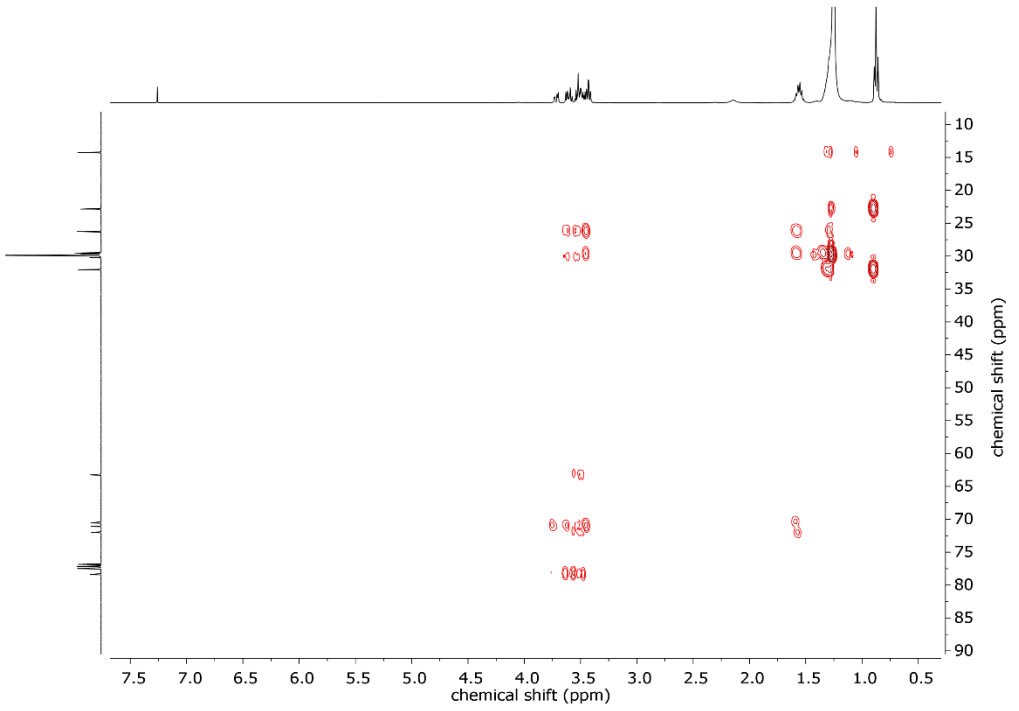

Figure S6. HMBC NMR (chloroform-*d*) of 1,2-bis-*n*-octadecyl glyceryl ether (BisOD).

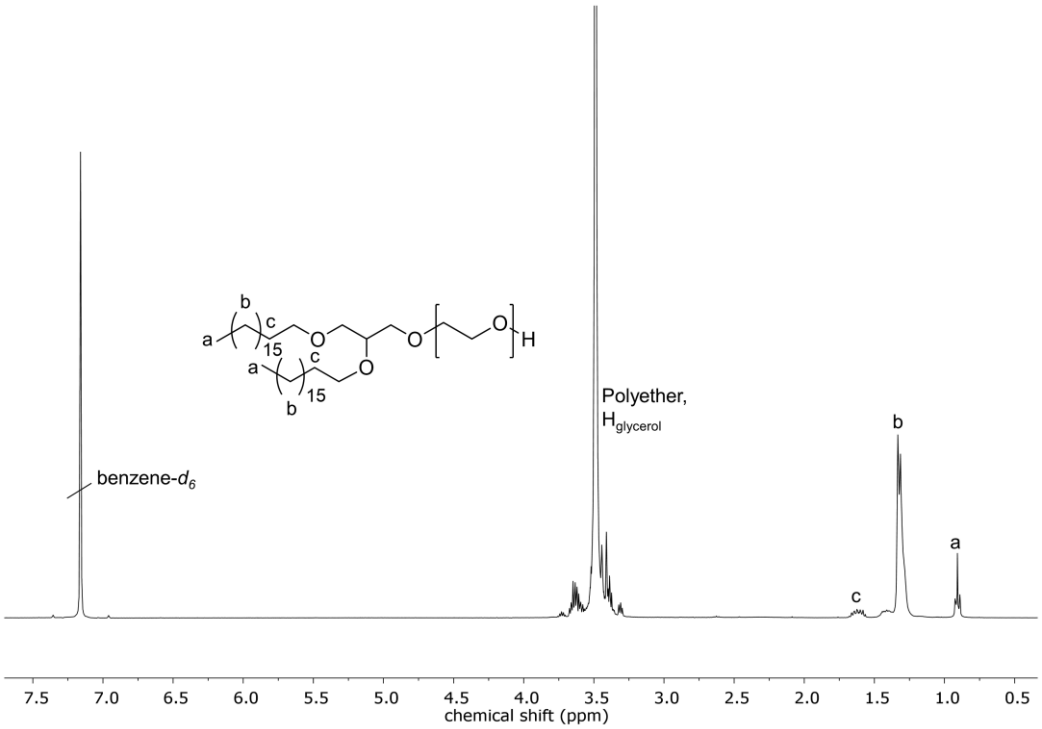

Figure S7. ^{1}H NMR (benzene-d_6, 400 MHz) of BisOD-PEG.

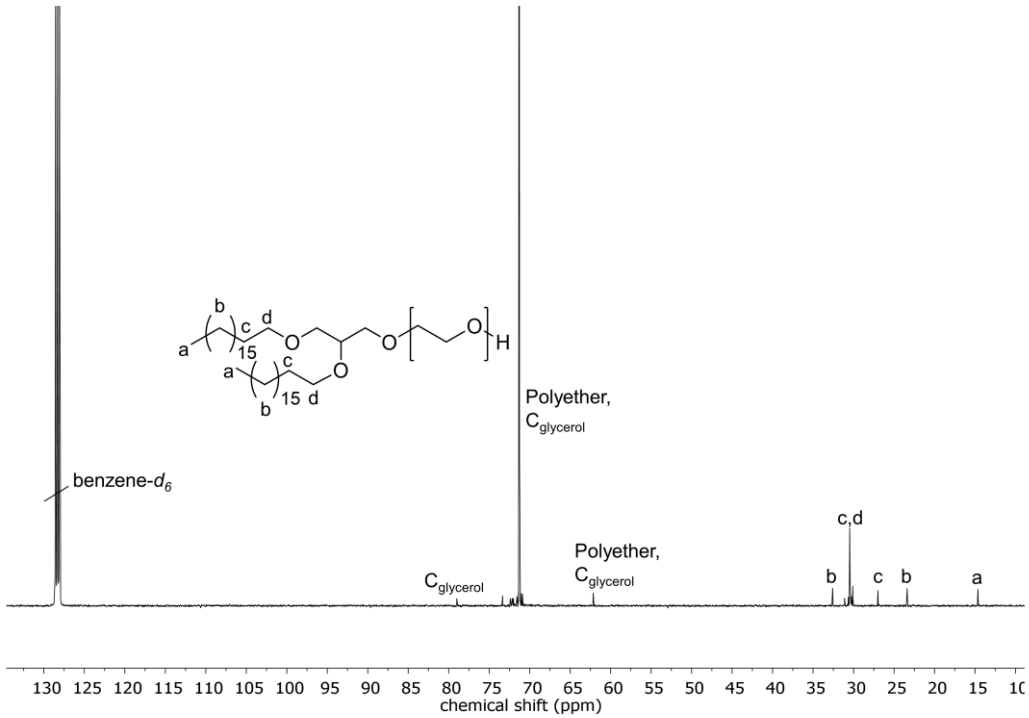

Figure S8. ^{13}C NMR (benzene-d_6, 101 MHz) of BisOD-PEG.

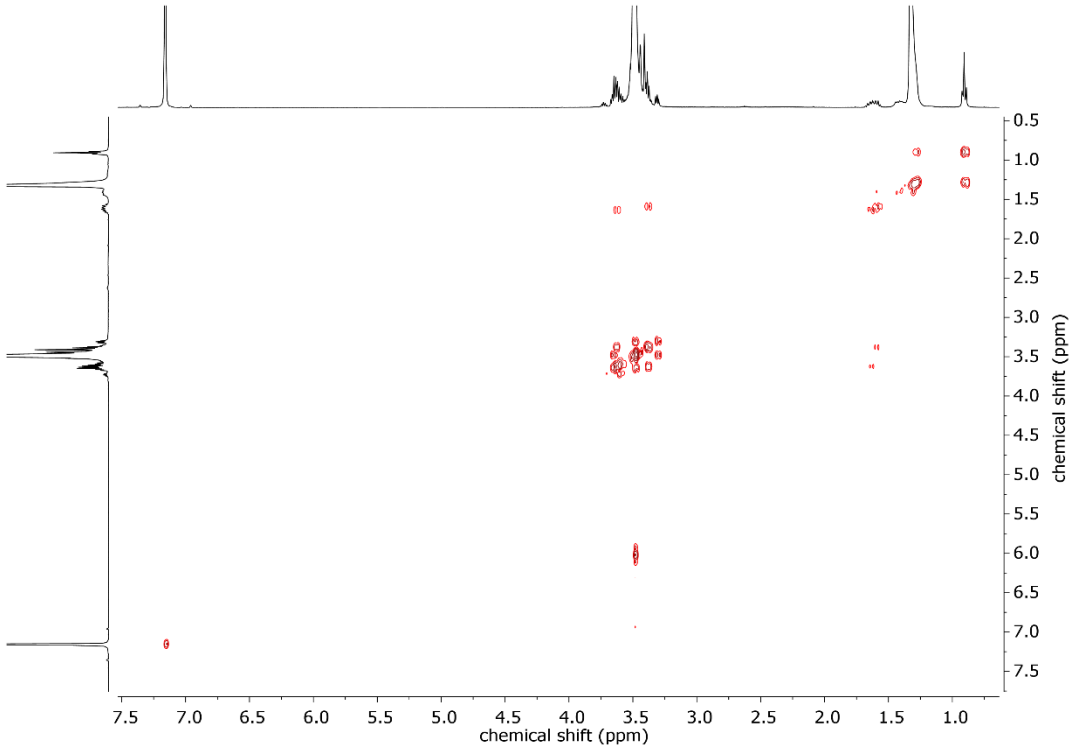

Figure S9. COSY NMR (benzene-d_6, 400 MHz) of BisOD-PEG.

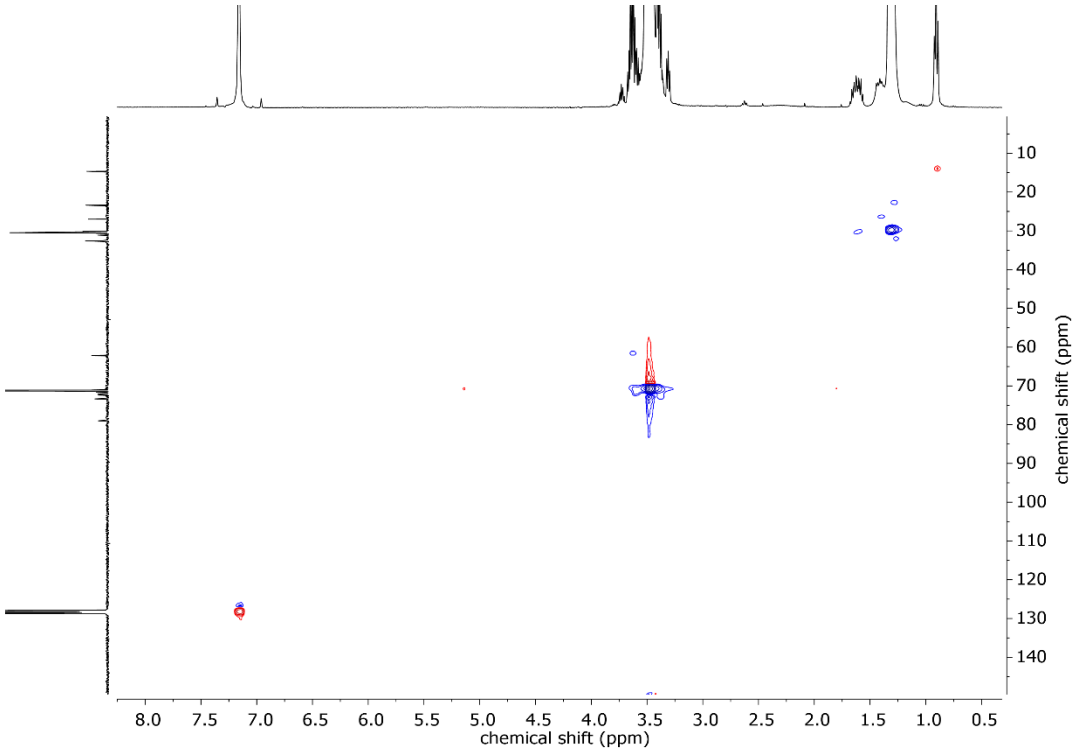

Figure S10. HSQC NMR (benzene-d_6) of BisOD-PEG.

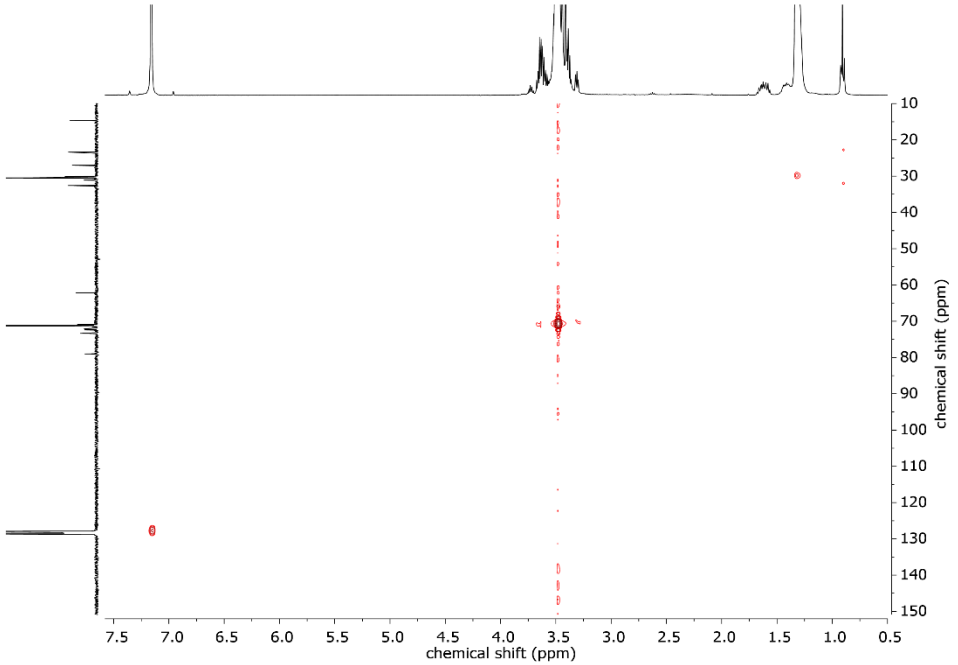

Figure S11. HMBC NMR (benzene-d_6) of BisOD-PEG.

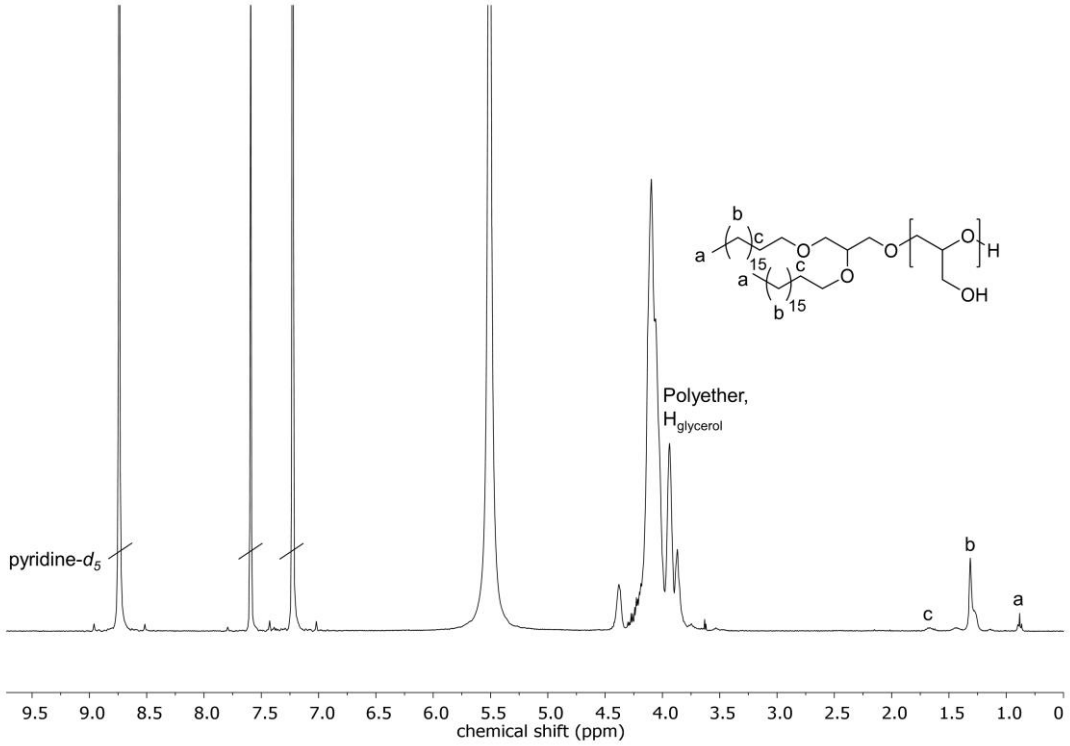

Figure S12. ^{1}H NMR (pyridine-d_5, 400 MHz) of BisOD-*lin*PG.

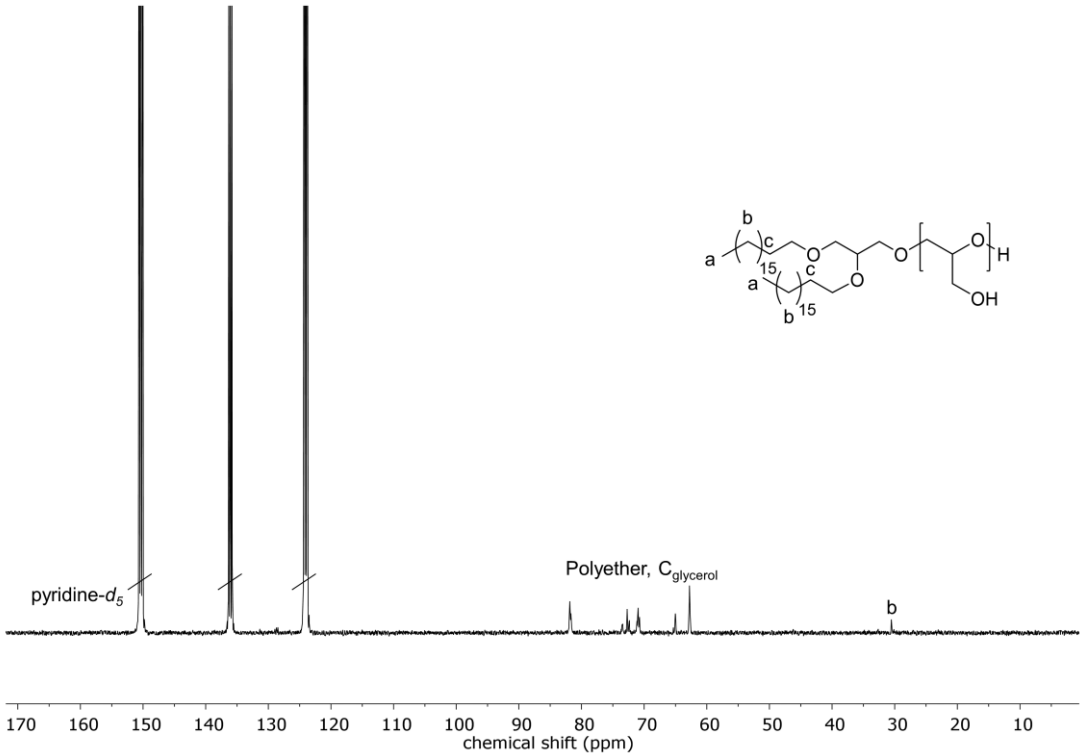

Figure S13. ^{13}C NMR (pyridine-d_5, 101 MHz) of BisOD-*lin*PG.

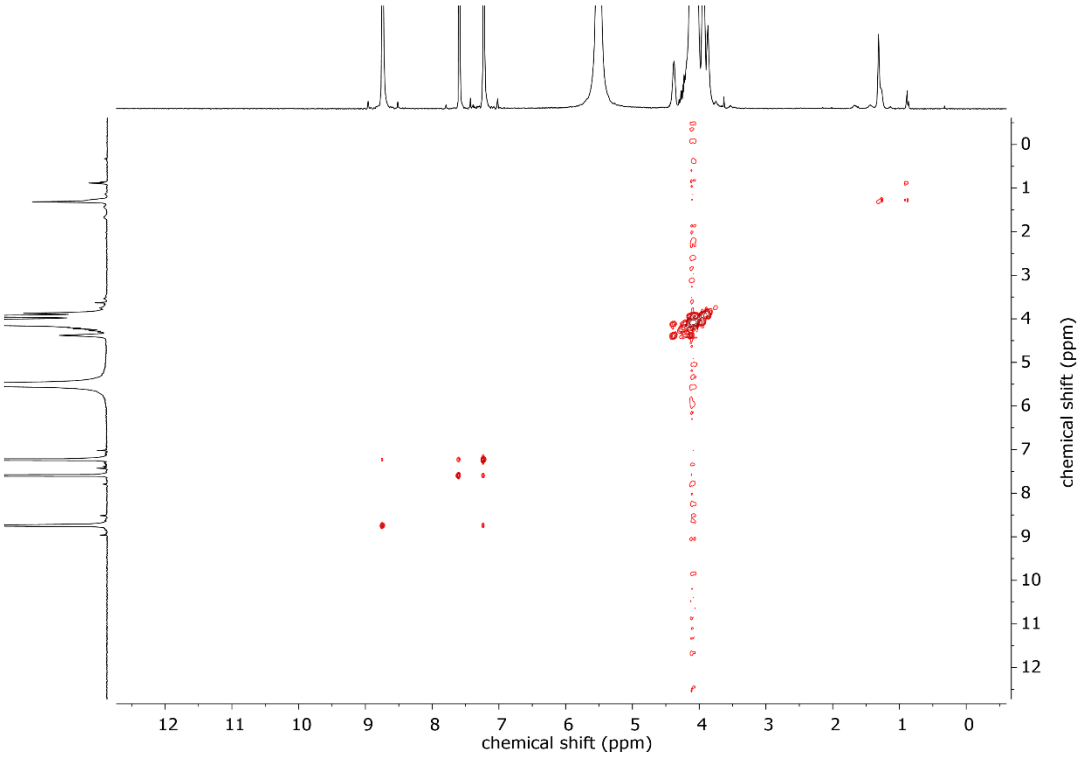

Figure S14. COSY NMR (pyridine-d_5, 400 MHz) of BisOD-*lin*PG.

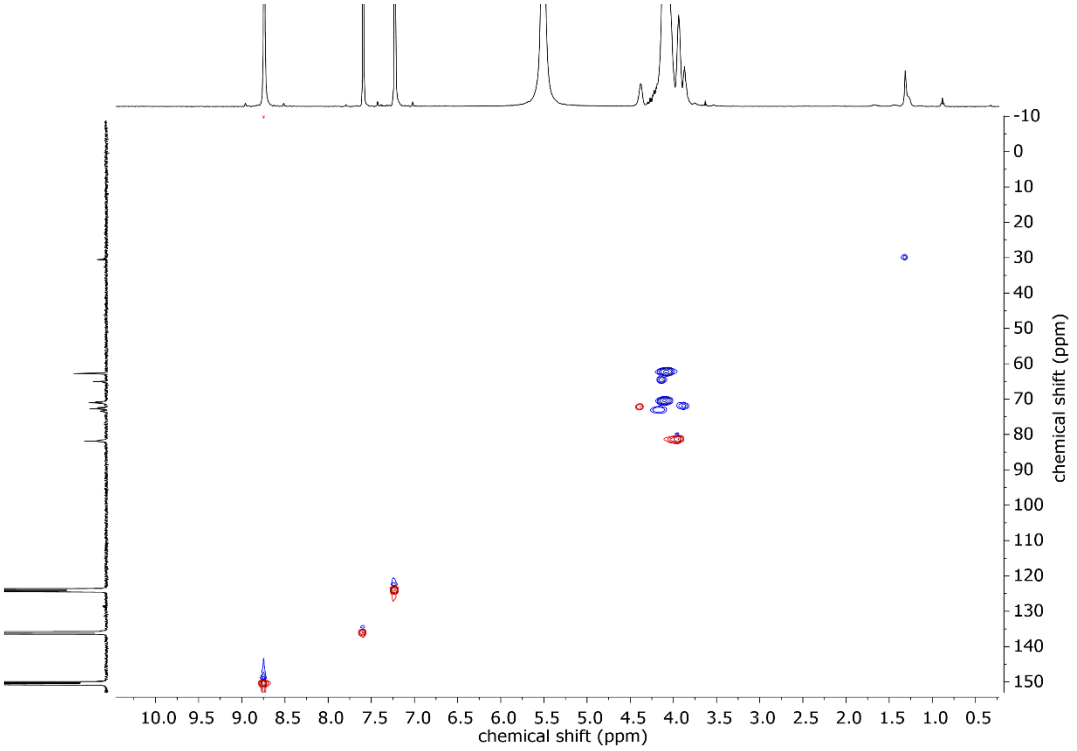

Figure S15. HSQC NMR (pyridine-d_5) of BisOD-*lin*PG.

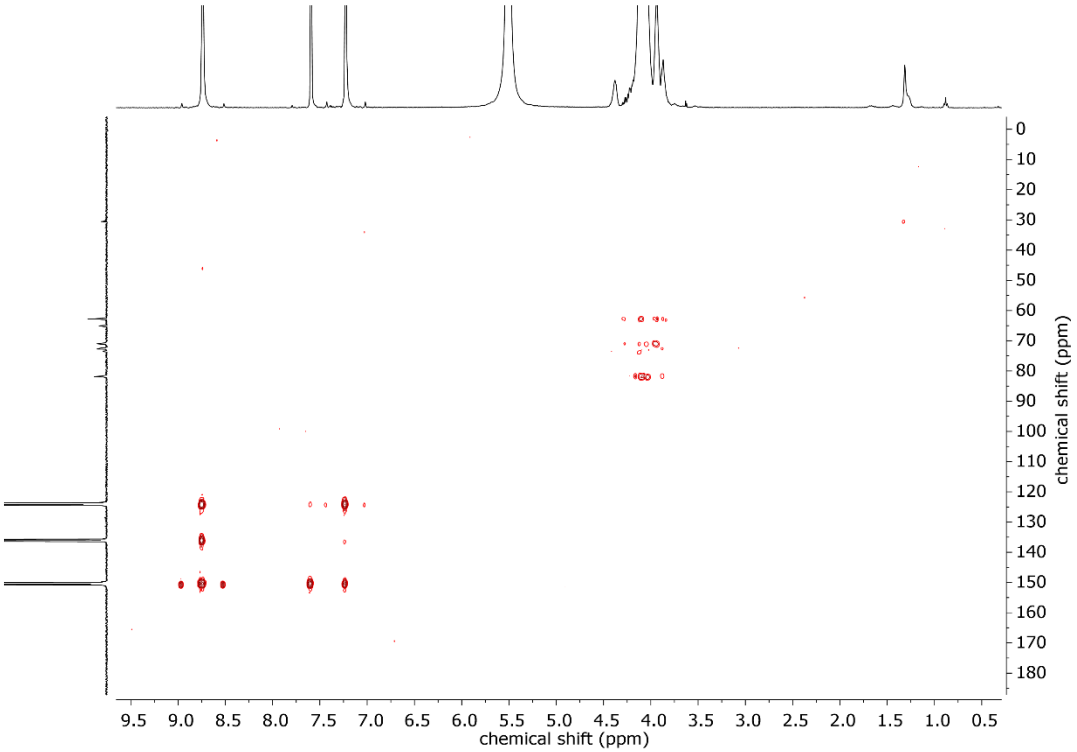

Figure S16. HMBC NMR (pyridine-d_5) of BisOD-*lin*PG.

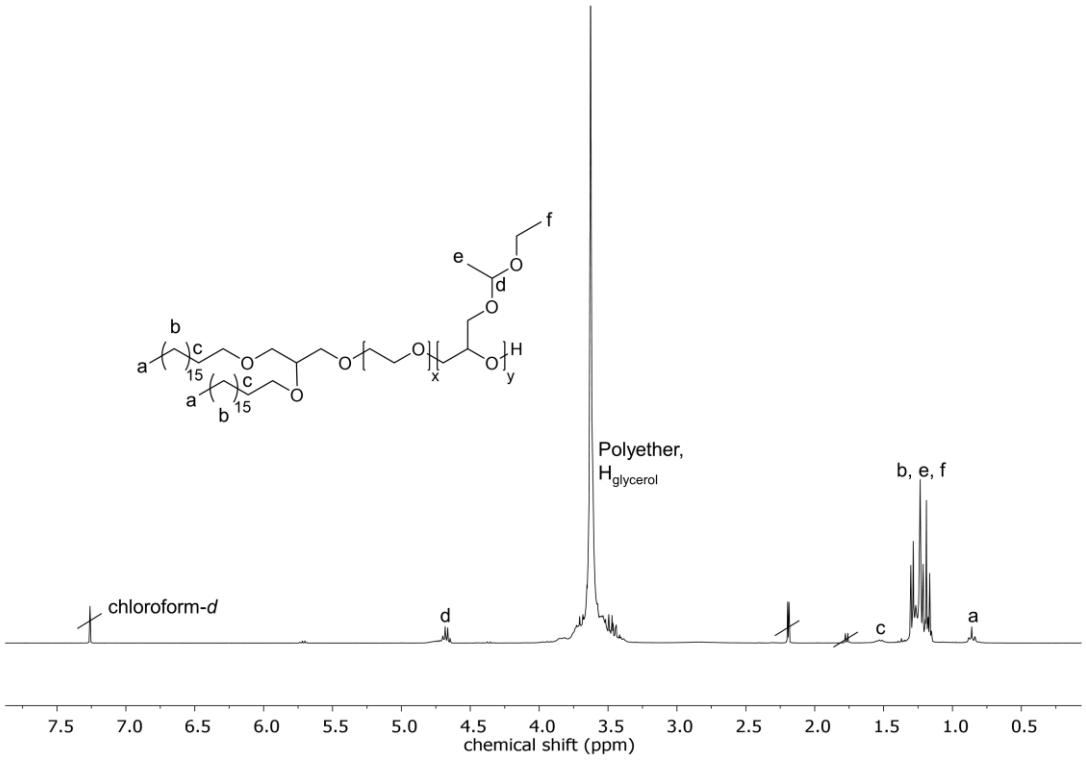

Figure S17. ^{1}H NMR (chloroform-*d*, 300 MHz) of BisOD-p(EEGE$_{0.12}$-*co*-EG$_{0.88}$).

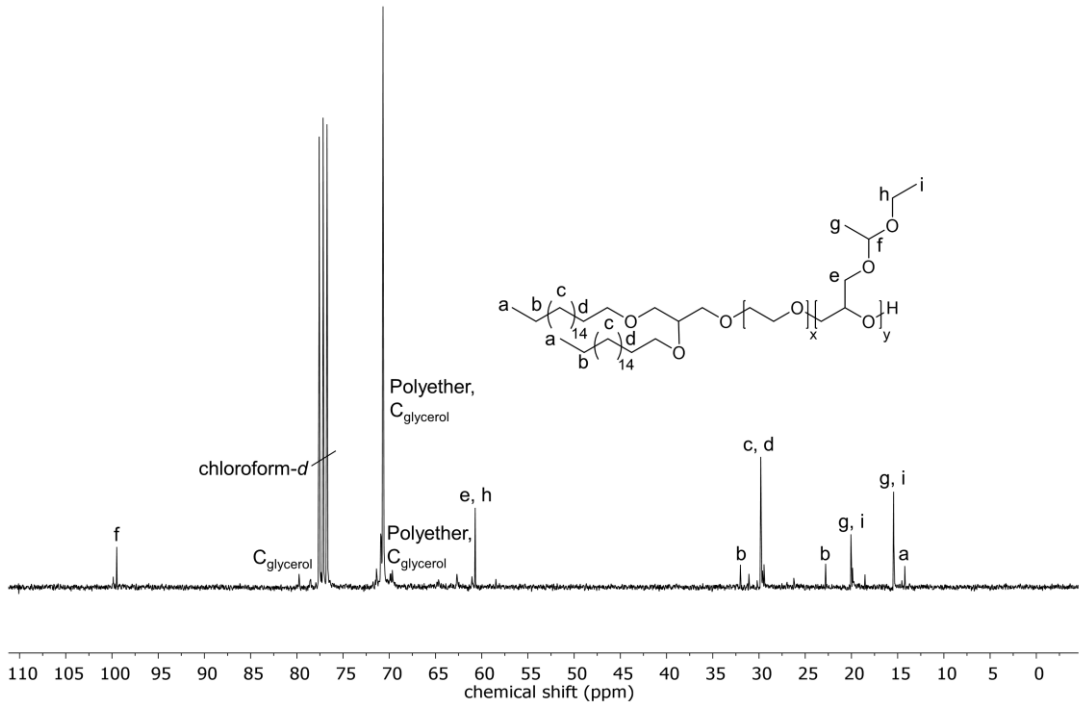

Figure S18. ^{13}C NMR (chloroform-*d*, 75 MHz) of BisOD-p(EEGE$_{0.12}$-*co*-EG$_{0.88}$).

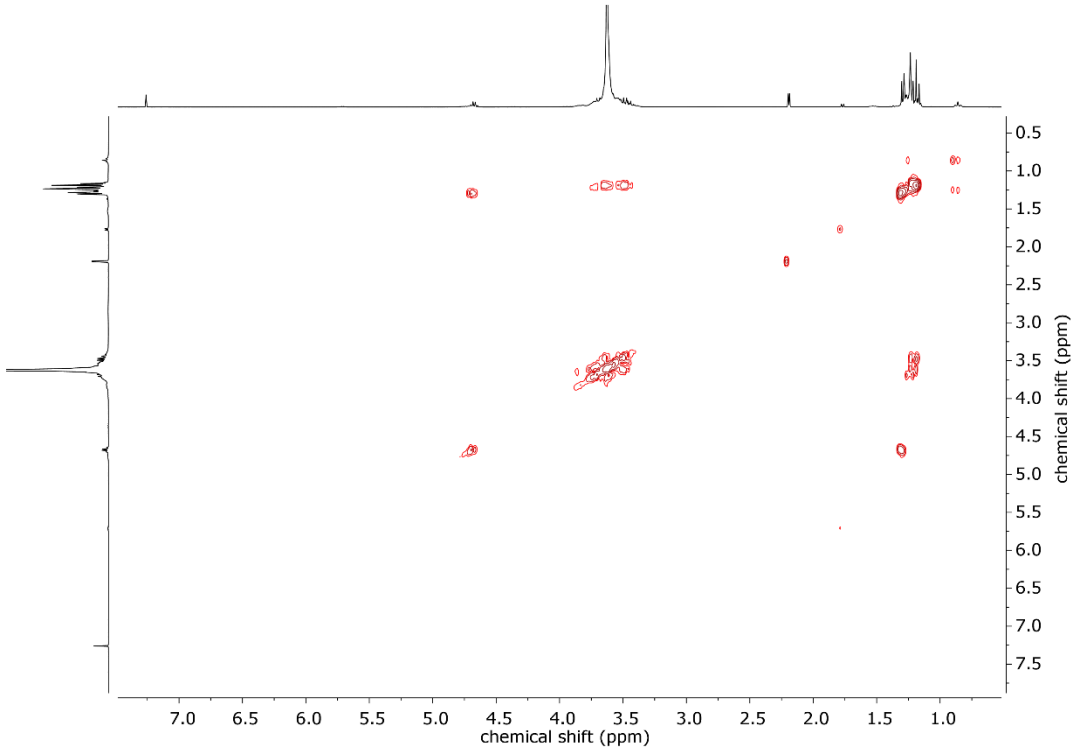

Figure S19. COSY NMR (chloroform-*d*, 300 MHz) of BisOD-p(EEGE$_{0.12}$-*co*-EG$_{0.88}$).

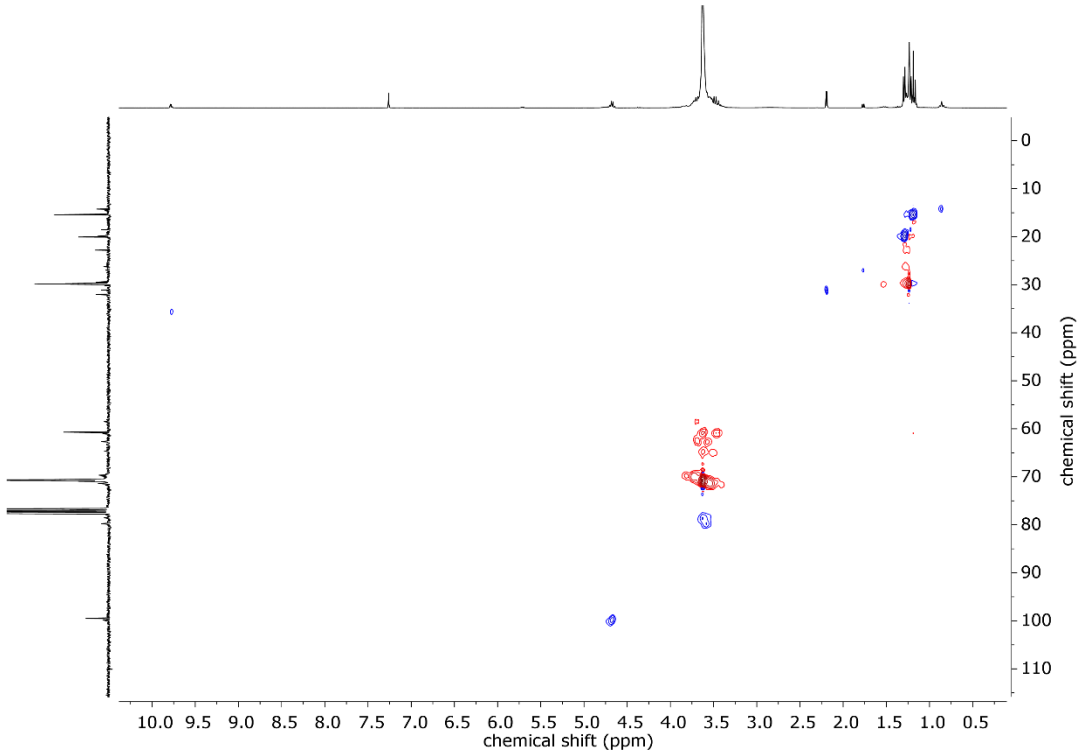

Figure S20. HSQC NMR (chloroform-*d*) of BisOD-p(EEGE$_{0.12}$-*co*-EG$_{0.88}$).

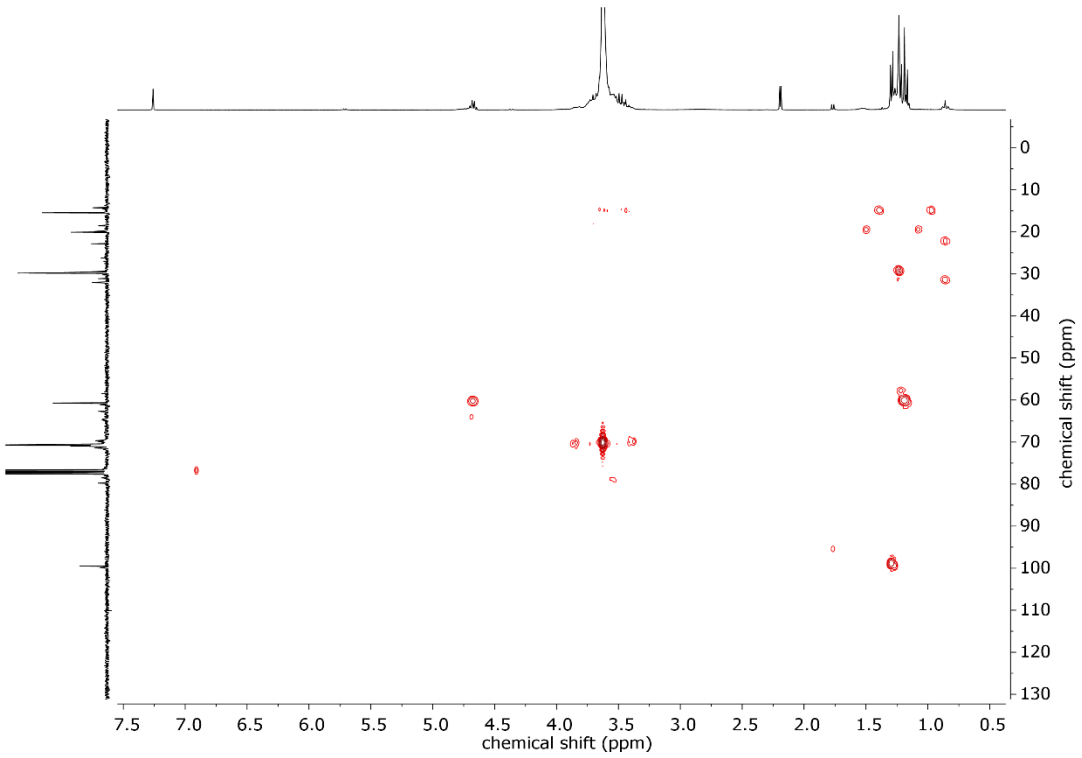

Figure S21. HMBC NMR (chloroform-*d*) of BisOD-p(EEGE$_{0.12}$-*co*-EG$_{0.88}$).

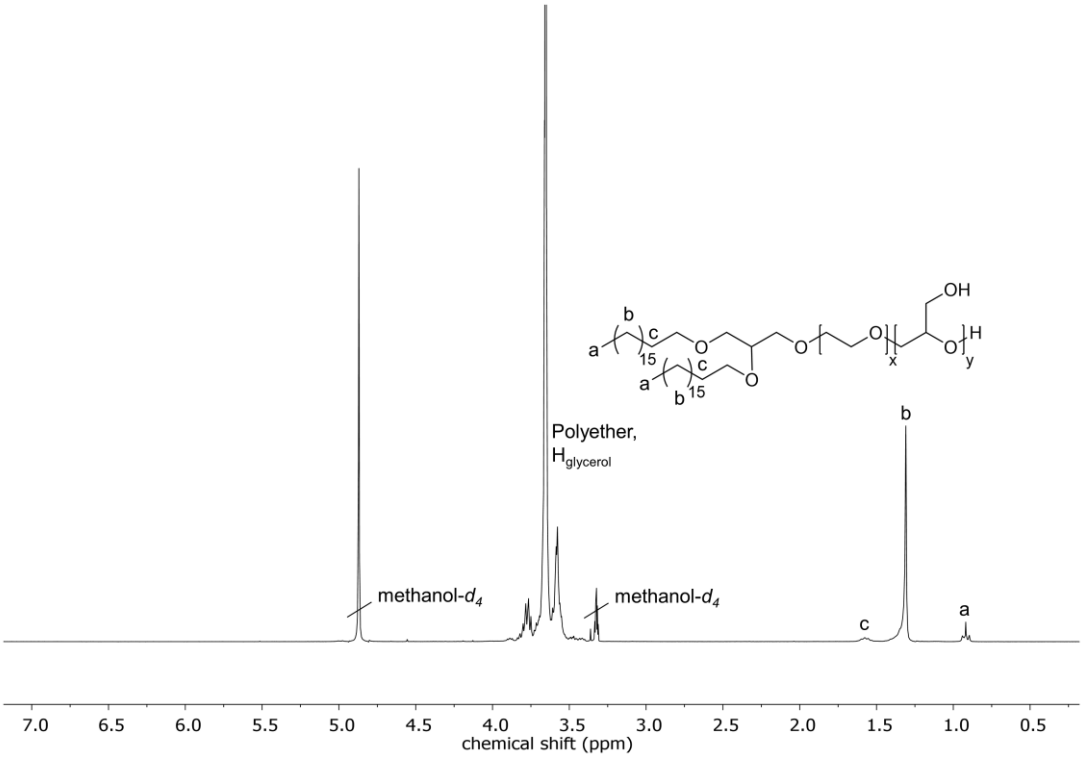

Figure S22. ^{1}H NMR (methanol-d_4, 300 MHz) of BisOD-p(G$_{0.12}$-*co*-EG$_{0.88}$).

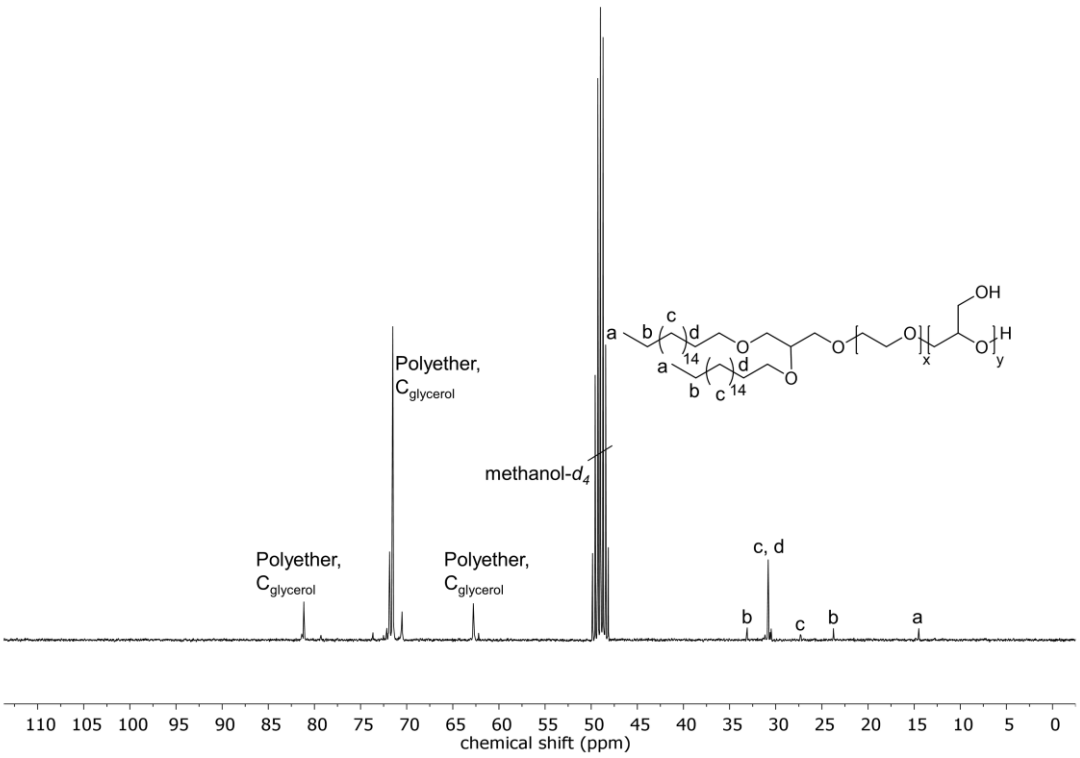

Figure S23. ^{13}C NMR (methanol-d_4, 75 MHz) of BisOD-p(G$_{0.12}$-*co*-EG$_{0.88}$).

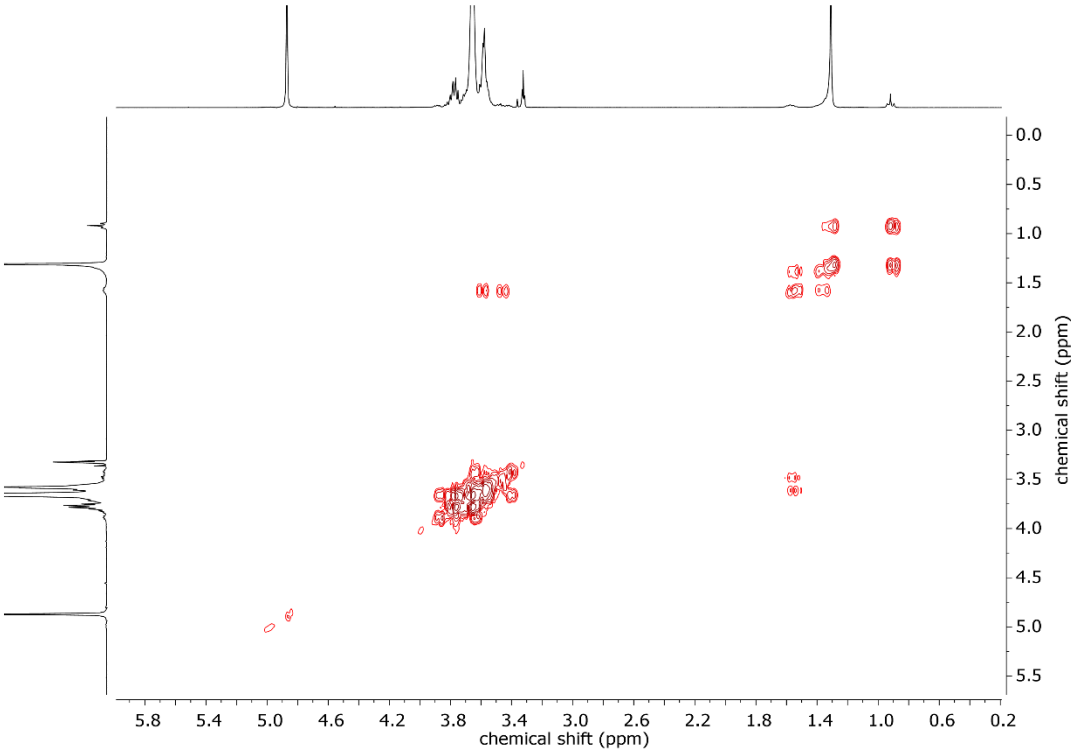

Figure S24. COSY NMR (methanol-d_4, 300 MHz) of BisOD-p(G$_{0.12}$-*co*-EG$_{0.88}$).

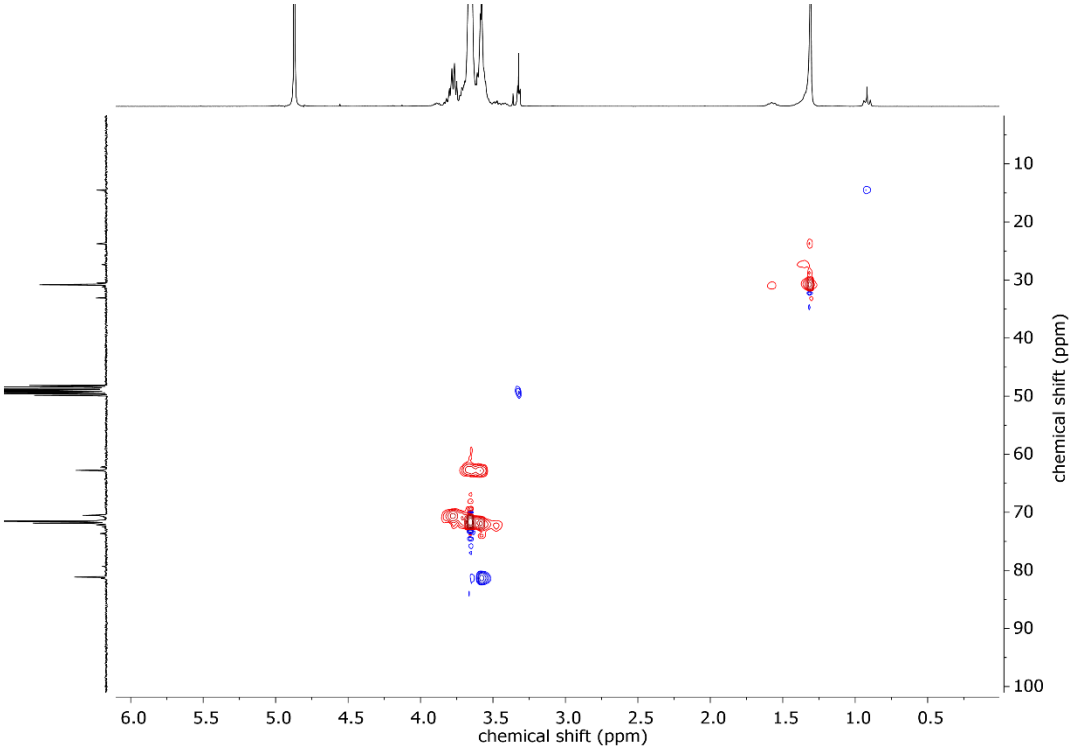

Figure S25. HSQC NMR (methanol-d_4) of BisOD-p($G_{0.12}$-*co*-$EG_{0.88}$).

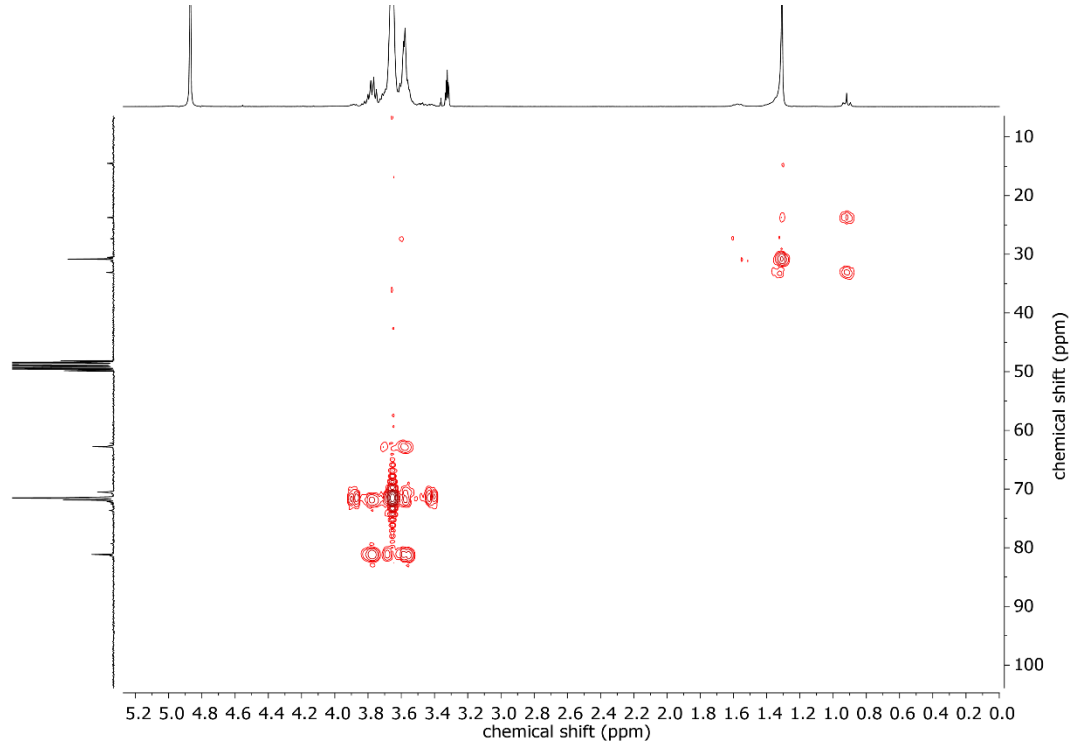

Figure S26. HMBC NMR (methanol-d_4) of BisOD-p($G_{0.12}$-*co*-$EG_{0.88}$).

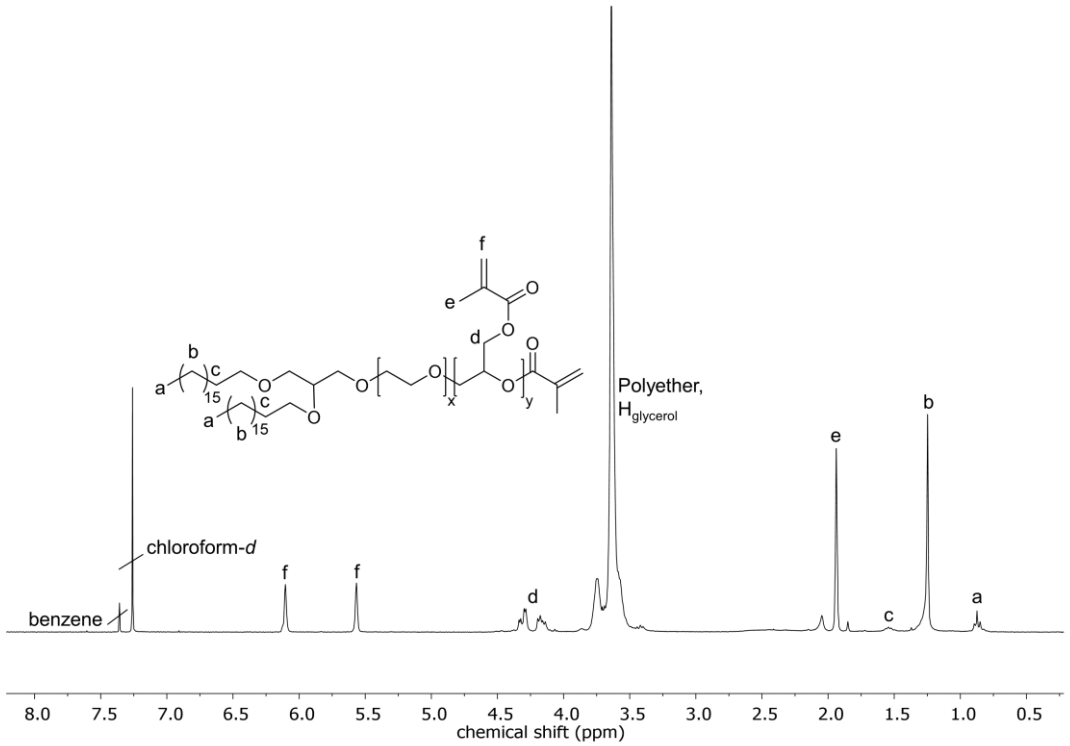

Figure S27. ^{1}H NMR (chloroform-*d*, 300 MHz) of BisOD-p($G^{MA}_{0.12}$-*co*-$EG_{0.88}$).

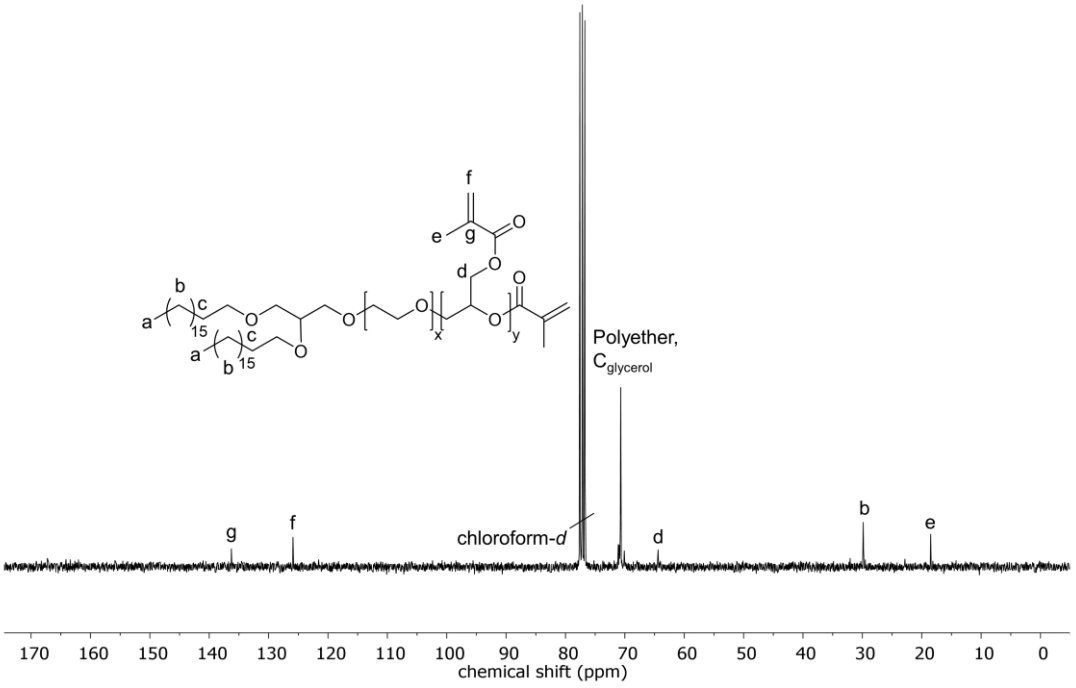

Figure S28. ^{13}C NMR (chloroform-*d*, 75 MHz) of BisOD-p($G^{MA}_{0.12}$-*co*-$EG_{0.88}$).

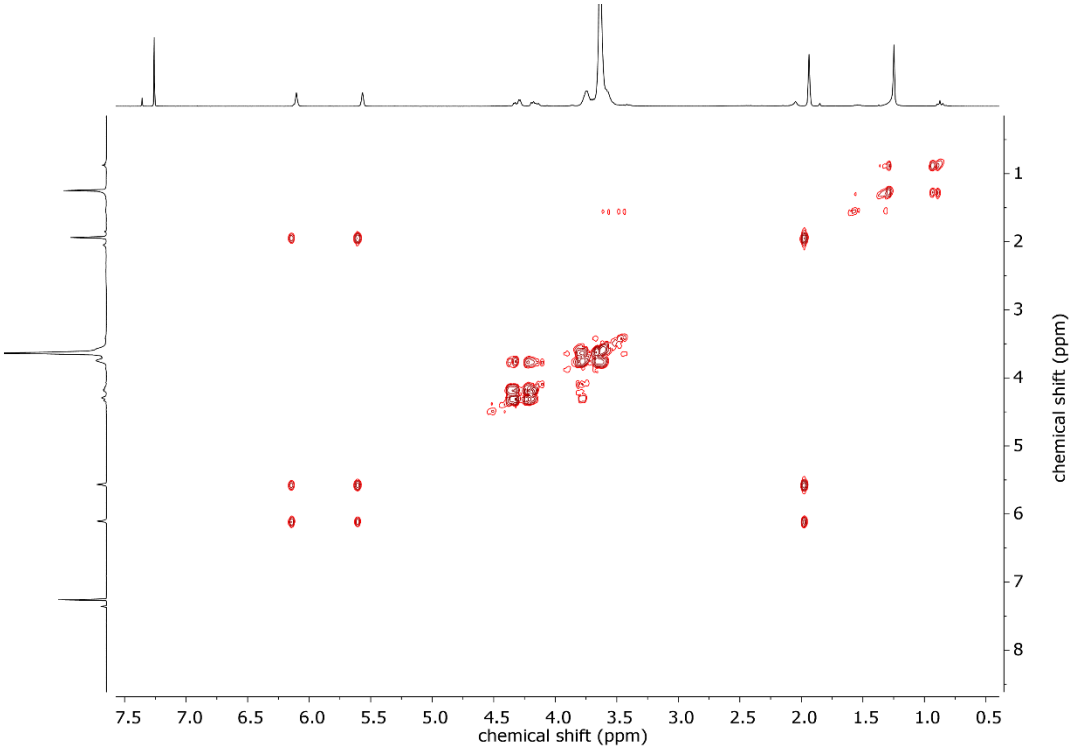

Figure S29. COSY NMR (chloroform-*d*, 300 MHz) of BisOD-p($G^{MA}_{0.12}$-*co*-$EG_{0.88}$).

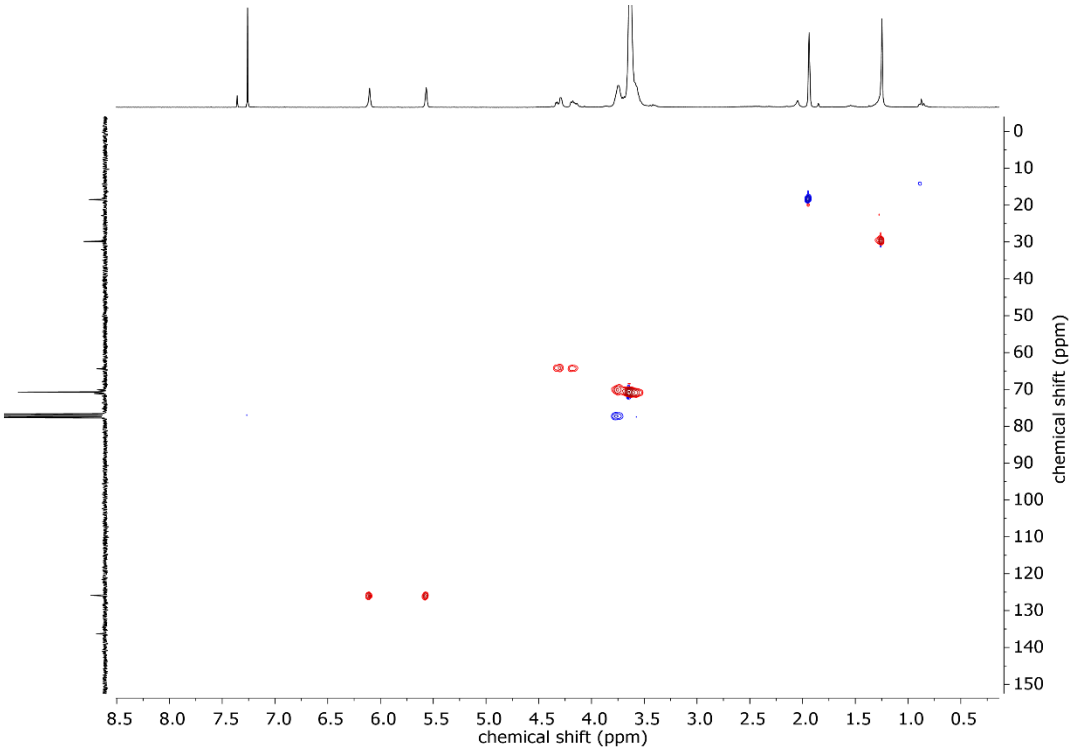

Figure S30. HSQC NMR (chloroform-*d*) of BisOD-p($G^{MA}_{0.12}$-*co*-$EG_{0.88}$).

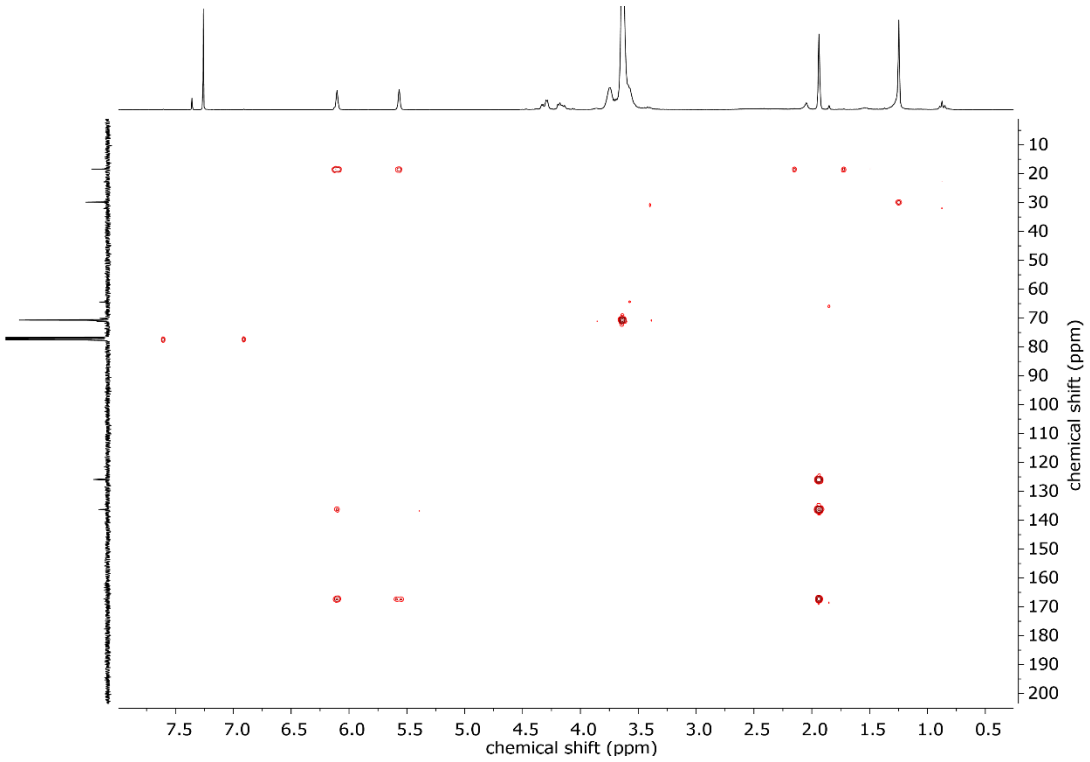

Figure S31. HMBC NMR (chloroform-*d*) of BisOD-p($G^{MA}_{0.12}$-*co*-$EG_{0.88}$).

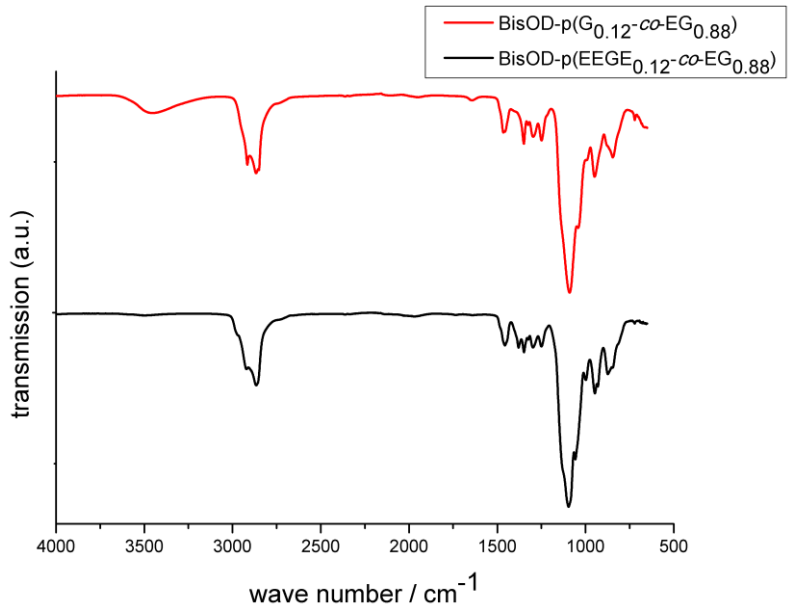

Figure S32. IR spectra of the synthesized copolymer BisOD-p($EEGE_{0.12}$-*co*-$EG_{0.88}$) (bottom, black) and BisOD-p($G_{0.12}$-*co*-$EG_{0.88}$) (top, red).

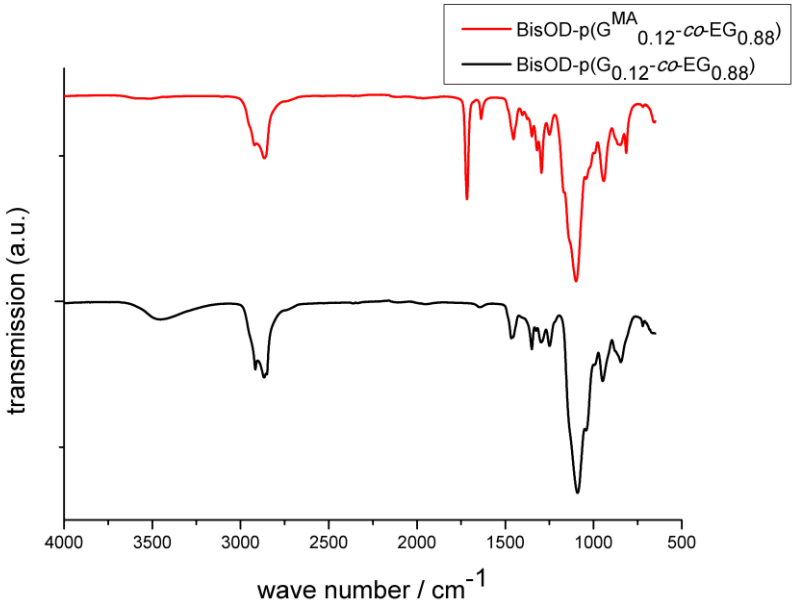

Figure S33. IR spectra of the synthesized copolymer BisOD-p(G$_{0.12}$-*co*-EG$_{0.88}$) (bottom, black) and BisOD-p(G$^{MA}_{0.12}$-*co*-EG$_{0.88}$) (top, red).

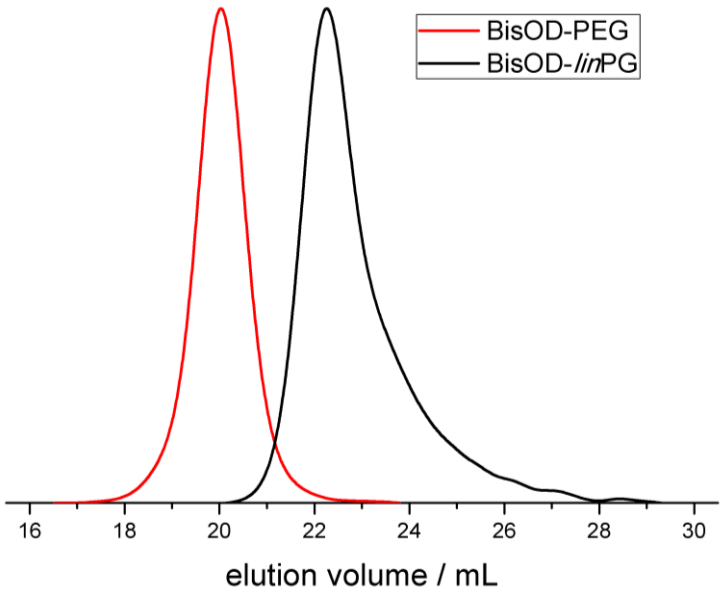

Figure S34. SEC traces (DMF, PEG standard, RI signal) of the BisOD-PEG and BisOD-*lin*PG.

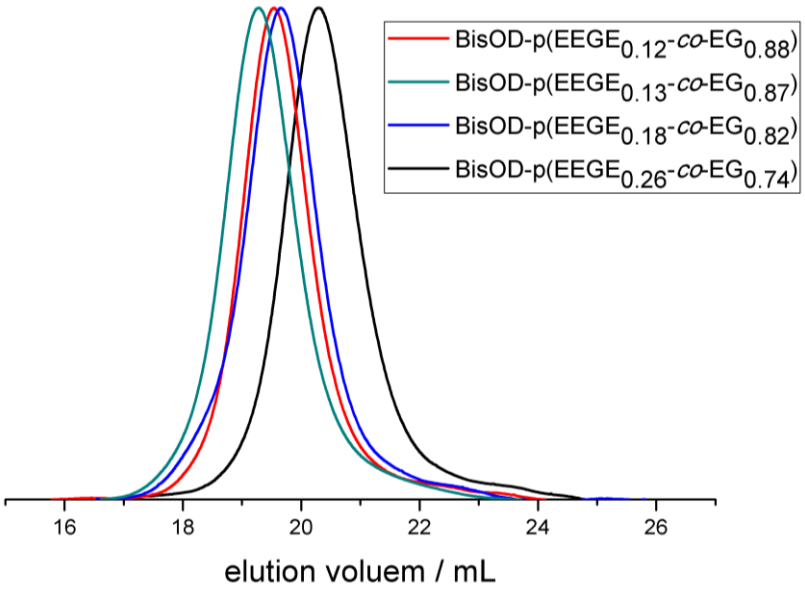

Figure S35. SEC traces (DMF, PEG standard, RI signal) of the synthesized copolymers BisOD-p(EEGE-*co*-EG).

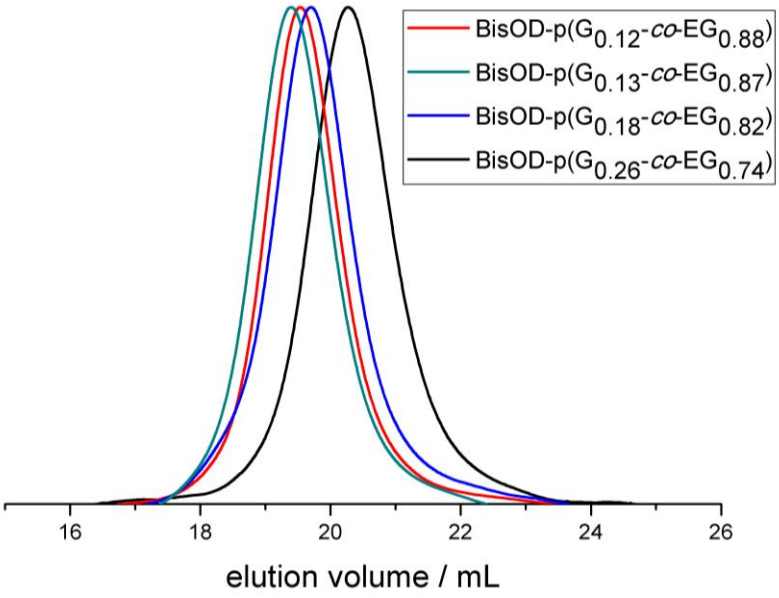

Figure S36. SEC traces (DMF, PEG standard, RI signal) of the synthesized BisOD-p(G-*co*-EG).

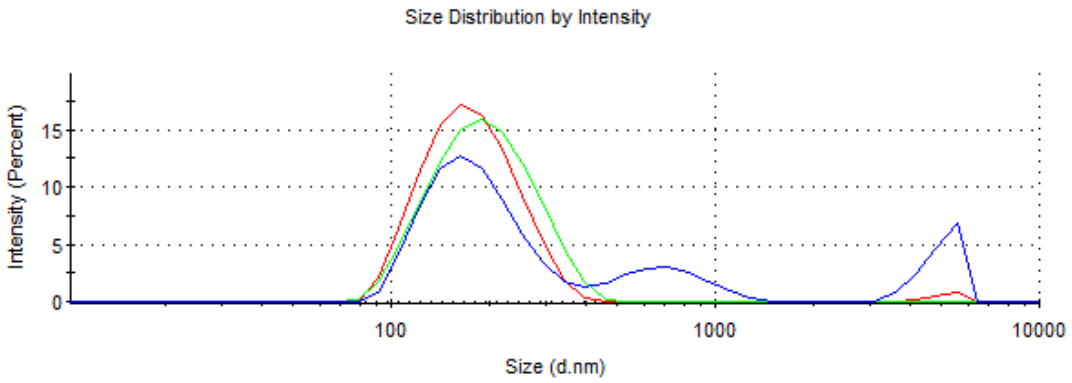

Figure S37. Size distribution of the liposomal formulation of BisOD-p($G^{MA}_{0.12}$-*co*-$EG_{0.88}$) (#8) before cross-linking (red curve) and after cross-linking with dilutions of 1:10 (blue curve) and 1:1000 (green curve).

4. References

(1) Fitton, A. O.; Hill, J.; Jane, D. E.; Millar, R. Synthesis of Simple Oxetanes Carrying Reactive 2-Substituents. *Synthesis* **1987**, 1140–1142.

(2) Stauch, O.; Uhlmann, T.; Fröhlich, M.; Thomann, R.; El-Badry, M.; Kim, Y.-K.; Schubert, R. Mimicking a Cytoskeleton by Coupling Poly(N -isopropylacrylamide) to the Inner Leaflet of Liposomal Membranes: Effects of Photopolymerization on Vesicle Shape and Polymer Architecture. *Biomacromolecules* **2002**, *3*, 324–332.

3. Functional Polyether-based Surfactants

3.1 Stealth Properties? How Adhesive Phosphonate Groups Control the Protein Corona of Polyglycerol-stabilized Nanocarriers

Ann-Kathrin Danner,[a,c] Susanne Schöttler,[b] Evandro Alexandrino,[b] Sophie Hammer,[a,c] Katharina Landfester,[b] Volker Mailänder,[b] Svenja Morsbach,[b,*] Holger Frey,[a,*] Frederik R. Wurm[b,*]

[a]Institute of Organic Chemistry, Johannes Gutenberg-University Mainz, Duesbergweg 10-14, 55128 Mainz, Germany.

[b]Max Planck Institute for Polymer Research, Ackermannweg 10, 55128 Mainz, Germany.

[c]Graduate School Materials Science in Mainz, Staudinger Weg 9, 55128 Mainz, Germany.

E-Mail: wurm@mpip-mainz.mpg.de

To be submitted.

Abstract

Nanocarriers in contact with biological fluids interact with plasma proteins, forming a protein corona. As a result a specific protein pattern depending on the nature of the particle is formed. Although the corona composition of PEGylated particles is currently being investigated, little is known regarding the protein pattern of PGylated particles and especially the influence of additional negative surface charges. Herein, PGylated nanocarriers with pendant phosphonate groups were prepared. The amount of phosphonate groups was adjusted precisely. The stealth behavior as well as the particles´ interaction with human plasma and their impact on protein corona formation was studied. It was shown that the protein corona resembled the pattern necessary for the stealth effect and that the introduced negative charges of the phosphonates can cancel out this effect in a controlled manner.

Table of Contents Graphics

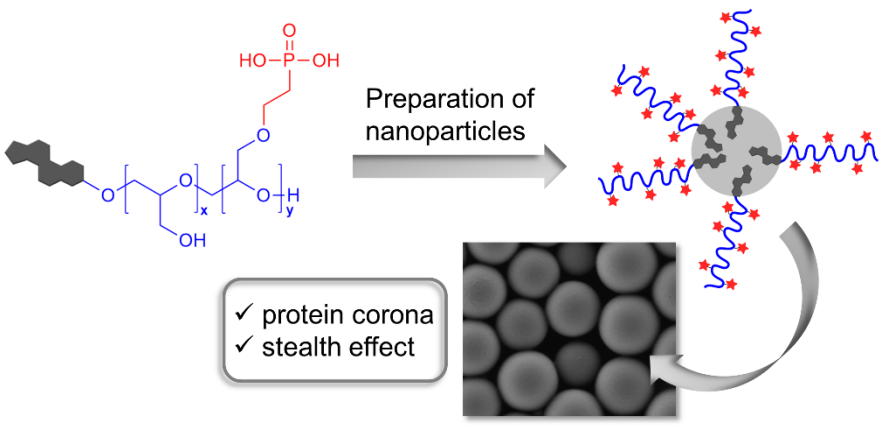

Introduction

Polymeric nanocarriers are envisioned to revolutionize modern pharmaceutical technology as multifunctional drug delivery devices.[1] In order to reach their place of action, nanocarriers have to be designed to avoid rapid clearance from the body in consequence of a fast recognition by the immune system. A "stealth" barrier on the surface of the nanocarriers is necessary to avoid unspecific cell uptake before the carrier has reached its destination. The reason for the stealth effect was recently redefined, and it was proven that a specific protein corona triggers the cellular uptake of nanocarriers.[2] This protein corona contains several stealth proteins that are responsible for the reduced uptake in macrophages. The suppression of nonspecific cellular uptake is achieved by the reduction of unspecific protein adsorption and at the same time selective enrichment of plasma proteins to the surface of the nanocarriers.[3] In most cases the surfaces are modified with poly(ethylene glycol) (PEG), which suppresses non-specific protein adsorption and enhances blood circulation times of the nanocarriers. This PEGylation, usually referred to as "stealth effect" has been known for decades,[4–10] and several PEGylated products are on the market.[11,12] However, it took until very recently to unravel the composition of the protein corona of PEGylated nanocarriers. The protein corona of nanocarriers has been studied both for covalent and non-covalent attachment of different stealth polymers, demonstrating that changes in the polymer structure distinctively alter the composition of the protein corona and the stability of such nanocarriers in human blood plasma.[2,13–18]

As PEG exhibits very limited functionality, polyglycerols (PGs) are promising due to their additional hydroxyl groups and thus various options for further functionalization. PGs are biocompatible and water-soluble; therefore they are currently discussed as alternatives for several biomedical applications.[19–22]

In this work, we study the protein pattern of PGylated particles. In addition, we investigate how the protein corona of nanocarriers can be influenced in a controlled manner by the chemical modification of the stealth polymer with a series of adhesive groups. We aim at a perfect balance between functionality and stealth effect that is, how many phosphonate groups can be attached to the polymer without extinguishing the stealth effect.

Results and Discussion

In our study a systematic variation of the phosphonate functionalization of the PG OH-groups with negative charges was carried out. Their effect on the stealth behavior of nanocarriers and how the pattern of their protein corona can be controlled was studied.

The attachment of PG to nanocarriers was achieved by noncovalent adsorption of amphiphilic PG-surfactants. They were prepared by anionic ring opening polymerization of ethoxyethyl glycidyl ether (EEGE), initiated with the cesium alkoxide of cholesterol and subsequent acidic removal of the acetal protecting groups to release the multiple hydroxyl moieties.[23] The amphiphilic PG (Ch-*lin*PG_{21}) was obtained with M_n^{NMR} = 1900 g mol^{-1} and narrow molecular weight distribution with low dispersity ($Đ$ = 1.25). These polyether-based surfactants were then modified with diethyl vinyl phosphonate in a tow-step procedure to prepare surfactants with a different, albeit precisely controlled number of negative charges at the polymer backbone to obtain Ch-*lin*P(G_x-*co*-G^{PE}_y) as shown in **Figure 1A**. The method applied for functionalization was recently developed by Koehler *et al*.[24] With this strategy the degree of modification was adjusted accurately. *i.e.* between 0 and 62 mol% of the hydroxyl groups were converted to phosphonates. All polymers were characterized by size exclusion chromatography (SEC) in DMF with PEG standards, ^{1}H NMR and ^{31}P NMR spectroscopy. The amphiphilic polymers exhibited narrow molecular weight distributions ($Đ \leq 1.36$) and molecular weights between 1900 and 4100 g mol^{-1}, as summarized in **Table 1**. The ^{1}H NMR spectra in **Figure 1B** show the typical resonances of Ch-*lin*PG (a and b) and for the functionalized surfactants also a characteristic signal for the methylene group adjacent to the phosphorus (red circle in b), confirming successful phosphonylation. **Figure 1C** shows the monomodal distribution of functionalized surfactants Ch-*lin*P(G_x-*co*-G^{DEPE}_y), as obtained from SEC. With increasing number of attached phosphonate groups there is a slight shift to higher elution volume translating to lower molecular weight, indicating hydrogen bonding and a change in the hydrodynamic radius with increasing number of functional groups.

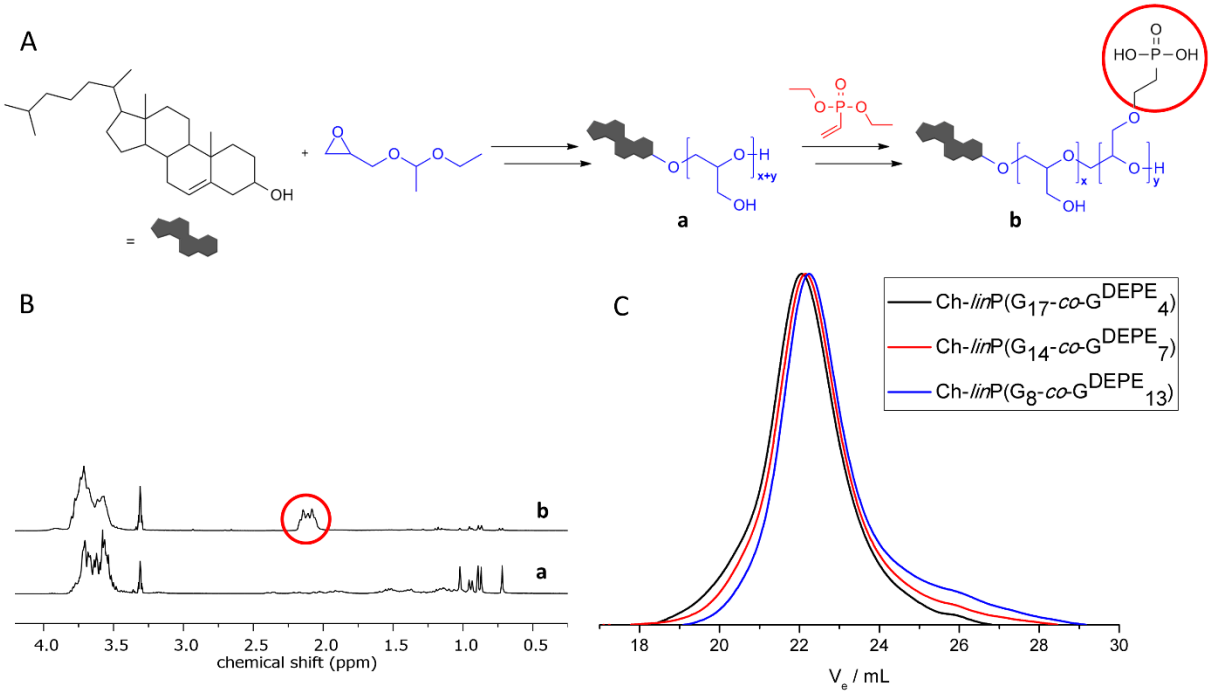

Figure 1. A: Synthesis strategy for polyether-based lipids with pendant phosphonate groups. B: ^{1}H NMR spectra of PG (Ch-*lin*PG$_{21}$) (a, bottom) and Ch-*lin*P(G$_x$-*co*-G$^{PE}_y$) (b, top). C: Typical SEC traces of a selection of Ch-*lin*P(G$_x$-*co*-G$^{DEPE}_y$).

Table 1. Properties of the synthesized amphiphilic polyethers including molecular weight, degree of functionalization and polydispersities.

Composition	***M*$_n$**[a] g mol^{-1}	**DEPE**[a] mol%	***Đ***[b]
Ch-*lin*PG$_{21}$	1940	-	1.25
Ch-*lin*P(G$_{17}$-*co*-G$^{DEPE}_4$)	2600	19	1.30
Ch-*lin*P(G$_{15}$-*co*-G$^{DEPE}_6$)	2920	29	1.35
Ch-*lin*P(G$_{14}$-*co*-G$^{DEPE}_7$)	3100	33	1.31
Ch-*lin*P(G$_{12}$-*co*-G$^{DEPE}_9$)	3410	43	1.25
Ch-*lin*P(G$_8$-*co*-G$^{DEPE}_{13}$)	4090	62	1.36

[a]calculated *via* ^{1}H NMR spectroscopy.
[b]determined using SEC measurements.

These novel amphiphilic structures were used as surfactants for the preparation of model polystyrene nanocarriers by the miniemulsion/solvent evaporation technique.[25] Polystyrene was dissolved in chloroform and dispersed in water containing the PG-amphiphiles as a

surfactant. After ultrasonication, solvent evaporation and dialysis against deionized water for 7 h as purification step, the model nanocarriers (with diameters between 170 and 280 nm, **Table 2**) with the respective polyglycerol layer were obtained (**Figure 2**).

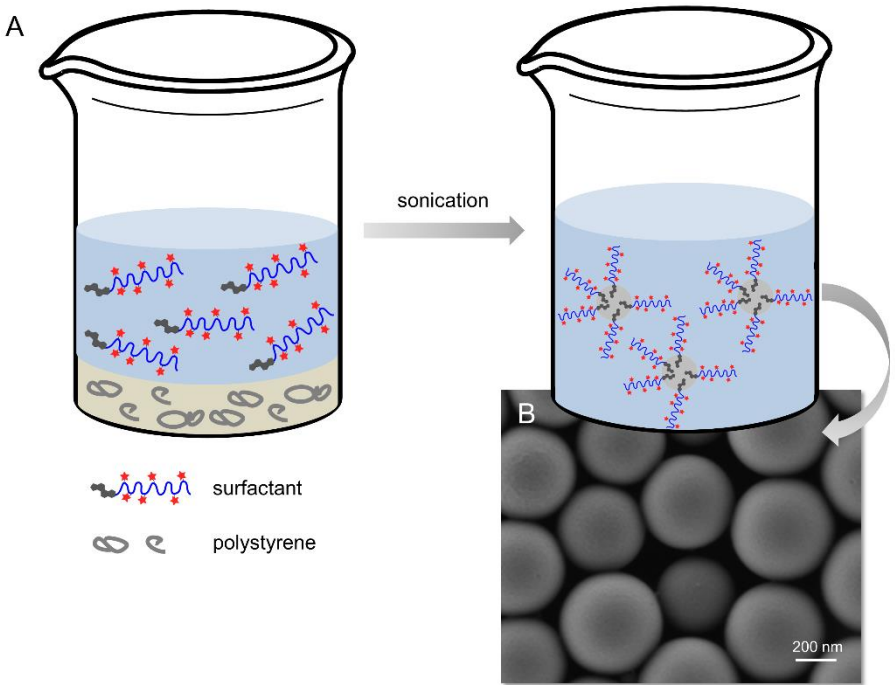

Figure 2. A: Schematic representation of the miniemulsion/solvent evaporation strategy for the preparation of nanoparticles. B: TEM image of the obtained polystyrene nanoparticles.

Characterization of the nanocarriers was performed by means of dynamic light scattering (**Table 2**). Zeta potential measurements and the obtained values are summarized in **Table 2**.The particles had, as already mentioned, diameters between 170 and 280 nm and showed narrow size distributions ($\mu_2 \leq 0.05$). Adsorption of the amphiphilic PG-surfactants with different numbers of functional groups was demonstrated by the reduction in the zeta potential that is with increasing amount of phosphonate groups in the surfactants, the zeta potential became increasingly negative in water (**Table 2** and **Figure 3A**).

Stability in human plasma is the first benchmark for nanocarriers. Therefore, the aggregation behavior of the nanoparticles in concentrated blood plasma was tested *via* dynamic light scattering (DLS) as described in literature.[26] It was found that nanocarriers loaded with polymers without phosphonates (Ch-*lin*PG_{21}) or with 29 mol% phosphonates (Ch-*lin*P(G_{15}-*co*-G^{PE}_6)) do not show any aggregation in plasma (see **Figures S18** and **S19**), while polymers with a higher phosphonate amount of 43 mol% (Ch-*lin*P(G_{12}-*co*-G^{PE}_9))

formed macroscopic aggregates (see **Figure S20**). This is in good agreement with previously obtained results by Rausch *et al.* who found that the aggregation tendency in blood plasma depends on the charge of the nanomaterial. The higher the charge (both positive and negative), the more prone is the system to aggregation.[26] In our case Ch-*lin*P(G_{12}-*co*-G^{PE}_{9}) exhibits the highest number of charged groups, which leads to the formation of macroscopic aggregates. This could be due to an insufficient compensation of the negative charges by the PG fraction.

Table 2. Overview of the properties of the obtained nanoparticles.

Surfactant	**DEPE**[a] mol%	**Rh** nm	**μ_2**[a]	**Zeta potential**
Ch-*lin*PG_{21}	0	280 ± 28	0.03	–26 ± 1
Ch-*lin*P(G_{15}-co-G^{PE}_{6})	29	236 ± 24	0.03	–64 ± 1
Ch-*lin*P(G_{12}-co-G^{PE}_{9})	43	172 ± 17	0.05	–66 ± 1

[a]μ_2 was determined *via* a cumulant fit of the correlation functions and describes the polydispersity of the sample.

Additionally, the zeta potential of the nanocarriers was determined after plasma incubation. The zeta potential values obtained (–22 to –44) were less negative than before incubation for all samples, which is indicative for the adsorption of plasma proteins, since they cover the initial charges of the surfactants. However, this effect was most pronounced for the nanoparticles with the highest surface charge and much less visible without phosphonate groups (see **Figure 3A**). The change in zeta potential can be seen as an indicator for the extent of protein adsorption. Similarly, the protein amount on the surface of the nanocarriers was determined *via* a Pierce 660 nm quantification assay. First of all, the protein amount found on the nanocarriers without any phosphoesters present (Ch-*lin*PG_{21}) was very low as expected for similar compounds like PEG.[27] This represents a first hint that *lin*PG indeed exhibits a stealth effect. In accordance with the zeta potential measurements, a trend depending on the amount of surface charges was observed. Although protein quantification showed a low overall protein adsorption on the investigated nanoparticles, for the particles with 43 mol% phosphonate groups (Ch-*lin*P(G_{12}-*co*-G^{PE}_{9})) the protein quantification revealed a slightly higher quantity of proteins (see **Figure S14**).

It should be emphasized that comparing these results with a hydrophobic control particle the protein adsorption is still very low.[17]

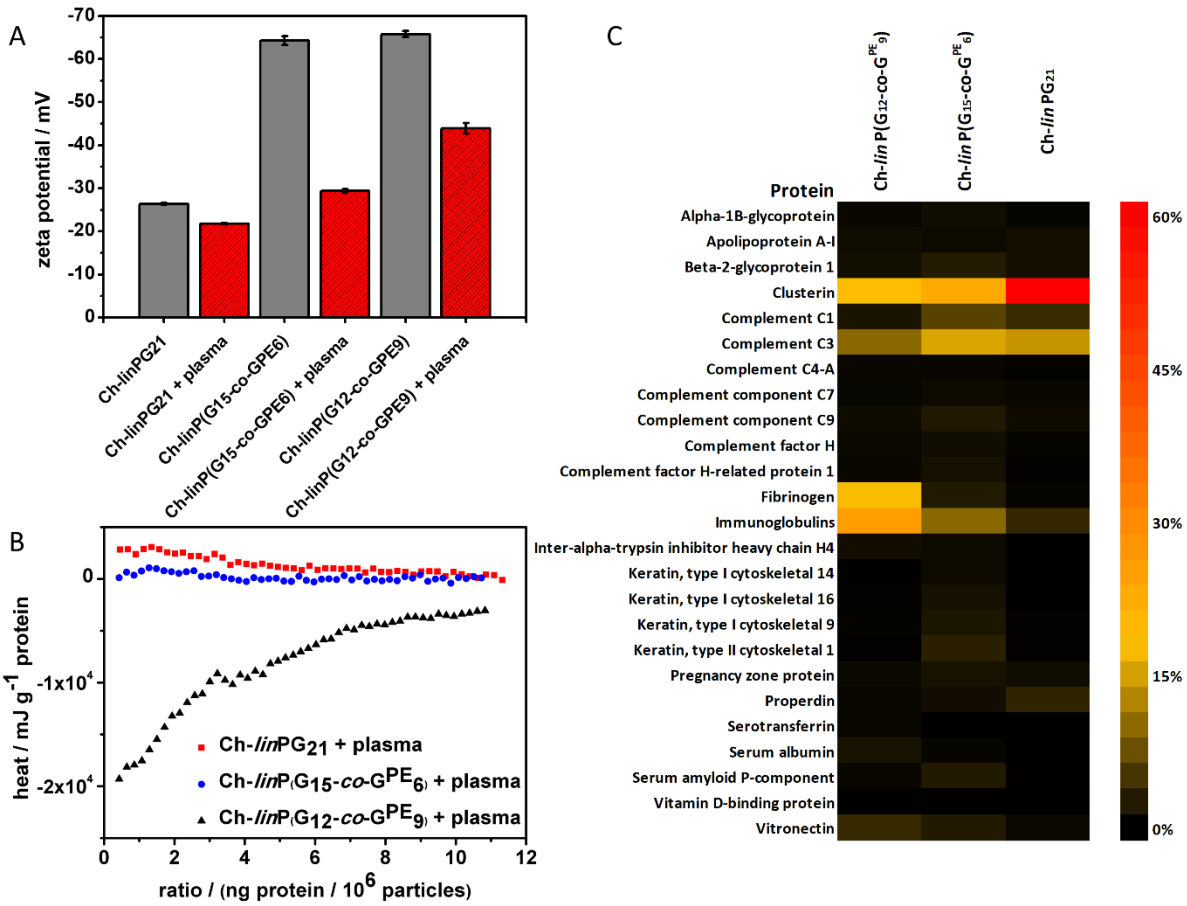

Figure 3. Zeta potential of the nanocarriers with and without protein corona (A), ITC binding isotherms for the adsorption of plasma proteins on nanocarriers with and without phosphonates: nanocarriers without phosphonates (red ■), nanocarriers with 29 mol% phosphonates (blue ●), nanocarriers with 43 mol% phosphonates (black ▲) (B) and heatmap of the most abundant proteins in the corona of the nanoparticles without and with phosphonate groups (C).

In order to determine the influence of the negative surface charge towards the thermodynamic properties of the protein adsorption we investigated the protein interactions from human plasma with the prepared nanocarriers *via* isothermal titration calorimetry (ITC) measurements. Diluted human plasma was titrated into the suspension of nanoparticles and the released heat was measured after each titration step. The heat of dilution was determined as a reference to correct the values of the adsorption heat. For the samples with 29 mol% (Ch-*lin*P(G_{15}-*co*-G^{PE}_6)) and without phosphonates (Ch-*lin*PG_{21}) a signal fluctuation around 0 was observed, which means that any kind of interaction

occurring is either enthalpically neutral or too small to be detected. Thus, the ITC measurements show that the attachment of a small amount of phosphonate groups does not influence the protein interaction in terms of thermodynamic properties compared to particles without additional phosphonate moieties. In contrast, there is a significant difference observable for nanocarriers with 43 mol% (Ch-*lin*P(G_{12}-*co*-G^{PE}_{9})) phosphonates per polymer chain. For this sample, a distinct exothermic process was observed, meaning that in that case the interaction mechanism is different and stronger interaction occurs. The binding affinity of plasma proteins is represented by the initial slope of the binding isotherm, which is clearly increased with 43 mol% (Ch-*lin*P(G_{12}-*co*-G^{PE}_{9})) phosphonates per polymer chain (see **Figure 3B**). Consequently, the ITC measurement gives insight into the protein corona and the results show that the protein affinity depends on the amount of phosphonate moieties on the particle surface.

Further, Lundqvist *et al.* found that a negative or positive surface charge on polystyrene nanoparticles entirely changes the protein pattern.[18] For our system this could mean that a stealth effect obtained by the introduction of PG could potentially be disturbed by the additional presence of charges. Hence, the protein pattern was investigated with liquid chromatography-mass spectrometry (LC-MS) and SDS-PAGE. LC-MS provides the possibility to investigate the protein corona by gaining insight into the protein pattern. Interestingly, the nanoparticles decorated with Ch-*lin*PG exhibited a protein pattern similar to the one reported for PEGylated nanoparticles. The dominant protein with a fraction of almost 60% was clusterin, which was highly enriched compared to all other plasma proteins. Another prominent protein was complement factor C3 with a fraction of around 14%. All other protein contributions were below 5%. Adding phosphonates to the system, this protein pattern shifts quite significant. With an increase in phosphonate content the fraction of clusterin decreases to around 20% where saturation seems to be reached. Additionally, the fractions of fibrinogen and especially immunoglobulins increase at the same time to roughly 18% and 25%, respectively. This result is also confirmed by the outcome of the SDS-PAGE (see **Figure S21**). It seems to be the case that the introduction of phosphonates first leads to a decrease of the enrichment of certain proteins and the overall protein pattern becomes much more unspecific. Upon further increase of the amount of charged groups again other proteins are specifically enriched. Those proteins like fibrinogen and immunoglobulins are rather undesired components of the protein corona since they promote uptake by phagocytic cells to clear the nanocarriers from the blood

stream. Those proteins are likely also responsible for the aggregation processes taking place, so that a high number of phosphonate groups is not favorable.

Conclusion

Cholesterol-based polyethers with varied amounts of pendant phosphonate groups were successfully synthesized and used as surfactants in the combined miniemulsion/solvent evaporation technique to prepare polystyrene nanoparticles. These model particles were characterized, revealing diameters between 170 and 280 nm and narrow size distributions. Furthermore, the behavior in human plasma was investigated and the resulting protein pattern was analyzed. In summary, the obtained results clearly show that the non-covalent attachment of polyglycerol results in a very similar stealth behavior as observed for PEGylated nanocarriers. Hence, polyglycerol is a promising multifunctional alternative for PEG: In addition, a certain amount of negative charges (29 mol% phosphonates per polymer chain) is tolerated by polyglycerol-stabilized nanocarriers before aggregation and alteration of the protein corona is observed, unrevealing the limit of applicable phosphonate moieties as functional groups. These findings will help to further understand and control the stealth behavior of nanocarriers and what chemists can change in their corona, *e.g.* to achieve a specific targeting of drugs.

Acknowledgments

A. Danner is a recipient of a DFG-funded position through the Excellence Initiative by the Graduate School Materials Science in Mainz (GSC 266). The authors thank Katja Klein and Monika Schmelzer for technical support.

References

(1) Banik, B. L.; Fattahi, P.; Brown, J. L. Polymeric nanoparticles: The future of nanomedicine. *Wiley interdisciplinary reviews. Nanomedicine and nanobiotechnology* **2016**, *8*, 271–299.

(2) Schottler, S.; Becker, G.; Morsbach, S.; Steinbach, T.; Mohr, K.; Landfester, K.; Mailander, V.; Wurm, F. R. Protein adsorption is required for stealth effect of poly(ethylene glycol)- and poly(phosphoester)-coated nanocarriers. *Nature nanotechnology* **2016**, *11*, 372–377.

(3) Schottler, S.; Landfester, K.; Mailander, V. Controlling the Stealth Effect of Nanocarriers through Understanding the Protein Corona. *Angewandte Chemie (International ed. in English)* **2016**, *55*, 8806–8815.

(4) Knop, K.; Hoogenboom, R.; Fischer, D.; Schubert, U. S. Poly(ethylene glycol) in drug delivery: pros and cons as well as potential alternatives. *Angew. Chem. Int. Edit.* **2010**, *49*, 6288–6308.

(5) Estanqueiro, M.; Amaral, M. H.; Conceição, J.; Sousa Lobo, José Manuel. Nanotechnological carriers for cancer chemotherapy: The state of the art. *Colloid. Surface. B* **2015,** DOI: 10.1016/j.colsurfb.2014.12.041.

(6) Lasic, D.; Papahadjopoulos, D. Liposomes revisited. *Science* **1995**, *267*, 1275–1276.

(7) Gabizon, A.; Papahadjopoulos, D. The role of surface charge and hydrophilic groups on liposome clearance in vivo. *BBA-Biomembranes* **1992**, *1103*, 94–100.

(8) Barenholz, Y. Doxil®--the first FDA-approved nano-drug: lessons learned. *J. Control. Release* **2012**, *160*, 117–134.

(9) Veronese, F. M.; Pasut, G. PEGylation, successful approach to drug delivery. *Drug Discov. Today* **2005**, *10*, 1451–1458.

(10) Alconcel, S. N. S.; Baas, A. S.; Maynard, H. D. FDA-approved poly(ethylene glycol)–protein conjugate drugs. *Polym. Chem.* **2011**, *2*, 1442.

(11) Allen, T. M.; Cullis, P. R. Drug delivery systems: entering the mainstream. *Science (New York, N.Y.)* **2004**, *303*, 1818–1822.

(12) Mero, A.; Schiavon, O.; Pasut, G.; Veronese, F. M.; Emilitri, E.; Ferruti, P. A Biodegradable Polymeric Carrier Based on PEG for Drug Delivery. *Journal of Bioactive and Compatible Polymers* **2009**, *24*, 220–234.

(13) Tenzer, S.; Docter, D.; Rosfa, S.; Wlodarski, A.; Kuharev, J.; Rekik, A.; Knauer, S. K.; Bantz, C.; Nawroth, T.; Bier, C. *et al.* Nanoparticle size is a critical physicochemical determinant of the human blood plasma corona: a comprehensive quantitative proteomic analysis. *ACS nano* **2011**, *5*, 7155–7167.

(14) Muller, J.; Bauer, K. N.; Prozeller, D.; Simon, J.; Mailander, V.; Wurm, F. R.; Morsbach, S.; Landfester, K. Coating nanoparticles with tunable surfactants facilitates control over the protein corona. *Biomaterials* **2017**, *115*, 1–8.

(15) Deng, Z. J.; Mortimer, G.; Schiller, T.; Musumeci, A.; Martin, D.; Minchin, R. F. Differential plasma protein binding to metal oxide nanoparticles. *Nanotechnology* **2009**, *20*, 455101.

(16) Bewersdorff, T.; Vonnemann, J.; Kanik, A.; Haag, R.; Haase, A. The influence of surface charge on serum protein interaction and cellular uptake: Studies with dendritic polyglycerols and dendritic polyglycerol-coated gold nanoparticles. *Int. J. Nanomed.* **2017**, *12*, 2001–2019.

(17) Kang, B.; Okwieka, P.; Schottler, S.; Morsbach, S.; Langhanki, J.; Mohr, K.; Opatz, T.; Mailander, V.; Landfester, K.; Wurm, F. R. Carbohydrate-Based Nanocarriers Exhibiting Specific Cell Targeting with Minimum Influence from the Protein Corona. *Angewandte Chemie (International ed. in English)* **2015**, *54*, 7436–7440.

(18) Lundqvist, M.; Stigler, J.; Elia, G.; Lynch, I.; Cedervall, T.; Dawson, K. A. Nanoparticle size and surface properties determine the protein corona with possible implications for biological impacts. *Proceedings of the National Academy of Sciences of the United States of America* **2008**, *105*, 14265–14270.

(19) Immordino, M. L.; Dosio, F.; Cattel, L. Stealth liposomes: review of the basic science, rationale, and clinical applications, existing and potential. *Int. J. Nanomed.* **2006**, *1*, 297–315.

(20) Mohr, K.; Müller, S. S.; Müller, L. K.; Rusitzka, K.; Gietzen, S.; Frey, H.; Schmidt, M. Evaluation of multifunctional liposomes in human blood serum by light scattering. *Langmuir* **2014**, *30*, 14954–14962.

(21) Reibel, A. T.; Müller, S. S.; Pektor, S.; Bausbacher, N.; Miederer, M.; Frey, H.; Rösch, F. Fate of linear and branched polyether-lipids in vivo in comparison to their liposomal formulations by (18)f-radiolabeling and positron emission tomography. *Biomacromolecules* **2015**, *16*, 842–851.

(22) Wurm, F.; Dingels, C.; Frey, H.; Klok, H.-A. Squaric acid mediated synthesis and biological activity of a library of linear and hyperbranched poly(glycerol)-protein conjugates. *Biomacromolecules* **2012**, *13*, 1161–1171.

(23) Köhler, J.; Keul, H.; Möller, M. Post-polymerization functionalization of linear polyglycidol with diethyl vinylphosphonate. *Chem. Commun.* **2011**, *47*, 8148–8150.

(24) Musyanovych, A.; Schmitz-Wienke, J.; Mailänder, V.; Walther, P.; Landfester, K. Preparation of biodegradable polymer nanoparticles by miniemulsion technique and their cell interactions. *Macromol. Biosci.* **2008**, *8*, 127–139.

(25) Rausch, K.; Reuter, A.; Fischer, K.; Schmidt, M. Evaluation of nanoparticle aggregation in human blood serum. *Biomacromolecules* **2010**, *11*, 2836–2839.

(26) Gref, R.; Lück, M.; Quellec, P.; Marchand, M.; Dellacherie, E.; Harnisch, S.; Blunk, T.; Müller, R.H. 'Stealth' corona-core nanoparticles surface modified by polyethylene glycol (PEG): Influences of the corona (PEG chain length and surface density) and of the core composition on phagocytic uptake and plasma protein adsorption. *Colloids and Surfaces B: Biointerfaces* **2000**, *18*, 301–313.

Supporting Information

Stealth Properties? How Adhesive Phosphonate Groups Control the Protein Corona of Polyglycerol-stabilized Nanocarriers

Ann-Kathrin Danner,[a,c] Susanne Schöttler,[b] Evandro Alexandrino,[b] Sophie Hammer,[a,c] Katharina Landfester,[b] Volker Mailänder,[b] Svenja Morsbach,[b,*] Holger Frey,[a,*] Frederik R. Wurm[b,*]

[a]Institute of Organic Chemistry, Johannes Gutenberg-University Mainz, Duesbergweg 10-14, 55128 Mainz, Germany.

[b]Max Planck Institute for Polymer Research, Ackermannweg 10, 55128 Mainz, Germany.

[c]Graduate School Materials Science in Mainz, Staudinger Weg 9, 55128 Mainz, Germany.

E-Mail: wurm@mpip-mainz.mpg.de

1. Reagents

All reagents and solvents were purchased from *Sigma-Aldrich, Acros Organics, Fisher Scientific* or *Deutero GmbH* and used as received, unless otherwise mentioned. Ethoxyethyl glycidyl ether (EEGE) was synthesized according to literature and dried over CaH_2 and cryo-transferred prior to use.[1]

2. Methods

2.1 NMR spectroscopy

^{1}H, ^{13}C and ^{31}P NMR spectroscopy as well as COSY (correlation spectroscopy), HSQC (heteronuclear single quantum coherence) and HMBC (heteronuclear multiple bond correlation) spectra were recorded using a Bruker Avance III HD 300 operated at 300 MHz. $CDCl_3$ or MeOD was employed as solvent and the spectra were referenced internally to proton signals of the deuterated solvent. The analysis of the NMR spectra was conducted applying the Software MestReNova (Version 9.0).

2.2 Size exclusion chromatography (SEC)

SEC measurements were performed in dimethylformamide with 0.25 g L^{-1} lithium bromide employing an Agilent 1100 Series equipped with PSS HEMA 300/100/40 column, RI and UV detector (275 nm). Calibration was carried out using poly(ethylene glycol) standards from Polymer Standards Service (PSS). SEC traces were analyzed with PSS WinGPC Unity.

2.3 Dynamic scanning calorimetry (DSC)

DSC measurements were carried out on a Perkin Elmer 8200 differential scanning calorimeter. 3 to 4 mg of a sample were measured in a temperature range of –90 to 20 °C (first cycle, heating rate 20 °C min^{-1}) respectively from –90 to 0 °C (second cycle, heating rate 10 °C min^{-1}). For analysis, the values for the second cycle were used. Calibration was performed using the melting points of indium (T_m = 156.6 °C) and Milli-Q water (T_m = 0 °C).

2.4 Scanning electron microscopy (SEM)

For scanning electron microscopy (SEM) a Zeiss LEO Gemini 1530 microscope from Carl Zeiss Microscopy GmbH was used.

2.5 Dynamic light scattering (DLS)

The multi-angle dynamic light scattering measurements were performed with an ALV/CGS3 compact goniometer system with a He / Ne laser 632.8 nm and a ALV/LSE-5004 correlator and evaluated with the ALV5000 software.

Pure nanoparticle samples were measured at a concentration of 0.1 g L^{-1} and filtered through 5 µm Millex SV filters before. For each plasma measurement 1 mL of human plasma was filtered through Millex GS filters with a pore size of 0.22 µm (Merck Millipore, USA) and 1 µL of the respective 1 wt% NP-dispersion was added. The corresponding reference measurements were conducted by replacing one of the components with an equal volume of MilliQ water. The samples were measured in dust-free quartz light scattering cuvettes (Hellma, Germany), which were cleaned with acetone in a Thurmond-apparatus before use.

2.6 DLS plasma measurements data evaluation

For analysis of the DLS data the method by Rausch *et al.* has been applied.[2] The sum of the autocorrelation functions (ACF) of the individual components (plasma and NPs) was used as fixed parameters and only the intensity fractions of the components as well as an additional diffusion process considering formed aggregates were used as variables.

The ACF of plasma could be well approximated by a sum of three exponential terms as given in equation S5:

$$g_{1,P}(t) = a_{1,P}\ \exp\left(-\frac{t}{\tau_{1,P}}\right) + \ a_{2,P}\ \exp\left(-\frac{t}{\tau_{2,P}}\right) + \ \ a_{3,P}\ \exp\left(-\frac{t}{\tau_{3,P}}\right) \qquad \text{(S1)}$$

Amplitudes are denoted by a_i and decay times by $\tau_i = \frac{1}{q^2 D_i}$ with the absolute scattering vector $q = \frac{4\pi n}{\lambda_0} \sin\left(\frac{\theta}{2}\right)$ and the Brownian diffusion coefficient of component i, D_i.

The ACF of NPs alone can be fitted by a biexponential function (equation S6):

$$g_{1,NP}(t) = a_{1,NP}\ exp\left(-\frac{t}{\tau_{1,NP}}\right) + a_{2,NP}\ exp\left(-\frac{t}{\tau_{2,NP}}\right) \qquad \text{(S2)}$$

The correlation function of the NPs in plasma could now be analyzed by consideration of both the ACF of plasma and NPs alone. Without any aggregation, the resulting ACF of the mixture $g_{1,m}(t)$ could be approximated by the sum of the individual ACFs, the so-called force fit, with the intensity contributions for plasma f_P and nanoparticles f_{NP} as the fit parameters (equation S7).

$$g_{1,m}(t) = f_P g_{1,P}(t) + f_{NP} g_{1,NP}(t) \quad \text{(S3)}$$

If aggregation occurred, the ACF could not be described by the simple sum of the two components. An additional ACF $g_{1,agg}(t)$ with a longer relaxation time for the larger aggregates needed to be considered:

$$g_{1,agg}(t) = a_{1,agg}\, exp\left(-\frac{t}{\tau_{1,agg}}\right) \quad \text{(S4)}$$

The final form for the correlation function with the intensity contribution of the aggregates f_{agg} is given in equation S9:

$$g_{1,m}(t) = f_P g_{1,P}(t) + f_{NP} g_{1,NP}(t) + f_{agg} g_{1,agg}(t) \quad \text{(S5)}$$

2.7 Zeta potential

The zeta-potential of the solutions wewas obtained using a Zetasizer NanoZ using as dispersive phase an aqueous $1x10^{-3}$ M KCl solution.

3. Synthesis

3.1 Synthesis of Ch-*lin*PG$_{21}$

Cholesterol (2 g, 5.2 mmol, 1 eq.) and CsOH monohydrate (0.78 g, 4.7 mmol, 0.9 eq.) were placed in a Schlenk flask and dissolved in benzene (10 mL). The mixture was stirred at 60 °C for 30 min to form the cesium alkoxide. Subsequently, the salt was dried under vacuum at 90 °C for 24 h and suspended in 60 mL anhydrous dioxane. The monomer EEGE (17.4 mL, 114 mmol, 22 eq.) was added and the mixture was heated to 80 °C for 48 h. The polymerization was stopped *via* the addition of an excess of methanol and the solvents were removed under reduced pressure. To cleave the acetal protecting groups of Ch-*lin*PEEGE the polymer was dissolved in methanol and 2N HCl was added. The solution was stirred for

48 h at 40 °C. Afterwards the solvent was removed and the crude product was precipitated twice in cold diethyl ether. The amphiphilic polymer Ch-*lin*PG_{21} was dried under vacuum. Yield: ~90%.

Before deprotection:

^{1}H-NMR, COSY (300 MHz, methanol-d_4): δ [ppm] = 5.29 (1H, C=CH cholesterol), 4.73–4.63 (m, 1H, CHOR acetal group, PEEGE), 3.86–3.35 (polyether backbone, CHOR cholesterol), 2.33–0.75 (40 H, CH_3, CH_2, CH cholesterol), 0.63 (s, 3H, CH_3 cholesterol).

After deprotection:

^{1}H-NMR, COSY (300 MHz, methanol-d_4): δ [ppm] = 5.38 (1H, C=CH cholesterol), 3.94–3.45 (polyether backbone, CHOR cholesterol), 2.41–0.81 (40 H, CH_3, CH_2, CH cholesterol), 0.72 (s, 3H, CH_3 cholesterol).

3.2 Synthesis of linear cholesterol-poly(glycerol-*co*-glycerol-diethylphosphonatoethyl) lipid

The synthesis was performed in analogy to literature.[3] The procedure is described for Ch-*lin*P(G_8-*co*-G^{DEPE}_{13}) as an example. The synthesis and characterization was carried out similarly for all polymers.

Ch-*lin*PG_{21} (1 g, 0.5 mmol, 1 eq.) was placed in a Schlenk tube and dissolved in dimethylfomamide (10 mL) under argon atmosphere. Over a time period of two hours, potassium *tert*-butoxide (1.0 M solution in THF, 0.6 mL, 0.6 mmol, 1.2 eq.) was added until the formation of small coagulates was observed. The formed *tert*-butanol was removed applying reduced pressure. Subsequently diethyl vinyl phosphonate (DEVP) (1.27 mL, 8.2 mmol, 16 eq.) was added slowly. The solution was stirred for 6 d at room temperature under an argon atmosphere. Afterwards, the precipitate was removed via filtration and the solvent was eliminated by applying reduced pressure. The polymer was dissolved in methanol and precipitated in an excess of cold diethyl ether. The polymer was dried in vacuum leading to Ch-*lin*P(G_8-*co*-G^{DEPE}_{13}) as highly viscous oil. Yield: 70-80%.

^{1}H-NMR, COSY (300 MHz, methanol-d_4): δ [ppm] =5.38 (1H, C=CH cholesterol), 4.147–4.09 (4H, POC$H_2$$CH_3$), 3.92–3.52 (polyether backbone; CHOR cholesterol), 2.23–2.10 (2H, $CH_2OCH_2CH_2P$), 1.38–1.30 (6H, $POCH_2CH_3$), 2.42–0.87 (40 H, CH_3, CH_2, CH cholesterol), 0.73 (3H, CH_3 cholesterol).

^{31}P-NMR (121.5 MHz, methanol-d_4): δ [ppm] = 30.0.

^{13}C-NMR, HSQC, HMBC (100.7 MHz, methanol-d_4): δ [ppm] = 81.6 (polyether backbone), 80.03 (polyether backbone), 71.93 (polyether backbone), 70.9 3 (polyether backbone), 66.2 3 (polyether backbone), 63.3–62.7 (polyether backbone; PO*C*$H_2$$CH_3$), 43.5 (cholesterol), 40.7 (cholesterol), 37.0 (cholesterol), 29.1 (cholesterol), 28.3 (cholesterol), 26.4 (CH_2OCH_2*C*H_2P), 23.2 (cholesterol), 19.2 (cholesterol), 16.9 (POCH_2*C*H_3).

3.3 Synthesis of linear cholesterol-poly(glycerol-*co*-glycerol-phosphonatoethyl) lipid

The synthesis was performed in analogy to the literature.[3] The procedure is described for Ch-*lin*P(G_8-*co*-G^{PE}_{13}) as an example. The synthesis and characterization was carried out similarly for all polymers.

Ch-*lin*P(G_8-*co*-G^{DEPE}_{13}) (0.15 g, 0.04 mmol, 1 eq.) was dissolved in anhydrous dichloromethane and bromotrimethylsilane was added (1.01 mL, 7.6 mmol, 16 eq. of silylating agent per diethylphosphonatoethyl group). The solution was stirred at 40 °C for 24 h. Subsequently, the solvent and other byproducts were removed applying vacuum. The polymer was redissolved in methanol (5 mL). After stirring for 24 h at room temperature, the solution was concentrated under reduced pressure. The crude polymer was precipitated in cold diethyl ether (40 mL). The product was obtained as highly viscous oil. Yield: 85-90%.

^{1}H-NMR, COSY (300 MHz, methanol-d_4): δ [ppm] = 5.37–5.30 (C=CH cholesterol), 3.93–3.40 (polyether backbone; CHOR cholesterol), 2.18–2.04 (2H, CH_2OCH_2C*H*$_2$P), 2.43–0.82 (40 H, CH_3,CH_2, CH cholesterol), 0.75–0.69 (3H, CH_3 cholesterol).

^{31}P-NMR (121.5 MHz, methanol-d_4): δ [ppm] = 26.7.

^{13}C-NMR, HSQC, HMBC (100.7 MHz, methanol-d_4): δ [ppm] = 81.5–79.9 (polyether backbone), 71.6-–70.8 (polyether backbone; CHOR cholesterol), 66.9 ($CH_2OCH_2CH_2$P), 62.5 (polyether backbone), 30.2–28.4 ($CH_2OCH_2CH_2$P).

3.4 Nanoparticle preparation

Polystyrene nanoparticles were synthesized using an adopted combination of the miniemulsion technique and the solvent-evaporation strategy.[4] 30 mg of the polymer were dissolved in 1.25 g of chloroform. 5 g of Milli-Q water containing 10 mg of SDS were

added to the chloroform solution and stirred during over a period of 60 min for the formation of the pre-emulsion. Then, the pre-emulsion was submitted to a pulsed ultrasonication process under an ice bath during 120 s (30 s sonicated and 10 s paused) at 70% amplitude in a ¼" tip Brason 450 W sonifier. The obtained miniemulsion was kept at 30 °C in an oil bath over a period of 8 h to completely evaporate the organic solvent. The obtained nanoparticles dispersion was further purified by exhaustive dialysis against water before being used for further studies.

3.5 Human material

Blood was taken from 10 healthy donors at the Transfusion Center of the University Clinics of the Johannes Gutenberg University Mainz after obtaining informed consent. The study was approved by the local ethics committee. To avoid blood clotting Li-Heparin was added. The blood was centrifuged and the remaining plasma from all donors was pooled. Aliquots of the plasma were stored at –80 °C. After thawing, the plasma was centrifuged at 20000 g for 1 h at 4 °C to remove remaining protein precipitates. Afterwards, a protein concentration of 66 g L^{-1} was determined for the plasma.

3.6 Isothermal titration calorimetry (ITC)

ITC measurements were carried out with a NanoITC Low Volume instrument (TA Instruments, Germany) with an effective cell volume of 170 µL. In an experiment 50 µL diluted human plasma (3,75 g·L^{-1}) were titrated into a suspension of each of the nanoparticle samples in water (Ch-*lin*PG_{21} - 9,4 g·L^{-1}, 1,64·10^{-7} mM; Ch-*lin*P(G_{15}-*co*-G^{PE}_6) - 6,0 g·L^{-1}, 1,73·10^{-7} mM; Ch-*lin*P(G_{12}-*co*-G^{PE}_9) - 2,3 g·L^{-1}, 1,71·10^{-7} mM). The temperature was kept constant at 25 °C. Additionally, the same volume of plasma was titrated into pure water to determine the heat of dilution as a reference. The number and volume of injections was kept constant for every measurement (25 x 2 µL). The time between injections was set to 300 s. The integrated heats of the reference measurements were then subtracted from the adsorption measurements to yield the adsorption isotherms. Each titration measurement was performed twice to ensure reproducibility.

3.7 Sample preparation for Protein Corona Analysis

Nanoparticle samples (0.05 m² of surface area in 300 µL) were incubated with 1 mL concentrated blood plasma for 1 h at 37 °C. The nanoparticles were then separated from the protein solution by centrifugation at 20000 g for 1 h. The pellet was resuspended in

PBS and again centrifuged at 20000 g for 1 h. This washing step was performed three times. Before the last washing step the suspension was transferred into a new Eppendorf tube. The proteins were then detached from the nanoparticles by adding 300 µL urea-thiourea buffer (7M Urea, 2M Thiourea, 4% CHAPS). The protein concentration was then determined by a Pierce 660nm protein assay according to manufacturer's instructions with BSA as a standard.

3.8 SDS polyacrylamide gel electrophoresis (SDS-PAGE)

For SDS-PAGE 16.25 µl of the protein sample was mixed with 6.25 µl NuPAGE LDS Sample Buffer and 2.5 µl NuPAGE Sample Reducing Agent and applied onto a NuPAGE 10% Bis-Tris Protein Gel (all Novex, Thermo Fisher Scientific). The electrophoresis was carried out in NuPAGE MES SDS Running Buffer at 150 V for 1.5 h with SeeBlue Plus2 Pre-Stained Standard (Invitrogen) as a molecular marker. The gel was stained using SimplyBlue SafeStain (Novex, Thermo Fisher Scientific).

3.9 Liquid-chromatography mass-sprectrometry (LC-MS) analysis

Proteins were digested following the protocol of *Tenzer et al.*[5] with following modifications: 25 µg of each protein sample was precipitated and trypsin was used with a 1:50 ratio (enzyme:protein). For LC-MS analysis the samples were diluted 10-fold with aqueous 0.1% formic acid and spiked with 50 fmol/µl Hi3 EColi Standard (Waters Corporation) for absolute quantification.

Quantitative analysis of protein samples was performed using a nanoACQUITY UPLC system coupled with a Synapt G2-Si mass spectrometer (Waters Corporation). Tryptic peptides were separated on the nanoACQUITY system equipped with a C18 analytical reversed-phase column (1.7 µm, 75 µm x 150 mm, Waters Corporation) and a C18 nanoACQUITY Trap Column (5 µm, 180 µm x 20 mm, Waters Corporation). Samples were processed with mobile phase A consisting of 0.1% (v/v) formic acid in water and mobile phase B consisting of acetonitrile with 0.1% (v/v) formic acid. The separation was performed at a sample flow rate of 0.3 µl/min, using a gradient of 2-37% mobile phase B over 70 min. As a reference compound 150 fmol/µl Glu-Fibrinopeptide was infused at a flow rate of 0.5 µl/min.

Data-independent acquisition (MS^E) experiments were performed on the Synapt G2-Si operated in resolution mode. Electrospray Ionization was performed in positive ion mode

using a NanoLockSpray source. Data was acquired over a range of m/z 50-2000 Da with a scan time of 1 s, ramped trap collision energy from 20 to 40 V with a total acquisition time of 90 min. All samples were analyzed in two technical replicates. Data acquisition and processing was carried out using MassLynx 4.1 and TansOmics Informatics software was used to process data and identify peptides. Data were post acquisition lock mass corrected. Noise reduction thresholds for low energy, high energy and peptide intensity were fixed at 120, 25, and 750 counts, respectively. During database searches, the protein false discovery rate was set at 4%. The generated peptide masses were searched against a reviewed human protein sequence database downloaded from Uniprot. The following criteria were used for the search: one missed cleavage, maximum protein mass 600 kDa, fixed carbamidomethyl modification for cysteine and variable oxidation for methionine. For identification a peptide was required to have at least three assigned fragments and a protein was required to have at least two assigned peptides and five assigned fragments. Quantitative data were generated based on the TOP3/Hi3 approach,[6] providing the amount of each protein in fmol.

4. Characterization Data

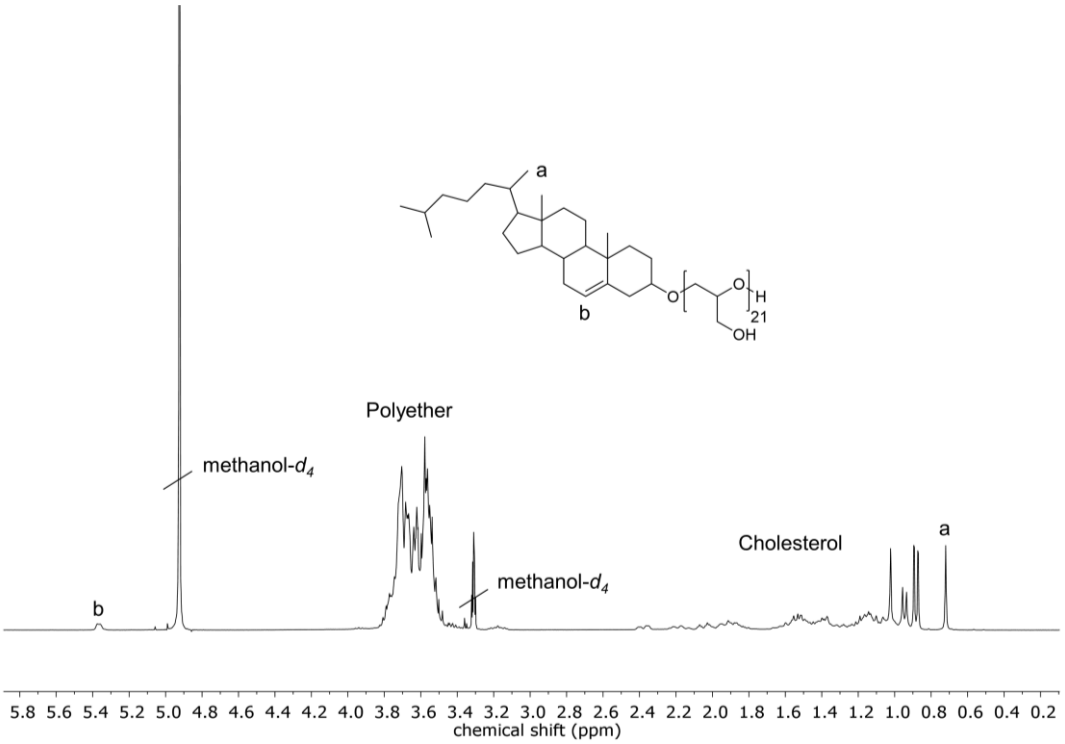

Figure S1. ^{1}H NMR spectrum of Ch*lin*PG$_{21}$ measured in methanol-d_4 at 300 MHz.

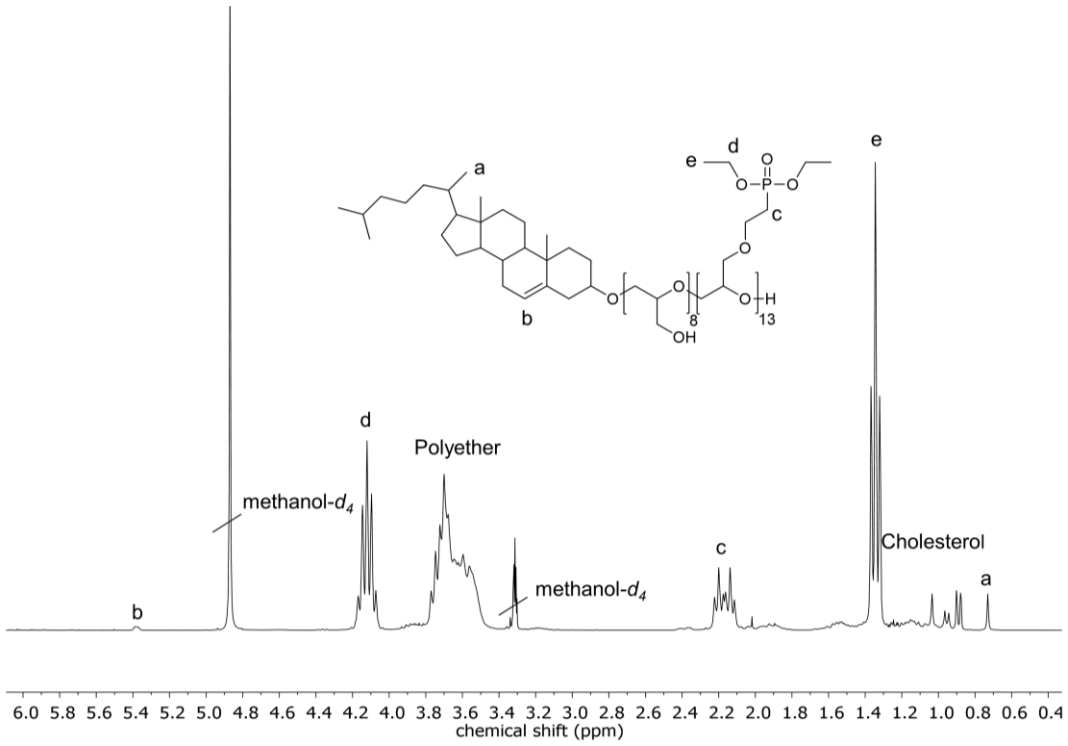

Figure S2. ^{1}H NMR spectrum of Ch-*lin*P(G$_8$-*co*-G$^{DEPE}_{13}$) measured in methanol-d_4 at 300 MHz.

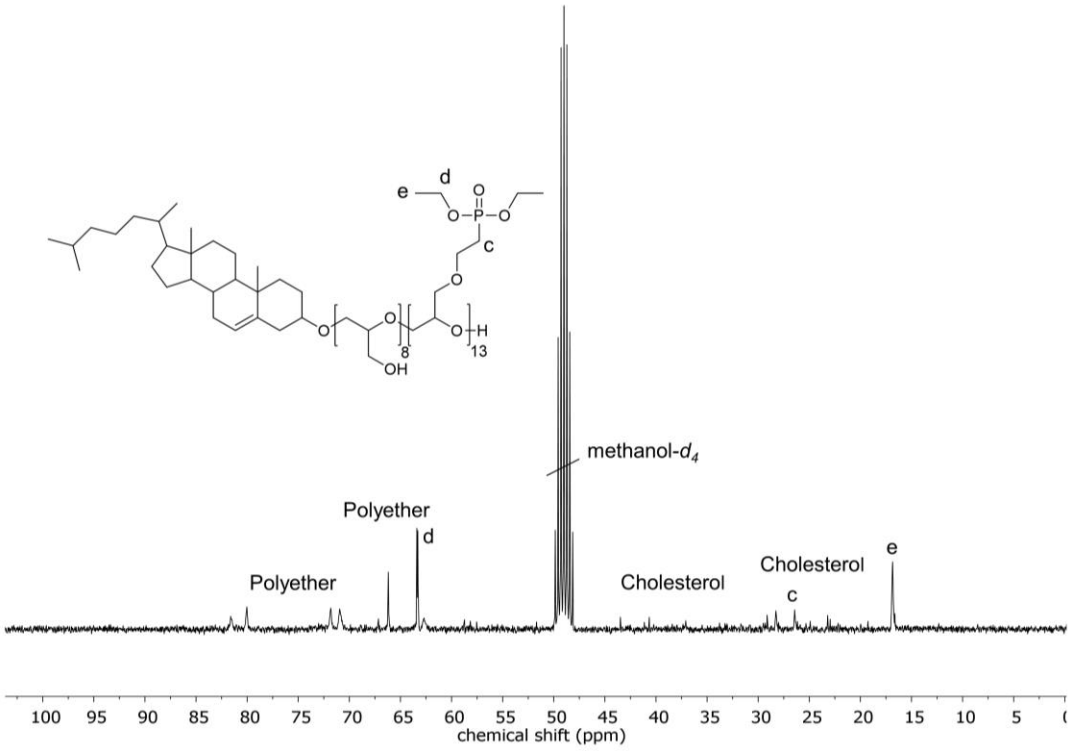

Figure S3. ^{13}C NMR spectrum of Ch-*lin*P(G$_8$-*co*-G$^{DEPE}_{13}$) measured in methanol-d_4 at 100.7 MHz.

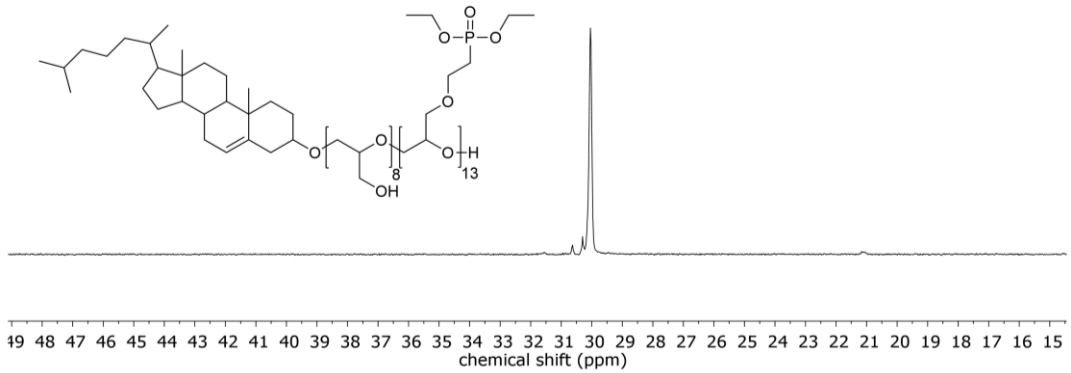

Figure S4. ^{31}P NMR spectrum of Ch-*lin*P(G$_8$-*co*-G$^{DEPE}_{13}$) measured in methanol-d_4 at 121.5 MHz.

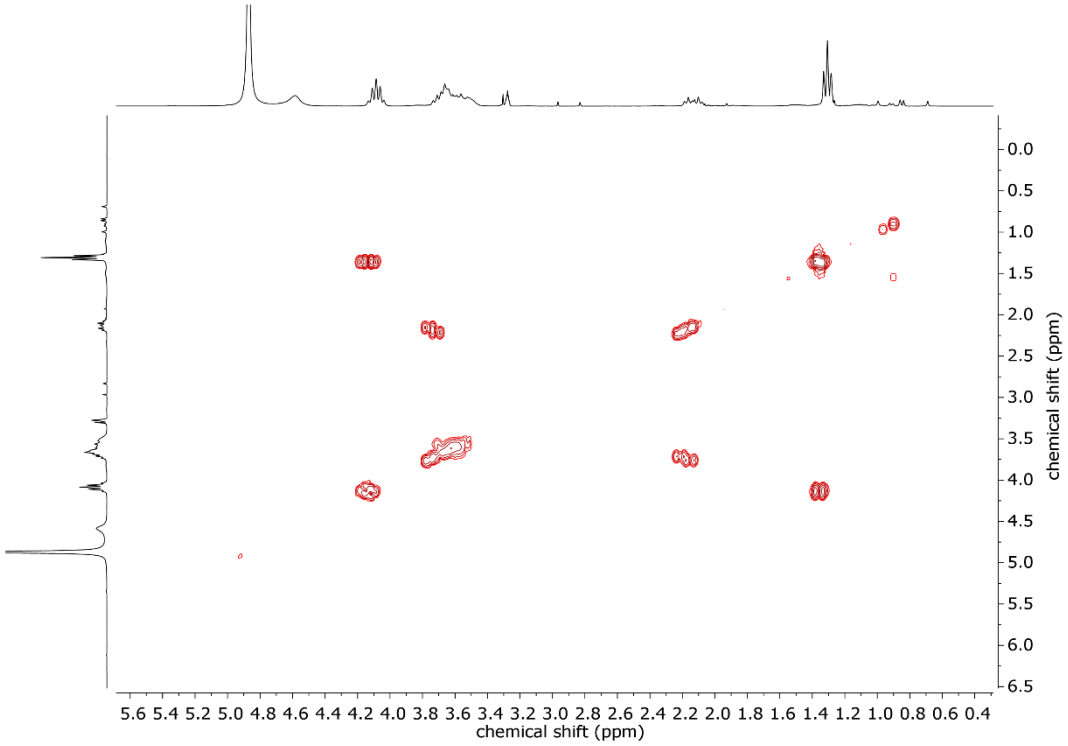

Figure S5. H,H-COSY NMR spectrum of Ch-*lin*P(G_8-*co*-G^{DEPE}_{13}) measured in methanol-d_4.

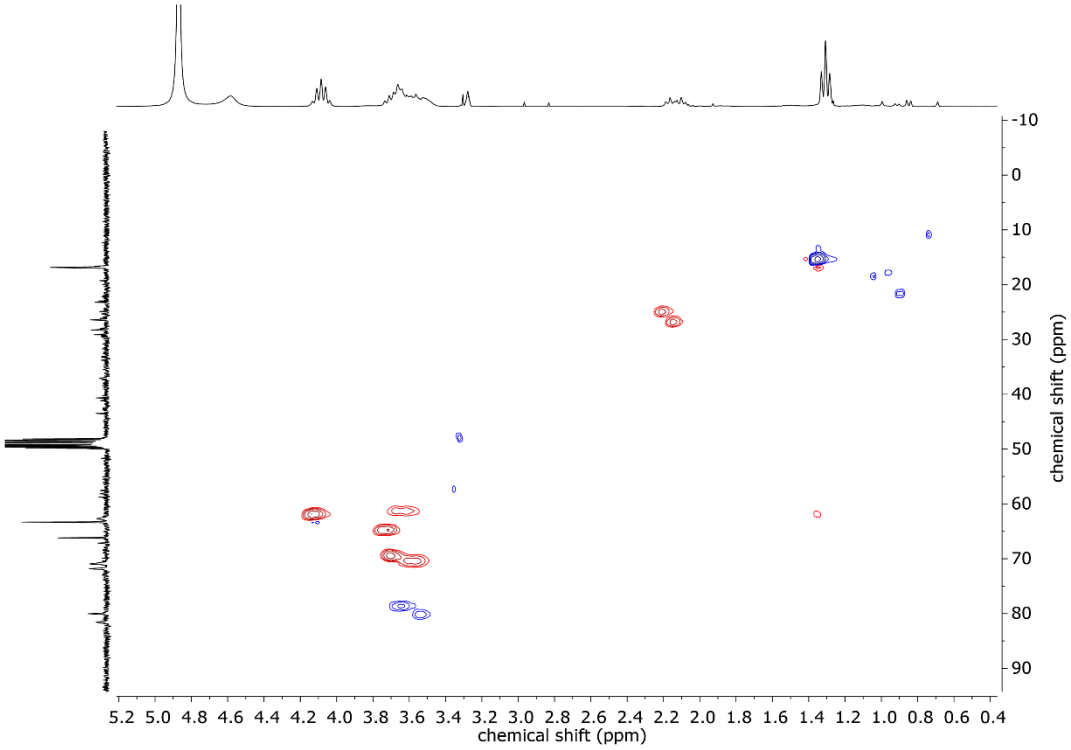

Figure S6. H,C-HSQC NMR spectrum of Ch-*lin*P(G_8-*co*-GDE^{PE}_{13}) measured in methanol-d_4. Methyl and methine groups appear as blue correlation peaks, whereas methylene groups appear as red correlation peaks.

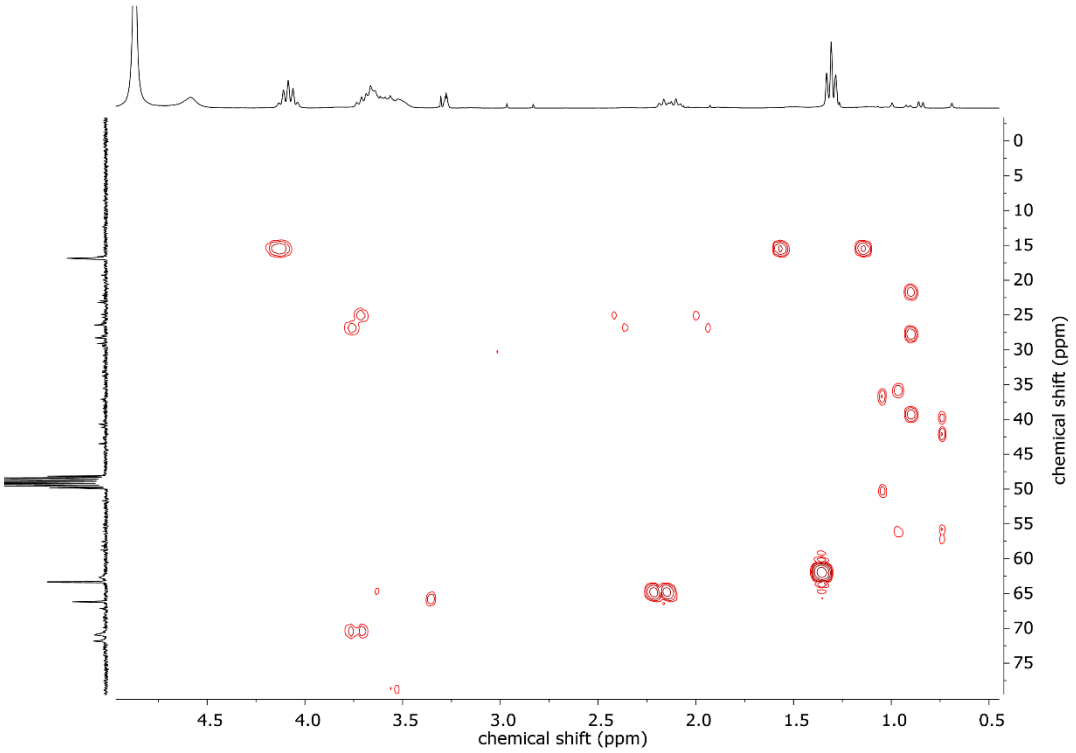

Figure S7. H,C-HMBC NMR spectrum of Ch-*lin*P(G_8-*co*-G^{DEPE}_{13}) measured in methanol-d_4.

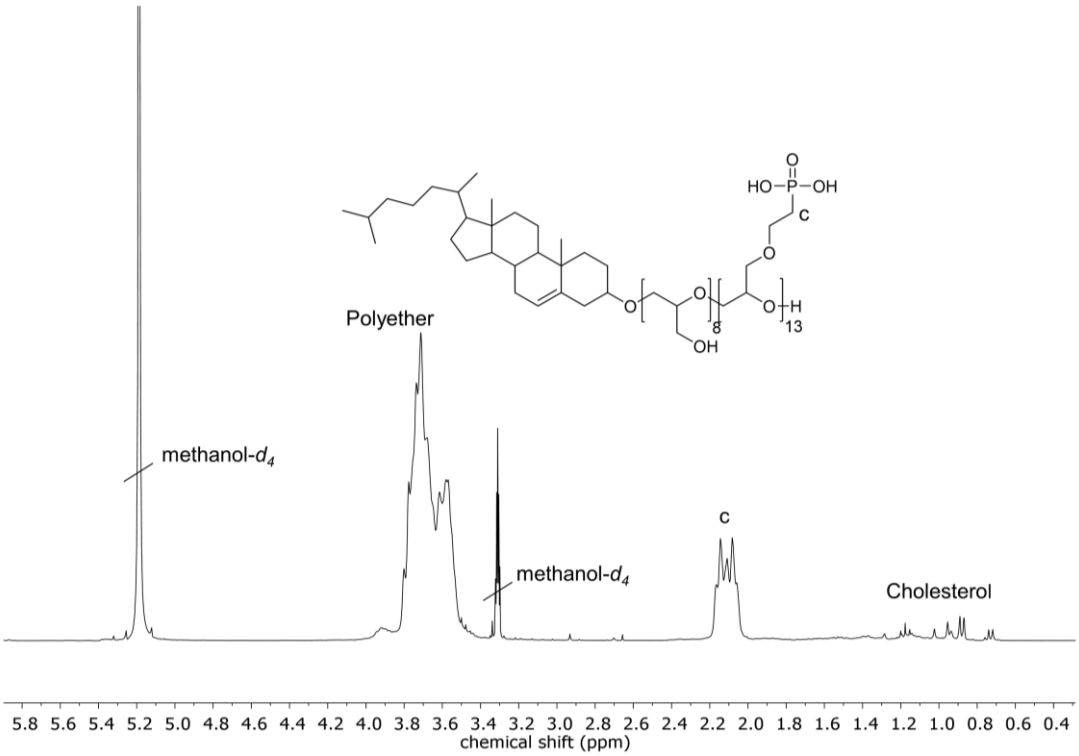

Figure S8. ^{1}H NMR spectrum of Ch-*lin*P(G_8-*co*-G^{PE}_{13}) measured in methanol-d_4 at 300 MHz.

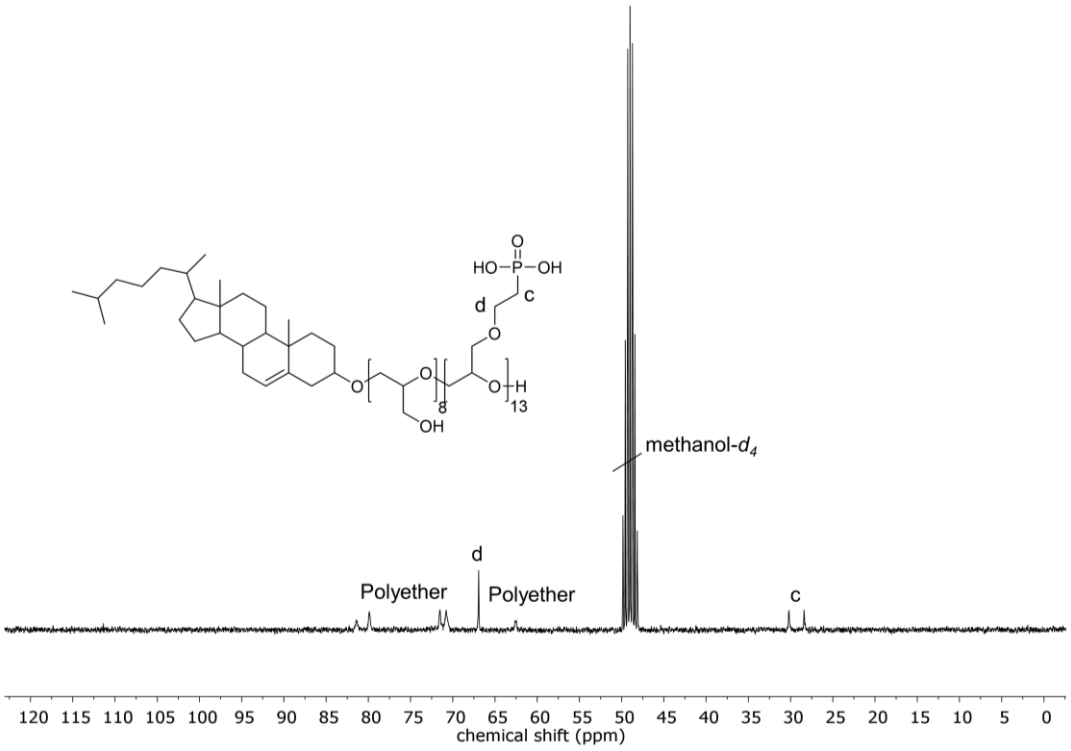

Figure S9. ^{13}C NMR spectrum of Ch-*lin*P(G$_8$-*co*-G$^{PE}_{13}$) measured in methanol-d_4 at 100.7 MHz.

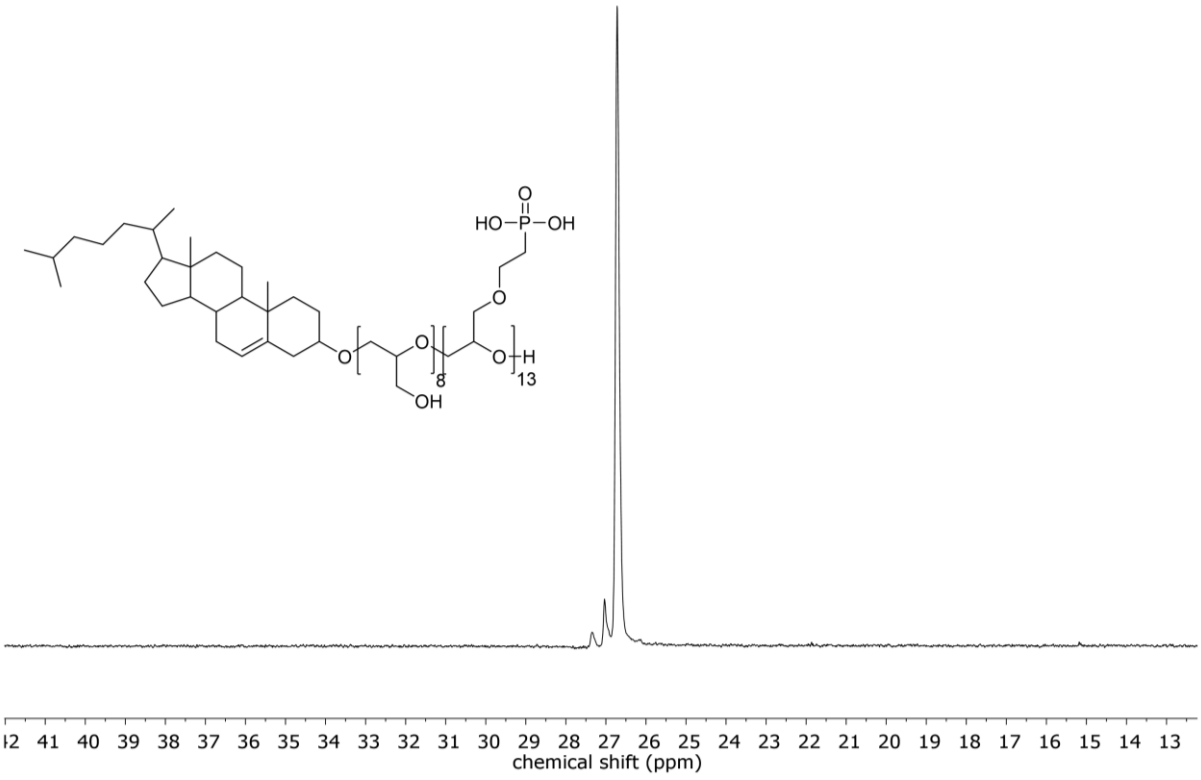

Figure S10. ^{31}P NMR spectrum of Ch-*lin*P(G$_8$-*co*-G$^{DEPE}_{13}$) measured in methanol-d_4 at 121.5 MHz.

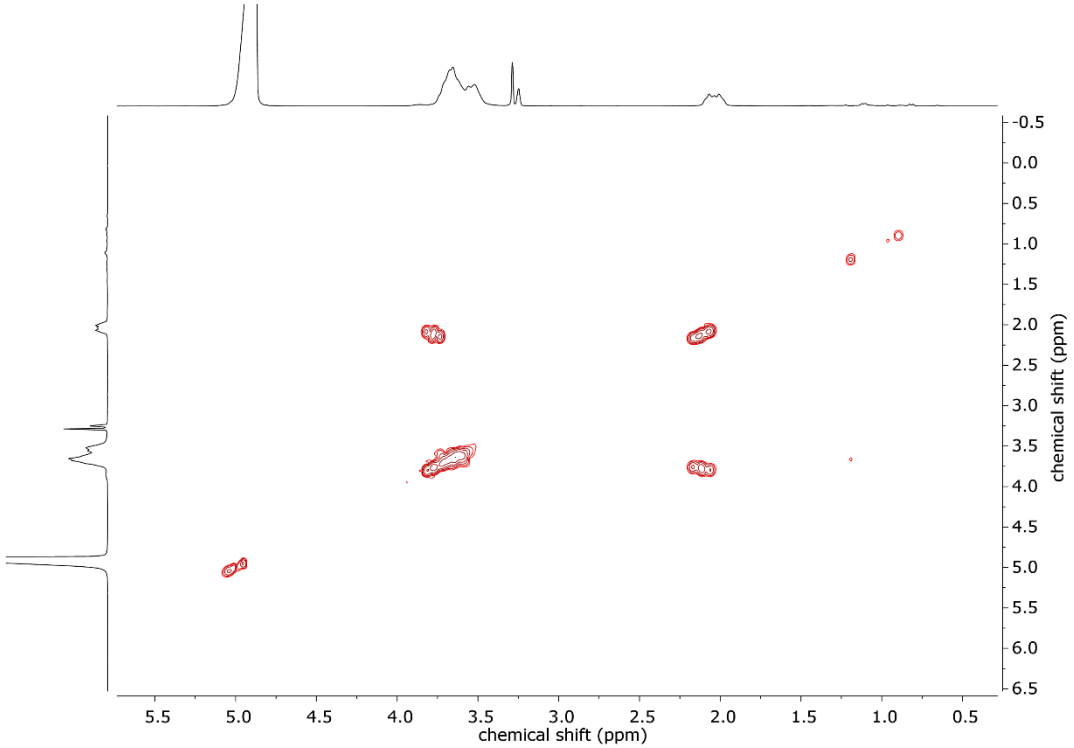

Figure S11. H,H-COSY NMR spectrum of Ch-*lin*P(G_8-*co*-G^{PE}_{13}) measured in methanol-d_4.

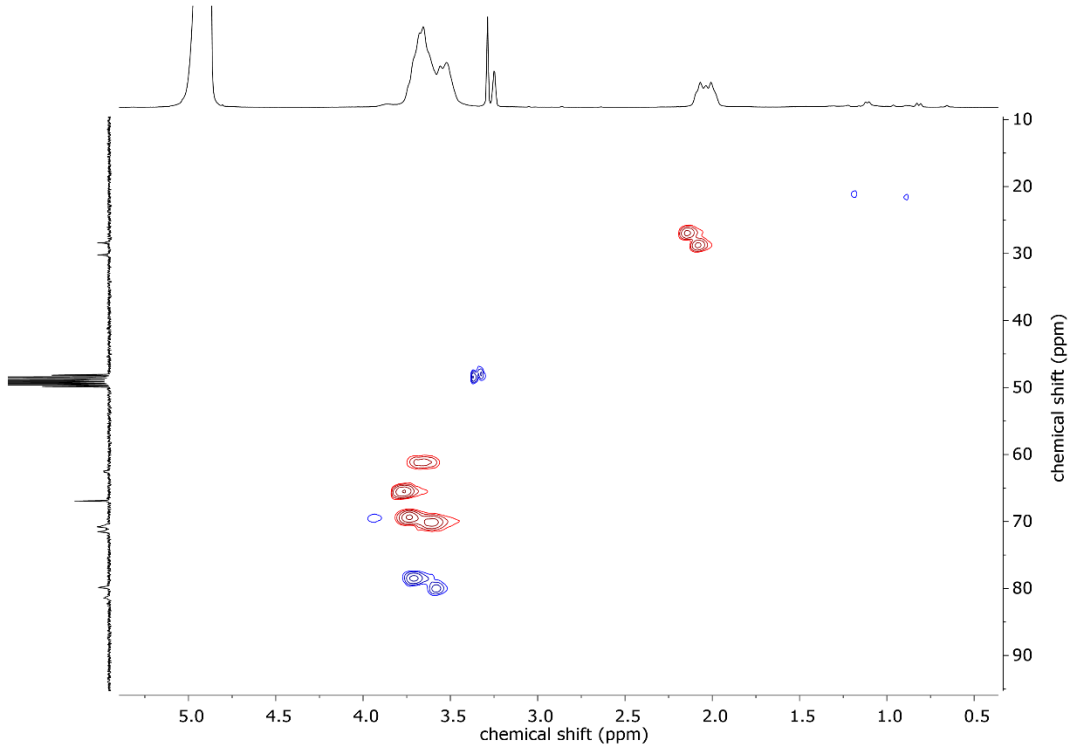

Figure S12. H,C-HSQC NMR spectrum of Ch-*lin*P(G_8-*co*-G^{PE}_{13}) measured in methanol-d_4. Methyl and methine groups appear as blue correlation peaks, whereas methylene groups appear as red correlation peaks.

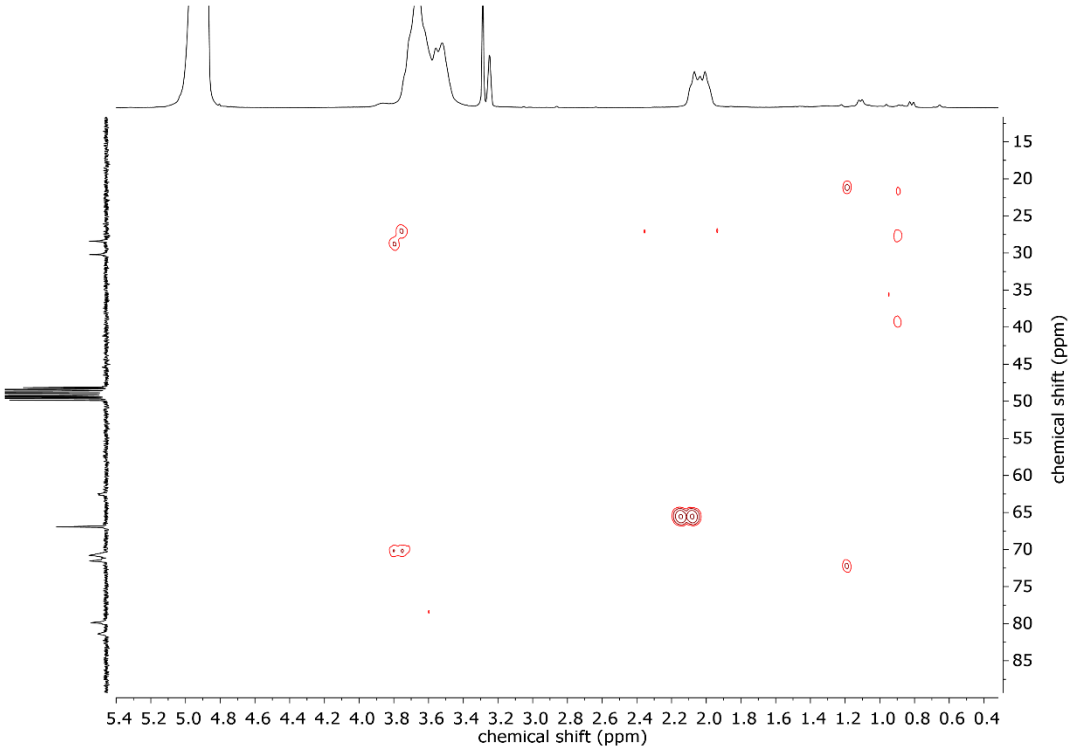

Figure S13. H,C-HMBC NMR spectrum of Ch-*lin*P(G_8-*co*-G^{PE}_{13}) measured in methanol-d_4.

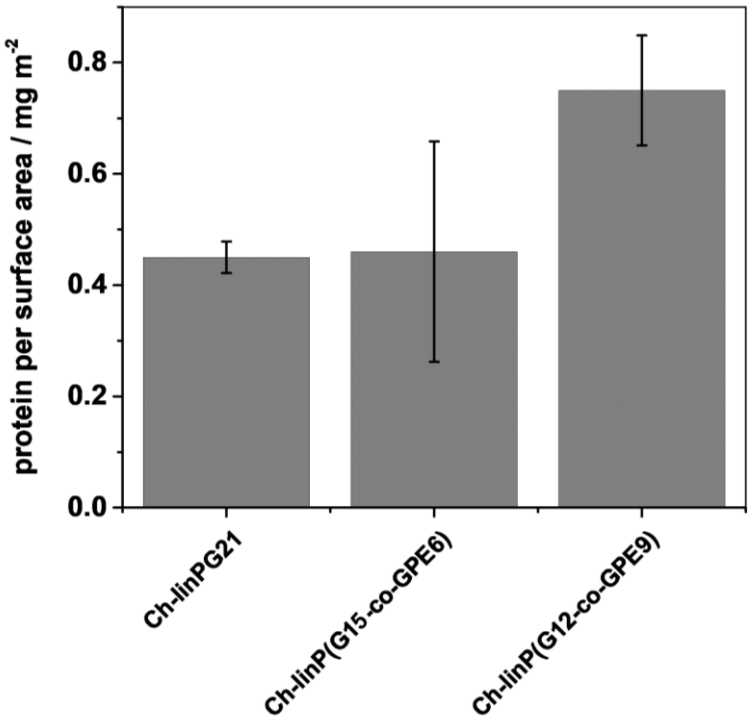

Figure S14. Amount of protein per particle surface area of the nanocarriers with and without phosphonate groups.

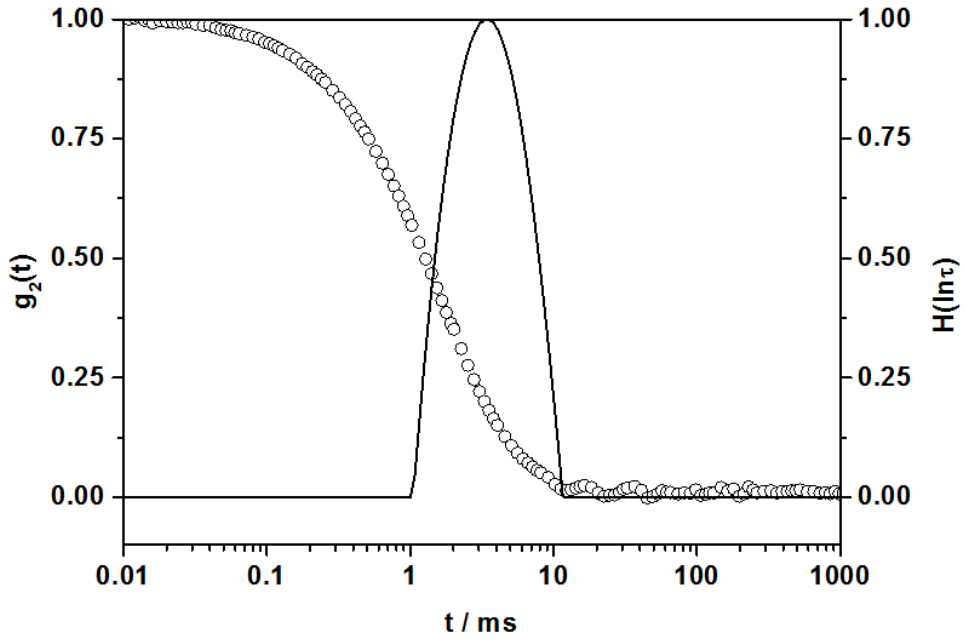

Figure S15. Autocorrelation function $g_2(t)$ (open circles o) and the distribution of relaxation times H(ln τ) (black line −) calculated by a CONTIN data analysis[7,8] are given for Ch-*lin*PG_{21}-decorated nanoparticles in water at a scattering angle of 90°

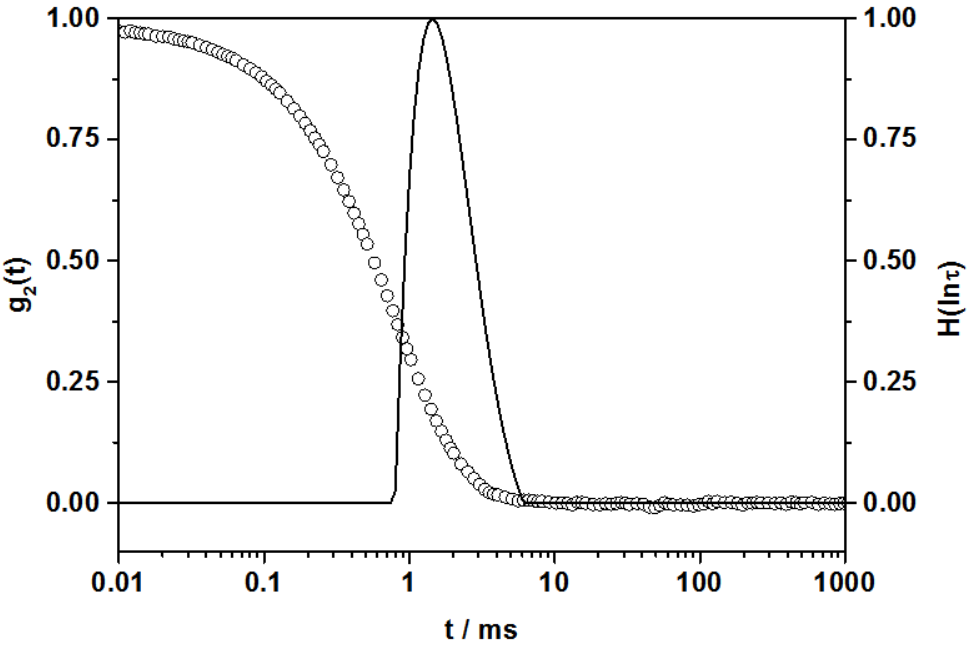

Figure S16. Autocorrelation function $g_2(t)$ (open circles o) and the distribution of relaxation times H(ln τ) (black line −) calculated by a CONTIN data analysis[7,8] are given for Ch-*lin*P(G_{15}-*co*-G^{PE}_6)-decorated nanoparticles in water at a scattering angle of 90°.

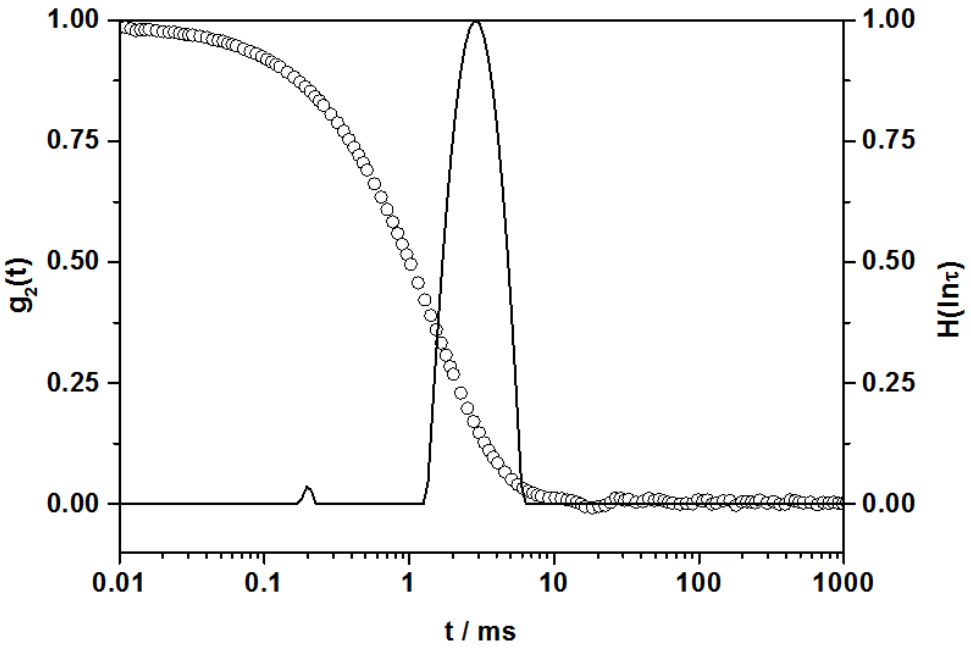

Figure S17. Autocorrelation function $g_2(t)$ (open circles o) and the distribution of relaxation times H(ln τ) (black line −) calculated by a CONTIN data analysis[7,8] are given for Ch-*lin*P(G_{12}-*co*-G^{PE}_9)-decorated nanoparticles in water at a scattering angle of 90°.

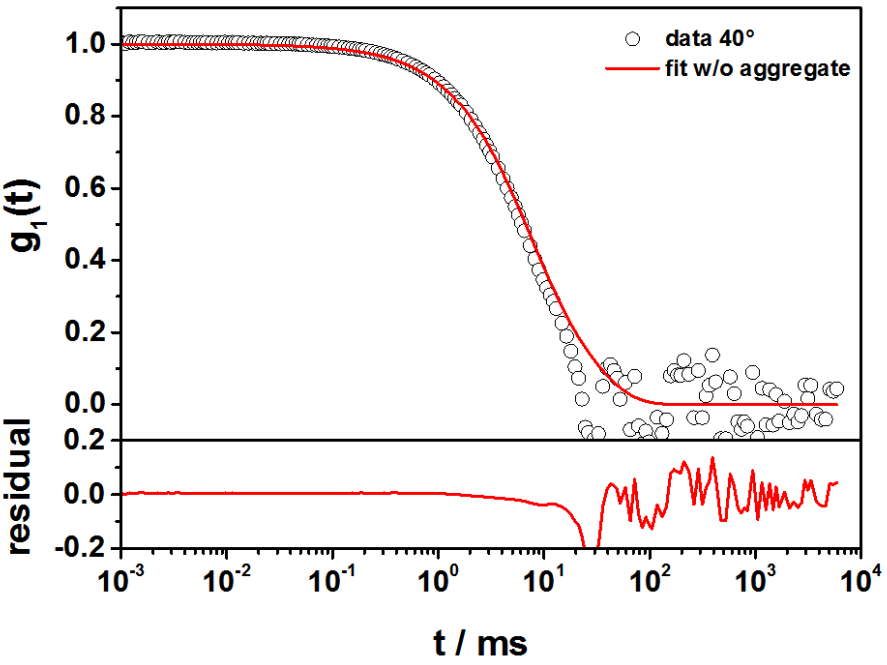

Figure S18. Upper graph: Autocorrelation function (empty circles ○) of the mixture of Ch-*lin*PG_{21}-decorated nanoparticles with concentrated human plasma at a scattering angle of 40°. The force fit generated from the sum of the individual components is represented by the red line. Lower graph: residual from subtraction of the fit from the data points.

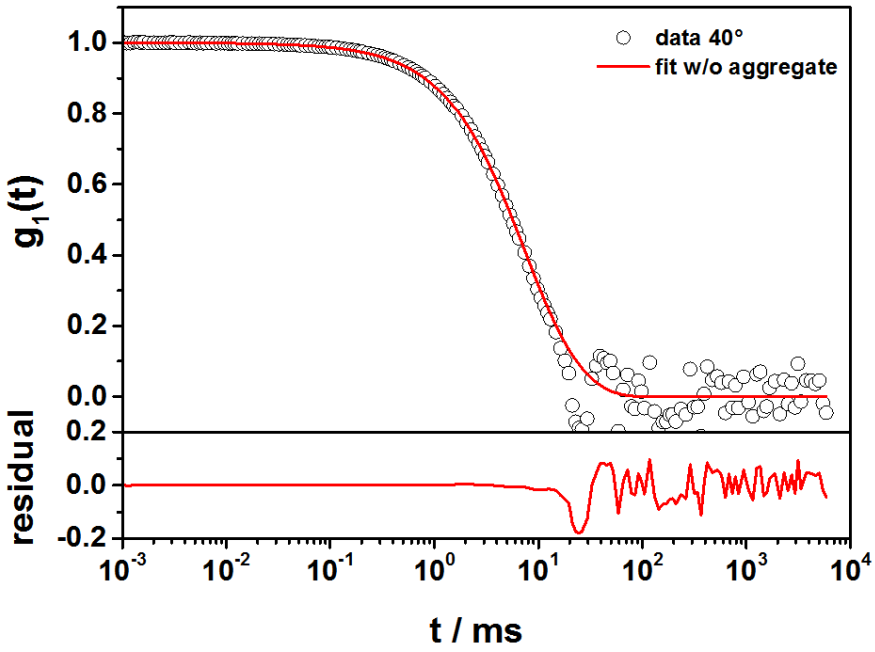

Figure S19. Upper graph: Autocorrelation function (empty circles ○) of the mixture of Ch-*lin*P(G_{15}-*co*-G^{PE}_{6})-decorated nanoparticles with concentrated human plasma at a scattering angle of 40°. The force fit generated from the sum of the individual components is represented by the red line. Lower graph: residual from subtraction of the fit from the data points.

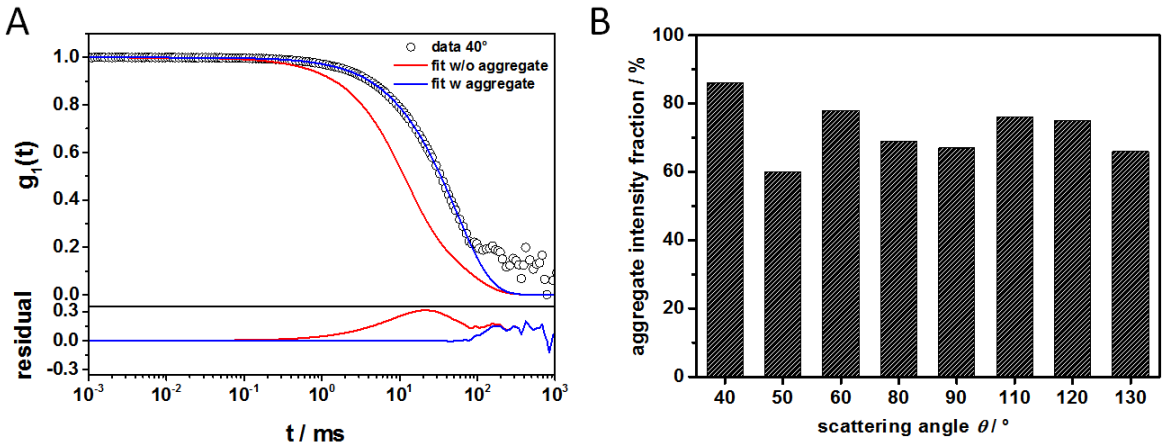

Figure S20. A) Upper graph: Autocorrelation function (empty circles ○) of the mixture of Ch-*lin*P(G_{12}-co-G^{PE}_{9})-decorated nanoparticles with concentrated human plasma at a scattering angle of 40°. The force fit generated from the sum of the individual components is represented by the red line. The fit including an additional aggregate term is represented by the blue line. Lower graph: residuals from subtraction of the fits from the data points. B) Aggregate fraction intensities for all measured scattering angles. The hydrodynamic

radius of the aggregate was determined to be ~1.6 µm, which is beyond the experimentally accurate regime of light scattering.

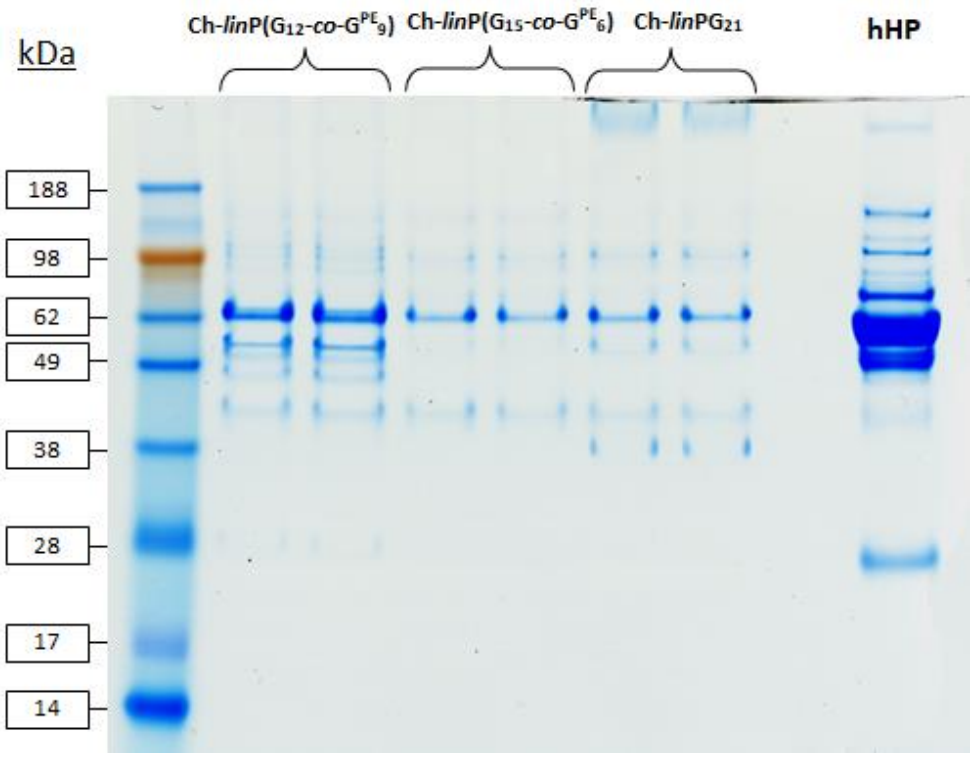

Figure S21. Coomassie Blue stained SDS-PAGE gel of Ch-*lin*P(G_{12}-*co*-G^{PE}_{9})-, Ch-*lin*P(G_{15}-*co*-G^{PE}_{6})- and Ch-*lin*PG_{21}-decorated after incubation in human heparin plasma (hHP) performed in duplicates. The pure plasma served as a reference (right lane).

Table S1. Most abundant proteins in the protein corona of PS nanocarriers with Ch-*lin*P(G_{12}-*co*-G^{PE}_9), Ch-*lin*P(G_{15}-*co*-G^{PE}_6) or Ch-*lin*PG_{21} as surfactant determined by proteomic mass spectrometry. Values were calculated from the molar masses of each protein identified by LC-MS.

	Ch-*lin*P(G_{12}-*co*-G^{PE}_9)	**Ch-*lin*P(G_{15}-*co*-G^{PE}_6)**	**Ch-*lin*PG_{21}**
Alpha-1B-glycoprotein	0.67%	1.28%	0.54%
Apolipoprotein A-I	1.16%	1.00%	1.41%
Beta-2-glycoprotein 1	1.33%	2.64%	1.44%
Clusterin	18.89%	22.71%	58.56%
Complement C1	1.86%	6.24%	4.11%
Complement C3	9.80%	15.53%	13.96%
Complement C4-A	0.72%	0.64%	0.30%
Complement component C7	0.62%	1.04%	0.76%
Complement component C9	1.06%	2.28%	1.09%
Complement factor H	0.83%	1.27%	0.51%
Complement factor H-related protein 1	0.69%	1.55%	0.28%
Fibrinogen	17.69%	2.39%	0.48%
Immunoglobulins	25.34%	9.82%	3.67%
Inter-alpha-trypsin inhibitor heavy chain H4	1.30%	0.98%	0.08%
Keratin, type I cytoskeletal 14	0.12%	1.02%	0.06%
Keratin, type I cytoskeletal 16	0.23%	1.63%	0.11%
Keratin, type I cytoskeletal 9	0.37%	2.02%	0.29%
Keratin, type II cytoskeletal 1	0.23%	3.04%	0.29%
Pregnancy zone protein	0.88%	1.78%	1.18%
Properdin	0.65%	1.30%	3.34%
Serotransferrin	0.74%	0.09%	0.01%
Serum albumin	1.76%	0.51%	0.15%
Serum amyloid P-component	0.66%	2.48%	0.17%
Vitamin D-binding protein	0.13%	0.19%	0.05%
Vitronectin	3.92%	2.37%	0.80%

5. References

(1) Fitton, A. O.; Hill, J.; Jane, D. E.; Millar, R. Synthesis of Simple Oxetanes Carrying Reactive 2-Substituents. *Synthesis* **1987**, 1140–1142.

(2) Rausch, K.; Reuter, A.; Fischer, K.; Schmidt, M. Evaluation of nanoparticle aggregation in human blood serum. *Biomacromolecules* **2010**, *11*, 2836–2839.

(3) Köhler, J.; Keul, H.; Möller, M. Post-polymerization functionalization of linear polyglycidol with diethyl vinylphosphonate. *Chem. Commun.* **2011**, *47*, 8148–8150.

(4) Musyanovych, A.; Schmitz-Wienke, J.; Mailänder, V.; Walther, P.; Landfester, K. Preparation of biodegradable polymer nanoparticles by miniemulsion technique and their cell interactions. *Macromol. Biosci.* **2008**, *8*, 127–139.

(5) Tenzer, S.; Docter, D.; Rosfa, S.; Wlodarski, A.; Kuharev, J.; Rekik, A.; Knauer, S. K.; Bantz, C.; Nawroth, T.; Bier, C. *et al.* Nanoparticle size is a critical physicochemical determinant of the human blood plasma corona: a comprehensive quantitative proteomic analysis. *ACS nano* **2011**, *5*, 7155–7167.

(6) Silva, J. C.; Gorenstein, M. V.; Li, G.-Z.; Vissers, J. P. C.; Geromanos, S. J. Absolute quantification of proteins by LCMSE: A virtue of parallel MS acquisition. *Molecular & cellular proteomics : MCP* **2006**, *5*, 144–156.

(7) Provencher, S. W. CONTIN: A general purpose constrained regularization program for inverting noisy linear algebraic and integral equations. *Computer Physics Communications* **1982**, *27*, 229–242.

(8) Provencher, S. W. Inverse problems in polymer characterization: Direct analysis of polydispersity with photon correlation spectroscopy. *Makromol. Chem.* **1979**, *180*, 201–209.

4. Chloride-functional Poly(ethylene glycol) Copolymers

4.1 Monomer-activated Copolymerization of Ethylene Oxide and Epichlorohydrin: *In Situ* Kinetics Evidences Tapered Block Copolymer Formation

Ann-Kathrin Danner,[a,b] Daniel Leibig,[a,b] Lea-Marie Vogt[a] and Holger Frey[a,*]

[a]Institute of Organic Chemistry, Johannes Gutenberg-University Mainz, Duesbergweg 10-14, 55128 Mainz, Germany.

[b]Graduate School Materials Science in Mainz, Staudinger Weg 9, 55128 Mainz, Germany.

E-Mail: hfrey@uni-mainz.de

To be submitted to *Polymer Chemistry*.

Abstract

The monomer-activated anionic ring-opening copolymerization (AROP) of ethylene oxide (EO) and epichlorohydrin (ECH) using tetraoctylammonium bromide as an initiator and triisobutylaluminum (*i*-Bu_3Al) as an activator was studied. The properties of the copolymers as well as the microstructure have been analyzed in detail via an *in situ* NMR kinetics study. The copolymers exhibit molecular weights ranging from 2,350 to 38,000 g mol^{-1} (measured by SEC) and moderate dispersities of 1.27–1.44. The thermal properties reveal both a glass transition and melting for all copolymers, supporting a block-like nature. Applying *in situ* NMR kinetic measurements, the reactivity ratios of EO and ECH were determined to be strongly disparate, *i.e.*, r_{EO} = 9.2 and r_{ECH} = 0.10. This shows that the simple one-pot statistical anionic copolymerization of EO and ECH *via* the monomer-activated AROP results in the formation of strongly tapered, block like structures. Furthermore, post-polymerization functionalization of the reactive chloromethyl groups by nucleophilic displacement was carried out at the copolymers. Copolymerization of EO and ECH offers a broad platform for further functionalization and therefore the possibility to prepare a variety of multifunctional PEGs.

Table of Contents Graphics

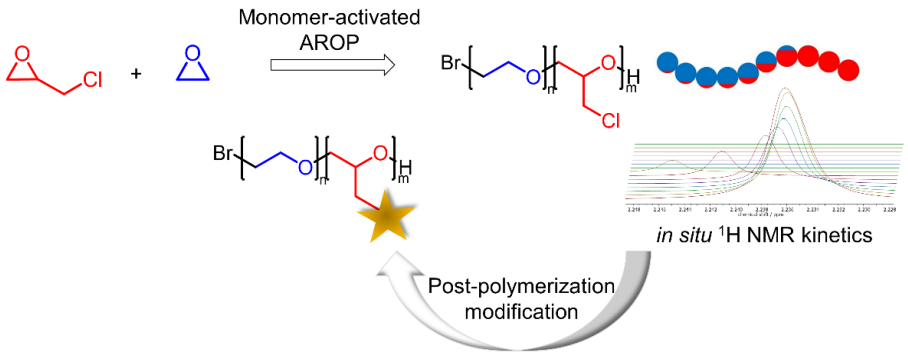

Introduction

Poly(glycidyl ether)s, such as polyglycerol and its derivatives are an emerging class of materials due to their biocompatibility and high functionality. In comparison to polyethylene glycol (PEG) also known as polyethylene oxide (PEO), poly(glycidyl ether)s offer multiple functional groups that can be used to further tailor the materials for biomedical applications.[1–6] In this context the copolymerization of ethylene oxide (EO) and epichlorohydrin (ECH) is a promising strategy, however the conventional anionic polymerization of epoxides is not applicable for the polymerization of epichlorohydrin (ECH) due to the reaction of the nucleophilic propagating chain end with the chloromethyl groups.[7] Cationic ring-opening polymerization or a polymerization via a coordinative mechanism is possible. Drawbacks of the cationic mechanism are backbiting, chain transfer and termination reactions during propagation, leading to cyclic oligomer side products and low molar mass polymers with molecular weights < 2500 g mol^{-1}.[8] In order to avoid this problem, Vandenberg was the first who reported a cationic coordination mechanism to synthesize high molar mass PECH with the aid of organometallic catalysts.[9] Subsequently, other groups further developed catalytic systems for the synthesis of high molar mass PECH.[10–13] Nevertheless, these systems also suffered from limitations regarding dispersity, conversion and limited molar masses when targeting high molar mass polymers.[10,14–19] The development of the monomer-activated polymerization led to new possibilities in the field of epoxide homo and copolymerization.

Over the past years the monomer-activated polymerization method gained in importance due to the possibility to polymerize monomers that cannot be polymerized via conventional anionic ring opening polymerization (AROP). By combining onium salts and triisobutylaluminum (*i*-Bu_3Al) (TIABL) it is possible to lower the nucleophilicity of the chain end and to suppress transfer reactions to monomers, permitting the controlled synthesis of high molar mass polyethers. In this strategy *i*-Bu_3Al serves as an epoxide-activator, and tetraalkylammonium salts are employed as initiator for the polymerization. To achieve fast initiation and high monomer conversion, an excess of activator compared to initiator is necessary.[7,20,21] Making use of these advantages, Carlotti, Deffieux and coworkers were the first to report the controlled polymerization of propylene oxide (PO) to achieve high molar masses.[22,23] Furthermore, copolymers of PO and ethylene oxide (EO) were prepared, and kinetic studies of the copolymerization revealed a higher reactivity of

EO in the monomer-activated approach.[24] In addition, Carlotti *et al.* used this strategy to synthesize polyepichlorohydrin (PECH) with high molar masses (M_n = 83,500 g mol^{-1}) and copolymers with varied amount of PO. Reactivity ratios were determined, indicating a higher reactivity of PO.[7] Furthermore, ethoxyethyl glycidyl ether (EEGE) and *tert*-butyl glycidyl ether (*t*BuGE) were polymerized and copolymers with PO and butylene oxide (BO) were prepared as well.[20] Copolymers of glycidyl methyl ether (GME) and EO with varied amount of GME (31–100 mol%)[25] and copolymers of GME and ethyl glycidyl ether (EGE) were synthesized to obtain thermoresponsive polyethers.[26] Moreover, Gervais *et al.* synthesized α-azido,ω-hydroxypolyethers of EO, PO, ECH and EEGE that exhibit an azide group enabling a 1,3-dipolar cycloaddition with an alkyne function.[27] Recently, Lynd and coworkers developed an organoaluminum initiator based on *N*,*N*-dibenzylethanolamine and polymerized PO, BO, ECH and AGE with molecular weights up to 95 kg mol^{-1}.[28] Several works rely on the reactive chloromethyl group in the side chain of PECH for a broad range of polymer modifications. For instance, Lynd and coworkers prepared degradable PEG via the copolymerization of EO and ECH followed by elimination of the chloride moieties leading to pH-sensitive methylene ethylene oxide (MEO) units.[29] Further modification reactions of the chloromethyl groups in copolymers led to glycidyl azides, glycidyl amines,[30] hydroxyurethane side groups[31] and poly(ionic liquids).[32] For all applications mentioned it is crucial to gain a detailed understanding of the microstructure of the copolymer of EO and ECH using the monomer-activated AROP. Consequently, in this study we investigate the monomer compositional profile and the characteristics of the copolymers.

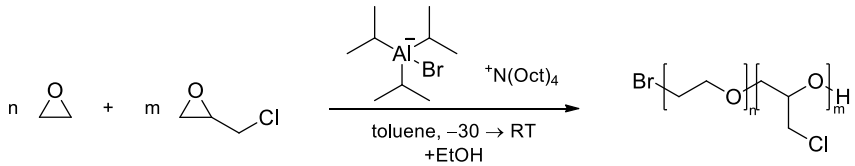

Scheme 1. Statistical copolymerization of ethylene oxide (EO) and epichlorohydrin (ECH) using the monomer-activated method.

Results and Discussion

A. Synthesis of Copolymers based on EO and ECH

Statistical copolymers of EO and ECH were synthesized using the monomer-activated AROP introduced by Carlotti, Deffieux and coworkers[23] in order to generate polyether copolymers with adjustable molecular weight and defined epichlorohydrin content. All copolymers were analyzed in detail using NMR spectroscopy, size exclusion chromatography (SEC) and differential scanning calorimetry (DSC). In addition *in situ* NMR kinetics studies were performed to determine the comonomer reactivity ratios and to gain detailed understanding of the microstructure of the copolymers. Furthermore, nucleophilic substitution reactions of the chloride moiety and a Michaelis-Arbuzov reaction was carried out as typical post-polymerization reactions of P(EO-*co*-ECH).

The direct (*i.e.*, statistical) copolymerization of EO and ECH was conducted in toluene with [*i*-Bu_3Al]/[$NOct_4Br$] ≥ 1.3 and temperatures ranging from –30 °C to room temperature with a reaction time of 24 h (**Scheme 1**). An excess of Lewis acid was necessary due to the formation of a $NOct_4Br$:triisobutylaluminum (1:1) aluminate complex and the simultaneous activation of the epoxide-monomer by the alkylaluminum as known from literature.[7] The polymerization was quenched by adding an excess of ethanol. In order to remove the aluminum catalyst and the initiator salt, the copolymers were first precipitated in cold diethyl ether, followed by dialysis against methanol/dichloromethane (MWCO 1000 DA). Nevertheless, it was not possible to remove the aluminum catalyst and initiator salt completely. However, all polymers exhibit a monomodal size distribution as displayed in **Figure 1**. The resulting copolymers had molecular weights in the range of 2350 to 38010 g mol^{-1} (SEC measurements in DMF using PEG standards) and moderate polydispersities from 1.27–1.44.

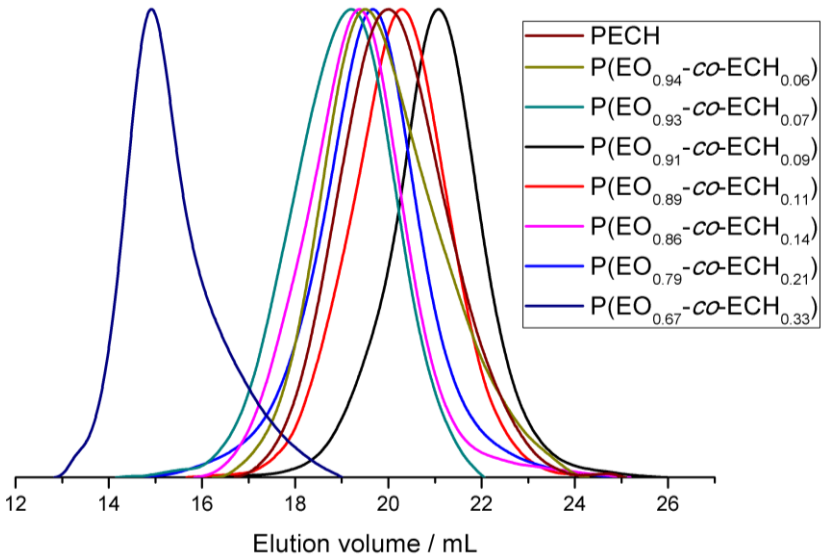

Figure 1. SEC traces (DMF, PEG standard, RI signal) of the synthesized PECH homopolymer and copolymers P(EO-*co*-ECH).

The molecular weights were close to expectation based on the amount of initiator employed. Only in some cases, slightly lower molecular weights were observed. This could be due to the complexation of trialkylaluminum by the oxygens of the formed copolymers at high conversion. Consequently, the concentration of the active monomer species decreases as reported earlier, resulting in slightly lower molecular weights.[7] The ECH comonomer content varied between 6 and 33 mol% in the copolymers and mirrored the concentration in the monomer feed (**Table 1**). The amount of ECH was kept low to preserve the properties of PEO on one hand, offering the possibility for functionalization leading to "multifunctional PEG" on the other. The fraction of incorporated ECH was calculated using ^{1}H NMR spectroscopy. For this purpose, the signal intensity of the methylene group next to the chlorine atom was compared to the signal intensity resulting from the backbone. The signals observed in the high field can be assigned to residual initiator salt, which could not be removed completely. The respective ^{1}H NMR spectrum is given in the Supporting Information (**Figure S7**). Characterization data like molecular weight, content of incorporated epichlorohydrin, polydispersity and thermal properties of the synthesized copolymers are summarized in **Table 1**.

Table 1. Properties of the synthesized PECH homopolymer and copolymers P(EO-*co*-ECH).

#	Composition[a]	[EO]/[ECH]th	M_n^{th}	$M_n^{SEC,b}$	$M_w/M_n^{SEC,b}$	T_g	T_m
		mol%	g mol^{-1}	g mol^{-1}		°C	°C
1	PECH	0:100	4710	3270	1.33	–32	-
2	P($EO_{0.94}$-co-$ECH_{0.06}$)	90:10	4970	3770	1.43	–55	46
3	P($EO_{0.93}$-co-$ECH_{0.07}$)	95:5	4730	6160	1.34	–54	49
4	P($EO_{0.91}$-co-$ECH_{0.09}$)	95:5	4730	2350	1.27	–49	51
5	P($EO_{0.89}$-co-$ECH_{0.11}$)	90:10	4970	3360	1.30	–54	42
6	P($EO_{0.86}$-co-$ECH_{0.14}$)	90:10	4970	5060	1.37	–52	40
7	P($EO_{0.79}$-co-$ECH_{0.21}$)	90:10	4970	4450	1.44	–53	38
8	P($EO_{0.67}$-co-$ECH_{0.33}$)	85:15	30870	38010	1.35	–50	38
9	PEO-4400	100:0	4400	4300[c]	-	–57[c]	59[c]

[a]Values determined by ^{1}H NMR spectroscopy.
[b]SEC measurements were performed in DMF using PEG standards.
[c]Data obtained from literature.[25]

The thermal properties of all polymers were analyzed using differential scanning calorimetry (DSC). The glass transition temperature T_g of PECH homopolymer (#**1**) is –32 °C, and no melting temperature T_m is detected, which is explained by the lack of tacticity. In literature, the T_g of PECH was reported to be between –36 °C and –18 °C for polymers with molecular weights ranging from 27500 g mol^{-1} to 1900 kg mol^{-1}.[30,33] The T_m of PEG strongly depends on the molecular weight.[34] The commercially available PEG-4400 with comparable molecular weight as the synthesized polymers exhibited a T_g of –57 °C and a T_m of 59 °C.[25] The copolymers prepared exhibit a T_g between –56 °C and –49 °C and a broad melting endotherm ranging from 38 °C to 51 °C (**Figure 2**). Thus, the thermal properties are similar to a PEG-4400 homopolymer. Remarkably, even copolymers with 33% ECH incorporation (sample 8, **Table 1**) still showed a melting endotherm at 38°C, indicating the presence of long PEG-homopolymer sequences in the statistical

copolymers. As can be seen in **Figure 2**, the melting point decreases with increasing ECH fraction, which can be explained by decreasing length of the PEG segments in the copolymers. Furthermore, the T_g increases with increasing ECH content (**Figure 2**). In general, the T_g is close to that of PEG-4400, because the ECH content was kept low (≤ 33 mol%) and hence had only little influence on the properties of the copolymers. In contrast to PECH (#**1**), which does not show melting, all copolymers exhibit a T_m. The measurements suggest the formation of long PEG segments and therefore a tapered structure for the copolymer P(EO-*co*-ECH). In order to obtain detailed information of the monomer gradient in the copolymer chains, *in situ* NMR kinetics of the statistical copolymerization under monomer-activated conditions was performed.

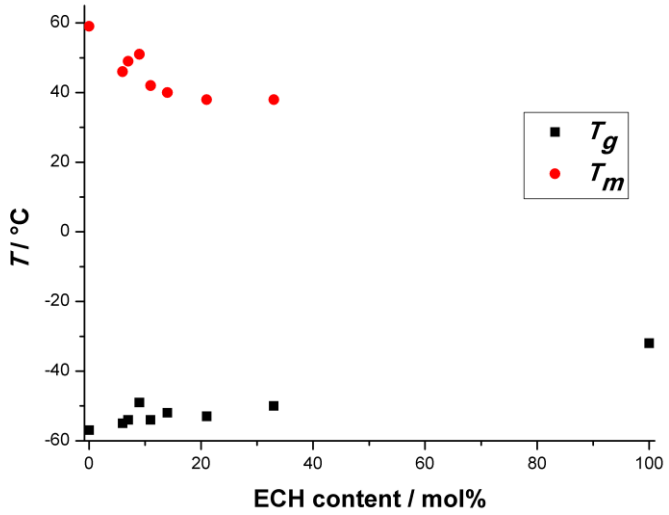

Figure 2. Thermal properties of the polymers synthesized. Glass transitions T_g vs. ECH content (mol%) and melting temperatures T_m vs. ECH content (mol%). Data for PEG-4400 was obtained from literature.[25]

B. *In situ* NMR kinetics

A ^{1}H NMR kinetics study was conducted to investigate the chain structure resulting from the statistical monomer-activated copolymerization of EO and ECH. In recent work, our group introduced a specific temperature program to monitor copolymerizations using the monomer-activated method via *in situ* NMR kinetics.[35] This study is challenging due to the low temperatures that have to be applied to monitor the monomer-activated copolymerization. In previous work from our group, the statistical copolymerization of EO and EEGE via the monomer-activated AROP revealed reactivity ratios of r_{EO} = 8.00 ± 0.16

and r_{EEGE} = 0.125 ± 0.003 resulting in a strongly tapered, block-like copolymer structure.[35] Heinen *et al.* recently investigated the copolymerization of glycidyl methyl ether (GME) and ethyl glycidyl ether (EGE) via the monomer-activated method, showing a random incorporation of these two glycidyl ether monomers.[26] Deffieux, Carlotti and coworkers studied the reactivity ratios of EO (r_{EO} = 2.05) and PO (r_{PO} = 0.013), under monomer-activation conditions, resulting in gradient copolymers and of PO (r_{PO} = 1.21) and ECH (r_{ECH} = 0.16), indicating a slightly higher reactivity of PO, resulting in isolated ECH units randomly distributed at the polymer chains.[7,24] To the best of our knowledge, the microstructure of copolymers from the two industrially relevant monomers EO and ECH via the monomer-activated AROP has not been investigated to date. Using the *in situ* NMR technique, it was possible to investigate the copolymerization of EO and ECH *in situ* and to calculate the corresponding reactivity ratios.[35]

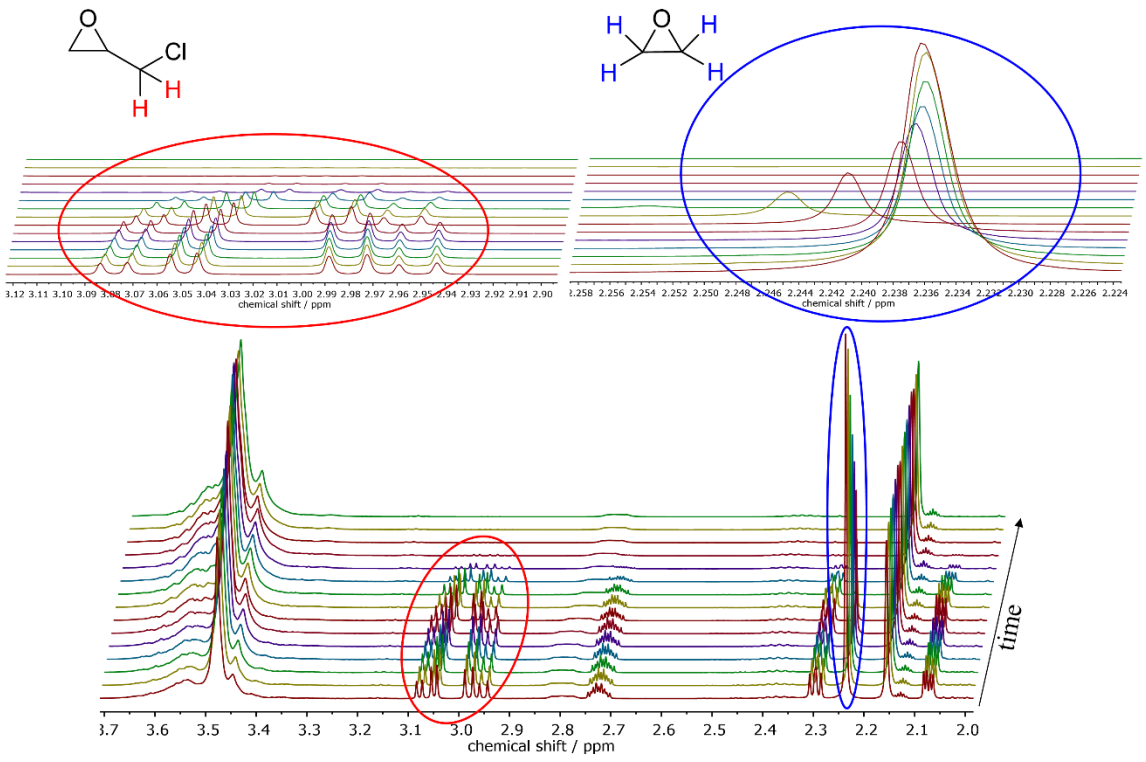

Figure 3. Selection of ^{1}H NMR spectra (400 MHz, toluene-d_8, 0 °C, 5 °C, 10 °C) of *in situ* NMR kinetics studies of the monomer-activated AROP of EO and ECH.

The monomer-activated AROP of EO and ECH was carried out in toluene-d_8 as a solvent. A sealed NMR tube was used for the measurement, providing the possibility for secure handling of EO and also to apply the same conditions for polymerization as in a conventional Schlenk flask. Due to the previous observation, that no significant

polymerization takes place below 0 °C,[35] the *in situ* NMR kinetics measurement was started at 0 °C.[35] The temperature was raised in 5 K steps every 70 min until full conversion was reached (174 min). A high ratio of catalyst/initiator ([*i*-Bu_3Al]/[$NOct_4Br$] ≥ 3.7) was chosen to achieve fast polymerization and full conversion without stirring. The SEC trace obtained from the crude sample (**Figure S16**) shows a monomodal size distribution and a moderate dispersity of 1.86, although stirring was not possible during ^1H NMR kinetics measurements. **Figure 3** shows a selection of NMR spectra of the kinetics experiment of EO (blue) and ECH (red). A decrease of the monomer signals as well as an increase of the broad backbone signal at 3.37–3.63 ppm with reaction progress can be observed. The measurement shows clearly that the incorporation of ECH is slower than of EO. As a result, EO rich segments are found in the proximity of the initiator, and ECH rich segments are situated at the termini of the chains.

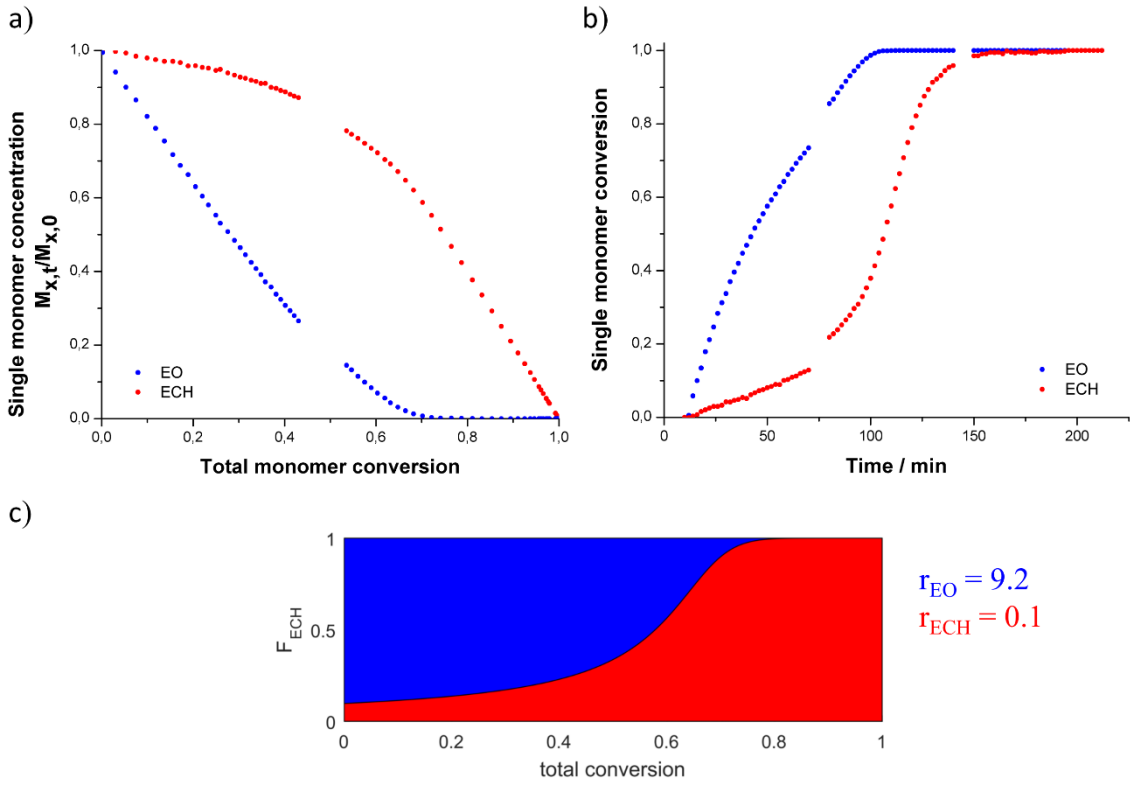

Figure 4. (a) Single monomer concentration vs. total monomer conversion for the monomer-activated AROP of EO (blue) and ECH (red); (b) single monomer conversion vs. time; (c) monomer distribution of a (hypothetical) P(EO-*co*-ECH) copolymer composed of 50 mol% EO (blue) and 50 mol% ECH (red), diagram according to a recently published procedure.[36]

The corresponding reactivity ratios were calculated using the Fineman-Ross formalism (**Figure S13**), and the resulting values were r_{EO} = 9.2 and r_{ECH} = 0.10. Single monomer concentration vs. total monomer conversion and the single monomer conversion vs. time plots are shown in **Figures 4a** and **4b**. In addition the distribution of EO and ECH units at the polymer chain of P(EO-*co*-ECH) with a (hypothetic) ratio of 50 mol% EO and 50 mol% ECH is visualized in **Figure 4c**. The reactivity ratios demonstrate that the statistical copolymerization of EO and ECH results in strongly tapered, block-like copolymer structures.

The thermal properties mentioned above mirror the strongly tapered structure, showing that P(EO-*co*-ECH) is a partially crystalline material with T_m in a range of 38 °C to 51 °C, depending on the amount of incorporated comonomer ECH. Long PEG segments that can crystallize are formed during the copolymerization. These results evidence that the simple statistical monomer-activated AROP of EO and ECH in a one-step, one-pot procedure leads to block copolymer like structures. Herzberger *et al.* observed the formation of tapered structures for the copolymerization of EO and ethoxyethyl glycidyl ether (EEGE) and proposed an interaction of all three oxygen atoms of EEGE with the Lewis acidic aluminum catalyst, leading to reduced interaction with the chain end shielded by the bulky ammonium counter ion and thus reduced reactivity.[35] Interestingly, also the copolymerization of EO and ECH studied in the current work leads to tapered block structures, despite the absence of oxygens capable of coordinating to the catalyst. Nevertheless, steric hindrance seems to play an important role. Carlotti and Deffieux and coworker also suggested steric hindrance for PO in the copolymerization with EO as a main reason for the reactivities observed, since bulky aluminum complexes are involved in the monomer addition.[24] This leads to the assumption that in case of the copolymerization of ECH steric hindrance is similarly relevant. Furthermore, Lewis-type interaction between the lone pairs of the chloride and the aluminum catalyst is possible. As a result, the activation of the epoxide ring is reduced, which decreases the reactivity of the ECH monomer.

C. Post-polymerization functionalization

The chloromethyl moieties in the copolymers enable further functionalization. Different functionalization reactions were carried out, resulting in a variety of multifunctional PEGs.[37] **Scheme 2** gives an overview of the post-polymerization reactions explored.

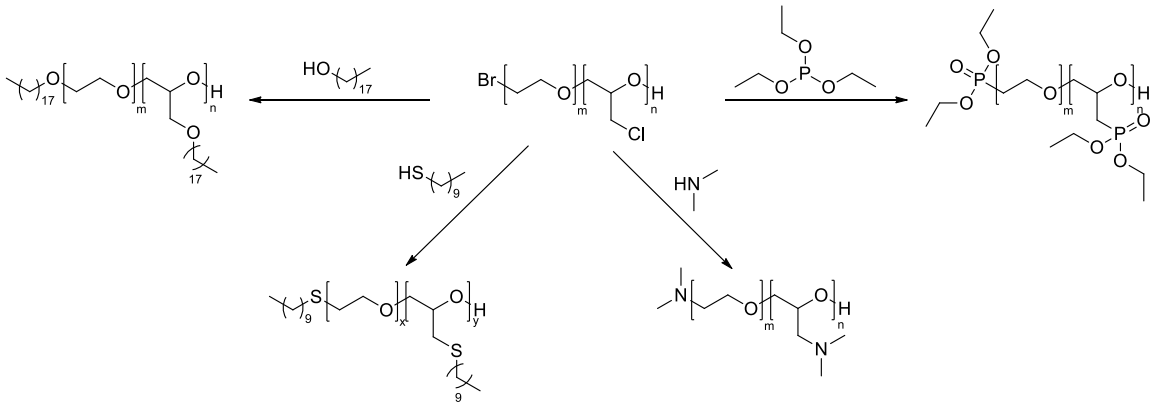

Scheme 2. Post-polymerization functionalizations of P(EO-*co*-ECH) with *n*-octadecanol (left) resulting in P(EO-*co*-ECH$^{n\text{-OD}}$), 1-decanthiol (middle, left) resulting in P(EO-*co*-ECH$^{1\text{-DT}}$), dimethylamine (middle, right) resulting in P(EO-*co*-ECH$^{\text{DMA}}$), and triethylphosphite (right) resulting in P(EO-*co*-ECH$^{\text{DEPE}}$).

Substitution of the chloride moiety with *n*-octadecanol was performed using sodium hydride (NaH), potassium *ter*t-butoxide (KOtBu), potassium naphthalenide and cesium hydroxide (CsOH). Using NaH the formed alkoxide was dried under vaccum for prolonged periods to remove moisture, and the reaction was carried out under an argon atmosphere. In order to ensure a complete deprotonation of the alkoxide, NaH and *n*-octadecanol was applied in a 1:1 ratio. The reaction was carried out for 5 h and 24 h, respectively, at elevated temperatures to obtain P(EO-*co*-ECH$^{n\text{-OD}}$). NMR spectroscopy and SEC measurements were carried out to confirm the functionalization. The attachment of the alkyl alcohol is observed by a shift of the SEC trace to lower elution volume, indicating an increase of molecular weight (**Figure S19**). Furthermore, the ^{1}H NMR spectrum (**Figure S17**) indicates successful functionalization, due to the new signals of the alkyl groups. Unfortunately, the ^{13}C NMR spectrum (**Figure S18**) reveals that a small signal for the chloromethyl group is still present. Hence, only partial functionalization was obtained. Also an increasing reaction time did not lead to full conversion. To generate a more reactive alkoxide, KOtBu, potassium naphthalenide and CsOH respectively were applied for deprotonation. In all three cases an elimination reaction instead of a substitution reaction was observed, which is due to the strongly basic nature of the alkoxide leading to an elimination instead of a substitution reaction with a primary, sterically hindered alkyl halide.[38] 2D NMR spectroscopy revealed that no covalent linkage between the polyether and the alkyl alcohol was formed and vinyl groups were observed. The signal for the chloromethyl group in the ^{13}C NMR spectrum vanished. In order to favor the substitution

reaction a weakly basic nucleophile, *i.e.* 1-decanthiol was used. The successful attachment of the alkyl thiol was proven by SEC measurement (**Figure S28**) and ^{1}H NMR spectroscopy. Nevertheless, in the ^{13}C NMR spectrum the signal of the chloromethyl group is also still present. Thus, also weakly basic nucleophiles only lead to partial substitution. In addition, a Michaelis-Arbuzov reaction and a substitution reaction using dimethylamine was performed. The functionalization was confirmed via ^{1}H NMR spectroscopy, SEC measurements (for the phosphonate-bearing polyether a lower molecular weight is observed due to interaction of the product with the column) and ^{31}P NMR spectroscopy. In the ^{13}C NMR spectra there is no shift observable between the chloromethyl groups and the functionalized methylene groups. Thus, full conversion is not absolutely certain although the applied reaction conditions were chosen to favor the formation of the functionalized product. However, due to the tapered structure of the copolymer all chloromethyl groups are in close proximity, which most likely limits conversion. Hence, the attachment of functional groups is possible, but full conversion is difficult to reach, due to the occurring competition between substitution and elimination reaction. In previous works also other groups reported only partial substitution of the chloromethyl groups of PECH prepared by cationic polymerization, *e.g.* Wang and coworkers applied a “grafting onto” strategy of poly(isoprene) (PI) and polystyrene (PS) and only reached grafting efficiencies up to 74% by applying 1,1-diephenylethylene (DPE) as coupling agent.[39]

Conclusion

The monomer-activated AROP was studied with respect to the statistical copolymerization of EO and ECH. The resulting copolymers showed molecular weights ranging from 2350 to 38010 g mol^{-1} (SEC) and moderate polydispersities of 1.27–1.44 (SEC measurements in DMF using PEG standards). The ECH content was kept low (6 to 33 mol%) to preserve the properties of PEG, but at the same time enable the attachment of functional groups, leading to multifunctional PEG.[39] An unexpected feature of the resulting copolymers is their tapered, *i.e.*, block-like structure obtained *via* statistical copolymerization, observed directly by *in situ* NMR kinetics. The reactivity ratios of EO and ECH were determined to be strongly disparate, *i.e.*, r_{EO} = 9.2 and r_{ECH} = 0.10. Consequently, the copolymers exhibit EO rich segments close to the initiator and ECH rich segments in proximity to the terminus.

These results are important findings to further understand the mechanism of the monomer-activated AROP and explain the thermal properties of the copolymers. A crystallizable PEG block was observed as a consequence of the block like structure. The resulting copolymers offer a broad platform for a variety of functionalization reactions. Nucleophilic substitution reactions as well as a Michaelis-Arbuzov reaction were performed to attach different groups at the polyether backbone. Nevertheless, a competition between substitution and elimination reaction as well as only partial functionalization was observed. Hence, the reaction conditions have to be chosen carefully. The results demonstrate that epichlorohydrin-based block copolymers with PEG block that are not accessible by oxyanionic sequential copolymerization can be prepared by monomer-activated statistical copolymerization.

Acknowledgments

A. Danner is a recipient of a DFG-funded position through the Excellence Initiative by the Graduate School Materials Science in Mainz (GSC 266). The authors thank Dr. Johannes C. Liermann and Nadine Schenk for technical assistance during *in situ* NMR kinetics measurements as well as Maria Mueller and Monika Schmelzer for DSC and SEC measurements. Jan Blankenburg is acknowledged for help with the evaluation of *in-situ* NMR data.

References

(1) Frey, H.; Haag, R. Dendritic polyglycerol: A new versatile biocompatible material. *Reviews in Molecular Biotechnology* **2002**, *90*, 257–267.

(2) Kainthan, R. K.; Janzen, J.; Levin, E.; Devine, D. V.; Brooks, D. E. Biocompatibility testing of branched and linear polyglycidol. *Biomacromolecules* **2006**, *7*, 703–709.

(3) Thomas, A.; Müller, S. S.; Frey, H. Beyond poly(ethylene glycol): linear polyglycerol as a multifunctional polyether for biomedical and pharmaceutical applications. *Biomacromolecules* **2014**, *15*, 1935–1954.

(4) Weinhart, M.; Grunwald, I.; Wyszogrodzka, M.; Gaetjen, L.; Hartwig, A.; Haag, R. Linear poly(methyl glycerol) and linear polyglycerol as potent protein and cell resistant alternatives to poly(ethylene glycol). *Chem. Asian J.* **2010**, *5*, 1992–2000.

(5) Gosecki, M.; Gadzinowski, M.; Gosecka, M.; Basinska, T.; Slomkowski, S. Polyglycidol, Its Derivatives, and Polyglycidol-Containing Copolymers—Synthesis and Medical Applications. *Polymers* **2016**, *8*, 227.

(6) Calderón, M.; Quadir, M. A.; Sharma, S. K.; Haag, R. Dendritic polyglycerols for biomedical applications. *Adv. Mater.* **2010**, *22*, 190–218.

(7) Carlotti, S.; Labbé, A.; Rejsek, V.; Doutaz, S.; Gervais, M.; Deffieux, A. Living/Controlled Anionic Polymerization and Copolymerization of Epichlorohydrin with Tetraoctylammonium Bromide−Triisobutylaluminum Initiating Systems. *Macromolecules* **2008**, *41*, 7058–7062.

(8) Biedron, T.; Kubisa, P.; Penczek, S. Polyepichlorohydrin diols free of cyclics: Synthesis and characterization. *J. Polym. Sci. A Polym. Chem.* **1991**, *29*, 619–628.

(9) Vandenberg, E. J. Organometallic catalysts for polymerizing monosubstituted epoxides. *J. Polym. Sci.* **1960**, *47*, 486–489.

(10) Xie, H.-Q.; Guo, J.-S.; Yu, G.-Q.; Zu, J. Ring-opening polymerization of epichlorohydrin and its copolymerization with other alkylene oxides by quaternary catalyst system. *J. Appl. Polym. Sci.* **2001**, *80*, 2446–2454.

(11) Wu, J.; Shen, Z. Rare Earth Coordination Catalysts for the Polymerization of Alkylene Oxides I. Polymerization of Epichlorohydrin. *Polym J* **1990**, *22*, 326–330.

(12) Hsieh, H. L. Polymerization of alkylene oxides with trialkylaluminum, metal acetylacetonates, and water. *J. Appl. Polym. Sci.* **1971**, *15*, 2425–2438.

(13) Kuntz, I.; Kroll, W. R. Polymerization of epoxides with dialkylaluminum acetylacetonate catalyst systems. *J. Polym. Sci. A-1 Polym. Chem.* **1970**, *8*, 1601–1621.

(14) Yagci, Y.; Serhatli, I. E.; Kubisa, P.; Biedron, T. Synthesis of block copolymers by combination of an activated monomer and free radical polymerization mechanism. *Macromolecules* **1993**, *26*, 2397–2399.

(15) Xie, H.-Q.; Pan, S.-B.; Guo, J.-S. Ring-opening copolymerization of epoxy-terminated polystyrene macromer with epichlorohydrin and study on properties of the copolymers. *European Polymer Journal* **2003**, *39*, 715–724.

(16) Royappa, A. T. On the copolymerization of epichlorohydrin and glycidol. *J. Appl. Polym. Sci.* **1997**, *65*, 1897–1904.

(17) Majid, M. A.; George, M. H.; Barrie, J. A. Living anionic synthesis and characterization of poly(epichlorohydrin-g-styrene) copolymers. *Polymer* **1981**, *22*, 1104–1111.

(18) Kohjiya, S.; Horiuchi, T.; Miura, K.; Kitagawa, M.; Sakashita, T.; Matoba, Y.; Ikeda, Y. Polymer solid electrolyte from amorphous poly[epichlorohydrin-co-(ethylene oxide)]/lithium perchlorate complex. *Polym. Int.* **2000**, *49*, 197–202.

(19) Kuntz, I.; Cozewith, C.; Oakley, H. T.; Via, G.; White, H. T.; Wilchinsky, Z. W. Epoxide Copolymerization with the Dialkylaluminum Acetylacetonate-Dialkylzinc-Water Catalyst System. *Macromolecules* **1971**, *4*, 4–10.

(20) Gervais, M.; Brocas, A.-L.; Cendejas, G.; Deffieux, A.; Carlotti, S. Synthesis of Linear High Molar Mass Glycidol-Based Polymers by Monomer-Activated Anionic Polymerization. *Macromolecules* **2010**, *43*, 1778–1784.

(21) Gervais, M.; Brocas, A.-L.; Cendejas, G.; Deffieux, A.; Carlotti, S. Linear High Molar Mass Polyglycidol and its Direct α-Azido Functionalization. *Macromol. Symp.* **2011**, *308*, 101–111.

(22) Billouard, C.; Carlotti, S.; Desbois, P.; Deffieux, A. "Controlled" High-Speed Anionic Polymerization of Propylene Oxide Initiated by Alkali Metal Alkoxide/Trialkylaluminum Systems. *Macromolecules* **2004**, *37*, 4038–4043.

(23) Labbé, A.; Carlotti, S.; Billouard, C.; Desbois, P.; Deffieux, A. Controlled High-Speed Anionic Polymerization of Propylene Oxide Initiated by Onium Salts in the Presence of Triisobutylaluminum. *Macromolecules* **2007**, *40*, 7842–7847.

(24) Rejsek, V.; Sauvanier, D.; Billouard, C.; Desbois, P.; Deffieux, A.; Carlotti, S. Controlled Anionic Homo- and Copolymerization of Ethylene Oxide and Propylene Oxide by Monomer Activation. *Macromolecules* **2007**, *40*, 6510–6514.

(25) Müller, S. S.; Moers, C.; Frey, H. A Challenging Comonomer Pair: Copolymerization of Ethylene Oxide and Glycidyl Methyl Ether to Thermoresponsive Polyethers. *Macromolecules* **2014**, *47*, 5492–5500.

(26) Heinen, S.; Rackow, S.; Schäfer, A.; Weinhart, M. A Perfect Match: Fast and Truly Random Copolymerization of Glycidyl Ether Monomers to Thermoresponsive Copolymers. *Macromolecules* **2017**, *50*, 44–53.

(27) Gervais, M.; Labbé, A.; Carlotti, S.; Deffieux, A. Direct Synthesis of α-Azido,ω-hydroxypolyethers by Monomer-Activated Anionic Polymerization. *Macromolecules* **2009**, *42*, 2395–2400.

(28) Rodriguez, C. G.; Ferrier, R. C.; Helenic, A.; Lynd, N. A. Ring-Opening Polymerization of Epoxides: Facile Pathway to Functional Polyethers via a Versatile Organoaluminum Initiator. *Macromolecules* **2017**, *50*, 3121–3130.

(29) Lundberg, P.; Lee, B. F.; van den Berg, S. A.; Pressly, E. D.; Lee, A.; Hawker, C. J.; Lynd, N. A. Poly(ethylene oxide)-co-(methylene ethylene oxide): A hydrolytically-degradable poly(ethylene oxide) platform. *ACS Macro Lett.* **2012**, *1*, 1240–1243.

(30) Meyer, J.; Keul, H.; Möller, M. Poly(glycidyl amine) and Copolymers with Glycidol and Glycidyl Amine Repeating Units: Synthesis and Characterization. *Macromolecules* **2011**, *44*, 4082–4091.

(31) Brocas, A.-L.; Cendejas, G.; Caillol, S.; Deffieux, A.; Carlotti, S. Controlled synthesis of polyepichlorohydrin with pendant cyclic carbonate functions for isocyanate-free polyurethane networks. *J. Polym. Sci. A Polym. Chem.* **2011**, *49*, 2677–2684.

(32) Hu, H.; Yuan, W.; Lu, L.; Zhao, H.; Jia, Z.; Baker, G. L. Low glass transition temperature polymer electrolyte prepared from ionic liquid grafted polyethylene oxide. *J. Polym. Sci. A Polym. Chem.* **2014**, *52*, 2104–2110.

(33) Chipara, M. I.; Barb, D.; Notingher, P. V.; Georgescu, L.; Sarbu, T. Spin probe investigation of molecular motions in polyepichlorohydrin: 1. *Polymer* **1996**, *37*, 707–712.

(34) Mandelkern, L. The Crystallization Of Flexible Polymer Molecules. *Chem. Rev.* **1956**, *56*, 903–958.

(35) Herzberger, J.; Leibig, D.; Liermann, J. C.; Frey, H. Conventional Oxyanionic versus Monomer-Activated Anionic Copolymerization of Ethylene Oxide with Glycidyl

Ethers: Striking Differences in Reactivity Ratios. *ACS Macro Lett.* **2016**, *5*, 1206–1211.

(36) Blankenburg, J.; Wagner, M.; Frey, H. Well-Defined Multi-Amino-Functional and Stimuli-Responsive Poly(propylene oxide) by Crown Ether Assisted Anionic Ring-Opening Polymerization. *Macromolecules* **2017**, *50*, 8885–8893.

(37) Obermeier, B.; Wurm, F.; Mangold, C.; Frey, H. Multifunctional Poly(ethylene glycol)s. *Angew. Chem. Int. Edit.* **2011**, *50*, 7988–7997.

(38) Clayden, J.; Greeves, N.; Warren, S. G. *Organic chemistry*, 2. ed.; Oxford Univ. Press: Oxford, 2012.

(39) Tang, T.; Fan, X.; Jin, Y.; Wang, G. Synthesis and characterization of graft copolymers with poly(epichlorohydrin- co -ethylene oxide) as backbone by combination of ring-opening polymerization with living anionic polymerization. *Polymer* **2014**, *55*, 3680–3687.

Supporting Information

Monomer-activated Copolymerization of Ethylene Oxide and Epichlorohydrin: *In Situ* Kinetics Evidences Tapered Block Copolymer Formation

Ann-Kathrin Danner,[a,b] Daniel Leibig,[a,b] Lea-Marie Vogt[a] and Holger Frey[a, *]

[a]Institute of Organic Chemistry, Johannes Gutenberg-University Mainz, Duesbergweg 10-14, 55128 Mainz, Germany.

[b]Graduate School Materials Science in Mainz, Staudinger Weg 9, 55128 Mainz, Germany.

E-Mail: hfrey@uni-mainz.de

1. Materials and Methods

1.1 Reagents

All reagents and solvents were purchased *from Sigma-Aldrich, Acros Organics* or *Fisher Scientific* and used as received, unless otherwise mentioned. Deuterated solvents were acquired from *Deutero GmbH*. Epichlorohydrin was dried over CaH_2 for at least 30 min and freshly distilled prior to use. For the anionic ring-opening polymerization (AROP) toluene was dried and stored over benzophenone/sodium. The flammable, toxic and gaseous ethylene oxide (EO) must be handled with care and was stored in pressure-proof gas bottles. EO is polymerized in flame-dried glassware to permit secure handling via cryo-transfer techniques and to convert EO inside the sealed and evacuated glass apparatus.

1.2 Characterization

^{1}H, ^{13}C and ^{31}P NMR spectroscopy as well as COSY (correlation spectroscopy), HSQC (heteronuclear single quantum coherence) and HMBC (heteronuclear multiple bond correlation) spectra were recorded using a Bruker Avance III HD 300 operated at 300 MHz and a Bruker AC 400 spectrometer operated at 400 MHz. DMSO-d_6, toluene-d_8, benzene-d_6, D_2O or MeOD was employed as solvent and the spectra were referenced internally to proton signals of the deuterated solvent. The analysis of the NMR spectra was conducted applying the Software MestReNova (Version 9.0). SEC measurements were performed in dimethylformamide or water (with 0.05 vol% TFA) with 0.25 g L^{-1} lithium bromide employing an Agilent 1100 Series equipped with PSS HEMA 300/100/40 column, RI and UV detector (275 nm). Calibration was carried out using poly(ethylene glycol) standards from Polymer Standards Service (PSS). SEC traces were analyzed with PSS WinGPC Unity. DSC measurements were carried out on a Perkin Elmer 8200 differential scanning calorimeter. 3 to 4 mg of a sample were measured in a temperature range of –90 to 100 °C (first cycle, heating rate 20 °C min^{-1}) respectively from –90 to 80 °C (second cycle, heating rate 10 °C min^{-1}). For analysis, the values for the second cycle were used. Calibration was performed using the melting points of indium (T_m = 156.6 °C) and Milli-Q water (T_m = 0 °C).

2. Synthesis

2.1 Poly(epichlorohydrin) (PECH) homopolymer

The synthesis was carried out in orientation to literature.[1]

The polymerization was carried out for 24 h in toluene with [*i*-Bu_3Al]/[$NOct_4Br$] = 3.0 and temperatures ranging from −10 °C to room temperature. After 24 h the polymerization was quenched by adding an excess of ethanol. The reaction mixture was precipitated in cold methanol and the resulting polymer dried in vacuo. Yield: 61%.

^{1}H NMR, COSY (400 MHz, DMSO-d_6): δ (ppm) = 3.80–3.75 (m, -CH_2Cl) 3.71–3.64 (m, polymer backbone).

^{13}C NMR, HSQC, HMBC (101 MHz, DMSO-d_6): δ (ppm) = 78.2 (-CH_2*C*HO-), 68.7 (-*C*H_2CHO-), 44.1 (-*C*H_2Cl).

2.2 Copolymerization of poly(ethylene oxide-*co*-epichlorohydrin) P(EO-*co*-ECH)

The copolymerization is described for P($EO_{0.94}$-co-$ECH_{0.06}$) as a representative example.

Tetra(*n*-octyl)ammonium bromide (TOAB) (0.268 g, 0.489 mmol, 1 eq.) was placed in a dry Schlenk flask and dissolved in benzene (10 mL). The mixture was stirred under reduced pressure and dried under vacuum to remove moisture for 16 h. To dissolve the initiator, toluene (10 mL) was cryo-transferred into the Schlenk flask. Subsequently, a 1.1 M solution of triisobutylaluminum (TIBAL) (0.578 mL, 0.636 mmol, 1.3 eq.) in toluene was added and the solution was stirred to allow the formation of the initiator complex. Epichlorohydrin was injected into the Schlenk flask via syringe at −80 °C and ethylene oxide (0.348 mL, 4.893 mmol, 10 eq.) was cryo-transferred using a graduated ampule. The polymerization was carried out for 24 h starting at −30 °C and rose slowly to room temperature. The polymerization was quenched by adding an excess of ethanol. The solvents were removed under reduced pressure and the crude product was precipitated in cold diethyl ether. In order to remove residual initiator the polymer was dialyzed against methanol/dichloromethane (1:1) for 48 h (MWCO 1000 DA) and dried in vacuo. Yield: 75%.

^{1}H NMR, COSY (300 MHz, DMSO-d_6): δ (ppm) = 3.75–3.61 (m, -CH_2Cl, -CH_2C*H*O-), 3.57–3.47 (m, polymer backbone).

^{13}C NMR, HSQC, HMBC (101 MHz, DMSO-d_6): δ (ppm) = 77.7 (-CH_2*C*HO-), 69.9 (polymer backbone), 44.8 (-*C*H_2Cl).

2.3 ^{1}H NMR kinetics study of the monomer-activated anionic ring opening copolymerization of P(EO-*co*-ECH)

The ^{1}H NMR kinetics study was carried out using a Norell S-500-VT-7 NMR tube sealed with a Teflon stop-cock. In order to prepare the initiator solution, 35.45 mg of tetra(*n*-octyl)ammonium bromide (TOAB) was placed in a Schlenk flask and freeze-dried with 3 mL benzene for 24 h. The dried initiator was then dissolved in 0.5 mL of toluene-d_8 to obtain the initiator solution. Epichlorohydrin (ECH) was dried over CaH_2 and cryo-transferred prior to use. Before conducting the ^{1}H NMR kinetics study the NMR tube was evacuated. Afterwards, 0.1 mL of the initiator solution (TOAB, 1 eq.) and 0.2 mL of toluene-d_8 was added under argon atmosphere while the NMR tube was cooled down in an aceton/dry ice bath. 60 µL of a 1.1 M solution of TIBAL (3.7 eq.) in toluene was added under argon atmosphere using a syringe, followed by 0.2 mL toluene-d_8 and 40 µL of the comonomer ECH (8 eq.). Further, 0.1 mL of toluene-d_8 was added. Prior to cryo-tranferring EO, the NMR tube was cooled with liquid nitrogen and evacuated under vacuum. EO (34 eq.) was transferred applying static vacuum. The NMR tube was closed with a Teflon stop-cock and further sealed with parafilm. The reaction mixture was cooled again in an aceton/dry ice bath until the measurement was conducted. Before the measurement was started, the tube was dried from the outside and shaken intensely to mix the solution. The tube was placed in the NMR spectrometer with the gas flow adjusted to 0 °C. Sample spinning was turned off and the first spectrum was recorded after the temperature was stable. Spectra were recorded every 2 minutes with 16 scans. The temperature was kept at 0 °C for 70 min, then raised to 5 °C for another 70 min whereas all other parameters were kept constant. The temperature was then set to 10 °C until full conversion (34 min). The copolymer obtained from the ^{1}H NMR kinetics study had a molecular weight of M_n^{SEC} = 6540 g mol^{-1} calculated via SEC measurement in DMF using PEG standards and a polydispersity of 1.86 (**Figure S14**).

2.4 Functionalization of P(EO-*co*-ECH) with *n*-octadecanol P(EO-*co*-ECH$^{n\text{-OD}}$)

n-Octadecanol (0.150 g, 0.557 mmol, 3.5 eq. per ECH unit) and sodium hydride (0.013 g, 0.557 mmol, 3.5 eq. per ECH unit) were placed in a dry Schlenk flask and dissolved in benzene. The solution was stirred at 60 °C for 1 h to enable the formation of the alkoxide

and dried under vacuum for 24 h. The polymer P($EO_{0.94}$-co-$ECH_{0.06}$) and the alkoxide was dissolved in dry toluene. The polymer solution was injected into the Schlenk flask via syringe and stirred for 5 h at 50 °C. The solvent was removed and the crude product was suspended in methanol and precipitated in cold diethyl ether to obtain the pure product. Yield: 42%.

^{1}H NMR, COSY (300 MHz, benzene-d_6): δ (ppm) = 3.79–3.21 (m, polymer backbone, -OCH_2CH_2-), 1.63–1.55 (m, -OCH_2CH_2-), 1.43–1.16 (m, -(CH_2)$_{15}$CH_3), 0.93–0.88 (m, -(CH_2)$_{15}$CH_3).

^{13}C NMR, HSQC, HMBC (101 MHz, benzene-d_6): δ (ppm) = 78.8 (-CH_2CHO-), 70.8 (polymer backbone), 59.7 (-OCH_2CH_2-), 31.3 (-(CH$_2$)$_{15}$CH$_3$), 29.8 (-(CH$_2$)$_{15}$CH$_3$).

2.5 Functionalization of P(EO-*co*-ECH) with 1-decanthiol P(EO-*co*-ECH$^{1\text{-DT}}$)

Sodium hydroxide (0.006 g, 0.160 mmol, 50 eq.) was dissolved in methanol at 0°C. 1-Decanthiol (0.001 mL, 0.004 mmol, 1.2 eq.) was added slowly at 0 °C and the solution was stirred for 1 h. Afterwards, P($EO_{0.94}$-*co*-$ECH_{0.06}$) (0.1 mg, 0.003 mmol, 1 eq.) was added and the solution was heated up to 75 °C and stirred for 14 h. The solvent was removed and the crude product was suspended in methanol and precipitated in cold diethyl ether to obtain the pure product as colorless powder. Yield: 69%.

^{1}H NMR, COSY (300 MHz, methanol-d_4): δ (ppm) = 3.90–3.84 (m, -CHCH$_2$S-), 3.80–3.38 (m, polymer backbone), 2.72–2.64 (m, -CH_2S-), 2.61–2.54 (m, -SCH_2-), 1.64–1.53 (m, -SCH$_2$CH_2-), 1.44–1.24 (m, -CH$_2$(CH_2)$_7$CH$_3$), 0.94–0.86 (m, -(CH$_2$)$_7$CH_3).

^{13}C NMR, HSQC, HMBC (101 MHz, methanol-d_4): δ (ppm) = 80.0 (-*C*HCH$_2$S-), 71.7 (polymer backbone), 33.1 (-*C*H$_2$S-, -S*C*H$_2$-), 32.3 (-SCH$_2$*C*H$_2$-), 30.8-29.9 (-CH$_2$(*C*H$_2$)$_6$CH$_2$-), 23.7 (-(CH$_2$)$_6$*C*H$_2$CH$_3$), 14.5 (-CH$_2$*C*H$_3$).

2.6 Functionalization of P(EO-*co*-ECH) with triethylphosphite in a michaelis-arbuzov reaction P(EO-*co*-ECH$^{\text{DEPE}}$)

P($EO_{0.94}$-*co*-$ECH_{0.06}$) (0.15 g, 0.004 mmol, 1 eq.) was placed in a flask and dissolved in triethylphosphite (0.6 mL,3.503 mmol, 880 eq.). The solution was stirred at 150 °C for 5h. In order to influence the chemical equilibrium, the formed chloroethane was removed during the reaction by distillation. At the end of the reaction, the remaining triethylphosphite was removed under reduced pressure and the crude product was

suspended in water and precipitated in cold diethyl ether. The product was dried via lyophilisation to obtain a colorless solid. Yield: 35%.

^{1}H NMR, COSY (300 MHz, D_2O): δ (ppm) = 4.19–4.08 (m, -POC*H*$_2$CH$_3$-), 3.95–3.60 (polymer backbone), 2.32–2.19 (m, -CHC*H*$_2$P-), 1.36–1.22 (m, -POCH$_2$C*H*$_3$-).

^{31}P NMR (121.5 MHz, D_2O): δ (ppm) = 32.4 (-*P*OCH$_2$CH$_3$-).

^{13}C NMR, HSQC, HMBC (101 MHz, D_2O): δ (ppm) = 77.7 (-CH$_2$*C*HO-), 69.5 (polymer backbone), 43.2 (-*C*H$_2$PO-), 15.6 (-POCH$_2$*C*H$_3$).

2.7 Functionalization of P(EO-*co*-ECH) with dimethylamine P(EO-*co*-ECH^{DMA})

P(EO$_{0.93}$-*co*-ECH$_{0.07}$) (0.10 g, 0.024 mmol, 1 eq.) was placed in a flask and dissolved in water (6 mL). The solution was cooled to 0 °C and dimethylamine (40 wt% in water) (0.11 mL, 2.10 mmol, 5 eq. per ECH unit) was added via syringe. The reaction mixture was stirred for 24 h at room temperature. At the end of the reaction, the remaining dimethylamine via evaporation and the crude product was dried by lyophilisation. To remove impurities, the polymer was dissolved in dichloromethane (4 mL) and extracted three times with 1M NaOH (3 mL) and once with saturated sodium chloride solution. The solvent was removed under reduced pressure to obtain the product as a colorless solid. Yield: 58%.

^{1}H NMR. COSY (400 MHz, benzene-d_6): δ (ppm) = 4.12–4.11 (m, -C*H*CH$_2$N-), 3.68–3.25 (polymer backbone), 2.56–2.49 (d, 15.7 Hz - CHC*H*$_2$N-), 2.19–2.12 (m, - N(C*H*$_3$)$_2$).

^{13}C NMR, HSQC, HMBC (101, benzene-d_6): δ (ppm) = 79.4 (-*C*HCH$_2$N-), 71.3 (polymer backbone), 70.4 (-CH*C*H$_2$N-), 44.7 (-N(*C*H$_3$)$_2$).

3. Characterization Data

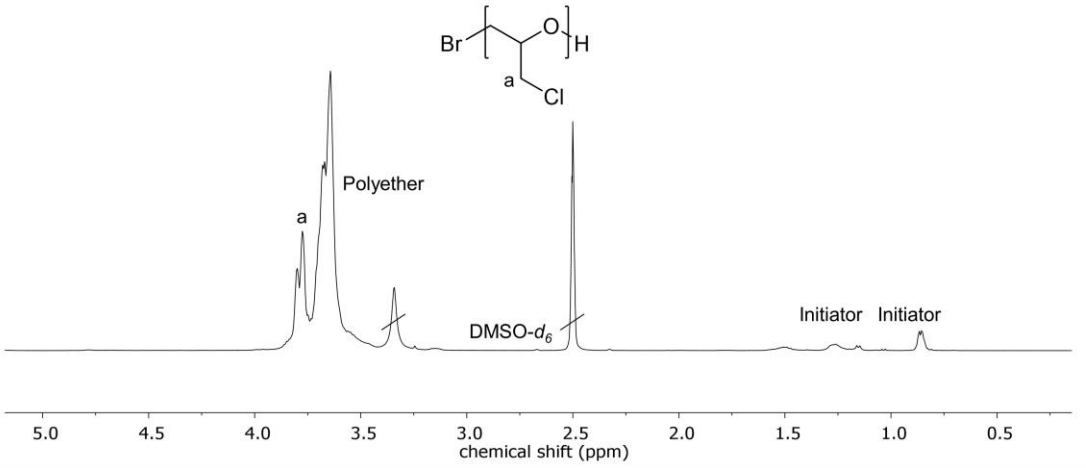

Figure S1. ^{1}H NMR (DMSO-d_6, 400 MHz) of PECH.

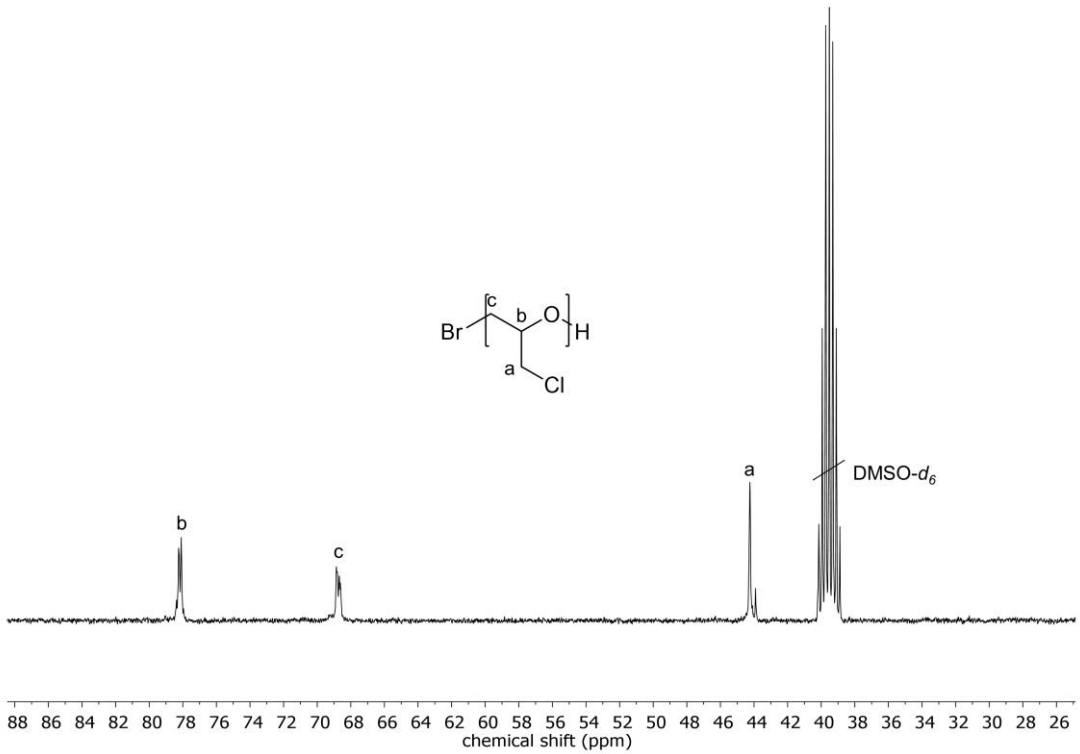

Figure S2. ^{13}C NMR (DMSO-d_6, 101 MHz) of PECH.

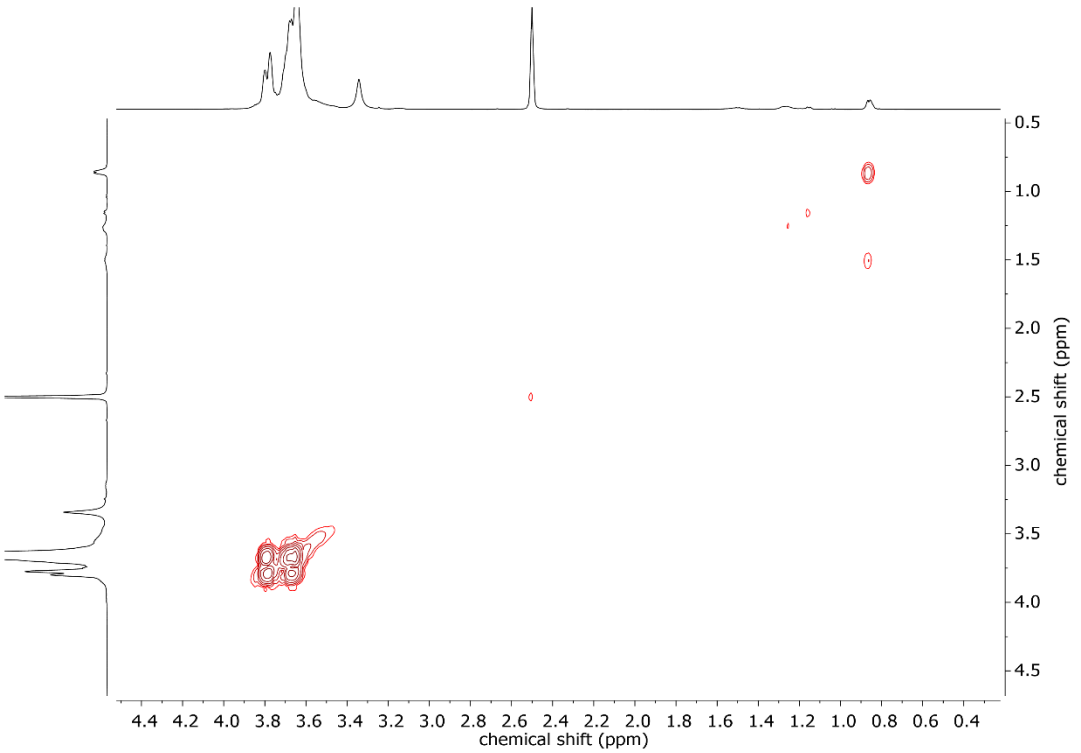

Figure S3. COSY NMR (DMSO-d_6, 400 MHz) of PECH.

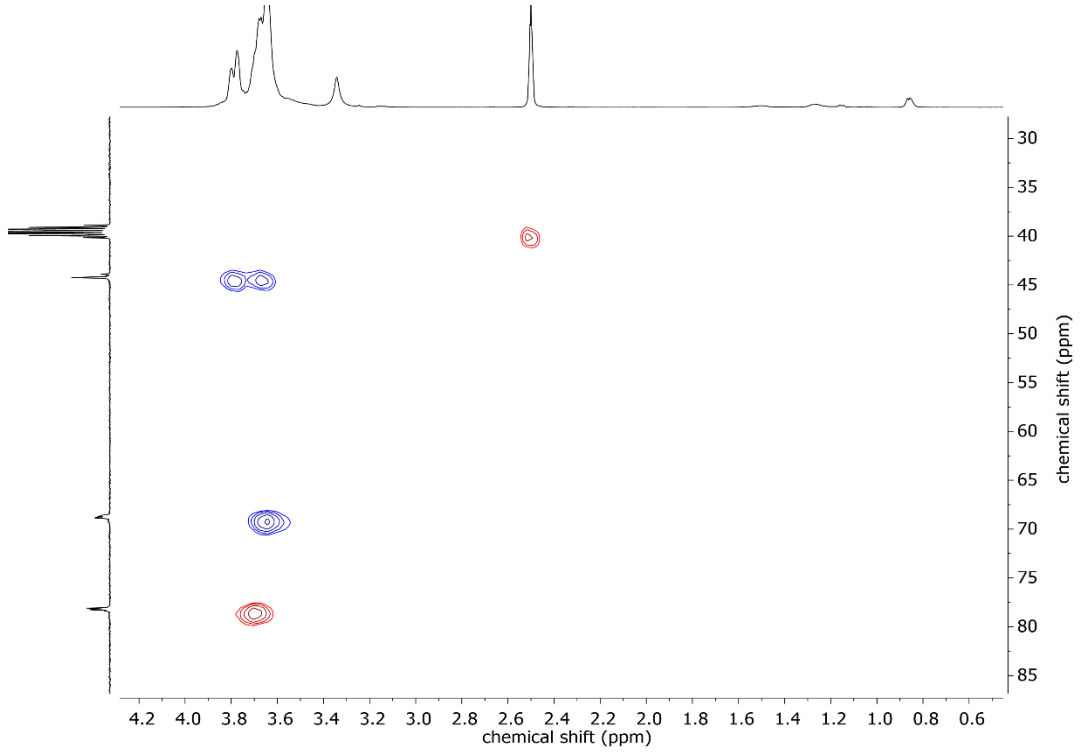

Figure S4. HSQC NMR (DMSO-d_6) of PECH.

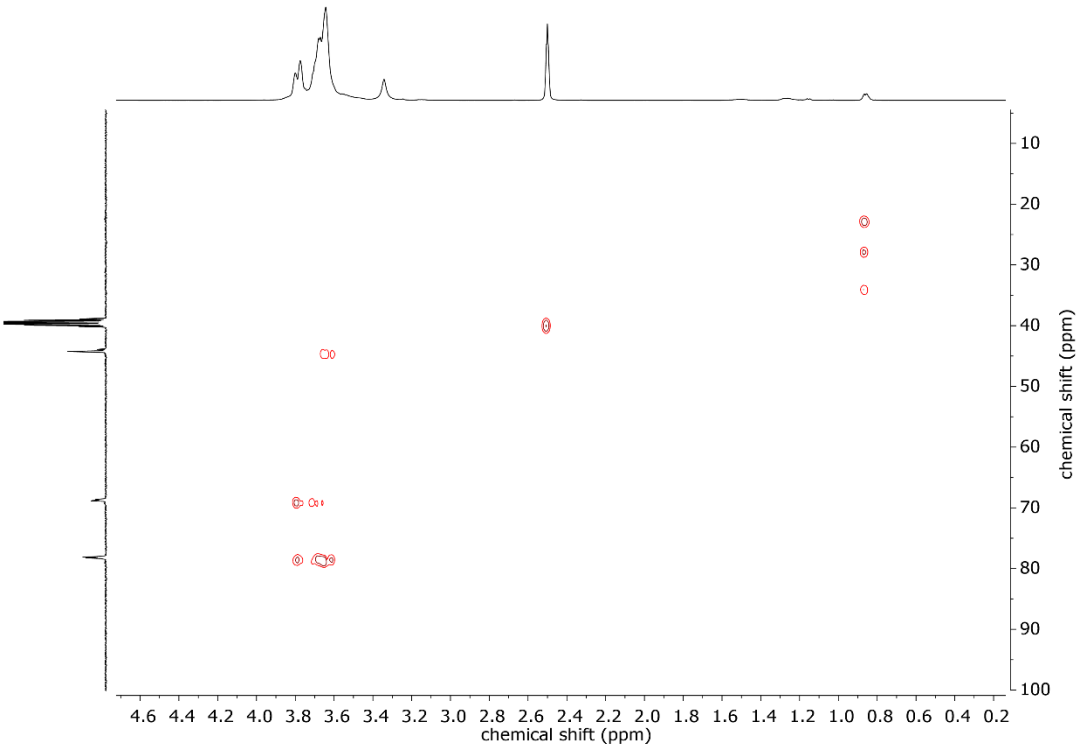

Figure S5. HMBC NMR (DMSO-d_6) of PECH.

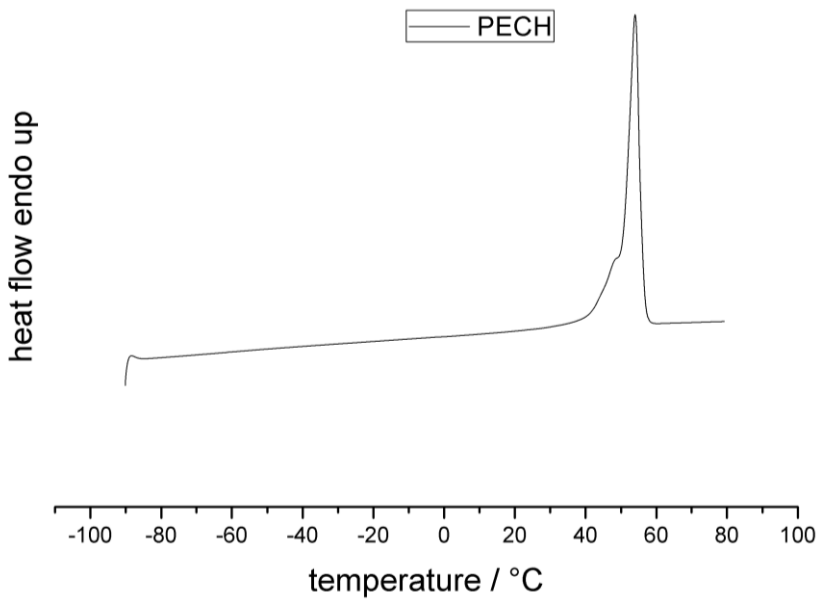

Figure S6. Plot of DSC measurement of PECH.

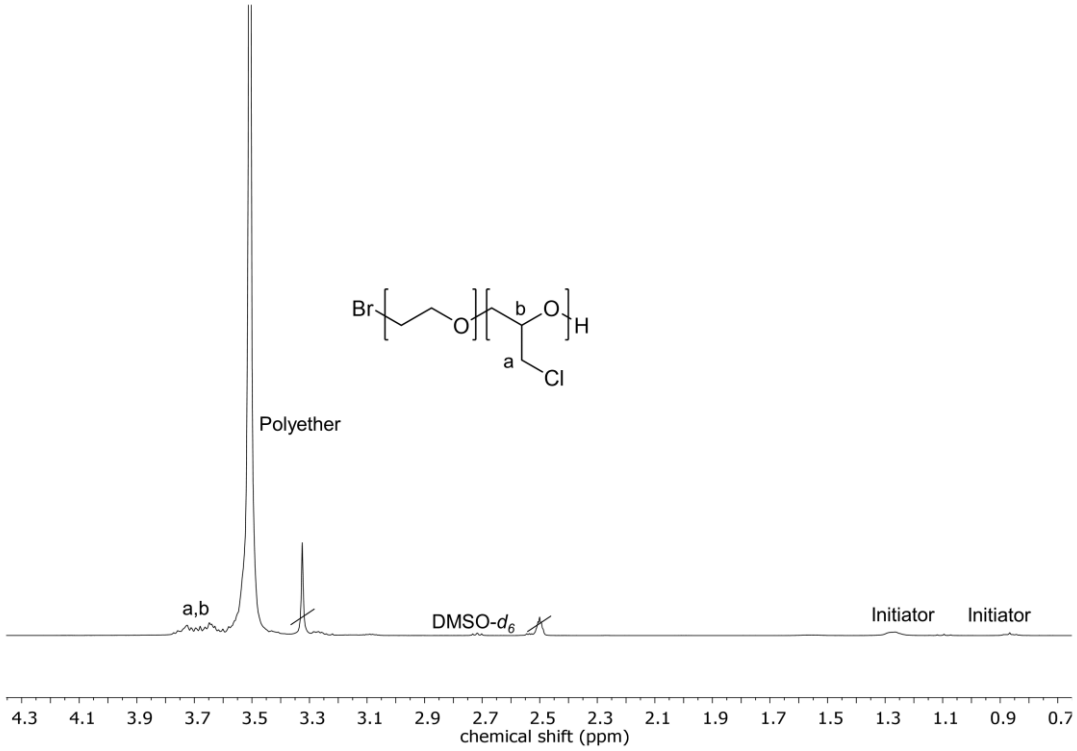

Figure S7. ^{1}H NMR (DMSO-d_6, 300 MHz) of P($EO_{0.94}$-*co*-$ECH_{0.06}$).

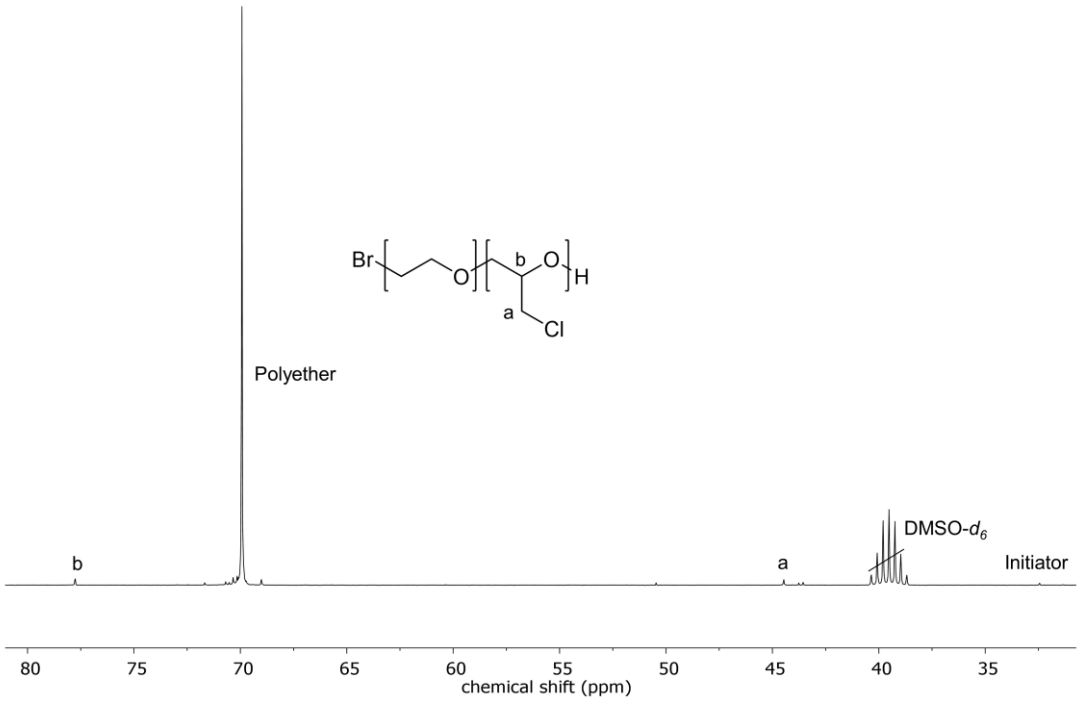

Figure S8. ^{13}C NMR (DMSO-d_6, 75 MHz) of P($EO_{0.94}$-*co*-$ECH_{0.06}$).

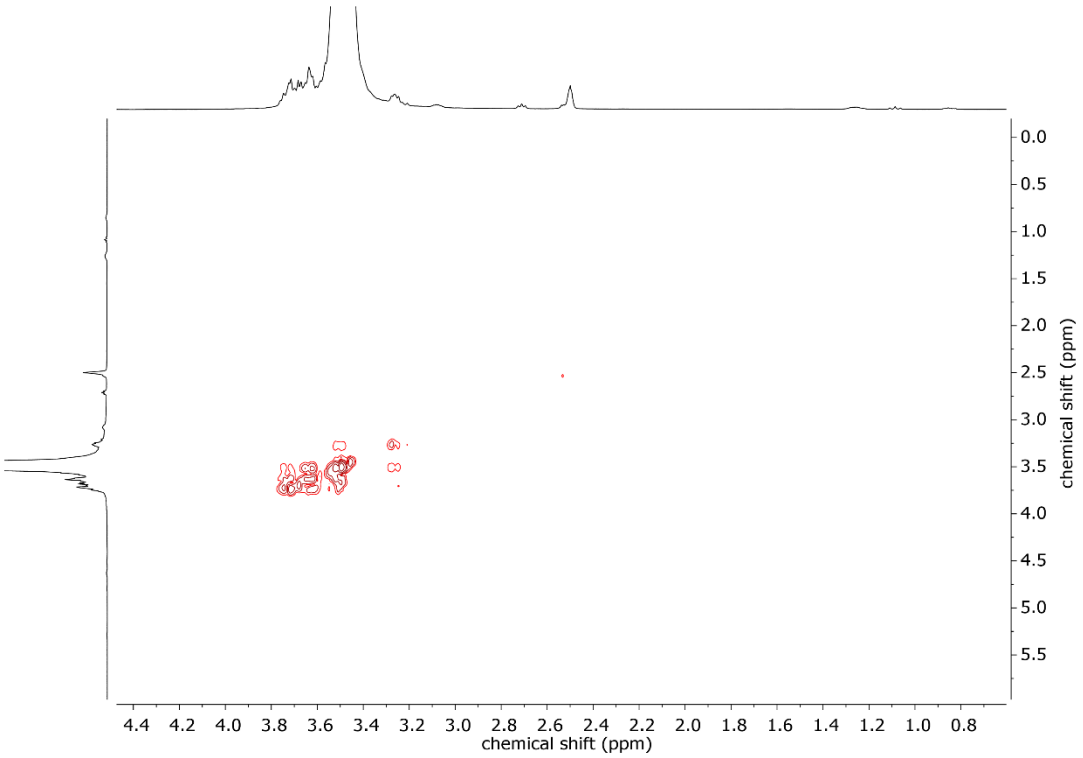

Figure S9. COSY NMR (DMSO-d_6, 300 MHz) of P($EO_{0.94}$-*co*-$ECH_{0.06}$).

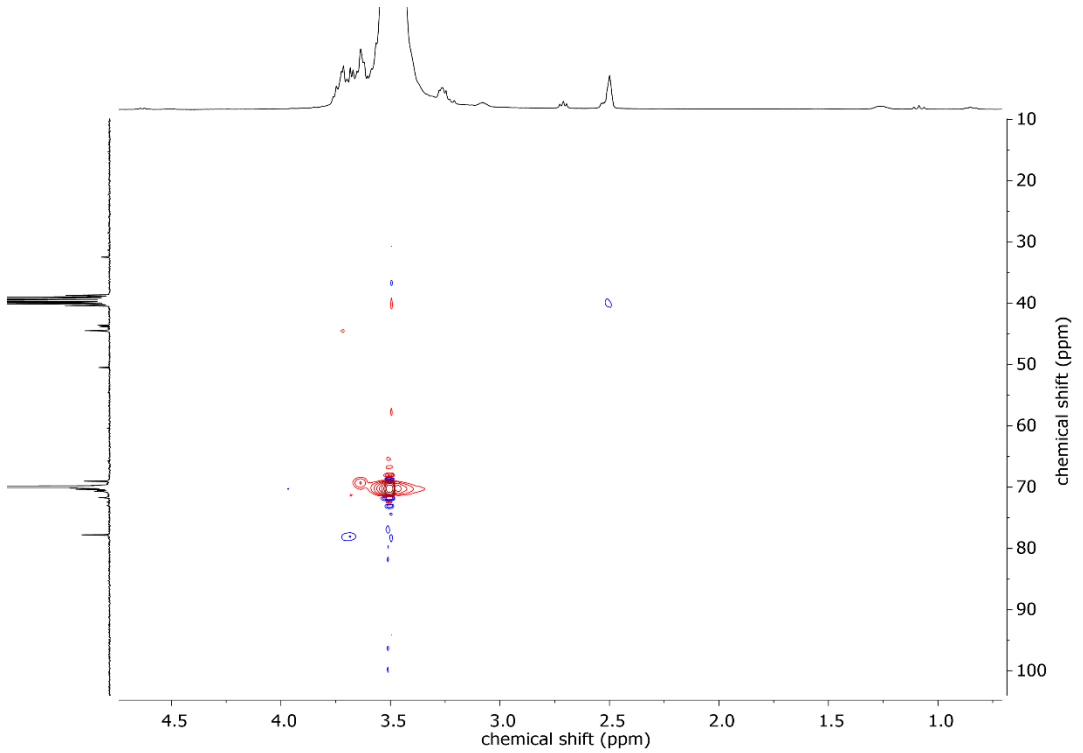

Figure S10. HSQC NMR (DMSO-d_6) of P($EO_{0.94}$-*co*-$ECH_{0.06}$).

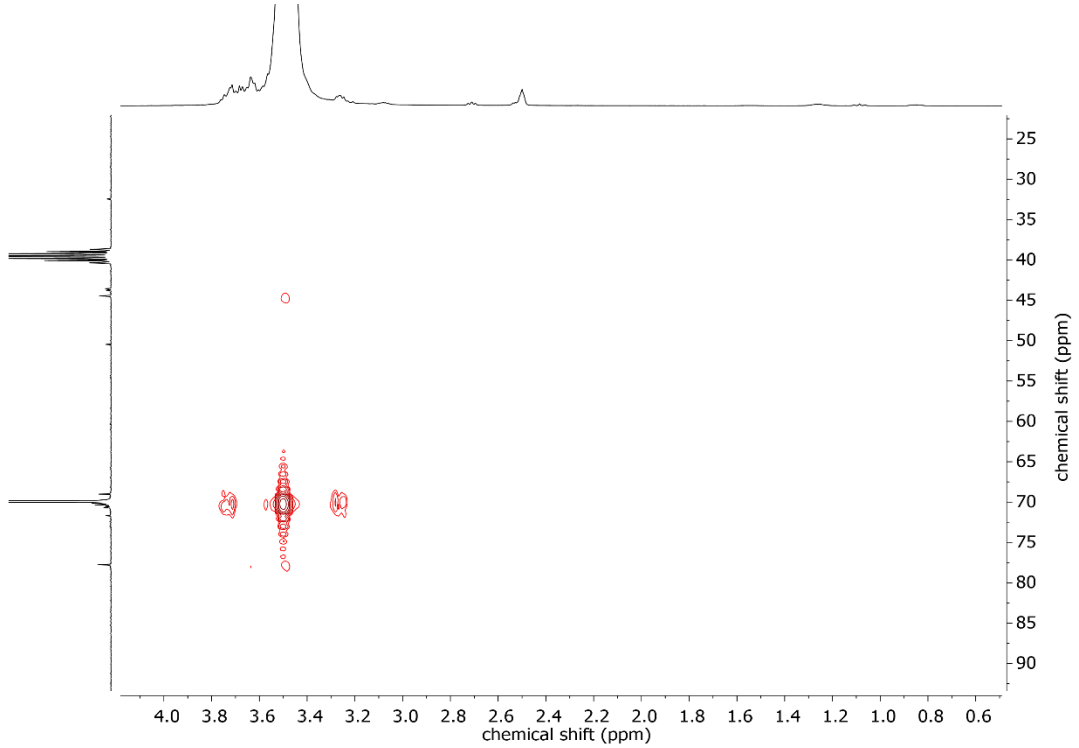

Figure S11. HMBC NMR (DMSO-d_6) of P($EO_{0.94}$-*co*-$ECH_{0.06}$).

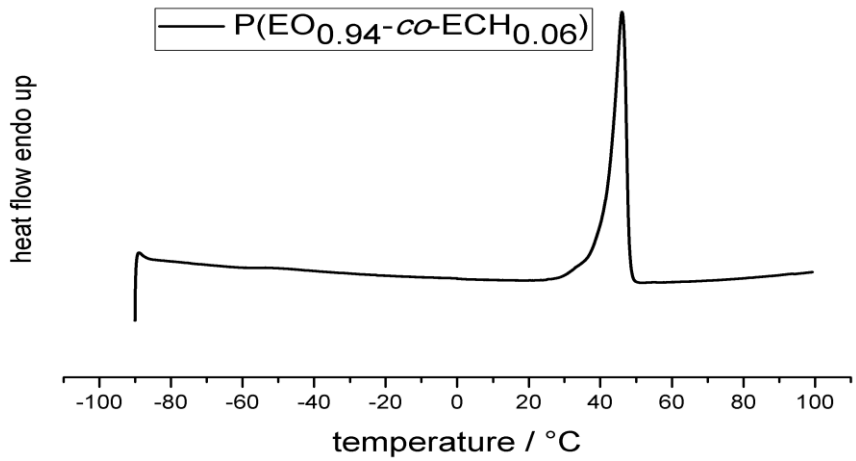

Figure S12. Plot of DSC measurement of P($EO_{0.94}$-*co*-$ECH_{0.06}$).

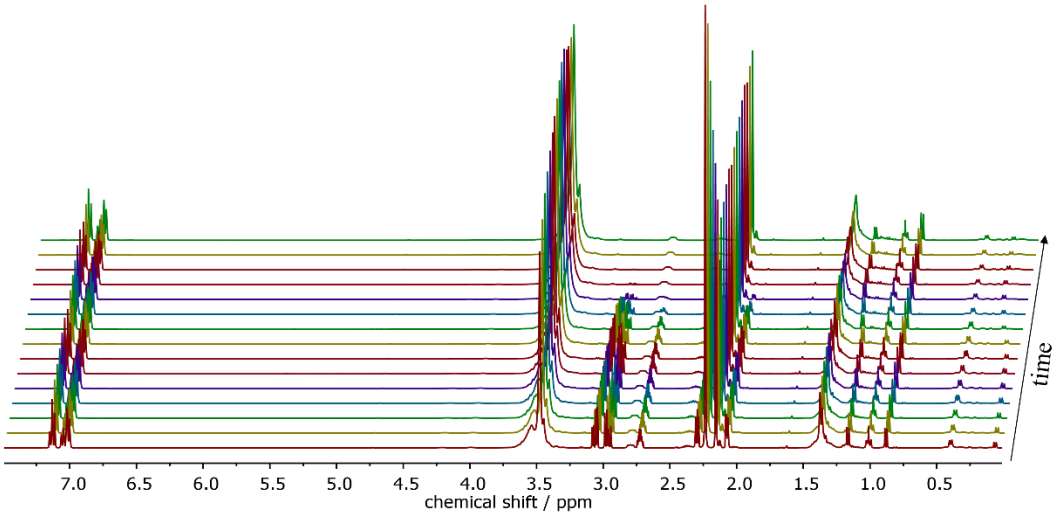

Figure S13. Selection of ^{1}H NMR spectra (400 MHz, toluene-d_8, 0 °C, 5 °C, 10 °C) of *in situ* NMR kinetics of the monomer-activated AROP of EO and ECH.

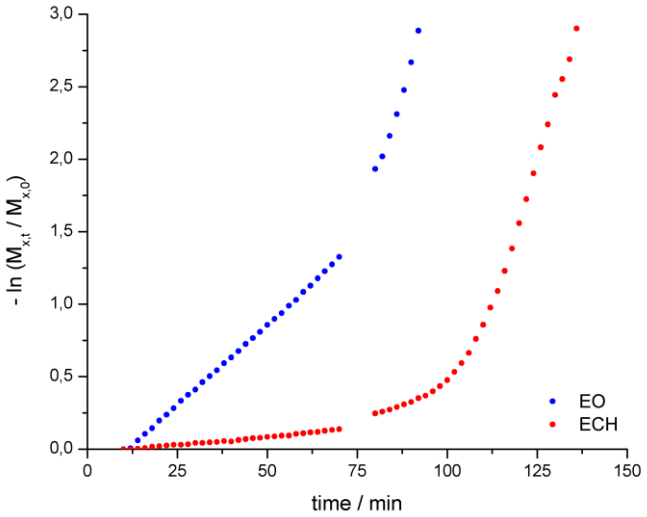

Figure S14. First-order time-conversion plot for the copolymerization of EO (blue) and ECH (red) via the monomer-activated method. When temperature was raised, no data was collected.

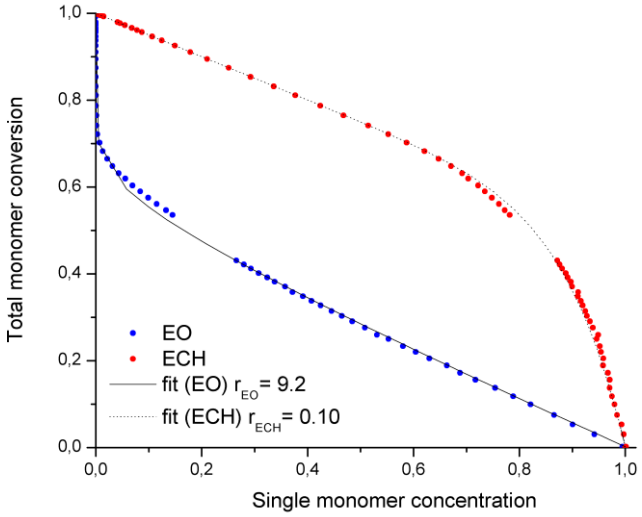

Figure S15. Total monomer conversion vs. single monomer concentration for the copolymerization of EO (blue) and ECH (red) via the monomer-activated method. The reactivity ratios were determined from the respective fits (EO solid line, ECH dashed line) in analogy to Lynd and coworkers.[2]

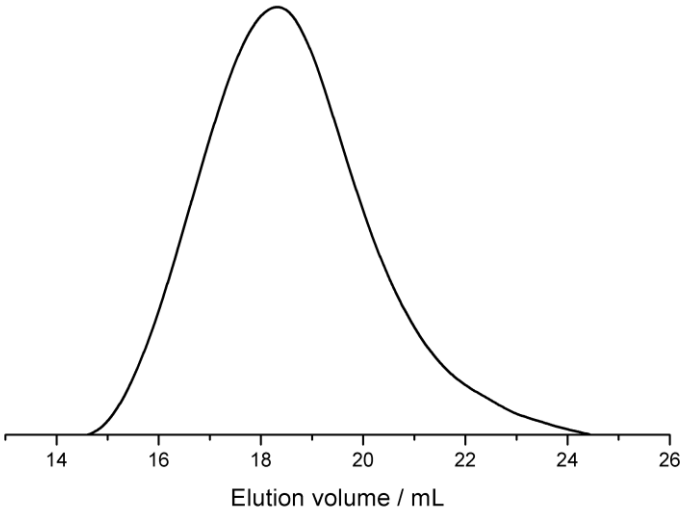

Figure S16. SEC elugram (DMF, PEG standard, RI signal) of P(EO-*co*-ECH) obtained from *in situ* NMR kinetics measurement.

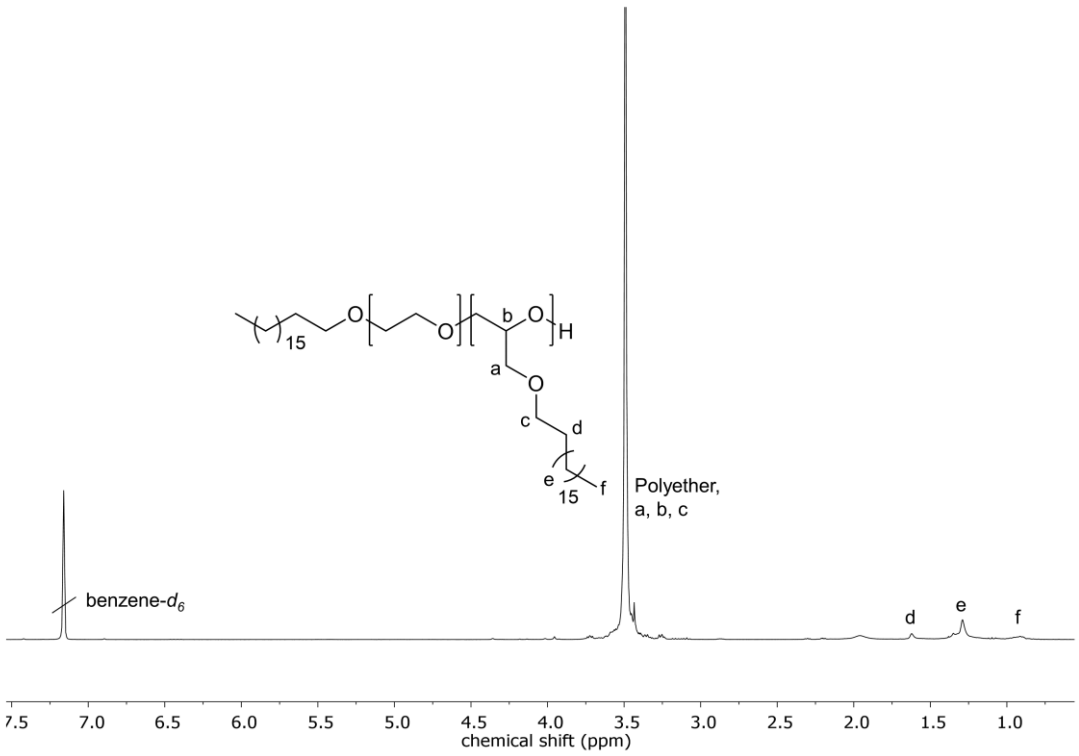

Figure S17. ^{1}H NMR (benzene-d_6, 300 MHz) of P($EO_{0.94}$-*co*-$ECH_{0.06}$) functionalized with *n*-octadecanol P(EO-*co*-ECH$^{n\text{-OD}}$).

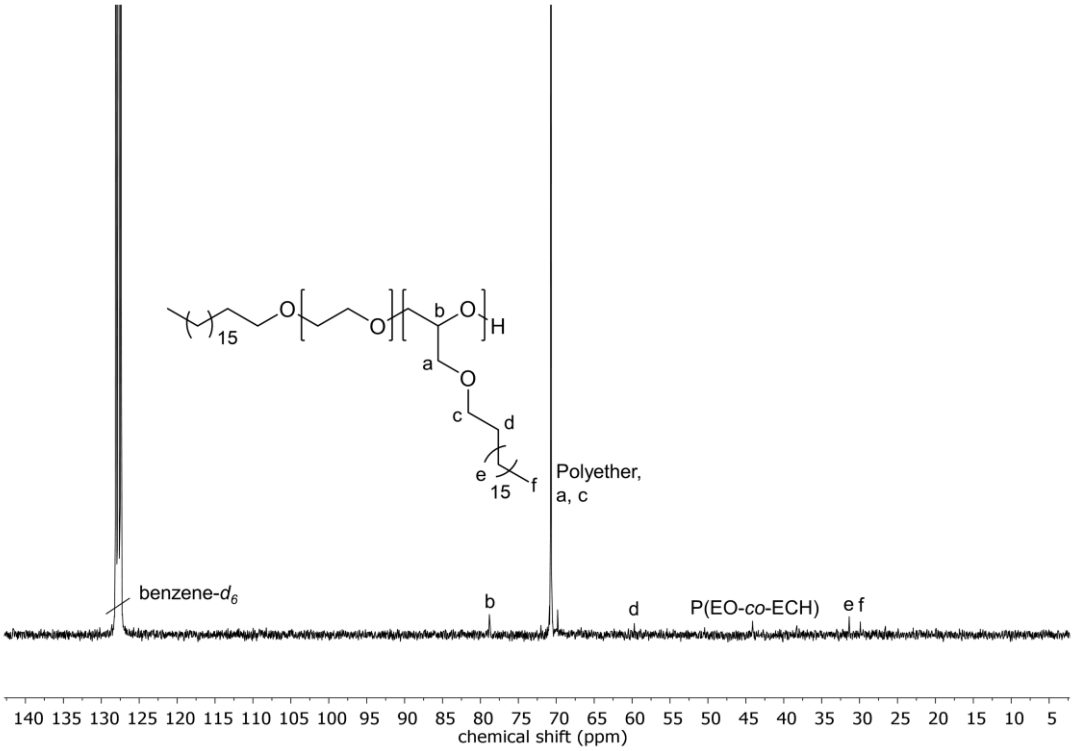

Figure S18. ^{13}C NMR (benzene-d_6, 75 MHz) of P(EO-*co*-ECH$^{n\text{-OD}}$).

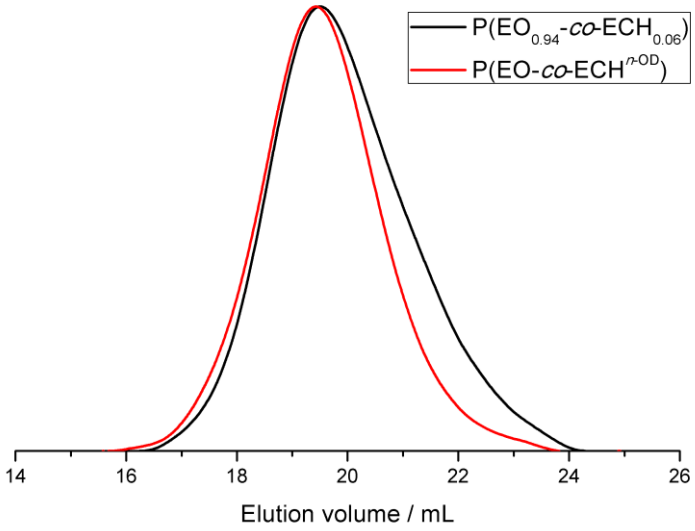

Figure S19. SEC elugram (DMF, PEG standard, RI signal) of P($EO_{0.94}$-*co*-$ECH_{0.06}$) and P(EO-*co*-$ECH^{n\text{-}OD}$).

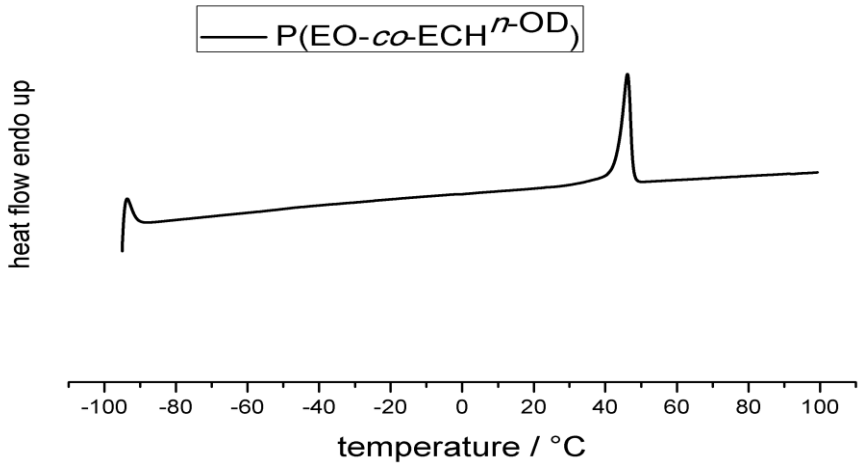

Figure S20. Plot of DSC measurement of P(EO-*co*-$ECH^{n\text{-}OD}$).

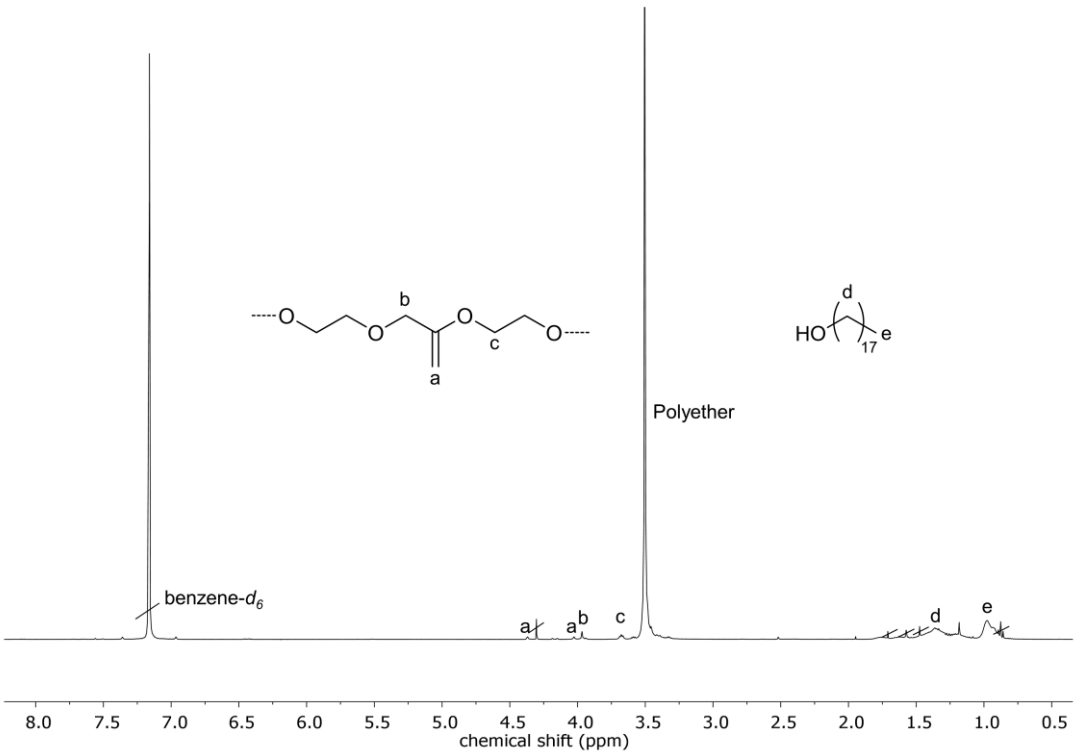

Figure S21. ^{1}H NMR (benzene-d_6, 400 MHz) of the occurring elimination of P($EO_{0.94}$-*co*-$ECH_{0.06}$) functionalized with *n*-octadecanol.

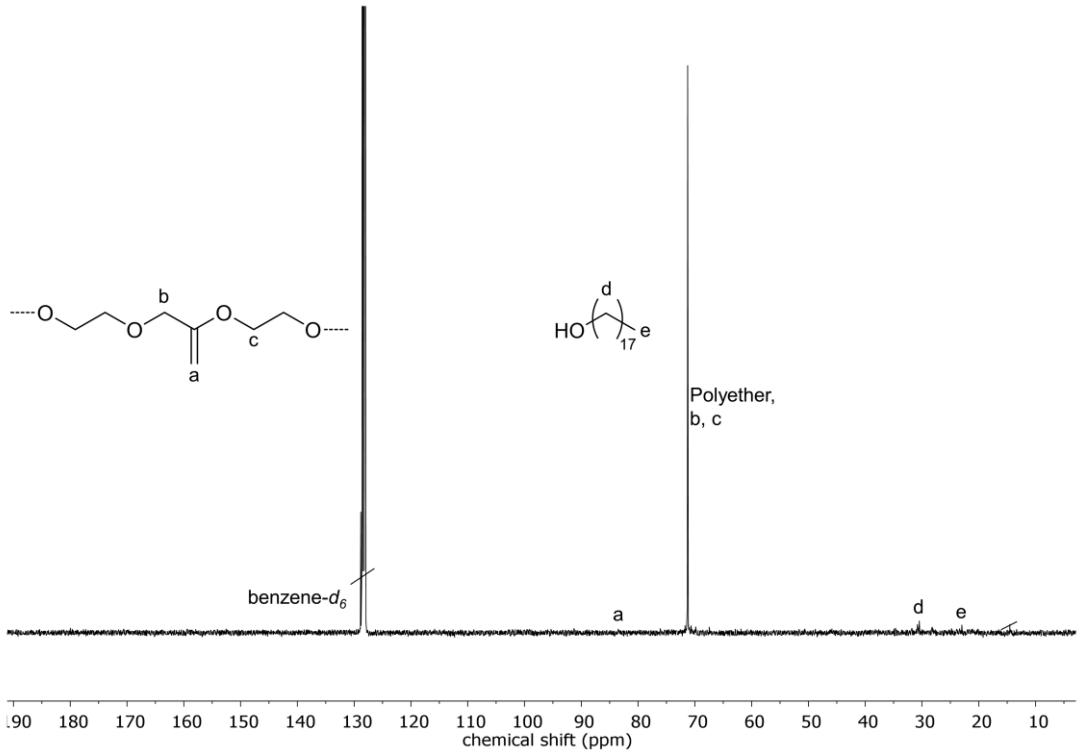

Figure S22. . ^{13}C NMR (benzene-d_6, 101 MHz) of the occurring elimination of P($EO_{0.94}$-*co*-$ECH_{0.06}$) functionalized with *n*-octadecanol.

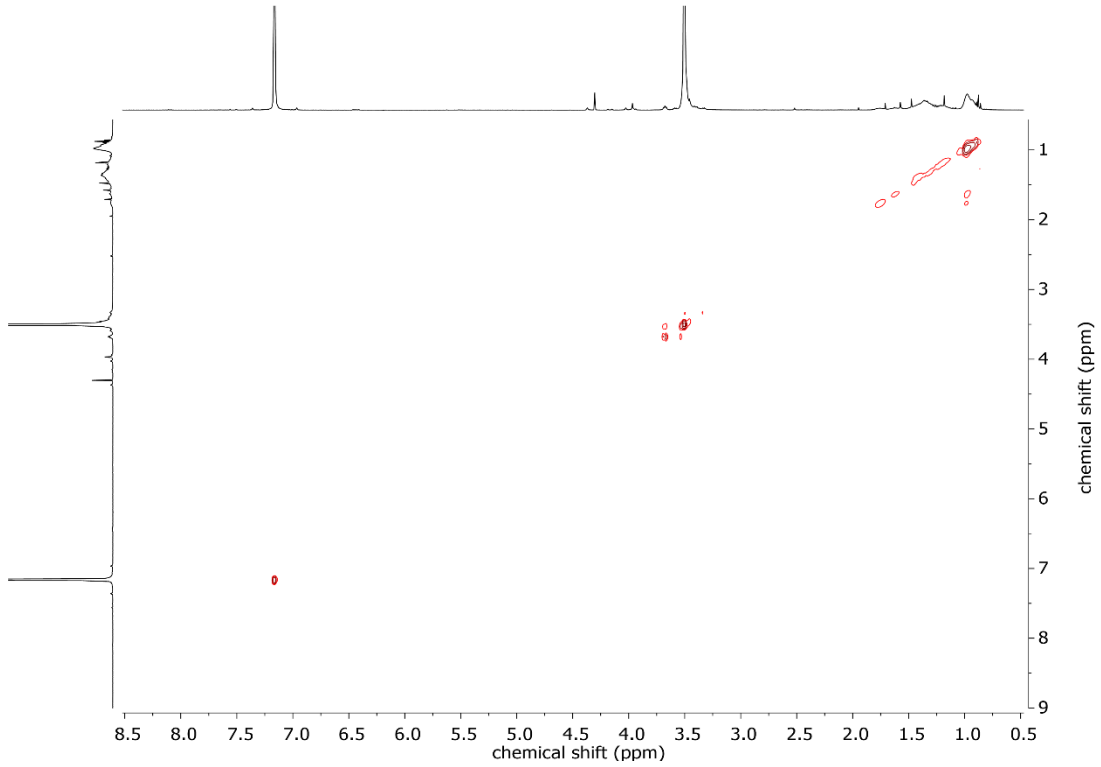

Figure S23. COSY NMR (benzene-d_6, 400 MHz) of the occurring elimination of P($EO_{0.94}$-*co*-$ECH_{0.06}$) functionalized with *n*-octadecanol.

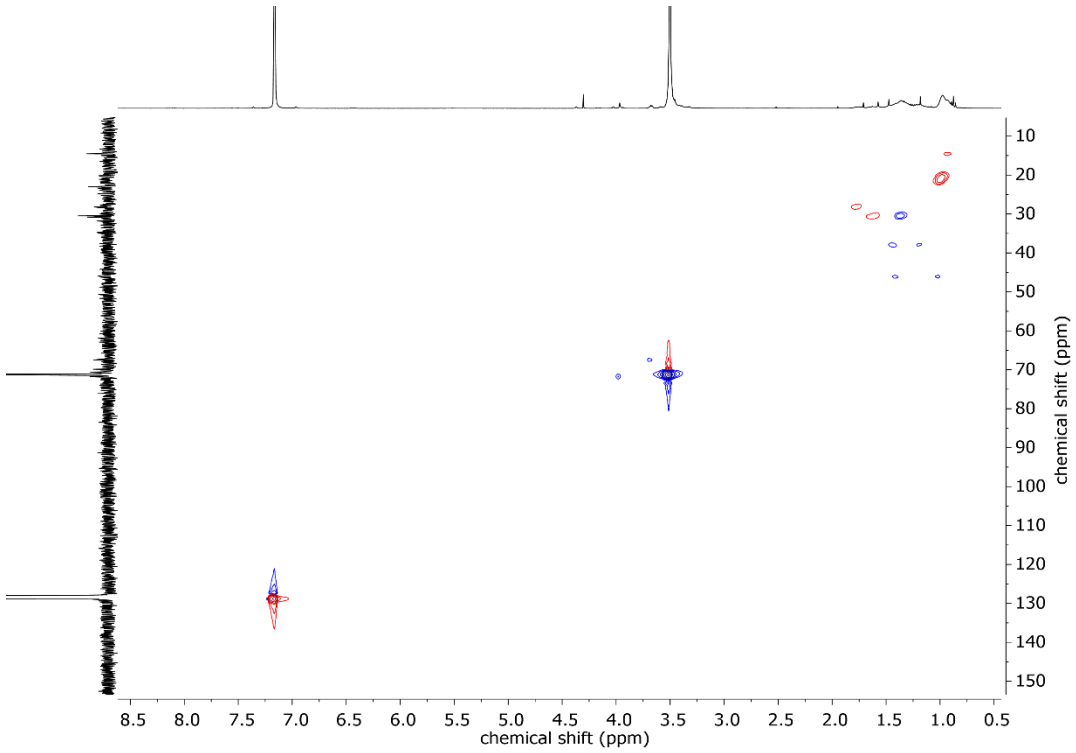

Figure S24. HSQC NMR (benzene-d_6) of the occurring elimination of P($EO_{0.94}$-*co*-$ECH_{0.06}$) functionalized with *n*-octadecanol.

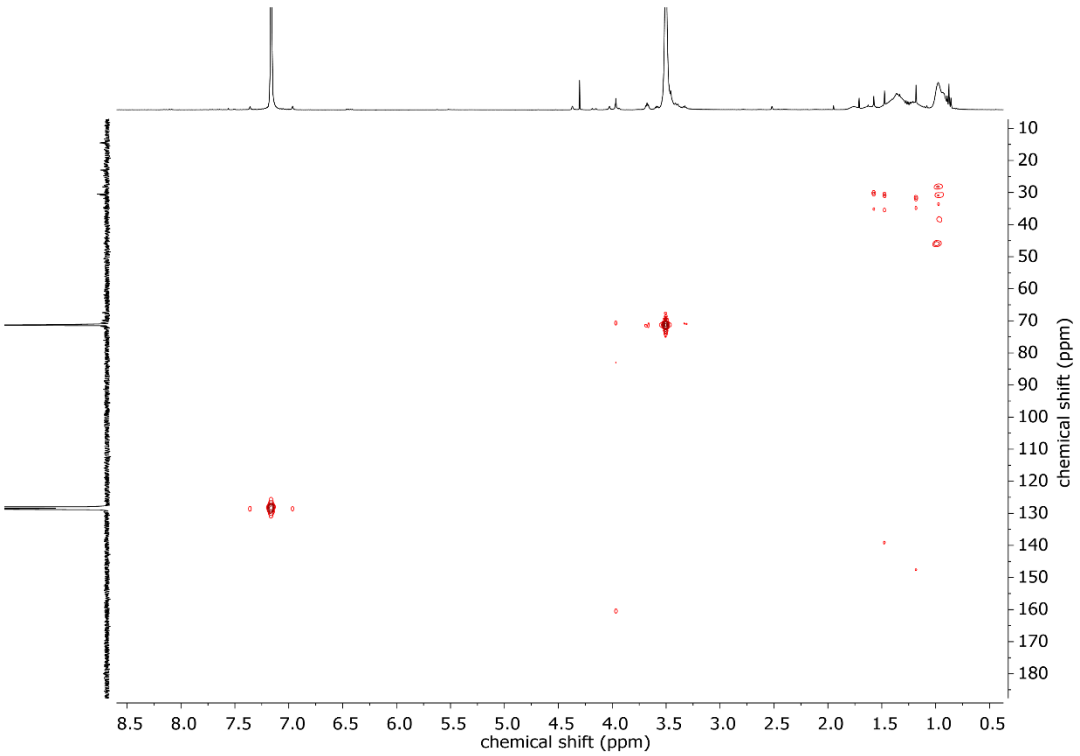

Figure S25. HMBC NMR (benzene-d_6) of the occurring elimination of P($EO_{0.94}$-*co*-$ECH_{0.06}$) functionalized with *n*-octadecanol.

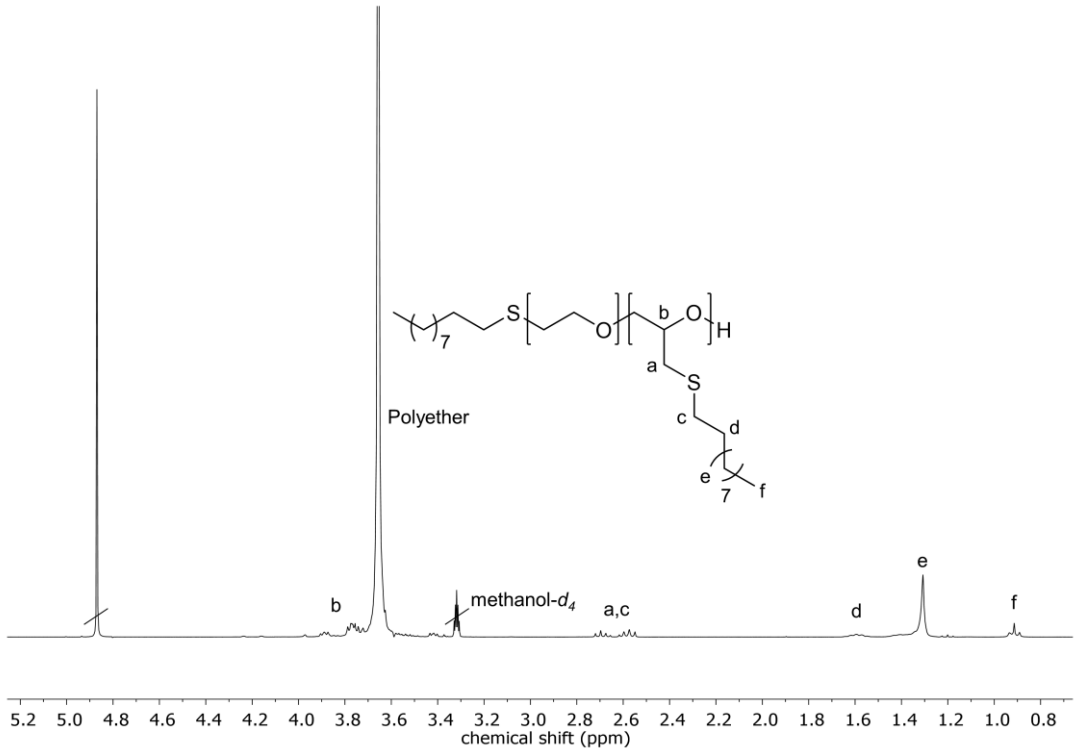

Figure 26. ^{1}H NMR (methanol-d_4, 300 MHz) of P($EO_{0.94}$-*co*-$ECH_{0.06}$) functionalized with 1-decanthiol P(EO-*co*-$ECH^{1\text{-}DT}$).

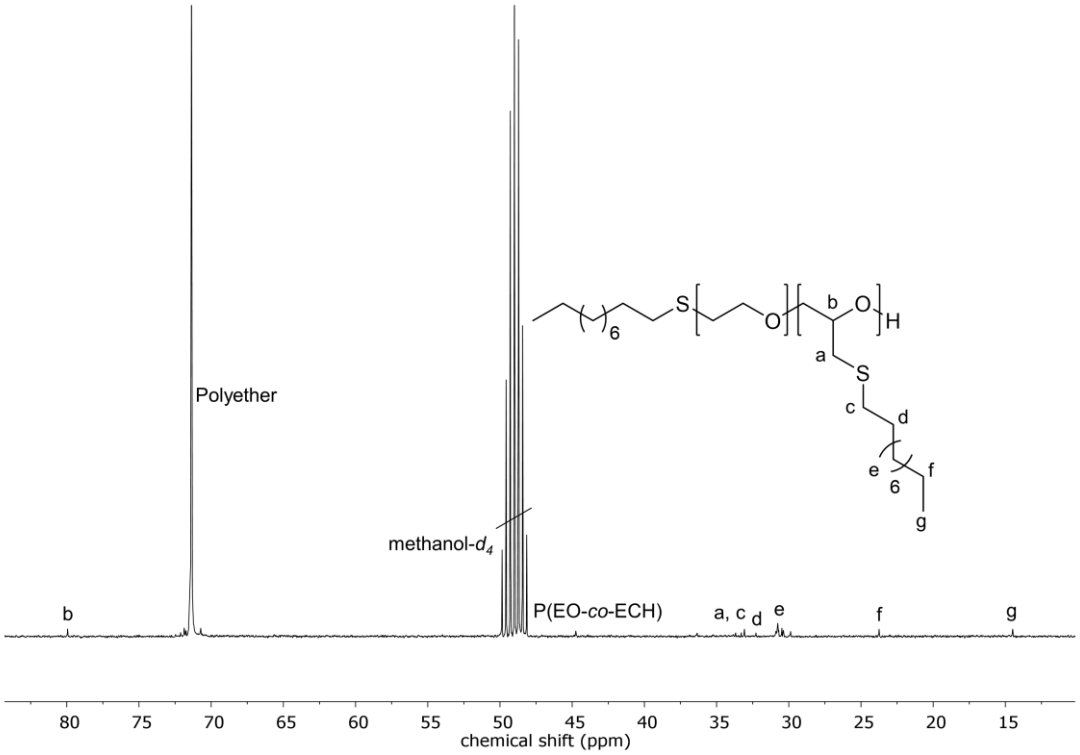

Figure S27. ^{13}C NMR (methanol-d_4, 75 MHz) of P(EO-*co*-ECH$^{1\text{-DT}}$).

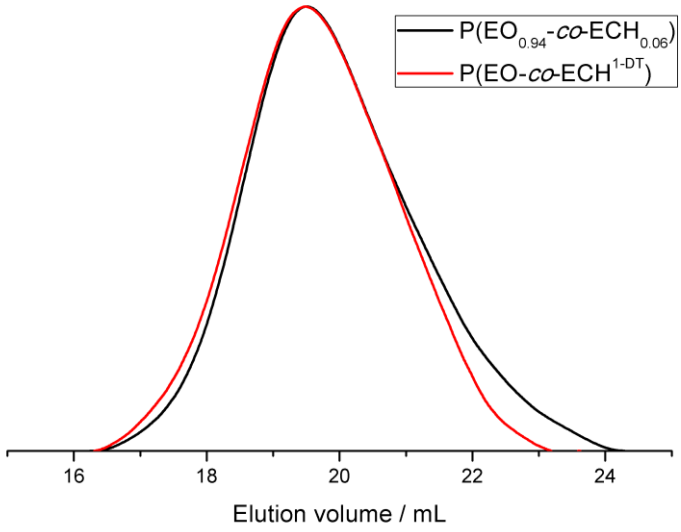

Figure S28. SEC elugram (DMF, PEG standard, RI signal) of P(EO$_{0.94}$-*co*-ECH$_{0.06}$) and P(EO-*co*-ECH$^{1\text{-DT}}$).

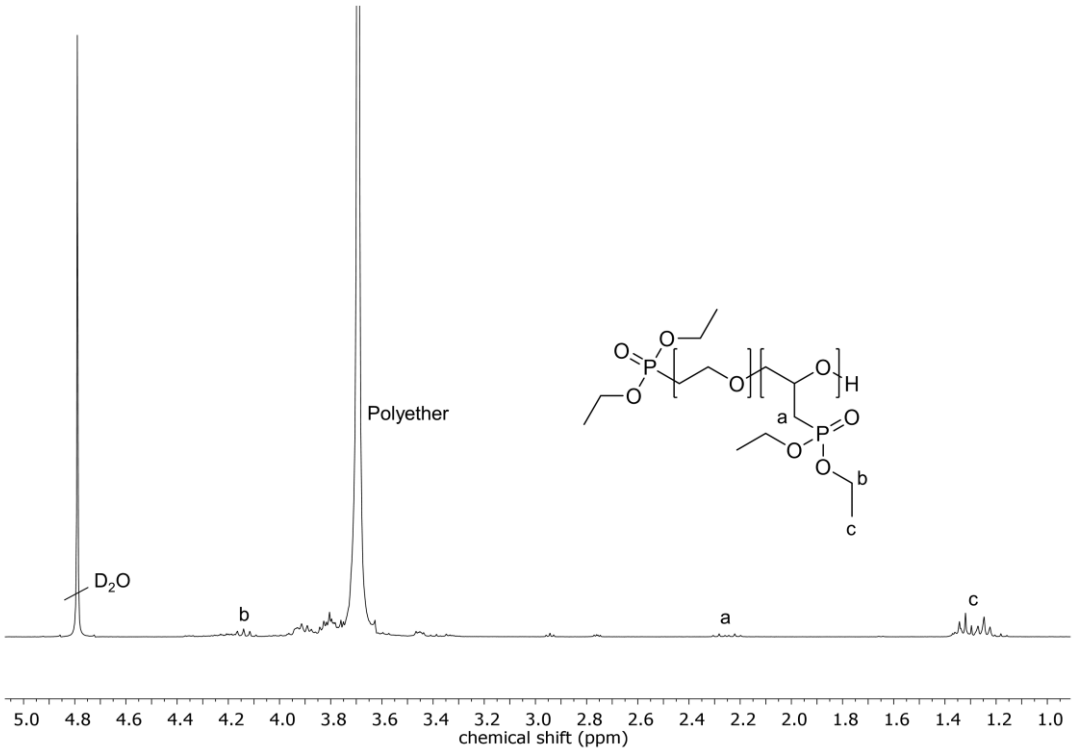

Figure S29. ^{1}H NMR (D_2O, 300 MHz) of P(EO-*co*-ECH^{DEPE}).

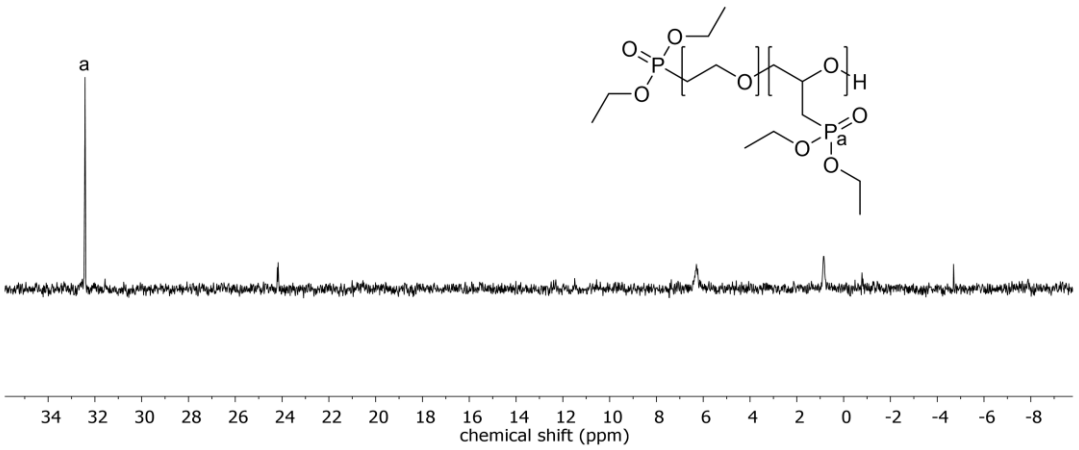

Figure S30. ^{31}P NMR (D_2O, 121.5 MHz) of P(EO-*co*-ECH^{DEPE}).

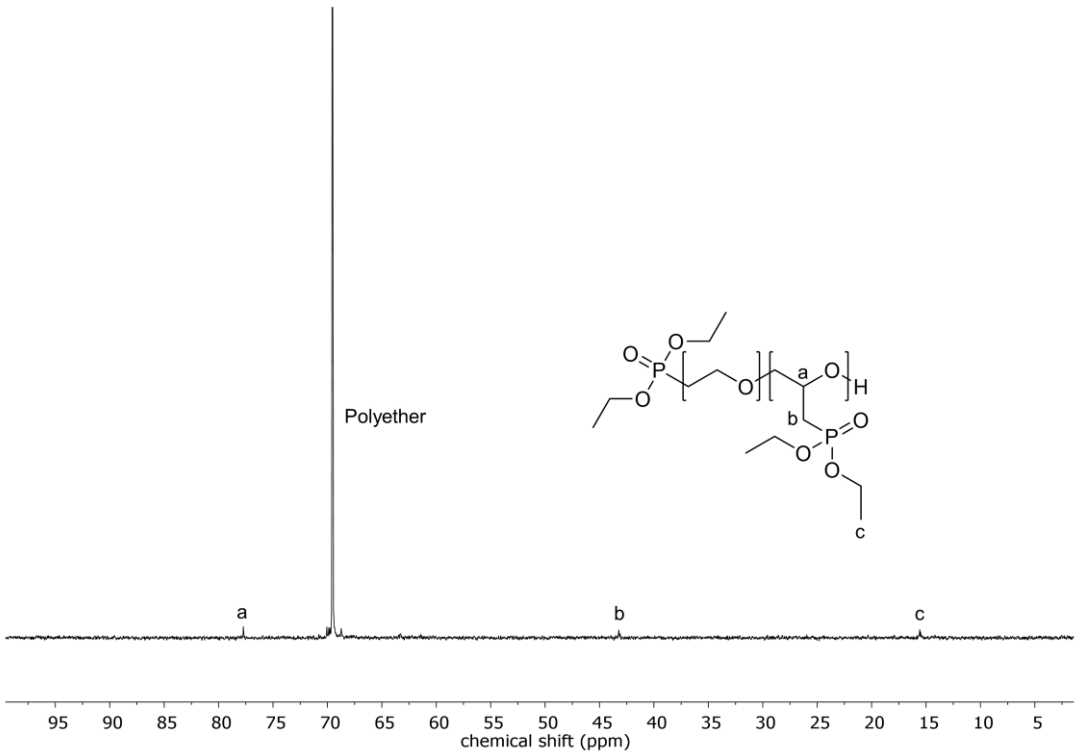

Figure S31. ^{13}C NMR (D_2O, 75 MHz) of P(EO-*co*-ECH^{DEPE}).

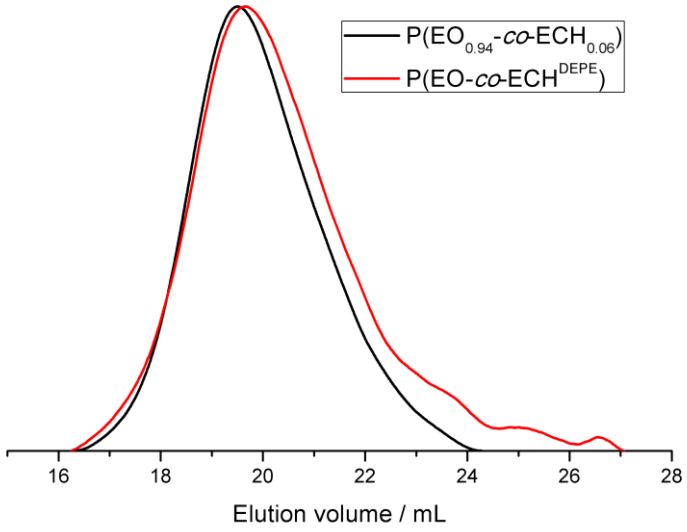

Figure S32. SEC elugram (DMF, PEG standard, RI signal) of P($EO_{0.94}$-*co*-$ECH_{0.06}$) and P(EO-*co*-ECH^{DEPE}).

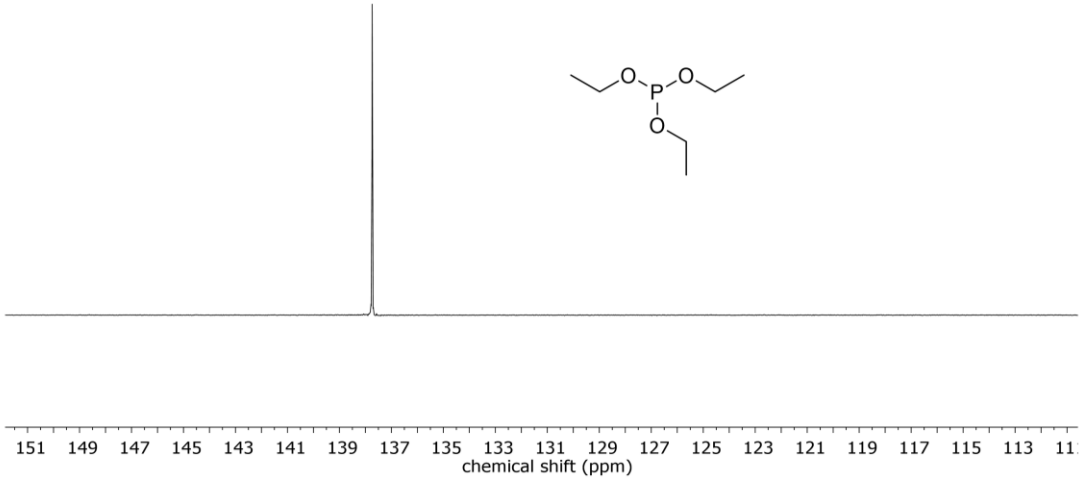

Figure S33. ^{31}P NMR (DMSO-d_6, 121.5 MHz) of triethylphosphite.

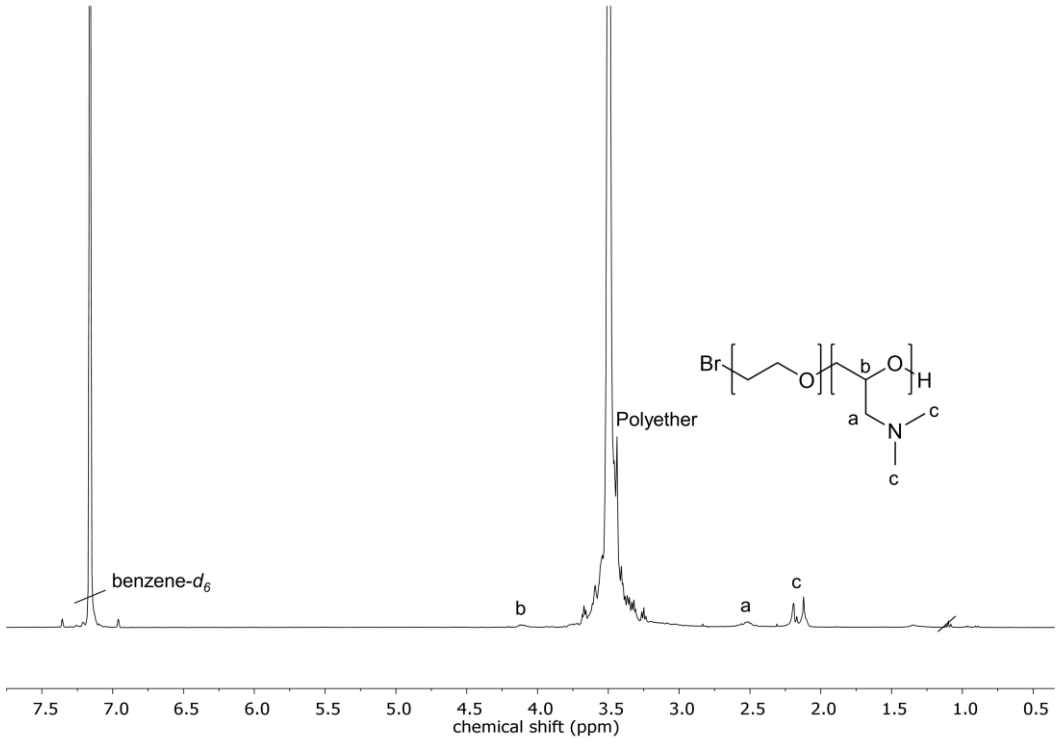

Figure S34. ^{1}H NMR (benzene-d_6, 400 MHz) of P(EO-*co*-ECH^{DMA}).

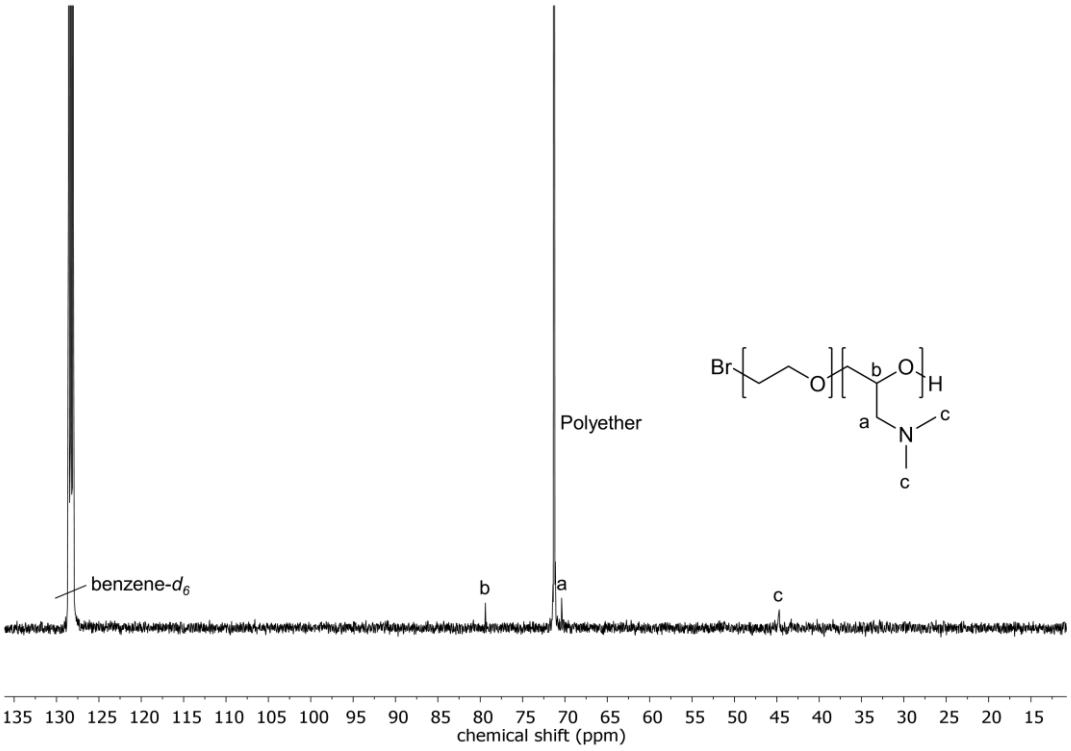

Figure S35. ^{13}C NMR (benzene-d_6, 101 MHz) of P(EO-*co*-ECH^{DMA}).

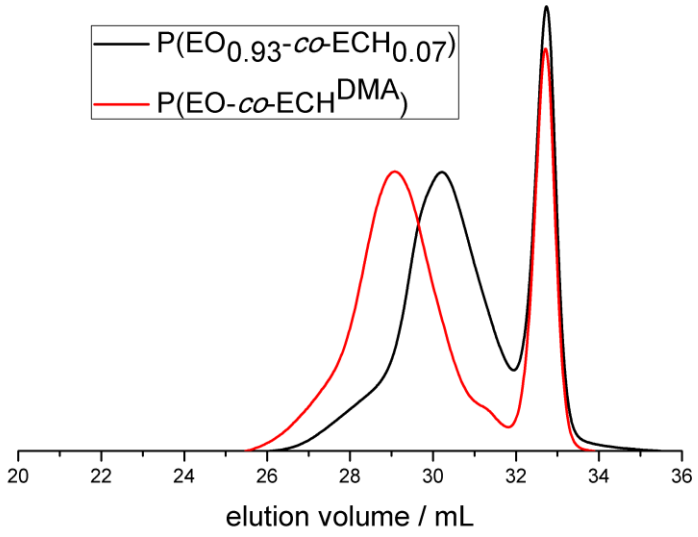

Figure S36. SEC elugram (H_2O (0.05 vol% TFA), PEG standard, RI signal) of P(EO$_{0.93}$-*co*-ECH$_{0.07}$) and P(EO-*co*-ECH^{DMA}). The second, overlapping trace displays a recurrent solvent peak.

Table S1. Summary of the properties of the functionalized copolymers P(EO-*co*-ECH$^{n\text{-OD}}$), P(EO-*co*-ECH$^{1\text{-DT}}$), P(EO-*co*-ECH^{DEPE}) and P(EO-*co*-ECH^{DMA}).

#	Composition	[EO]/[ECH] mol%	$M_n^{SEC,\,a}$ g mol^{-1}	$M_w/M_n^{SEC,\,a}$	T_g °C	T_m °C
10	P(EO-*co*-ECH$^{n\text{-OD}}$)	94:6	4750	1.31	–51	46
11	P(EO-*co*-ECH$^{1\text{-DT}}$)	94:6	4160	1.29	–54	41
12	P(EO-*co*-ECH^{DEPE})	94:6	3640	1.31	–58	41
13	P(EO-*co*-ECH^{DMA})	93:7	6960[a]	1.43[b]	–60	30

[a]SEC measurements were performed in DMF using PEG standards.
[b]SEC measurements were performed in H_2O (0.05 vol% TFA) using PEG standards.

4. References

(1) Carlotti, S.; Labbé, A.; Rejsek, V.; Doutaz, S.; Gervais, M.; Deffieux, A. Living/Controlled Anionic Polymerization and Copolymerization of Epichlorohydrin with Tetraoctylammonium Bromide−Triisobutylaluminum Initiating Systems. *Macromolecules* **2008**, *41*, 7058–7062.

(2) Beckingham, B. S.; Sanoja, G. E.; Lynd, N. A. Simple and Accurate Determination of Reactivity Ratios Using a Nonterminal Model of Chain Copolymerization. *Macromolecules* **2015**, *48*, 6922–6930.

5. Outlook

This section presents a selection of further projects initiated within the scope of this thesis and gives an outlook on future activities related to the preceding chapters.

I) Polyether-lipids with variable hydrophobic initiators and different polymer architectures

In **chapter 2.1** the synthesis of linear and hyperbranched polyether lipids was presented using dialkyl-based initiators with different alkyl chain lengths. In addition, the polymer architecture was varied, resulting in linear and hyperbranched structures of polyethylene glycol (PEG) as well as polyglycerol (PG). Subsequently, the polyether lipids were functionalized with alkyne moieties to enable the attachment of functional groups *via* click chemistry. In an ongoing collaboration with Matthias Voigt and Prof. Dr. Mark Helm from the Institute of Pharmacy and Biochemistry, Johannes Gutenberg-University Mainz, the stability of lipid anchorage will be investigated. Based on recent work,[1] these investigations will be carried out by labeling the polyether lipids with fluorophores *via* an azide-alkyne cycloaddition after the preparation of liposomes as displayed in **Figure 1**. The interaction of these structures with cells and especially the cell membranes will be studied. Furthermore, the stability of lipid anchorage could be studied *via* positron emission tomography (PET) studies. The already attached alkyne-functions enable ^{18}F-radiolabeling to investigate the *in vivo* distribution of liposomes carrying the different polyether lipids.[2,3] Moreover, therapeutic agents could be integrated into the liposomal structures and stability of encapsulation could be investigated to ensure secure transport of the cargo.

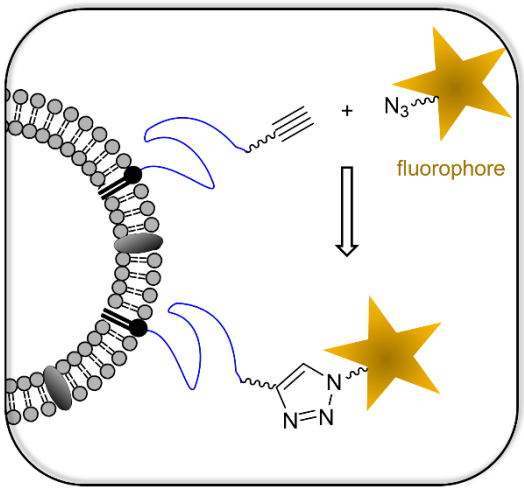

Figure 1. Schematic representation of an azide-alkyne cycloaddition for post-functionalization of the polyether lipid.

II) pH-sensitive copolymers to obtain degradable PEG

In **section 2.2** the synthesis of amphiphilic polyethers with pendant pH-sensitive moieties was presented. By applying potassium as the counter ion for the alkoxide and crown ethers for complexation, the polymerization in less polar solvents was achieved and hence was the use of hydrophobic initiators. In addition, the applied conditions led to a direct formation of vinyl ether moieties and an additional post-polymerization isomerization was avoided. Studies of the pH-sensitive cleavage of the polymers revealed full degradation at pH 3.5 within 5 days (at 37 °C) and a very good stability at pH 7.0 (no degradation after 32 days at 37 °C). The hydrolysis might be further accelerated if full conversion of the isomerization of the side-chain double bond could be achieved during polymerization. This could allow fine-tuning of the kinetics for the cleavage. In this process, the reaction temperature and amount of applied crown ethers might play a key role.

Another important future objective is the investigation of the stability and fragmentation properties of the pH-dependent cleavage of the polymers in liposomal formulations, as the preparation of liposomes was already presented to be successful. For this purpose, a fluorescent label could be attached *via* click chemistry and subsequent fluorescence spectroscopy could allow for the investigation of the cleavage process.[4] Furthermore, encapsulation efficiencies of different cargo molecules as well as investigations on the kinetics of drug release might be interesting to study.

By combining pH-sensitive moieties and an attachment of target functions, liposomes with pH-dependent release and the ability of active targeting could be accessible. Due to the available hydroxyl group at the polyether lipids, post-polymerization modification could be easily performed to attach functional moieties. This might serve as promising innovation to tackle current challenges of liposomal drug carrier systems.

III) PEG-lipids with multifunctional moieties for active targeting

In **chapter 2.3** multifunctional PEG with tailored molecular weights and adjustable comonomer content was obtained *via* the copolymerization of ethylene oxide (EO) and mannose-carrying epoxides. The mannose moieties enable active targeting to macrophages and dendritic cells due to an overexpression of carbohydrate-receptors on cells of the immune system.[5] In further investigations, the preparation of liposomes and the influence of the mannose-moieties on cellular uptake could be investigated. The amount of attached functional groups will also influence the cellular uptake and has to be taken into account.

In order to investigate this cellular uptake, a labeling of the polymers with dyes might be necessary. Therefore, alkyne moieties could be attached to the polyether lipids to enable an azide-alkyne cycloaddition in the previously described fashion (*vide supra*).

Moreover, a combination of the synthesized BisOD-*hb*PGs (presented in **section 2.1**) and carbohydrate moieties as target functions are another promising strategy to exploit the multifunctionality of *hb*PG and to develop polyether lipids for active targeting. First results of this ongoing project are presented herein after. The project is carried out in collaboration with Prof. Dr. Martina Stenzel, School of Chemistry, Centre for Advanced Macromolecular Design (CAMD), University of New South Wales, Sydney, Australia.

i) *hb*PG lipids with variable amount of carbohydrate-moieties for targeted delivery of therapeutics:

Carbohydrate-based derivatives, which mimic natural glycosylation patterns are known to facilitate targeted drug delivery, *i.e.* active targeting is promoted and carbohydrate-binding proteins on cell surfaces (so-called lectins) can recognize the glycopolymers.[6] Cell-cell interactions are initiated by ligand-receptor recognition, leading to increased cellular uptake *via* receptor-mediated endocytosis.[7] Due to the weakness of one single interaction, multiple carbohydrate-moieties are necessary to obtain a "cluster glycoside effect".[8,9] Thus, a high local concentration of carbohydrate moieties should help to achieve a "cluster glycoside effect". In general, fructose moieties are known to target breast cancer cells due to an overexpression of GLUT-5 receptors on these cell surfaces.[10] In this context, carbohydrate moieties, *i.e.* fructose-based structures, will be attached to *hb*PG to enable the preparation of liposomes, exhibiting recognition patterns for active targeting.

In first experiments, *β*-D-fructopyranose was converted to 1-*O*-bromoacetate-2,3:4,5-di-*O*-isopropylidene-*β*-D-fructopyranose (**5**) in two steps as shown in **Scheme 1**. The successful synthesis was confirmed using ^{1}H NMR, ^{13}C NMR and 2D spectroscopy. **Figure 2** displays the ^{1}H NMR spectrum of 1-*O*-bromoacetate-2,3:4,5-di-*O*-isopropylidene-*β*-D-fructopyranose and the respective assignments of the chemical shifts.

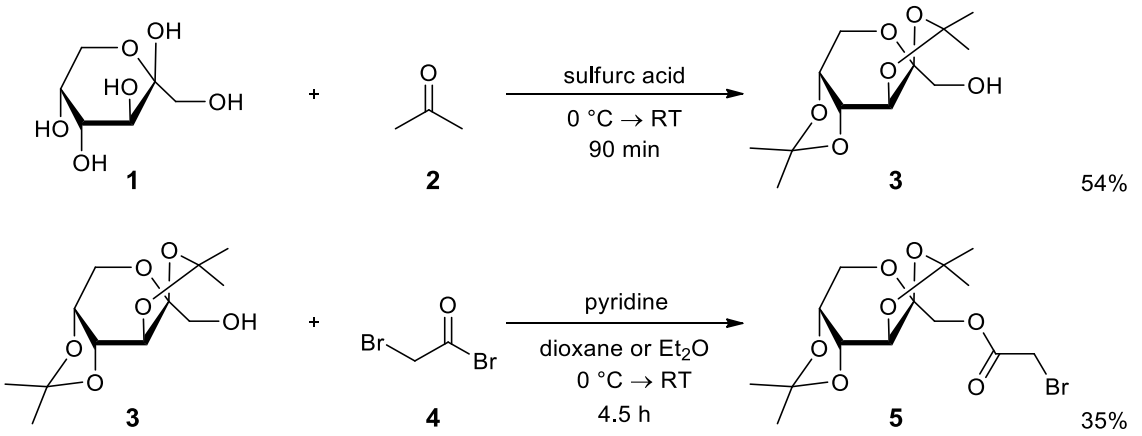

Scheme 1. Two step procedure to convert *β*-D-fructopyranose to 1-*O*-bromoacetate-2,3:4,5-di-*O*-isopropylidene-*β*-D-fructopyranose.

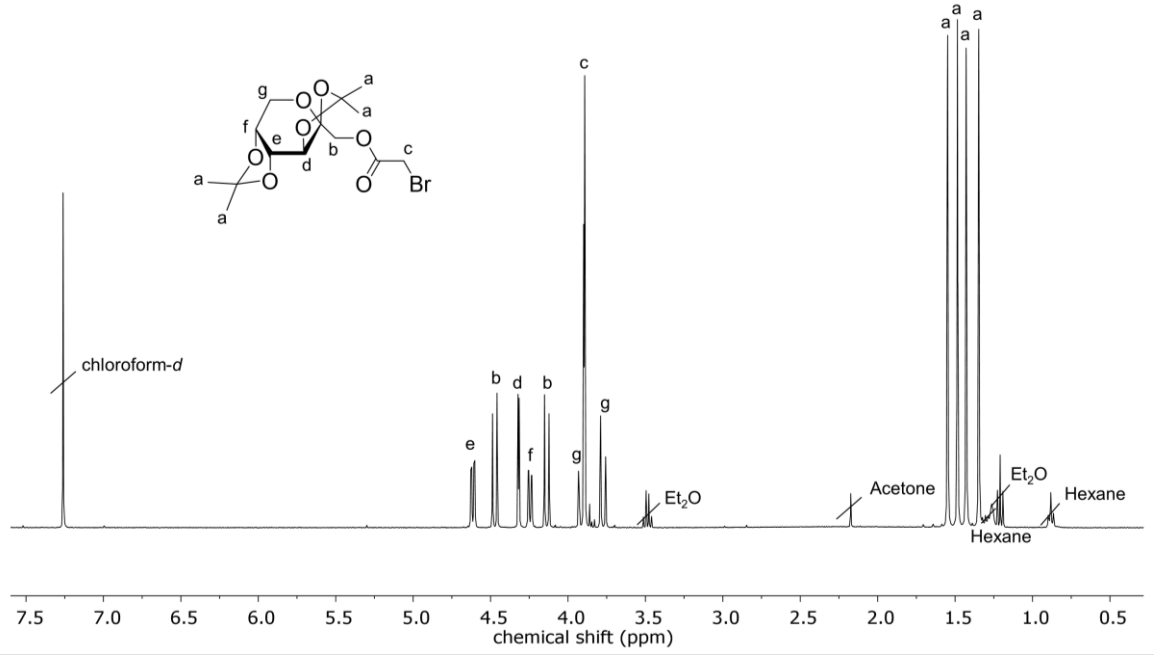

Figure 2. ^{1}H NMR (300 MHz, chloroform-*d*) of 1-*O*-bromoacetate-2,3:4,5-di-*O*-isopropylidene-*β*-D-fructopyranose.

A model reaction of glycerol and 1-*O*-bromoacetate-2,3:4,5-di-*O*-isopropylidene-*β*-D-fructopyranose (**5**) was performed to study the attachment of the carbohydrate derivative *via* nucleophilic substitution as well as the subsequent cleavage of the isopropylidene protecting groups. Nucelophilic substitution was carried out under basic conditions, using sodium hydride, leading to 1-*O*-glycerol-2,3:4,5-di-*O*-isopropylidene-*β*-D-fructopyranose (**7**). The cleavage of the isopropylidene groups was studied *via* ^{1}H NMR kinetics, revealing integrity of the protecting groups in a mixture of acetic acid (AcOH) and deuterated water

(D_2O) (1:1) even after 8 days, whereas cleavage was obtained in trifluoroacetic acid (TFA)/D_2O (1:1) in less than four hours (**Figure 3**). The ester-functionality was stable under these conditions, providing a suitable protocol for the generation of 1-*O*-glycerol-*β*-D-fructopyranose (**8**).

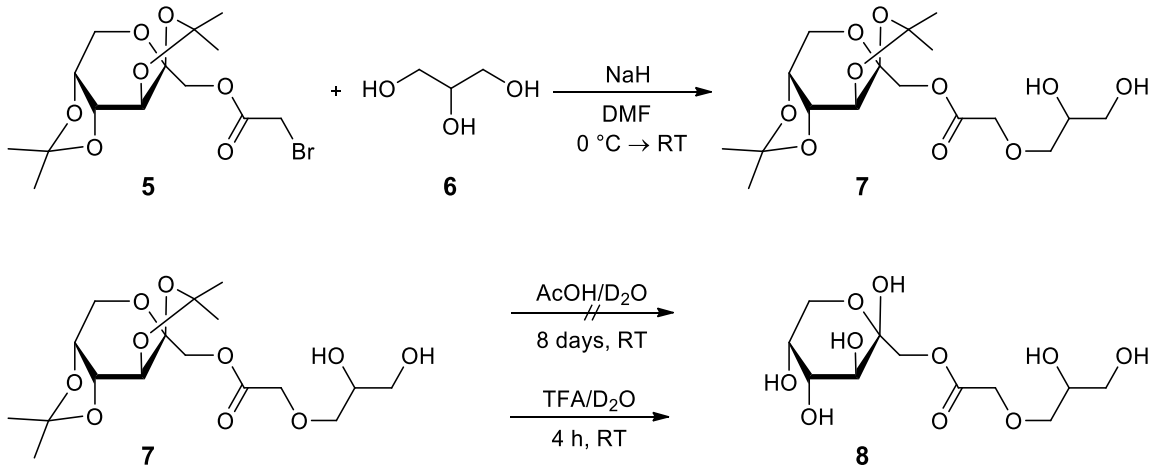

Scheme 2. Nucleophilic substitution reaction of 1-*O*-bromoacetate-2,3:4,5-di-*O*-isopropylidene-*β*-D-fructopyranose (**5**) and glycerol (**6**) to obtain 1-*O*-glycerol-2,3:4,5-di-*O*-isopropylidene-*β*-D-fructopyranose (**7**) (top) and acidic cleavage of the isopropylidene protecting groups to obtain 1-*O*-glycerol-*β*-D-fructopyranose (**8**) (bottom).

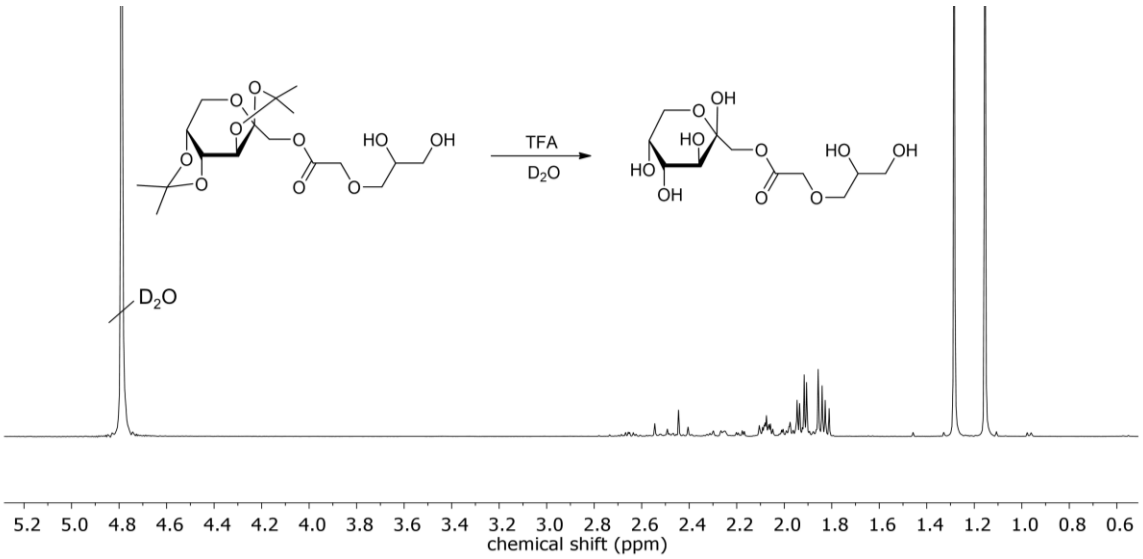

Figure 3. ^{1}H NMR spectrum (300 MHz, D_2O) 1-*O*-glycerol-*β*-D-fructopyranose.

In first attempts these reaction conditions were also applied to the functionalization of the polyether lipids. The carbohydrate-based derivative (**5**) was attached to BisOD-*hb*PG *via* a nucleophilic substitution reaction under basic conditions to obtain BisOD-*hb*P(G-*co*-G^{Fru})

(**10**) (S**cheme 3**). Upon varying the amount of applied 1-*O*-bromoacetate-2,3:4,5-di-*O*-isopropylidene-*β*-D-fructopyranose tailored degrees of functionalization (15 and 25 mol%) were obtained. So far, the successful attachment of the functional moieties was confirmed *via* ^{1}H NMR spectroscopy (**Figure 4**). Due to the formation of aggregates in methanol-d_4 the degree of functionalization as well as the molecular weight of the polyether lipids could not be calculated *via* end group analysis.

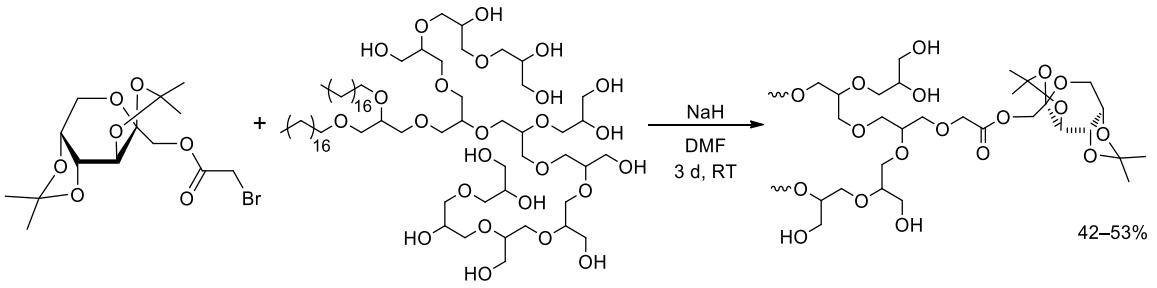

Scheme 3. Functionalization of BisOD-*hb*PG (**9**) with 1-*O*-bromoacetate-2,3:4,5-di-*O*-isopropylidene-*β*-D-fructopyranose (**5**) to obtain BisOD-*hb*P(G-*co*-G^{Fru}) (**10**).

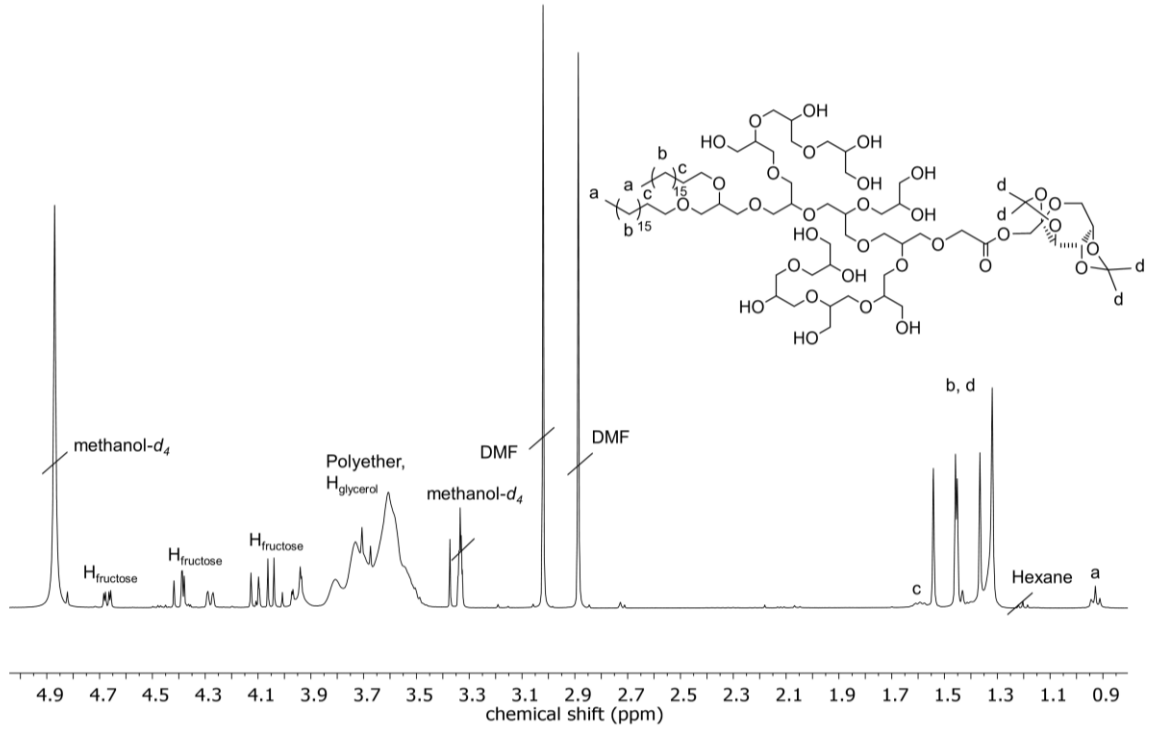

Figure 4. ^{1}H NMR spectrum (300 MHz, methanol-d_4) of BisOD-*hb*P(G-*co*-G^{Fru}) (**10**).

Table 1. Summary of the functionalized polyether lipids BisOD-*hb*P(G-*co*-G^{Fru}).

#	M_n^{th} g mol^{-1}	M_n^{NMR} g mol^{-1}	Degree of functionalizationth mol%
10a	10560	[a]	15
10b	13230	[a]	25

[a]calculation not possible due to the formation of aggregates.

The cleavage of the isopropylidene protecting groups still needs to be performed in a mixture of TFA/H_2O (1:1). Due to the preliminary results obtained from the model reaction, cleavage should be possible using the conditions described above. These first results already demonstrate the addressability and multifunctionality of BisOD-*hb*PG. Further attempts have to be carried out to functionalize and characterize the fructose-carrying polyether lipids. In addition, the cleavage of the protecting groups as well as the application of these lipids in liposomes still needs to be investigated.

IV) Multifunctional PEG-lipids enabling cross-linking

In **section 2.4** methacrylate-moieties were introduced into copolymers of polyethylene glycol and polyglycerol by enzymatic esterification of pendant hydroxyl groups. The double bonds can be cross-linked upon irradiation with UV light to enable the preparation of liposomes with enhanced stability due to a cross-linking of the polyether stealth layer. First results for cross-linking of the liposomes were already achieved. Nevertheless, the cross-linking of liposomal formulations as well as the influence of cross-linking on the stability still has to be investigated. A possible next step could be an introduction of pH-cleavable moieties to facilitate cleavage of the cross-linked stealth layer at the site of action. For this purpose, acetal or ketal functions could be integrated in the polyether lipid using recently established protocols.[14] In addition, the pendant double bonds could serve to attach functional moieties by using thiol-ene click chemistry, leading to functional polyether lipids.

V) Polyether-lipids for sterically stabilized nanoparticles

In **chapter 3** the successful application of cholesterol-based polyglycerol as surfactant in the miniemulsion/solvent evaporation technique was presented. Investigation of the protein

corona of the polystyrene particles revealed similar properties as PEGylated nanoparticles, *i.e.* a comparable stealth effect. Due to the pendant phosphonate moieties, these polyether lipids possess peculiar properties, which renders them interesting for targeted drug delivery *e.g.* considering bone tissue. For this application biocompatibility of the nanocarriers is indispensable, which can be achieved by using polylactide, leading to biodegradable carriers.[11] Furthermore, an encapsulation of a therapeutic cargo inside the nanoparticle can be carried out.

In addition, the phosphonate moieties are also promising to promote a crystallization of minerals, *e.g.* bone related material. In order to investigate the influence of the phosphonate-bearing polyether lipids on mineral formation, crystallization experiments using the prepared nanoparticles were performed in collaboration with Dr. Romina Schröder, Mirko Montigny and Prof. Dr. Wolfgang Tremel, Institute of Inorganic Chemistry and Analytical Chemistry, Johannes Gutenberg-University Mainz. In first attempts calcium carbonate was crystallized on the particle-surfaces. Amorphous $CaCO_3$ is known as potential precursor to initiate the formation of bone minerals.[12] Crystallization of calcite, the most stable crystalline polymorph of $CaCO_3$,[13] was possible, whereas a selective crystallization of vaterite, the less stable crystalline polymorph of $CaCO_3$,[15] was not successful, yet. Especially the crystallization of vaterite might be promising, because it still exhibits sufficient reactivity for a transformation to hydroxyapatite (HA).[15] So far, the particles were investigated using scanning electron microscopy (SEM) and XRD-measurements. **Figure 5** shows nanoparticles with calcite crystallized on the surface. Further attempts have to be carried out to investigate the possibility of crystallization and the ability of these nanoparticles to stimulate, *e.g.* bone regeneration.

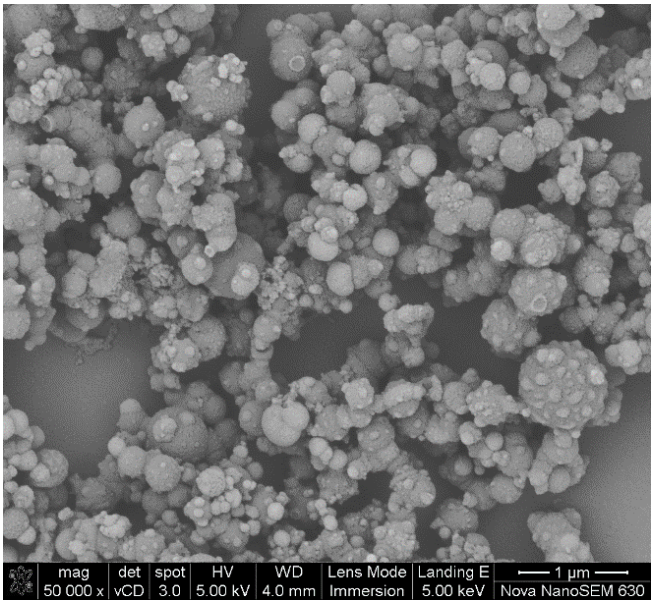

Figure 5. Crystallization of calcite on polystyrene nanoparticles stabilized with phosphonate-bearing polyether lipids.

VI) Extending the scope of multifunctionality by applying the monomer-activated AROP

In **chapter 4** the monomer-activated copolymerization of ethylene oxide (EO) and epichlorohydrin (ECH) was studied, revealing the formation of a tapered, block like structure. Furthermore, the obtained copolymers possess numerous chloride moieties which enable post-polymerization modification *via* nucleophilic substitution, rendering these structures versatile for multiple applications. The performed functionalization reactions still have to be improved to obtain full conversion. Moreover, the properties of the functional polyethers as well as the respective applications depending on the functional groups could be investigated in more detail. For example the introduction of long alkyl chains leads to amphiphilic copolymers that could be applied as non-ionic surfactants for various applications depending on the hydrophilic-lipophilic balance (HLB).[16,17] In addition, the successful attachment of dimethyl amine to the polymer is interesting because it can not be introduced directly during polymerization and consequently broadens the scope of amine-bearing polyethers. Quaternarization of the dimethyl amines could be performed to obtain a cationic PEG-based polyether, which might be promising for gene delivery.[18]

References

(1) Fritz, T.; Voigt, M.; Worm, M.; Negwer, I.; Müller, S. S.; Kettenbach, K.; Ross, T. L.; Roesch, F.; Koynov, K.; Frey, H. *et al.* Orthogonal Click Conjugation to the Liposomal Surface Reveals the Stability of the Lipid Anchorage as Crucial for Targeting. *Chem. Eur. J.* **2016**, *22*, 11578–11582.

(2) Reibel, A. T.; Müller, S. S.; Pektor, S.; Bausbacher, N.; Miederer, M.; Frey, H.; Rösch, F. Fate of linear and branched polyether-lipids in vivo in comparison to their liposomal formulations by (18)f-radiolabeling and positron emission tomography. *Biomacromolecules* **2015**, *16*, 842–851.

(3) Wagener, K.; Worm, M.; Pektor, S.; Schinnerer, M.; Thiermann, R.; Miederer, M.; Frey, H.; Rösch, F. Comparison of Linear and Hyperbranched Polyether Lipids for Liposome Shielding by 18F-Radiolabeling and Positron Emission Tomography. *Biomacromolecules* **2018,** DOI: 10.1021/acs.biomac.8b00115.

(4) Müller, S. S.; Fritz, T.; Gimnich, M.; Worm, M.; Helm, M.; Frey, H. Biodegradable hyperbranched polyether-lipids with in-chain pH-sensitive linkages. *Polym. Chem.* **2016**, *7*, 6257–6268.

(5) Irache, J. M.; Salman, H. H.; Gamazo, C.; Espuelas, S. Mannose-targeted systems for the delivery of therapeutics. *Expert Opin. Drug Deliv.* **2008**, *5*, 703–724.

(6) Ting, S. R. S.; Chen, G.; Stenzel, M. H. Synthesis of glycopolymers and their multivalent recognitions with lectins. *Polym. Chem.* **2010**, *1*, 1392.

(7) David, A.; Kopecková, P.; Kopecek, J.; Rubinstein, A. The role of galactose, lactose, and galactose valency in the biorecognition of *N*-(2-hydroxypropyl)methacrylamide copolymers by human colon adenocarcinoma cells. *Pharm. Res.* **2002**, *19*, 1114–1122.

(8) Ponader, D.; Maffre, P.; Aretz, J.; Pussak, D.; Ninnemann, N. M.; Schmidt, S.; Seeberger, P. H.; Rademacher, C.; Nienhaus, G. U.; Hartmann, L. Carbohydrate-lectin recognition of sequence-defined heteromultivalent glycooligomers. *J. Am. Chem. Soc.* **2014**, *136*, 2008–2016.

(9) Lundquist, J. J.; Toone, E. J. The Cluster Glycoside Effect. *Chem. Rev.* **2002**, *102*, 555–578.

(10) Zhao, J.; Lai, H.; Lu, H.; Barner-Kowollik, C.; Stenzel, M. H.; Xiao, P. Fructose-Coated Nanodiamonds: Promising Platforms for Treatment of Human Breast Cancer. *Biomacromolecules* **2016**, *17*, 2946–2955.

(11) Musyanovych, A.; Schmitz-Wienke, J.; Mailänder, V.; Walther, P.; Landfester, K. Preparation of biodegradable polymer nanoparticles by miniemulsion technique and their cell interactions. *Macromol. Biosci.* **2008**, *8*, 127–139.

(12) Gower, L. B. Biomimetic model systems for investigating the amorphous precursor pathway and its role in biomineralization. *Chem. Rev.* **2008**, *108*, 4551–4627.

(13) Hagiya, K.; Matsui, M.; Kimura, Y.; Akahama, Y. The crystal data and stability of calcite III at high pressures based on single-crystal X-ray experiments. *J. Miner. Petrol. Sci.* **2005**, *100*, 31–36.

(14) Matthias Worm. pH-Cleavable and Hyperbranched Polyether Architectures: From Novel Synthesis Strategies to Applications in Nanotechnology and Biomedicine. Dissertation, Johannes Gutenberg-Universität Mainz, Mainz, 2016.

(15) Schröder, R.; Pohlit, H.; Schüler, T.; Panthöfer, M.; Unger, R. E.; Frey, H.; Tremel, W. Transformation of vaterite nanoparticles to hydroxycarbonate apatite in a hydrogel scaffold: Relevance to bone formation. *J. Mater. Chem. B* **2015**, *3*, 7079–7089.

(16) McKenzie, D. A. Nonionic surfactants. *J. Am. Oil Chem. Soc.* **1978**, *55*, 93–97.

(17) Pasquali, R. C.; Sacco N.; Bregni, C. The Studies on Hydrophilic-Lipophilic Balance (HLB): Sixty Years after William C. Griffin´s Pioneer Work (1949-2009). *Lat. Am. J. Pharm.* **2009**, *28*, 313–317.

(18) Xu, F. J.; Yang, W. T. Polymer vectors via controlled/living radical polymerization for gene delivery. *Prog. Polym. Sci.* **2011**, *36*, 1099–1131.

6. Appendix

6.1 Examples of Xylochemistry: Colorants and Polymers

Jonas Kühlborn,[a] Ann-Kathrin Danner,[a,b] Holger Frey,[a] Rishab Iyer,[c] Anthony J. Arduengo III,[c] and Till Opatz[a,*]

[a]Institute of Organic Chemistry, Johannes Gutenberg-University Mainz, Duesbergweg 10-14, 55128 Mainz, Germany.

[b]Graduate School Materials Science in Mainz, Staudinger Weg 9, 55128 Mainz, Germany.

[c]Department of Chemistry, The University of Alabama, Tuscaloosa, Alabama 35487, United States.

Published in *Green Chemistry*, **2017**, *19*, 3780-3786.

Available *via* the Royal Society of Chemistry´s website:

http://pubs.rsc.org/en/content/articlelanding/2017/gc/c7gc01244f#!divAbstract

ROYAL SOCIETY OF CHEMISTRY View Article Online
DOI: 10.1039/C7GC01244F

Journal Name

ARTICLE

Examples of Xylochemistry: Colorants and Polymers

Jonas Kühlborn[a], Ann-Kathrin Danner[a,b], Holger Frey[a], Rishab Iyer[c], Anthony J. Arduengo III[c,*], and Till Opatz[a,*]

Received 00th January 20xx,
Accepted 00th January 20xx

DOI: 10.1039/x0xx00000x

www.rsc.org/

Dedicated to Prof. Dr. Hans-Günther (Hagga) Schmalz on the occasion of his 60th birthday

Against the backdrop of modern sustainable chemistry and valorization of biomass for chemical raw materials, the syntheses of indigo dyes and polyamides as representatives of two classes of everyday chemical products based on xylochemicals are described. Wood-derived starting materials were transformed into functional materials using the principles of *green chemistry* to expand the scope of products gained from renewable resources. The indigo dyes were synthesized in a short, straightforward sequence starting from vanillin without the use of organic solvents. Two polyamides, representatives of todays most important class of polymers, were obtained from 4-propylcyclohexanol, which is one of the longest known (and most abundant) hydrogenative depolymerization products of lignin.

Introduction

The current chemical infrastructure relies mainly on petroleum and other fossil resources, the supplies of which are finite and which become increasingly difficult to extract from underground deposits. Furthermore, their use leads to a carbon imbalance in our ecosystem[1] and they contribute to a significant degree to the anthropogenic pollution of our environment. As a result of these issues, a paradigm change in the chemical infrastructure towards a sustainable production and use of chemical intermediates needs to be established. Possible solutions have been presented in the concepts of Anastas and Warner, who also postulated the 12 principles of *green chemistry*. One major aspect of these principles is the use of renewable feedstocks to provide chemical building blocks, intermediates and reagents.[2] Attention is recently turning to the use of biomass as a new raw material for energy and chemical production[3, 4] which bears several advantages such as an ecologically benign production and the "renewability" of the resources in contrast to the continual depletion of coal and petroleum. Besides these ecological factors there are also chemical advantages including the abundance of complex substituents and groupings found in naturally occurring chemical building blocks such as the presence of functional groups or heteroatoms, and, importantly, the chiral content of these materials.[5] Such preexisting functionalities should be maintained and utilized rather than destroyed and rebuilt in order to seize the full potential of the raw material employed. In the area of biomass valorization, lignin has received great attention as a promising feedstock in the past decades.

Lignin is part of lignocellulose and accounts for approximately 30% of the organic carbon in the biosphere. It consists of phenylpropanoid units derived from *p*-coumaryl, coniferyl and sinapyl alcohol.[6] These assemble through C–O and C–C bonds to the unique heterogenic, aromatic, hyperbranched polymer lignin (figure 1), which can serve as a starting point for the preparation of a variety of useful chemical intermediates. Although the depolymerization of lignin is known since 1938,[7] great effort has been put into its valorization as an effective source of low-

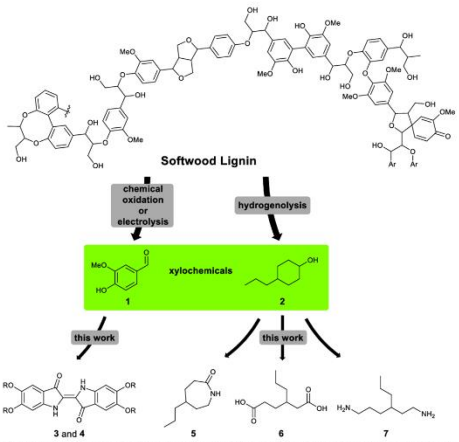

Figure 1 Conversion of lignin through key xylochemicals to dyes and bifunctional A_2/B_2 monomers.

[a] Institute of Organic Chemistry, Johannes Gutenberg University, Duesbergweg 10–14, 55128 Mainz, Germany.
[b] Graduate School Materials Science in Mainz, Staudingerweg 9, 55128 Mainz.
[c] Department of Chemistry, The University of Alabama, Tuscaloosa, Alabama 35487, United States.

† Footnotes relating to the title and/or authors should appear here.
Electronic Supplementary Information (ESI) available: [details of any supplementary information available should be included here]. See DOI: 10.1039/x0xx00000x

molecular-weight compounds in recent years.[8] A variety of depolymerization methods have been developed to this end which include pyrolysis, hydrolysis, hydrogenolysis, liquid-phase reforming, chemical oxidation, and gasification. These methods mainly produce aromatic compounds of six to nine carbon atoms with functional groups such as hydroxyl, carbonyl or carboxyl.[9]

We recently reported the xylochemical synthesis of the berberine-type alkaloid Ilicifoline B in a sequence in which all carbon atoms are exclusively derived from wood.[10, 11] In order to enhance the portfolio of products available through this strategy, we now report a synthesis of chemically well-defined colorants and unconventional polyamides based on wood derived molecules (xylochemicals). Furthermore, all steps of the synthesis are conducted with methods according to the principles of *green chemistry* to maximize the sustainability of the entire process and minimize environmental impact.

Indigo dyes as well as polyamides belong to the most common functional materials and have a long history in chemical industry and marketplace. Indigo itself is known and used since the time of the ancient Egyptians and has received even more attention since its structural elucidation by von Baeyer in 1883.[12] A variety of indigo syntheses and derivatives have since been developed. Furthermore new applications for indigos have been investigated, for example their use as semiconductors.[13]

Polyamides received popularity by the development of the synthetic fibers nylon (polyamide 6,6, PA66) by Carothers in 1937[14] and Perlon® (polyamide 6, PA6) by Schlack in 1938.[15] Because of their unmatched stability and unique properties like high toughness and good wear properties, polyamides are still an important class of materials. Today's production of indigo dyes as well as that of polyamides heavily relies on petroleum raw materials and environmentally deleterious processes.[16, 17] Here, we present an alternative and sustainable access to both compound classes.

Results and discussion

Indigo dye syntheses

The synthesis of the indigo derivatives started from veratraldehyde (**8**) which can be directly isolated from biomass or can be obtained from vanillin (**1**) by O-methylation with dimethyl sulphate[18] (available from the reaction of methanol with oleum or SO_3). The conversion of lignin to vanillin through chemical oxidation[19] or electrolysis[20] is widely explored. Veratraldehyde was nitrated as described in the literature with 65% aqueous nitric acid to the corresponding 6-nitro derivative (**9**) in 91% yield (figure 2).[21]

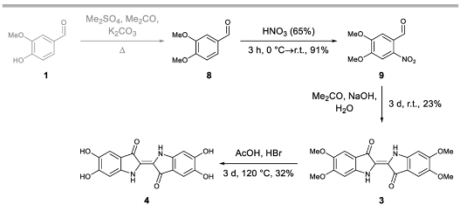

Figure 2 Synthetic route to the indigos **3** and **4** based on the xylochemical **1**.

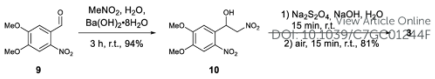

Figure 3 Alternative sustainable route to **3** based on **2**.

The latter could be transformed into 5,5‘,6,6‘-tetramethoxyindigo (**3**) in 23% yield according to a procedure by Harley-Mason through reaction with acetone and aqueous sodium hydroxide in a Baeyer-Drewsen indigo synthesis.[22] Acetone and methanol (also known as wood alcohol) are available from wood by the long known processes of wood pyrolysis and distillation.[23] The Baeyer-Drewsen indigo synthesis is the oldest synthetic method to produce indigo derivatives.[12] Although it was eventually replaced by routes starting from aniline, it represents the most sustainable route because of the use of aromatic aldehydes and acetone, which can easily be obtained from renewable sources.[8] Its low yield was suspected to be a result of the complex reaction mechanism. Indigo derivative **3** could further be transformed into 5,5‘,6,6‘-tetrahydroxyindigo (**4**) in 32% yield with HBr/acetic acid (figure 2).

While this route already fulfils the criteria of xylochemistry, we sought to prepare **3** by an alternative procedure to maximize synthetic efficiency. Starting from aldehyde **9**, a catalytic Henry-reaction with $Ba(OH)_2{\cdot}8H_2O$ and nitromethane in water provided the corresponding nitroaldol product **10** in 94% yield (figure 3).[24] This compound could be converted to indigo **3** using a method also developed by Harley-Mason. Treatment of **10** with sodium dithionite in aqueous alkaline solution and subsequent aerial oxidation produced **3** in 81% yield.[25]

Although the synthesis of indigos from 1-(2-nitrophenyl)-2-nitroethanol derivatives is a very rarely used, it is in accord with the principles of *green chemistry*. Nitromethane can be generated from dimethyl sulfate and potassium or sodium nitrite in high yield and purity on an industrial scale.[26] All steps of the synthesis were conducted in water using catalytic methods and mild reaction conditions.

Like most indigo dyes, indigos **3** and **4** are poorly soluble in organic solvents and water. Compounds **3** and **4** are known since 1948[22] and 1947,[27] respectively, but apart from a report on some photophysical properties of **3** by De Melo et al.,[28] no further information or spectroscopic data have been reported. Indigo **3** can be used for vat dyeing textiles after dithionite reduction (see ESI, S50).

Polyamide syntheses

For the synthesis of the polyamide monomers, we chose 4-propylcyclohexanol (**2**) as the key xylochemical. It is one of the first compounds obtained through the depolymerization pathway by means of catalytic hydrogenolysis of hardwood lignin over copper chromite developed by Adkins et al. in 1938 with 11 wt% yield.[7, 8] Because of the more suitable implementation on a laboratory scale, we prepared **2** from inexpensive 4‘-hydroxypropiophenone (**11**) through hydrogenation over Pd/C in the presence of lactic acid to obtain **2** in 92% yield (figure 4).[29] As with the actual xylochemical, **2** was obtained as a mixture of both possible diastereomers with a ratio of cis:trans 1:1 (^{1}H-NMR, see the ESI, S27). These could easily be separated by flash chromatography for characterization, but all

View Article Online
DOI: 10.1039/C7GC01244F

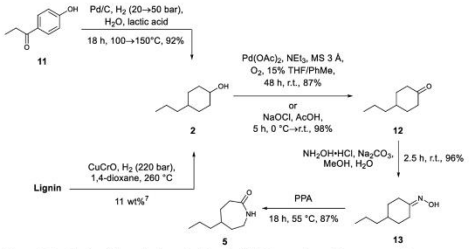

Figure 4 Synthesis of the xylochemical **2** and of AB-type polyamide monomer **5**.

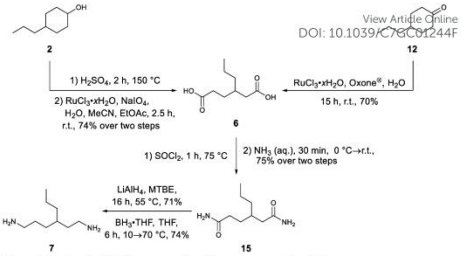

Figure 5 Synthesis of A_2/B_2-type polyamide monomers **6** and **7**.

further syntheses were carried out with the isomeric mixture. Based on **2**, the corresponding *ε*-lactam **5** as well as the corresponding hexanedioic acid **6** and hexanediamine **7** were synthesized. These compounds represent xylochemical versions of the most common monomers for polyamide synthesis.

Lactam **5** was produced according to an industrial *ε*-caprolactam synthesis[30] by oxidation of **2** to the ketone **12** which was converted to the corresponding oxime **13** followed by Beckmann-rearrangement (figure 4).

For the oxidation of **2**, several green aerobic oxidation methods were evaluated. Aerobic procedures can be considered as the most sustainable oxidation methods because they guarantee good atom-economy and the only side-product is water.[5] While the most common procedures based on the nitroxyl radical TEMPO (**14a**)[31] did not show any conversion of **2** (table 1, entries 1–3) other nitroxyl radicals like ABNO (**14b**),[32] keto-ABNO (**14c**)[33] or PINO (**14d**)[34] led to moderate yields of **12** (table 1, entries 4–6). Remarkably, only the *cis*-diastereomer of **2** could be converted to the ketone **12** with keto-ABNO (**14c**, table 1, entry 5).

The best yield (87%) among the aerobic oxidation procedures was provided by a method based on $Pd(OAc)_2$/triethylamine in a toluene/THF mixture under oxygen atmosphere (table 1, entry 7).[35]

Table 1 Used nitroxyl radicals and tested reaction conditions for the aerobic oxidation of **2** to **12**.

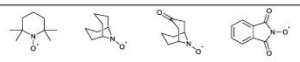

Entry	Oxidation system	Solvent	Conditions (yield, %)
1	**14a**, NH_4NO_3, HCl, air	MeCN	60 °C, 35 h (0)
2	**14a**, $Cu(OAc)_2$, air	MeCN:H_2O	r.t., 18 h (0)
3	**14a**, $NaNO_2$, HBr, air	MeCN	r.t., 38 h (0)
4	**14b**, $Fe(NO_3)_3{\cdot}9H_2O$, air	MeCN	r.t., 6 h (60)
5	**14c**, $NaNO_2$, HNO_3, O_2	MeCN	r.t., 38 h (40)[a]
6	**14d**, $Fe(NO_3)_3{\cdot}9\ H_2O$, O_2	MeCN	r.t., 48 h (45)
7	$Pd(OAc)_2$ (3 mol%), NEt_3 (6 mol%), O_2	PhMe:THF	r.t., 48 h (87)
8	NaOCl (1.2 eq)	AcOH	r.t., 5 h (98)

[a] full conversion of *cis*-**2**; *trans*-**2** could still be detected by TLC and NMR.

The failure of the nitroxyl radical based methods is suspected to be the result of steric hindrance. As an inexpensive and simple alternative procedure, treatment with NaOCl in acetic acid readily oxidized **2** to **12** in 98% yield on a 10 gram scale (table 1, entry 8).[36] The following synthesis of the oxime **13** was conducted with hydroxylamine hydrochloride and sodium carbonate in methanol and water in 96% yield.[37] Beckmann-rearrangement with polyphosphoric acid at 55 °C[38] provided **5** in 87% yield.

The monomers for the A_2/B_2-type polyamide, compounds **6** and **7**, could be obtained from alcohol **2** by acidic dehydration and catalytic oxidative cleavage or from ketone **12** by oxidation to yield diacid **6** followed by ammonolysis of the corresponding acyl chloride and reduction to obtain diamide **7** (figure 5).

Direct oxidation of **2** to **6** with tungstic acid and H_2O_2, with NaOCl under sonication or $RuCl_3{\cdot}xH_2O$ and Oxone® failed. Thus, dehydration was performed by catalytic amounts of sulfuric acid at 150 °C.[39] The resulting cyclohexene was then subject to catalytic oxidative cleavage with sodium periodate as the oxidizing agent using $RuCl_3{\cdot}xH_2O$ as a catalyst.[40] Through this sequence, **6** could be obtained in 74% yield over two steps. The outcome of this reaction strongly depends on the amount of oxidizing reagent. While the use of two equivalents of $NaIO_4$ gives the corresponding dialdehyde, three or more equivalents are necessary to obtain the dicarboxylic acid.[40] Although the use of large amounts of oxidizing reagent is in contrast to the precepts of sustainable chemistry, the periodate could be regenerated from the formed iodate by electrochemical oxidation.[41] Alternatively **12** could be oxidized to **6** in 70% yield using the water soluble and inexpensive Oxone®, in combination with as little as 0.5 mol% of $RuCl_3{\cdot}xH_2O$ as a catalyst and water as the solvent.[42] After conversion of **6** into the acyl chloride with thionyl chloride, ammonolysis with aqueous ammonia provided diamide **15** in 75% yield over two steps.[43] This diamide could be reduced to the corresponding diamine **7** either with lithium aluminium hydride (LAH) in MTBE in 71% yield or with borane·THF complex in THF in 74% yield.[44] The reduction step can still be further optimized to improve its sustainability and e.g.

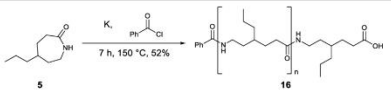

Figure 6 Anionic ring-opening polymerization of **5** to the corresponding polyamide **16**.

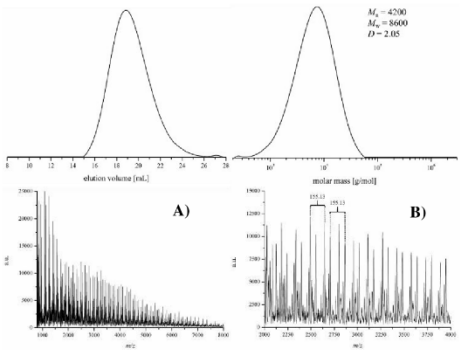

Figure 7 SEC result (top left: elution volume, right: molar mass) and MALDI-ToF spectrum (below) **A)** full spectrum, **B)** enlarged region (m/z = 2000–4000) of AB-type polyamide **16**.

electrochemical reductions[45] or catalytic hydrogenations[46] of amides to amines have been developed to this end.

Polymerizations

We have investigated several polymerization/oligomerization methods for **5** (which was previously claimed to be barely polymerizable due to an inhibitory effect of the propyl moiety).[47, 48] While anionic ring-opening polymerization (AROP) with sodium hydride and *N*-acteyl caprolactam as well as nucleophilic polymerization with octylamine and tin(II) 2-ethylhexanoate did not lead to promising results, AROP with potassium as the initiator and benzoyl chloride as a termination agent worked well (figure 6).[49]

The resulting polyamide **16** is soluble in most organic solvents except for ethereal solvents and chloroform. The yield was diminished due to the volatilization of the monomer **5** at the high temperature and low pressure that were necessary for the polymerization. In order to obtain entirely monomer-free polyamide **16**, dialysis was conducted while washing with hexane/ethyl acetate and water or precipitation in cold diethyl ether did not remove low molecular compounds to a sufficient extent to allow analytical characterization. Characterization of the polyamide thus obtained was performed by SEC, MALDI-ToF-MS and NMR, all of which indicated a successful polymerization. The NMR data show the aliphatic main chain and the terminal benzoyl group (ESI, S45).

Determination of the chain length with the end group analysis method leads to n = 25 and therefore M_n = 4200 g mol^{-1} including the terminal groups. This is in accordance with the result of the SEC experiment showing a value of 8600 g mol^{-1} for M_w and 4200 g mol^{-1} for M_n with a dispersity ($Đ$) of 2.05 (figure 7). The high dispersity is ascribed to the bulk polymerization, which leads to quick solidification and poor stirring of the mixture. Consequently not all chains can be terminated at the same time after addition of the termination agent. This leads to unequal distribution of the chain length and of the molecular weight. SEC shows a unimodal product distribution.

The MALDI-ToF experiment (figure 7) also shows successful polymerization, but two peak series with the peak distance of the repeating unit (M = 155.13 g mol^{-1}) can be identified. According to our calculations, one series originates from the polyamide with the benzoyl group (M = 105.03 g mol^{-1}) attached to the terminal nitrogen and with a terminal carboxylic acid moiety as a potassium adduct (figure 7, **B**)). The second peak series results from polyamide matrix adducts (HABA-Matrix (M = 242.07 g mol^{-1}), figure 7, **B**)). The MALDI experiment therefore confirms that the benzoyl group is attached to the polyamide and no cyclic polymers were formed. Furthermore, the terminal lactam ring was hydrolyzed to the corresponding amino acid, most probably during the work up of the polymer.

The recorded spectra cannot be used to determine the average molecular weight or dispersity of the polymer since the peak intensity cannot be considered proportional to the abundance (mass discrimination). These properties are rather determined using SEC or NMR experiments.

The thermal behavior of **16** was investigated by differential scanning calorimetry (DSC) displaying a glass transition temperature (T_g) of 15 °C, but no distinct melting point (T_m, figure 8). The most important factor influencing T_g is the efficiency of hydrogen bonding of the amide group between the polymer chains. As expected, the flexible propyl side chain in **16** reduces the ability to form interchain hydrogen bonds and of effective alignment of the polymer chains in comparison with T_g of Nylon 6 (T_g = 51 °C).[50] The substitution increases the flexibility of the polymer.

We have tested several polycondensation methods with derivatives of dicarboxylic acid **6** for the synthesis of A_2/B_2-type polyamides, but neither the activated pentachlorophenyl ester nor the diethyl ester of **6** reacted with **7**. On the other hand, polycondensation of the acyl chloride with diamine **7** in *N*,*N*-dimethylacetamide (DMAc) in the presence of triethylamine at room temperature worked well (figure 9).[51] Again, the polyamide proved to be soluble in most organic solvents except for ethereal solvents and chloroform. It was also purified using dialysis for analytical characterization. It is suspected that the preceding formation of the acid chloride lowered the yield because it might not have resulted in quantitative conversion, but rather in formation of the cyclic anhydride and therefore leads to a slight excess of diamine although dicarboxylic acid and diamine were used in equimolar amounts. Nevertheless, a moderate yield of 62% of polymer **17** was achieved.

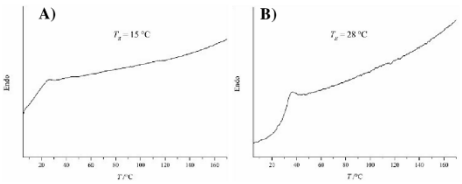

Figure 8 DSC scans of **A)** AB-type polyamide **16** and **B)** A_2/B_2-type polyamide **17**.

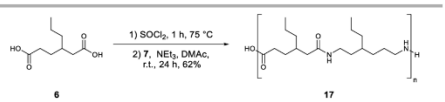

Figure 9 Synthesis of A_2/B_2-type polyamide **17**.

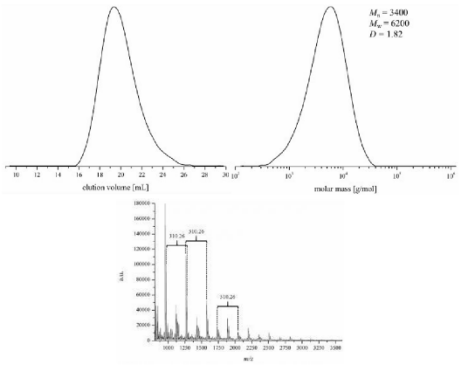

Figure 10 SEC result (top left: elution volume, right: molar mass) and MALDI-ToF spectrum (below) of A_2/B_2-type polyamide **17**.

The polyamide thus obtained was investigated by SEC, MALDI-ToF-MS and NMR and indicated a successful polymerization. The NMR data show two sets of alkyl side chains as well as two carbonyl groups (ESI, S47–S48). In lack of an end group, the molecular weight could only be determined using SEC (figure 10). This experiment results in values of 3400 g mol^{-1} for M_n and 6200 g mol^{-1} for M_w with a dispersity ($Đ$) of 1.82. MALDI-ToF data also confirm successful polymerization, but three peak sets with a peak distance of the repeating unit (M = 310.26 g mol^{-1}) can be identified (figure 10). The most intensive peaks belong to the sodium adduct of the cyclic polymer. The second intensive peak set originates from the corresponding linear polymer **17** (figure 10, sodium adduct). The difference between these two peak sets adds up to M = 18 g mol^{-1}. The third peak series belongs to a polyamide with two terminal amine functionalities. This polyamide is most probably the result of the acid depletion mechanism outlined above.

Differential scanning calorimetry (DSC) investigations of **17** resulted in a glass transition (T_g) of 28 °C and, as with **16**, no distinct melting point was observed (figure 10), which is clearly due to the branched nature of the monomer units. The propyl branches impede crystallization and lead to strong softening, i.e., low T_g of the A_2/B_2-type polyamides compared to the T_g of unsubstituted PA66 (T_g = 70 °C)[52] as in the case of the AB-type polyamide. The low T_g is based on the impeded order of the polyamide main chains and conesequently the reduced possibility of hydrogen bonding between the chains. On the other hand, the hydrogen bonding capability of the A_2/B_2-type polyamides appears to be somewhat higher than of the AB-type polyamides, as is manifest in the higher value for T_g of **17** compared to **16**. We believe the monomers **5**–**7** are of interest as a component in other polyamides to reduce melting points and degree of crystallization.

Conclusion

We have successfully established a sustainable synthesis for two colorants, the indigo dyes **3** and **4**, as well as for the polyamide monomers **5**–**7** along with the respective polymers from the xylochemicals vanillin (**1**) and 4-propylcyclohexanol (**2**). 6-Nitroveratraldehyde (**9**), available from vanillin in two steps, was transformed to **3** along two different routes. Baeyer-Drewsen indigo synthesis with acetone and NaOH[22] provided **3** with low yield in a single step, whereas the two-stage synthesis using a catalytic Henry-reaction and subsequent reduction provided **3** with an overall yield of 89% over three steps. Both sequences were conducted without using organic solvents and extensive purification. Cleavage of the methyl ether moieties of **3** yielded tetrahydroxy-indigo **4**. Starting from the xylochemical 4-propylcyclohexanol (**2**), the polyamide monomers **5**–**7** were synthesised in moderate to high yields using methods of green chemistry. Lactam **5** was produced in 93% yield over three steps using a sequence of catalytic aerobic oxidation of **2** followed by oxime synthesis and Beckmann-rearrangement. The A_2/B_2-type polyamide monomers were obtained by acid catalyzed elimination of **2** followed by catalytic oxidative olefin cleavage or by direct oxidation of **12** to obtain **6** in 74% or in 84% over two steps, respectivley. Subsequent formation of the acid chloride of **6**, ammonolysis and reduction provided the diamine **7** in 63% over five steps. Polymerization of these monomers was achieved using anionic ring-opening polymerization for **5** and polycondensation for **6** and **7**, leading to polyamides with unusual properties. The xylochemistry-derived monomers could also be used for copolymerization to tune the aggregation behavior of classical polyamides. In summary, sustainable and straightforward synthetic procedures of functional materials like colorants and polymers were established that could potentially substitute petroleum based methods and products. All carbon atoms in the products originate from renewable resources.

Acknowledgements

The authors thank Monika Schmelzer for SEC measurements (Mainz), Maria Müller (Mainz) for measuring DSC scans, Dr. Elena Berger-Nicoletti (Mainz) for MALDI-ToF-MS measurements, Dr. Johannes C. Liermann (Mainz) for his support concerning NMR measurements and Dr. Norbert Hanold (Mainz, deceased) for HR-ESI-MS measurements. This work was supported by the Carl-Zeiss foundation (project ChemBioMed) as well as by the German Federal Ministry of Education and Research (grant no. 01DG17013). A. Danner is a recipient of a DFG-funded position through the Excellence Initiative by the Graduate School Science in Mainz (GSC 266). A.J.A. acknowledges support through a University of Alabama Research Award: RG14648 "Technology for a Sustainable Chemical Economy" – STANCE.

Notes and references

1 J. R. Trabalka, *Atmospheric Carbon Dioxide and the Global Carbon Cycle*, U.S. Department of Energy, Office of Energy Research, Office of Basic Energy Sciences, Carbon Dioxide Research Division, 1985.
2 P. T. Anastas and J. C. Warner, *Green Chemistry Theory and Practice*, Oxford University Press, New York, 1998.
3 P. Gallezot, *Chem. Soc. Rev.*, 2012, **41**, 1538–1558.
4 J. F. Jenck, F. Agterberg and M. J. Droescher, *Green Chem.*, 2004, **6**, 544–556.
5 R. A. Sheldon, *Green Chem.*, 2007, **9**, 1273–1283.

6 W. Boerjan, J. Ralph and M. Baucher, *Annu. Rev. Plant Biol.*, 2003, **54**, 519–546.
7 E. E. Harris, J. D'Ianni and H. Adkins, *J. Am. Chem. Soc.*, 1938, **60**, 1467–1470.
8 M. D. Kärkäs, B. S. Matsuura, T. M. Monos, G. Magallanes and C. R. J. Stephenson, *Org. Biomol. Chem.*, 2016, **14**, 1853–1914.
9 J. Zakzeski, P. C. A. Bruijnincx, A. L. Jongerius and B. M. Weckhuysen, *Chem. Rev.*, 2010, **110**, 3552–3599.
10 D. Stubba, G. Lahm, M. Geffe, J. W. Runyon, A. J. Arduengo and T. Opatz, *Angew. Chem., Int. Ed. Engl.*, 2015, **54**, 14187–14189.
11 D. Stubba, G. Lahm, M. Geffe, J. W. Runyon, A. J. Arduengo and T. Opatz, *Angew. Chem.*, 2015, **127**, 14394–14396.
12 A. von Baeyer and V. Drewsen, *Ber. Dtsch. Chem. Ges.*, 1883, **16**, 2205–2208.
13 M. Irimia-Vladu, E. D. Głowacki, P. A. Troshin, G. Schwabegger, L. Leonat, D. K. Susarova, O. Krystal, M. Ullah, Y. Kanbur, M. A. Bodea, V. F. Razumov, H. Sitter, S. Bauer and N. S. Sariciftci, *Adv. Mater.*, 2012, **24**, 375–380.
14 *US Pat.,* 2071253 A, 1937.
15 *US Pat.,* 2142007 A, 1938.
16 S. Van de Vyver and Y. Román-Leshkov, *Catal. Sci. Technol.*, 2013, **3**, 1465–1479.
17 R. Beerthuis, G. Rothenberg and N. R. Shiju, *Green Chem.*, 2015, **17**, 1341–1361.
18 L. Gavara, T. Boisse, J.-P. Hénichart, A. Daïch, B. Rigo and P. Gautret, *Tetrahedron*, 2010, **66**, 7544–7561.
19 E. A. B. d. Silva, M. Zabkova, J. D. Araújo, C. A. Cateto, M. F. Barreiro, M. N. Belgacem and A. E. Rodrigues, *Chem. Eng. Res. Des.*, 2009, **87**, 1276–1292.
20 D. Schmitt, C. Regenbrecht, M. Hartmer, F. Stecker and S. R. Waldvogel, *Beilstein J. Org. Chem.*, 2015, **11**, 473–480.
21 S. Kumar, E. J. Wachtel and E. Keinan, *J. Org. Chem.*, 1993, **58**, 3821–3827.
22 J. Harley-Mason, *J. Chem. Soc.*, 1948, 1244–1247.
23 O. Beaumont and Y. Schwob, *Industrial & Engineering Chemistry Process Design and Development*, 1984, **23**, 637–641.
24 M. Pandi, P. K. Chanani and S. Govindasamy, *Applied Catalysis A: General*, 2012, **441–442**, 119–123.
25 R. H. Horn, R. B. Miller, S. N. Slater, M. W. Partridge, F. Bell, W. H. Hunter, G. Anderson, N. Campbell, G. T. Newbold, W. F. Beech, N. Legg, J. Harley-Mason, A. G. Sharpe and H. Kacser, *J. Chem. Soc.*, 1950, 2900–2908.
26 J. Liu, *Liquid Explosives*, Springer, Berlin, Heidelberg, 2015.
27 J. Harley-Mason, *Nature (London, U. K.)*, 1947, **159**, 338–339.
28 J. S. S. de Melo, R. Rondão, H. D. Burrows, M. J. Melo, S. Navaratnam, R. Edge and G. Voss, *ChemPhysChem*, 2006, **7**, 2303–2311.
29 *WO Pat.,* 2002014253 A1, 2002.
30 G. Bellussi and C. Perego, *CATTECH*, 2000, **4**, 4–16.
31 R. Prebil, G. Stavber and S. Stavber, *Eur. J. Org. Chem.*, 2014, **2014**, 395–402.
32 L. Wang, S. Shang, G. Li, L. Ren, Y. Lv and S. Gao, *J. Org. Chem.*, 2016, **81**, 2189–2193.
33 M. B. Lauber and S. S. Stahl, *ACS Catalysis*, 2013, **3**, 2612–2616.
34 H. Zhao, W. Sun, C. Miao and Q. Zhao, *J. Mol. Catal. A: Chem.*, 2014, **393**, 62–67.
35 M. J. Schultz, S. S. Hamilton, D. R. Jensen and M. S. Sigman, *J. Org. Chem.*, 2005, **70**, 3343–3352.
36 R. V. Stevens, K. T. Chapman and H. N. Weller, *J. Org. Chem.*, 1980, **45**, 2030-2032.
37 *WO Pat.,* 2011075699 A3, 2011.
38 D. G. Powell and L. J. Mathias, *J. Am. Chem. Soc.*, 1990, **112**, 669–675.
39 G. H. Coleman and H. F. Johnstone, *Org. Synth.*, 1925, **5**, 33.
40 F. Zimmermann, E. Meux, J.-L. Mieloszynski, J.-M. Lecuire and N. Oget, *Tetrahedron Lett.*, 2005, **46**, 3201–3203.
41 L. J. J. Janssen and M. H. A. Blijlevens, *Electrochim. Acta*, 2003, **48**, 3959–3964.
42 L. Rokhum and G. Bez, *Synth. Commun.*, 2011, **41**, 548–552.
43 A. Treibs and F. Neumayr, *Chem. Ber.*, 1957, **90**, 76–79.
44 A. V. Malkov, L. Gouriou, G. C. Lloyd-Jones, I. Starý, V. Langer, P. Spoor, V. Vinader and P. Kočovský, *Chemistry – A European Journal*, 2006, **12**, 6910-6929.
45 C. Edinger, V. Grimaudo, P. Broekmann and S. R. Waldvogel, *ChemElectroChem*, 2014, **1**, 1018–1022.
46 G. Beamson, A. J. Papworth, C. Philipps, A. M. Smith and R. Whyman, *Adv. Synth. Catal.*, 2010, **352**, 869-883.
47 H. K. Hall, *J. Am. Chem. Soc.*, 1958, **80**, 6404–6409.
48 L. E. Wolinski and H. R. Mighton, *Journal of Polymer Science*, 1961, **49**, 217–223.
49 M. Winnacker, S. Vagin, V. Auer and B. Rieger, *Macromol. Chem. Phys.*, 2014, **215**, 1654–1660.
50 A. Siegmann and Z. Baraam, *Die Makromolekulare Chemie, Rapid Communications*, 1980, **1**, 113 –117.
51 A. Sudo and S. Sugita, *Journal of Polymer Science Part A: Polymer Chemistry*, 2016, **54**, 3436-3443.
52 F. Gao and A. J. Daugulis, *J. Chem. Technol. Biotechnol.*, 2010, **85**, 302–306.

View Article Online DOI: 10.1039/C7GC01244F

View Article Online
DOI: 10.1039/C7GC01244F

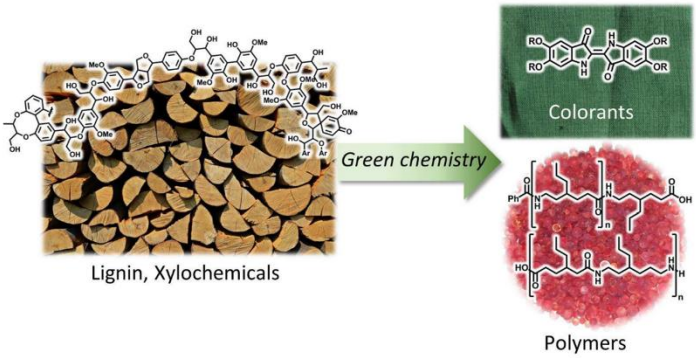

204x104mm (300 x 300 DPI)

Curriculum Vitae

Publications & Contributed Presentations

Publications

- *Amphiphilic PEG with pH-sensitive Units Introduced via Anionic Ring-opening Copolymerization of EO and EPB Using a Hydrophobic Initiator*
  A.-K. Danner, L. Bessler, H. Frey, **2018**, *to be submitted.*
- *Synthesis of Mannose-carrying Lipids via Anionic Copolymerization of Ethylene Oxide and Mannose-bearing Glycidyl Ethers*
  A.-K. Danner, J. Langhanki, T. Opatz, H. Frey, **2018**, *to be submitted.*
- *Stealth Properties? How Adhesive Phosphonate Groups Control the Protein Corona of Polyglycerol-stabilized Nanocarriers*
  A.-K. Danner, S. Schöttler, E. Alexandrino, S. S. Hammer, K. Landfester, V. Mailänder, S. Morsbach, H. Frey, F. R. Wurm, **2018**, *to be submitted.*
- *Monomer-activated Copolymerization of Ethylene Oxide and Epichlorohydrin: In Situ Kinetics Evidences Tapered Block Copolymer Formation*
  A.-K. Danner, D. Leibig, L.-M. Vogt, H. Frey, **2018**, *to be submitted.*
- *Examples of Xylochemistry: Colorants and Polymers*
  J. Kühlborn, A.-K. Danner, H. Frey, R. Iyer, A. J. Arduengo, T. Opatz, Green Chem. **2017**, *19*, 3780.

Contributed Presentations

- JCF Frühjahrssymposium, Konstanz, Germany, 2018
  Multifunctional and pH-responsive Polyether-based Lipids for Targeted Drug Delivery (Poster)
- 134th BASF International Summer Course, Ludwigshafen, Germany, 2017
  Multifunctional and pH-responsive Polyether-based Lipids for Targeted Drug Delivery (Presentation & Poster)
- The 12th International Conference on Advanced Polymers via Macromolecular Engineering, Ghent, Belgium, 2017
  Amphiphilic Polyether-based Architectures as Versatile Structures for Biomedical Applications (Poster)
- 253rd ACS National Meeting & Exposition, San Francisco, USA, 2017
  Multifunctional Polyether-based Lipids for Liposomal Nano Drug Carrier Systems (Presentation & Poster)
- International Conference on Advanced Polymers, Biomaterials, Bioengineering & Nano Drug Delivery, Flic-en-Flac, Mauritius, 2016
  Polyether-based Lipids with Targeting Functions for Drug Delivery Systems (Poster)
- Leibniz Young Polymer Scientist Forum, Aachen, Germany, 2016
  Versatility of Cholesterol-initiated, Multifunctional Polyethers in Nano Drug Carrier Systems (Presentation & Poster)
- JCF Frühjahrssymposium, Kiel,Germany, 2016
  Polyether-based Lipids for the Synthesis of Nanocarriers with Stealth-Effect (Poster)
- 250th ACS National Meeting & Exposition, Boston, USA, 2015
  Polyether-based Lipids with Targeting Functions for Biomedical Applications (Poster)